



**U.S. Department of Energy
Office of Energy Efficiency and Renewable Energy
Fuel Cell Technologies Program
Hydrogen Sorption Center of Excellence (HSCoE)**

HSCoE Final Report Executive Summary

September 30, 2010

***Lin Simpson
Director, HSCoE
National Renewable Energy Laboratory (NREL)
Golden, Colorado***

NREL is a national laboratory operated by the Alliance for Sustainable Energy, LLC, for the United States Department of Energy under contract DE-AC36-08GO28308.

HSCoE Final Report, Executive Summary

Acronyms and Abbreviations

ANL	Argonne National Laboratory
APCI	Air Products and Chemicals Inc.
B	boron
Be	beryllium
BET	Brunauer-Emmett-Teller
C	carbon
CA	carbon aerogel
Ca	calcium
Caltech	California Institute of Technology
COF	covalent organic framework
Cr	chromium
Cu	copper
DOE	U.S. Department of Energy
DRIFTS	diffuse reflectance infrared Fourier transform spectroscopy
Duke	Duke University
EERE	DOE Office of Energy Efficiency and Renewable Energy
F	fluorine
Fe	iron
FY	fiscal year
g	gram
g/mol	grams per mole
H	hydrogen
H ₂	dihydrogen
K	kelvin
kJ	kilojoule
kW	kilowatt
L	liter
Li	lithium
LLNL	Lawrence Livermore National Laboratory
m ²	square meter
Met-Cars	metallocarbohedrenes
Mg	magnesium
Michigan	University of Michigan
Missouri	University of Missouri-Columbia
mL	milliliter
Mn	manganese
Mo	molybdenum
MOF	metal-organic framework
mol	mole
N	nitrogen
Na	sodium
Ni	nickel
NIST	National Institute of Standards and Technology
nm	nanometer

NMR	nuclear magnetic resonance
NREL	National Renewable Energy Laboratory
O	oxygen
ORNL	Oak Ridge National Laboratory
PEEK	polyetheretherketone
Penn	University of Pennsylvania
Penn State	Pennsylvania State University
POP	porous organic polymer
Pt	platinum
Rice	Rice University
Ru	ruthenium
S	sulfur
Sc	scandium
SSA	specific surface area
SWNH	single-walled carbon nanohorn
SWNT	single-walled carbon nanotube
TAMU	Texas A&M University
TC	templated carbon
Ti	titanium
TPD	temperature-programmed desorption
UCLA	University of California, Los Angeles
UNC	University of North Carolina, Chapel Hill
V	vanadium
vdW	van der Waals
W	tungsten
wt %	weight percent
Zn	zinc

Abstract

The U.S. Department of Energy (DOE) Hydrogen Sorption Center of Excellence (HSCoE) was formed in 2005 as a 5-year project to develop hydrogen storage materials primarily for application with light-duty vehicles. The HSCoE was competitively selected (DOE 2003), led by the National Renewable Energy Laboratory (NREL), and comprised partners from U.S. national laboratories, universities, and industry (see Figure ES-1). The HSCoE concluded operations in September 2010 as per its planned schedule.

Because dihydrogen (H_2) has relatively low volumetric energy density compared to typical liquid transportation fuels, the primary focus of the HSCoE was to develop sorbent materials that could be used to meet DOE 2010 and 2015 on-board hydrogen storage system targets. These targets included on-board fuel storage in which the system contains more than ~5.5 percent by weight (wt %) and ~40 grams of hydrogen per liter (g/L). State-of-the-art, compressed-gas H_2 systems operate at pressures between 350 and 700 bar at ambient temperature and store 3–4 wt % and less than 25 g/L. In addition, current liquid-hydrogen systems use more than 30% of the energy in the hydrogen for liquefaction and cannot meet the DOE long-term targets for volumetric capacity. Thus, the HSCoE's goal was to develop sorbents that enable systems to operate at temperatures closer to ambient and at nominal pressure (less than 350 bar), to help meet all DOE performance targets simultaneously.

In general, sorbents increase hydrogen storage capacities compared to high-pressure, compressed-gas systems at a given pressure and temperature, thus enabling lower pressure to be used to achieve a capacity that's comparable or higher. At sufficiently high pressures where compressed H_2 becomes very dense (typically 250 to 300 bar at ambient temperature), sorbents no longer improve hydrogen storage capacities. Sorbent materials embody a tremendous potential for transportation technologies and offer a range of advantages compared to existing systems. They allow fast hydrogen fill-up and discharge rates, nominal thermal-management requirements during refueling, ease of engineering, the ability to provide required pressures, and favorable system energy efficiencies, which decrease costs. Sorbents may also be used in other hydrogen storage applications such as delivery and stationary power generation.

When the HSCoE was established, the main challenge for sorbents revolved around the low binding energies of H_2 with interfaces, and thus the need to use cryogenic temperatures to achieve high capacity. Thus, from the outset, the HSCoE focused on adjusting the binding energies to achieve higher capacity at temperatures closer to ambient. Overall, the main issues for hydrogen storage with sorbents involve achieving required volumetric and gravimetric capacities as well as system cost. These issues are related, because system costs are directly addressed by increased capacities and storage at temperatures closer to ambient and at lower pressures.

HSCoE principals identified four main mechanisms for hydrogen storage by sorbents and created specific development plans to ensure that the appropriate resources were applied to solving the very difficult technical issues with each one. To ensure efficiency and accelerate development, the HSCoE formed complementary research focus areas/groups loosely aligned with the four sorption-based hydrogen storage mechanisms: (1) Optimized Nanostructures, (2) Substitution, (3) Strong/Multiple H_2 Binding by Metal Centers, and (4) Weak Chemisorption/Spillover.

Specific partners with the right skill sets were assigned to each research group; these partners worked closely together on the most difficult issues for each focus area. Selection criteria were established for each focus area, and the HSCoE quickly selected specific sorbents/classes for focused development efforts based on their hydrogen storage potential and/or performance—along with material classes that *should not* be developed further.

Regardless of the specific elements used, a pure physisorption material needs to have a specific surface area (SSA) of more than about 3,000 m²/g to have the potential to meet DOE hydrogen storage targets (see *DOE Fuel Cells Technologies Multi-Year Research, Development and Demonstration Plan* [DOE 2007]). This requirement alone eliminates hundreds of elements and materials that are just too heavy.

During its 5-year life, the major findings of the HSCoE included:

1. **Cryogenic Storage:** New materials increase gravimetric (>60%, i.e., from ~5 to >8.5 wt % at ~80 K) and volumetric (~150%, i.e., from ~15 to >35 g/L at ~80 K) hydrogen storage on high-SSA sorbents by optimizing pore size distributions (0.7 to 1.5 nm) to increase SSA and packing density. Standard physisorption-based H₂ gravimetric capacity scales with SSA. Thus, no substantial increase in capacity can be achieved with geometric structures alone. Although binding energies can be approximately doubled with very small pores that enable multiple wall interactions with the H₂ molecules, effectively, the space for adsorption is decreased, thus decreasing the overall capacity.
2. **Toward Ambient-Temperature Storage:** Substitutional materials such as boron in carbon or metal-organic frameworks (MOFs) exhibit enhanced dihydrogen binding energy (i.e., 8 to 12 kJ/mol) that increases capacities (e.g., doubles or triples) on a per-SSA basis at near-ambient temperatures.
3. **Ambient-Temperature Storage:** Reversible high-capacity sorbents that were designed and made via ambient-temperature hydrogenation techniques such as spillover store 1 to 4 wt % at ambient temperatures, with the potential for 7 wt % and 50 g/L at ambient temperatures and less than 200 bar. In addition, *coordinated unsaturated metal centers* are a new class of H₂ storage materials with the potential to store at ambient temperature >10 wt % and >100 g/L. More fundamental experimental work is needed to fully prove these concepts and provide validation for the model predictions.
4. **Improved Measurements:** Unique measurement capabilities developed by the HSCoE accurately and reproducibly characterize H₂ storage properties of small, laboratory-scale samples (1–200 mg). These measurement capabilities enhanced high-throughput, rapid-screening analyses. In addition to capacity measurements, a high-pressure nuclear magnetic resonance spectroscopy system was developed to help identify hydrogen interactions in micropores versus those in macropores. The HSCoE also used several different techniques including neutron scattering, Raman and Fourier transform infrared spectroscopies, and differential volumetric measurements to provide unique hydrogen storage materials' characterization. In addition, the HSCoE led the publication of DOE's "Best Practices" guide for hydrogen storage measurements—a reference guide for kinetics, capacity, thermodynamics, and cycling measurements (DOE 2008).

5. ***Predictive Theory:*** Research approaches used by the HSCoE that combined iterative and coupled theory and experimental efforts accelerated materials design and development. First-principles theorists designed synthesis pathways and accompanying materials with optimal hydrogen storage properties. These predictive approaches sped identification of materials with the potential to meet DOE hydrogen storage targets, including novel heterogeneous materials, paths to creating high-capacity, fast-filling spillover materials, and new classes of sorbents with the potential for greater than 100 g/L and 10 wt % at ambient temperature. If these materials were to be reproducibly synthesized, they would have the potential of enabling systems that exceed DOE's 2015 system targets.

The HSCoE accelerated development by working closely among groups with the right skill sets to increase appropriate-material synthesis rates of optimized sorbents with access to as many higher-energy binding sites as possible. The sorbent-development efforts were also accelerated by iteratively using first-principles theory with known materials and processes to design rational synthetic pathways and materials with optimal hydrogen storage properties. These predictive approaches helped to speed the identification of materials and approaches that have the potential to meet DOE hydrogen storage targets, including novel heterogeneous materials, paths to creating high-capacity, high-rate spillover materials, and entirely new classes of sorbents, one of which uses the unique properties of calcium, with viable synthetic routes. These revolutionary materials could store hydrogen at densities greater than 100 g/L and 10 wt % at ambient temperature, which is well in excess of liquid-hydrogen densities and exceeds DOE's ultimate system targets including cost, volumetric capacity, and gravimetric capacity.

The HSCoE made substantial progress in developing sorbents for hydrogen storage. This includes identifying numerous materials and entire material classes for which development efforts either were not started or were ended, and for which the HSCoE recommends that future efforts not be performed. The HSCoE also created high-SSA sorbents that can be used to construct systems that meet DOE's 2010 hydrogen storage targets. Furthermore, although only a very limited number of viable routes exist, the HSCoE identified clear development paths for constructing sorbents with the potential to meet DOE's 2015 and even DOE's ultimate full-fleet targets for light-duty vehicles (DOE 2009).

The HSCoE believes that the on-vehicle refueling capability of sorbent materials is unique and offers tremendous advantages that should be exploited for hydrogen storage. Thus, the HSCoE highly recommends that future development efforts be performed with the focus on reducing material and system costs by improving material storage capacities at near-ambient temperatures. Future efforts should leverage the work performed by the HSCoE to minimize repetition, gain insights on lessons learned, and use the materials and capabilities developed. For example, the rapid-throughput, highly accurate characterization capabilities for hydrogen storage materials developed by the HSCoE were essential to quickly identify material properties and validate results so that minimal efforts were wasted on poor materials or erroneous results. This is absolutely critical to eliminating the hundreds of thousands of dollars and years of effort often associated with rooting out what ultimately turns out to be erroneous results. Furthermore, any future efforts must also investigate additional material properties related to hydrogen storage systems so that thermal conductivity, heat dissipation, refill and discharge rates, durability, and other engineering issues are fully addressed.

Table of Contents

Introduction	8
HSCoE Partners	10
R&D Approach and Research Activities	12
Optimized Nanostructures for Physisorption	14
Substitution	15
Strong/Multiple Dihydrogen Binding	16
Weak Chemisorption/Spillover	16
Major Results and Findings	17
Cryogenic Storage via Physisorption on High-SSA Materials	19
Toward Ambient-Temperature Storage with Increased H ₂ Binding	22
Increasing Ambient-Temperature Storage with Strong/Multiple Dihydrogen Binding	25
Weak Chemisorption/Spillover	29
Major Accomplishments	33
Recommendations	36
Review of Go/No-Go Decisions	36
Recommendations for Continued R&D	37
Suggestions for New Materials Systems To Be Investigated	40
Identification of Remaining Issues for Recommended Systems	40
Identification of Systems Recommended for No Further Investigation	42
Recommended Storage Options and Material Systems for Early Market Applications	42
Lessons Learned from the Center Approach	42
Lessons Applicable to All R&D Efforts	43
Summary of Accomplishments	43
Conclusions	45
References	48

Introduction

The U.S. Department of Energy (DOE) Hydrogen Sorption Center of Excellence (HSCoE) was competitively selected and formed in 2005 to develop materials for hydrogen storage systems to be used in light-duty vehicles. The HSCoE and two related centers of excellence were created as follow-on activities to the DOE Office of Energy Efficiency and Renewable Energy's (EERE's) Hydrogen Storage Grand Challenge Solicitation issued in fiscal year (FY) 2003 (DOE 2003).

Because dihydrogen (H_2) has relatively low volumetric energy density compared to typical liquid transportation fuels, the primary focus of the HSCoE was to develop sorbent materials that could be used to meet DOE 2010 and 2015 on-board hydrogen storage system targets. These targets included on-board fuel storage in which the system contains more than ~5.5 percent by weight (wt %) and ~40 grams of hydrogen per liter (g/L). State-of-the-art, compressed-gas H_2 systems operate at pressures between 350 and 700 bar at ambient temperature and store 3–4 wt % and less than 25 g/L. In addition, current liquid-hydrogen systems use more than 30% of the energy in the hydrogen for liquefaction and cannot meet the DOE long-term targets for volumetric capacity. Thus, the HSCoE's goal was to develop sorbents that enable systems to operate at temperatures closer to ambient and at nominal pressure (less than 350 bar), to help meet all DOE performance targets simultaneously. Sorbents allow fast on-vehicle hydrogen fill-up and discharge rates, nominal thermal management requirements during refueling, ease of engineering, the ability to provide required pressures, and favorable system energy efficiencies. The last benefit affects hydrogen and storage costs, a vital consideration in designing storage systems. In addition, sorbents may also be used in other hydrogen storage applications such as stationary power generation, portable power, backup power, and niche, early-market vehicles.

Hydride species often have high binding energies (typically 40–60 kilojoules per mole [kJ/mol]) with the hydrogen, which can result in poor energy efficiencies for reversible storage and may require off-vehicle regeneration of the spent material. By comparison, the hydrogen sorbents investigated by the HSCoE typically rely on non-covalent interactions (for example, typically 5 to ~30 kJ/mol), thus providing a range of advantages compared to hydride and high-pressure physical storage systems for transportation applications. The optimal hydrogen interactions with sorbents could enable fast hydrogen on-vehicle fill and discharge rates, nominal thermal management requirements during fueling, lower pressure requirements for on-board storage and fueling, ease of engineering on the vehicle, and favorable “well-to-fuel cell” energy efficiencies that decrease vehicle and station costs.

In general, sorbents increase hydrogen storage capacities compared to high-pressure, compressed-gas systems at a given pressure and temperature, thus enabling lower pressure to be used to achieve a capacity that's comparable or higher. At sufficiently high pressures where compressed H_2 becomes very dense (typically 250 to 300 bar at ambient temperature), sorbents no longer improve hydrogen storage capacities. When the HSCoE was established, the main challenge for sorbents revolved around the low binding energies of H_2 with interfaces, and thus the need to use cryogenic temperatures to achieve high capacity. Thus, from the outset, the HSCoE focused on adjusting the binding energies to achieve higher capacity at temperatures closer to ambient. Overall, the main issues for hydrogen storage with sorbents involve achieving required volumetric and gravimetric capacities as well as system cost. These issues are related,

because system costs are directly addressed by increased capacities and storage at temperatures closer to ambient and at lower pressures.

Detailed system analysis is needed to project actual H₂ storage system capacities, but, because this was outside the scope of the HSCoE, the HSCoE typically reported what is termed “excess” H₂ storage material values. Excess values represent the H₂ actually stored on the sorbent surfaces and thus what the material is contributing to storage in the system/tank. Because sorbents tend to have additional pore and intraparticle volume where H₂ gas also resides, a given material will typically “contain” more (i.e., material “total”) H₂ than the reported material excess value. However, DOE-directed detailed analyses indicate that systems using sorbents will have usable system capacities close to the excess values, and thus these excess values can be used to gauge differences between materials and what an actual system may store (ANL 2010). Specifically, although the exact details will vary based on the storage pressure, temperature, and storage mechanism, the HSCoE focused on developing sorbents with excess capacities greater than ~6 wt % and 40 g/L, and on reducing system and station costs by limiting storage pressures to less than 200 bar and temperatures to higher than ~77 degrees Kelvin (K) (–200 degrees Celsius, °C), with the ultimate goal of higher than 200 K (–80°C). Note that material “total” capacities are only normalized to the sorbent weight and are often misleading, because they typically translate to far lower system capacities when the weight of the entire system is used.

The HSCoE's critical goals included the following hydrogen storage system targets: net available capacity of 45 g/L and 6 wt % and system cost of \$133/kg H₂. However, in FY 2009, DOE revised the hydrogen storage system targets for light-duty vehicles, some of which are shown in Table ES-1 (DOE 2009). In light of this change, all DOE targets discussed in the remainder of this document will reference the revised DOE hydrogen storage system targets. The targets for the HSCoE are nominally reflected by the 2015 DOE hydrogen storage targets shown in Table ES-1.

Table ES-1. Revised (in 2009) Selected High-Level DOE Hydrogen Storage System Targets for Light-Duty Vehicles*

Target	2010	2015	Ultimate Full Fleet
System Gravimetric Density (% wt)	4.5 (1.5 kWh/kg)	5.5 (1.8 kWh/kg)	7.5 (2.5 kWh/kg)
System Volumetric Density (g/L)	28 (0.9 kWh/L)	40 (1.3 kWh/L)	70 (2.3 kWh/L)
System Fill Time for 5-kg fill, min (fueling rate, kg/min)	4.2 min (1.2 kg/min)	3.3 min (1.5 kg/min)	2.5 min (2.0 kg/min)

*http://www1.eere.energy.gov/hydrogenandfuelcells/storage/pdfs/targets_onboard_hydro_storage_explanation.pdf

To ensure that the development activities were performed as efficiently as possible, the HSCoE formed complementary, focused development teams or clusters based on the following four sorption-based hydrogen storage mechanisms:

1. Physisorption on high-specific surface area (SSA) and nominally single-element materials
2. Enhanced H₂ binding in substituted/heterogeneous materials

3. Strong and/or multiple H₂ binding from coordinated, but electronically unsaturated, metal centers
4. Weak chemisorption/spillover.

From the outset, HSCoE partners were chosen to provide the specific expertise and capabilities necessary to develop materials that could fulfill DOE requirements. The National Renewable Energy Laboratory (NREL) led the HSCoE, with partners at other U.S. national laboratories and universities, and at Air Products and Chemicals, Inc., a corporate partner (see Figure ES-1). The NREL team included HSCoE Director Lin Simpson, Anne Dillon, Philip Parilla, Thomas Gennett, Yufeng Zhao, Jeff Blackburn, and Chaiwat Engtrakul, as well as Michael Heben (who subsequently went to the University of Toledo) and Shengbai Zhang (now at Rensselaer Polytechnic Institute).

HSCoE Partners

Under NREL's coordination, a center was established that included development activities at more than 20 renowned institutions throughout the United States and direct collaborations with institutions around the world. The HSCoE partners/projects are described briefly in the following.

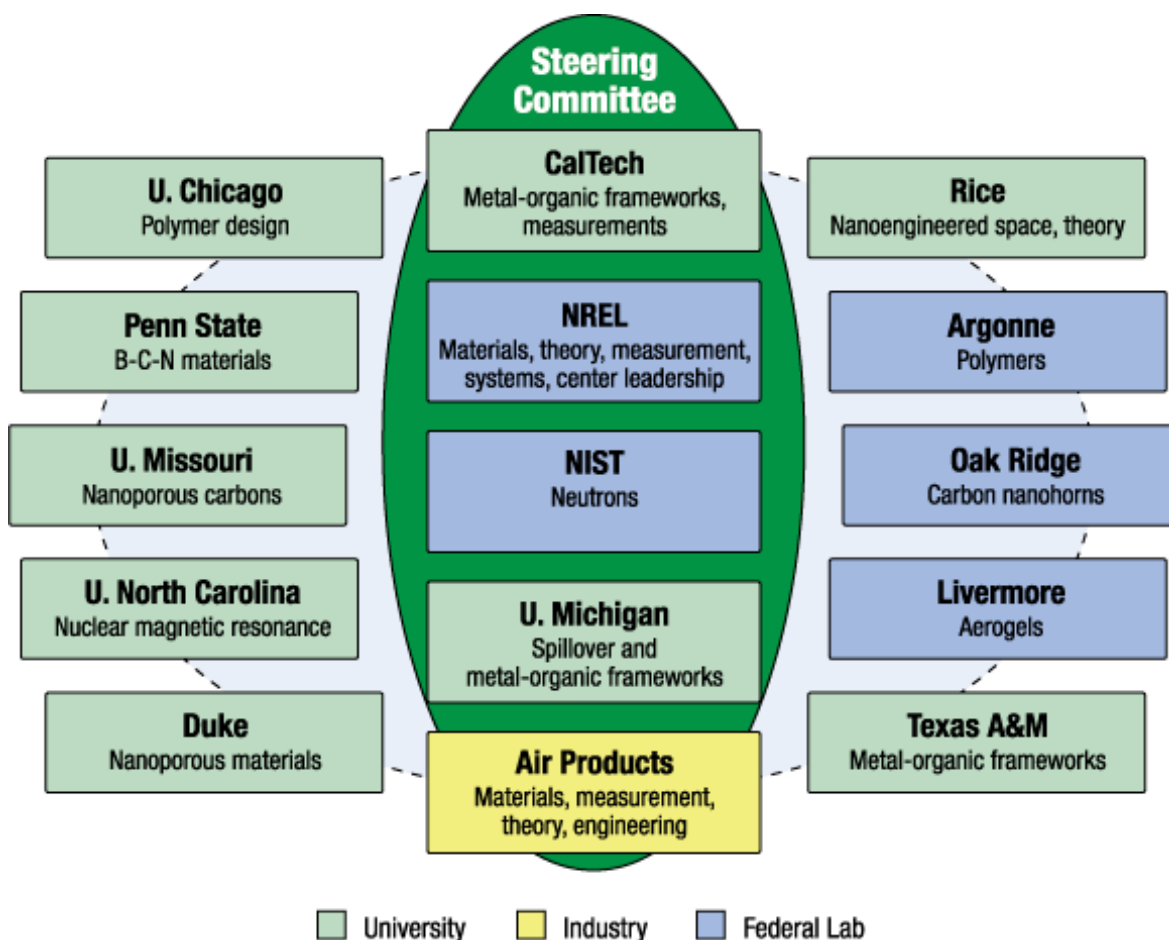


Figure ES-1. Overview of the HSCoE partners. Rice, NREL, and Air Products and Chemicals formed the HSCoE Steering Committee during Phase I.

- ***Air Products and Chemicals Inc. (APCI)***, Alan Cooper and Guido Pez (retired). APCI enabled and executed discovery of materials with "practical heats" of hydrogen absorption.
- ***Argonne National Laboratory (ANL)***, Di-Jia Liu, University of Chicago, Yuping Lu. ANL developed new hydrogen adsorbents based on nanostructured porous organic polymers (POPs). ANL collaborated with the University of Chicago researchers who constructed the POPs.
- ***California Institute of Technology (Caltech)***, Channing Ahn. Caltech focused efforts on determining the optimal microporous size distributions necessary for maximizing volumetric densities and producing uniform binding for the entire capacity range of the sorbent.
- ***Duke University***, Jie Liu. Duke initially synthesized and purified gram quantities of single-walled carbon nanotubes (SWNTs) with well-controlled small diameters via chemical vapor deposition methods. After no significant improvement in sorption properties was found, the project was redirected to developing low-cost and scalable synthesis of microporous carbon materials with well-controlled pore sizes suitable for hydrogen storage.
- ***Lawrence Livermore National Laboratory (LLNL)***, Ted Baumann. The LLNL team concentrated on the design and synthesis of new nanostructured carbon aerogels (CAs) that could meet the DOE 2010 targets for on-board vehicle hydrogen storage.
- ***University of Michigan (Michigan)***, Ralph T. Yang. Michigan pioneered the development of new nanostructured sorbents optimized for hydrogen spillover.
- ***University of Missouri-Columbia (Missouri)***, Peter Pfeifer. Missouri investigated high-SSA carbons from corn cobs, which show considerable promise for reversible on-board storage of hydrogen with high gravimetric and volumetric storage capacities.
- ***National Institute of Standards and Technology (NIST)***, Dan Neumann and Craig Brown. NIST performed state-of-the-art, neutron-scattering measurements to probe the amount, location, bonding states, dynamics, and morphological aspects of hydrogen storage materials. NIST performed this role within both the HSCoE and the Metal Hydride Center of Excellence.
- ***Oak Ridge National Laboratory (ORNL)***, Dave Geohegan and Alexander A. Puzos. ORNL worked on synthesis, processing, and tuning of single-walled carbon nanohorn (SWNH) structures for effective hydrogen storage to meet the DOE 2010 targets.
- ***Pennsylvania State University (Penn State)***, Peter C. Eklund (deceased), Michael Chung, Henry Foley, and Vincent Crespi. Penn State developed new high-SSA materials that have enhanced hydrogen binding (i.e., isosteric heats of adsorption) through a direct chemical modification of the framework via chemically substituting boron (B) into sp^2 -carbon (C) frameworks.
- ***Rice University (Rice)***, James Tour, Carter Kittrell, and Richard E. Smalley (deceased). Rice's primary objective was to design and develop nanostructured materials using sp^2 carbon.

- **Rice**, Boris Yakobson and Robert Hauge. For this project, Rice modeled the interaction of hydrogen with material structures, optimized them for storage, and assessed their capacity.
- **Texas A&M University (TAMU)**, Hongcai Zhou (formerly of Miami University-Ohio). TAMU designed, synthesized, and characterized high-SSA, metal-organic frameworks (MOFs) with active metal centers aligned in porous channels and accessible by H₂ molecules.
- **University of North Carolina, Chapel Hill (UNC)**, Yue Wu and Alfred Kleinhammes. UNC developed unique characterization tools based on nuclear magnetic resonance (NMR) to provide simultaneously detailed information on microscopic structures of nanoporous materials and their hydrogen storage capacities, binding energies, and kinetics.
- **University of Pennsylvania (Penn)**, Alan G. MacDiarmid (deceased), Pen-Cheng Wang. Penn focused on the synthesis, processing, characterization, and selection of polyaniline-based materials.
- **Former Partner: Michigan/University of California, Los Angeles (UCLA)**, Omar Yaghi. This project, which developed MOFs for hydrogen storage, left the HSCoE at the end of Phase I, which concluded 18 months after the start, to pursue development independently.

R&D Approach and Research Activities

A guiding principle the HSCoE used in developing the required materials is that a continuum of energies existed for hydrogen bound to substrates and molecules. On the weak side of the continuum is non-dissociative (hydrogen remains a molecule, H₂) physisorption, which is due purely to van der Waals (vdW) forces (~4 kJ/mol). On the opposite end is the full C-H chemical bond in methane with an energy of ~400 kJ/mol. As shown in Figure ES-2, between these two limits, with nominal binding energies between 5 and 40 kJ/mol, are:

- *Physisorption* related to key parameters affecting vdW forces
- *Enhanced dihydrogen binding* via the formation of complexes that exhibit electron transfer interactions from the hydrogen as in substituted/heterogenous materials
- *Multiple dihydrogen interactions*, i.e., forward- and back-electron donation, between the sorbent and hydrogen that induces a significant molecular bond stretching between the hydrogen atoms
- *Weak chemisorption*, which is weak, reversible, chemical bonding of mono-atomic hydrogen to lightweight receptor materials (via a “spillover” mechanism).

The DOE targets can be met with sorbents if: (1) the energy for hydrogen adsorption (i.e., the enthalpy) can be designed to be in a nominal optimal range of ~10–40 kJ/mol, depending on the entropy (i.e., effectively the state of the sorbed hydrogen compared to the relatively disordered state of the hydrogen gas), desired operating pressure, and temperature (see Figure ES-3); and/or

(2) an efficient volumetric arrangement (see Figure ES-4) of a sufficient number of suitable binding sites can be achieved with a low-weight material.

By focusing on specific mechanisms, the HSCoE leveraged appropriate materials and synthetic capabilities and expertise of the different partners to create optimized-pore-size and high-SSA materials; heterogeneous materials with enhanced dihydrogen binding; materials with coordinated metal centers; and spillover or chemisorbed hydrogen materials.

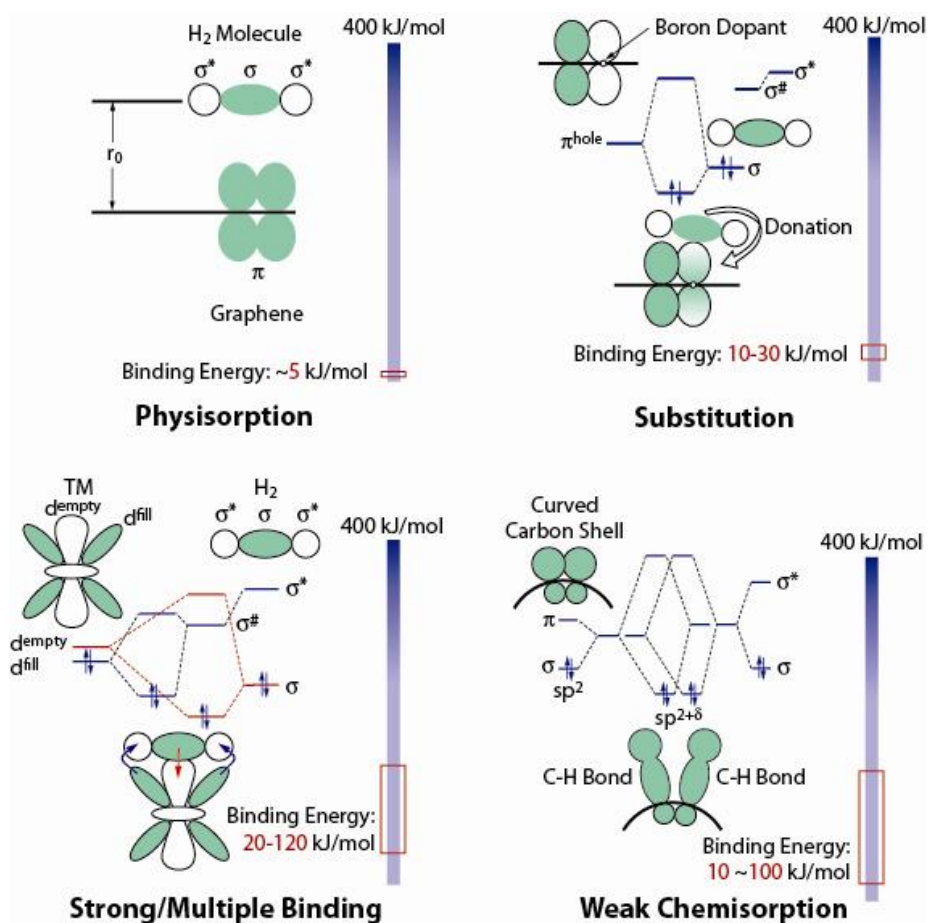


Figure ES-2. Illustration of the four types of sorbent binding mechanisms the HSCoE investigated

From the outset, to facilitate selection from among a relatively large number of potential sorbent materials, HSCoE researchers placed greater emphasis on identifying and developing mechanisms that led to higher volumetric capacity and more favorable operating conditions rather than on specific individual materials. This enabled efficient and rapid progress by focusing resources on identifying and optimizing specific properties and critically evaluating hydrogen storage material classes. This is why the HSCoE was organized into four focused efforts, each of which was designed to address a specific set of issues associated with a specific hydrogen-sorption mechanism (Figure ES-2).

These focused research efforts were complementary, with lessons learned and materials developed in one effort often proving applicable to another. For example, the main issues for physisorption are optimized pore sizes and very high SSAs. Similar issues arise for other sorbent material classes, and thus lessons learned for physisorption materials were directly applied to other HSCoE development activities. The key advantage of the mechanism-focused approach is that selection criteria could be identified for each material class based on a limited amount of experimental and calculation work. This enabled identification of the most promising materials, and thus eliminated the vast majority that lacked the potential to meet DOE targets. This approach substantially reduced the HSCoE's overall work while prioritizing development efforts.

Optimized Nanostructures for Physisorption

In most hydrogen-sorption materials with the potential to meet DOE targets, almost every atom must be accessible and lightweight. Therefore, materials with high SSA are required. In addition, to meet volumetric targets, the sorption sites need to be arranged to minimize the amount of open space (Figure ES-4) so that the bulk density can be as high as possible. This suggests that porous structures should be optimized to allow hydrogen egress in and out, but the hydrogen should be in contact with some kind of sorption site. Logically, the materials should have no macroporosity (pores greater than ~50 nm diameter) and minimal mesoporosity (pores between 2 and 50 nm diameter), and, depending on the specific sorption mechanism, the materials should have pore sizes between 0.7 and ~1.5 nm.

In general, to allow sorption on all surfaces of a pore, the distance between the surfaces should be at least twice that of the kinetic diameter of dihydrogen (2.89 Å). In addition, multilayer adsorption effects, H-H repulsion, and other space-optimization considerations suggest that the pore sizes may need to be ~1.2 nm. Finally, calculations suggest that some enhanced binding may occur if the pore structure is on the order of 0.7 to 1.2 nm.

The "Optimized Nanostructures" effort focused on designing and synthesizing lightweight, high-SSA, optimal-pore-size materials with the findings being applicable to almost all sorption materials. The effort focused on stabilizing large quantities of hydrogen directly by physisorption. Specific activities involved performing theoretical modeling and experiments to determine potential mechanisms for higher storage capacities and to provide guidance for materials development. The thrust of these efforts involved optimizing both sorption sites and

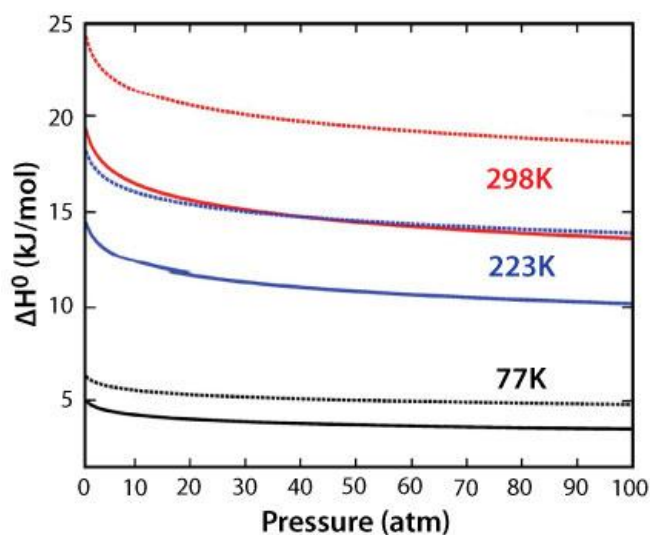


Figure ES-3. The optimal enthalpy (ΔH) for hydrogen storage depends on the pressure, temperature, and sorption interaction (i.e., entropy: dotted lines $\Delta S=-10R$, and solid lines $\Delta S=-8R$). For example, as shown in this plot (Source: Bhatia and Myers 2006), if materials with enthalpies between ~13 and 25 kJ/mol can be made, then ambient-temperature hydrogen storage is possible with pressures between ambient and 100 bar. For lower binding energies, lower storage temperatures will be needed.

space to enhance binding without loss of volumetric capacity. In addition, these efforts developed and/or improved scalable and reproducible synthesis methods of nanoporous materials. Several different synthetic pathways were investigated, including templated carbon/boron, polymers, MOFs, aerogels, SWNHs, and scaffolded SWNTs. Synthesized materials were characterized to determine their hydrogen storage properties and, when appropriate, to identify unique sorption mechanisms. In some cases, this involved optimizing materials for other storage processes beyond physisorption.

Substitution

The HSCoE formed the “Substitution” development effort to focus on increasing the intrinsic binding energy of storage materials and thus their storage capacity at higher temperatures. In general, increasing the intrinsic heats of dihydrogen adsorption is difficult, and the HSCoE identified only a few potential pathways.

For most pure materials, or materials with electronic configurations that induce no significant adsorption, the primary adsorption mechanism is physisorption, which typically has enthalpies of ~ 5 kJ/mol or less for interaction with a single surface. Enhanced physisorption binding energies (i.e., 5 to 10 kJ/mol) are often observed with high-SSA materials. This is primarily a result of interaction with multiple adsorption sites that then limits the total gravimetric capacities. In general, physisorbed dihydrogen on single surfaces has relatively low binding energies, and capacity requires operation at lower cryogenic temperatures and higher intermediate pressures. Typically, increased binding energies, lower temperature, and higher pressure are required to overcome the intrinsic repelling force between dihydrogens to yield higher storage capacities on the sorbent surface at a specific temperature and/or pressure.

Going beyond pure physisorption requires enhanced electron interactions between the sorption material and dihydrogen. In general, heterogeneous elemental structures or surface functionalization can induce enhanced electron interactions. However, the HSCoE’s relatively comprehensive investigations revealed very few material systems with the potential to enhance dihydrogen binding.

In general, the exchange of a different atom species in an elementally homogeneous lattice induces an electronic perturbation that may enhance dihydrogen binding. Based on initial

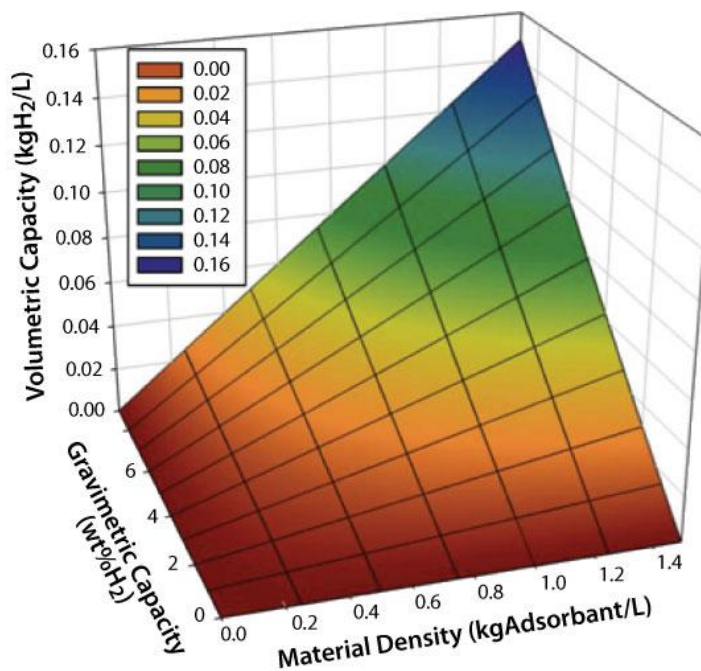


Figure ES-4. Graph from ANL showing the dependence of volumetric density on gravimetric and bulk density for sorption materials. The plot indicates that to have the potential to meet the DOE 2015 volumetric target (0.04 kgH₂/L, yellow band on chart), bulk material densities between 0.7 and 1 g/L will be required for sorbent materials with 6 to 7 wt % gravimetric capacities.

predictions and experimental results, the HSCoE partners developed scalable synthesis methods to form substituted and intercalated materials that demonstrate enhanced dihydrogen storage properties. Boron substitution was achieved by either starting with chemical compounds with high concentrations of B and forming high-SSA materials, forming B-substituted activated and graphitic carbons (e.g., BC₃), or substituting boron for carbon atoms in preformed materials. In addition, the HSCoE partners developed anion-intercalated graphitic and other intercalated/functionalized materials with enhanced hydrogen storage properties.

Strong/Multiple Dihydrogen Binding

The final set of methods to improve dihydrogen binding is characterized by forward- and back-electron donation from the sorption material that induces a significant molecular bond stretching between the hydrogen atoms (Kubas 2001). Typically, this is achieved when the sorption sites are electronically and coordinately unsaturated. In these cases, electrons are donated from the hydrogen to electronic states in the sorbent, and some electron transfer occurs where other sorbent electronic states donate to the hydrogen molecule. These types of sorption sites can bind a dihydrogen molecule more strongly (10 to 200 kJ/mol), but more importantly, they can also bind multiple dihydrogen molecules to a single sorption site. This method enables a substantial increase in volumetric densities if these sites can be densely arrayed.

As stated previously, the HSCoE focused on materials with an optimal range between ~10 and 40 kJ/mol to enable reversible, near-ambient temperature and pressure hydrogen storage. The HSCoE investigated integrating appropriate metal centers with binding energies to 40 kJ/mol with materials such as aerogels, carbon nanohorns, carbon nanotube scaffolds, polycyclic aromatic hydrocarbons, graphene, and MOFs. These efforts included using the higher Coulomb repulsion between alkaline metals to facilitate metal/substrate binding and/or enhancing charge transfer to stabilize the metal/substrate interaction with substitutional integration of different atoms in the support materials. One key issue with the use of open metal centers is that their higher reactivity makes them susceptible to an array of issues. Such issues include agglomeration of the metals and reaction with contaminants, both of which reduce or eliminate the hydrogen storage enhancement, which makes durability and synthetic processing more challenging.

Weak Chemisorption/Spillover

The HSCoE also actively investigated methods to efficiently store dissociated hydrogen. In general, dissociated or atomic hydrogen forms strong bonds with other materials (e.g., metal hydrides or chemical hydrides) that require high temperatures (>500 K) or catalysts to break the bonds. However, it is possible for hydrogen atoms to be adsorbed to surfaces in such a way that the bonding is weaker and conducive to nominal reversible storage capacities at near-ambient temperature and under moderate pressure. From a practical standpoint, a catalyst is typically needed to dissociate the dihydrogen gas; this is a known technology in the chemical process industry. Because most common industrial catalysts (e.g., Pt, Pd, Ni) are relatively heavy and expensive (e.g., platinum group metals), reaching the DOE targets will require catalysts that are appropriately integrated with a lightweight and compact material such as carbon or boron so that the dissociated hydrogen can “spillover” and be stably and reversibly stored, primarily on the lightweight, inexpensive receptor material.

Maximizing performance and costs via spillover involves focused development efforts to optimize catalyst performance and dispersion and to integrate with receptor material properties

and hydrogen surface transport/diffusion mechanisms. This involves performing systematic experiments to quantify spillover processes, determining the causes for material degradation and irreproducibility, and developing scalable and reproducible synthesis methods of spillover materials. For example, because of the mechanisms associated with hydrogen diffusion on the receptor material surfaces, low refueling rates and small materials' surface properties are major challenges that must be resolved. To address these issues, the HSCoE leveraged modeling to identify and to construct new spillover materials with improved properties and to chemically modify known spillover materials to improve spillover performance.

Major Results and Findings

During its 5-year tenure, the HSCoE made substantial progress in developing sorbents that can be used for light-duty vehicle and other applications. The HSCoE developed high-SSA sorbents that could be used to construct systems that meet DOE's 2010 system targets (i.e., 4.5 wt % and 28 g/L). Furthermore, the HSCoE identified development paths for designing and synthesizing sorbents with the potential to meet DOE's 2015 and DOE's ultimate full-fleet system targets for light-duty vehicles (DOE 2009). The HSCoE systematically developed or investigated hundreds of different materials and/or processes; this resulted in more than 200 peer-reviewed publications, with more than 25% of them involving multiple U.S. and international institutions as co-authors. Based on the huge number of framework materials alone (e.g., MOFs), as well as the huge number of potential new materials identified, the exact number of materials developed/studied is impossible to quantify. However, the efforts led by DOE and the HSCoE helped accelerate sorbent development worldwide, as demonstrated by the thousands of papers that have been published in hydrogen sorption during the last few years. In addition to hundreds of conference presentations, proceedings, and published reports, the HSCoE partners submitted and/or received more than 40 patents.

The HSCoE also determined more than 100 pathways (e.g., synthesis routes) and/or materials that were down-selected as not being applicable to meeting current light-duty vehicle targets. However, some of the down-selected materials and the materials developed for light-duty vehicles may have many other transportation applications and portable or stationary power applications. Many may be useful in today's major high technology applications including carbon capture/CO₂ sequestration, energy storage, batteries, semiconductor electronics, composites, drilling fluids, inks, drug delivery, transparent conductors, photovoltaics, purification, biomass catalysts, fuel cell catalysts, and energy generation.

In general, the major findings for the HSCoE are aligned with the specific sorption mechanisms investigated. However, one of the more important conclusions of the center is related directly to the experimental measurements. During the past 5 years, the HSCoE has measured the hydrogen storage properties of thousands of different sorbents from its partners and from development groups around the world. The lack of consensus and the inability to validate storage-capacity measurements stands out as a major problem that plagues the community. This problem is highlighted by the recent European Commission JRC report showing round-robin test results from the "Novel Efficient Solid Storage for Hydrogen" partners (Zlotea et al. 2009), which showed more than 100% deviation in capacities for the same relatively low-capacity sorption material. Reproducibility and measurement-error problems tend to only get worse with higher-

capacity, laboratory-scale materials where only 50 to 100 mg may be available for measurement. The results from a couple of the laboratories were similar, but interestingly, the agreement between the laboratories was different depending on the storage temperature of the measurements.

Early on, the HSCoE partners also had significant deviations in measurement results between different partners, but the partners worked together to identify measurement differences and to work through the problems. This included working closely with the writing of DOE's best-practices document (DOE 2008), which provides a comprehensive and detailed set of methodologies for performing measurements. Paradoxically, implementation of, and the specific protocols used for, some of the methodologies still results in significant measurement differences, especially for high-capacity sorbents.

As shown in Figure ES-5, it is possible for two institutions that developed measurement systems completely independently to get virtually the same isotherm for the same material. The HSCoE was fortunate to have three groups—NREL, Caltech, and NIST—that had good agreement in hydrogen storage capacity isotherm results at different temperatures and pressures. The center members worked together to help all the different groups develop protocols to measure isotherms accurately, but equipment and training limitations kept even a close group such as the HSCoE partners from achieving complete agreement. In general, though, when partners worked together, hydrogen storage capacity measurements could be brought into close agreement for sorbents, and validation by specific laboratories is sufficient to ensure the competency of the results.

The important issue here is that the HSCoE, sorbent development groups, and the hydrogen storage community as a whole continue to waste valuable resources dealing with reports of exceptional hydrogen storage results that ultimately in months or years turn out to be basic problems with measurements. As discussed below, one of the HSCoE recommendations directly addresses this issue by calling for sorbent standards and qualification practices to be implemented that go well beyond what can be accomplished with the best-practices document (DOE 2008). The other reason for spotlighting this issue is that actual progress and major findings must be compared to validated results—not to unsubstantiated claims that ultimately cannot be reproduced. With this in mind, the HSCoE successfully advanced hydrogen storage sorbents in a number of ways, including improving nanostructures for optimal hydrogen storage and enhancing isosteric heats of adsorption along with capacities.

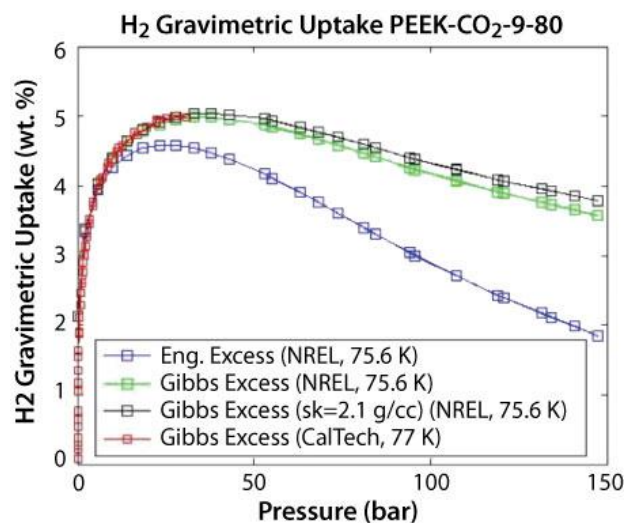


Figure ES-5. Excess H₂ gravimetric uptake isotherms (± 0.1 % error) of a pyrolyzed polyetheretherketone (PEEK) material measured at NREL and Caltech. The agreement of the data from two different laboratories is exceptional, providing strong evidence of the outstanding hydrogen storage properties of this sorbent. The estimated error of the excess H₂ gravimetric uptake for the data from Caltech is ± 0.1 %.

Cryogenic Storage via Physisorption on High-SSA Materials

The HSCoE developed rational designs and methods to synthesize sorbents with the appropriate nanostructures and compositions for optimal hydrogen storage. The center had groups that investigated methods to enhance physisorption through geometric configurations and to form nanostructures with just the right pore sizes, which allowed as much access to the surfaces as possible for hydrogen sorption.

In general, storage capacities increase with higher SSAs and bulk densities. Here, the bulk density is calculated based on the actual volume of the lightweight highly porous sorbent powder or pellets. Although these are necessary requirements for high capacity, other factors, including optimized pore sizes (i.e., 0.7 to 1.5 nm) and enhanced binding energies (i.e., >5 kJ/mol) for the entire capacity range, are also important.

However, it continues to be non-trivial to achieve both the high SSAs and the micropore diameters (i.e., 0.7 to 1.5 nm) necessary for optimized H₂ storage. Many methods, such as activation (Guo et al. 2008) and inorganic or organic templating (Yang et al. 2007; Sakintuna and Yurum 2005), SWNT scaffolds, SWNHs (Poretzky et al. 2008; Geohegan et al. 2007), self-organizing MOFs (Wong-Foy et al. 2006; Collins and Zhou 2007), or equivalent materials were used to make porous materials. With a vast library of ligand “building blocks” and different coordination chemistries, the HSCoE literally made hundreds of frameworks that were characterized by X-ray diffraction, SSA analysis, and H₂ capacities. The HSCoE was at the forefront of formulating and synthesizing frameworks for hydrogen storage (Wong-Foy et al. 2006) and the first to make materials that exceed 3,800 m²/g SSA and have 7 wt % excess H₂ storage capacities. Subsequently, frameworks with ~6,500 m²/g and ~8.5 wt % excess H₂ storage were reported (Farha et al. 2010). The main issues with these framework materials are the need for cryogenic temperatures and the trade-off between very high SSAs that achieve good gravimetric capacities and lower bulk densities (i.e., 0.1 to 0.5 g/ml) that have relatively low volumetric storage capacities (at best, less than ~30 g/L).

As part of the HSCoE efforts, predictive models were developed to understand the physisorption interactions of hydrogen with high-SSA materials and to understand the relationship between geometrical configurations and storage capacities. In general, the volumetric capacity scales directly with the gravimetric capacity through material density. Thus, simultaneous increases of the volumetric and gravimetric capacities require increasing both SSA and material density, which means that larger voids should be removed. For physisorption, H₂ binding energy is determined by the effective contact area per H₂. Perhaps the simplest H₂ sorbent is a sp²-bonding network of pure carbon, in which the closed electronic shell and strong C-C bonds leave no reactive sites for hydrogen chemisorptions, thus only physisorption of hydrogen molecules is allowed in a weak dispersive force field (vdW interaction).

Typical high-SSA carbons such as activated carbons and carbon aerogels generally show great promise for use in storage tanks, but the pore size distributions in these materials range from microporous (<2 nm) to macroporous (>50 nm), resulting in poor volumetric densities. Framework structures also typically have a range of free-space dimensions that can be in the mesoporous regime (2 to 50 nm), which makes a number of these materials less than ideal for hydrogen storage applications. Moreover, typical sorption enthalpies of 4 to 6 kJ/mol are close to thermal energies, requiring low temperatures if large quantities of hydrogen are to be stored.

Within the HSCoE, different synthetic techniques and geometric structures were investigated to determine which provided the best materials for physisorption-based hydrogen storage. The processes included using synthesis techniques to create appropriately sized pores in dense materials and constructing self-assembled crystal structures with open pores.

Previous to the start of the center, a substantial amount of work had been performed on developing “activated” and “superactivated” carbons, with materials such as AX-21 representing the state of the art in sorbents. Sorbents such as AX-21 have ~5 wt % maximum excess hydrogen storage capacity at ~80 K with ~30-bar pressures, but because of their relatively large pore sizes (1 to 4 nm), their bulk densities are relatively low (~0.3 g/ml), and thus their volumetric hydrogen storage capacities are only ~15 g/L. These superactivated carbons are formed using pyrolysis and/or chemical-treatment techniques that create pores in bulk natural carbons.

In general, the HSCoE focused most of its efforts from the outset on creating high-SSA sorbents with optimal and uniform pore sizes. Whether with frameworks, activated carbons, polymers, nanotube scaffolds, or intercalated graphite, the goals remained the same. This focused set of efforts proved successful in creating materials with extremely high SSAs (~6500 m²/g) and gravimetric capacities (>8.5 wt %) at 77 K, high bulk densities in the range of 0.7 to 1.4 g/ml, and in a few cases, materials with both good surface areas and bulk densities (Simpson 2010). This latter set of results is ultimately where all sorbent materials need to be. In the best case, where the best SSAs and best bulk densities via optimal pore sizes can be combined, it may ultimately be possible to synthesize physisorption materials with >7 wt % and >50 g/L capacities at ~80 K and ~40 bar (See Figure ES-6)

It may be possible to meet DOE 2010 hydrogen storage targets with presently demonstrated sorbents at ~80 K storage temperatures. In addition, even though present projections for sorbents are a little low to be able to meet DOE 2015 targets at ~80 K, because sorbent capacities can easily be increased by ~30% (i.e., >9 wt % and >65 g/L) using storage temperatures at ~50 K, there are definitely paths forward for sorbent-based hydrogen storage systems to meet DOE 2015 capacity targets. These increased capacities need to be balanced with system costs and efficiency. However, storage system costs will be significantly lower at the 20 bars needed for 50 K storage compared to the 350- or 700-bar pressures needed for ambient-temperature storage. Even though physisorption-based sorbents will require cryocompression, they have no significant heat-transport issues, can operate at moderate

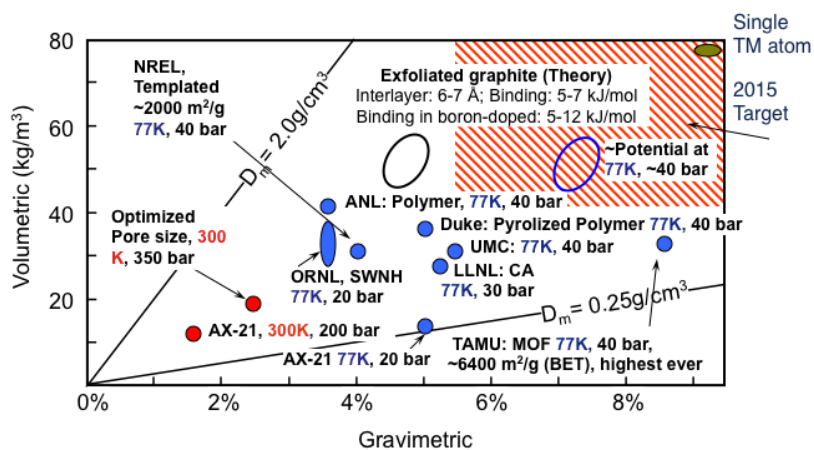


Figure ES-6. Summary plot of excess volumetric and gravimetric capacities achieved for different sorbents. Note that the “AX-21” data are representative of sorbent materials before the HSCoE started.

pressures, and may require the least engineering (compared to metal or chemical hydrides) to design and construct a system that could meet the DOE 2015 targets.

At the outset of the HSCoE's activities, numerous publications had reported extraordinary results for high-SSA materials in which the enhanced capacities were potentially a result of novel geometries or structures within the material (Zlotea et al. 2009). In general, heats of adsorption can be increased with multiple-wall interactions, but this ultimately reduces capacities based on the decrease in space for the hydrogen molecules (Purewal et al. 2009). The HSCoE did not validate any single-element material or any materials with unexceptional electronic states that have substantially higher capacities beyond those expected based on SSA and specific storage conditions. For example, at one time carbon nanotubes were thought to possibly have unique H₂-storage properties, but after a dedicated focused effort, the HSCoE made a No-Go decision on using carbon nanotubes as an ambient-temperature hydrogen storage material. Ultimately, carbon nanotubes may still provide excellent hydrogen storage at cryogenic temperatures. Specific experiments demonstrated that materials with near-single pore sizes did not provide the constant heats of adsorption expected as a function of loading. These results suggest that even in materials with uniform pore sizes, other effects or features (e.g., edge, exterior surfaces, or surface functional groups) may be important for hydrogen storage.

Alkali-intercalated graphite materials were used to demonstrate that higher isosteric heats of adsorption can be achieved with appropriate geometric structures. However, as seen in Figure ES-6, the overall gravimetric hydrogen storage capacity is substantially reduced (i.e., to ~2 wt % maximum excess at 77 K). This is because the higher heat of adsorption is being provided by the hydrogen molecule interacting with two graphene layers (instead of one), thus substantially decreasing the number of adsorption sites for other hydrogen molecules. Thus, although geometric structures can provide higher heats of adsorption that enable a higher hydrogen capacity at higher temperatures, the overall maximum achievable capacity is substantially decreased.

Specifically, the storage capacity of the alkali-metal intercalated graphite at 195 K is ~1.3 wt % or ~65% of the 2 wt % maximum excess at ~80 K. This is substantially higher than the 25% to 35% observed at ~195 K for typical single-walled physisorption materials (Richard et al. 2009), demonstrating that materials with enhanced isosteric heats retain more of their hydrogen storage capacities at higher temperatures. However, the ultimate storage capacity of typical high-SSA carbons at 195 K is ~2 wt %, so even though the retained component is less and has lower binding energy, the increased SSA of typical activated carbons creates a higher overall capacity. These intercalated graphite results support the predictions of higher isosteric heats with narrower pore sizes in the range of 0.6 to 0.9 nm, the ability of intercalated graphite to monoatomically disperse alkali metals, and/or the potential enhanced heats of adsorption by electron donation to the lattice from the alkali atoms, resulting in enhanced (10 to 15 kJ/mol) heats of adsorption. However, even if stage 1 (i.e., graphite layers and intercalated layers alternate) alkali metal or similar intercalated graphite materials could be made, effectively doubling or possibly tripling the capacities reported in Figure ES-7, the substantially smaller pore sizes needed to obtain the higher heats of adsorption results in capacities that are too low to enable meeting the DOE 2015 targets.

The HSCoE found that sorbents have the potential to meet DOE hydrogen storage targets with physisorption alone, but cryogenic temperatures (see Table ES-2) are required, which impacts fueling station, system, and H₂ costs. The relatively low binding energies associated with physisorption means that only ~50 kilowatts (kW) of heat will need to be removed during refueling. This will have minimal impact on the fueling station costs compared to materials with higher binding energies such as metal hydrides, which could require 800 kW of cooling. To meet the DOE 2015 targets, the HSCoE recommends that the only physisorption materials that should be considered for development are those with SSAs greater than ~3000 m²/g, optimized uniform pore sizes in the range of ~0.7 to ~1.5 nm, excess material H₂-storage capacities >50 g/L and 7 wt % at temperatures between ~80 and 200 K, and moderate pressures (less than 200 bar).

Toward Ambient-Temperature Storage with Increased H₂ Binding

Typically, increased binding energies, lower temperature, and/or higher pressures are required to overcome the intrinsic repelling forces between dihydrogens to yield higher storage capacities on the sorbent surface at a specific temperature and pressure. To have higher capacities at temperatures closer to ambient, and compared to pure physisorption, enhanced electronic interactions between the sorption material surface and H₂ are required. For example, the empty p-orbitals created by substituting boron (B) for carbon (C) in a C-matrix induces electron donation from the hydrogen molecule to enhance binding energies by a factor of three (i.e., from ~5 to 10–15 kJ/mol [Kim et al. 2006]) and thus increase capacities, especially at operating temperatures >200 K. Similar enhanced physisorption binding energies can also be achieved through interactions with multiple adsorption surfaces, but the achievable capacity is substantially reduced because there is less surfaces for adsorption. The predicted enhanced binding achieved by appropriately substituting B in C was measured with a number of different techniques and agreed with the theoretical predictions of 10–15 kJ/mol. Challenges remaining include optimization of B loading levels with the required bonding coordination (i.e., sp² electronic coordination) and simultaneously obtaining high SSA. Several other low-molecular-weight heterogeneous materials (i.e., materials with lithium, beryllium, nitrogen, oxygen,

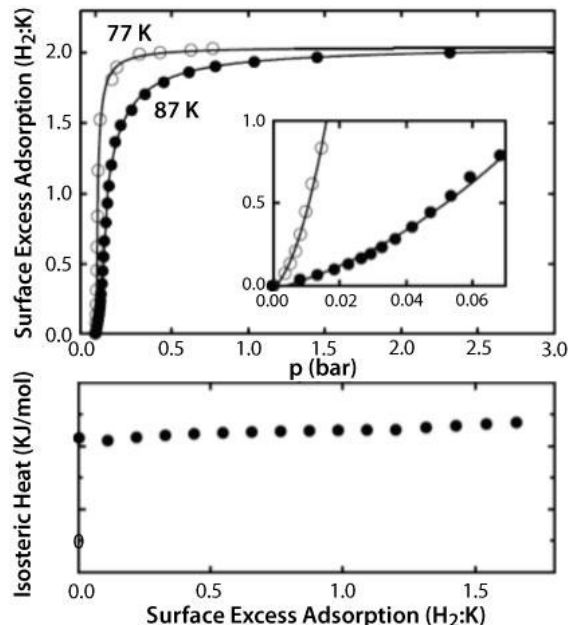


Figure ES-7. (Upper) 77 and 87 K isotherms of KC24 (K-intercalated graphite) with a blowup of the low-pressure regime in the inset. (Lower) Plot of the isosteric enthalpy of adsorption demonstrating nearly constant sorption enthalpy values with loading.

Table ES-2. Capacities of High-SSA (~3,000 m²/g) Sorbents at Different Temperatures

Temperature (K)	Excess Gravimetric Capacity (wt %)	Excess Volumetric Capacity (g/L)	Nominal Pressure (Bar)
30	~14	~90	3
50	~8	~55	8
80	~5	~35	20
300	~1	~7	350

fluoride, sodium, magnesium, potassium, and/or sulfur) were investigated (Kim et al. 2006). Other B-C or C-C coordination, the presence of other elements such as nitrogen (N) in the lattice, or other (except for Be) substituted lightweight elements (e.g., Li, N, O, F, Na) in carbon lattices do not significantly enhance dihydrogen binding (Kim et al. 2006). Boron-substituted carbon was found to be the most promising substituted material. However, in addition to needing to be in the correct coordination state, calculations predict that enhanced binding may occur only if the B remains both electronically and structurally “frustrated,” such that the B atoms are out of the plane of the carbon matrix, thus potentially expanding the lattice (Figure ES-8).

In addition to direct substitution, initial efforts identified that materials with intercalated and/or absorbed ions may enhance dihydrogen binding. For example, anions with high charge/volume ratio (e.g., fluoride) (Cooper 2008) can donate electron density to s^* -orbitals of dihydrogen. Similarly, other intercalated species (e.g., alkali and alkaline metals, anions) may induce charge interactions to improve hydrogen adsorption enthalpies (Q. Sun et al. 2009). Some of these effects may have been observed in the alkali metal-intercalated graphite materials that produce higher and uniform binding energies that are due to multiwall interactions. In some cases, it is theorized (Yoon et al. 2007) that molecular dopants complexed with nanostructures can generate sufficient electric fields to enhance H_2 storage. Finally, some of these substituted or functionalized materials may improve sorption of other elements/molecules for different hydrogen mechanisms associated with back-donation (Zhao et al. 2005; Kim et al. 2009; Y.Y. Sun et al. 2009; Yoon et al. 2008) and/or spillover.

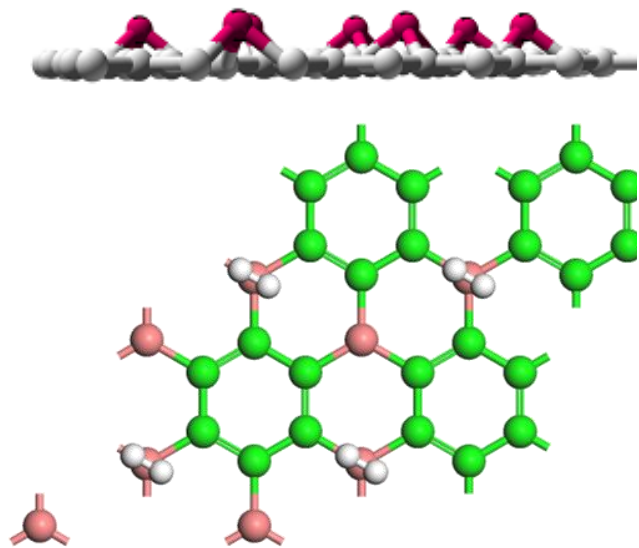


Figure ES-8. Schematic of the BC_3 structures that are predicted to have enhanced dihydrogen adsorption

Based on these initial predictions and experimental results, the HSCoE partners developed scalable synthesis methods to form substituted and intercalated materials that demonstrated enhanced dihydrogen storage properties. Because Be has substantial health-related issues, boron is the only lightweight element left to substitute in carbon. In addition, the center partners developed anion-intercalated graphitic and other intercalated/functionalized materials with enhanced hydrogen storage properties. APCI performed similar calculations for F-based systems, but subsequent experimental validation remained elusive. However, these experiments were only a very minor component of the HSCoE efforts. Several techniques were used by the HSCoE to form high-SSA and high-B-content porous carbon materials. For example, Penn State formed porosity in B-containing precursors (Chung et al. 2008); NREL formed B-substituted SWNTs in gas-phase synthesis; Penn State, APCI, and NREL deposited ultrathin BC_x layers in templates; and Missouri used B-ion implantation.

Contrary to literature reports (Marchand 1971), all attempts by HSCoE partners to use boron oxide in physical contact with graphene materials at high temperatures did not produce any significant B-substituted carbons with the correct coordination. Similarly, initial attempts to form sp^2 -coordinated B substituted in carbons with ion-beam implantation have not yet succeeded. These ion-beam implantation experiments began in 2009 and will continue beyond the center with the project at Missouri. In general, pyrolyzation and templating of B-C precursors produced $\sim 500 \text{ m}^2/\text{g}$ materials with $\sim 15\%$ B. However, materials with higher SSAs could be formed, but with lower boron concentrations.

Furthermore, most materials made to date demonstrate multiple binding states (see Figure ES-9). This is probably because B goes into amorphous and other carbon coordinations more easily than sp^2 . However, it is the higher-energy sp^2 coordination that has the greater electronic affinity and perhaps the structural stress needed for enhanced dihydrogen binding.

As discussed above, the predicted enhanced binding provided by appropriately substituted B in carbon was detected with a number of different spectroscopic techniques. The HSCoE used X-ray photoelectron spectroscopy to determine the specific coordination states of B in C; prompt gamma neutron spectroscopy, electron dispersive spectroscopy, and electron energy loss spectroscopy to determine the concentration of B in C; inelastic neutron scattering and diffuse reflectance infrared Fourier transform spectroscopy (DRIFTS) to determine the hydrogen binding state in the BC materials; and NMR spectroscopy and temperature-programmed desorption (TPD) to quantify the hydrogen binding energy and amount of interaction in the BC materials.

As shown in Figure ES-10, the resulting porous BC_x materials had substantially higher hydrogen adsorption on a per-SSA basis compared to pure carbon materials. In general, maximum excess gravimetric hydrogen adsorption capacities of $\sim 3 \text{ wt } \%$ are observed at 77 K for materials with 600

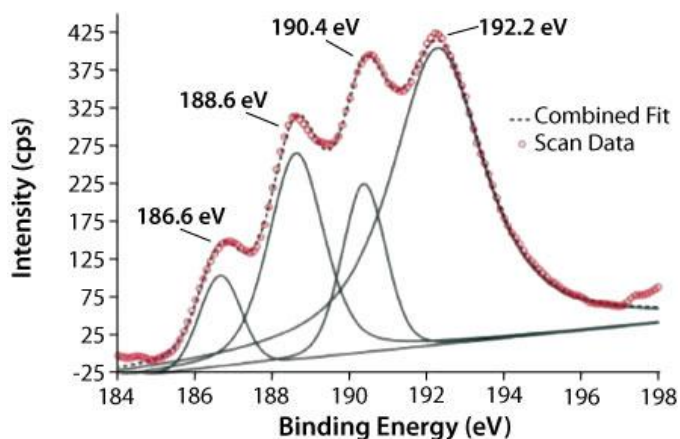


Figure ES-9. High-resolution B 1s spectrum and associated boron binding energies of deposited BC_x material

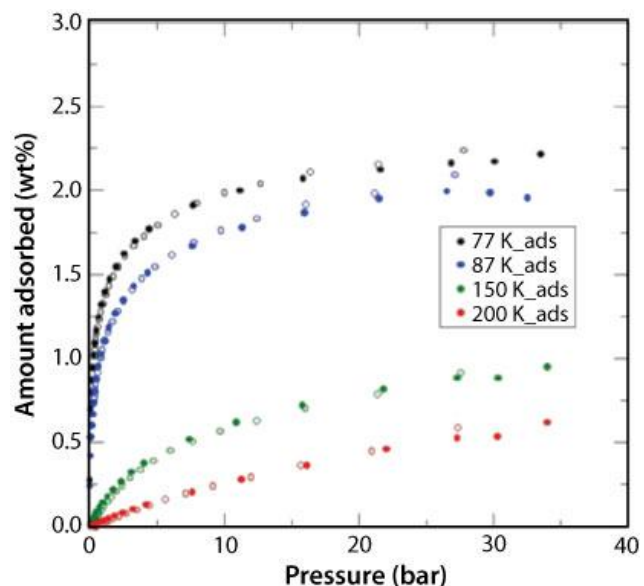


Figure ES-10. Representative example of hydrogen adsorption (solids) and desorption (open) excess gravimetric isotherms of porous BC_x sorbents. Because this material has only 600 to 800 m^2/g SSA, the maximum excess hydrogen adsorptions of $\sim 2.3 \text{ wt } \%$ at 77 K is much higher than is typically seen for pure carbon sorbents (i.e., 1.2 to 1.6 wt %).

to 800 m²/g SSAs. In addition, ~65% of the 77 K capacity is retained with some porous BC_x materials at ~200 K. This compares to 25% to 30% with pure carbon materials at the same temperature.

Calculations and experimental measurements both show that stronger dihydrogen binding of between 10 and 15 kJ/mol (see Figure ES-11) occurs when B is substituted with sp² coordination with carbons. This is sufficient to substantially increase the storage temperature compared to typical cryo-compressed materials and to potentially enable BC₃-like materials to

be used to meet DOE hydrogen storage capacity targets at 150–250 K temperatures if sufficient SSAs can be obtained. Any significant storage temperature increase toward ambient significantly reduces weight and costs, thus making it easier to meet DOE system targets. The effect of enhanced hydrogen binding and perhaps smaller pore structures associated with BC_x materials is also observed with TPD. In general, as the B content of the BC_x materials is increased, the hydrogen requires higher temperatures or takes a much longer time to desorb under vacuum conditions. This is consistent with a higher binding energy and/or the more tortuous path associated with the potential formation of smaller porous structures. That said, similar effects are not observed with nitrogen-substituted templated carbon materials, suggesting that the higher binding energies associated with boron substitution plays a major roll.

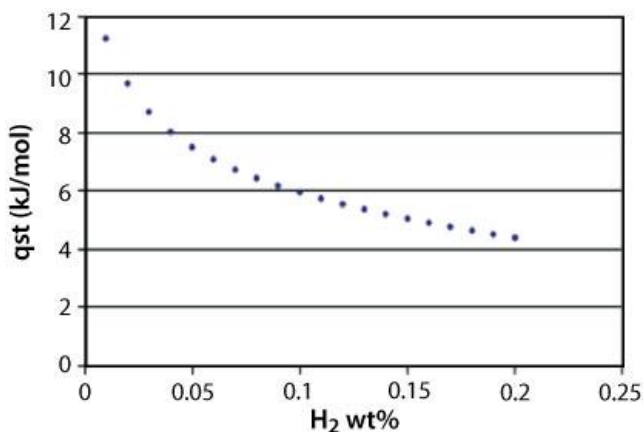


Figure ES-11. Representative example of the hydrogen isosteric heat of adsorption for a porous templated BC_x sorbent

Increasing Ambient-Temperature Storage with Strong/Multiple Dihydrogen Binding

As discussed above, materials such as sp²-coordinated boron substituted into a carbon lattice provide enhanced dihydrogen binding of 10 to 15 kJ/mol. However, going beyond this requires the use of materials with higher chemical potentials such as metals. The HSCoE championed the use of unsaturated coordinated metal centers to increase H₂ binding energies (predicted values of greater than 20 kJ/mol) and to enable the potential of multiple H₂-molecule binding at a single adsorption metal site. In these materials, the metal atoms interact with a lattice, but are sufficiently configured to have enhanced interactions with H₂ via both forward and back donation of electrons. Zhao et al.'s 2005 seminal paper in this area was the first to predict unique structures that may have the potential to hold multiple (i.e., 2 or more) H₂ molecules at a specific metal site. This paper, which has been referenced more than 220 times, has opened up an entirely new area of investigation for hydrogen storage. The key findings on this topic since the inception of the HSCoE are that lightweight alkali, alkaline earth, and 3d transition metals may be configured to enhance binding and have the potential to bind multiple H₂ molecules to a single metal atom (see Figure ES-12). More fundamental experimental work is needed to fully prove these concepts and provide experimental validation for the model predictions. However, the potential is promising. For example, substantial amounts of work within the HSCoE identified the unique properties of Ca for hydrogen storage (Ataca et al. 2009; Kim et al. 2009; Y.Y. Sun et al. 2009; Yoon et al. 2008). As discussed in more detail below, Ca coordinated in the correct way

may reversibly stores more than 100 g/L and 10 wt % at ambient temperatures (see Figure ES-13). This is substantially higher than liquid hydrogen, but at ambient temperature. Based on initial designs from ANL, storage systems that achieve >75% of the material capacities should be possible under these conditions. Thus, these inexpensive materials that bind multiple hydrogen molecules per site could provide a reasonable path toward meeting DOE's ultimate storage targets (i.e., 7.5 wt % and 70 g/L).

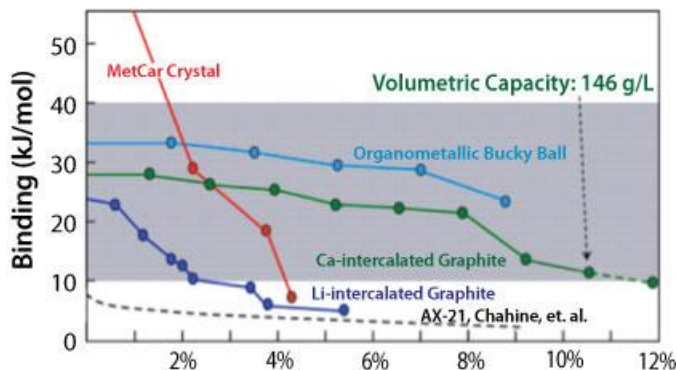


Figure ES-12. Some coordinated metal center materials designed by the HSCoE maintain optimum hydrogen binding energies for their entire capacity range. This helps with engineering and enhances the material capacity.

In general, the specific partially coordinated atom sites needed for strong and multiple dihydrogen binding can be attained in a number of ways. These include stabilizing single metal atoms on high-SSA materials (e.g., Li/tetrahydrofuran co-intercalation compounds or Ca on graphene lattices) or in crystalline structures such as MOFs or metallocarbohedrenes (Met-Cars). Thus, the HSCoE focused on methods to develop hydrogen interactions with coordinated but unsaturated metal centers and to design and synthesize these types of sorbents. This involved using calculations to identify and guide tractable reactions that balance reactivity with stability and capacity.

From the outset, the HSCoE strictly adhered to the criteria of synthesizing stable materials that have the potential to meet DOE hydrogen storage targets. Thus, theorists not only identified new materials, they worked with experimentalists to identify thermodynamically viable synthetic paths to form stable materials. A class of materials that can enhance dihydrogen binding was first identified by Kubas (Kubas 2007); it involves creating materials and structures in which individual metal atoms are coordinated to or in structures to keep them from agglomerating, but with electrons that are not fully compensated.

Although initial work demonstrated enhanced dihydrogen adsorption, the key finding since the inception of the HSCoE is that lightweight alkali, alkaline earth, and 3d transition metals can be configured to enhance binding and perhaps to bind multiple dihydrogen molecules with a single metal atom. This can occur at the metal atom site itself, or potentially charge-transferred to the matrix material, which may enhance adsorption over the entire exposed surface. Metal clustering and reaction with other elements reduce or eliminate the enhanced capacities, and thus materials must be designed to stabilize the atoms.

The main challenges with coordinated metal center approaches to hydrogen storage include being able to uniformly disperse these higher binding sites in such a way that they are accessible to the dihydrogen, are stable and do not degrade with time/refueling cycles, and provide relatively uniform dihydrogen binding throughout as much of the material storage capacity range as possible. This latter point is important from an engineering perspective so that the net available capacity can be maximized over as small a temperature and pressure range as possible,

which reduces the overall system costs. Overall, the HSCoE developed several ways to synthesize materials with coordinated metal centers, including:

- Integration of metals in structures such as Met-Cars or frameworks
- Full metal coordination with electronic transfer to the support
- Single metal atoms coordinated (but electronically unsaturated) to bonding sites of supports.

Metal centers in MOFs or equivalent materials bind dihydrogen in the 10–15 kJ/mol range, which is sufficient for near-ambient-temperature (150 to 220 K)

storage. The main issue with this type of material is that a high number of binding sites must be uniformly dispersed and accessible to enable significantly enhanced dihydrogen adsorption properties/capacities. The main issue with framework materials is that the high SSAs often obtained are mutually exclusive to the high density of metal centers needed to provide the higher-binding energy sites. Furthermore, the open pore structures often needed to attain high SSAs make them less stable with low crystal densities that reduce volumetric capacities.

Thus, framework materials must be designed with densely packed metal centers that are open for hydrogen adsorption to increase the binding energy for most of their capacity range. This is especially critical because the metal centers in framework materials will typically be able to adsorb only a single hydrogen molecule. Some of the initial experimental studies demonstrated that exposed transition metal sites in framework materials have H₂ isosteric heats of adsorption of ~10 kJ/mol (Dincă et al. 2006). This binding is significantly smaller than that observed in other metal center hydrogen storage systems (Kubas 2001). Ab initio calculations quantitatively account for the experimental findings and further show that the splitting and occupation of the spin orbitals in MOF systems are why their binding energies result in one dihydrogen being smaller than that observed in other materials (Sun et al. 2007). However, these calculations also predict that if other transition metals are used (e.g., Sc, Ti, V, Cr, or Mn), the H₂ binding energy by the MOF metal centers can be tuned to between 10 and 50 kJ/mol.

NIST worked with Dr. Jeffrey Long's group at the University of California, Berkeley, which created a set of MOF materials that were structurally similar but with different transition metals. NIST used inelastic neutron scattering to show that the primary H₂ adsorption sites were at the metal sites, and that these sites had the highest enthalpies. Furthermore, NIST showed that the metal-H₂ distance, which is inversely proportional to the binding energy, was greatest for the Cu²⁺ ion and least for the Fe²⁺ ion MOF. Thus, the binding was strongest for the Fe-MOF and weakest for the Cu-MOF. These results contradicted predictions by Zhou, Wu, and Yildirim (Zhou et al. 2008) that suggested that enthalpies and thus adsorption distance should be related to the ionic radius of the metals. Because the ionic radius of Mn²⁺ is greater than Fe²⁺, which is

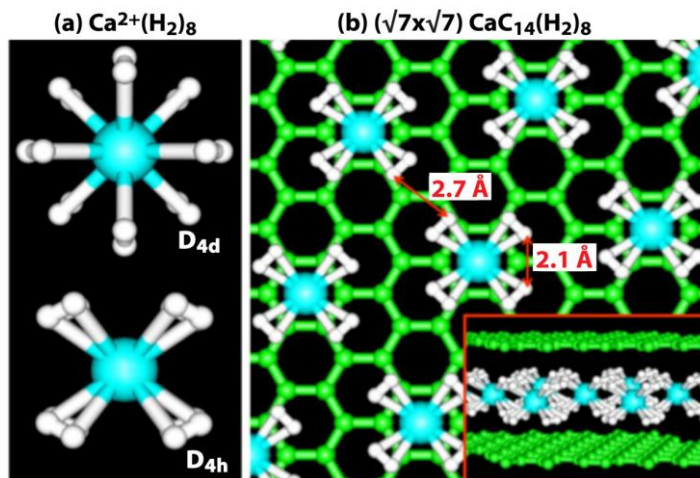


Figure ES-13. Illustration of a Ca-graphene structure that may sorb 8 H₂ per Ca, creating a hydrogen storage material with capacities of more than 100 g/L and 10 wt %

greater than Cu^{2+} , NIST's results showed that this is not the case. Subsequent work needs to be performed to see if spin-polarization effects (Sun et al. 2007) fully account for the observed behavior.

In general, metal centers in structures are sterically hindered and thus can adsorb one or at most two hydrogen molecules. To exceed this limit and enable adsorption of multiple hydrogen molecules to each metal site, the single metal atoms must have more access to the hydrogen. However, this access must be balanced against the need to coordinate the metal atoms so that they are sufficiently immobile to prevent agglomeration and are not sufficiently active to form hydrides. In general, single metal atom coordination on the surface of pure elemental supports such as carbon is relatively weak and predicted to be insufficient in many cases to prevent agglomeration and/or hydride formation.

It is synthetically challenging to avoid metal agglomeration (clustering) in all carbon frameworks. The metal must be bound to well-defined sites on high-SSA substrates with precisely tuned energetics (see Yildirim and Ciraci 2005; Sun et al. 2006; Ataca et al. 2009; Kim et al. 2009). However, based on some initial predictions (Yildirim and Ciraci 2005; Sun et al. 2006) and the unavailability of appropriately functionalized materials at the beginning of the center's efforts, a significant amount of work was performed on integrating metals with materials such as fullerenes and SWNTs. Ultimately, pure carbon materials are probably not sufficient to stabilize transition metal atoms, and thus materials with functionalized or higher binding sites must be used.

NREL demonstrated one- and two-dihydrogen adsorption to single metal atoms coordinated with functionalized activated carbon, $\text{Ni}(\text{BF}_4)_2(\text{PPh}_2)_2 - \text{SiO}_2$ aerogel, BC_x materials, as cointercalants in graphite, and other material systems. In each of these cases, the dihydrogen was strongly bound such that desorption temperatures of 150 K to greater than 300 K were required. All the results to date have been in quantitative agreement with predictions based on the coordination of the metals and the specific elements being used. The HSCoE was the first to identify the special properties of Ca, which is abundant and inexpensive. NREL applied its unique predictive M_xH_2 theories to investigate the hydrogen storage properties of group I and II metals. Unlike Li, Na, and Mg, Ca can be coordinated to matrix materials in such a way that a pseudo-3d band state forms, enabling substantial amounts of dihydrogen to be reversibly adsorbed. For example, Ca-intercalated graphene (see Figure ES-11) with the graphene layers separated sufficiently to allow dihydrogen molecules access around the Ca atoms has the potential to have net hydrogen capacities in excess of 100 g/L and 10 wt %. In this case, the Ca atoms are stabilized by the carbon with a +1.3 charge transfer at 50–90 kJ/mol. Furthermore, the Ca atoms adsorb dihydrogen at 20–40 kJ/mol. The Ca-C binding and charge transfer are sufficiently strong to prevent Ca clustering; they become weaker as more dihydrogens adsorb. The Ca_xH_2 binding is sufficient to store and release dihydrogen at densities much higher than liquid hydrogen, but at ambient temperatures and moderately low pressures (i.e., 4 to 30 bar). Even though the synthetic pathways remain a challenge, this set of work provides a breakthrough that clearly defines sorbent materials that could be used to meet DOE's ultimate storage targets.

In addition to the initial Ca-graphene work, NREL also found that graphitic B-C and some covalent organic framework (COF) and MOF materials stabilize open Ca centers. In the case of COFs, two Ca atoms will be bound to benzene linkers at ~120 kJ/mol, which in turn will adsorb

four dihydrogen molecules with an average binding energy of 15 kJ/mol. Although this particular material will have a hydrogen storage capacity of only ~44 g/L and 5.6 wt %, the theorists and experimentalists have worked together to identify materials with viable synthetic pathways.

Finally, although most efforts focused on stable hydrogen sorption to single metal sites, the HSCoE also identified processes and materials in which metals induce stronger hydrogen sorption to the support materials, another potential storage route. The key future efforts must focus on materials/process optimization to increase the number of viable binding sites and ultimately the overall storage capacities.

Weak Chemisorption/Spillover

The HSCoE also investigated methodologies to store dissociated hydrogen molecules (i.e., hydrogen atoms). Unlike the work discussed previously to increase binding for dihydrogen, the key issue here was actually developing ways to store dissociated hydrogen with binding energies substantially lower than those typically observed for hydride formation. The HSCoE investigated several ways to do this including endohedral fullerenes, boron-substituted materials, and Met-Cars. Among the more promising material classes, the HSCoE demonstrated that catalyzed hydrogen dissociation followed by “spillover” (see Figure ES-14) onto lightweight receptor support materials enabled ambient-temperature storage with binding energies that range from 10 to 25 kJ/mol.

In general, chemical covalent bonding between hydrogen and carbon is relatively strong (i.e., 50 to 400 kJ/mol) and requires high temperature to dissociate the bond. However, hydrogen atoms can interact with materials such as graphene in a way that does not change the graphite structures substantially (irreversibly), and the hydrogen interaction is more like adsorption (Lin et al. 2008). Spillover is a metal-catalyzed process in which the hydrogen molecule dissociates to H-atoms on the metal catalyst, followed by migration of hydrogen atoms onto the surface of a receptor material and subsequent diffusion away from the catalyst site. For this process to occur, the diffusion and storage of atomic hydrogen on the receptor surfaces must have substantially weaker bonding/barriers to migration than typically observed with chemical covalent bonding (i.e., weak chemisorption). Although the phenomenon of spillover has been known for decades for petrochemical and refining catalysis applications with ~0.01 wt % hydrogen adsorption (Conner and Falconer 1995), the HSCoE

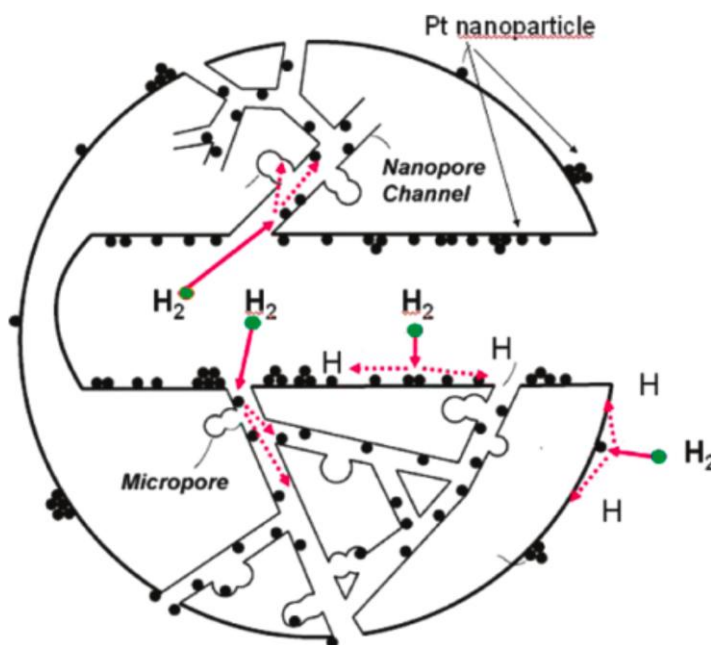


Figure ES-14. Conceptual diagram of hydrogen spillover processes. Reversible room-temperature spillover hydrogen storage involves a series of steps: (a) molecular H₂ dissociates on metal catalyst particles; (b) atomic H migrates to the receptor; (c) diffusion of atomic H across the receptor surfaces.

partners demonstrated that this process could be used to reversibly store substantially more hydrogen (>30 g/L and >4 wt %, Yang et al. 2006) at ambient temperatures and nominal pressures (less than 200 bar). This is an increase of more than 300% compared to H₂ storage on a sorbent or as gas in a compressed tank at the same pressure and temperature. The HSCoE demonstrated spillover both experimentally and by confirming agreement with thermodynamic principles as a revolutionary new process for ambient-temperature, reversible hydrogen storage. However, the materials tend to be very sensitive to processing conditions, the material synthesis procedures lacked reproducibility, and the accuracy of the measurement techniques varied, all of which can lead to substantial variations in sorption capacities. For example, although the work performed by the HSCoE at Michigan on “bridged” framework materials has been reproduced by international groups (Wang and Yang 2010), and the hydrogen uptake was measured by DOE’s validation laboratory at the Southwest Research Institute, the base materials for this particular sample are very air sensitive and thus full evaluations of these materials were difficult. Ultimately, theoretical predictions and non-reversible hydrogenation experiments demonstrate that capacities of close to one hydrogen atom per receptor atom (e.g., carbon) should be achievable via spillover. This translates to a potential for excess capacities greater than 7 wt % and 50 g/L at ambient temperatures and less than 200 bar. At the end of the HSCoE, DOE formed an international team led by NREL to validate the measurement and synthesis methods of spillover materials to improve reproducibility. In addition, the team is determining the specific hydrogen-receptor interactions using spectroscopic techniques to fully understand the mechanisms involved. This is important to understanding the significant difference between fill and discharge rates as well as issues that limit capacities. Ultimately, the issues with slow fill rates and lower than expected capacities may be related, and once the mechanisms are fully understood, these issues should be addressable.

Spillover is a process that dissociates dihydrogen onto a metal catalyst, followed by migration of hydrogen atoms onto the surface of a receptor material and subsequent diffusion away from the catalyst site—all of which leads to significant storage of hydrogen. The concept of hydrogen spillover has its genesis in fundamental studies with heterogeneous metal catalysts, particularly with the type of systems used for chemical hydrogenation reactions (Connor and Falconer 1995). Within catalytic processes, the metal has the role of “activating” hydrogen by reversibly dissociating H₂ into metal-H atom (hydride) species on its surface. For example, it has been observed that by heating Pt dispersed on carbon at 623 K, Pt/Al₂O₃ at 473–573 K, Pd/C at 473 K, and Pt/WO₃, under hydrogen pressure, the amount of H₂ absorbed exceeds the known H₂-sorption capacity of the metal alone (Sermon and Bond 1974). In these seminal reports, the “excess quantity” of this hydrogen on the support is usually very small, amounting to only several atoms of H for every H that's bound to the metal. Several comprehensive reviews of hydrogen spillover in catalysis have been published (e.g., Conner and Falconer 1995). Spillover is highly dependent on the metal catalysts, the support/receptor chemical composition, and the synergistic interaction.

Computations by Rice, APCI, and NREL identified that it is thermodynamically possible for hydrogen atoms to be stably stored in groups or clusters. The main step that is not well understood is that of hydrogen atom diffusion on the receptor. These efforts demonstrated that it is thermodynamically possible for hydrogen atoms to be stably stored in groups or clusters. Groups of H atoms tend to form compact clusters, influenced by aromaticity rules and the pyramidalization strain compensation, so that the lowest energy clusters consist of closed six-

hydrogen rings. Evaluation of the Gibbs formation energy as a function of temperature and pressure indicate that the H cluster formation has phase-nucleation dependencies, guided by nucleus barriers and corresponding critical cluster size. One important aspect of this analysis is that the calculated balance between the fluidic gas phase and the immobilized storage-phase indicates that spillover can store ~7.7 wt % H and be changed in either direction by changing pressure and temperature not too far from ambient conditions. Thus, these analyses indicate that, thermodynamically, spillover is a reasonable option for reversible, ambient-temperature hydrogen storage processes.

The HSCoE team was the first to identify that barriers to migration are lowered sufficiently via structural (e.g., hopping between closely spaced surfaces) and electronic features. Collaborative work using inelastic neutron scattering spectroscopy observed spillover hydrogen on carbon supports. Deuterium tracer investigations demonstrated that, effectively, the spillover process is sequential with the first hydrogen adsorbed being the last desorbed. The results are direct evidence that (1) atomic species are formed during the spillover processes, as shown by hydrogen-deuterium formation, and (2) the desorption follows a reverse spillover process in which atoms migrate back onto the metal particle to recombine and desorb as molecules. In general, the size, dispersion, and type of catalyst affect the efficiency and thus the capacity of spillover.

Furthermore, Rice demonstrated that the thermodynamics and kinetics for the catalysts and from the catalysts to the receptors are energetically downhill (Singh et al. 2009). Effectively then, thermodynamic calculations show that the presence of the hydrogenated phase of graphene makes the spillover step from metal to receptor thermodynamically favorable. Under the right conditions, spillover from the catalysts to the receptor will occur before hydride formation, and thus spillover is not kinetically limited by the metal-hydride properties. Ultimately, all the thermodynamic calculations that modeled the well-known spillover phenomenon associated with hydrogen bronzes from metal oxides (e.g., MoO₃ and WO₃) and metal sulfides (e.g., ZnS and MoS₂) were validated by APCI (Mitchell et al. 2003a).

Pioneering studies by the HSCoE partners revealed a novel process to store substantial quantities of hydrogen via hydrogen spillover (Lueking and Yang 2002; Li and Yang 2007). High hydrogen storage capacities at near-ambient conditions were achieved and were subsequently validated in several independent experiments (Dutta et al. 2007; Chen and Huang, 2007). Hydrogen spillover has been investigated using many carbon-based materials such as carbon nanofibers (Marella and Tomaselli 2006), amorphous activated carbon (Zielinski et al. 2005), graphite (Mitchell et al. 2003b), SWNTs (Yang et al. 2006), and MOF complexes (Li and Yang 2006). In one example, a hydrogen spillover-induced increase of hydrogen storage capacity for activated carbon and SWNTs by factors of 2.9 and 1.6, respectively, was reported (Lachawiec et al. 2005). Inelastic neutron scattering spectroscopy directly identified spillover hydrogen on a carbon support (Mitchell et al. 2003a).

For spillover (Li and Yang 2007) to occur to any significant extent in solid materials, it is essential that the H atoms be able to move from the vicinity of catalyst particles to substrate sites far from where the catalysts reside. Within the HSCoE, active research was performed to understand hydrogen spillover processes. These studies point to certain elements of spillover mechanisms that can satisfactorily explain the observed large storage capacity (as much as 4

wt.% of H₂) and facile hydrogen desorption kinetics from the carbon-based storage compounds at near-ambient temperatures (Mavrandonakis and Klopper 2008).

In general, the size, dispersion, and type of catalyst used can affect the efficiency and thus the capacity of spillover (Glugla et al. 1989; Chen et al. 1991; deLeon et al. 1997). Although spillover results vary tremendously with materials, processes, and treatments, a number of techniques are available for direct catalyst integration. These include incipient wetness impregnation, other chemical processes, vapor processes, and dispersion of nanocatalysts. The HSCoE optimization efforts investigated the use of different catalysts and different porous carbons to find the materials with the highest capacities. To date, the highest activated carbon capacities have been observed with an EMC-2 zeolite templated carbon (developed at Mulhouse University, France) with an initial Brunauer-Emmett-Teller SSA of 3839 m²/g and nanoparticle Ru catalysts (see Figure ES-15, Teichner 1990). The storage capacities depended on the catalyst material (i.e., Ru > Pt > Ni) and dispersion. The apparent isostatic heats of adsorption (ΔH_{ads}) for the catalyst-activated carbon spillover materials were measured to be in the range of 15 to 23 KJ/mol. Deuterium isotope tracer in conjunction with TPD studies demonstrated that, effectively, the spillover process is sequential with the first hydrogen adsorbed being the last desorbed or removed. The results are direct evidence that (1) atomic species are formed during the spillover processes, as shown by the hydrogen-deuterium formation, and (2) the desorption follows a reverse spillover process in which atoms migrate back onto the metal particle to recombine and desorb as molecules.

To increase spillover capacities beyond those observed for activated carbons, the HSCoE investigated several routes including the use of substituted materials, physical mixtures of catalyst- and non-catalyst-containing materials, and “bridged” structures. Michigan demonstrated that Pt on carbon materials combined with framework materials substantially increases spillover capacities in excess of 4 wt % at ambient temperature (see Figure ES-16) (Wang et al. 2009; Olson et al. 2010). Subsequent work by NREL demonstrated that spillover effects continue well past 100 bar, so these results with the bridged IRMOF8 material indicate that spillover well in excess of 4 wt % should be achievable if higher pressures are applied. NREL also determined that pyrolyzed sucrose is an excellent spillover material in and of itself. These results were validated by other groups around the world and at DOE’s validation laboratory, the Southwest Research Institute. Although the use of the bridge material and the specific features of IRMOF8 that have not been observed to the same degree with other framework materials must be studied and understood in greater detail, the Michigan work developed a simple and effective technique to build spillover materials with secondary receptor materials that have substantially higher

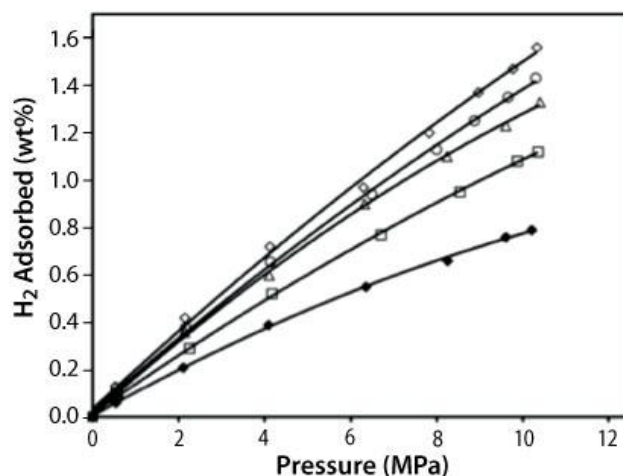


Figure ES-15. Ru/EMC. H₂ isotherms at 298 K on templated carbon (TC) and 6 wt % metal catalysts. All materials were H₂-reduced at 300°C except Ru/TC-T, which was thermally reduced (in N₂) at 900°C (1 hr). Brunauer-Emmett-Teller SSAs for each sample were (m₂/g): Ru/TC-T = 2090 (open diamonds); Ru/TC = 3004 (open circles); Pt/TC = 3120 (open triangles); Ni/TC = 3091 (open squares); TC = 3839 (closed diamonds).

capacities. The bridge-building process appears to be receptor specific, and optimization and/or use of other receptors may yield even greater hydrogen storage capacities.

Work by the HSCoE identified several factors that can increase adsorption rates; they include using higher pressures during the initial loading step, integrating trace amounts of gasses such as methane (Wang and Yang 2008) and water, and chemically modifying the catalysts and/or receptors. Ultimately, the HSCoE demonstrated that, depending on the capacity needed, it may be possible to meet the DOE 2015 refill rate target of ~3 minutes by reaching only 80% to 90% of the maximum excess capacity. In general, desorption rates are more than sufficient to meet DOE's fuel supply rates.

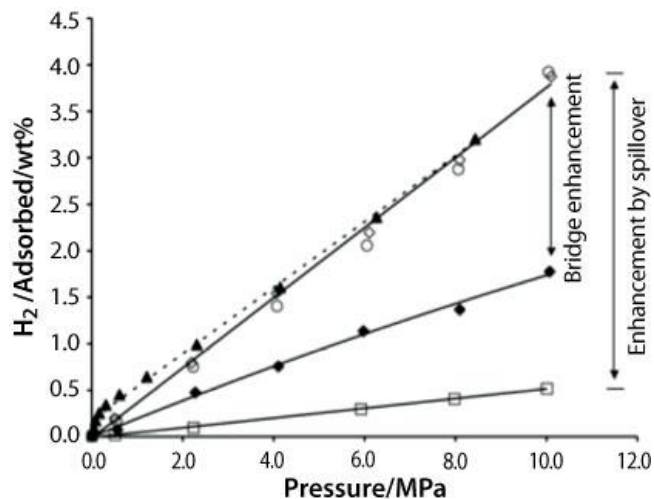


Figure ES-16. High-pressure hydrogen isotherms at 298 K for pure IRMOF-8 (\square), Pt/AC and IRMOF-8 physical mixture (1:9 weight ratio) (solid diamonds), and for bridged sample of Pt/AC-bridges-IRMOF-8: first adsorption (solid triangles), desorption (open diamonds) and second adsorption (open circles).

Overall, the HSCoE demonstrated that substantial increases in hydrogen storage capacity can be achieved at ambient temperatures with weak chemisorption processes such as spillover. Future work must improve adsorption rates via improved catalyst dispersion and integration and improved receptor properties. Care must be taken to ensure that irreversible chemical reactions with the receptor materials do not occur and that the measured hydrogen uptake is truly representative of the amount of hydrogen that can be delivered to the fuel cell. Although a significant amount of work is still required to develop highly reproducible and robust materials that have the high capacities demonstrated by the HSCoE with less durable materials, the clear indication is that weak chemisorption is a viable path for on-vehicle, refuelable hydrogen storage.

Major Accomplishments

During its 5 years of operation, the HSCoE improved sorbent properties to the point that they could be used to meet DOE on-vehicle hydrogen storage system targets. Specific accomplishments are described in the following.

1. Designed and developed reversible sorbents via ambient-temperature hydrogenation/storage techniques (e.g., weak chemisorption) that demonstrated >4 wt % storage capacities with isosteric heats of adsorption between 10 and 30 kJ/mol.

The center pioneered the development of materials that have relatively low chemical binding of hydrogen, potentially allowing efficient, reversible on-vehicle refueling. This class of materials enables hydrogen storage system designs with more than 75% of the volumetric and gravimetric capacities of the materials and substantially reduces system costs and complexity. Hydrogen

spillover has been observed on numerous materials for decades. However, previous to the HSCoE, spillover was observed only at the ~0.01 wt % level. The HSCoE demonstrated much higher capacities experimentally and developed a substantially improved thermodynamic and kinetic understanding of the processes involved, in which the models were validated with known spillover materials, e.g., “hydrogen bronze.” The main issues researchers probed included improving capacities, stability, and charging (refueling) rates.

Calculations indicate that 7%–8 wt % (50–60 g/L) capacities at ambient temperature are possible. Hydrogenation experiments have demonstrated 7.5 wt % on carbon samples, albeit these specific results used chemical processes rather than spillover to hydrogenate the carbon. First-principle calculations indicate that spillover is thermodynamically viable, with binding in agreement with observed measurements. Improved understanding of spillover kinetics is needed to enable materials to be designed with higher capacities and sorption rates that can meet DOE 2015 targets.

In general, weak chemisorption-based hydrogen storage may be able to meet DOE targets if kinetics and stability issues can be appropriately balanced with the thermodynamics needed to create the optimal isosteric heats of adsorption (i.e., 10 to 30 kJ/mol). The kinetics and thermodynamics depend on the functional groups and/or electronic properties on the surface of the receptor materials, which must be appropriately adjusted to be stable over repeated reversible hydrogen loading/discharge cycles. Charging rates, pressures, and receptor-materials compositions can all be adjusted to achieve the desired hydrogen storage properties. Although additional development and optimization work needs to be done, the principles of high-capacity, weak chemisorption-based hydrogen storage have been demonstrated, and the higher storage capacities measured to date have been validated in separate synthesis and measurement laboratories. However, reproducibility and stability remain major issues.

2. Developed new materials that increased the gravimetric (~50%, from ~5 to >7 wt % at 77 K) and volumetric (~150%, from ~15 to >35 g/L at 77 K) hydrogen storage capacities by physisorption onto high-SSA sorbents by optimizing pore sizes (0.7 to 1.5 nm) to increase SSA and packing density.

The HSCoE partners synthesized new high-SSA physisorption materials with optimized uniform pore sizes using a variety of scalable/inexpensive processes including aerogels, pyrolyzed carbons, templated carbons, and MOFs. These optimized pore-structured sorbents can be used to construct hydrogen storage systems that meet DOE 2015 delivered capacity targets of 5.5 wt % and 40 g/L if appropriate storage temperatures (i.e., 50 to 80 K) and pressures (i.e., 10 to 100 bar) are used. The decreased pressures (compared to high-pressure, 350–700-bar storage systems) that are enabled by relatively inexpensive carbon-based sorbents could substantially reduce tank and balance-of-plant costs.

3. Discovered and demonstrated coordinated, unsaturated metal centers as a new class of hydrogen storage materials that could meet DOE’s targets. Several material systems were demonstrated, and specific synthetic paths based on known materials were identified.

This class of materials includes systems that use low-cost elements/materials that have the potential to meet DOE’s ultimate capacity targets with uniform isosteric heats of adsorption

ranging from 15 to 30 kJ/mol for almost the entire capacity. Thus, this class of materials offers the potential to far exceed capacity and energy efficiency capabilities of any other on-vehicle refueling material-based and/or high-pressure storage system.

The HSCoE explored strong multiple binding to great effect. The center discovered and championed an entirely new class of viable materials that uses lightweight (e.g., 3d electron, alkali, and alkali earth metals) metal centers to enhance H₂ isosteric heats of adsorption and enable multiple H₂ binding on each metal site. The pioneering work done by HSCoE partners spurred substantial R&D efforts and resulted in hundreds of publications. To meet DOE targets, the HSCoE team leveraged known materials to develop and optimize routes to stabilize multiple hydrogen molecules on a metal atom that exhibit moderate H₂ binding energies. Individual transition-metal atoms have been experimentally observed to adsorb 1–7 H₂ molecules with appropriate binding energies, and the theoretical predictions are in quantitative agreement with all known experimental results involving 3d metals. The key has been and continues to be stably coordinating the metal atoms so that the H₂ molecules can reversibly adsorb/desorb in a hydrogen storage system.

4. Designed and developed substitutional materials with enhanced dihydrogen binding energy to increase capacities at near-ambient temperatures, on a per-SSA basis.

By substituting one element into that of another single-element structure, materials with enhanced hydrogen isosteric heats of adsorption (e.g., ~11 kJ/mol for B-substituted carbon, compared to ~5 kJ/mol for pure carbon) can be created to increase storage capacities at near-ambient (e.g., ~200 K) temperatures. Thus, substituted materials have the potential to meet DOE's 2015 hydrogen storage system capacity targets. Increasing storage temperatures to near ambient helps decrease system costs by reducing the costs of insulation, tanks, and balance of plant.

HSCoE researchers created high-SSA, B-C material using several different scalable and inexpensive methods. In complete agreement with theoretical calculations, the HSCoE found that these substituted materials required the B to be electronically frustrated with the correct coordination in the carbon lattice (i.e., sp² coordination) to increase H₂ binding (e.g., ~11 kJ/mol) and capacities at temperatures approaching ambient. Neutron spectroscopy data showed, for the first time, a large rotational splitting indicative of enhanced H₂ interactions in a B-substituted carbon. DRIFTS measurements showed reversible hydrogen interaction with the B-C material. Future efforts must focus on increasing simultaneously both the boron concentration and SSAs of these substituted materials.

5. Developed unique measurement capabilities to accurately and reliably characterize hydrogen storage properties of laboratory-scale (1–100 mg) samples to enhance high throughput and rapid screening analysis (isotherms, SSA, pore size distribution, isosteric heats of adsorption, TPD, and NMR).

Accurately measuring hydrogen storage properties has been a major problem in the community for decades. This has been due partly to having only small quantities of the most novel laboratory-scale materials to characterize. The center's investment in developing protocols and measurements capable of providing accurate results from small amounts of sample have

substantially enhanced throughput by eliminating the need to develop larger-scale synthetic methods or repeating synthesis processes numerous times to make enough material.

6. Confirmed that standard physisorption-based dihydrogen adsorption scales with SSA. To date, no validated experimental evidence exists that any substantial capacity enhancement occurs as a result of geometric configurations.

At the outset of the HSCoE's activities, numerous publications had reported extraordinary results for high-SSA materials in which the enhanced capacities were potentially a result of novel geometries or structures within the material. In general, heats of adsorption can be increased with multiple-wall interactions, but this ultimately reduces capacities. The center did not validate any single-element material or any materials with unexceptional electronic states that have substantially higher hydrogen storage capacities beyond what is expected based on the SSA and specific storage conditions. For example, at one time carbon nanotubes were thought to possibly have unique hydrogen storage properties, but after a dedicated focused effort, the HSCoE made a No-Go decision on using carbon nanotubes as an ambient-temperature hydrogen storage material (DOE 2006). The emphasis here is that even though the heats of adsorption can be increased, the overall capacity cannot be significantly increased based on geometrical structures alone. Ultimately, if appropriately arrayed, carbon nanotubes may still provide excellent hydrogen storage at cryogenic temperatures.

7. Performed hundreds of systematic investigations, after which the ultimate conclusion for dozens of specific materials and/or processes was that they should not be investigated further for vehicular hydrogen storage applications.

By identifying paths, processes, and/or materials that should no longer be investigated, the HSCoE provided DOE and the hydrogen storage community with valuable information that can be used to better define and identify future efforts.

Recommendations

Review of Go/No-Go Decisions

As mentioned previously, the HSCoE's focused development efforts identified a substantial number of materials/material classes that should not be investigated further based on a number of considerations, including detailed selection criteria developed specifically for sorption materials. Based on the nature of the HSCoE's development of hydrogen storage mechanisms (rather than specific materials), the exact number of materials down-selected is difficult to identify. Through these efforts, the HSCoE was able to quickly pinpoint the few selected material classes and their required properties and focus on them for present and future development. For example, regardless of the specific elements used, a pure physisorption material needs to have a SSA of more than 2000 to 3000 m²/g (depending on storage temperature used). This requirement alone eliminates hundreds of elements and materials that are just too heavy to be able to meet it if a solely physisorption-based hydrogen storage mechanism is used. Thus, the HSCoE eliminated most alumina-silica-based zeolites from further consideration basically from the outset.

Furthermore, through calculations and a limited number of specific experimental investigations, it became clear that only correctly coordinated boron substituted in graphitic carbon is a viable

route to improved hydrogen storage for substituted carbon materials, and thus the use of other lightweight elements received little or no additional investigations. In terms of carbon materials, this eliminated the need to perform experimental investigations on hundreds of potential element/process combinations for this material class. Similarly and from the outset, the HSCoE continually evaluated different sorbents to identify the material classes and their corresponding properties that should receive focused development based on their potential ability to be able to meet DOE hydrogen storage targets.

In FY 2009, the HSCoE formally evaluated the status of sorbents that could meet DOE hydrogen storage targets and wrote a report for the the DOE EERE Fuel Cell Technologies Program. This HSCoE project deliverable, the [*Hydrogen Sorption Center of Excellence \(HSCoE\) Materials Go/No-Go Recommendation Document*](#), is available on the DOE website (HSCoE 2009). It provides an overview of the work performed by the HSCoE through November 2009; specific recommendations to DOE for materials development efforts that should, and should not, be continued; and a list of key research priorities remaining to be resolved. The center identified clear development paths for constructing sorbent materials that have the potential to meet DOE's revised 2015 and ultimate full-fleet targets (DOE 2009) for light-duty vehicles. The center recommended that development efforts for specific materials/classes be continued where viable routes existed for synthesizing sorbents that could be used to meet DOE's targets.

Recommendations for Continued R&D

Because this sorbents go/no-go recommendation was made within the last year, a substantial amount of the recommendations remains pertinent, feeding directly into the recommendations that follow here. At this point in time, which is the formal completion of the HSCoE's research, a specific set of recommendations are as follows:

Overall recommendation: The HSCoE recommends that development efforts for specific material classes be continued where viable routes exist for synthesizing sorbents that can be used to meet the appropriate set of targets. The specific selection criteria for future efforts should focus on the DOE 2015 and the ultimate full-fleet hydrogen storage targets. The focus has been, and should remain, on capacity, kinetics, thermodynamics, and costs. The HSCoE recommends these focus areas because the majority of the other DOE 2015 and ultimate targets for sorbents will be more of a systems-engineering issue than an intrinsic material property issue.

Even when hydrogen binding energies are substantially increased to enable near-ambient-temperature storage, these binding energies (typically 10 to 25 kJ/mol) and the associated entropies of hydrogen should not be an issue. They are low enough that the relatively small amount of heat generated during refueling should be easily removed with the typical sorption material's intrinsic thermal conductivity properties and/or appropriately designed integration of thermal conductivity materials in condensed "pelletized" materials. In addition, because most sorbent materials will likely operate at moderate pressures (i.e., 10 to 100 bar), delivery rates and system pressures should not be significant issues.

In general, a range of temperatures and pressures can be used as long as the materials and systems can be constructed to meet the DOE targets. However, the closer to ambient conditions the system operates, the less expensive the system costs. This must be traded against overall

system performance, which includes the potential need for added heat removal. This need for balance leads to four specific recommendations related to materials, system, and classes.

1. Develop materials for hydrogen storage by weak chemisorption. Ambient-temperature storage via catalytic hydrogen dissociation and transfer to high-SSA receptor materials (e.g., spillover) demonstrates 10 to 30 kJ/mol reversible hydrogen binding energies, which enable ambient-temperature storage. Furthermore, because the binding energies for spillover are much lower than for typical metal or chemical hydrides, thermal management issues for heat removal during refueling and delivery rate issues should be moderate, and thus should not significantly impact the overall storage system. Thus, the center recommends that spillover or equivalent materials continue to be developed for hydrogen storage.

Although some of the processes involved have been demonstrated experimentally and by thermodynamic principles, additional development is needed to further understand and improve atomic hydrogen transport on the receptor material (for uptake/refill and discharge kinetics) and to improve the performance reproducibility and effectiveness of the synthetic processes. Once these issues are addressed, initial analyses indicate that because spillover enables ambient-temperature storage, systems with more than 75% of the material capacities can be achieved using basic pressurized (~100 bar) tanks.

Initial analysis indicates that excess material storage capacities of more than 7 wt % should be possible with spillover. In addition, because spillover should be applicable to materials with more than 1 g/ml bulk density, storage systems with more than 50 g/L and more than 5.5 wt % capacities should be achievable at ambient temperature and ~100 bar. Thus, with inexpensive, carbon-based materials and the development of inexpensive, highly dispersed catalysts (e.g., nanoparticle Ni), spillover materials should be usable in systems that meet DOE's 2015 targets.

2. Develop materials for multiple-dihydrogen storage on designed sites. Although substantial efforts will be needed to form the novel structures, development of multiple-dihydrogen adsorption on designed sites should be continued because the resulting structures could meet DOE ultimate targets—making it one of the few solutions identified with this potential.

Multiple-dihydrogen adsorption on designed sites provides a reasonable path toward meeting DOE's ultimate full-fleet targets (DOE 2009), with the provision that this may require substantial development efforts. Several inexpensive material systems have been predicted that may be used to meet these targets at near-ambient temperature. One prediction includes the use of inexpensive Ca with inexpensive carbon supports to form materials that may be able to store hydrogen at ambient temperature with twice the gravimetric and volumetric densities of liquid hydrogen. Such a structure, if it is possible to synthesize and stabilize, would be a tremendous breakthrough. Meeting DOE's ultimate targets will enable hydrogen to become a viable energy carrier for transportation and other important renewable energy applications.

3. Develop substituted/heterogeneous materials with demonstrated hydrogen binding energies in the range of 10–25 kJ/mol. The center recommends that researchers develop substituted/heterogeneous materials that can be used to enhance dihydrogen isosteric heats of adsorption in the range of 10–25 kJ/mol. These materials will enable near-ambient-temperature (150–250 K) hydrogen storage. Development efforts should focus on creating materials with the

appropriate chemical and electronic structures, sufficient composition, and high SSAs. These materials could potentially decrease system hardware costs and constraints and may be used to meet DOE's 2015 hydrogen storage system targets (40 g H₂/L; 5.5 wt %).

For single-element materials such as carbon, only a few elements (e.g., boron substituted in sp² coordination) substantially enhance dihydrogen binding. However, other heterogeneous systems (e.g., certain MOFs) have demonstrated enhanced dihydrogen binding. In general, the principle is well established; the main issues include access and creating enough high-binding-energy sites to substantially increase capacities. In addition, these heterogeneous materials also demonstrate substantial stabilization of single metal centers and other absorbed species that improve hydrogen storage.

4. Limit development of materials in which the storage mechanism is physisorption to only those with optimized structures. The center recommends that present and future development be performed only on a select set of materials in which the primary storage mechanism is physisorption. To meet the DOE 2015 targets, the only physisorption materials that should be considered for development are those that can have SSAs greater than ~3,000 m²/g, optimized uniform pore sizes in the range of ~0.7 to ~1.5 nm, and excess material hydrogen storage capacities greater than 50 g/L and 7 wt % at cryogenic temperatures (~80–200 K) and moderate pressures (less than 100 bar).

- Although it may be possible to meet the DOE 2015 system targets with high-SSA materials, isosteric heats of adsorption between 10 and 25 kJ/mol will be required to increase storage temperatures to greater than 200 K to significantly improve system capacity and/or costs. Furthermore, near-ambient temperatures will probably be required to meet DOE's ultimate full-fleet storage targets (DOE 2009). Such targets can be met in a number of ways, including developing specific heterogeneous materials, coordinated but unsaturated metal centers, and weak hydrogenation processes such as spillover.

With currently demonstrated bulk-material packing densities and hydrogen storage properties, sorbents will substantially decrease the volume and pressure now used for high-pressure (350 to 700 bar) compressed tanks, and thus could significantly reduce overall system costs. Future selection criteria should focus further on identifying materials that can be used to meet DOE's ultimate targets. In addition to the specific performance issues for each material class discussed previously, developing material synthetic processes and pathways that are scalable, inexpensive, and reproducible—and producing materials that can meet the DOE system cost targets—remains a challenge that must be pursued aggressively in all cases.

Again, in general, the main issues for sorbents are the relatively low dihydrogen binding energies, which directly affect storage temperature. This adversely impacts system costs, volumetric capacity, and available gravimetric capacity. Thus, the main focus of future applied development efforts must be on enhancing and/or optimizing hydrogen binding energies. This focus will require balancing improved hydrogen storage system costs and capacities with perhaps adversely affected material-contamination sensitivity, durability, refill rates, and materials' cost issues.

Suggestions for New Materials Systems To Be Investigated

As discussed above and in more detail in the full report, the HSCoE identified several material classes that include numerous material systems with the potential to meet DOE 2015 and even ultimate hydrogen storage targets and therefore should be investigated further. The main emphasis for developing new sorbents should be placed on performing systematic investigations with model systems within the material classes recommended for further development in the preceding pages. For example, within the multiple-dihydrogen adsorption class of materials, the Ca-graphene and equivalent systems have been identified as having very good storage capacities and viable synthetic routes. Thus, the HSCoE suggests that future efforts focus on developing sorbents that use the unique properties of coordinated Ca atoms. Similar examples of material systems exist within all the material classes recommended for further investigation. Thus, the main focus for sorbents should be on developing new material systems within the substituted/heterogeneous, multiple-dihydrogen adsorption site, and weak chemisorption material classes.

Identification of Remaining Issues for Recommended Systems

Each material system and material class has individual and unique challenges that cannot be adequately summarized here (but are discussed in the body of the full report). However, sorbents as a whole have common issues that must be adequately addressed. These include the need to:

1. *Develop robust, reproducible, and scalable synthetic methods that create materials in which all adsorption sites are accessible to the hydrogen.* Whether for high-SSA physisorption materials, weak-chemisorption spillover materials, or other sorption materials, the main issue has been and remains development of improved synthetic methods to create the materials that have been designed for optimum hydrogen storage. Although substantial progress has been made, clear improvements are needed with synthetic processes to form the requisite materials that can be used reproducibly and be scaled up for commercial manufacturing.

2. *Improve computational methods to more accurately predict the ability to synthesize designed materials and hydrogen storage capacity as a function of temperature and pressure.* In general, HSCoE theorists and experimentalists worked very closely together to design materials that have good hydrogen storage properties and that can be synthesized. However, to advance these efforts further will require that each step and precursor in a process be accurately modeled (as compared to just the end state) so that viable routes to designed materials can be quickly identified computationally before the experiments are performed.

In addition, presently there are no good computational platforms that accurately predict a material capacity as a function of pressure and temperature. Models based on grand canonical Monte Carlo simulation use non-first-principle and/or empirical force fields that require calibration and thus tend to lack the required accuracy for predicting capacities.

3. *Develop a better understanding of atomic hydrogen transport on receptor materials.*

Clearly, the main issue with weak chemisorption is a fundamental lack of understanding of how hydrogen atoms diffuse along the receptor materials. Eliminating this deficiency is critical to ultimately predicting the full potential of and designing optimized spillover materials.

4. Develop a better understanding of metal center coordination and its effect on hydrogen adsorption. Although a rudimentary first-principles understanding exists, a more robust and predictive set of computational tools is needed to enable designing coordinated metal centers that are more stable to environmental contaminants and other degradation mechanisms (i.e., cluster formation), while at the same time are optimized for storing the maximum number of hydrogen molecules.

5. Develop materials in concert with designs for hydrogen storage systems. Development efforts should continue on optimizing the materials needed for specific storage systems. Based on the successes achieved since the center's inception, researchers have created sorbents that have the potential to meet DOE's revised 2010 targets, assuming that storage systems are optimized for the material being used. If sorbents are to be used to meet DOE's 2015 and ultimate targets, it will be even more imperative that storage systems be optimized for the new sorbent materials with higher binding energies and other substantially different but critical performance characteristics. For example, compared to compressed (350 to 700 bar) or cryo-compressed hydrogen storage technologies, which have demonstrated material packing densities and storage properties, the main benefits of sorption materials include substantial (twofold) reductions in volume, reductions in pressure (~20-fold), and a fourfold or more increase in storage temperature. All of these benefits substantially improve system costs, resonance times for boil-off, and resolution of engineering-design issues. However, capacity and other performance characteristics must be balanced against system costs and overall well-to-tank and in-tank efficiencies.

6. Develop sorbent material measurements standards and certifications. In conjunction with DOE's *Recommended Best Practices for the Characterization of Storage Properties of Hydrogen Storage Materials* (DOE 2008), specific standards, mechanisms for measurement qualifications, and certifications need to be developed with regard to hydrogen storage capacity and some material property measurements. As with standards, qualifications, and certificates that are available for measuring SSAs in highly porous materials, a similar set needs to be developed to ensure that hydrogen storage capacities, isosteric heats of adsorption, and even sub-nanometer pore size distributions are being measured accurately and calculated and reported uniformly.

The cornerstone of materials development is the accurate determination of material properties and performance. For decades, claims of spectacular results that ultimately turned out to be erroneous have plagued the gas-storage community, resulting in loss of valuable time and resources. As interest in hydrogen storage ramps up, the number of publications and results—and the desire to publish/report outstanding results quickly—increases commensurately. This rush to publish results that push the envelope is often at odds with performing detailed measurements that ensure that all of the hydrogen storage metrics being published are rigorously validated. In addition, presently there are no national or international established standards, procedures, or certifications that provide independent qualification of measurement systems and procedures. Thus, the HSCoE recommends that planning and implementation of useful standards and certifications be performed to help the community accelerate materials development and to minimize wasting limited resources on efforts that ultimately serve only to resolve poor measurements.

Identification of Systems Recommended for No Further Investigation

The HSCoE assembled a complete list of materials and processes recommended for no further R&D (HSCoE 2009). Because sorbent materials are arranged more by a specific mechanism than by a system, down-selections can occur only with a given material/process. Thus, in general, future sorbent development should follow the recommendations above and minimize repeating work that has already been done. Again, only a select few elements and materials used in sorbents will be able to meet DOE hydrogen storage system targets. The key is arranging those elements and materials for optimal hydrogen storage. Thus, future development should eliminate any materials that cannot be used to meet DOE's 2015 targets. For sorbents, specifically, capacity and cost targets must be addressed fully. This indicates that certain high-SSA materials, including many of the MOFs, with good gravimetric capacities but poor bulk densities cannot meet DOE volumetric capacity targets even using crystal densities; these should be eliminated from further investigation. This will free up resources to focus on MOFs and other materials that are more stable with higher bulk densities and thus higher volumetric capacities—and minimize wasting efforts developing inappropriate materials.

Recommended Storage Options and Material Systems for Early Market Applications

In general, DOE has not defined criteria for early market hydrogen storage applications and the HSCoE did not develop sorbents optimized for any application except light-duty vehicles. With that said, in general sorbents provide unique engineering solutions that will be of benefit to many early market applications. For example, optimized high-SSA materials in slightly modified compressed and cryo-compressed tanks will provide substantial improvements compared to present storage systems for forklifts, buses, and other high-use, short-term storage transportation and portable power applications. The main benefits of sorbents—ease of engineering and enhanced volumetric capacities compared to high-pressure hydrogen—make them ideal for reducing the volume and increasing the capacity of storage systems for buses and forklifts.

Lessons Learned from the Center Approach

The HSCoE approach opened up collaborations in ways that could not have been attained with any other format. Central to this is the knowledge that the complexity of the problems encountered required skills and talents of multidisciplinary investigators. Efforts based on material classes enabled focus-area experts to work closely together to solve difficult problems. Further, the synthesis of optimized materials required integration of complementary approaches, including joint synthesis, measurement, and structural-characterization facilities, that enabled comprehensive capabilities for all partners. Beyond this, such collaborative work enabled unified support for wider (non-center) research efforts. Such collaborations accelerate R&D efforts by months or even years. The center joined partners together in a precompetitive environment. Similarly, it established research directions based on broad expertise and capabilities. This in turn enabled rapid/flexible response to new development. Also important, this team approach enabled fast validation of results.

From an institutional standpoint, consistent funding spanning 5 or more years encourages the focus on the longer-term efforts that are needed to solve complex and difficult problems. Given

this span, it becomes incumbent upon participants to make sure that the R&D momentum is retained in detailed knowledge, which assures that past funding is not wasted. The core knowledge gained should be retained within government systems to enable work with all stakeholders and partners throughout the world. The HSCoE's focus on on-board refueling was the most challenging approach possible, but it was clearly needed, because otherwise a migration to easier goals (e.g., off-board regeneration and higher-pressure storage) would have been too tempting.

Lessons Applicable to All R&D Efforts

The joint non-disclosure agreement and direct interaction between partners was absolutely essential to success. For efficient use of resources, feasibility analyses should be performed for materials-development selection, materials deliverables for the DOE Hydrogen Storage Engineering Center, and for scale-up. In general, cost analyses should be an integral part of the decision process for all future efforts. Materials design via modeling is an effective tool that should be incorporated in all materials- and process-development activities.

Furthermore, high-throughput combinatorial methods should be incorporated for materials optimization. However, because not all materials discovered can benefit from combinatorial methods, this should not be a requirement for all future materials-development efforts. In general, durability (and thus reactivity) studies should be part of any materials-development effort for materials selected as "promising" and being considered for engineering evaluations. For the engineering center to develop systems that can meet the DOE 2015 targets, continued new materials (and thus material scale-up) must be integrated into the effort. Thus, materials-synthesis groups must work closely with the engineering center to ensure efficient use of limited resources in this type of activity. Based on this provision, material quantities and qualities may need to be adjusted based on delivery and testing requirements. Markets that can support the initial high cost of new storage systems should be included as part of DOE's overall plan. As such, those involved in materials-development efforts should take these other potential applications into consideration in their development plans.

Summary of Accomplishments

The HSCoE seamlessly integrated diverse, multidisciplinary expertise and sorbent development efforts. Prior to the HSCoE, state-of-the-art H₂ sorbents were exemplified by commercial activated high-SSA carbon (AX-21, now sold as MSC-30). These H₂ sorbents had ~5 wt % and 15 g/L storage capacities at 77 K and ~30 bar. In addition, there was substantial uncertainty and controversy about the measurement and capacity reproducibility of many sorbents. Specific HSCoE accomplishments include:

- 1. Developed and demonstrated hundreds of sorbents with as much as 300% improvement in hydrogen storage capacities, some of which may be used to meet DOE hydrogen storage targets.***
 - a. Cryogenic Storage: Developed new materials that increased the gravimetric (~60%, from ~5 to >8.5 wt % at 77 K) and volumetric (~150%, from ~15 to >35 g/L at 77 K) hydrogen storage capacities by physisorption onto high-SSA sorbents by optimizing pore sizes (0.7 to 1.5 nm) to increase SSA and packing density.

- i. Duke, NREL, UNC, and Caltech worked together to synthesize and characterize pyrolyzed PEEK materials with controlled pore sizes of 0.7 to 1.5 nm.
 - ii. Michigan's MOF-177 publication (Wong-Foy et al. 2006) has been cited ~750 times.
 - iii. TAMU's porous coordination network (PCN) material was shown to store >8.5 wt % excess H₂ storage at 77 K.
 - b. ***Toward Ambient-Temperature Storage:*** Through close collaboration between theorists and experimentalists, systematically searched through potential lightweight materials and determined that, without using metals, appropriately coordinated boron substituted in carbon is one of the very few viable methods to increase H₂ binding in a heterogeneous high-SSA material. The HSCoE championed this new approach, developing BC_x substitutional materials that achieved the theoretically predicted ~11 kJ/mol H₂ binding, and on a per-SSA basis, had >2 times the H₂ storage capacities compared to typical activated carbons, even at near-ambient temperatures. The HSCoE partners collaborated closely to synthesize and characterize these BC_x materials. The HSCoE also developed a new class of materials that is predicted to have high capacities (i.e., potentially >10 wt % and 100 g/L at ambient temperature) by creating sorption sites that store multiple (i.e., 2 to 8) H₂ molecules with binding energies between 10 and 30 kJ/mol. If the predictions can be demonstrated with fundamental experimental investigations, then the materials could have more than twice the H₂ storage densities of liquid H₂, but at ambient temperature.
 - i. The seminal paper in this area was published by HSCoE partners, has been cited more than 200 times, and spurred R&D resulting in hundreds of new publications.
 - ii. Substantial fundamental discovery and systematic development efforts are needed.
 - c. ***Ambient-Temperature Storage:*** The center pioneered the design and development of reversible sorbents via ambient-temperature spillover (e.g., weak chemisorption) that demonstrated 1 to 4 wt % storage capacities (more than two orders of magnitude gain compared to previous materials, i.e., ~0.01 wt %) with isosteric heats of adsorption between 10 and 30 kJ/mol.
2. ***Six Nature and Science publications with more than 3000 citations and 17 scientific journal cover articles.***
 3. ***More than 200 publications in peer-reviewed journals, with more than 50 co-authored by multiple U.S. and international institutions. These publications include three book chapters and a reference book.***
 4. ***More than 40 hydrogen storage material patents (12 issued) or applications submitted by HSCoE partners.***
 5. ***Two small businesses start-ups associated with HSCoE partners involving nanomaterials (i.e., CNT, Inc., and Unidym) and the scaled production of frameworks (e.g., BASF) that can be used as hydrogen storage materials.***
 6. ***Worked with world-class investigators around the world, including three Nobel Laureates.***
 7. Major awards including a President's Young Investigator Award, American Physics Society Fellow Appointment, Academy of Engineers Appointment, Neutron Scattering Society of America Science Prize, Neutron Scattering Society of America Fellow Appointment, Endowed Academic Chairs, Discover Magazine R&D 100, Materials

Research Society Medal, Department of Commerce Silver Medal, AAAS Newcomb Cleveland Prize, Top 10 Green-Tech Breakthroughs of 2008, and multiple DOE awards for scientific excellence.

8. Mentored more than 50 postdocs, and approximately 40 Ph.D. and 5 M.S. candidates. ***More than 10 accepted tenure-track academic appointments*** and 10 accepted scientist positions at national laboratories.
9. More than 800 conference presentations, proceedings, and published reports.
10. Accelerated hydrogen storage material development around the world by organizing more than a dozen technical conference sessions on hydrogen storage, an entire Materials Research Society Conference, and more than 20 national and international workshops on hydrogen sorption.
11. Performed hundreds of systematic investigations, after which the ultimate conclusion for most of the specific materials and/or processes was that they should not be investigated further for vehicular hydrogen storage applications. For example, elements with molecular weights that exceed ~16 grams per mole (g/mol) probably cannot be used to meet DOE 2015 storage targets at temperatures greater than ~80 K with physisorption. Furthermore, if stronger H₂ bonding is produced, then elements with molecular weights higher than ~32 g/mol will require multiple H₂ adsorption per sorbent atom to be able to meet DOE targets. In addition, nearly all the atoms must be accessible to the hydrogen to have sufficient capacities. These simple criteria virtually eliminate many typical sorbents such as zeolites.
12. ***Developed unique measurement capabilities*** to accurately and reliably characterize hydrogen storage properties of laboratory-scale (1–100 mg) samples to enhance high throughput and rapid screening analysis (isotherms, SSA, pore size distribution, isosteric heats of adsorption, temperature-programmed desorption, Raman and Fourier transform infrared spectroscopies, neutron scattering, and nuclear magnetic resonance).

The HSCoE's close interactions enabled substantially more development to occur more quickly than could have ever been done as independent projects. The synthesis, predictive theory, and materials directly address the issues of on-vehicle hydrogen storage and have uses in most of today's major high-technology applications including carbon capture, CO₂ sequestration, batteries, energy storage, semiconductor electronics, composites, drilling fluids, inks, drug delivery, transparent conductors, photovoltaics, purification, biomass catalysts, fuel cell catalysts, and energy generation.

Conclusions

At the inception of the HSCoE, the required hydrogen storage performance criteria and a number of other factors were used to quickly identify potential development materials and sorption mechanisms that could be used to meet DOE targets. Thus, from the outset, the center quickly eliminated entire classes of materials and processes that received no further development effort. Instead, the center focused activities on developing novel, scalable synthetic processes to form high-SSA, lightweight materials with optimum pore structures and compositions that had the potential to be used to meet DOE's 2015 and even DOE's ultimate full-fleet, on-vehicle refueling system targets (DOE 2009). The HSCoE focused exclusively on solving the very difficult challenges of developing materials only for on-vehicle refueling and storage. Based on

the intrinsic low isosteric heats of adsorption associated with sorbents, system capacity and costs are typically the main issues that must be resolved, and thus the center focused most of its efforts on improving these factors.

To accelerate development to the maximum, the HSCoE quickly identified focused efforts and directed specific partners and capabilities toward solving the most challenging problems. These focused development efforts included optimizing structures, substitution/heterogeneous materials, strong/multiple H₂ binding, weak chemisorption, and cross-cutting theory. Also, substantial efforts were performed in improving sorbent measurements to provide accurate characterization of the most important properties needed for developing materials. These measurement development efforts included improving accuracies to accelerate development so that laboratory-scale samples could be quickly characterized without the need for scaling up.

The HSCoE's organization, evaluation processes, and accelerated development efforts were used to continually identify promising new materials/processes as well as sorbents that did not make the cut and received no additional development. For example, at the outset of the HSCoE, a great deal of literature reported that materials such as carbon nanotubes and pyrolyzed conducting polymers could provide high-capacity, ambient-temperature hydrogen storage based on their unique structures. Thus, the HSCoE initially established significant activities to reproduce the results and resolve the exact capabilities of these different materials. The center determined that even though isosteric heats of adsorption may be increased, no significant gravimetric capacity improvements can be attained simply by improved geometrical structures for physisorption-based hydrogen storage beyond that expected based on material properties such as SSA. This was a critical finding for the center that led to [no-go decisions on carbon nanotubes](#) (DOE 2006) and conducting polymers for ambient-temperature hydrogen storage.

Ultimately, measurement calibration and control is at the heart of many of the erroneous results reported in the literature. For sorbents, the relatively light, low-density materials used, as well as the relatively low binding with hydrogen, can easily lead to inaccurate measurements. Thus, the center identified measurement standards, qualification, and certification as potential efforts that should be supported in the future. Measurement issues aside, the HSCoE did develop novel sorbents with improved capacities that can be used to meet DOE 2010 hydrogen storage system targets. Furthermore, the HSCoE developed and identified materials that may be able to be used to meet DOE 2015 and ultimate targets. In general, physisorption-based sorbents will need lower temperatures to meet DOE 2015 targets, and thus overall hydrogen energy efficiencies, system and hydrogen costs, and dormancy times must be balanced against capacities to engineer an appropriate system.

The HSCoE identified that increasing the isosteric heat of adsorption of sorbents for hydrogen, beyond that typically observed for physisorption, lowers system engineering constraints and costs. Thus, the HSCoE identified that properly structured heterogeneous materials such as boron-substituted carbon can substantially increase hydrogen storage capacities at near-ambient temperatures (i.e., ~220 K). The main issue here is developing materials with enough accessible sorption sites that the overall capacities at near-ambient temperatures can meet DOE targets. However, heterogeneous materials also help improve other sorbents including stabilizing coordinated metals and weak chemisorption. To increase heats of adsorption beyond what substituted/heterogeneous materials can do, the center identified coordinated but electronically

unsaturated metals and weak chemisorption of hydrogen as two viable mechanisms that enable ambient-temperature hydrogen storage.

The center championed the development of weak chemisorption (spillover) for large-capacity, ambient-temperature hydrogen storage. The center developed several new materials and catalyst processes that improved capacity and charging rates. An improved understanding of surface functionalization, catalyst size, and dispersion enhanced the sorption processes involved. The center also began investigating the barriers to migration based on structural and electronic features to provide development paths to create high-capacity, high-rate, hydrogen storage spillover materials that meet DOE targets. These factors, along with decreasing processing times, increasing scalability, and improved kinetic performance, accelerated the materials-development activities, enabling the HSCoE to identify viable paths forward to create weak-chemisorption materials that have the potential to be used to meet DOE 2015 hydrogen storage system targets.

The successful marriage of theory and experiment was most evident in the HSCoE's design of feasible materials based on multiple hydrogen storage per sorption site. From the center's outset, the ability to synthesize, the stability, and the DOE targets were selection criteria for the design of new materials. This along with interesting results reported in the literature led to the HSCoE championing the development of extremely novel sorbents. Such sorbents directly address the volumetric issues associated with ambient-temperature storage with high-SSA materials, while maintaining most of the advantages of sorbents to create materials that can meet even DOE's ultimate targets. For example, the HSCoE identified new inexpensive materials that use unique properties of Ca with highly viable synthetic routes. These revolutionary new materials could reversibly store hydrogen at twice the volumetric capacities (i.e., >100 g/L and >10 wt %) of liquid hydrogen, but at ambient temperature (i.e., ~300 K higher).

Sorbent materials, which will be refilled on the vehicle, enable the potential for substantially higher refueling efficiencies (and thus lower costs), because storage-material transport and regeneration will not be needed. Thus, the center believes that the on-vehicle refueling capability of sorbent materials is a tremendous advantage that should be exploited for hydrogen storage. However, to fully leverage this advantage, it is imperative that discovery and development efforts focus on reducing material and system costs. This cost reduction can be achieved by improving material storage capacities at near-ambient temperatures. Furthermore, any future efforts must also investigate the material properties related to hydrogen storage systems so that thermal conductivity, heat dissipation, refill and discharge rates, durability, and other engineering issues can be quantified fully.

References

- ANL (2010). "Hydrogen Storage through Nanostructured Porous Organic Polymers (POPs)," *DOE Fuel Cell Technologies Annual Progress Report*; pp. 495–498. http://www.hydrogen.energy.gov/pdfs/progress10/iv_c_1f_liu.pdf.
- Ataca, C.; Akturk, E.; Ciraci, S. (2009). "Hydrogen Storage of Calcium Atoms Adsorbed on Graphene: First-Principles Plane Wave Calculations." *Phys. Rev. B* (79:4); pp. 0414061-1–0414061-4. <http://link.aps.org/doi/10.1103/PhysRevB.79.041406>.
- Bhatia, S.K.; Myers, A.L. (2006). "Optimum Conditions for Adsorptive Storage." *Langmuir* (22:4); pp. 1688–1700. <http://pubs.acs.org/doi/full/10.1021/la0523816>.
- Chen, B.S.; Falconer, J.L.; Chang, L. (1991). "Formation and Decomposition of Methoxy Species on a Ni/Al₂O₃ Catalyst." *J. Catal.* (127:2); pp. 732–743. [http://dx.doi.org/10.1016/0021-9517\(91\)90195-A](http://dx.doi.org/10.1016/0021-9517(91)90195-A).
- Chen, C.H.; Huang, C.C. (2007). "Hydrogen Storage by KOH Modified Multi-Walled Carbon Nanotubes." *Int. J. Hydrogen Energy* (32:2); pp. 237–246. <http://dx.doi.org/10.1016/j.ijhydene.2006.03.010>.
- Chung, T.C.M.; Jeong, Y.; Chen, Q.; Kleinhammes, A.; Wu, Y. (2008). "Synthesis of Microporous Boron-Substituted Carbon (B/C) Materials Using Polymeric Precursors for Hydrogen Physisorption." *J. Am. Chem. Soc.* (130:21); pp. 6668–6669. <http://pubs.acs.org/doi/full/10.1021/ja800071y>.
- Collins, D.J.; Zhou, H.-C. (2007). "Hydrogen Storage in Metal-Organic Frameworks." *J. Mater. Chem.* (17:30); pp. 3154–3160. <http://dx.doi.org/10.1039/b702858j>.
- Conner, W.C.; Falconer, J.L. (1995). "Spillover in Heterogeneous Catalysis." *Chem. Rev.* (95:3); pp. 759–788. <http://dx.doi.org/10.1021/cr00035a014>.
- Cooper, A. (2008). "IV.C.1.m Enabling Discovery of Materials with a Practical Heat of Hydrogen Adsorption." *DOE Hydrogen Program Annual Progress Report 2008*. pp. 674–678. http://www.hydrogen.energy.gov/pdfs/progress08/iv_c_1m_cooper.pdf.
- de Leon, S.A.G.; Grange, P.; Delmon, B. (1997). "Characterization by Temperature-Programmed Reduction of Non-Conventional Catalysts for Hydrotreatment." *Catal. Lett.* (47:1); pp. 51–55. <http://dx.doi.org/10.1023/A:1019099309001>.
- Dinca, M., Han, W.S.; Liu, Y.; Dailly, A.; Brown, C.M.; Long, J.R. (2006). "Hydrogen Storage in a Microporous Metal-Organic Framework with Exposed Mn²⁺ Coordination Sites." *J. Am. Chem. Soc.* (128:51); pp. 16876–16883. <http://dx.doi.org/10.1021/ja0656853>.
- DOE (2003). "Grand Challenge" for Basic and Applied Research in Hydrogen Storage; Solicitation Number DE–PS36–03GO93013.
- DOE (2006). *Go/No-Go Decision: Pure, Undoped Single Walled Carbon Nanotubes for Vehicular Hydrogen Storage U.S. Department of Energy (DOE) Hydrogen Program*. http://www.hydrogen.energy.gov/pdfs/go_no_go_nanotubes.pdf.
- DOE (2007). *Fuel Cells Technology Program Multi-Year Research, Development and Demonstration Plan: Planned Program Activities for FY 2005–2015*. <http://www.eere.energy.gov/hydrogenandfuelcells/mypp/index.html>.
- DOE (2008). *Recommended Best Practices for the Characterization of Storage Properties of Hydrogen Storage Materials*. http://www.eere.energy.gov/hydrogenandfuelcells/pdfs/bestpractices_h2_storage_materials.pdf.
- DOE (2009). *Targets for Onboard Hydrogen Storage Systems for Light-Duty Vehicles*. http://www.eere.energy.gov/hydrogenandfuelcells/storage/pdfs/targets_onboard_hydro_storage_explanation.pdf.
- Dutta, G.; Waghmare, U.V.; Baidya, T.; Hegde, M.S. (2007). "Hydrogen Spillover on CeO₂/Pt: Enhanced Storage of Active Hydrogen." *Chem. Mat.* (19:26); pp. 6430–6436. <http://dx.doi.org/10.1021/cm071330m>.
- Farha, O.K.; Yazaydin, A.O.; Eryazici, I.; Malliakas, C.D.; Hauser, B.G.; Kanatzidis, M.G.; Nguyen, S.T.; Snurr, R.Q.; Hupp, J.T. (2010). "De Novo Synthesis of a Metal-Organic Framework Material Featuring Ultrahigh Surface Area and Gas Storage Capacities." *Nat. Chem.* (2); pp. 944–948. <http://dx.doi.org/10.1038/nchem.834>.

- Geohegan, D.B., et al. (2007). "In Situ Time-Resolved Measurements of Carbon Nanotube and Nanohorn Growth." *Phys. Status Solidi B* (244:11); pp. 3944–3949. <http://dx.doi.org/10.1002/pssb.200776204>.
- Glugla, P.G.; Bailey, K.M.; Falconer, J.L. (1989). "Activated Formation of a H-CO Complex on Ni/Al₂O₃ Catalysts." *J. Catal.* (115:1); pp. 24–33. [http://dx.doi.org/10.1016/0021-9517\(89\)90004-3](http://dx.doi.org/10.1016/0021-9517(89)90004-3).
- Guo, J.; Gui, B.; Xiang, S.X.; Bao, X.T.; Zhang, H.J.; Lua, A.C. (2008). "Preparation of Activated Carbons by Utilizing Solid Wastes from Palm Oil Processing Mills." *J. Porous Mat.* (15:5); pp. 535–540. <http://dx.doi.org/10.1007/s10934-007-9129-z>.
- HSCoE (2009). *Hydrogen Sorption Center of Excellence (HSCoE) Materials Go/No-Go Recommendation*. http://www.eere.energy.gov/hydrogenandfuelcells/pdfs/hscoe_recommendation_feb_10.pdf.
- Kim, Y.-H., Zhao, Y.; Williamson, A.; Heben, M.J.; Zhang, S.B. (2006). "Nondissociative Adsorption of H₂ Molecules in Light-Element-Doped Fullerenes." *Phys. Rev. Lett.* (96:1); pp. 016102-1–016102-4. <http://link.aps.org/doi/10.1103/PhysRevLett.96.016102>.
- Kim, Y.-Y.; Sun, Y.Y.; Zhang, S.B. (2009). "Ab initio Calculations Predicting the Existence of an Oxidized Calcium Dihydrogen Complex to Store Molecular Hydrogen in Densities up to 100 g/L." *Phys. Rev. B* (79:11); pp. 115424-1–115424-5. <http://link.aps.org/doi/10.1103/PhysRevB.79.115424>.
- Kubas, G.J. (2001). "Metal–Dihydrogen and σ -Bond Coordination: the Consummate Extension of the Dewar–Chatt–Duncanson Model for Metal–Olefin π Bonding." *J. Organomet. Chem.* (635:1–2); pp. 37–68. [http://dx.doi.org/10.1016/S0022-328X\(01\)01066-X](http://dx.doi.org/10.1016/S0022-328X(01)01066-X).
- Kubas, G.J. (2007). "Fundamentals of H₂ Binding and Reactivity on Transition Metals Underlying Hydrogenase Function and H₂ Production and Storage." *Chem. Rev.* (107:10); pp. 4152–4205. <http://dx.doi.org/10.1021/cr050197j>.
- Lachawiec, A.J.; Qi, G.S.; Yang, R.T. (2005). "Hydrogen Storage in Nanostructured Carbons by Spillover: Bridge-Building Enhancement." *Langmuir* (21:24); pp. 11418–11424. <http://dx.doi.org/10.1021/la051659r>.
- Li, Y.W.; Yang, R.T. (2006). "Hydrogen Storage in Metal–Organic Frameworks by Bridged Hydrogen Spillover." *J. Am. Chem. Soc.* (128:25); pp. 8136–8137. <http://dx.doi.org/10.1021/ja061681m>.
- Li, Y.W.; Yang, R.T. (2007). "Hydrogen Storage on Platinum Nanoparticles Doped on Superactivated Carbon." *J. Phys. Chem. C* (111:29); pp. 11086–11094. <http://dx.doi.org/10.1021/jp072867q>.
- Lin, Y.; Ding, F.; Yakobson, B.I. (2008). "Hydrogen Storage by Spillover on Graphene as a Phase Nucleation Process." *Phys. Rev. B*; (78); p. 041402-R. <http://dx.doi.org/10.1103/PhysRevB.78.041402>.
- Lueking, A.; Yang, R.T. (2002). "Hydrogen Spillover from a Metal Oxide Catalyst onto Carbon Nanotubes—Implications for Hydrogen Storage." *J. Catal.* (206:1); pp. 165–168. <http://dx.doi.org/10.1006/jcat.2001.3472>.
- Marchand A. (1971). "Electronic Properties of Doped Carbon." Walker P.L., ed. *Chemistry and Physics of Carbon*, Vol. 7, New York: Marcel Dekker; pp. 155–188.
- Marella, M.; Tomaselli, M. (2006). "Synthesis of Carbon Nanofibers and Measurements of Hydrogen Storage." *Carbon* (44); pp. 1404–1413. <http://dx.doi.org/10.1016/j.carbon.2005.11.020>.
- Mavrandonakis, A.; Klopper, W. (2008). "Comment on 'Kinetics and Mechanistic Model for Hydrogen Spillover on Bridged Metal–Organic Frameworks.'" *J. Phys. Chem. C* (112:8); pp. 3152–3154. <http://dx.doi.org/10.1021/jp074758h>.
- Mitchell, P.C.H.; Ramirez-Cuesta, A.J.; Parker, S.F.; Tomkinson, J.; Thompsett, D. (2003a). "Hydrogen Spillover on Carbon-Supported Metal Catalysts Studied by Inelastic Neutron Scattering. Surface Vibrational States and Hydrogen Riding Modes." *J. Phys. Chem. B* (107:28); pp. 6838–6845. <http://dx.doi.org/10.1021/jp0277356>.
- Mitchell, P.C.H.; Ramirez-Cuesta, A.J.; Parker, S.F.; Tomkinson, J. (2003b). "Inelastic Neutron Scattering in Spectroscopic Studies of Hydrogen on Carbon-Supported Catalysts—Experimental Spectra and Computed Spectra of Model Systems." *J. Mol. Struct.* (651–653); pp 781–785. [http://dx.doi.org/10.1016/S0022-2860\(03\)00124-8](http://dx.doi.org/10.1016/S0022-2860(03)00124-8).
- Olson, T.S.; Pylypenko, S.; Atanassov, P.; Asazawa, K.; Yamada, K.; Tanaka, H. (2010). "Anion-Exchange Membrane Fuel Cells: Dual-Site Mechanism of Oxygen Reduction Reaction in Alkaline Media on

- Cobalt–Polypyrrole Electrocatalysts.” *J. Phys. Chem C* (114:11); pp. 5049–5059. <http://dx.doi.org/10.1021/jp910572g>.
- Puretzky, A.A.; Geoghegan, D.B.; Styers-Barnett, D.; Rouleau, C.M.; Zhao, B.; Hu, H.; Cheng, M.D.; Lee, D.W.; Ivanov, I.N. (2008). “Cumulative and Continuous Laser Vaporization Synthesis of Single Wall Carbon Nanotubes and Nanohorns.” *Appl. Phys. A* (93:4); pp. 849–855. <http://dx.doi.org/10.1007/s00339-008-4744-3>.
- Purewal, J.; Kieth, J.B.; Ahn, C.C.; Fultz, B.; Brown, C.M.; Tyagi, M. (2009). “Adsorption and Melting of Hydrogen in Potassium-Intercalated Graphite,” *Phys. Rev. B*; Vol. 79; p. 054305. <http://dx.doi.org/10.1103/PhysRevB.79.054305>.
- Richard, M.A.; Bernard, P.; Chahine, R. (2009). “Gas Adsorption Process in Activated Carbon over a Wide Temperature Range above the Critical Point. Part 1: Modified Dubinin-Astakhov Model.” *Adsorption* (15:1); pp. 43–51. <http://dx.doi.org/10.1007/s10450-009-9149-x>.
- Sakintuna, B.; Yurum, Y. (2005). “Templated Porous Carbons: A Review Article.” *Ind. Eng. Chem. Res.* (44:9); pp. 2893–2902. <http://dx.doi.org/10.1021/ie049080w>.
- Sermon, P.A.; Bond, G.C. (1974). “Hydrogen Spillover.” *Catal. Rev.* (8:1); pp. 211–239. <http://www.tandfonline.com/doi/abs/10.1080/01614947408071861>.
- Simpson, L. (2010). “Overview of the DOE Hydrogen Sorption Center of Excellence.” *2010 DOE Annual Merit Review*. http://www.hydrogen.energy.gov/pdfs/review10/st014_simpson_2010_o_web.pdf.
- Singh, A.K.; Ribas, M.A.; Yakobson, B.I. (2009). “H-Spillover through the Catalyst Saturation: An *Ab Initio* Thermodynamics Study.” *ACS Nano* (3:7); pp. 1657–1662. <http://dx.doi.org/10.1021/nn9004044>.
- Sun, Q.; Jena, P.; Wang, Q.; Marquez, M. (2006). “First-Principles Study of Hydrogen Storage on Li₁₂C₆₀.” *J. Am. Chem. Soc.* (128:30); pp. 9741–9745. <http://dx.doi.org/10.1021/ja058330c>.
- Sun, Q.; Wang, Q.; Jena, P. (2009). “Functionalized Heterofullerenes for Hydrogen Storage.” *App. Phys. Lett.* (94:1); pp. 013111-1–013111-3. <http://link.aip.org/link/APPLAB/v94/i1/p013111/s1>.
- Sun, Y.Y.; Kim, Y.-H.; Zhang, S.-B. (2007). “Effect of Spin State on the Dihydrogen Binding Strength to Transition Metal Centers in Metal-Organic Frameworks.” *J. Am. Chem. Soc.* (129:42); pp. 12606–12607. <http://dx.doi.org/10.1021/ja0740061>.
- Sun, Y.Y.; Lee, K.; Kim, Y.-H.; Zhang, S.B. (2009). “*Ab Initio* Design of Ca-Decorated Organic Frameworks for High Capacity Molecular Hydrogen Storage with Enhanced Binding.” *Appl. Phys. Lett.* (95:3); pp. 33109-1–33109-3. <http://link.aip.org/link/APPLAB/v95/i3/p033109/s1>.
- Teichner, S.J. (1990). “Recent Studies in Hydrogen and Oxygen Spillover and Their Impact on Catalysis.” *Appl. Catal.* (62:1); pp. 1–10. [http://dx.doi.org/10.1016/S0166-9834\(00\)82232-0](http://dx.doi.org/10.1016/S0166-9834(00)82232-0).
- Wang, Y.H.; Yang, R.T. (2008). “Increased Hydrogen Spillover by Gaseous Impurity - Benson-Boudart Method for Dispersion Revisited,” *J. Catalysis*; (260:1); p. 198-201. <http://dx.doi.org/10.1016/j.jcat.2008.09.013>
- Wang, L.; Yang, F.H.; Yang, R.T. (2009). “Hydrogen Storage Properties of B- and N-Doped Microporous Carbon.” *AICHE Journal* (55:7); pp. 1823–1833. <http://dx.doi.org/10.1002/aic.11851>.
- Wang, L.; Yang, R.T. (2010). “Hydrogen Storage on Carbon-Based Adsorbents and Storage at Ambient Temperature by Hydrogen Spillover,” *Catalysis Reviews – Sci. & Eng.*; Vol. 52(4); pp. 411–461. <http://www.tandfonline.com/doi/full/10.1080/01614940.2010.520265>.
- Wong-Foy, A.G.; Matzger, A.J.; Yaghi, O.M. (2006). “Exceptional H₂ Saturation Uptake in Microporous Metal-Organic Frameworks.” *J. Am. Chem. Soc.* (128:11); pp. 3494–3495. <http://dx.doi.org/10.1021/ja058213h>.
- Yang, F.H.; Lachawiec, A.J.; Yang, R.T. (2006). “Adsorption of Spillover Hydrogen Atoms on Single-Wall Carbon Nanotubes.” *J. Phys. Chem. B* (110:12); pp. 6236–6244. <http://dx.doi.org/10.1021/jp056461u>.
- Yang, Z.; Xia, Y.; Mokaya, R. (2007). “Enhanced Hydrogen Storage Capacity of High Surface Area Zeolite-Like Carbon Materials.” *J. Am. Chem. Soc.* (129:6); pp. 1673–1679. <http://dx.doi.org/10.1021/ja067149g>.

- Yildirim, T.; Ciraci, S. (2005). "Titanium-Decorated Carbon Nanotubes as a Potential High-Capacity Hydrogen Storage Medium." *Phys. Rev. Lett.* (94:17); pp. 175501-1–175501-4. <http://link.aps.org/doi/10.1103/PhysRevLett.94.175501>.
- Yoon, M.; Yang, S.; Wang, E.; Zhang, Z. (2007). "Charged Fullerenes as High-Capacity Hydrogen Storage Media." *Nano. Lett.* (7:9); pp. 2578–2583. <http://dx.doi.org/10.1021/nl070809a>.
- Yoon, M.; Yang, S.Y.; Hicke, C.; Wang, E.G.; Geohegan, D.; Zhang, Z.Y. (2008). "Calcium as the Superior Coating Metal in Functionalization of Carbon Fullerenes for High-Capacity Hydrogen Storage." *Phys. Rev. Lett.* (100:20); pp. 206806-1–206806-4. <http://link.aps.org/doi/10.1103/PhysRevLett.100.206806>.
- Zhao, Y.; Kim, Y.-H.; Dillon, A.C.; Heben, M.J.; Zhang, S.B. (2005). "Hydrogen Storage in Novel Organometallic Buckyballs." *Phys. Rev. Lett.* (94:15); pp. 155504-1–155504-4. <http://link.aps.org/doi/10.1103/PhysRevLett.94.155504>.
- Zhou, W.; Wu H.; Yildirim, T. (2008). "Enhanced H₂ Adsorption in Isostructural Metal-Organic Frameworks with Open Metal Sites: Strong Dependence of the Binding Strength on Metal Ions." *J. Am. Chem. Soc.* (130:46); pp. 15268–15269. <http://dx.doi.org/10.1021/ja807023q>.
- Zielinski, M.; Wojcieszak, R.; Monteverdi, S.; Mercy, M.; Bettahar, M.M. (2005). "Hydrogen Storage on Nickel Catalysts Supported on Amorphous Activated Carbon." *Catal. Commun.* (6:12); pp. 777–783. <http://dx.doi.org/10.1016/j.catcom.2005.07.001>.
- Zlotea, C.; Moretto, P.; Steriotis, T. (2009). "A Round Robin Characterisation of the Hydrogen Sorption Properties of a Carbon Based Material." *Int. J. Hydrogen Energy* (34:7); pp. 3044–3057. <http://dx.doi.org/10.1016/j.ijhydene.2009.01.079>.

[This page left blank intentionally]



**U.S. Department of Energy
Office of Energy Efficiency and Renewable Energy
Fuel Cell Technologies Program
Hydrogen Sorption Center of Excellence (HSCoE)**

HSCoE Final Report

September 30, 2010

***Lin Simpson
Director, HSCoE
National Renewable Energy Laboratory (NREL)
Golden, Colorado***

Preface

The U.S. Department of Energy's Hydrogen Sorption Center of Excellence (HSCoE) was formed in 2005 as a 5-year project to develop hydrogen-storage materials primarily for light-duty vehicle applications. The HSCoE was competitively selected under the "Grand Challenge" for Basic and Applied Research in Hydrogen Storage (solicitation number DE-PS36-03GO93013) and led by the National Renewable Energy Laboratory. The center comprised partners from U.S. national laboratories, universities, and industry. The HSCoE concluded operations in September 2010 as per its planned schedule.

This report documents the HSCoE's organizational structure and research findings. It also contains the HSCoE's recommendations for classes of sorption materials that merit further research and development for light-duty vehicle applications.

Acknowledgements

Funding for this effort was provided by the U.S. Department of Energy's (DOE's) Office of Energy Efficiency and Renewable Energy within the Hydrogen Sorption Center of Excellence as part of DOE's National Hydrogen Storage Grand Challenge. We gratefully acknowledge the contributions made to this report by all of our partners and collaborators. The list of contributors is far too numerous to include here, but many of them are mentioned within the body of this report. We thank them all. The success of this project was directly related to their tremendous contributions and willingness to work closely together to solve very difficult problems. Finally, we especially thank and acknowledge all of the people at DOE and their collaborators for valuable and insightful input and direction.

Acronyms and Abbreviations

Å	angstrom
AC	activated carbon
AIMD	<i>ab initio</i> molecular dynamics
ANL	Argonne National Laboratory
APCI	Air Products and Chemicals Inc.
at. %	atomic percent
atm	atmosphere
B	boron
BC _x	boron-substituted carbon
B-SWNT	boron-substituted single-walled carbon nanotube
Be	beryllium
BET	Brunauer-Emmett-Teller
C	carbon
C ₆₀	fullerene
CA	carbon aerogel
Ca	calcium
Caltech	California Institute of Technology
Cl	chloride
CNT	carbon nanotube
Co	cobalt
COF	covalent organic framework
Cr	chromium
Cs	cesium
Cu	copper
CUMC	coordinatively unsaturated metal center
CVD	chemical vapor deposition
D ₂	deuterium
DFT	density functional theory
DMF	dimethylformamide
DOE	U.S. Department of Energy
DRIFTS	diffuse reflectance infrared Fourier transform spectroscopy
Duke	Duke University
DWNT	double-walled carbon nanotubes
EDS	electron dispersive spectroscopy
EDX	energy dispersive X-ray
EELS	electron energy loss spectroscopy
EERE	DOE Office of Energy Efficiency and Renewable Energy
EPR	electron paramagnetic spin resonance
F	fluorine
Fe	iron
FTIR	Fourier transform infrared
FY	fiscal year
g	gram
GCMC	Grand Canonical Monte Carlo

GGA	generalized gradient approximation
GIC	graphite intercalation compound
GO	graphite or oxide
h	hour
H	hydrogen
H ₂	dihydrogen
HD	hydrogen deuteride
HF	hydrogen fluoride
HRTEM	high-resolution transmission electron microscopy
HSCoE	Hydrogen Sorption Center of Excellence
INS	inelastic neutron scattering
IR	infrared
K	Kelvin
	potassium
kg	kilogram
kJ	kilojoule
L	liter
LDA	local density approximation
LDOS	local density of states
Li	lithium
LiH	lithium hydride
LLNL	Lawrence Livermore National Laboratory
LSX	low-silica type X
m ²	square meter
MAS	magic angle spinning
MAS-NMR	magic angle spinning nuclear magnetic resonance
MD	molecular dynamics
mdip	methylene-di-isophthalate
Met-Car	metallocarbohedrene
Mg	magnesium
MHCoE	Metal Hydride Center of Excellence
Michigan	University of Michigan
Missouri	University of Missouri-Columbia
mL	milliliter
Mn	manganese
min	minute
Mo	molybdenum
MOF	metal-organic framework
mol	mole
MPa	megapascal
MWNT	multi-walled nanotubes
N	nitrogen
N ₂	dinitrogen
Na	sodium
NDA	non-disclosure agreement
Ni	nickel

NIST	National Institute of Standards and Technology
NMR	nuclear magnetic resonance
NREL	National Renewable Energy Laboratory
O	oxygen
ORNL	Oak Ridge National Laboratory
PANI	polyaniline
Pd	palladium
PEEK	polyetheretherketone
Penn	University of Pennsylvania
Penn State	Pennsylvania State University
PGAA	prompt-gamma activation analysis
<i>p</i> -H ₂	para-hydrogen
POP	porous organic polymer
ppm	parts per million
PPy	polypyrrole
psia	pounds per square inch absolute
Pt	platinum
PVD	physical vapor deposition
QENS	quasielastic neutron spectroscopy
Qst	isosteric heats of adsorption
Rb	rubidium
Rice	Rice University
RPI	Rensselaer Polytechnic Institute
RT	room temperature
Ru	ruthenium
S	sulfur
SANS	small-angle neutron scattering
SBU	secondary building unit
Sc	scandium
SEM	scanning electron microscopy
SPD	surface packing density
SSA	specific surface area (per unit of mass)
STP	standard temperature and pressure
SWNH	single-walled carbon nanohorn
SWNT	single-walled carbon nanotube
TAMU	Texas A&M University
TBB	benzenetristetrazolate
TC	templated carbon
TEB	triethylboron
TEM	transmission electron microscopy
TGA	thermal gravimetric analysis
THF	tetrahydrofuran
Ti	titanium
TM	transmission metal
TMS	tetramethylsilane
TPD	temperature-programmed desorption

UC	University of Chicago
UCLA	University of California, Los Angeles
UNC	University of North Carolina, Chapel Hill
UV	ultraviolet
V	vanadium
VASP	Vienna <i>Ab initio</i> Simulation Package
vdW	van der Waals
vol %	volume percent
W	tungsten
wt %	weight percent
XPS	X-ray photoelectron spectroscopy
XRD	X-ray diffraction
Zn	zinc

Table of Contents

1.0 Introduction/Background	22
1.1 Mission and Scope.....	22
1.2 Partners.....	25
1.3 References.....	32
2.0 Development	33
2.1 Approach/Overview	33
2.2 Optimized Nanostructures	38
2.3 Substituted Materials.....	38
2.4 Strong/Multiple Dihydrogen Interactions	40
2.5 Weak Chemisorption/Spillover	41
2.6 Crosscutting Theory	41
2.7 Specialty Characterization	43
2.8 Overview of Analyses Performed.....	43
2.9 Specific Analytical Tools Used by the HSCoE Partners	44
2.9.1 Adsorption Isotherm	44
2.9.1.1 Surface Area Analysis/Pore Size Analysis	44
2.9.1.2 Excess Hydrogen Adsorption	44
2.9.2 Temperature-Programmed Desorption	45
2.9.3 Microscopies and Morphologies.....	46
2.9.3.1 X-Ray Diffraction	46
2.9.3.2 Electron Microscopies	46
2.9.3.3 Small-Angle Neutron Scattering.....	46
2.9.4 Hydrogen Interactions.....	47
2.9.4.1 Neutron Scattering Spectroscopy.....	47
2.9.4.2 Quasielastic Neutron Spectroscopy	47
2.9.4.3 Nuclear Magnetic Resonance	48
2.9.5 Composition and Atomic Content	49
2.9.5.1 Prompt Gamma Activation Analysis	49
2.9.5.2 X-Ray Photoelectron Spectroscopy	49
2.9.5.3 High-Resolution Electron Energy-Loss Spectroscopy	49
2.10 Analyses Performed for Specific Sorbent Classes	50
2.10.1 Optimized Nanospaces.....	50
2.10.2 Substituted Materials	50
2.10.3 Strong/Multiple Dihydrogen Interactions	51
2.10.4 Weak Chemisorption/Spillover.....	51
2.11 Cross-Cutting Theory	52
2.11.1 Density Functional Theory	53
2.11.2 Continuum and Other Modeling Approaches	54
2.12 Down-Select Criteria	55
2.13 Material Properties and Systems Investigated	57
2.13.1 Overview	57
2.13.2 Optimized Nanostructures	59
2.13.2.1 Pyrolyzation of Organic Materials.....	63
2.13.2.2 Chemical Synthesis and/or Intercalation of Exfoliated Graphite/Graphene	64

2.13.2.3 Vapor Synthesis and Scaffolding/Foams of Carbon Nanotubes and Nanohorns	65
2.13.2.4 Templating	66
2.13.2.5 Inexpensive/Scalable Aerogels for H ₂ Storage and Metal Hydride Scaffolding.....	67
2.13.2.6 Crystalline Porous Frameworks or Polymers	69
2.13.3 Substituted Materials	71
2.13.3.1 Predicted Heterogeneous Sorbents for Hydrogen Storage.....	73
2.13.3.2 Elucidation of Desired Sites.....	75
2.13.3.3 BC ₃ Graphene Versus C Graphene	76
2.13.3.4 Fluoride-Intercalated Carbon Materials	78
2.13.3.5 Boron-Substituted Sorbent Synthesis	79
2.13.3.6 Pyrolysis of B-Containing Precursor	80
2.13.3.7 Templating BC _x and NC _x	81
2.13.3.8 Direct Assembly of B-Substituted Carbon	82
2.13.3.9 B, N, and P Atom Substitution into Chemically Synthesized Graphene	82
2.13.3.10 Cross-Cutting Calculations for Substituted Materials	83
2.13.4 Strong/Multiple Dihydrogen Interactions	85
2.13.4.1 Overview of First-Principles and Materials Design.....	85
2.13.4.2 Effectiveness and Accuracy of Density Functional Theory for Hydrogen Adsorption.....	86
2.13.4.3 Integration of Metals in Framework Structures	88
2.13.4.4 Coordination of Metals to High-Surface-Area Supports	91
2.13.4.5 Unique Properties of Coordinated Ca Metal Centers	96
2.13.4.6 Coordinated Metal Centers for Storing Hydrogen.....	96
2.13.5 Weak Chemisorption/Spillover.....	98
2.13.5.1 Spillover Thermodynamics	100
2.13.5.2 Spillover Kinetics.....	105
2.13.5.3 Thermodynamic Calculations Validation	106
2.13.5.4 Spillover via Physisorbed Atomic Hydrogen	108
2.13.5.5 Hydrogen Storage via Spillover.....	110
2.13.5.6 Other Weak Chemisorption Hydrogen Storage Materials	115
2.13.6 Cross-Cutting Theory.....	115
2.13.6.1 Hydrogenation of Boron-Nitride Materials	116
2.13.6.2 Met-Cars	117
2.13.6.3 Endohedral Fullerene	118
2.14 References	119
3.0 Results	132
3.1 Major Findings.....	132
3.2 Optimized Nanostructures	134
3.2.1 Enhancing Physisorption Enthalpies Through Geometric Structures.....	134
3.2.2 Increasing Specific Surface Area.....	137
3.2.2.1 Carbon Aerogels	137
3.2.2.2 Carbon Aerogel Scaffolds for Complex Hydrides.....	139
3.2.2.3 Frameworks.....	146

3.2.3 Increasing Volumetric Capacity	151
3.2.4 Go/No-Go Decision for Nanotube-Based Storage at Ambient Temperature	155
3.3 Substituted Materials.....	156
3.3.1 First-Principles Materials Design	156
3.3.1 Synthesis and Hydrogen Storage Results of B-Substituted Carbons.....	158
3.3.1.1 Pyrolysis Synthesis of BC _x	158
3.3.2 Other Benefits of Heterogeneous Sorbents.....	184
3.4 Strong/Multiple Dihydrogen Interactions	189
3.4.1 Frameworks.....	190
3.4.2 Coordination of Metals to High-Surface-Area Supports	197
3.4.1.1 Metal Coordination on Pure Carbon Supports.....	198
3.4.2.2 Solution-Phase Hydrogenation of Carbon Nanostructures	207
3.4.2.3 Metal Intercalation in Graphite Compounds.....	209
3.4.3 Metal Coordination to Functionalized Substrates.....	211
3.4.3.1 Metal-Phosphine Coordination	212
3.4.3.2 Metal-Graphene Oxide.....	215
3.4.4 Strong/Multiple Dihydrogen Interactions: Conclusions	216
3.4.4.1 Practical Paths Forward for Sorbent Materials	217
3.4.5 Strong/Multiple Dihydrogen Interaction No-Go Decisions.....	219
3.4.5.1 Tractable Solution-Phase Reactions Involving Organometallic Sc Complexes.....	219
3.4.5.2 Reducible Fulvalene-Based MOF Linkers.....	220
3.5 Weak Chemisorption/Spillover	221
3.5.1 Spillover Storage on Metal-doped Superactivated Carbon.....	223
3.5.2 Irreversible Chemical Reactions	227
3.5.3 High-Capacity Experimental Spillover Results	228
3.5.4 Spillover on Boron-Substituted Carbon Materials.....	230
3.5.5 Accelerated Sample Activation Process	233
3.5.6 Synergistic Spillover with Core Shell Materials.....	233
3.5.7 Spillover on Ru-Activated Carbon Matrix via Pyrolysis.....	236
3.5.8 Spillover of Hydrogen on Pt/Carbon from Pyrolyzed Sucrose Templated on Silica Sphere Templates.....	237
3.6 Summary of Development Efforts and Results	247
4.0 Major Technical Accomplishments of Center	266
5.0 Recommendations.....	270
5.1 Review of Go/No-Go Decisions	270
5.2 Materials/Systems/Classes Recommended for Continued R&D	271
5.3 Suggestions for New Materials Systems To Be Investigated	274
5.4 Identification of Remaining Issues for Recommended Systems	274
5.5 Identification of Systems Recommended for No Further Investigation.....	276
5.6 Recommended Storage Options and Material Systems for Early Market Applications	277
5.7 References.....	277
6.0 Lessons Learned from the Center Approach	278
6.1 Lessons Applicable to All R&D Efforts.....	278

7.0 Conclusions	280
7.1 References	282
Appendix A: Hydrogen Sorption Center of Excellence Bibliography	283
A.1 Publications	283
A.2 People Who Worked in the Hydrogen Sorption Center of Excellence.....	304
A.3 Awards and Special Accomplishments	306
A.4 Patents, Patent Applications, and Records of Invention	308
Appendix B: Updated Table (June 2009) of DOE Targets	314
Appendix C: HSCoE Materials Go/No-Go Recommendation Document (September 2009).....	316

List of Figures

Figure 1-1. Overview of the HSCoE Partners. UCLA/Michigan and Penn State left the center at the end of Phase I. Also, Rice, NREL, and Air Products formed the Steering Committee during Phase I.	26
Figure 2-1. Illustrations of the four types of sorbent binding mechanisms investigated by the HSCoE	34
Figure 2-2. The optimal enthalpy (ΔH) for hydrogen storage depends on the pressure, temperature (black is 77 K, blue is 223 K, and red is 298 K), and sorption interaction (i.e., entropy: e.g., dotted lines $\Delta S = -10R$, and solid lines $\Delta S = -8R$). For example, as shown in this plot if materials with enthalpies between ~ 13 and 25 kJ/mol can be made, then ambient temperature hydrogen storage is possible with pressures between ambient and 100 bar. For lower binding energies, lower storage temperatures will be required.	35
Figure 2-3. Graph from Argonne National Laboratory showing the dependence of volumetric density on gravimetric and bulk density for sorption materials. The plot indicates that to have the potential to meet DOE 2015 volumetric target (0.04 kg H ₂ /L, yellow band on chart), bulk material densities between 0.7 and 1 g/L will be required for sorbent materials with 6 to 7 wt % gravimetric capacities.	35
Figure 2-4. Overview of the HSCoE partners' roles and specialties associated with rational design of sorbents	42
Figure 2-5. Optimal pore size for maximization of volumetric capacity: low density and large pore size (left) may lead to low volumetric capacity because of the unused voids. Optimal pore size and material density can maximize the volumetric capacity (right).	61
Figure 2-6. Binding of H ₂ to activated carbon sites with various types of dangling bonds (left) in comparison to that bound to carbon sites without dangling binding (right). The atomic structures of small hydrocarbon segments with dangling sp ³ σ -bonds and sp ² π -bonds mimic activated carbon surfaces. The H ₂ binding energy was calculated, and no noticeable enhancement of binding energy was observed. This result indicates that activation of carbon surfaces does not lead to stronger physisorption.	62
Figure 2-7. Aggregates of “short” and “long” single-wall carbon nanohorns produced by laser vaporization. Schematic representation of individual nanohorns is shown.	66
Figure 2-8. Calculations predict that only electronically frustrated B and Be substituted in carbon with correct coordination significantly increase H ₂ binding (e.g., ~ 11 kJ/mol) and capacities at temperatures approaching ambient.	72
Figure 2-9. (a) and (b) are the differential planar electron density, $\Delta\rho(x,y)$, for B and Be, respectively. Solid and dotted contours indicate electron accumulation and depletion, respectively. The contour interval is 0.003 and the cutoffs are ± 0.08 e/Å ² . (c) Linear $\Delta\rho(x)$, for B and Be along the x axis shown in (a) and (b), respectively. The positions of the H ₂ and B (Be) are indicated.	74
Figure 2-10. Modeled amorphous carbon with pore sizes of 1–2 nm (a), and H ₂	

binding after substitution with boron at different sites (b-d). Black, green, and yellow balls are carbon, boron, and hydrogen atoms.....	75
Figure 2-11. Calculations show that the increased amount of B substituted in carbon supports increases the stabilization of Ti atoms.....	76
Figure 2-12. Schematic of bottom-up preparation of heteroatom-substituted synthetic graphenes by a solution-phase process. The all-carbon synthetic graphenes were prepared in the same manner, but with deletion of the boron-, phosphorous- and nitrogen-containing precursors.....	83
Figure 2-13. Example of a B-substituted structure (Schwartzite) with heptagonal carbon rings, negative Gaussian curvature, and small pore size that enhances hydrogen binding (blue is carbon, red is boron, and green is hydrogen).....	84
Figure 2-14. Examples of metal-based materials designed by the HSCoE that maintain optimum hydrogen binding energies (shaded area) throughout their entire H ₂ capacity range	85
Figure 2-15. (Left) Simulated model for Mn-based MOF systems. Four H ₂ molecules are adsorbed on the four Mn centers. (Right) Electron density plot of an anti-bonding state between the H ₂ σ and Mn d_{z^2} orbitals. These calculations quantitatively agree with experimentally measured binding energies and indicate that splitting and occupation of the spin orbitals reduces the binding.	89
Figure 2-16. Structure of (a) a Met-Car dimer and (b) corresponding tetrahedral Met-Car crystal	90
Figure 2-17. A Cp polymer decorated by Mn atoms (orange). Each Mn binds three H ₂ molecules (white).....	90
Figure 2-18. Design of a co-intercalated-graphite compound, in which Li and THF are the co-intercalation species.....	93
Figure 2-19. H ₂ storage in Li-intercalated BC _x graphite.....	93
Figure 2-20. Binding energy vs. capacity. Hydrogen binding energy versus loading in intercalated graphite with and without B doping.	94
Figure 2-21. Concept for synthesizing transition metal-decorated aerogel supports.....	95
Figure 2-22. Mechanism for Kubas coordination. The shading (green) represents charge density. Donation and back donation are denoted in blue and red, respectively.	97
Figure 2-23. Conceptual diagram of hydrogen spillover processes. Reversible RT hydrogen storage on metal-doped carbon materials via a “spillover” mechanism involves a series of steps: (a) molecular H ₂ dissociates on the metal catalyst particles; (b) atomic H migrates to the receptor; and (c) atomic H diffuses across the receptor surfaces.	99
Figure 2-24. Average binding energy of the chemically absorbed hydrogen atom blocks (size of 2, 6, 24, ∞ of hydrogen atoms) on graphene, compared to the cohesive energy of the free hydrogen molecule, H ₂	101
Figure 2-25. a) Left: Schematics of spillover process in real space. The inequality shows the range of chemical potential μ_H favorable for spillover. Right: model of spillover in energy space displays the relative energy (chemical potential) of H in different states. The gray, dark-red, and blue lines show the μ_H in fully hydrogenated graphene (CH), in metal hydride, and in the H ₂	

<p>molecule, respectively. The pink and dark red blocks show the range of energies of H at the catalyst and at the Pd(111) surface with the H coverage varying from 0.25 to 1 mL. The family of thin dark blue lines corresponds to the energies of H bound to graphene. b) The optimized structure of Ni₄H_{2n} (n = 2 to 10). The plot of incremental energy E_{incr} vs. number of H atoms. The gray line shows the H binding energy in the fully hydrogenated phase. The E_{incr} crosses this line after the 6th H₂ molecule, indicating the thermodynamic onset of spillover.....</p>	102
Figure 2-26. Weak C-H bonds formed through sp ² +d rehybridization	103
Figure 2-27. Schematic illustration of binding energy vs. hydrogen coverage in nanosorbents and the requirement for binding energy tuning	103
Figure 2-28. Initial calculations at NREL identified that, compared to migration along a surface, hopping between closely spaced surfaces substantially lowers the barrier for hydrogen diffusion.....	106
Figure 2-29. TPD result from 6 wt % Pt on templated carbon (3400 m ² /g) after dosing with 0.4 atm H ₂ followed by D ₂ at 298 K for 5 min (followed by quench, gas phase removal, and TPD).....	113
Figure 2-30. Rates of adsorption (a), and desorption (b) at different pressures using Pt/AX-21 samples (T = 298 K)	114
Figure 2-31. Atomic structure and charge contour of small boron-nitride molecules	116
Figure 2-32. Bonding framework in a Ti ₈ C ₁₂ Met-Car molecule	118
Figure 2-33. Energy of H binding to pure C ₆₀ (black curve) and Ca-encapsulated C ₆₀ (blue curve). When metal atoms are encapsulated, the charge transfer from the metal to the cage decreases and then increases again as H coverage increases, as shown by the insets, where the charge density is contributed by the four electrons just below the Fermi level.....	119
Figure 3-1. Excess H ₂ gravimetric uptake isotherms (± 0.1 % error) of a pyrolyzed PEEK material measured at NREL and Caltech. The agreement of the data from two different laboratories is exceptional, providing very good evidence of the outstanding hydrogen-storage properties of this sorbent. (A) Shows a full pressure range (0–150 bar) and (B) focuses on the lower-pressure region (0–50 bar). The estimated error of the excess H ₂ gravimetric uptakes for the data from Caltech is ± 0.1%.....	133
Figure 3-2. The H ₂ isosteric enthalpy of adsorption for ACF10, ACF20, and CNS201 as a function of excess adsorption. Inset: the isosteric heat is plotted as a function of the fractional amount of adsorption (excess adsorption divided by the saturation adsorption amount at 77 K).....	135
Figure 3-3. (Upper) 77 and 87 K isotherms of KC ₂₄ (K intercalated graphite) with a blowup of the low-pressure regime in the inset. (Lower) Plot of the isosteric enthalpy of adsorption demonstrating nearly constant sorption enthalpy values with loading.	136
Figure 3-4. Representative thermal gravimetric analysis data for LiBH ₄ incorporated into various CA scaffolds showing the influence of pore size and carbon nanotubes on the dehydrogenation reaction. The black curve is LiBH ₄ mixed with nonporous graphite. The weight losses indicate dehydrogenation	

and scale with LiBH ₄ loading.	141
Figure 3-5. Schematic of TAMU's PCN-12 and 12' materials. Small adjustments enable metal centers to be more open and accessible for hydrogen storage.....	148
Figure 3-6. Isotherms of PCN materials made by TAMU. Note that the data labeled PCN-69 in this graph actually correlate to PCN-68. The data were measured by Dailly and coworkers at General Motors.....	149
Figure 3-7. Schematic of one of ANL/UC's porous polymers in which the conductive backbone has been incorporated with different elements	152
Figure 3-8. (a)–(d): The calculated local density of states (LDOS) for B (Be) in C ₃₅ B(Be)-H ₂ . The LDOS for B (Be) are solid lines, whereas the LDOS for H ₂ are open circles. (e) and (f): The square changes of the carbon states caused by H ₂ sorption, namely $\sigma^2=[\delta\text{LDOS}(\text{carbon})]^2$ between the non-bonding and bonding states.....	157
Figure 3-9. Example of a B-precursor synthesis route using poly(diethynylphenylborane) chloride for preparing porous BC _x materials.....	158
Figure 3-10. Solid-state ¹¹ B MAS-NMR spectra of BC _x materials prepared from pyrolysis of a B-precursor (with LiCl salts) at (a) 600°C (run A-1), (b) 800°C (run A-2), (c) 1100°C (run A-3), and (d) 1500°C (run A-5).	160
Figure 3-11. TE images of (top) BC ₁₁ (run A-1) and (bottom) BC ₄₀ (run A-6).....	161
Figure 3-12. Schematics of BC _x materials: (left) top view and (right) side view.....	162
Figure 3-13. SEM images of BC _x materials obtained after pyrolysis of B-precursors (with LiCl) at (a) 600°C (run A-1) and (b) 1800°C (run A-6), and (c) B-precursor (without LiCl) at 600°C.....	163
Figure 3-14. SEM image of BC ₁₁ materials (run A-1).....	163
Figure 3-15. Pore size distribution of (a) BC ₁₁ (run A-1), (b) BC ₁₃ (run A-2), (c) BC ₁₃ (run B-1), and (d) BC ₁₇ (run B-2)	164
Figure 3-16. X-ray diffraction patterns of LiCl salts in B-precursor after pyrolysis at various temperatures: (a) 150°C, (b) 400°C, (c) 450°C, and (d) 600°C	165
Figure 3-17. Hydrogen adsorption vs. H ₂ pressure for two porous (BC ₆ and BC ₁₂) materials at (a) 77 and (b) 293 K	166
Figure 3-18. ¹ H NMR of boron-substituted graphitic carbon exposed to H ₂ gas at 295 K and 10 MPa. The thick continuous line is the spectrum, and the dashed lines are the three components used to fit the spectrum: (A) H ₂ in capillary, (B) H ₂ in large voids, (C) H ₂ in nanopores. Inset: SEM image of sample granule.....	167
Figure 3-19. RT isotherms based on the intensities of lines (A), (B), and (C) in Figure 3-18. The inset shows the isotherms of the two components of peak C, identified by T ₁ measurements. C1 is associated with the long-T ₁ component, and C2 is associated with the short-T ₁ component. The lines are fits with Langmuir isotherms.	168
Figure 3-20. TEM images of CM-Tec parent material (left) and BC _x deposited onto CM-Tec (right). Red arrow in right figure denotes the turbostratic overlayer of deposited BC _x	169
Figure 3-21. High-surface-area, porous BC ₆ material produced by direct pyrolysis of triethylboron at 900°C	170
Figure 3-22. Sieverts capacity at 77 K and 2 bar, and TPD capacity, as a function	

of nitrogen BET surface area for a variety of BC _x -templated activated carbons. CM-Tec is the parent activated carbon material for all samples.	170
Figure 3-23. Representative example of hydrogen temperature-programmed desorption for a templated BC _x sorbent. The hydrogen desorption from templated BC _x materials with higher B concentration is much slower than from materials with less B.	171
Figure 3-24. B and C XPS of templated BC _x materials.	172
Figure 3-25. (a) Static and magic angle spinning (MAS) ¹³ C NMR spectra of BC ₅ powder. (b) Static and MAS ¹¹ B NMR spectra of BC ₅ powder.	173
Figure 3-26. Diagrams of boron-containing precursors used to form porous boron-substituted carbon materials.	174
Figure 3-27. Representative example of hydrogen adsorption (solids) and desorption (open) excess gravimetric isotherms of porous BC _x sorbents. Because this material SSAs of only 600 to 800 m ² /g, the maximum excess hydrogen adsorption of ~2.3 wt % at 77 K is much higher than what is typically observed for pure carbon sorbents (i.e., 1.2 to 1.6 wt %).	178
Figure 3-28. Representative example of the hydrogen isosteric heat of adsorption for a porous templated BC _x sorbent.	179
Figure 3-29. INS measurement of the intensity of hydrogen remaining on the sample as a function of temperature. The data show that the B-containing samples hold hydrogen to a greater extent at temperatures below ~65 K.	180
Figure 3-30. Isotherm comparison of volumetric hydrogen storage capacities of laser-produced and arc-produced C-SWNTs and B-SWNTs.	181
Figure 3-31. EELS spectrum for boron-doped SWNTs prepared by laser vaporization; laser target contained 11% NiB catalyst.	182
Figure 3-32. Neutron spectra for arc-produced C-SWNTs (open symbols) and B-SWNTs (filled symbols). A mass fraction of 0.1% is equivalent to a 1 H ₂ :B atomic ratio of the B-SWNT samples. Right panel displays the different spectra.	182
Figure 3-33. Comparison of neutron spectra for laser-produced C-SWNT (open symbols) and B-SWNTs (filled symbols). Data are labeled for H ₂ :B atomic ratios of the B-SWNT samples with the equivalence of 0.2% mass fraction being equivalent to 1 H ₂ . Right panel displays the different spectra between 0.5 H ₂ :B and 1 H ₂ :B and 1 H ₂ :B and 2 H ₂ :B.	183
Figure 3-34. Elemental mapping of C, B, N, and P in substituted graphene structures using EELS.	185
Figure 3-35. SSA measurements from nitrogen BET at 77 K vs. hydrogen uptake at 77 K and 2 bar. The data for all-carbon and substituted synthetic graphenes are indicated by the different colored symbols, as shown in the legend. The solid lines with the matching colors are the linear fits and extrapolations obtained from the sample data.	186
Figure 3-36. Simulated model for Mn-based MOF systems. Four deuterium (D ₂) molecules are adsorbed on the four Mn centers. Light blue spheres represent D ₂ centroids, and the orange spheres show the position of a partially occupied, extra framework Mn ²⁺ ion site. Sites are labeled I to IV in order of the observed adsorption sites.	191

Figure 3-37. Diagrams of the Fe, Mn, and Cu MOF materials made by the University of California at Berkeley that were used by NIST to measure the hydrogen interactions with the metal centers. NIST performed INS that identified that the H ₂ adsorption strength was strongest for Fe ²⁺ > Mn ²⁺ > Cu ²⁺ , which correlates to the metal-H ₂ distance: Fe ²⁺ < Mn ²⁺ < Cu ²⁺ (i.e., 2.17 < 2.27 < 2.47 Å, respectively). However, this does not correlate to the metal ionic radius (i.e., Mn ²⁺ > Fe ²⁺ > Cu ²⁺). NIST also found that the Fe ²⁺ site catalyzes hydrogen conversion to para-H ₂ (completely at low loading, partially at high loading).	192
Figure 3-38. D ₂ Adsorption Sites in MOF-74 at a loading of 4.2 D ₂ :Zn. (a) Superpositions of Fourier difference map together with the crystal structure of MOF-74 projected down the <i>c</i> -axis. The red-yellow regions indicate the high scattering regions of the first two adsorption sites. (b) The four D ₂ adsorption sites identified by neutron powder diffraction (labeled 1–4, spheres of green and light blue). (c) The first three D ₂ adsorption sites are shown with the first site directly interacting with the Zn ²⁺ ions (blue balls) at a distance of 2.6 Å.....	193
Figure 3-39. Different INS spectra of <i>p</i> -H ₂ loaded HKUST-1 and the bare substrate measured on FANS. The displayed spectra result from <i>p</i> -H ₂ scattering only, and peaks of significant intensity are labeled as either rotations (Rot) or a combination of rotation and transition (Trans). Ratios of <i>p</i> -H ₂ to copper are 0.26 (blue circles, adsorption at Cu site only) and 1.1 (green circles, adsorption at Cu site and second site).	194
Figure 3-40. The synthesis and open metal site alignment (top), hydrogen uptake (bottom, left), and heat of adsorption (bottom, right) of the two MOF polymorphs: PCN-12 and PCN-12'.....	196
Figure 3-41. Solid-state ¹³ C NMR spectra of the fullerene compounds in which C ₆₀ interacts with Li, Fe, Sc, Co, and Cr.....	200
Figure 3-42. HRTEM and EDX analysis of the Fe(C ₆₀) compound.....	201
Figure 3-43. XRD pattern of the Fe(C ₆₀) compound	202
Figure 3-44. Cartoon representation of Fe(C ₆₀) chains.....	202
Figure 3-45. Raman spectra of pure C ₆₀ , K ₆ C ₆₀ , and all of the metal fullerene products (Li, Co, Cr, Sc, and Fe)	203
Figure 3-46. Hydrogen TPD spectra of the metal fullernene complexes in which C ₆₀ is interacting with Cr, Sc, Fe, or Co. The samples were degassed to 130°C and exposed to hydrogen at RT and 500 torr for ~5 min.....	204
Figure 3-47. TPD spectra revealing that the hydrogen-adsorption capacity of the Li(C ₆₀) complex (excess Li metal present) is more than two orders of magnitude greater than that of the Sc, Co, Cr, and Fe complexes.....	205
Figure 3-48. Solid-state ¹³ C NMR spectra of Li ₁₂ C ₆₀ (top) and Li(C ₆₀) (excess Li metal present, bottom).	206
Figure 3-49. Representative TPD spectra for hydrogenated SWNT (Na-SWNT, blue) and Pt-AC/SWNT (Pt/Na-SWNT, red) samples. The addition of a Pt-AC catalyst material lowered desorption temperature by nearly 75°C and enabled reversible RT H ₂ loading of the material. The Pt-AC/SWNT mixture was first degassed to 300°C and then exposed to ~500 torr of H ₂ gas at RT.	208
Figure 3-50. FTIR spectrum of a reduced SWNT material (left) and theoretical	

representation of C-H bonds on a nanotube surface (right).....	209
Figure 3-51. XRD spectrum of Li-THF co-intercalation in graphite.....	210
Figure 3-52. TPD for Li-BC ₆ (black), BC ₆ (red), and Li on AC (blue). Samples were degassed to 300°C prior to a 500-torr, RT H ₂ dose.	212
Figure 3-53. XPS of C 1s spectra for CM-Tec AC (black), BC ₆ on CM-Tec AC (red), and Li-BC ₆ on CM-Tec AC (blue). Right: High-resolution TEM of Li-BC ₆ material.....	212
Figure 3-54. Reaction pathways to reactive Ni intermediates with reactive ligands that are easily displaced.	214
Figure 3-55. Hydrogen TPD data for a Ni(BF ₄) ₂ -PPh ₂ -SiO ₂ aerogel. The sample was degassed to 300°C prior to a RT 500-torr H ₂	214
Figure 3-56. TEM micrograph of Ni nanoparticles (dark spots, 2–5 nm) on a functionalized SiO ₂ aerogel	215
Figure 3-57. H ₂ binding to Ti fragments on graphene oxide (Ti, blue; oxygen, red).....	216
Figure 3-58. Schematic representation of the grafting of benzyl Ti fragments onto GO substrates	216
Figure 3-59. H ₂ binding in a LiSiO ₂ nanotube viewed toward the wall (left) and along the axial direction (right). Gold, red, purple, and grey balls denote, respectively, Si, O, Li, and H atoms.	217
Figure 3-60. Atomic structures of (a) H ₂ -loaded Ca(H ₂) ₈ complexes with the D _{4d} and D _{4h} symmetries, and (b) Ca(H ₂) ₈ -intercalated graphite in a $\sqrt{7}\times\sqrt{7}$ pattern. Inset shows the side view. Green, blue, and white atoms are C, Ca, and H, respectively.....	218
Figure 3-61. Building blocks and structure of COF- α (viewed along the [001] direction).....	218
Figure 3-62. Schematic of the tractable reaction for the synthesis of CpScH ₂ (H ₂) ₄	219
Figure 3-63. Reaction pathway for the synthesis of a Sc metal complex with multiple dihydrogen ligands	220
Figure 3-64. Chemical structures for three new fulvalene-based MOF linkers.....	221
Figure 3-65. Typical and consistent results on hydrogen isotherms at 298 K on 6 wt % Pt/AX-21 are shown.	224
Figure 3-66. TPD result for 6 wt % Pt on carbon (3400 m ² /g) after dosing with 0.4 atm H ₂ followed by D ₂ at 298 K for 5 min (followed by quench, gas-phase removal, and TPD).....	225
Figure 3-67. High-pressure hydrogen isotherms at 298 K on 6 wt % Pt/AX-21 (○, upper curve) by direct integration technique (error bars are based on 1 σ of 4 separately prepared samples). Undoped AX-21 (□, lower curve).	226
Figure 3-68. H ₂ isotherms at 298 K on templated carbon (TC) and 6 wt % metal catalysts. All materials were H ₂ -reduced at 300°C except Ru/TC-T, which was thermally reduced (in N ₂) at 900°C (1 h). BET SSAs for each sample were (m ² /g): Ru/TC-T = 2090 (open diamonds); Ru/TC = 3004 (open circles); Pt/TC = 3120 (open triangles); Ni/TC = 3091 (open squares); TC = 3839 (closed diamonds).	226
Figure 3-69. Representative diffusion time constants for H spillover on Pt/TC at 298 K.....	227
Figure 3-70. The graph on the left illustrates how an adsorption curve can be	

affected by side reactions. The squares illustrate the first adsorption cycle of a highly oxidized carbon-receptor-pt catalyst, and the triangles, diamonds, and circles show the next cycles with drastically reduced sorption capacities. This is a direct effect of water formation. The curve on the right illustrates a TPD after a typical high-pressure hydrogen adsorption. This illustrates how easily one can identify the formation of water.	228
Figure 3-71. High-pressure hydrogen isotherms at 298 K for pure IRMOF-8 (□), Pt/AC, and IRMOF-8 physical mixture (1:9 weight ratio) (solid diamonds), and for a bridged sample of Pt/AC-bridges-IRMOF-8: first adsorption (solid triangles), desorption (open diamonds), and second adsorption (open circles).	229
Figure 3-72. TEM image of Ru catalyst on BC _x sorbents (left) and ambient-temperature isotherm data (right) of BC _x and Ru catalyst on BC _x sorbents. These results demonstrate the enhanced reversible hydrogen-storage capacity of the BC _x sorbent with a Ru catalyst, consistent with a spillover mechanism. Each hydrogen pressure step in the isotherm required only ~10 min to equilibrate, substantially shorter than for carbons. Also note that these data have not been corrected for He adsorption during calibration.	232
Figure 3-73. Hydrogen spillover results indicate that improved catalyst processing enhances capacity (top). Irreproducibility in the processing often results in limited hydrogen spillover. However, with appropriate processing, hydrogen spillover (e.g., Ru on CM-Tec data) is observed (bottom).	234
Figure 3-74. TEM image of the core-shell platinum-ceria catalyst that improved hydrogen spillover for storage	235
Figure 3-75. Pt-Ceria core shell materials mixed with an MSC-30 activated carbon matrix. Typically, the isolated core-shell nanoparticles were on the order of 3–5 nm. The hydrogen-sorption properties of the resultant materials were evaluated via low- to high-pressure volumetric adsorption at RT from 1–140 bar. The total gravimetric hydrogen adsorption is almost double that expected from the mixture if there were no synergistic/catalytic effect. Improving the catalyst/receptor interface appears to enhance spillover.	235
Figure 3-76. Hydrogen spillover capacity of a ruthenium-activated carbon material made via pyrolysis of Ru(acac) in the presence of activated carbon	236
Figure 3-77. Microscopic images of silica-templated carbon matrix of ~600 m ² /g prepared according to literature procedures. The platinum-doping level was ~10 wt %. The hydrogen-sorption properties of the material were unique and successful.	237
Figure 3-78. Volumetric hydrogen-adsorption isotherms that compare the sorption properties of: (a) black line is a 3600 m ² /g activated carbon blank (MSC-30 an ax-21 like material); (b) blue line is a 600 m ² /g carbon matrix blank; (c) green line is the 900 m ² /gram silica-templated carbon matrix blank; (d) red line illustrates the hydrogen sorption properties of the Pt-carbon silica-templated matrix.	238
Figure 3-79. Adsorption isotherm of H ₂ on Pt/AX-21 at 298 K with presorbed CH ₄ at P(CH ₄) = 0 (●), 5.0×10 ⁻⁴ (◇), 1.2×10 ⁻³ (□), and 3.4×10 ⁻³ atm (△). The three presorbed CH ₄ points fall essentially on the origin, which is due to the large Y-axis scale.	239

Figure 3-80. Adsorption isotherm of H ₂ on Pt/AX-21 at 298K with presorbed CH ₄ at P(CH ₄)=0 (○), 1.0×10 ⁻³ (●), 5.0×10 ⁻³ (▲), 1.0×10 ⁻² (■), and 0.1 atm (◆) (Wang and Yang 2008).....	240
Figure 3-81. High-pressure hydrogen isotherms at 298 K for 10% Pd/graphite oxide (○), 10% Pd/AX-21-O (◇), and 10% Pd/AX-21 (△), normalized by the BET SSA. The BET SSAs are: 2466 m ² /g for Pd/AX-21 and 2362 m ² /g for Pd/AX-21-O, and 687 m ² /g for Pd/graphite oxide (Wang et al. 2009).....	242
Figure 3-82. (Left) High-pressure hydrogen isotherms at 298 K for 6 wt % Pt doped on various carbons. Adsorption (■) and desorption (□) on Pt/TC-O (via O ₂ plasma); adsorption (▲) and desorption (△) on Pt/TC (not oxidized). (Right) Cyclic adsorption/desorption of H ₂ on 6 wt % Pt/TC-plasma: first cycle (■), 1.75 wt % at 100 atm; second cycle (▲), 1.36 wt %; third cycle (●), 1.32 wt %; and fourth cycle (◆), 1.32 wt % (Wang, Yang, and Yang 2010).	243
Figure 3-83. Hydrogen desorption rates on Pt/Maxsorb, Pt/Maxsorb-TiF ₃ -A, and Pt/Maxsorb-TiF ₃ -B at 298 K. Pressure step: (a) 77.7–52.8 atm for Pt/Maxsorb; (b): 78.1–53.1 atm for Pt/Maxsorb-TiF ₃ -A; (c) 77.9–52.9 atm for Pt/Maxsorb-TiF ₃ -B.	244
Figure 3-84. These results illustrate the change in hydrogen-sorption behavior from a receptor only (pure CM-Tec) to a Ru-decorated CM-Tec material. The significance of this accomplishment is that based on the new enhanced kinetics, it should be possible to charge a spillover sample so that it could reach the theoretical limit and be saturated at 6.6 wt % in 5 min, at ~100 bar and RT. Thus, the new results indicate that the spillover process may meet the DOE 2010 gravimetric targets and approach the 2010 rate targets. Additionally, assuming a realistic density of the carbon material of 1 g/cm ³ , it would be possible to exceed the 2010 volumetric targets with a system value of 0.06 kg H ₂ /L.	245
Figure 3-85. High-pressure hydrogen isotherms on CVD-Pt/Li-LSX. Adsorption (▲); desorption (△) at 298 K and 10 MPa (Wang and Yang 2010).....	246
Figure 3-86. High-pressure hydrogen isotherms on 10 wt % Ni/Ca-LSX (○) at 298 K and 10 MPa (Wang and Yang 2010).....	247

List of Tables

Table 1-1. Revised (in 2009) Selected High-Level DOE Hydrogen Storage System Targets for Light-Duty Vehicles*	23
Table 1-2. Status of Sorption Materials' Ability to Meet DOE Storage System Targets.....	25
Table 2-1. Overview of the HSCoE Partners' Roles and Responsibilities.....	36
Table 2-2. Selection Criteria for Sorbent Material Classes	57
Table 2-3. Formation Energy of Boron Dopants and H ₂ Binding Energy in Different Sites of Amorphous Carbon	75
Table 2-4. The H ₂ Gravimetric Density, Calculated Lattice Spacing (d), Average Bader Charge on F (Q _F), and Average H ₂ Adsorption Energy (ΔE) at 300 K.....	79

Table 2-5. A Summary of Porous BC _x Materials Prepared by B-Precursor Containing Inorganic Salts under Various Pyrolysis Conditions	81
Table 2-6. Comparison of the H ₂ Binding Energies (in kJ/mol H ₂) from the Nine Density Functionals with Accurate Benchmark Results.....	87
Table 2-7. Total energy (eV, in red) of metal-clustered structures relative to the metal-dispersed structures and nearest Li–Li distance (Å, in blue). It is demonstrated that Li-clustered structures become energetically more favorable at Li ₁₀ C ₆₆ B ₆	94
Table 2-8. Reaction Heat (kJ/mol H ₂) of Hydrogenation of Small Hydrocarbon Molecules and Graphene Sheet.....	104
Table 2-9. Overview of the Different Sorbents and Catalysts Used by HSCoE Partners To Construct Spillover Materials for Hydrogen Storage.....	111
Table 2-10. Overview of Predictive Efforts for Designed Hydrogen Storage Materials	115
Table 2-11. Reaction Heat (kJ/mol H ₂) of Hydrogenation of Small Hydrocarbon and Ammonia-Borane Molecules	117
Table 3-1. Adsorption Energy (in eV units) of H ₂ for Doped C ₃₆ . Endo- and Sub- Stand for Endohedral and Substitutional Doping, Respectively.....	156
Table 3-2. Lattice Parameters of BC _x Materials Measured by X-Ray Diffraction Patterns.....	161
Table 3-3. Summary of Specific Surface Area and Pore Volume of Four BC _x Materials	165
Table 3-4. Orientational potential obtained from GGA calculations and the corresponding rotational levels. The calculated classical harmonic H ₂ phonons for a fixed H ₂ orientation perpendicular to the Cu-Cu bond are $\omega(x') = 9.56$ meV, $\omega(y') = 13.44$ meV, and $\omega(z') = 22.87$ meV. The coupling of phonons with rotational transitions explains the observed INS spectra.	194
Table 3-5. Volumetric Hydrogen Adsorption Capacities at 2 Bar for Both RT and 77 K, Following No Degas and Degassing to 100° and 250°C for Li-THF Co- Intercalated and Li-Intercalated Graphite	211
Table 3-6. Results of CH ₄ and H ₂ Adsorption on Pt/AX-21.....	239
Table 3-7. XPS Relative Subpeak Area of C _{1s} of the Untreated and Oxygen Plasma-Treated Carbon (Wang, Yang, and Yang 2010)	243
Table 3-8. Summary of Hydrogen Storage Properties for Systems Developed and Investigated for van der Waals-Based, High-Specific-Surface-Area Sorbents	247
Table 3-9. Summary of Hydrogen Storage Properties for Systems Developed and Investigated for Substituted Sorbents	249
Table 3-10. Summary of Hydrogen-Storage Properties for Systems Developed and Investigated for Strong/Multiple Dihydrogen Binding-Based Sorbents.....	250
Table 3-11. Summary of Hydrogen Storage Properties for Systems Developed and Investigated for Weak Chemisorption Materials	254

1.0 Introduction/Background

1.1 Mission and Scope

The U.S. Department of Energy (DOE) Hydrogen Sorption Center of Excellence (HSCoE) was formed in 2005 to develop materials for hydrogen storage systems to be used in light-duty vehicles. The HSCoE and two related centers of excellence were created as follow-on activities to the DOE Office of Energy Efficiency and Renewable Energy's (EERE) Hydrogen Storage Grand Challenge Solicitation issued in fiscal year (FY) 2003.

For transportation applications, sorbents offer tremendous advantages compared to existing hydrogen storage systems; i.e., high pressure (350 to 700 bar) or liquid hydrogen. Sorbents allow fast on-vehicle hydrogen fill-up and discharge rates, nominal thermal management requirements during refueling, ease of engineering, the ability to provide required pressures, and favorable system energy efficiencies. The last benefit affects hydrogen and storage costs, a vital consideration in designing storage systems. In addition, use of sorbents may significantly reduce the volume and weight of storage systems compared to 350- and 700-bar high-pressure tanks. An added benefit of this development, beyond the primary focus of vehicular applications, is that sorbents may also be used in other hydrogen storage applications such as stationary power generation, portable power, backup power, and niche, early-market vehicles.

When the HSCoE was established, there were a number of challenges for sorbents. One revolved around the relatively low binding energies with hydrogen, and thus the need to use cryogenic temperatures (e.g., 77 K, -193°C , liquid nitrogen temperature at 1 bar). In addition, the HSCoE had to work through the wide range of irreproducible values reported for sorbents. This involved developing reproducible measurement calibrations and procedures that are adaptable to different characterization laboratories, as well as developing a sound understanding of the hydrogen sorption processes involved and their ultimate limitations or boundaries. The HSCoE's critical goals included the following hydrogen storage system targets: net available capacity of 45 g/L and 6 wt % and system cost of \$133/kg H_2 (dihydrogen).

However, in FY 2009, DOE revised the hydrogen storage system targets for light-duty vehicles, some of which are shown in Table 1-1 (DOE 2009). In light of this change, all DOE targets discussed in the remainder of this document will reference the revised DOE hydrogen storage system targets. The targets for the HSCoE are nominally reflected by the 2015 DOE hydrogen storage targets shown in Table 1-1. To ensure that the development activities were performed as efficiently as possible, the HSCoE formed complementary, focused development clusters based on the following four sorption-based hydrogen storage mechanisms:

1. Physisorption on high-specific-surface-area (SSA) and nominally single-element materials
2. Enhanced H_2 binding in substituted/heterogeneous materials

3. Strong and/or multiple H₂ interactions from coordinated, but electronically unsaturated, metal centers
4. Weak chemisorption/spillover.

Table 1-1. Revised (in 2009) Selected High-Level DOE Hydrogen Storage System Targets for Light-Duty Vehicles*

Target	2010	2015	Ultimate Full Fleet
System Gravimetric Density (% wt)	4.5 (1.5 kWh/kg)	5.5 (1.8 kWh/kg)	7.5 (2.5 kWh/kg)
System Volumetric Density (g/L)	28 (0.9 kWh/L)	40 (1.3 kWh/L)	70 (2.3 kWh/L)
System Fill Time for 5-kg fill, min (fueling rate, kg/min)	4.2 min (1.2 kg/min)	3.3 min (1.5 kg/min)	2.5 min (2.0 kg/min)

*http://www1.eere.energy.gov/hydrogenandfuelcells/storage/pdfs/targets_onboard_hydro_storage_explanation.pdf

The HSCoE worked toward the goal of developing high-capacity sorbents that could be operated at temperatures and pressures approaching ambient and be charged efficiently and quickly in the tank with minimal energy requirements and minimal penalties to the hydrogen fuel infrastructure. The work was directed at overcoming barriers to achieving DOE system goals and identifying pathways to meet the hydrogen storage system targets.

Specifically, the HSCoE:

- Developed high-SSA sorbents with optimal hydrogen (H) binding energies with the focus on increasing binding to ~25 kJ/mol H₂ for room-temperature (RT) operation. This enables:
 - High-capacity systems that operate at modest pressures (e.g., less than 100 bar) and below fuel-cell operating temperatures (<70°C)
 - Meeting both gravimetric and volumetric targets simultaneously with rapid kinetics
 - Efficient and rapid on-board refueling with minimal energy requirements.
- Rapidly correlated capacity, structural, and energetic information to reduce time between discovery, assessment, and down-selection of materials.
- Integrated experiment and theory seamlessly in both “feedback” (explanation) and “feed-forward” (discovery) modes.
- Devised facile synthetic routes using low-cost approaches.
- Created a nimble and flexible, yet structured, teaming environment to accelerate discovery, evaluation, and selection of promising development directions.
- Organized partners in focused groups to optimize development and avoid duplication of effort, with seamless integration of experiment/theory.
- Used quantitative down-select criteria prior to beginning R&D and at go/no-go points.

The HSCoE developed novel high-SSA hydrogen-storage materials for advanced fuel cell technologies. The HSCoE's development efforts comprised 17 active projects at 22 institutions. HSCoE partners conducted a wide range of applied research and engineering studies on available sorbent materials and developed design principles and synthetic methods for next-generation materials that may be used to meet the critical DOE system hydrogen storage targets. The technical barriers addressed by these projects from the *Hydrogen, Fuel Cells and Infrastructure Technologies Program Multi-Year Research, Development and Demonstration Plan* (DOE 2009) include the following.

General:

- (A) System Weight and Volume
- (B) System Cost
- (C) Efficiency
- (D) Durability/Operability
- (E) Charging/Discharging Rates
- (J) Thermal Management

Reversible On-Board:

- (P) Lack of Understanding of Hydrogen Physisorption and Chemisorption
- (Q) Reproducibility of Performance.

The HSCoE developed sorption materials for hydrogen storage systems. As shown in Table 1-2 the HSCoE focused on addressing the higher-risk targets for sorbents that are associated with capacity and costs. These include:

- Cost: \$4/kWh net
- Specific energy: 1.8 kWh/kg
- Energy density: 1.3 kWh/L
- Charging/discharging rate: 3.3 min.

Table 1-2. Status of Sorption Materials' Ability to Meet DOE Storage System Targets

Storage Parameter	Units	2010	2015	Ultimate
System Net Gravimetric ^a	kWh/kg (kg H ₂ /kg system)	L 1.5 (0.045)	M 1.8 (0.055)	H 2.5 (0.075)
System Volumetric Capacity: Usable energy density from H ₂ (net useful energy/max system volume)	kWh/L (kg H ₂ /L system)	L 0.9 (0.028)	M 1.3 (0.040)	H 2.3 (0.070)
Storage System Cost ^b (& fuel cost) ^c	\$/kWh net (\$/kg H ₂) \$/gge at pump	L 4* (133) 2-3	M 2* (67) 2-3	H TBD 2-3
Durability/Operability <ul style="list-style-type: none"> Operating ambient temperature ^d Min/max delivery temperature Cycle life (1/4 tank to full) ^e Cycle life variation ^f Min delivery pressure from storage system; FC= fuel cell, ICE= internal combustion engine Max delivery pressure from storage system^g 	°C °C Cycles % of mean (min) at % confidence Atm (abs) Atm (abs)	L -30/50 (sun) -40/85 1000 90/90 4FC/35 ICE 100	M -40/60 (sun) -40/85 1500 99/90 3FC/35 ICE 100	H -40/60 (sun) -40/85 1500 99/90 3FC/35 ICE 100
Charging/discharging Rates <ul style="list-style-type: none"> System fill time (for 5-kg H₂) Minimum full flow rate Start time to full flow (20°C) ^h Start time to full flow (-20°C) ^h Transient response 10%-90% and 90% -0%^l 	min (kg H ₂ /min) (g/s)/kW s s s	L 4.2 min (1.2 kg/min) 0.02 5 15 0.75	M 3.3 min (1.5 kg/min) 0.02 5 15 0.75	H 2.5 min (2.0 kg/min) 0.02 5 15 0.75
Fuel Purity (H ₂ from storage) ^j	% H ₂	L 99.99 (dry basis)		
Environmental Health & Safety <ul style="list-style-type: none"> Permeation & leakage ^k Toxicity Safety Loss of usable H₂ ^l 	Standard cubic centimeters per hour - - (g/h)/kg H ₂ stored	Meets or exceeds applicable standards		
		L 0.1	M 0.05	H 0.05

See Appendix B for table notes..

L: Green: low risk, high probability to meet.

M: Yellow: medium risk, medium probability to meet.

H: Red: high risk, low probability to meet.

1.2 Partners

From the outset, HSCoE partners were chosen to provide the specific expertise and capabilities necessary to develop materials that could fulfill DOE requirements. The National Renewable Energy Laboratory (NREL) led the HSCoE, with partners at other U.S. national laboratories and universities, and at Air Products and Chemicals, Inc., a corporate partner. The NREL team included HSCoE Director Lin Simpson, Anne Dillon, Philip Parilla, Thomas Gennett, Yufeng Zhao, Jeff Blackburn, and Chaiwat Engtrakul, as

well as Michael Heben (who subsequently went to University of Toledo), and Shengbai Zhang (now at Rensselaer Polytechnic Institute).

Under NREL's coordination, a center was established that included development activities at more than 20 renowned institutions throughout the United States and direct collaborations with institutions around the world (see Figure 1-1).

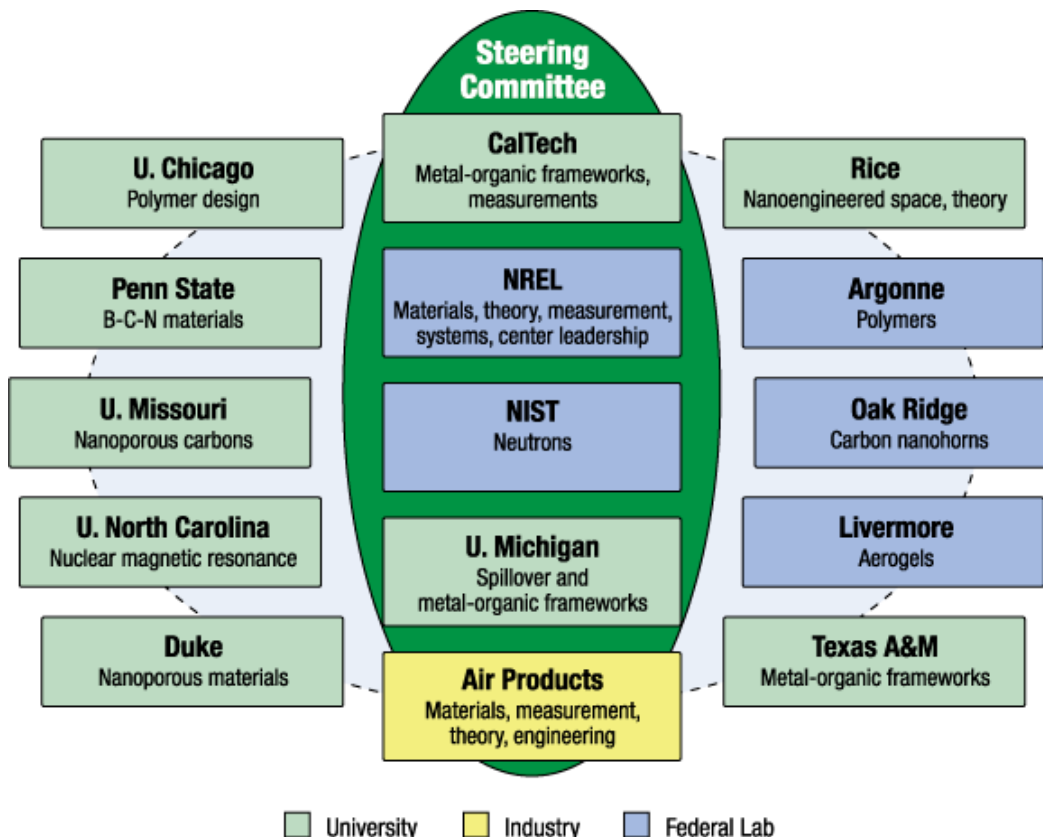


Figure 1-1. Overview of the HSCoE Partners. UCLA/Michigan and Penn State left the center at the end of Phase I. Also, Rice, NREL, and Air Products formed the Steering Committee during Phase I.

The HSCoE partners are described below:

- National Renewable Energy Laboratory (NREL):** NREL's role was to lead the HSCoE and to develop reversible sorbents for hydrogen storage focused on light-duty vehicle applications. This included developing the science base and technology advances required to meet DOE storage goals by investigating a range of hydrogen sorption materials. NREL performed R&D within the HSCoE on a variety of nanostructured and high-SSA materials, which included carbon, metals, oxides, and/or other lightweight elements. NREL's H₂ storage material goals involved providing DOE with viable solutions with the potential to meet even the ultimate technical targets. Meeting DOE's ultimate technical targets will likely require the

development of revolutionary materials. NREL's research was targeted at addressing key technical barriers:

- Weight and volume: System capacities approach material capacities as the tank operation moves toward ambient temperatures and pressures with materials that have optimum binding energies. In general, sorbents already meet the vast majority of DOE hydrogen storage targets and have minimal heat transport requirements. NREL's development efforts focused on the remaining targets—cost and capacity. Because volumetric and gravimetric capacities are closely linked in sorbents, the approach centered on:
 - Increasing material density (i.e., >0.7 g/mL) to decrease size
 - Increasing SSA and optimizing pore sizes to decrease tank weight/size.
 - Optimization of binding energies to increase capacities and operating temperature. This included
 - Developing the highest-efficiency storage system by optimizing sorbent materials that operate reversibly on board with a hydrogen binding energy in the range of 15–20 kJ/mol (for RT operation).
 - Decreasing heat-transfer requirements to increase on-board refueling times.
 - Ensuring that sorption materials would typically meet DOE refueling and delivery rate targets.
 - Closing the gap between the idealized sorption materials that have been predicted and the synthesis of actual materials using low-cost source materials and synthesis processes such that cost target will be achieved.
 - Cost: The goal was to develop sorption materials using inexpensive materials and processes. Typical high-SSA, lightweight materials (e.g., activated carbon) are commercially manufactured in bulk at ~\$1/kg with carbon costs being only a small fraction. Thus, material costs for a system could be ~\$15/kg-H₂ (assume 7 wt %).
- **Air Products and Chemicals Inc. (APCI):** Alan Cooper and Guido Pez (retired) led the team. APCI enabled and executed discovery of materials with “practical heats” of hydrogen absorption. These practical heats are hydrogen adsorption enthalpy ranges that allow for the charging and discharging of hydrogen storage materials at near-ambient temperatures and reasonable hydrogen pressures (i.e., 3–100 bar). APCI also performed computational work to design materials with enhanced heats of adsorption and to understand reversible hydrogen spillover processes using metal oxides and carbon-based materials. Materials that were predicted to have exceptional heats of adsorption include lithium-intercalated single-walled carbon nanotubes (SWNTs), fluoride graphite intercalation complexes (theoretical heat of adsorption ~8–20 kJ/mol H₂), and boron-substituted carbons (experimental isosteric heat of adsorption ~11–12 kJ/mol H₂). Once well-characterized samples of the potential hydrogen storage materials were synthesized, accurate measurement techniques, such as APCI's unique differential pressure adsorption method, were employed to obtain

hydrogen isotherms and heats of adsorption. Advanced techniques such as correction for helium adsorption effects on H₂ isotherms were employed as necessary.

- **Argonne National Laboratory (ANL):** Di-Jia Liu, University of Chicago, and Yuping Lu led the ANL team, which addressed combined volumetric and gravimetric challenges by exploring a new class of hydrogen adsorbent—nanostructured porous organic polymers (POPs). ANL collaborated with the University of Chicago researchers who constructed the POPs. In general, POPs have excellent thermal stability and tolerance to gas contaminants such as moisture. They also have low skeleton density and high intrinsic porosity via covalent bonds, which makes them capable of maintaining SSA during high-pressure pelletizing for better volumetric density. The team’s approach focused on improving hydrogen uptake capacity and the heat of adsorption by enhancing SSA, porosity control, and framework-adsorbate interactions through rational design and synthesis at the molecular level. The design principles aimed at improving the following attributes of the polymers: (1) high SSA to provide sufficient interface with H₂; (2) narrow pore diameter to enhance van der Waals (vdW) interactions in the confined space; and (3) “metallic” features, either through π -conjugation or metal doping, to promote electronic orbital interactions with hydrogen. Since joining the HSCoE in the summer of 2007, the ANL team prepared more than 60 samples of POP materials in three different polymeric categories. In addition to polymer design and synthesis, the team also conducted various characterization studies on POP surface properties, hydrogen uptake capacity, isosteric heat of adsorption, and hydrogen-POP interaction. This work was done independently and through collaboration with HSCoE partners. The team also conducted ab initio and density functional theory (DFT) calculations to compare with the experimental results for a better understanding of the hydrogen-polymer interaction on the surface or inside of confined space.
- **California Institute of Technology (Caltech):** Channing Ahn led the Caltech team, which focused its efforts on determining the behavior of unmodified carbons and the optimal microporous size distributions necessary for maximizing volumetric densities. High-SSA-based physisorbents are a class of materials that are closer to engineering viability for high gravimetric density reversible on-board storage applications, than other on-board reversible candidate materials, provided that cryogenic storage is acceptable. Further optimization of this class of materials was necessary to increase volumetric densities. This optimization required promoting narrow pore distribution in these materials, and modifications to the surface to increase the sorption enthalpy.
- **Duke University:** Led by Jie Liu, the Duke team initially synthesized and purified gram quantities of SWNTs with well-controlled small diameters via chemical vapor deposition methods. Once no significant improvement in sorption properties could be observed, the project was redirected in 2008 to developing low-cost and scalable synthesis of microporous carbon materials with well-controlled pore sizes that would be suitable for hydrogen storage. The Duke team studied several approaches, including the use of different zeolites as a template, the use of organic micelle

structures as a template, and the slow oxidation of polymer precursors. Among them, the slow activation of polyetheretherketone (PEEK) under a carbon dioxide (CO₂) environment or water vapor produced microporous carbon with an average pore size <2 nm. Initial testing at 77 K by both NREL and the Caltech team showed that these materials can store ~5.1 wt % (~35 g/L with a measure bulk density at ~0.7 g/L) hydrogen at 40 bar and 77 K. The high density of the materials makes them a good choice for high-volumetric storage capacity.

- **Lawrence Livermore National Laboratory (LLNL):** Ted Baumann led the LLNL team, which concentrated on the design and synthesis of new nanostructured carbon aerogels (CAs) that could meet the DOE 2010 targets for on-board vehicle hydrogen storage. CAs are a unique class of porous materials that possess a number of desirable structural features for the storage of hydrogen, including high SSAs (>3000 m²/g), continuous and tunable porosities, and variable densities. CAs are also promising candidates for porous scaffolds for metal hybrids based on their large pore volumes and the tunable porosity. In addition, the synthesis of CAs allows for the dispersion of secondary materials into the carbon matrix that can serve as catalysts or destabilizing agents for the metal hydride and potentially influence the transport properties of the scaffold.
- **National Institute of Standards and Technology (NIST):** Dan Neumann and Craig Brown led this team. As background, the successful application of neutron-scattering techniques to hydrogen research has a history spanning almost 50 years. NIST performed state-of-the-art, neutron-scattering measurements to probe the amount, location, bonding states, dynamics, and morphological aspects of hydrogen storage materials. They measured the HSCoE-developed materials that showed the most promise of meeting the 2010 DOE goals. NIST performed this role within both the HSCoE and the Metal Hydride Center of Excellence (MHCoe), another DOE center.
- **Oak Ridge National Laboratory (ORNL):** Dave Geohegan and Alexander A. Puretzky led the ORNL team, which worked on synthesis, processing, and tuning of single-walled carbon nanohorn (SWNH) structures for effective hydrogen storage to meet the DOE 2010 targets. SWNHs are single-walled, closed-shell carbon structures that form ball-shaped agglomerates (50–100 nm in diameter) that are excellent supports for metal catalyst nanoparticles. ORNL developed a high-temperature, tunable pulse-width laser vaporization technique to synthesize SWNHs with variable morphology at ~20 g/h rates. *In situ* diagnostics including high-speed videography of the synthesis process, fast pyrometry of the graphite target, and differential mobility analysis monitoring of particle size distributions are applied to understand growth times and provide in situ process control of SWNH morphology. ORNL demonstrated that the morphology of the SWNHs (i.e., the shape and size of the individual units as well as interstitial pore size) can be changed by varying synthesis conditions. Therefore, synthesis and processing of metal-decorated SWNH structures with variable morphologies provides a strong and versatile test bed to nano-engineer materials for optimal hydrogen uptake.

- Pennsylvania State University (Penn State):** Peter C. Eklund (now deceased), Michael Chung, Henry Foley, and Vincent Crespi led this team, which developed the new high-SSA materials that have enhanced hydrogen binding (i.e., isosteric heats of adsorption) through a direct chemical modification of the framework; specifically chemically substituting boron into sp^2 carbon frameworks. New boron-carbon materials were synthesized by high-temperature plasma, pyrolysis of boron-carbon precursor molecules, and post-synthesis modification of carbons. Hydrogen uptake was assessed, and first-principles theory identified novel mechanisms of enhancement and guided the development of improved synthetic strategies and materials properties.
- Rice University (Rice):** James Tour, Carter Kittrell, and Richard E. Smalley (now deceased) led this team with a primary objective of designing and developing nanostructured materials using sp^2 carbon. The original focus was on carbon nanotubes (CNTs), with subsequent emphasis on graphene based on cost considerations. CNTs are now being made in ton quantities for incorporation into battery electrodes, which could bring CNTs back into play in the future. Nanoporous sp^2 carbon scaffolds tend to have 2x higher uptake than Chahine's rule for 77 K, although low SSA remains a challenge. Graphene media without the proppants behave similarly to other carbon materials. Addition of nitrogen atoms' substitution increases the uptake per unit surface area; values as high as 28 at % have been achieved. Boron and phosphorous substitution enhances binding enthalpy to 8.6 kJ/mol, but much higher percentage substitution is needed to exceed 10 kJ/mol. These substituted graphene materials will provide suitable binding sites for charged intercalants, which is now being tested. The effort also investigated the use of intercalants to boost binding energies sufficiently to enable storage at temperatures much closer to ambient.
- Rice:** Another Rice team, led by Boris Yakobson and Robert Hauge, modeled materials structures' interaction with hydrogen, optimized their makeup for storage, and assessed their volumetric and gravimetric capacity. The team designed basic carbon foams with the optimized porosity for enhanced dihydrogen binding and storage capacity. By varying the separation and diameters, foams with different porosity were generated. Grand Canonical Monte Carlo (GCMC) simulations allow them to evaluate the storage in these foams. For more realistic storage capacities, quantum corrections were incorporated. The accessible surface areas have also been calculated using nitrogen (N_2) as the probe gas, which enables a direct comparison with Brunauer-Emmett-Teller (BET) SSA data. Among the similar mass density foams, the (5,5)+(10,0) welded tubes yield the optimum for storage with the gravimetric (6 wt %) and volumetric (60 g/L) capacities at 77 K, exceeding the DOE targets. Rice also advanced the understanding of thermodynamics and kinetics of hydrogen spillover into the chemisorbed state on graphene. Rice demonstrated that it is energetically possible for spillover of H to occur from a metal cluster to the hydrogenated graphene, both from the free-standing and from the receptor-supported catalyst. Their work provided an explanation of the “nano-thermodynamics” of spillover and hints toward improved materials.

- Texas A&M University (TAMU):** Led by Hongcai Zhou (formerly of Miami University-Ohio, the TAMU team designed, synthesized, and characterized high-SSA metal-organic frameworks (MOFs) with active metal centers aligned in porous channels and accessible by H₂ molecules. MOFs are synthetic nanoporous crystalline materials composed of inorganic and organic building blocks. Through optimized, cooperative binding, the MOFs were designed with enhanced affinity to H₂ to help reach the DOE hydrogen storage targets. TAMU enhanced H₂ uptake by (1) preparing catenation isomer pairs to evaluate the contribution from catenation to the hydrogen uptake of a MOF material; (2) synthesizing porous MOFs with high hydrogen adsorption affinities based on different coordinatively unsaturated metal centers (CUMCs); (3) using MOFs that contain nanoscopic cages based on double-bond-coupled di-isophthalate linkers; and (4) obtaining stable MOFs with high SSA by the incorporation of mesocavities with microwindows.
- University of Michigan (Michigan):** Ralph T. Yang led this project designed to develop new nanostructured sorbent materials optimized for hydrogen spillover. Spillover is broadly defined as the transport (i.e., via surface diffusion) of dissociated hydrogen formed on a catalyst and stably storage on a receptor surface. To exploit spillover for storage, among the key questions are whether spillover is reversible at ambient temperature and if the desorption rates at ambient temperature are fast enough for automotive applications. Michigan developed new sorbents by using a transition metal (e.g., Pt, Ru, Pd and Ni) as H₂ dissociation source and difference high-SSA sorbents as the hydrogen receptors. Different metal doping methods have been used successfully to achieve high metal dispersion thereby significant spillover enhancements, as well as a bridging technique used for bridging to MOFs. This report summarizes the progress made in the project.
- University of Missouri-Columbia (Missouri):** Peter Pfeifer led this team, which examined high-SSA carbons developed by the university from corncobs. These porous carbon sorbents show considerable promise for reversible on-board storage of hydrogen with high gravimetric and volumetric storage capacities. Missouri designed, fabricated, characterized, and evaluated the sorbents, adjusting the pore architecture and surface composition for optimum capacity and deep potential wells.
- University of North Carolina at Chapel Hill (UNC):** Yue Wu and Alfred Kleinhammes led a team that developed unique characterization tools based on nuclear magnetic resonance (NMR) to provide simultaneously detailed information on microscopic structures of nanoporous materials, their hydrogen storage capacities, binding energies, and H₂ kinetics. UNC worked with all the synthetic groups in the HSCoE to conduct unique NMR experiments with the different partner material *in situ* under controlled H₂ pressure. Such NMR studies provided critical information for identifying promising approaches used by HSCoE partners for enhancing binding energies and storage capacities. In addition to ¹H NMR investigation of H₂ adsorption, NMR was also employed to measure the atomic content of substituted elements (i.e., boron in boron-substituted graphitic materials) as well as the local

environment and the local symmetry of these substituted nuclei. Such studies were carried out on nearly all samples developed by HSCoE.

- **University of Pennsylvania (Penn; Former Partner):** Led by Alan G. MacDiarmid (now deceased) and Pen-Cheng Wang, the Penn team focused primarily on the synthesis, processing, characterization, and selection of polyaniline (PANI)-based materials. This was based on a publication by Cho and colleagues (2002) that reported more than 8 wt % (reversible) hydrogen gas storage at RT in doped (metallic) forms of organic conducting polymers (“synthetic metals”), PANI and polypyrrole (PPy). The conclusions of the research group at Penn in collaboration with measurements at NREL agree with those of Panella and coinvestigators (2005) in that under the incompletely described experimental conditions given by Cho and coworkers (2002), no significant adsorption of H₂ was observed. Ultimately, the effort was not able to demonstrate any significant hydrogen storage enhancement by conducting polymer materials and the project was stopped at the end of Phase 1.
- **Michigan/University of California, Los Angeles (UCLA; Former Partner):** Omar Yaghi led a team that investigated the hydrogen affinity of MOFs and optimized hydrogen storage performance by testing and evaluating various structures, synthetic methods, and activation procedures. Synthesized MOFs were evaluated by different partners that performed different characterizations, such as NMR spectroscopy, to provide additional insights into the mechanism of hydrogen storage. This project left the HSCoE at the end of Phase 1 to pursue development independently.

1.3 References

Cho, S.J.; Song, K.S.; Kim, J.W.; Kim T.H.; Choo, K. (2002). “Hydrogen Sorption in HCl-Treated Polyaniline and Polypyrrole: New Potential Hydrogen Storage Media.” *Fuel Chemistry Division, 224th National Meeting of the American Chemical Society: August 18–22, 2002, Boston, Massachusetts*, Vol. 47; pp. 790–791.

DOE (2009). *Fuel Cells Technology Program Multi-Year Research, Development and Demonstration Plan: Planned Program Activities for FY 2005–2015*.
www.eere.energy.gov/hydrogenandfuelcells/mypp/index.html.

Panella, B.; Kossykh, L.; Dettlaff-Weglikwska, U.; Hirscher, M.; Zerbi, G.; Roth, S. (2005). Volumetric Measurements of Hydrogen Storage in HCl-Treated Polyaniline and Polypyrrole.” *Synthetic Metals*, Vol. 151, pp. 208–210.

2.0 Development

2.1 Approach/Overview

A guiding principle in developing the required materials is that a continuum of energies exists for hydrogen bound to substrates and molecules. On the weak side of the continuum is nondissociative (hydrogen remains a molecule, H₂) physisorption, which is due purely to van der Waals (vdW) forces (~4 kJ/mol). On the opposite end is the full C-H chemical bond in methane with an energy of ~400 kJ/mol. As shown in Figure 2-1, between these two limits, with nominal binding energies between 5 and 40 kJ/mol, are:

- Physisorption—related to key parameters affecting vdW forces
- Enhanced dihydrogen binding—via the formation of complexes that exhibit electron transfer interactions from the hydrogen as in substituted/heterogenous materials
- Multiple dihydrogen binding—forward- and back-electron donation, between the sorbent and hydrogen that induces a significant molecular bond stretching between the hydrogen atoms.
- Weak chemisorption—weak, reversible, chemical bonding of mono-atomic hydrogen to lightweight receptor materials (via a “spillover” mechanism).

The U.S. Department of Energy (DOE) targets can be met with sorbents if (1) the energy for hydrogen adsorption (i.e., the enthalpy) can be designed to be in a nominal optimal range (~10–40 kJ/mol: depending on the entropy, which is effectively the state of the sorbed hydrogen compared to the relatively disordered state of the hydrogen gas), desired operating pressure, and temperature (see, for example, Bhatia and Myers 2006, Figure 2-2); and/or (2) efficient volumetric arrangement (see Figure 2-3) of a sufficient number of suitable binding sites can be achieved with a low-weight material. These goals are difficult to reach in conventional adsorbents with high specific surface areas (SSAs), which are limited by low physisorption binding energies, heterogeneity of the adsorbent surfaces and adsorption sites, and excessive macroporosity and poor volumetric packing.

By focusing on specific mechanisms, the Hydrogen Sorption Center of Excellence (HSCoE) leveraged appropriate materials and synthetic capabilities and expertise of the different partners to create optimized pore size and high-SSA materials; heterogeneous materials with enhanced dihydrogen binding; materials with coordinated metal centers; and spillover or chemisorbed hydrogen materials.

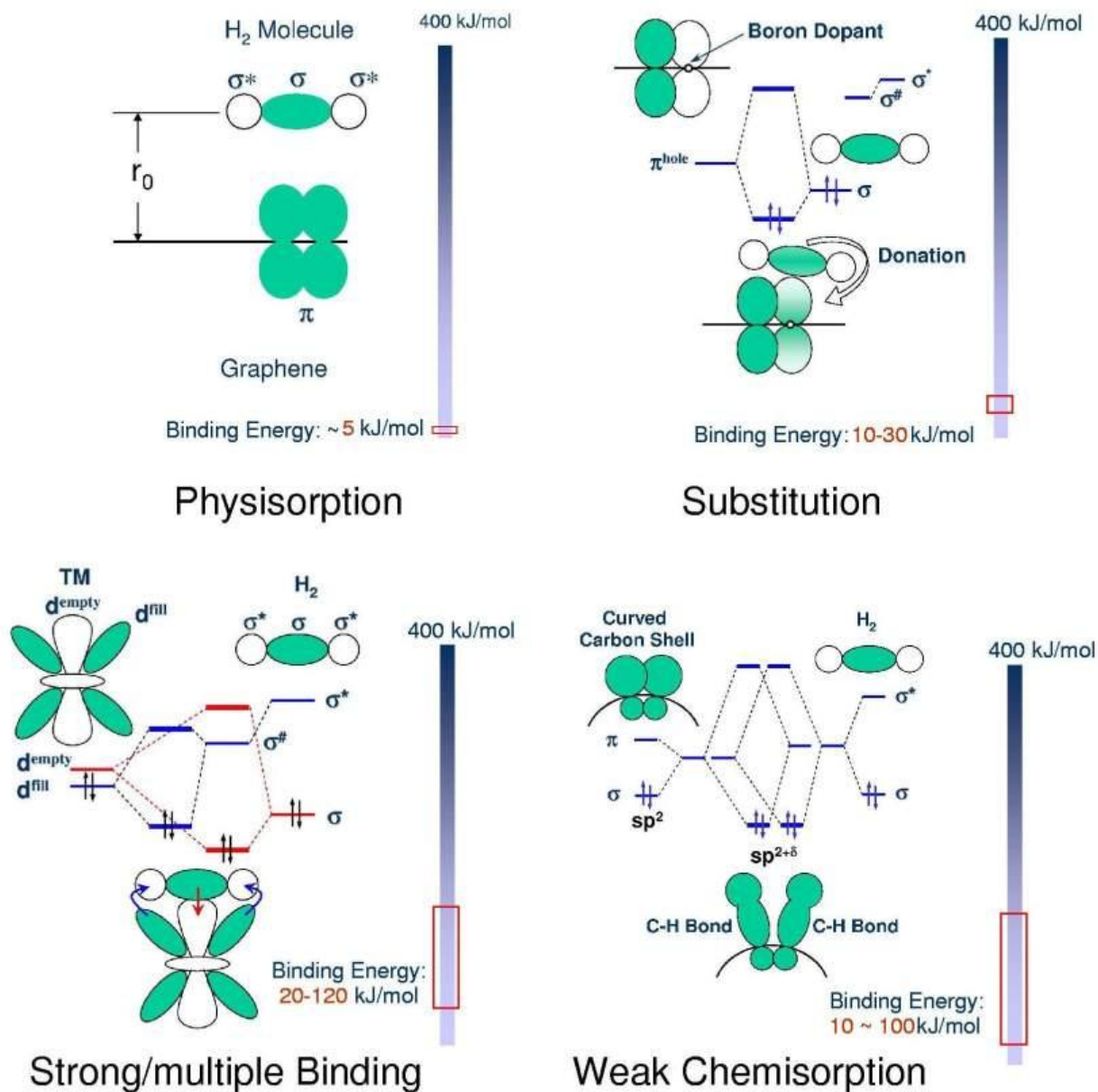
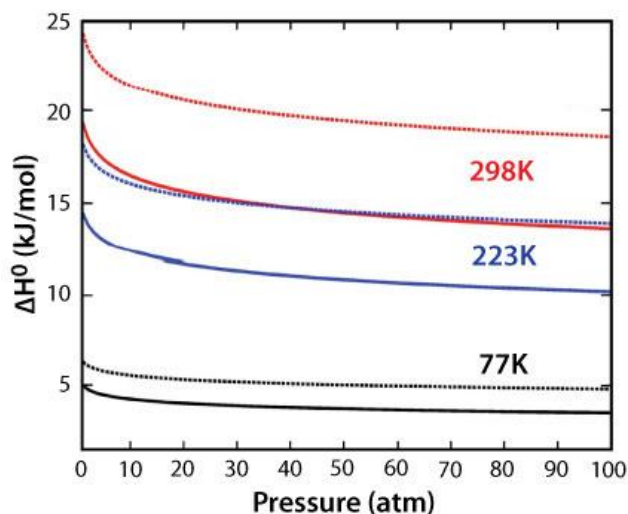


Figure 2-1. Illustrations of the four types of sorbent binding mechanisms investigated by the HSCoE



Source: Adapted from Bhatia and Myers 2006.

Figure 2-2. The optimal enthalpy (ΔH) for hydrogen storage depends on the pressure, temperature (black is 77 K, blue is 223 K, and red is 298 K), and sorption interaction (i.e., entropy: e.g., dotted lines $\Delta S = -10R$, and solid lines $\Delta S = -8R$). For example, as shown in this plot if materials with enthalpies between ~ 13 and 25 kJ/mol can be made, then ambient temperature hydrogen storage is possible with pressures between ambient and 100 bar. For lower binding energies, lower storage temperatures will be required.

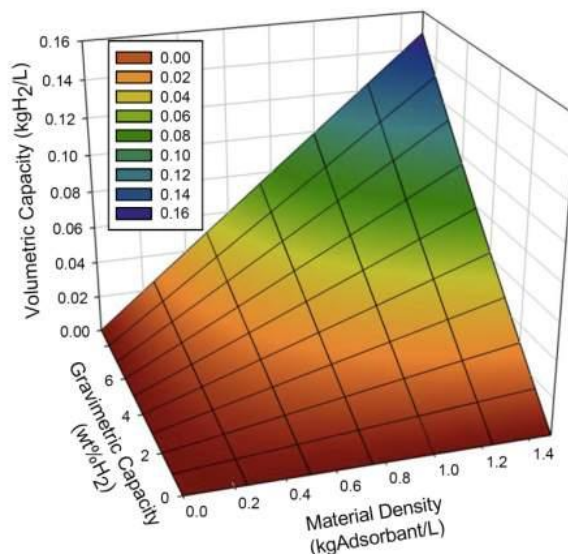


Figure 2-3. Graph from Argonne National Laboratory showing the dependence of volumetric density on gravimetric and bulk density for sorption materials. The plot indicates that to have the potential to meet DOE 2015 volumetric target (0.04 kg H₂/L, yellow band on chart), bulk material densities between 0.7 and 1 g/L will be required for sorbent materials with 6 to 7 wt % gravimetric capacities.

From the outset, in order for the HSCoE to select among a relatively large number of potential sorbent materials, researchers placed more emphasis on identifying and developing mechanisms that led to higher volumetric capacity and more favorable operating conditions rather than on specific, individual materials. This enabled efficient and rapid progress by focusing resources on identifying and optimizing specific

properties and critically evaluating hydrogen storage material classes. This is why the HSCoE was organized into four focused efforts (see Table 2-1), each of which was designed to efficiently address a specific set of issues associated with a specific hydrogen sorption mechanism (Figure 2-1).

Table 2-1. Overview of the HSCoE Partners' Roles and Responsibilities

HSCoE Partners' Development Areas														
HSCoE Partners	ANL	APCI	Caltech	Duke	LLNL	NIST	NREL	ORNL	Penn State	Rice	TAMU	Michigan	Missouri	UNC
Research Focus Groups														
1. Optimized Nanostructures (Ahn, Simpson)	S		P	P	P	P	P	P		P	P		P	P
2. Substituted Materials (Cooper, Blackburn)	P	P		S	S	P	P		P				S	P
3. Strong/Multiple Dihydrogen Interactions (Brown, Engtrakul)						P	P		S	S	P			P
4. Weak Chemisorption/Spillover (Yang, Gennett)		S		S	S	P	P	S		S		P		P
P = primary and S = secondary focus														
Goals of Development Areas														
1. Create and stabilize optimized high-SSA structures														
2. Enhance storage directly and create anchor points for other species														
3. Implement improved binding on solid supports, array active metals (e.g., MOFs)														
4. Understand and improve capacities, kinetics, reproducibility														

Notes: ANL = Argonne National Laboratory; APCI = Air Products and Chemicals Inc.; Caltech = California Institute of Technology; Duke = Duke University; LLNL = Lawrence Livermore National Laboratory; NIST = National Institute of Standards and Technology; NREL = National Renewable Energy Laboratory; ORNL = Oak Ridge National Laboratory; Penn State = Pennsylvania State University; Rice = Rice University; TAMU = Texas A&M University; Michigan = University of Michigan; Missouri = University of Missouri-Columbia; UNC = University of North Carolina at Chapel Hill; SSA = specific surface area

These focused research efforts were complementary, with lessons learned and materials developed in one effort often proving applicable to another. For example, for physisorption the main issues are optimized pore sizes and very high SSAs. Similar issues arise for other sorbent material classes, and thus lessons learned for physisorption materials were directly applied to other HSCoE development activities. The key advantage of the mechanism-focused approach was that selection criteria could be identified for each material class based on a limited amount of experimental and calculation work. This enabled identification of the most promising materials and thus eliminated the vast majority without the potential to meet DOE targets. This approach substantially reduced the HSCoE's overall work while prioritizing development efforts.

The main goals of the HSCoE were to discover the performance limits of various sorbents that could be used to meet the DOE system targets for reversible hydrogen storage (i.e., for motive applications). This involved the design and synthesis of materials that bind large amounts of hydrogen on both a per-weight and a per-volume basis as either: (1) weakly and reversibly bound atoms and/or (2) strongly bound molecules. The HSCoE focused on determining binding mechanisms and energies, and the manner in which suitable sites may be organized in space to achieve a high-volumetric density using low-weight frameworks. This involved determining the effects of geometry, introduction of defects, adventitious dopants, and catalytic species as well as elemental substitution. The HSCoE investigated a range of different lightweight, nanostructured materials and porous frameworks. The HSCoE strove to be nimble, flexible, and responsive to incorporating promising new ideas, materials, and concepts as they arose.

By working closely together and drawing on the unique capabilities of the various partners, HSCoE members were highly successful in accelerating the development of hydrogen storage materials. This close interaction resulted in more than 40 joint projects per year, in which the rapid materials development was illustrated by upward of 30 joint publications per year. In addition, the HSCoE worked with more than 40 groups from around the world and directly with the Chemical Hydride and Metal Hydride Centers of Excellence to ensure that its development efforts leveraged other research activities for efficient utilization of resources. Finally, the HSCoE also ensured that its development efforts were transparent and were provided to the scientific community in a timely manner to again help speed the storage materials' development progress. This was done through the active organization by HSCoE partners of hydrogen storage materials conferences around the world, and through hundreds of presentations at conferences and hundreds of publications in peer-reviewed journals (see Appendix A).

In general, the HSCoE focused exclusively on developing materials for on-vehicle refueling and hydrogen storage, and made substantial progress, sufficient to where sorbents may be used to meet DOE 2010 hydrogen storage system targets. In addition, progress was sufficient to identify sorbents that may be developed to meet DOE 2015 and possibly even DOE ultimate hydrogen storage targets. The HSCoE approach enabled direct development of a detailed understanding of different sorption mechanisms that led to identification of new materials and synthetic routes with well-vetted predictions grounded in experimental observations. The tremendous results obtained by close interaction between theory and experiment were also aided by a strong focus on reproducible rapid-throughput hydrogen storage property measurements and unique materials characterization techniques. The overall center approach involved organizing and bringing together different partners/capabilities to focus on specific aspects of the development cycle, including:

1. Focused experimental development efforts
2. Crosscutting theory
3. Unique hydrogen sorbent characterization techniques.

2.2 Optimized Nanostructures

In most hydrogen sorption materials with the potential to meet DOE targets, almost every atom must be accessible and lightweight. Therefore, materials with high SSAs are required. In addition, to meet volumetric targets, the sorption sites need to be arranged to minimize the amount of open space (Figure 2-3) so that the bulk density can be as high as possible. This suggests that porous structures should be optimized to allow hydrogen egress in and out, but the hydrogen should be in contact with some kind of sorption site. Logically, the materials should have no macroporosity (pores greater than ~50 nm in diameter) and minimal mesoporosity (pores between 2 and 50 nm in diameter), and, depending on the specific sorption mechanism, the materials should have pore sizes between 0.7 and ~1.5 nm.

In general, to allow sorption on all surfaces of a pore, the distance between the surfaces should be at least twice that of the kinetic diameter of dihydrogen (2.89 Å). In addition, multilayer adsorption effects, H-H repulsion, and other space-optimization considerations suggest that the pore sizes may need to be ~1.2 nm. Also, calculations suggest that some enhanced binding may occur if the pore structure is on the order of 0.7 to 1.2 nm.

The Optimized Nanostructures effort focused on designing and synthesizing lightweight, high-surface-area, optimal-pore-size materials, with the findings being applicable to almost all sorption materials. The effort focused on stabilizing large quantities of hydrogen directly by physisorption. Researchers investigated methods to optimize sorption properties and increase dipole-dipole interaction (i.e., vdW forces) binding energies via appropriate geometrical pore structures by arraying high-SSA structures (e.g., scaffolds). This was done by forming high-surface areas directly during synthesis or by creating porosity in dense structures. The thrust of these efforts involved optimizing sorption sites and optimizing space to enhance binding without loss of volumetric capacity.

Specific activities for the optimized nanospace effort involved performing theoretical modeling and experiments to determine potential mechanisms for higher storage capacities and to provide guidance for materials development. In addition, these efforts developed and/or improved scalable and reproducible synthesis methods of nanoporous materials. Several different synthetic pathways were investigated, including templated carbon/boron, polymers, metal-organic frameworks (MOFs), aerogels, single-walled nanohorns (SWNHs), and scaffolded single-walled nanotubes (SWNTs). Synthesized materials were characterized to determine their hydrogen storage properties and, when appropriate, to identify unique sorption mechanisms. In some cases, this involved optimizing materials for other storage processes beyond physisorption.

2.3 Substituted Materials

The HSCoE formed the substitution development effort to focus on increasing the intrinsic binding energy of storage materials and thus their storage capacity at higher temperatures. In general, increasing the intrinsic heats of dihydrogen adsorption is difficult, and the HSCoE identified only a few potential pathways. For most pure

materials, or materials with electronic configurations that induce no significant adsorption, the primary adsorption mechanism is physisorption, which typically has enthalpies at ~5 kJ/mol or less for interaction with a single surface. Enhanced physisorption binding energies (i.e., 5 to 10 kJ/mol) are often observed with high-SSA materials. This is primarily a result of interaction with multiple adsorption sites that then limits the total gravimetric capacities. In general, physisorbed dihydrogen on single surfaces has relatively low binding energies, and capacity requires operation at lower cryogenic temperatures and higher intermediate pressures. Typically, increased binding energies, lower temperature, and higher pressure are required to overcome the intrinsic repelling force between dihydrogens to yield higher storage capacities on the sorbent surface at a specific temperature and/or pressure.

Going beyond pure physisorption requires enhanced electron interactions between the sorption material and dihydrogen. In general, heterogeneous elemental structures or surface functionalization can induce enhanced electron interactions. However, after relatively comprehensive investigations, very few material systems were identified with the potential to enhance dihydrogen binding. In general, the exchange of a different atom species in an elementally homogeneous lattice induces an electronic perturbation that may enhance dihydrogen binding. For example, the empty p orbitals on boron (B)-substituted [for] carbon (C) induces electron donation from H₂ to provide a reasonable enhancement in binding (i.e., 10 to 15 kJ/mol) and capacities. However, it was determined that only boron substituted with a sp² or similar coordination produced the enhanced dihydrogen binding. Other B-C or C-C coordination, the presence of other elements such as nitrogen (N) in the lattice, or other (except for beryllium [Be]) substituted lightweight elements (e.g., Li, N, O, F, Na) in carbon lattices do not significantly enhance dihydrogen binding. Furthermore, in addition to needing to be in the correct coordination state, calculations predict that enhanced binding may occur only if the B remains both electronically and structurally “frustrated” such that the B atoms are out of the plane of the carbon matrix, thus potentially expanding the lattice.

In addition to direct substitution, initial efforts identified that materials with intercalated and/or absorbed ions may enhance dihydrogen binding. For example, anions with high charge/volume ratio (e.g., fluoride) can donate electron density to s*-orbitals of dihydrogen. Similarly, other intercalated species (e.g., alkali and alkaline metals, anions) may induce charge interactions to improve hydrogen adsorption enthalpies. In some cases, it is theorized (Yoon et al. 2007) that nanostructures can be created to generate sufficient electric fields to enhance H₂ storage. Finally, some of these substituted or functionalized materials may improve sorption of other elements/molecules for different hydrogen mechanisms associated with back-donation and/or spillover.

Based on initial predictions and experimental results, the HSCoE partners developed scalable synthesis methods to form substituted and intercalated materials that demonstrate enhanced dihydrogen storage properties. Boron substitution was achieved by either starting with chemical compounds with high concentrations of B and forming high-SSA materials, forming boron-substituted activated and graphitic carbons (e.g., BC₃), or substituting boron for carbon atoms in preformed materials. In addition, the HSCoE

partners developed anion-intercalated graphitic and other intercalated/functionalized materials with enhanced hydrogen storage properties.

2.4 Strong/Multiple Dihydrogen Interactions

The final set of methods to improve dihydrogen binding is characterized by forward- and back-electron donation from the sorption material that induces a significant molecular bond stretching between the hydrogen atoms (Kubas 2001). Typically, this is achieved when the sorption sites are electronically and coordinately unsaturated. In these cases, electrons are donated from the hydrogen to electronic states in the sorbent, and some electron transfer occurs where other sorbent electronic states donate to the hydrogen molecule. These types of sorption sites can bind a dihydrogen molecule more strongly (10 to 200 kJ/mol), but more importantly, can also bind multiple dihydrogen molecules to a single sorption site. This method enables a substantial increase in volumetric densities if these sites can be densely arrayed. As stated previously, the HSCoE focused on materials with an optimal range between ~10 and 40 kJ/mol to enable reversible near-ambient temperature and pressure hydrogen storage.

In general, the specific partially coordinated atom sites needed for strong and multiple dihydrogen binding can be attained in a number of ways. These include stabilizing single metal atoms on high-surface materials (e.g., Li/THF co-intercalation compounds or Ca on graphene lattices) or in crystalline structures such as MOFs or metallocarbohedrenes (Met-Cars). Thus, the HSCoE focused on methods to develop hydrogen interactions with coordinated but unsaturated metal centers and to design and synthesize these types of sorbents. This involved using calculations to identify and guide tractable reactions that balance reactivity with stability and capacity.

The HSCoE investigated integrating appropriate metal centers with binding energies to 40 kJ/mol, with materials such as aerogels, carbon nanohorns, carbon nanotube scaffolds, polycyclic aromatic hydrocarbons, graphene, and MOFs. These efforts included utilizing the higher Coulomb repulsion between alkaline metals to facilitate metal/substrate binding and/or enhancing charge transfer to stabilize the metal/substrate interaction with substitutional integration of different atoms in the support materials. One key issue with the use of open metal centers is the fact that their higher reactivity makes them susceptible to an array of issues. Such issues include agglomeration of the metals and reaction with contaminants, both of which reduce or eliminate the hydrogen storage enhancement, which makes durability and synthetic processing more challenging.

2.5 Weak Chemisorption/Spillover

The HSCoE also actively investigated methods to efficiently store dissociated hydrogen. In general, dissociated or atomic hydrogen forms strong bonds with other materials (e.g., metal hydrides or chemical hydrides) that require high temperatures (e.g., more than 500 K) or catalysts to break the bonds. However, it is possible for hydrogen atoms to be adsorbed to surfaces in such a way that the bonding is weaker and conducive to nominal reversible storage capacities at near-ambient temperature and under moderate pressure. From a practical standpoint, a catalyst is typically needed to dissociate the dihydrogen gas; this is a known technology in the chemical process industry. Because most common industrial catalysts (e.g., Pt, Pd, Ni) are relatively heavy and expensive (e.g., platinum group metals), reaching the DOE targets will require catalysts that are appropriately integrated with a lightweight and compact material such as carbon or boron so that the dissociated hydrogen can “spillover” and be stably and reversibly stored, primarily on the lightweight inexpensive receptor material.

Maximizing performance and costs via spillover involves focused development efforts to optimize catalyst performance and dispersion and to integrate with receptor material properties and hydrogen surface transport/diffusion mechanisms. This involves performing systematic experiments to quantify spillover processes, determining the causes for material degradation and irreproducibility, and developing scalable and reproducible synthesis methods of spillover materials. For example, because of the mechanisms associated with hydrogen diffusion on the receptor material surfaces, low refueling rates and small materials surface properties are major challenges that must be resolved. To address these issues, the HSCoE leveraged modeling to identify and construct new spillover materials with improved properties and to chemically modify known spillover materials to improve spillover performance.

2.6 Crosscutting Theory

As discussed above, the HSCoE integrated experimental development with predictive theory closely to build a detailed understanding of the sorption mechanisms involved. This understanding was used to rationally design new sorbents and viable synthetic pathways. To ensure optimal integration and utilization of the limited resources, the complementary theoretical efforts within the HSCoE were actively coordinated (see Figure 2-4).

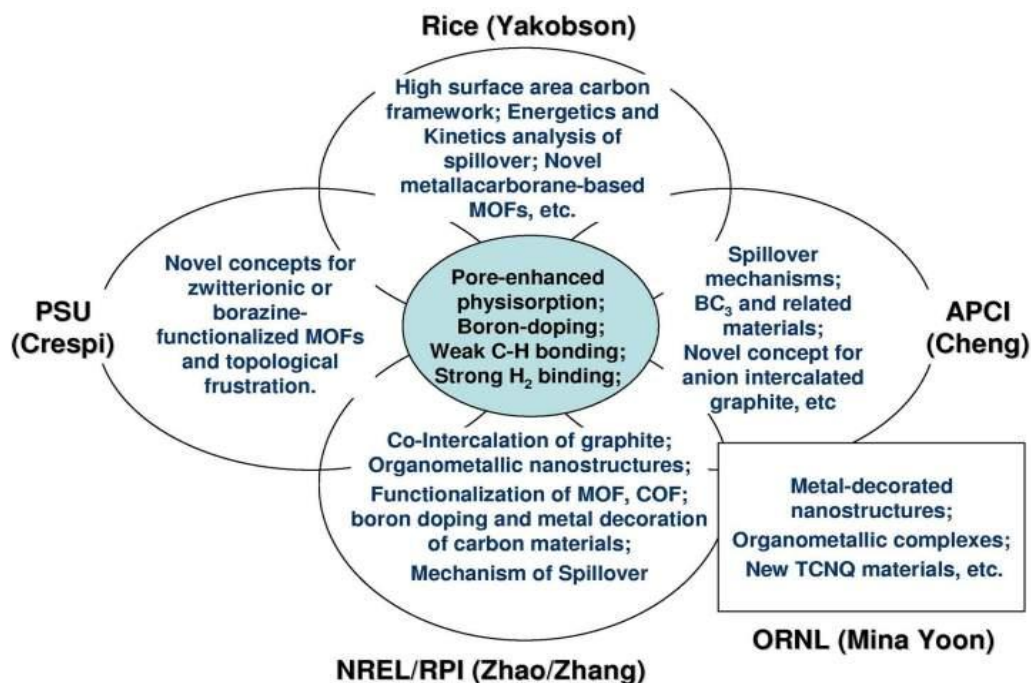


Figure 2-4. Overview of the HSCoE partners' roles and specialties associated with rational design of sorbents

The theory team consisted of 10–20 researchers throughout the different HSCoE partners and was led by key investigators. The theoretical work used a variety of methods and modes of simulation to provide highly accurate simulations of experimental results, and, once validated, predictions of designed sorbent performance. Specific methods included:

- Different levels and methods of density functional theory (DFT). Most of the theoretical work performed by HSCoE partners employed the state-of-art first-principles atomistic simulation based on the density functional theory as implemented in the Vienna Ab initio Simulation Package (VASP) or Gaussian distribution. However, other packages and methods within the DFT family were used as appropriate.
- Energetics and structural optimization-based calculations. Total energy and structural optimization are the most frequently used modes of simulation for determining stable/metastable structures of materials, characterization of reactivity, and interaction with hydrogen.
- Kinetics calculations/simulations were particularly useful for simulation of H spillover effects. A climbing nudged elastic band method was typically used to calculate the H diffusion barriers in carbon substrates.
- Molecular dynamics (MD) simulation at finite temperature is the most effective simulation mode to test the stability of a material and to identify atomistic processes

- Electronic structure analysis is a powerful method to disclose the mechanism of hydrogen interaction with storage materials and provides deep insights into electron-counting rules (e.g., 18-electron rule), tunability of hydrogen binding energy, and acceleration of kinetics of H spillover.
- Bridging atomistic and parameterized continuum modeling was developed to simulate systems with larger numbers of atoms or molecules.

2.7 Specialty Characterization

The HSCoE developed or improved measurement techniques to help characterize sorbent properties and accelerate materials development. This included efforts to understand the sources of errors associated with reported hydrogen storage capacity measurements, development of in-situ nuclear magnetic resonance (NMR) spectroscopy measurements at high pressure and low temperature, and adaptation of the suite of neutron scattering techniques to optimally characterize hydrogen sorption on high-SSA materials. The improved understanding of errors enabled sorption capacity systems to be constructed that provided accurate results from very small “laboratory scale” (e.g., a few milligrams) samples to accelerate materials development by providing useful characterization without the need to scale up the processing and make larger samples. The NMR system built by The University of North Carolina, Chapel Hill (UNC) provided information about the porous structures, hydrogen storage capacities, binding energies, and H₂ kinetics for sorbents. The neutron scattering analysis performed by the National Institute of Standards and Technology (NIST) provided critical structural, hydrogen interaction, composition, and other important material property information to the HSCoE in its quest to understand current systems and develop new materials for hydrogen storage. These and other measurement techniques enabled sorbents to be quickly characterized to select materials based on a true understanding of their hydrogen storage properties.

2.8 Overview of Analyses Performed

Although the HSCoE focused on a subset of all the possible hydrogen storage media, this still encompasses a large class of materials and a wide range of types (engineered nanospaces, substituted materials, metal-centered-based materials, and weak chemisorption/spillover materials). The approach and focus of each of these subgroups also varied widely as the hydrogen storage mechanisms and their optimization differed among the groups. Therefore, understanding and investigating these materials encompasses almost the entire range of present-day analytical techniques. Each of these techniques has advantages and disadvantages and only with a coordinated analytical approach does any sensible and coherent understanding arise that provides insight toward the mission’s goals. Within each subclass of materials, specific analytical techniques reveal themselves over time as being particularly useful as either routine and facile techniques to provide baseline information or to probe for deeper insights into the scientific mechanisms that are needed to fully understand and develop these materials.

Another critical factor to consider in such a large and coordinated effort with its large quantity and variety of samples to be measured is the efficiency and quality of

characterization. Unfettered access to the needed instrumentation is paramount as well as optimized screening procedures, reliable and reproducible measurement protocols, and verification procedures to ensure accurate measurements. Access to instrumentation is an important pragmatic consideration in defining routine measurement protocols needed for the high throughput of samples. Establishing the necessary facilities to handle the measurements took considerable effort and resources as did developing the measurement protocols. These resources and the centerwide expertise provided the foundation for the measurement effort. Below is a brief listing of some of the more useful techniques and the information that they provide.

2.9 Specific Analytical Tools Used by the HSCoE Partners

2.9.1 Adsorption Isotherm

In general, adsorption/desorption measurement of gasses as a function of temperature and pressure are used to characterize sorbents in a number of ways. For example, analysis of isotherms measured close to the liquid/gas transition temperature of the probe molecule (e.g., ~77 K for nitrogen and ~195 K for CO₂) can be used to analyze the pore size distribution and the SSA of the sorbent. These same measurements can be performed with hydrogen at ~19 K, and the excess gravimetric capacity of hydrogen can be measured at different temperatures to provide an information that can be used to estimate a hydrogen storage system capacity using a given sorbent.

2.9.1.1 Surface Area Analysis/Pore Size Analysis

Surface-area and pore-size analysis are a very important analysis tools for this class of sorption materials, and most samples are analyzed for surface area. The methodology is very similar to the volumetric technique discussed below, except that the gas used for the measurement is usually nitrogen. The adsorption isotherm is analyzed according to particular adsorption models that have the SSA as a parameter thereby yielding an estimate for the surface area. The most widely used models are the Brunauer-Emmett-Teller (BET) and Langmuir models. The Langmuir model was developed first and describes adsorption as gas atoms or molecules sticking to a surface in a single layer. In contrast, the BET model allows for multiple layers to form. Regardless of the model, the number of first-layer sites is a parameter and the adsorption data can be fit to the model yielding the number of sites. The surface area of the material can then be calculated by knowing the number of sites and the size of the gas atoms or molecules. The BET model is most frequently used to determine the surface area.

2.9.1.2 Excess Hydrogen Adsorption

Adsorption isotherms with hydrogen can be used to determine the “excess” hydrogen adsorbed on to the material of interest at a fixed temperature and as a function of pressure. The term “excess” refers to the hydrogen on or near the sample surface that has a local density above that of the surrounding free gas. Specifically, it is also known as the “Gibbsian surface excess” or “Gibbsian excess,” and it directly measures the ability of the material of interest to adsorb hydrogen. This is contrasted with the “engineering excess” and the “total capacity.” The latter measures the total amount of hydrogen stored in the container and includes both the Gibbsian excess and the amount in the free gas above the sample. The former takes the total capacity and subtracts the corresponding

total capacity of an empty identical container; it addresses the question of, “Is it better to use an empty container to store the gas or an identical container containing the material of interest?” As the center was mainly interested in the ability of the material of interest to adsorb hydrogen, measurements within the HSCoE focused on the Gibbsian excess.

There are two common methods to measure adsorption isotherms: volumetric and gravimetric. Volumetric determines adsorption by application of the gas law to calculate mass balance of the gas. It uses calibrated volumes at known temperatures and measured pressures to determine the amount of gas above the sample before and after applied gas pressure changes and assumes that any missing gas was adsorbed onto the sample or extra gas was desorbed from the sample. It is very important the temperature profile of the apparatus is constant over time and that the volumes are calibrated very accurately. Gravimetric methods measure the combined mass of the sample and any hydrogen adsorbed. This mass is compared with the mass with no hydrogen. The volume of the sample, sample container, and relevant volumes of the balance support must be accurately known to compensate for buoyancy effects. One weakness of the gravimetric method when measuring hydrogen adsorption is that it is sensitive to impurities in the gas, because hydrogen is the lightest gas and all impurities are heavier. Any adsorption of the impurities by the sample will affect the results more than that of a volumetric system. The HSCoE primarily used the volumetric method to measure adsorption isotherms, but corresponding gravimetric measurements were made with some sorbents.

Within the HSCoE, several partners performed volumetric measurements including the National Renewable Energy Laboratory (NREL), NIST, Pennsylvania State University (Penn State), Air Products and Chemicals Inc. (APCI), the California Institute of Technology (Caltech), Argonne National Laboratory (ANL), the University of Missouri-Columbia (Missouri), and Texas A&M University (TAMU). NREL has three volumetric systems, one low pressure (~2 bar maximum) and two high pressure (~200 bar maximum). The low-pressure system is used as a screening tool to roughly gauge the quality of samples. It is also useful for samples where only small quantities are available, as it needs only a few milligrams to perform a measurement. The high-pressure systems typically require ~100 mg for an optimum measurement. Both low- and high-pressure systems can measure samples at room temperature (RT) and at liquid nitrogen temperature. Regardless of the sample temperature, it is crucial that the apparatus's temperature profile remain constant over the course of the measurement including both the calibration and adsorption measurement cycles. NREL has gone to great effort to ensure that this condition is satisfied. This is especially important for samples displaying the spillover phenomenon, as the measurement cycle is very long based on the relatively slow kinetics. NREL and NIST can perform isotherm measurements from ~10 K to ambient temperature, and APCI developed a differential pressure volumetric system.

2.9.2 Temperature-Programmed Desorption

Temperature-programmed desorption (TPD) effectively heats a sample at a prescribed rate and monitors the effluent released. Because a mass spectrometer is often used to measure the atomic and molecular species released, the sample is typically held at vacuum pressures of $\sim 10^{-6}$ torr prior to heating. Often the sample is cryogenically cooled with liquid nitrogen or a cryo-cooler to 77 K or lower to capture the adsorbed species on

the sample while the sample vessel is being evacuated. Even with this cooling, TPD typically underestimates capacities because no overpressure is present. For example, with high-SSA sorbents, hydrogen that is adsorbed at ambient temperature would be completely removed during evacuation, unless the sample is cooled. Once cooled, most other adsorbed gasses that become solids or liquids at, for example, 77 K are then held on the sample during evacuation, and an accurate accounting of these gasses can be measured when the sample is heated back up to ambient or higher temperatures. However, unless the sample is cooled to ~5 K, hydrogen will partially be evacuated and thus an accurate accounting of the amount stored cannot be obtained. TPD provides a quick method to monitor the different components in the effluent, including potential break-down materials from the sorbent and chemically reacted species that may have formed and are released from the sample at higher temperatures. In general, TPD can be used to quickly determine if enhanced bonding is present and/or quantitatively measure the binding energies of the gases to the sorbents. TPD can be used to accurately determine the composition of the effluent and the binding energies of even sub-milligram samples. TPD is also routinely used to monitor the reaction and degassing processes associated with sorbent syntheses.

2.9.3 Microscopies and Morphologies

2.9.3.1 X-Ray Diffraction

X-ray diffraction (XRD) occurs when X-rays are scattered elastically off the electrons surrounding the atoms in the sample and produce an interference pattern (diffraction). Detecting this diffraction pattern provides information about the samples, specifically concerning the arrangements of the atoms in the sample. The measurement may identify the crystal structure and measure lattice constants, particle sizes, etc. of the sample. In the context here, XRD is most often used to ascertain whether, in synthesizing materials, the desired crystal structure has been obtained. It can also be used to monitor the crystal structure over time with additional sample processing to check for changes in the sample or the stability of the crystal structure. As many of the materials studied under this program are considered to have amorphous atomic structure, this particular technique had limited utility.

2.9.3.2 Electron Microscopies

Both scanning electron microscopy (SEM) and transmission electron microscopy (TEM) provide critical information on the samples. SEM scans an electron beam across the sample and detects scattered electrons from the surface, thereby giving information on surface morphology and pore structure. TEM also scans an electron beam across very thin samples and detects the transmitted electron beam. This provides information on microcrystallinity, particle size, and particle distribution. Both microscopies can have energy dispersive spectroscopy analysis to provide compositional information, including modes to help enhance morphologies based on the elemental compositions.

2.9.3.3 Small-Angle Neutron Scattering

Small-angle neutron scattering (SANS) measurements on HSCoE materials such as nanoporous carbons have been used to gain insights into the morphology of the pore structure and how hydrogen is adsorbed (mobility or motion of H₂) into these types of

materials, respectively. SANS probes structure in materials on the nanometer-to-micrometer scale and therefore is ideal to probe pore structure and morphology. In SANS, the neutron wavelength, λ , and scattering angle, θ , determine the length scale probed through the relationship, $d \approx \lambda / \theta$.

2.9.4 Hydrogen Interactions

2.9.4.1 Neutron Scattering Spectroscopy

Powder neutron diffraction measurement for the HSCoE were performed at the National Institute of Standards and Technology Center for Neutron Research to structurally characterize sorbent materials using the BT1 powder diffractometer (Stalick et al. 1995), and then to probe the rotational potential felt by adsorbed hydrogen as a function of temperature with the BT4 filter-analyzer inelastic spectrometer (Copley, Neumann, and Kamitakahara 1995).

Hydrogen behaves as a three-dimensional quantum rotor in the solid with energy levels given by $E_J = BJ(J + 1)$, where J is the rotational quantum number and $B = 7.35$ meV is the rotational constant. Here $J = 0 \rightarrow 1$, or para \rightarrow ortho transition, is used as a probe of hydrogen binding sites. This transition occurs at an energy close to $2B = 14.7$ meV in the pure molecular solid because the molecules are essentially free quantum rotors with no center-of-mass translation. In the gas phase, the continuous spectrum of recoil energies broadens the rotational transition, so the technique is able to discern adsorbed molecules which do not diffuse. Relatively weak interactions between the rotating molecule and its environment will alter this simple energy level scheme; given sufficient spectroscopic resolution, accurate information can be deduced about the adsorbate site symmetry and the nature of the hydrogen-substrate interaction (FitzGerald et al. 1999; Eckert et al. 1996; Smith et al. 1996). A further advantage of neutron scattering in this context is the low absorption in most materials, which facilitates *in situ* measurements involving cryostats and pressure vessels (Brown et al. 2000).

Inelastic neutron scattering (INS) spectroscopy of H_2 quantum transitions provides detailed knowledge of the H_2 adsorption sites. The information provided includes determination of the highest enthalpy sites at lowest loadings; lower energy sites are filled with subsequent loading. Difference data from INS can be used to infer the amount of hydrogen spillover. Furthermore, INS can be used to determine some of the H_2 :substrate interaction parameters that are useful for guiding theory.

2.9.4.2 Quasielastic Neutron Spectroscopy

Quasielastic neutron spectroscopy (QENS) is used to determine the self-diffusion of H_2 adsorbed in materials. The diffusion constant and activation energies measured for H_2 in/on the substrate are important parameters for kinetic and thermodynamic modeling.

QENS is an inverse geometry time-of-flight instrument in which a pulsed polychromatic beam is incident on the sample. An array of graphite analyzers allow only those neutrons with energies low enough (3.6 meV) to reach the detectors. The incident neutron energy is scanned by time-of-flight. Standard data reduction programs are used for normalization

of the data and conversion to a linear energy scale in neutron energy loss (reproduced from Brown et al. 2009, p. 204025).

2.9.4.3 Nuclear Magnetic Resonance

Proton nuclear magnetic resonance (NMR) spectroscopy has the ability to characterize conformational and dynamic processes in materials, and therefore, allows for the study of interfacial phenomena on the nanoscale. NMR with in-situ, high-pressure H₂ loading is very sensitive (detectable at below 0.1 wt % level) for selectively detecting H₂ molecules confined in nanopores, and therefore, offers the unique ability to monitor the dynamic interaction between a sorbent material and H₂. For example, 1H NMR peaks can be shifted upfield from non-interacting H₂ when H₂ is in the proximity to the graphitic basal plane where strong anisotropic diamagnetic susceptibility leads to an additional upfield isotropic chemical shift $\sigma_{iso} = (2/3)(\chi_{||}-\chi_{\perp})/\langle R^3 \rangle$ (Tabony 1980; Carrington and McLachlan 1967). Here, R is the distance of the nucleus to the basal plane and $\langle \rangle$ is the average over time; $\chi_{||}$ and χ_{\perp} are the magnetic susceptibilities along and perpendicular to the c axis, respectively (Heremans, Olk, and Morelli 1994). The presence of different shifts is associated with H₂ in different types of confined regions with different average proximity to the surface (Kleinhammes et al. 2010).

Individual isotherms associated with 1H NMR peak intensities can be obtained by measuring the peak intensities versus pressure P. Typically a linear pressure dependence of the intensities of the proton peaks is as expected from H₂ gas. The isotherm data can be used to extract the binding energy based on the Langmuir model that is expected to describe the H₂ adsorption behavior in the supercritical region with sufficient accuracy (Bhatia and Myers 2006) and is given by de Boer (1968):

$$n_{H_2}(P, T) = n_{H_2,\infty} [bP/(1+bP)]; b = \sigma/[v_0 \sqrt{(2\pi m_{H_2} k_B T)}] \bullet \exp[E_{ad}/(k_B T)] \quad (1)$$

Here, $n_{H_2,\infty}$ is the saturation coverage, σ is the area occupied by a H₂ molecule on the surface and is about 0.16 nm² based on the commensurate filling measurement of a graphite plane (Nielsen and Ellenson 1977), v_0 is the attempt frequency of about 10¹³ Hz, m_{H_2} is the mass of H₂, and E_{ad} is the binding energy (Kleinhammes et al. 2010).

It is important to realize that disordered porous materials are not homogeneous, e.g., boron-substituted carbons. Spin-lattice-relaxation time (T₁) measurements provide a unique tool for analyzing such structural heterogeneity because T₁ is sensitive to the size of nanopores and the kinetics of H₂. It is known that T₁ of H₂ gas depends sensitively on molecular collisions described by Johnson and Waugh (1962):

$$T_1^{-1} = \omega^2 \tau_c / (1 + \omega_0^2 \tau_c^2) \quad (2)$$

Here, ω^2 is a known constant related to dipolar and rotation-induced (for $J = 1$) effective field at the proton, $\omega_0/2\pi$ is the Larmor frequency of the magnetic field, and τ_c is the lifetime of the state $|1m\rangle$ determined by H₂-H₂ collisions, thus, $1/\tau_c \propto P$. For H₂ gas of $P = 1$ MPa and RT $\tau_c = \sim 0.3$ ns (Johnson and Waugh 1962). Thus, $\omega_0^2 \tau_c^2 \ll 1$ and Equation 2 predicts $T_1 \propto P$ above 1 MPa in such fast-motion limit. For proton NMR peaks in a given spectrum, the saturation recovery curve of the nuclear magnetization,

$M(t)$, exhibits an exponential dependence on the recovery time t , $[M_0 - M(t)]/M_0 = \exp(-t/T_1)$ where M_0 is the magnetization in equilibrium (Kleinhammes et al. 2010).

2.9.5 Composition and Atomic Content

2.9.5.1 Prompt Gamma Activation Analysis

The use of non-destructive bulk elemental determination from prompt-gamma activation analysis (PGAA) of HSCoE-synthesized materials steered synthetic approaches and gave valuable feedback to researchers pertaining to the elemental composition of a given sorbent material (e.g., boron or nitrogen doping levels).

2.9.5.2 X-Ray Photoelectron Spectroscopy

X-ray photoelectron spectroscopy (XPS) relies on the photoelectric effect, whereupon electrons are emitted from a material upon absorption of high-energy (low wavelength) photons. In XPS, a photon from a monochromatic X-ray beam of known energy, $h\nu$, displaces an electron, e^- , from an electronic orbital with binding energy E_b :



In Equation 3, A can be an atom, molecule, or ion and A^{+*} is an electronically excited ion with a positive charge one greater than that of A . An electron spectrometer measures the kinetic energy of the emitted electron E_k , which can be used to determine the binding energy, E_b , of the electron:

$$E_b = h\nu - E_k - \Phi \quad (4)$$

In Equation 4, Φ is the work function of the spectrometer, a factor that corrects for the electrostatic environment in which the electron is formed and measured.

The binding energy, E_b , of the measured electrons gives detailed information about the identity and bonding environment of atoms and molecules within a given sample. Specifically for boron-substituted carbon materials, boron can be identified by photoelectrons with binding energies in the range of ~180 to 200 eV, whereas carbon binding energies are in the range of ~280 to 300 eV. Within these envelopes, further detail about the atomic binding environments can be gleaned by the exact position of the observed peaks. For example, boron in a sp^2 bonding geometry (e.g., BC_3 , BN) has a binding energy of 190–192 eV. In contrast, the binding energy is 192–193 eV for B_2O_3 , and is much lower (187–189 eV) for elemental boron and B_4C . The specific binding energies observed in the carbon region can also convey information about carbon orbital hybridization, with sp^2 C appearing around 284.5 eV and sp^3 C around 285.5–286 eV. Furthermore, substitutional incorporation of boron into the sp^2 C lattice has been shown to lead to a lower energy shoulder in the carbon spectrum around 282–283 eV.

2.9.5.3 High-Resolution Electron Energy-Loss Spectroscopy

The fundamental mechanisms underlying electron energy loss spectroscopy (EELS) are similar to those involved in photoelectron spectroscopies such as XPS. In EELS, the energy source is a high-energy electron beam with a known, narrow range of kinetic energies. The electron beam is generated by TEM and is sent through a sample located on a TEM grid. Upon passing through the sample, some of the electrons undergo inelastic scattering events by interacting with the material being measured, and these scattering events transfer energy to the material causing an energy loss for the transmitted electron.

The energy imparted to the material can cause a variety of excitations including inner shell ionizations in which a core electron is emitted from an electronic orbital, analogous to the photoelectron process utilized in the XPS measurement. However, in contrast to XPS where the energy of the ejected photoelectrons is measured, in EELS the energy of the transmitted electrons (from the incident high-energy electron beam) is measured. Thus, the energy loss associated with transmission of the electron beam through the sample can be used to calculate the binding energy of electrons emitted through scattering events, which in turn can be used to identify atoms and deduce atomic bonding environments within the material.

The primary advantage of EELS is the high spatial resolution associated with using a narrow electron beam, which is why the technique is often qualified as high-resolution (HR-) EELS. In a high-resolution TEM instrument, the electron beam can be focused down to diameters of a few nanometers, meaning that the atomic composition and bonding environment can be resolved on similar spatial scales. HR-EELS was used by the HSCoE to determine boron, nitrogen, and phosphorous incorporation into carbon materials with superb spatial resolution. Similar to XPS, the specific binding energies observed for a given sample convey information about the boron/phosphorous/nitrogen content and bonding environment, but EELS allows this information to be mapped out with nanometer-scale resolution. This advantage allows for tracking the spatial uniformity of substitutional atom incorporation and also for correlating the bonding environment to specific morphological features that may be observed in a TEM image.

2.10 Analyses Performed for Specific Sorbent Classes

2.10.1 Optimized Nanospaces

The most important properties of physisorption-based materials are SSA and pore size. Thus, the main characterization performed measured the sorbent's SSA and pore size distributions with nitrogen (sometimes H₂ and CO₂) using standard isotherm measurement techniques. These measurements provided accurate information that ultimately relates to the measured hydrogen storage capacities as measured with hydrogen isotherms. In some cases to get a better mechanistic understanding of specific adsorption sites, other characterization was performed, including inelastic neutron spectroscopy of H₂ quantum transitions, quasielastic neutron spectroscopy of H₂ diffusion, neutron imaging of adsorption processes in bulk briquettes of high-surface-area activated carbon, small-angle neutron scattering for pore morphology, and 1H NMR for hydrogen-sorbate interactions. Through these different measurements, it became clear that physisorption was primarily affected by the number of surfaces involved with the adsorption, and that the capacity was primarily related to the SSA. Thus, many of the tools used to study other adsorption mechanisms were not particularly useful for investigating vdW sorption.

2.10.2 Substituted Materials

In addition to the standard suite of measurements used to characterize high-SSA sorbents, the enhanced binding and other properties provided by appropriately substituted B in carbon was measured with a number of different spectroscopic techniques. The HSCoE employed XPS to determine the specific coordination states of B in C; prompt gamma

neutron spectroscopy, electron dispersive spectroscopy (EDS), and EELS to determine the concentration of B in C; INS and diffuse reflectance infrared Fourier transform spectroscopy (DRIFTS) to determine the hydrogen binding state in the BC materials; and NMR spectroscopy and TPD to quantify the hydrogen binding energy and amount of interaction in the BC materials.

NREL used XPS to investigate the coordination state of boron incorporation into the graphitic lattice. The boron 1s and carbon 1s spectra are useful in determining the exact state of boron binding. XPS identified four main coordination states including boron carbide, elemental boron, sp^2 boron, and boron oxide. Compilation of all the boron coordination states also provides an estimate of the total amount of boron in each state and in the material as a whole. Nanoprobe EELS measurements go one step beyond standard EDS to determine the local B content and B bonding geometry. PGAA is one of many tools in the suite of neutron scattering that provides elemental composition. In this case, PGAA provided another complementary method to determine the amount of B in the carbon materials. INS can determine hydrogen binding energies, sorbent-hydrogen and H-H bond lengths, and even more subtle effects associated with pore sizes and compositions. Measurements performed for the HSCoE efforts marked the first time that this splitting was observed with any carbon- or boron-substituted carbon, providing definitive proof that the B in the sample significantly affects the interaction with H_2 .

2.10.3 Strong/Multiple Dihydrogen Interactions

Identifying and characterizing strong H_2 binding sites in sorbent materials is critical to help design new materials that store H_2 under realistic conditions. Neutron scattering and TPD experiments were carried out to probe the adsorption/desorption of H_2 on various materials. Hydrogen has the largest scattering interaction with neutrons, making neutron scattering techniques ideal for studying strong H_2 binding sites. Neutron diffraction techniques provided the atomic locations of H_2 within crystalline materials and enabled a detailed understanding of the mechanism of hydrogen storage. INS measures the dynamics of H_2 at strong H_2 binding sites. INS is instrumental in determining the major contributions to the binding energies (i.e., improved overall adsorption enthalpy). For example, INS shows that the highest hydrogen binding enthalpies in MOFs result from the open metal sites. TPD measurements were highly reliable and were used to quickly determine enhanced hydrogen binding enthalpies. Higher temperature TPD peaks (>150 K) typically represented populations of structurally unique, stronger H_2 binding sites. In addition, TPD was used to discriminate between dissociative and non-dissociative adsorption mechanisms.

2.10.4 Weak Chemisorption/Spillover

In general, most of the materials used for spillover investigations were high-SSA sorbents, and the typical analyses for these types of materials (discussed above) were routinely performed to provide baseline information of the receptors before and after catalyst integration. Because of the novelty of the entire mechanism, specific spectroscopic tools and methods have not been fully developed to provide the material property information needed to fully understand the processes. Thus, standard tools such as ambient-temperature adsorption isotherms and TPD provided the most direct evidence for enhanced capacities resulting from spillover and in some cases resulting from

chemical reactions of species on the receptors with the dissociated hydrogen. Routinely monitoring the effluents of weak chemisorption and spillover materials with TPD is very important to ensure that the hydrogen storage capacities provided by the isotherm measurements are fully reversible at the conditions of interest for light-duty vehicles. NMR, inelastic neutron, Raman, and Fourier transform infrared (FTIR) spectroscopies were all investigated as possible ways to directly observe the carbon-hydrogen bonding. However, the bonds associated with spillover are sufficiently different that only indirect observations of the effect have been made to date with these tools. That said, more strongly bonded hydrogen has been observed with these measurements where relatively weaker chemical C-H bonds are clearly seen and provide a platform from which to develop/improve these methods in order to observe the weaker spillover effects.

2.11 Cross-Cutting Theory

The HSCoE used several different methods at several different institutions (see Figure 2-4) to provide predictive hydrogen sorbent design and performance evaluations. The HSCoE developed an integrated theory for hydrogen storage within a paradigm of “interaction-structure-properties” based on thermodynamics and quantum mechanics. The concept of hydrogen sorbents is introduced to describe optimal types of hydrogen storage materials, in which the interaction between hydrogen and the sorbent is much weaker than the internal interactions in the sorbents so that fast kinetics and high energy efficiency can be achieved. Optimal hydrogen binding energies that enable highly reversible hydrogen charge/discharge are discussed for near-ambient operating conditions. Mechanism of hydrogen-material interaction is analyzed through a unified bond theory. Statically, the internal interactions hold the components together for them to form a stable sorbent structure. Dynamically, the internal interactions provide the driving force for structure formation. Of crucial importance for hydrogen storage, the internal interactions affects the interaction between the sorbent and hydrogen. In total, the internal interactions not only determine how to form a stable sorbent, but also allows for the hydrogen binding properties to be tuned purposely. In this theory, a hydrogen sorbent is viewed as arrays of sorption sites on the surfaces, and key quantities such as the density of sorption sites, SSA, and their relationship with hydrogen-storage properties are analyzed. Typical nanoscale building blocks for construction of hydrogen sorbents are used. The design principles of hydrogen sorbents are derived from practical requirements such as energy efficiency, charging/discharge rate, cost, reversibility, and durability. A detailed account of this integrated theory can be found in Zhao and coauthors (2010). In the 5-year life time of the HSCoE, one of the major achievements of the theory team was the prediction of strong H₂ binding to coordinately unsaturated metal centers (Zhao et al. 2005) and boron substituted in carbon materials (Kim et al. 2006).

For most of the theoretical work performed by the HSCoE, state-of-art atomistic simulation was used based on DFT as implemented in VASP or Gaussian. Total energy and structural optimization is the most frequently used mode of simulation for determination of stable/meta-stable structures of the materials, characterization of reactivity, and interaction with hydrogen. The kinetics calculation mode is particularly useful for simulation of H spillover effects. A climbing nudged elastic band method was normally used to calculate the H diffusion barriers of the receptor materials. Molecular

dynamics simulation at finite temperature is the most effective simulation mode to test the stability of a material and to identify atomistic processes. Electronic structure analysis provided information about the mechanism of hydrogen interaction with the storage materials and provided deep insights into electron-counting rules (e.g., 18-electron rule), tunability of hydrogen binding energy, and acceleration of kinetics of hydrogen spillover. To bridge atomistic and continuum modeling, parameterized continuum models were developed for simulation of scale-up systems.

2.11.1 Density Functional Theory

DFT in the local density and generalized gradient approximations allows for accurate first-principles calculation of structural energetics, including charge-transfer and hybridization components of adsorbates binding. Van der Waals components of the interaction require extension of the exchange-correlation potential to include non-local electrostatics effects, but the enhancements required for practical hydrogen storage will require interactions beyond vdW to obtain the required binding energetics, with either empirical or more computationally intensive first-principles treatments of this non-local exchange-correlation. Molecular dynamics in the first-principles and empirical approximations provide insights into the structures and stabilities of the host adsorbents and spectroscopic properties useful to interpreting various experimental probes.

Atomic structure analysis is a basic step in characterization of materials. It allows for quantitative determination of symmetry of bonding networks, bond lengths, bond angles, and coordination number. DFT analysis is especially useful to determine the atomic structures of nanoscale and non-crystalline materials, which are very difficult or even impossible to determine experimentally. Many of the new materials (e.g., metal-decorated buckyballs, Met-Car molecules and crystals, amorphous and activated carbon, MOFs, boron-substituted carbon [BC_x], intercalated graphite) developed by the HSCoE experimentalists have been characterized atomistically via DFT calculations. Electronic analysis consists of a series of quantum-mechanical approaches such as eigen states hybridization, density of states, charge density, charge occupancy, charge transfer and rehybridization, delocalization (resonant effect) and electron counting, and bonding mechanisms. Systematic electronic analysis provides insights into the hydrogen interaction with the sorbent materials. Within the HSCoE, four fundamental hydrogen bonding mechanisms were used as part of the hydrogen storage materials development efforts.

Kinetics analyses are effective in characterizing hydrogen adsorption/desorption and H diffusion in spillover processes. In these well-defined processes, kinetic barriers are first calculated within the so-called nudged elastic band method and the rate constant of the event can be evaluated based on an Arrhenius equation. Thermodynamic analysis can be used to search unknown atomistic processes in synthesis and reactions, and to assess the thermo-stability of a rationally designed sorbent material.

The effectiveness and accuracy of DFT has been well tested for strongly binding systems. For example, the cohesive energy of typical metal and semiconductor materials can be accurate to within 0.2 eV per atom (or 5%). When the systems involve primarily vdW interactions, however, the accuracy of DFT calculations quickly deteriorates because of

the small magnitude of the interaction energy (which can be as small as 0.05 eV per atom). DFT typically overestimates vdW interactions in the local density approximation (LDA), but underestimates or even gives no binding in the generalized gradient approximation (GGA). For H₂ sorbents based on weak chemisorption (e.g., Kubas interactions), the H₂ binding is typically 0.15 to 0.50 eV/H₂, which falls between vdW interactions and traditional chemical bonding. The accuracy for the DFT approach in the common approximations for these weaker interactions between metal centers and dihydrogen depends on the exchange-correlation functionals used. Initially, four representative systems were selected (i.e., Ti-C₂H₄, Sc-C₅H₅, Ca-BDC, and Li-BDC), which cover a wide range of sorbent materials proposed for high-capacity RT H₂ storage. Highly accurate calculations at the MP2/cc-PVQZ level and further corrections for the correlation energy at the CCSD(T)/cc-pVTZ level were used to obtain the dihydrogen binding energies on these systems. These accurate results were used to evaluate nine exchange-correlation functionals widely used in standard DFT calculations. As discussed below, the comparison revealed that the H₂ binding energy obtained with PBE and PW91 functionals are accurate to within a few hundredth of an eV/H₂, validating the predictions where these two functionals were used.

HSCoE partners at NREL and Rensselaer Polytechnic Institute developed DFT-based atomistic modeling of vdW forces. Quantum mechanic (H₂ particle) corrections for H₂ physisorption were also investigated by Rice University (Rice). Quantum corrections were incorporated by Feynman-Hibbs variational treatments and showed that corrections can be significant even at RT and are essential for realistic comparison of simulations with the experiments.

2.11.2 Continuum and Other Modeling Approaches

Continuum models were used in to help engineer nanospaces for optimal capacity of hydrogen adsorption. Basic quantities, such as density of sorption sites and intrinsic microscopic capacity, are introduced for characterization of the sorbent. Based on these equations, the relationship between the volumetric and gravimetric capacities can be deduced through material density. Based on this model, the maximum SSA and optimal pore size for physisorption materials are derived.

In general, two different groups within the HSCoE investigated the use of Grand Canonical Monte-Carlo (GCMC) simulations to provide accurate predictions of hydrogen capacities for sorbents. The GCMC calculation accuracy hinges on the choice of the interaction potential. Because there are several available potentials, it becomes really difficult to select one prior to the measurement so that good predictions can be made. Because of the light weight of the H₂ molecule, it cannot be treated as a fully classical fluid. To achieve a reasonable accuracy for comparisons, quantum corrections must be included via the Feynman-Hibbs variational treatment. HSCoE results indicate that quantum effects always reduce the capacity, and they should be accounted for even at RT. At best, the GCMC calculations can be used to determine lower and upper bounds for hydrogen storage capacities at different temperatures and pressures. Thus, the calculated values provide a range between what the actual sorbent capacity should be. However, all too often researchers report only the upper bound capacity and do not provide well-founded predictions for material capacities.

2.12 Down-Select Criteria

The HSCoE development efforts were grouped into four focus areas, which were based on material classes that could be used to meet DOE hydrogen storage system targets for light-duty vehicles. The four classes were entitled Optimized Nanostructures, Substituted Materials, Strong Binding/Multiple Dihydrogen Interactions, and Weak Chemisorption/Spillover. Within each area, the HSCoE developed a set of selection criteria for the most critical material properties to help quickly identify sorbents that should be developed and those that should not be investigated further. These criteria are summarized in Table 2-2.

The selection criteria did not replace the DOE hydrogen-storage targets, but allowed materials to be developed that did not yet meet some of the targets. In most cases, the materials being developed had to have a clear potential to either meet the DOE hydrogen storage targets or provide useful insights into specific properties of interest to help make materials that could meet them. An important consideration was the fact that the sorbent's binding energy significantly affects the hydrogen storage system cost, net available volumetric and gravimetric capacities, and operating conditions. Thus, as the binding energies increase, the gravimetric capacity increases at higher temperatures and lower pressures. This critical point means that hydrogen storage systems become less expensive with optimal binding energies. Thus, the selection criteria used for each material class were adjusted to allow less developed materials to be considered, because, in principle, meeting the DOE targets becomes easier with higher hydrogen binding energies.

Because each material class has unique issues for meeting DOE's targets, a separate set of selection criteria was used to help address the critical development needs that must be met to be successful. The specific selection criteria for each class are provided below.

- Optimized Nanostructures for Physisorption (nominally 77 K storage)
 - The material's gravimetric storage capacity should be approximately 0.03 kg H₂/kg with a volumetric storage capacity of approximately 0.03 kg H₂/L, a possible temperature range of 77–200 K, and a nominal pressure range of 30–100 bar—with a clear potential for further improvement.
 - The high-pressure adsorption isotherm should be >80% reversible, i.e., at least 80% of the stored hydrogen is desorbed or discharged between 77 and 200 K, at nominal fuel cell operating pressures.
 - The desorption or discharge rate at 77–200 K should be more than 0.4 g/s.
 - The charge rate should have 90% of the H₂ adsorbed by the material at 77–200 K within 3.3 min.
 - Material cost projections should be less than half the system cost targets.
- Substituted Materials
 - The initial binding energy should be in the range of 10–25 kJ/mol, and the material should operate within a temperature range of 77–353 K and pressure range of 30–100 bar. There should be a clear potential for gravimetric and volumetric capacity optimization.

- The high-pressure adsorption isotherm should be >80% reversible, i.e., at least 80% of the stored hydrogen is desorbed or discharged between 77 and 353 K, for nominal fuel cell operating pressures.
- The desorption or discharge rate at 77–200 K should more than 0.4 g/s.
- The charge rate at 77–353 K should meet or be within 90% of the DOE target of 3 min for 5 kg H₂.
- Material cost projections should be less than half of the system cost targets.
- Strong/Multiple Dihydrogen Interactions
 - The initial binding energy should be in the range of 10–25 kJ/mol, and the material should operate within a temperature range of 77–353 K and pressure range of 30–100 bar. There should be a clear potential for gravimetric and volumetric capacities optimization.
 - The high-pressure adsorption isotherm should be >80% reversible, i.e., at least 80% of the stored hydrogen is desorbed or discharged between 77 and 353 K, for nominal fuel cell operating pressures.
 - The desorption or discharge rate at 77–200 K should more than 0.4 g/s.
 - The charge rate at 77–353 K should meet or be within 90% of the DOE target of 3.3 min for 5 kg H₂.
 - Materials cost projections should be less than 75% of the system cost targets.
- Weak Chemisorption/Spillover
 - The material's gravimetric storage capacity should be approximately 0.01 kg H₂/kg with a volumetric storage capacity of approximately 0.01 kg H₂/L, a possible temperature range of 298–353 K at 100 bar, and with a clear potential for further improvement.
 - The high-pressure adsorption isotherm should be >80% reversible, i.e., at least 80% of the stored hydrogen is desorbed or discharged with a temperature that does not exceed 353 K, for a nominal fuel cell operating pressure.
 - The desorption or discharge rate at 77–200 K should more than 0.4 g/s.
 - The charge rate at 298–353 K should not exceed 10 h for a full charge of 5 kg H₂.
 - Materials cost projections should be less than 75% the system cost targets.

Table 2-2. Selection Criteria for Sorbent Material Classes

	Cryogenic Sorbents^a	Substituted Materials	Strong Binding/Multiple H₂ Metal Centers	Weak Chemisorption/Spillover
Volumetric Storage Capacity (kg H ₂ /L)	0.03	Potential to be >0.04	Potential to be >0.04	0.01 ^d
Excess Gravimetric Storage Capacity (kg-H ₂ /kg)	0.03	Potential to be >0.06	Potential to be >0.06	0.01 ^d
Pressure Range (bar)	30–100	30–100	30–100	~100
Binding Energy (kJ/mol)	NA	10–25	10–40	10 to 30
Temperature Range (K)	77–200	77–353	77–353	298–353
Adsorption Isotherm Reversibility ^b	>80%	>80%	>80%	>80%
Desorption Rate for 5-kg H ₂ Storage Total	>0.4 g/s	>0.4 g/s	>0.4 g/s	>0.4 g/s
Charge Rate in 3.3 min. for 5 kg H ₂ ^c	90%	90%	90%	e
Full-Scale Material Cost Projections by System Cost Targets	<50%	<50%	<75%	<75%

^a At nominal 77 K storage

^b At nominal fuel cell operating pressures (i.e., ~4 bar)

^c DOE target. For spillover, charge rates adjusted for materials with potential to meet target.

^d Must have clear potential for improvement

^e Since loading is still a substantial issue for spillover, charge rates should not exceed 10 h for full charge of 5 kg H₂ and there must be a clear path to meeting DOE targets.

2.13 Material Properties and Systems Investigated

2.13.1 Overview

As stated above, sorbents have relatively low dihydrogen binding energies, which directly affect storage temperature. This adversely impacts system costs, volumetric capacity, and available gravimetric capacity. Thus, the HSCoE's applied development efforts focused on optimizing hydrogen storage adsorption spaces and enhancing hydrogen binding energies. This required balancing improved hydrogen storage system costs and capacities with perhaps adversely affected material contamination sensitivity, durability, refill rates, and material costs issues. The HSCoE used material and material class selection criteria to identify potential sorbents and mechanisms for focused development efforts. Thus, the HSCoE quickly identified a few selected material classes and their required properties, which then received the bulk of the development work.

As discussed in Section 2.1, the HSCoE focused on four main classes of sorbents for hydrogen storage: Optimized Nanostructures, Substituted Materials, Strong/Multiple Dihydrogen Interactions, and Weak Chemisorption. Within these main sorbent classes,

efforts were typically limited to development of materials with clear viability for meeting DOE targets. For example, regardless of the specific elements used, a pure physisorption material needed to have high SSA (2500 to 3000 m²/g) in order to have the required space to store sufficient amounts of hydrogen. This requirement alone eliminated hundreds of elements that are just too heavy if only a physisorption-based hydrogen storage mechanism is used. Thus, lightweight elements such as carbon, boron, and nitrogen in open-pore structures received the bulk of the development efforts for physisorption-based materials.

Improving sorbent properties for hydrogen storage beyond that attained with weak physisorption materials requires substantial increases in binding energy that improves capacities at higher temperatures, toward ambient. In the select few cases where binding energies can be increased, the stringent SSA and pore-size distribution criteria applied to weak physisorbents is different, even though material space optimization will still be important. From its inception, the HSCoE investigated several methodologies and material systems to increase the intrinsic binding energy of H₂. Based on these efforts, numerous materials were down-selected, and a select few materials/material classes were identified as having the potential to be used to meet DOE system targets. For example, almost all lightweight elements (e.g., Li, N, O, and F) substituted in a carbon matrix do not significantly increase dihydrogen binding. Only Be and B substantially increase dihydrogen binding energy when substituted in carbon in the appropriate coordination. Through calculations and a limited number of specific experimental investigations, it became clear that only correctly coordinated B substituted in graphitic carbon was a viable route to improve hydrogen storage for substituted carbon materials; thus the use of other lightweight elements was limited. In terms of carbon materials, this eliminated the need to perform experimental investigations on hundreds of potential element/process combinations for this material class.

Metal centers in MOFs or equivalent materials bind dihydrogen in the 10–15 kJ/mol range, which is sufficient for near-ambient temperature (150 to 220 K) storage. The main issue with all of these types of materials is that a high number of these binding sites must be uniformly dispersed and accessible in to have the enhanced hydrogen adsorption properties available for a significant fraction of the material storage capacity. Thus, the HSCoE also investigated sorbents with the ability to adsorb multiple dihydrogens on designed sites. Several inexpensive material systems and synthetic pathways (e.g., calcium [Ca] integrated with graphene and other framework materials) were identified that may be used to meet DOE's ultimate targets. These systems and pathways, however, require substantial applied development efforts to achieve the breakthroughs necessary to form the novel structures that have enhanced dihydrogen binding for the entire capacity range. Even so, the basic principles of forming multiple-dihydrogen bonding on these sites with 15 to 40 kJ/mol binding energies were demonstrated experimentally. Furthermore, the potential to store H₂ at ambient temperature and nominal pressures between 10 and 50 bar with theoretical densities greater than twice that of liquid hydrogen make these development efforts highly promising.

The HSCoE also investigated methodologies to store dissociated hydrogen molecules (e.g., hydrogen atoms). Unlike the work to increase binding for dihydrogen, the key issue

here was actually developing ways to store dissociated hydrogen with binding energies substantially lower than those typically observed for hydride formation. Among the more promising material classes, the HSCoE demonstrated that catalyzed hydrogen molecule dissociation followed by “spillover” onto lightweight receptor support materials enable ambient-temperature storage with binding energies in the range of 10 to 25 kJ/mol. Although the phenomenon of spillover has been known for many decades, HSCoE partners demonstrated that this material class could be used to store substantial (>30 g/L and >4 wt %) amounts of hydrogen at near-ambient temperature and at nominal pressures. The HSCoE demonstrated spillover both experimentally and by thermodynamic principles as a process for ambient-temperature, reversible hydrogen storage. However, the materials have tended to be very sensitive to synthetic processing conditions, resulting in substantial irreproducibilities.

With currently demonstrated bulk-material packing densities and hydrogen storage properties, sorbent materials substantially decrease the volume and pressure now used for high-pressure (350 to 700 bar) compressed tanks, and thus could significantly reduce overall system costs. In addition to the specific performance issues for each material class discussed previously, developing material synthetic processes and pathways that are scalable, inexpensive, and reproducible—and producing materials that can meet the DOE system cost targets—remains a challenge that must be aggressively pursued in all cases.

2.13.2 Optimized Nanostructures

The HSCoE rationally designed and developed methods to synthesize sorbents with the appropriate nanostructures and compositions for optimal hydrogen storage. The HSCoE had groups that investigated methods to enhance physisorption through geometric configurations, and to form nanostructures with just the right pore sizes where as much access to the surfaces as possible was available for hydrogen sorption. In general, storage capacities increase with higher SSAs and higher bulk densities. While these are necessary requirements for high storage capacities, other factors, including optimized pore sizes and enhanced binding energies for the entire capacity range, are also important. The HSCoE focused efforts to improve all of these material properties independently and simultaneously. However, it continues to be non-trivial to achieve both the high SSA and the micropore diameters (i.e., 0.7 to 1.5 nm) necessary for optimized H₂ storage (see, for example, Patchkovskii et al. 2005). Many methods such as activation (Guo et al. 2008) and inorganic or organic templating (see, for example, Yang, Xia, and Mokaya 2007; Sakintuna and Yurum 2005) SWNT scaffolds, SWNHs (see, for example, Poretzky et al. 2008; Geohegan et al. 2007), and self-organizing MOFs (see, for example, Collins and Zhou 2007; Wong-Foy, Matzger, and Yaghi 2006) or equivalent materials were used to achieve such porous materials.

As part of the HSCoE efforts, predictive models were developed to understand the physisorption interactions of hydrogen with high-SSA materials and to understand the relationship between geometrical configurations and storage capacities. The number of sorption sites per unit mass is:

$$D_s = N_s/M = S_{SSA}/S_o \quad (5)$$

where, N_s , M , S_{SSA} , and S_0 are, respectively, the number of sorption sites, mass of the sorbent material, SSA, and area per sorption site. The gravimetric capacity (C_w) and volumetric capacity (C_v) can be expressed as:

$$C_w = N_s n_H / M = D_s n_H, \text{ and } C_v = D_s n_H D_{HSM} = C_w D_{HSM} \quad (6)$$

where n_H and D_{HSM} are the number of H atoms per site and density of the hydrogen storage material. Based on these equations, it can be inferred that (i) volumetric capacity scales with gravimetric capacity through material density, and (ii) simultaneous increase of the volumetric capacity and the gravimetric capacity requires increasing both the SSA and the material density, which means that larger voids should be removed.

For physisorption, the H_2 binding energy is determined by the effective contact area. The simplest H_2 sorbent is perhaps a sp^2 -bonding network of pure carbon, in which the closed electronic shell and strong C-C bonds leave no reactive sites for hydrogen chemisorption, thus only physisorption of hydrogen molecules is allowed in a weak dispersive force field (i.e., vdW interaction). Strict computation of the vdW force quantum mechanically at the atomic level is still a challenge. Even if the continuum dispersive force potential is known, because of its small mass, a H_2 molecule often has to be treated as a quantum-mechanical particle. An accurate and efficient calculation of vdW interactions within density functional theory may be achieved using a local atomic potential approach (Sun et al. 2008). Here, a simple continuum model is employed in which the binding energy of physisorbed H_2 is proportional to the effective contact area, s , per hydrogen molecule on the surface of the sorbent. That is $E_b = s B_0$, where B_0 can be calibrated with the binding energy of a hydrogen molecule encapsulated in an ideally spherical shell with a radius of $r\Omega$, which is the equilibrium distance of the vdW interaction between the H_2 molecule and the shell. Using $H_2@C60$ as a gauging system with a known binding energy of 0.3 eV/ H_2 or 7 kcal/mol (Slanina et al. 2006) and an effective contact area of $S\Omega = 4\pi r\Omega^2 = 1.453 \text{ nm}^2$, then $B_0 = 0.207 \text{ eV/nm}^2$ is obtained. It is known that the binding energy of an H_2 physisorbed to a flat surface is $\sim 0.04 \text{ eV}/H_2$, therefore, the effective contact surface area of an H_2 molecule to such a flat surface is $S\Pi = 0.19 \text{ nm}^2/H_2$. Interestingly, this effective contact area is comparable to the geometrical occupancy area of $0.14 \text{ nm}^2/H_2$, estimated within different methods (Panella et al. 2005; Nijkamp et al. 2001), and that of $0.17 \text{ nm}^2/H_2$, measured at 77 K and 1 bar (Zuttel et al. 2004). These equations and the parameters B_0 , $s\Pi$ measure the binding strength of H_2 molecules in the dispersive force field, independent of the material. Based on these results for physisorption, a capacity of 6 wt % and 50 g/L at a binding energy of 15 kJ/mol requires a material with a SSA of 11,500 m^2/g and optimized pore sizes of 3.2 Å. This is a big challenge from a sorbent standpoint. While this model is very simplistic, it highlights the intrinsic difficulty in creating sorbents with sufficient SSA and binding energy to meet the challenging DOE 2015 hydrogen storage targets.

Additional calculations indicated that other coordination states (e.g., sp and sp^3) do not improve binding energy or capacities, and thus the HSCoE had to develop other methods besides physisorption for ambient-temperature hydrogen storage. Because SSAs and physisorption binding energies of typical carbons are only in the range of 2500 to 4000 g/m^2 and $\sim 5 \text{ kJ}/\text{mol}$, respectively, it is clear that achieving the desired capacities

requires substantially different approaches. For physisorption, this means the pore sizes need to be increased to the point that a hydrogen molecule interacts with only one wall to allow enough space for a sufficient capacity to be achieved. However, this decreases binding energies, and thus substantially lower storage temperatures are required to achieve the desired capacities. However, because volumetric capacity scales directly with the gravimetric capacity through material density, to simultaneously increase volumetric and gravimetric capacities, both SSA and material density must be increased while minimizing void size (see Figure 2-5).

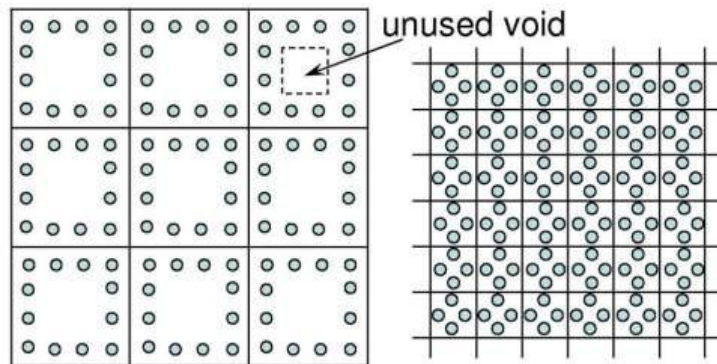


Figure 2-5. Optimal pore size for maximization of volumetric capacity: low density and large pore size (left) may lead to low volumetric capacity because of the unused voids. Optimal pore size and material density can maximize the volumetric capacity (right).

Typical high-SSA carbons such as activated carbons and carbon aerogels generally show great promise for use in storage tanks, but the pore size distributions in these materials range from microporous (<2 nm) to macroporous (>50 nm), resulting in poor volumetric densities. Framework structures also typically have a range of free-space dimensions that can be in the mesoporous regime (2 to 50 nm), making a number of these materials less than ideal for hydrogen storage applications. Moreover, typical sorption enthalpies of 4 to 6 kJ/mol are close to thermal energies, requiring low temperatures if large quantities of hydrogen are to be stored. At the outset of the HSCoE, the literature was replete with reports of hydrogen storage materials where exceptional sorption capacities were attributed to novel geometric structures (see Zlotea, Moretto, and Steriotis 2009). In addition, researchers predicted that structures with accessible vdW spaces and pore sizes in the 0.6 to 0.9 nm² range could increase hydrogen binding and capacity via a superposition of potentials.

Within the HSCoE, different synthetic techniques and geometric structures were investigated to determine which provided the best materials for physisorption-based hydrogen storage. The processes included using synthesis techniques, creating appropriately sized pores in dense materials, and constructing self-assembled crystal structures with open pores. Previous to the start of the HSCoE, considerable work had been done developing “activated” and “superactivated” carbons, with materials such as AX-21 representing the state of the art in sorbents. Sorbents such as AX-21 have ~5 wt % maximum excess hydrogen storage capacity at ~80 K with ~30 bar pressures, but resulting from their relatively large pore sizes (e.g., 1 to 4 nm), their bulk densities are

relatively low (e.g. ~ 0.3 g/mL), and thus their volumetric hydrogen storage capacities are only ~ 15 g/L. These superactivated carbons are formed from using pyrolysis and/or chemical treatment techniques that create pores in bulk natural carbons. The HSCoE investigated ways to optimize similar techniques to create sorbents with more optimal pore sizes for hydrogen that range from ~ 0.7 to 2 nm. These efforts were supported by predictions that the different types of physisorption sites have limited effects on molecular hydrogen (see Figure 2-6). Thus, the focus remained on geometries, and the HSCoE investigated a number of routes to creating sorbents with optimal pore structures.

Specifically, the HSCoE synthesized new high-SSA physisorption materials with optimal uniform pore sizes using a variety of scalable/inexpensive processes, including:

- Pyrolyzation of organic materials such as polyetheretherketone (PEEK) and corncobs
- Chemical synthesis and/or intercalation of exfoliated graphite/graphene
- Vapor synthesis and scaffolding/foams of carbon nanotubes and nanohorns
- Templating to form structures such as zeolite templated carbons and BC_x
- Inexpensive and scalable aerogel synthesis for H_2 storage and metal hydride scaffolding
- Crystalline porous MOFs or polymers.

Although not exhaustive, the processes and materials investigated by the HSCoE provided a good representative set of sorbents from which specific conclusions and recommendations for future efforts were made.

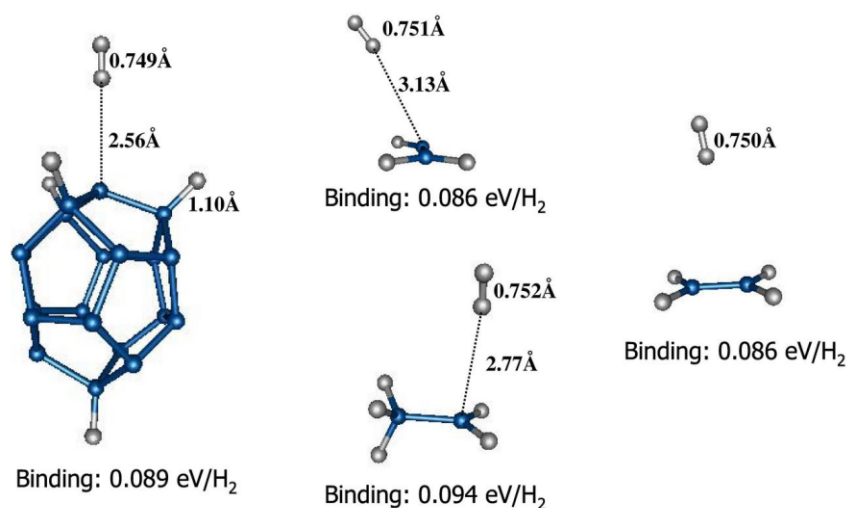


Figure 2-6. Binding of H_2 to activated carbon sites with various types of dangling bonds (left) in comparison to that bound to carbon sites without dangling binding (right). The atomic structures of small hydrocarbon segments with dangling sp^3 σ -bonds and sp^2 π -bonds mimic activated carbon surfaces. The H_2 binding energy was calculated, and no noticeable enhancement of binding energy was observed. This result indicates that activation of carbon surfaces does not lead to stronger physisorption.

2.13.2.1 Pyrolyzation of Organic Materials

The University of Missouri leveraged its capabilities to synthesize high-SSA carbons produced from pyrolysis and potassium hydroxide (KOH) activation of corncobs to form reversible on-vehicle hydrogen storage sorbents with relatively high gravimetric and volumetric storage capacities. Missouri adjusted its processes to form sorbents with pore sizes between 0.5 and 2 nm, with 2500 to 3300 m²/g SSAs. Missouri's ultimate goal, which includes performing work that will continue past the HSCoE, is to increase SSAs further by inducing fission tracks from boron implantation where the B creates more holes in the graphene materials and perhaps raises the isosteric heat of adsorption. Initial porous carbon sorbents with approximately 5 wt % excess gravimetric capacities have been synthesized. As yet, the boron implantation has not produced sorbents with significant hydrogen storage capacities.

Conducting Polymers

Based on reports by Cho and coauthors (2002), Penn within the HSCoE investigated the use of doped (metallic) forms of the organic conducting polymers ("synthetic metals") polyaniline and polypyrrole. These materials reportedly stored approximately 8 wt % (reversible) hydrogen gas at ambient temperature. Polyaniline is a unique type of conducting polymer in which the charge delocalization can, in principle, offer multiple sites on the polymer backbone for the adsorption and desorption of hydrogen, involving weakening of the H-H bond followed by spillover adsorption of this hydrogen onto the adjacent nano-fibrous network. Thus, the Penn group members, who are world-renowned experts in conducting polymers, investigated the use of polyaniline in its different oxidation states (doped and non-doped forms) and other conducting polymers (e.g., polypyrrole) for optimization of hydrogen storage applications. Specific activities were performed to understand the fundamental mechanisms involved and to determine the hydrogen sorption performance.

Polyaniline nanofibers were synthesized systematically with different oxidation states (e.g., emeraldine), and measurements were performed to characterize their hydrogen storage properties. For example, UNC conducted 1H-NMR measurement on the polyaniline nanofibers, but did not observe any significant hydrogen adsorption. However, both TPD and 1H-NMR results showed unusual features during the hydrogen adsorption process, which seemed to depend on the amount of water previously adsorbed by the polyaniline sample. Based on the work from this ~2-year effort, which was not able to synthesize any samples with significant hydrogen storage capacities, the project was stopped at the end of Phase 1 of the HSCoE.

PEEK-Derived Microporous Carbon Materials

Unlike other activation processes that use KOH treatments (Guo et al. 2008), Duke University (Duke) used water and CO₂ treatments to create highly porous sorbents from PEEK (Cansado et al. 2007). This simple, robust method does not require the removal of caustic chemicals while enabling sufficient control to adjust pore sizes and SSAs. This method relies on the oxidization of the PEEK structure to create well-defined pores. Using these techniques, Duke produced samples with large SSAs (>3000 m²/g), small pore-diameter distributions (predominantly ≤3 nm), and large cumulative pore volumes (~1.7 cm³/g). Thus, Duke developed methods that could be used to tune sorbents for

optimal storage of H₂. These techniques should be applicable to other structured starting materials like the porous polymers synthesized by ANL.

2.13.2.2 Chemical Synthesis and/or Intercalation of Exfoliated Graphite/Graphene

Graphene, a 2-D carbon nanomaterial (Stankovich et al. 2006; Novoselov et al. 2004) and graphene-based pillared nanostructures may have potential for hydrogen storage (Jin et al. 2011). The graphene layers in materials such as graphite are very chemically stable and potentially have very high SSA. These layers in graphite are accessible to intercalants including protons and alkali metals. However, the space between graphene layers is too small for dihydrogen to access, and even if it could, the capacity would be too small to meet DOE hydrogen storage targets. Experimental results indicate that the hydrogen uptake capacity of thermally exfoliated graphene derived from graphite oxide (GO) (McAllister et al. 2007; Schniepp et al. 2006) increases linearly with the surface area (Ghosh et al. 2008). But these materials need further improvement in hydrogen capacity to be able to meet DOE hydrogen storage targets. Rice leveraged its expertise with SWCNs to develop sorbents based on graphene and insertion of proppants to engineer appropriate nanostructures.

The original graphene material was obtained by rapidly heating GO, synthesized by the Hummers method (Hummers and Offeman 1958) to 1000°C in 1 min under a H₂/Ar (50 sccm/500 sccm) gas flow. The graphene was then annealed at 1000°C in the H₂/Ar gas flow for 15 min. In this modified procedure, H₂ was introduced to remove most of the oxygen content. The graphene was functionalized and crosslinked using diazonium modification in super acids such as chlorosulfonic acid or oleum (Behabtu et al. 2010; Hudson, Casavant, and Tour 2004). In this form, proppants that worked well for carbon nanotubes as sidewall functional groups, including aryl sulfonates, methyl di-aniline, and t-butyl aniline, were incorporated to hold the graphene apart (Lomeda et al. 2008). These graphene-based sorbents had a significantly higher hydrogen storage capacity compared to typical porous carbons on a per-SSA basis. However, substantial improvement is needed to reach the predicted SSAs and hydrogen storage capacities for these types of materials. Based on the materials and procedures used, Rice estimates that commercial production of these types of materials with the potential to storage ~7 wt % hydrogen could cost less than 45/kg (less than \$70/kg H₂ stored). In addition, the functionalized procedures developed for these scaffolded graphene materials may be used for incorporation of metal centers and materials with enhanced electrostatic attraction of the hydrogen into the nanopore.

In a complementary effort, Caltech used alkali metal-intercalated graphite to study the effects of multiple walled binding, uniform isosteric heats of adsorption for the entire capacity range, and alkali metal-enhanced storage of hydrogen. The alkali metals intercalate readily into graphite, forming a hydrogen storage material with the alkali metal between every third graphene layer. Caltech demonstrated that the multiple walls double or triple the hydrogen isosteric heat of adsorption; the uniform slit pores provide uniform binding over the entire storage capacity range, and the alkali metal atoms provide enhanced dihydrogen binding.

2.13.2.3 Vapor Synthesis and Scaffolding/Foams of Carbon Nanotubes and Nanohorns

Carbon Nanotubes

At the outset of the HSCoE, considerable effort was dedicated to investigating the use of single-walled carbon nanotubes (SWCNTs) for hydrogen storage. This level of interest resulted from numerous reports in the literature of hydrogen storage capacity results ranging from 0 to more than 20 wt % at ambient temperature. These diverse results were initially explained by unique geometric features of nanotubes along with substantial differences in nanotube synthesis and purification. The HSCoE used laser vaporization (NREL), arc (NREL, Penn State), and chemical vapor (NREL, Duke, Rice) synthesis techniques, along with systematically controlled purification processes to make an array of different nanotube materials with different properties. Different nanotubes were made by different HSCoE partners and evaluated at multiple institutions to ensure the accuracy of the measurements. For example, NREL used materials from different institutions to prepare a number of samples where the hydrogen storage capacities were validated at both NREL and Southwest Research Institute (SwRI). Rice developed carbon nanotubes, nanotube foams, and nanotube scaffolds, along with capabilities that estimated the potential capacities of the different structures. Duke synthesized very small diameter (i.e., less than 1 nm) carbon nanotubes to investigate curvature effects on hydrogen storage.

Ultimately, at the end of the approximate 2-year focused effort, the HSCoE found that differences in measured hydrogen storage capacity could not be correlated with specific carbon nanotube synthesis methods or with various properties of the carbon nanotube structure. Furthermore, no exceptional hydrogen storage capacities were identified. In general, the hydrogen storage capacities of carbon nanotubes are similar to other porous carbon sorbents, with similar SSAs and isosteric heats of adsorption. Although the number of publications and the worldwide level of effort on carbon nanotube research and development for hydrogen storage have continued to grow in the last decade and important progress has been achieved, the HSCoE could not rectify the uncertainty in many reported hydrogen storage capacity results for pure, undoped samples.

Ultimately, the DOE Fuel Cell Technologies Program used input obtained through a Federal Register Notice, the open peer-reviewed literature, and technical feedback from the FreedomCAR and Fuel Partnership and DOE researchers to make a “No-Go” decision on future investment in pure, undoped SWCNTs for ambient-temperature vehicular hydrogen storage applications. At ambient temperature, carbon nanotubes typically had less than 0.2 wt % excess hydrogen adsorption, and the best samples only had approximately 800 to 1100 m²/g SSAs. Regardless of size, scaffolding, or functionalization, the best carbon nanotube materials had only ~3 wt % excess adsorption at 77 K and ~20 bar pressures. While the HSCoE concluded that it should be possible to make an idealized array of carbon nanotubes that may be able to exceed 6 wt % at 77 K, the focused efforts by the center were not able to get close to this capacity, and ultimately, most of the carbon nanotube activities were redirected to other development efforts with a greater potential to synthesize materials that could be used to meet DOE targets.

Single-Walled Carbon Nanohorns

One of the main problems associated with carbon nanotubes is that their long uniform geometries result in significant bundling, making substantial amounts of the surfaces inaccessible to hydrogen. Although the vdW forces that induce this bundling are relatively weak, the long lengths of the nanotubes creates sufficient attraction that it proved difficult to keep the tubes separated, even with cross-linked ligands. To directly address this issue, HSCoE partner Oak Ridge National Laboratory (ORNL) investigated the use of single-walled carbon nanohorns (SWNHs). SWNHs are carbon nanostructures with a unique morphology in which cone-shaped carbon structures are joined at the center, thus eliminating bundling and automatically creating high-SSA materials. Carbon nanohorn aggregates are assembled from the “bottom up” from individual nanohorns. Nanohorns are cone-shaped, atomic-layer-thick nanostructures that contain preferred hydrogen adsorption sites in their tips and have variable internal and interstitial pores that have been shown to contain hydrogen at liquid hydrogen density or higher (Figure 2-7). SWNHs are easily produced in large quantities, and have been shown to serve as excellent metal catalyst supports for fuel cells and batteries in addition to their potential as sorbents. Thus, SWNHs can be functionalized by tailoring their pores and by metal decoration to optimize their hydrogen storage capacities.

ORNL developed SWNHs with high SSAs (>2100 m²/g) and optimized their geometries for containing high volumetric densities while increasing their binding strength to hydrogen with incorporation of functional groups, substitutions, and incorporation of metal. The shape of individual nanohorns was tuned during synthesis to find morphologies with adsorption sites and high binding energies. For example, NMR results performed by UNC demonstrated that the hydrogen was preferentially stored in sub-nm pores in large and small nanohorns, opened and unopened by oxidation. The interstitial pores in large nanohorns store hydrogen in smaller pores than the internal pores of small nanohorns. The nanohorn innate interstitial pores were tuned by oxidative treatments and other processing techniques (e.g., heat, compression). ORNL synthesized pure SWNH materials with >3.5 wt % excess hydrogen adsorption at 77 K, and bulk densities >1 g/ml.

2.13.2.4 Templating

In general, materials with high SSA can be created via pyrolysis processing of non-porous materials. However, materials made this way tend to have heterogeneous surface structures and a broad range of pore sizes, many of which are too large and thus have a substantial fraction of the hydrogen residing in the gas state rather than adsorbed onto

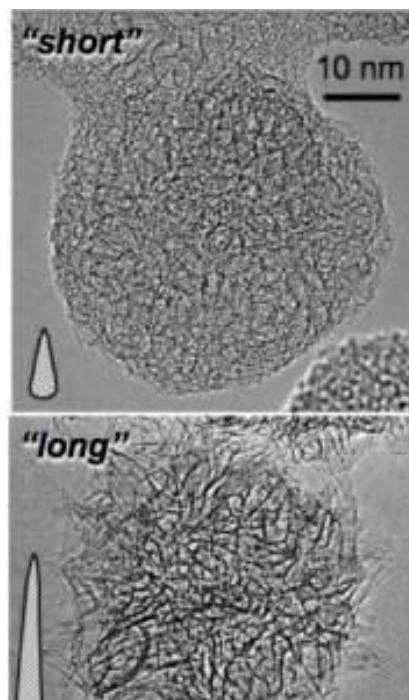


Figure 2-7. Aggregates of “short” and “long” single-wall carbon nanohorns produced by laser vaporization. Schematic representation of individual nanohorns is shown.

surfaces. Creating optimized geometric structures in which all of the sorption sites are accessible to hydrogen requires the careful design of materials and the processes used.

This issue is the same regardless of the sorption mechanism being employed, but does require that the structures be optimized for the desired type and conditions of the hydrogen storage. Templating is one technique employed by HSCoE partners, including NREL, Penn State, Caltech, and Duke, to enable systematic investigations of how specific structures and compositions affect hydrogen storage properties. Templating involves the vapor or chemical-phase deposition of a partial or full layer of material onto a porous structure. If, for example, carbon is coated onto a zeolite template, the zeolite template can be removed via chemical or vapor processing, leaving behind a porous carbon material that matches the geometric structure of the removed zeolite template. This type of process has been used to make highly porous carbon materials (i.e., with SSAs $>3500 \text{ m}^2/\text{g}$) with pores that are nearly identical to the zeolite, resulting in materials with $\sim 7 \text{ wt } \%$ hydrogen storage capacities (Yang, Xia, and Mokaya 2007).

Most of the template work performed by the HSCoE was focused on forming heterogeneous (substituted) materials and is discussed more in these sections later in the document. However, NREL developed templating techniques specifically to make novel lightweight hydrogen storage materials with optimal pore structures mimicking the template chosen. This technique accelerated development by increasing the synthesis rate of appropriate materials in which all the higher hydrogen binding sites are accessible. In general, NREL found that templated carbons with SSAs in the range of $\sim 2000 \text{ m}^2/\text{g}$ are easily synthesized. However, higher SSAs with smaller pore sizes are more difficult. Furthermore, NIST, in collaboration with Monash at the University of Australia, investigated the general hydrogen dynamics in zeolite-templated microporous carbons. The pore structures in the templated carbon are such that the inelastic neutron scattering of the hydrogen spectra are broad and liquidlike; there seems to be two types of hydrogen diffusing on two different timescales at 77 K as determined by QENS.

2.13.2.5 Inexpensive/Scalable Aerogels for H_2 Storage and Metal Hydride Scaffolding

Carbon aerogels (CAs) comprise another class of carbons/processing that can serve as effective physisorbents for molecular hydrogen. In general, aerogels can be made from inexpensive solution-phase sol-gel polymerization followed by pyrolyzation. Thus, aerogel synthesis is scalable and applicable to commercial manufacturing. However, prior to the HSCoE, little was known about the hydrogen sorption properties of CAs.

To close that gap, Lawrence Livermore National Laboratory (LLNL) leveraged its expertise with aerogels to perform focused development of CA synthesis techniques that produced hydrogen sorbents with optimal SSAs, pore sizes, and compositions. Carbon aerogels are typically prepared through the sol-gel polymerization of resorcinol with formaldehyde in aqueous solution to produce organic gels that are supercritically dried and subsequently pyrolyzed in an inert atmosphere (Fricke and Petricevic 2002; Pekala 1989). As prepared, CAs can have SSAs ranging from 200 to $1200 \text{ m}^2/\text{g}$, depending on the reaction formulation. The accessible surface areas in these materials can be further increased through chemical or thermal activation processes. Chemical activation can be

performed through heating the carbon (or carbon precursor) in concentrated acids (H_3PO_4) or bases (i.e., KOH). Thermal activation of CAs involves the controlled burn-off of carbon from the network structure in an oxidizing atmosphere such as steam, air, or carbon dioxide at elevated temperatures. In both cases, activation creates new micropores and opens closed porosity in the CA framework, leading to an increase in the overall SSA.

Thermal activation using carbon dioxide proved to be the most effective method for generating high-SSA CAs. Access to high SSAs in activated CAs also required careful design of the pre-activated carbon framework, because the morphology of the network structure ultimately determines the textural properties of the activated material. CAs with larger structural features (micron-sized pores and ligaments) yielded higher-SSA materials with thermal activation. By contrast, the microstructure of traditional CAs, consisting of nanometer-sized carbon particles and tortuous pore structures, both limited the surface areas attainable through activation and led to inhomogeneous burn-off in monolithic samples. By using CAs with larger pore and particle sizes, LLNL was able to prepare activated CA monoliths with BET SSAs in excess of $3200 \text{ m}^2/\text{g}$ (Baumann et al. 2008). These SSA values are the highest that we are aware of for CAs and are comparable to those of the highest-SSA activated carbons. These values are also greater than the SSA of a single graphene sheet ($2630 \text{ m}^2/\text{g}$, if both graphene surfaces are taken into account). Presumably, edge-termination sites constitute a substantial fraction of the SSA in these activated CAs, as is the case for traditional high-SSA activated carbons.

Interestingly, the activated CA materials remained monolithic despite the significant mass loss during thermal treatment. This observation is important, because the ability to readily fabricate monolithic sorbents could provide advantages in both material handling and design of storage tanks. Examination of the CAs following activation shows that the general framework structure was retained, but the network ligaments were smaller relative to those of the unactivated material, which is due to burn-off of carbon from the aerogel framework. Although the SSAs for these materials increased with increasing activation time, the average size of the micropores formed during activation also increased. Thus, materials with intermediate surface areas ($\sim 1500 \text{ m}^2/\text{g}$) exhibit an average pore size of $\sim 1 \text{ nm}$, while the formation of “supermicropores” and/or small mesopores (pores larger than 2 nm) are observed in the higher-SSA material (e.g., $\sim 3200 \text{ m}^2/\text{g}$).

Previous studies have shown that size and shape of the pores in hydrogen physisorbents play a critical role in hydrogen uptake, and that the optimal pore structure are slit-shaped pores with diameters between 0.7 and 1 nm (Patchkovskii et al. 2005; Murata et al. 2002). Therefore, LLNL focused on developing new activation approaches that limit the formation of these larger pores. For example, chemical activation of CAs with KOH was examined. Although this method created CAs with narrow size distributions of micropores and large micropore volumes, LLNL was not able to prepare materials with SSAs comparable to those of the CO_2 -activated materials. Based on these results, a hybrid activation approach might prove promising in which both thermal and chemical activation are used to produce high-SSA CA sorbents with average micropore size of $\sim 1 \text{ nm}$. In general, LLNL successfully synthesized high-SSA CAs that had $>5 \text{ wt } \%$ (29 g/L)

excess hydrogen adsorption at 77 K. This is comparable to other activated carbon materials. However, the flexibility in the processing enabled the CAs to be optimized for other hydrogen storage mechanisms including dispersion of single-metal atoms, spillover, and metal hydrides.

In a parallel effort, LLNL also designed CA materials as nanoporous scaffolds for metal hydride systems. Recent work by others (see, for example, Gross et al. 2008; Stephens et al. 2009) demonstrated that nanostructured metal hydrides show enhanced kinetics for reversible hydrogen storage relative to the bulk materials. This effect is diminished, however, after several hydriding/dehydriding cycles, because the material structure coarsens. Incorporation of the metal hydride into a porous scaffolding material can potentially limit coarsening and, therefore, preserve the enhanced kinetics and improved cycling behavior of the nanostructured metal hydride. Successful implementation of this approach, however, requires the design of nanoporous solids with large accessible pore volumes ($>4 \text{ cm}^3/\text{g}$) to minimize the gravimetric and volumetric capacity penalties associated with the use of the scaffold. In addition, these scaffold materials should be capable of managing thermal changes associated with the cycling of the incorporated metal hydride. CAs are promising candidates for the design of such porous scaffolds based on large pore volumes and tunable porosity of aerogels. Also, the synthesis of CAs allows for the dispersion of secondary materials into the carbon matrix that can serve as catalysts or destabilizing agents for the metal hydride and potentially influence the transport properties of the scaffold. For example, LLNL demonstrated that the incorporation of carbon nanotubes into the CA framework not only improves the thermal conductivity of the scaffold, but may also affect the kinetics of dehydrogenation for certain metal hydrides. This research is a joint effort with HRL Laboratories, a member of the DOE Metal Hydride Center of Excellence. LLNL's efforts focused on the design of new CA materials that can meet the scaffolding requirements, while metal hydride incorporation into the scaffold and evaluation of the kinetics and cycling performance of these composites were performed at HRL.

2.13.2.6 Crystalline Porous Frameworks or Polymers

Most of the sorbent materials discussed to this point involve a large amount of disorder or amorphous structures either at the atomic or at the larger pore size scales. However, there are a large number of crystalline materials that have substantial porosity. As discussed previously, many of these materials (e.g., silica and alumina-based zeolites) will probably not be able to meet DOE hydrogen storage targets, because the elements used to construct their frameworks are too heavy and substantial SSAs approaching $3000 \text{ m}^2/\text{g}$ cannot be achieved. However, there are a number of crystalline materials such as MOFs, other organic-based frameworks, and porous polymers that use lightweight elements like carbon in the majority of their structure so that high SSAs can be achieved.

In the past decade, there has been an escalation of interest in the study of MOFs and other framework materials based on their fascinating structures and intriguing application potential. Their exceptionally high SSAs, uniform yet tunable pore sizes, and well-defined adsorbate-framework interaction sites make them suitable for hydrogen storage. Various strategies to increase the hydrogen capacity of frameworks, such as using pore size comparable to hydrogen molecules, increasing surface area and pore volume, using

catenation, and introducing coordinatively unsaturated metal centers (CUMCs) have been widely explored to increase the hydrogen uptake of the frameworks. Recently, inelastic neutron scattering and neutron powder diffraction as well as computational studies suggest that the choice of both metal centers and ligands can play an important role in tailoring the gas-framework interactions. In addition, those ligands containing phenyl rings have been proven favorable for hydrogen adsorption. Frameworks with hydrogen-uptake capacities in systems have been shown to exceed the DOE 2010 gravimetric storage targets under reasonable pressures and cryogenic temperatures (typically 77 K). However, the weak interaction between hydrogen molecules and frameworks is a major hurdle limiting the hydrogen storage capacities at ambient temperature.

Within the HSCoE, TAMU (and at the start of the HSCoE, Michigan/UCLA) developed framework materials focused on enhanced hydrogen storage capacities, especially at temperatures approaching ambient. TAMU investigated several strategies to improve hydrogen uptake in frameworks, including:

- Using catenation isomer pairs to evaluate the contribution from catenation to the hydrogen uptake of a framework material. Catenation can be used to reduce pore sizes in porous frameworks and has also been explored as an efficient method to improve hydrogen capacity.
- Synthesizing porous frameworks with high hydrogen adsorption capacities based on different CUMCs. The implementation of CUMCs into porous frameworks has been considered one of the most attractive ways to improve their affinities to hydrogen.
- Hydrogen storage studies in frameworks containing nanoscopic cages based on double-bond-coupled di-isophthalate linkers. Those ligands containing phenyl rings in frameworks have been proven favorable for hydrogen adsorption.
- Designing and synthesizing porous frameworks based on an anthracene derivative, which can provide additional hydrogen binding sites to increase the hydrogen uptake.
- Obtaining stable frameworks with high SSAs by the incorporation of mesocavities with microwindows.
- Constructing frameworks with “close-packing” alignment of open metal sites, which can increase the number of nearest-neighbor open metal sites of each H₂-hosting void in a 3-D framework so that they can interact directly with the guests (H₂ molecules) inside the void.
- Building up porous lanthanide frameworks and studying their potential application in gas adsorption.

Within the HSCoE, additional framework investigations and characterizations were performed as part of effort throughout the world to construct framework materials with optimal hydrogen storage properties. Other efforts included:

- Synthesis and characterization of frameworks such as MOF-177, MIL-53, U. Nottingham Cu-based MOFs, and covalent organic frameworks (COFs) by Caltech.
- NIST in collaboration with A. Dailly at General Motors investigated the origin of hysteretic sorption curves in flexible MIL-53 frameworks. NIST determined that the framework flexes without the influence of the adsorbate on cooling and located the hydrogen adsorption sites at 4 K and through the hysteresis loop at 77 K. NIST determined the relative magnitude of the breathing effect through adsorption of other gases and determined that an H₂-saturated closed pore can trap hydrogen to about 110 K, but that this retention competes with the tendency of the framework to open with increasing temperature.

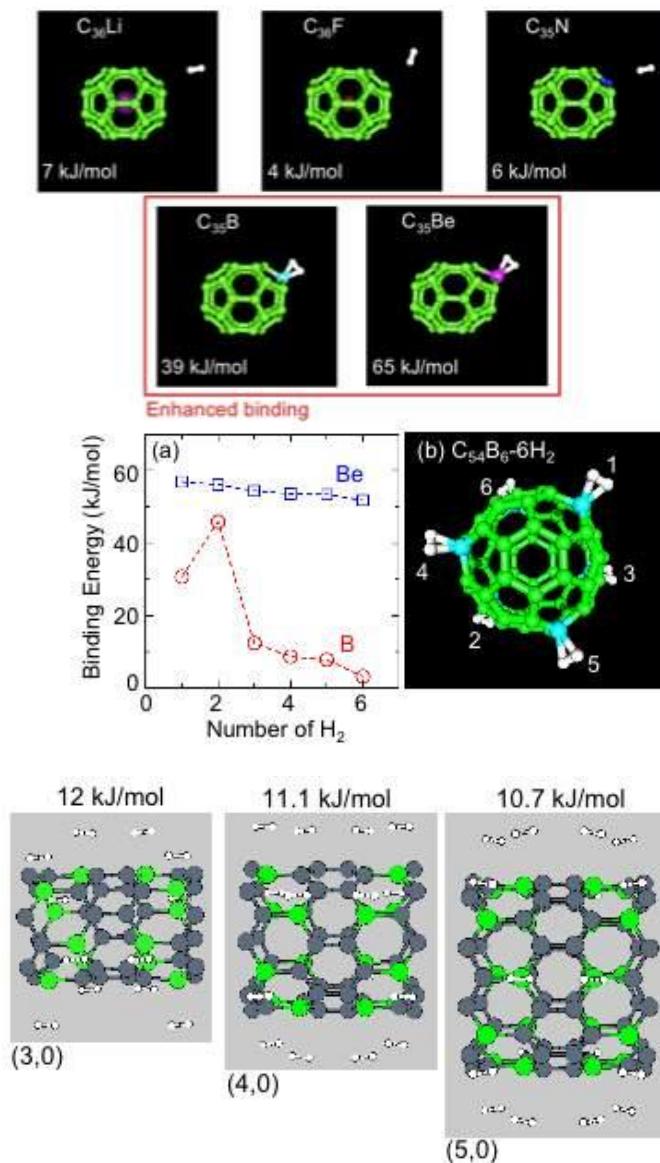
Similar to framework materials, porous polymers provide another set of crystalline materials with potential for hydrogen storage. Polymers have excellent thermal stability, tolerance to moisture and other contaminants, low skeleton density, and intrinsic porosity via covalent bonds and are capable of maintaining high SSA under the high pressures used in pelletizing for better volumetric density. Furthermore, they can be produced at the commercial scale with existing industrial infrastructure. Significant progress has been made in developing polymers as gas adsorbents (see for example McKeown et al. 2006 and Yuan et al. 2009)

Within the HSCoE, ANL in partnership with the University of Chicago focused on improving hydrogen uptake capacity and the heat of adsorption by enhancing SSA, porosity, and framework-adsorbate interaction through rational design and synthesis at the molecular level. ANL focused on improving the SSA of polymers and making porous polymers with narrow pore diameters. ANL also investigated adding “metallic” features, either through π -conjugation or metal substitution, to promote electronic orbital interaction with hydrogen. The SSAs and porosity were systematically adjusted using simple aromatic monomers with contorted cores and hyper-crosslinking chemistry. In addition, nanoporous polymers with monomers containing heterocyclic functional groups for better conductivity or polarizability were investigated. Through these efforts, dozens of different structures were synthesized and characterized. Porous polymers with SSAs as high as $\sim 1900 \text{ m}^2/\text{g}$ and tunable pore sizes from 0.6 to 0.9 nm were prepared. Additional work will need to focus on increasing the SSAs and hydrogen storage capacities further, and study the H₂-polymer interactions with high-pressure ¹H NMR measurement to determine the state of hydrogen in the micropores.

2.13.3 Substituted Materials

For most pure materials, or materials with electronic configurations that induce no significant adsorption, the primary adsorption mechanism is physisorption, which typically has enthalpies of $\sim 5 \text{ kJ/mol}$ for interaction with a single surface. Enhanced physisorption binding energies (i.e., 5 to 15 kJ/mol) are often observed with high-SSA materials. This is primarily a result of interaction with multiple adsorption surfaces that then limits the ultimate achievable capacity. Typically, increased binding energies, lower temperature, and/or higher pressures are required to overcome the intrinsic repelling

forces between dihydrogens to yield higher storage capacities on the sorbent surface at a specific temperature and/or pressure.



Surface curvature (sp^2 - sp^3 hybridization) affects the binding.

Figure 2-8. Calculations predict that only electronically frustrated B and Be substituted in carbon with correct coordination significantly increase H₂ binding (e.g., ~11 kJ/mol) and capacities at temperatures approaching ambient.

To go beyond pure physisorption requires enhanced electron interactions between the sorption material and dihydrogen. In general, heterogeneous elemental structures or surface functionalization can induce enhanced electron interactions. However, after relatively comprehensive investigations, very few material systems were identified with the potential to enhance dihydrogen binding (Kim et al. 2006; Chung et al. 2008). In general, the exchange of a different atom species in an elementally homogeneous lattice induces an electronic perturbation that may enhance dihydrogen binding. For example, the empty p orbitals on boron (B)-substituted [for] carbon induces electron donation from

H₂ to provide a reasonable enhancement in binding (i.e., 10 to 15 kJ/mol) and capacities. However, it was determined that only boron substituted with a sp² or similar coordination produced the enhanced dihydrogen binding. Other B-C or C-C coordination (Kim et al. 2006), the presence of other elements such as N in the lattice, or other (except for Be) substituted lightweight elements (e.g., Li, N, O, F, Na) in carbon lattices do not significantly enhance H₂ binding (Figure 2-8). Furthermore, in addition to needing to be in the correct coordination state, calculations predict that enhanced binding may occur only if the B remains both electronically and structurally “frustrated,” such that the B atoms are out of the plane of the carbon matrix, thus potentially expanding the lattice.

2.13.3.1 Predicted Heterogeneous Sorbents for Hydrogen Storage

For Li, although the volume of the cage is slightly increased, which is consistent with electron transfer from Li to the cage, there is no significant increase in the adsorption energy, $E_a = 0.07$ eV/H₂. The situation is worse for F where the electron transfer reverses its direction and the adsorption energy decreases to $E_a = 0.04$ eV/H₂. A substitutional nitrogen also has no advantage for H₂ adsorption. Here, $E_a = 0.06$ eV/H₂, with no sign that charge transfer between N and H₂ takes place. In contrast, H₂ binds to substitutional B or Be with significantly larger binding energies, i.e., calculations using LDA predicts ~0.39 and 0.65 eV/H₂, respectively. Highly accurate quantum Monte Carlo calculations predict 0.2 ± 0.05 eV/H₂ adsorption energy for C₃₅B-H₂. Although this value is about 0.2 eV/H₂ smaller than that from LDA calculations, it is still significantly larger than the vdW energy of about 0.04 eV/H₂.

To understand the enhanced adsorption of H₂ in doped fullerenes, the site-decomposed local densities of states for B and Be were calculated. For unbound C₃₅B-H₂, the doubly occupied H₂ σ state shows a single peak about 5 eV below the Fermi level, whereas the B p_z -like state shows two peaks about 1 and 3 eV above the Fermi level. The presence of this doublet is the result of a strong hybridization of B p_z state with carbon π -states. For bound C₃₅B-H₂, the H₂ σ state spreads out with two main peaks about 10 eV below the Fermi level, whereas the B p_z states move to higher energies. These level shifts are consistent with the notion that H₂ binds to B through an electronic hybridization. A similar hybridization is also seen for C₃₅Be-H₂. Because of a larger separation of the Be p_z state, the magnitude of the shift of the H₂ σ level (about 3 eV) is smaller than that of B. The models also show that the Be-H₂ coupling perturbs the carbon host states less than the B-H₂ coupling.

In contrast, no such hybridization was observed between H₂ and the other substitutional and endohedral impurities that were studied. This is understandable because in endohedral doping with species such as Li and F, there is no localized empty impurity state on the fullerene that the H₂ σ state can hybridize with. In the case of substitutional N, the p_z -like N lone pair is already doubly occupied. A hybridization with the low-lying H₂ σ state would increase its energy and is therefore not favored. In other words, the presence of a highly localized empty p_z orbital is essential for the non-dissociative adsorption of H₂ to doped fullerenes. It should be noted that although the initial calculation used fullerenes as a model system, as discussed below and shown in Figure 2-8, the results are similar for other B-substituted C systems like nanotubes, graphene, and even amorphous carbon.

More direct physical insights were obtained by examining the electron density difference, $\Delta\rho = \rho(\text{C}_{35}\text{X-H}_2) - \rho(\text{C}_{35}\text{X}) - \rho(\text{H}_2)$, where $\rho(x,y)$ is the planar electron density, integrated over the z direction (out of the plane in Figure 2-9) and $X = \text{B}$ or Be . Note that when calculating $\rho(\text{C}_{35}\text{X})$ and $\rho(\text{H}_2)$, the atoms are fixed in their respective final, relaxed positions in $\text{C}_{35}\text{X-H}_2$. The $\Delta\rho$ for B and Be indicate that the adsorption of H_2 causes significantly larger disturbance to $\rho(\text{C}_{35}\text{B})$ than to $\rho(\text{C}_{35}\text{Be})$. Noticeably, a new three-center bond forms between H_2 and B (Be), at the expense of a weaker H-H bond. The linear electron density, $\Delta\rho(x)$, from which was calculated the total amount of charge transferred from the ($x \geq 0$) region to the ($x \leq 0$) region where $x = 0$ corresponds to the position of H_2 , indicates that 0.21 and 0.12 electrons are transferred for B and Be, respectively. In the case of B, however, only about 29% = 0.06 electrons are directly involved in the three-center bond. In contrast, in the case of Be, the full 0.12 transferred electrons are involved in the bond formation. Therefore, E_a for Be is significantly larger than that for B. These observations are consistent with the notion that a highly localized p_z orbital is essential for non-dissociative adsorption. It leads to a smaller disturbance to the fullerene as evidenced by the smaller tail for Be, as well as a smaller disturbance to the H_2 as evidenced by the shorter H_2 bond length of 0.8 Å for Be versus 0.85 Å for B.

As shown in Figure 2-8, multi- H_2 sorption using C_{54}B_6 and C_{54}Be_6 were modeled. In the case of Be, the number of adsorbed H_2 has little effect on the adsorption energy (E_a) up to the sixth adsorbed H_2 . This is consistent with the analysis that Be states involved in the H_2 binding are more localized, and are hence less perturbed by the presence of other Be- H_2 subunits. In the case of C_{54}B_6 , E_a increases initially to a peak at $n = 2$ (about 0.47 eV/ H_2). After that, E_a decreases with n and reaches the minimum at $n = 6$ with an E_a similar to pure physisorption.

The multi- H_2 sorption was also calculated using C_{54}B_6 and C_{54}Be_6 . In the case of Be, the number of adsorbed H_2 has little effect on the adsorption energy (E_a) up to the sixth adsorbed H_2 . This is consistent with the analysis that Be states involved in the H_2 binding are more localized, and are hence less perturbed by the presence of other Be- H_2 subunits.

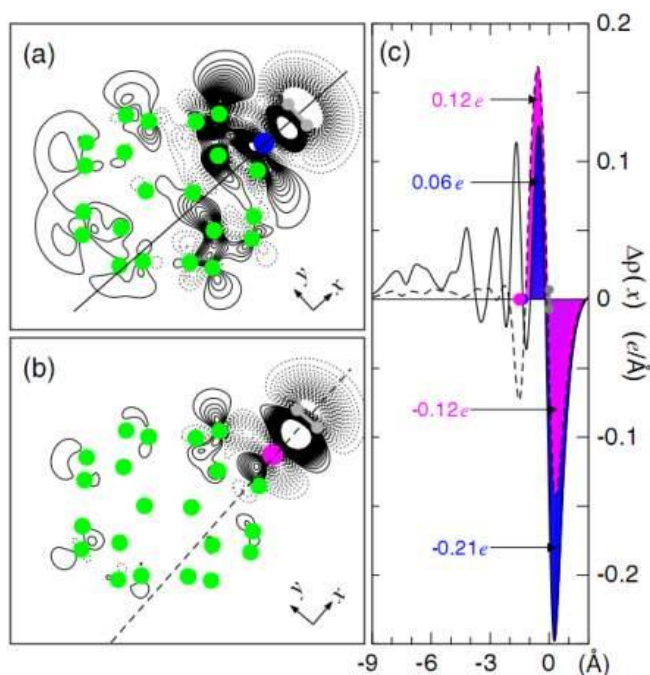


Figure 2-9. (a) and (b) are the differential planar electron density, $\Delta\rho(x,y)$, for B and Be, respectively. Solid and dotted contours indicate electron accumulation and depletion, respectively. The contour interval is 0.003 and the cutoffs are $\pm 0.08 e/\text{\AA}^2$. (c) Linear $\Delta\rho(x)$, for B and Be along the x axis shown in (a) and (b), respectively. The positions of the H_2 and B (Be) are indicated.

In the case of $C_{54}B_6$, E_a increases initially to a peak at $n = 2$ (about 0.47 eV/H₂). After that, E_a decreases with n and reaches the minimum at $n = 6$ with an E_a similar to pure physisorption.

2.13.3.2 Elucidation of Desired Sites

Boron substitution in amorphous carbon was investigated within the DFT-LDA method. Ten substitution sites were chosen in such a way that the boron is fully open to the pore space (see Figure 2-10). The binding enhancement due to B substitution was calculated for each of the different sites, and the results are shown in Table 2-3. As discussed above, the ability to substitute B in carbon nanotubes or cages is difficult, but the hydrogen binding enhancement is significant. However, in the amorphous carbon, the B can more easily be incorporated, but little to no enhanced H₂ binding occurs. Of ten boron substitution sites, only one can enhance H₂ binding and all the rest have similar binding energy to that of a pure vdW force field, i.e., 15.6 kJ/mol H₂, within the DFT-LDA method used here.

The structure of site 10 that enhances H₂ binding is shown in Figure 2-10(b). The reactivity of this site can be seen from the three four-member rings. Site 5 has a slightly smaller binding energy than the pure vdW binding energy, because the surrounding space is slightly narrow for a H₂ molecule.

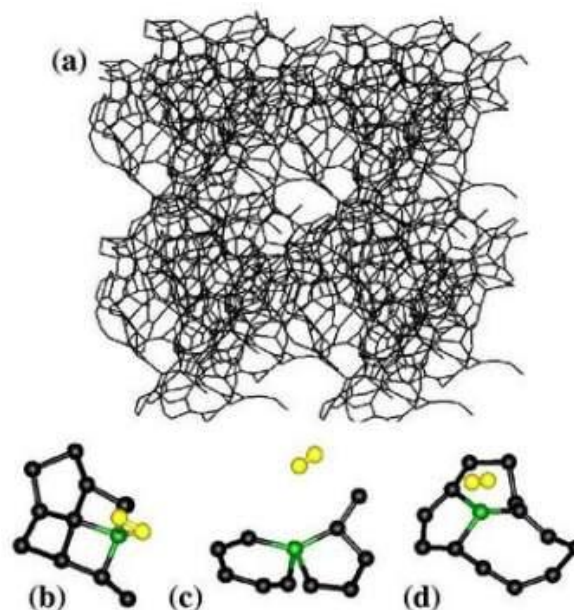


Figure 2-10. Modeled amorphous carbon with pore sizes of 1–2 nm (a), and H₂ binding after substitution with boron at different sites (b-d). Black, green, and yellow balls are carbon, boron, and hydrogen atoms.

Table 2-3. Formation Energy of Boron Dopants and H₂ Binding Energy in Different Sites of Amorphous Carbon

Sites	Formation Energy (eV)	H ₂ Binding
1	1.064	22.0
2	3.467	18.7
3	4.385	17.1
4	3.276	18.4
5	2.621	15.2
6	2.974	18.6
7	2.465	15.6
8	2.052	20.2
9	2.330	20.8
10	3.177	85.7

As discussed previously, these results apply only to hydrogen binding. Substitution of other elements may enhance binding of other gases or metals. For example, NREL identified that B substitution in C_{60} is essential to stabilize dispersion of transition metal atoms to create materials with hydrogen storage capacities of nearly 9 wt % at near-ambient temperatures (Zhao et al. 2005). Similar predictions were made by Penn State where boron substitution stabilizes the atomic dispersion of metal atoms on high-SSA BC_x materials. For example, titanium dispersed on a BC_x sheet obtains increased stabilization with increasing boron content (Figure 2-11). This general mechanism, which applies to several metals, provides a means to stabilize low-coordinate metal sites that are attractive for hydrogen storage and for catalysis.

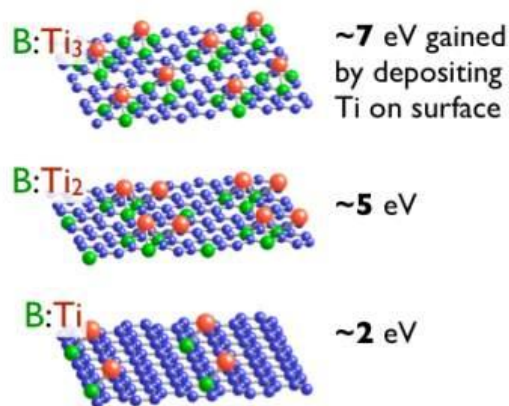


Figure 2-11. Calculations show that the increased amount of B substituted in carbon supports increases the stabilization of Ti atoms.

2.13.3.3 BC_3 Graphene Versus C Graphene

Following Zhang and Alavi (2007), APCI performed DFT LDA calculations to examine whether it is energetically possible to move H_2 molecules into bulk BC_3 through the edge planes. Given an equilibrated initial position for the H_2 molecule of about 3.5 Å away from the edge, the molecule was gradually moved (i.e., computationally) toward the slit pore, passing through the edge, and ending in a location between two B atoms of adjacent BC_3 layers in the middle of the selected unit cell. The potential energy increases as the molecule approaches the edge and reaches the transition state where the H_2 molecule is slightly activated (bond distance of 0.77 Å) at the edge of the BC_3 lattice. The c-axis spacing expands by 1.28 Å at the transition state to accommodate the H_2 with a slightly tilted horizontal orientation. Continuing on this pathway, the c-axis spacing increases by an additional 0.36 Å beyond the transition state spacing as the H_2 molecule orientation changes to a tilted vertical alignment with the BC_3 layers to interact more effectively with the two B atoms residing in the two adjacent layers near the edge. At this point, the H-H bond distance again increases slightly and the potential energy is reduced by ~10 kJ/mol from the transition-state energy. It is remarkable that the lattice parameter c, which is twice the interlayer distance, increases substantially to 8.44 Å from its initial value of 6.79 Å.

The potential energy continues to decrease commensurately as the activated H₂ molecule moves toward the center of the unit cell. The c-axis spacing then gradually decreases to nearly its original value. At the site of chemisorption, the H-H bond becomes significantly elongated and the two H atoms form covalent bonds with C atoms adjacent to the B atoms. The calculated C-H bond distance is 1.18 Å, which is considerably longer than the typical C-H bond found in most hydrocarbons. The apparently modest strength of this bond is due likely to the geometric bond angle strain on the C and B atoms next to the binding sites, imposed by the change of carbon atom hybridization from sp² to sp³ on forming the C-H bonds.

The overall calculated activation barrier for H₂ migration and dissociative chemisorption in bulk BC₃ is quite modest (~30 kJ/mol). Thus, it is expected that H₂ diffusion through the slit pore into the bulk BC₃ lattice would be facile at near-ambient conditions. This is in sharp contrast to the analogous process in graphite where H₂ diffusion from the gas phase into the bulk is known to be very difficult (Mitchell et al. 2003). Within the BC₃ lattice, the H₂ molecule is partially activated on arrival at the transition state, as evidenced by the elongated H-H bond distance. This quasi-dissociated state is maintained as the H₂ molecule continues its migration toward the center of the unit cell where the H-H bond is abruptly ruptured to form the C-H bonds. The relaxation of the C atom where H is chemisorbed is relatively modest, and the neighboring B atom moves out of the BC₃ plane toward the opposite direction of the absorbed H. The lattice relaxation on H absorption in BC₃ is significantly smaller than that for graphite, in which the C atom that forms a bond with H is puckered out of the plane by several tenths of an angstrom (Sha and Jackson 2002).

The LDA results suggest that H₂ diffusion into the slit pore of BC₃ is facile, and the intercalated H₂ will undergo spontaneous dissociation to form covalent bonds with C atoms. These C-H bonds might be sufficiently labile to allow the H atoms to diffuse throughout the lattice in a thermally activated process, which would make BC₃ a highly promising hydrogen storage material with good capacity and facile desorption kinetics. In particular, we note that BC₃ would be an ideal media to store hydrogen via hydrogen spillover. It should be more efficient than the materials that have been used as hydrogen spillover substrates to date, because it would require no metal catalyst to promote the release of storage hydrogen by the dissociation of molecular H₂. Thus, a critical issue is related to the reliability of the LDA calculations, because LDA is known to overestimate binding energies. Furthermore, because the intercalation of H₂ into the BC₃ lattice leads to H-H bond dissociation and C-H bond formation, GGA should be a more appropriate method to describe the energetics. In contrast to the exothermic process predicted by the LDA calculation, this process was found to be moderately endothermic by ~46 kJ/mol. The calculated energy barrier of ~60 kJ/mol is also higher than the value obtained with LDA. Nevertheless, both the GGA-calculated thermochemistry and the activation barrier are modest, suggesting that H₂ diffusion into bulk BC₃ and the subsequent dissociative chemisorption near the edge could be facile at near-ambient conditions.

2.13.3.4 Fluoride-Intercalated Carbon Materials

In gas-phase calculations, “naked” fluoride anions (Nyulasi and Kovacs 2006) and charge-separated ammonium fluoride salts (Trewin et al. 2008) have been shown to interact strongly with molecular hydrogen. Sweany et al. (1997) have reported an experimental characterization of adducts of H₂ with CsF ion pairs. The normally infrared-silent H₂ was perturbed by the salt, yielding spectra interpreted as arising from H₂ and CsF adducts, with as many as three H₂ molecules per CsF, whereas H₂ interacts primarily with the F⁻ anion. Based on frequency shifts showing a lengthening of the H-H bond, the interaction was attributed to the donation of electron density from the F⁻ anion to the H₂ antibonding σ^* orbital. APCI’s conceptual challenge was to devise solid-state materials that incorporate both the strong hydrogen interactions of naked fluoride and sufficient porosity. Chemical intercalation of graphite has been demonstrated to increase H₂ adsorption capacity by creating porosity through intercalation and separation of the graphene layers, as well as increasing the hydrogen affinity of the graphite through increased electron density. For example, the second-stage graphite intercalation complex KC₂₄ has been shown to adsorb 2 H₂/K at 77 K corresponding to 1.2 wt % H₂ (Watanabe et al. 1971). Electron transfer from K to the graphene layers in this “donor type” graphite intercalation compound (GIC) increases the heat of adsorption from -4 kJ/mol in native graphite to about -10 kJ/mol in KC₂₄. To date, there have been no examples of “acceptor type” GIC with a demonstrated appreciable hydrogen adsorption. Graphite fluorides represent a well-studied subset of acceptor GIC. A range of fluorination levels are accessible, and the nature of the C-F bonding evolves from ionic to semi-ionic to covalent as the decreasing C:F ratio approaches 1:1 (Perdew and Zunger 1981).

APCI conducted *ab initio* molecular dynamics (AIMD) simulations at RT on H₂ in a GIC containing fluoride anions and subsequently synthesized fluoride GICs for isotherm measurements. Upon F⁻ intercalation, significant lattice expansion (~2.3Å) occurs, based on the DFT structural optimization, and the intercalated F atoms form long C-F bonds with the graphene sheets. Compared to the typical C-F bond lengths in organofluorine compounds and perfluorinated graphite (~1.35Å), the C-F bonds in the partially fluorinated graphite GIC are considerably longer, ranging from 1.417 to 1.533Å. The significantly elongated, semi-ionic bonds arise from bond angle distortions resulting from the partial fluorination, as only some of the C atoms change their electronic configuration from sp² to sp³. As shown in Table 2-4, Bader population analysis indicates that the average charge (Q_F) on the F atoms ranges from -0.655 to -0.659. At low H₂ loadings, the spacing between adjacent graphene layers shrinks slightly, because the H₂ molecules interact more strongly with the semi-ionic F atoms (Table 2-4). At higher H₂ loadings, however, the interlayer distance increases substantially to accommodate the large number of H₂ molecules. A detailed analysis of the AIMD trajectories indicates that H₂ molecules in the lattice interact with the fluoride ions, but are highly mobile in the interlayer spaces at 300 K. The H₂ molecules are confined to the interlayer spaces between F atoms and are rarely in close contact with graphene sheets. No dissociative chemisorption of H₂ was observed in the entire course of AIMD simulations. These results suggest that the calculated average H₂ adsorption energy decreases as H₂ loading increases. At high H₂ loadings, the H₂-H₂ repulsion is largely responsible for the decrease of H₂ adsorption energy. At lower H₂ loadings, however, the simulation suggests that the average adsorption energy is substantially higher than those observed in most porous carbons.

Table 2-4. The H₂ Gravimetric Density, Calculated Lattice Spacing (d), Average Bader Charge on F (Q_F), and Average H₂ Adsorption Energy (ΔE) at 300 K

Complex	H ₂ (wt %)	d (Å)	Q _F	ΔE (kJ/mol·H ₂)
C ₃₂ F ₈		5.698	-0.659	
C ₃₂ F ₈ ·2 ₂	0.37	5.613	-0.656	-23.3
C ₃₂ F ₈ ·23 ₂	0.74	5.602	-0.655	-19.6
C ₃₂ F ₈ ·29 ₂	4.29	6.556	-0.657	-10.5
C ₃₂ F ₈ ·20 ₂	8.22	7.723	-0.656	-3.6

Based on these initial predictions and experimental results, the HSCoE partners developed scalable synthesis methods to form substituted and intercalated materials that demonstrate enhanced dihydrogen storage properties. Because Be has substantial health issues, B is the only lightweight element left to investigate for substitution in carbon. Potentially, heavier elements like phosphorous substitution in carbon may also provide enhanced hydrogen binding. In addition, the HSCoE partners developed anion-intercalated graphitic and other intercalated/functionalized materials with enhanced hydrogen storage properties. APCI's similar calculations for F-based systems were investigated as well, but subsequent experimental validation remains elusive. However, these experiments were only a very minor component of the HSCoE efforts.

2.13.3.5 Boron-Substituted Sorbent Synthesis

Boron substitution was achieved by either starting with chemical compounds with high concentrations of B and forming high-SSA materials, forming boron-substituted activated and graphitic carbons (e.g., BC₃), or substituting B for C atoms in preformed materials. The main challenge is being able to create materials with high substitution concentrations (>20 at %) and high SSAs (>1000 m²/g) with the substituted element in the correct electronic state. Because the specific concentration and SSA requirements depend on many factors including the binding energy, it is difficult to quantify the exact properties needed. As a general rule, as the binding energy increases, the more tightly the hydrogen can be packed on the surfaces, and thus the less SSA is required for a given temperature and pressure.

To form the requisite B-C materials, approaches similar to those discussed for creating high-SSA materials with optimized pore sizes were investigated. In general, pyrolyzation and templating of B-C precursors produced ~500 m²/g materials with ~15% B. However, materials with higher SSAs have lower boron concentrations. Attempts to sublime boron into carbon materials have not proven to be reproducible. Furthermore, most materials made to date demonstrate multiple binding states. This is probably because B goes into amorphous and other carbon coordinations more easily than sp² frameworks. However, it is the higher energy sp² coordination that has the greater electronic affinity and perhaps the structural stress needed for enhanced dihydrogen binding. Similarly, APCI investigated the use of F to enhance dihydrogen binding. The overarching goal of this work was to increase the isosteric heats of adsorption so that temperatures approaching ambient could be used for storage. Increasing the storage temperature reduces system costs and thus provides a potential path to meeting the DOE targets.

2.13.3.6 Pyrolysis of B-Containing Precursor

The Penn State group made significant advances in a precursor approach to preparing BC_x materials with controlled B content and morphology (i.e., surface area). The idea is based on the thinking that B has similar atomic size as C, and B forms a strong tri-valence bonding structure with C. Therefore, it is possible that B can be effectively substituted in the C (graphene) structure without significantly distorting its planar structure. In fact, there are some existing organoborane compounds that have similar B-substituted fused-ring structures. The key concept here is to design suitable B-precursors that can be thermally transformed into a fused-ring structure without losing the B and C elements. At the same time, the precursors must create a micro-porous structure with high SSA in the resulting BC_x material. It is highly desirable to have strong acidic B moieties (i.e., electron deficiency) in the resulting BC_x , which will engage in p-electron delocalization in the fused-ring structures and serve as p-type internal dopants to activate the surfaces and increase the H_2 binding energy.

Penn State designed and synthesized several organic and polymeric B-precursors and subjected them to pyrolysis to form BC_x materials. One successful example used poly(diethynylphenylborane chloride). In this B-precursor, the combination of alkynyl and B-Cl moieties is very favorable for inter-polymer reactions at low temperature (<150°C), which involve chloroboration and cyclization (2p + 4p electrons). The precursor changes color from white to brown and also increases its molecular mass without losing weight. Both reactions offer an important stabilization step to assure a high pyrolysis yield at high temperatures. Beyond 150°C, the precursor quickly deepens in color with the continuous evolution of HCl gas, which may be related to an electrophilic substitution on aromatic rings involving B-Cl moieties to incorporate B in the fused-ring structures. After an initial weight loss up to 400°C—which is due mostly to the HCl by-product—the weight loss becomes relatively small. At 600°C, the total weight loss is about 20%, which is close to the expected value when removing all H and Cl atoms in the B-precursor. PGAA indicated that the resulting porous BC_x material (after water-washing to remove LiCl salts) is composed almost entirely of B and C elements in a BC_{11} composition. This material has a 7.7 wt % of B, which is only slightly below the 8.4 wt % in the starting B-precursor (considering only B and C contents).

In addition, Penn State incorporated substitutional boron into high-SSA microporous carbons by pyrolysis of a blend of microporous-forming polymer precursors (polyfurfuryl alcohol) and boron-containing organic precursors (tetraethylammonium borohydride). The as-prepared pyrolyzed samples had 1–5 wt % boron incorporation. However, activation with CO_2 selectively removed some of the carbon, which increased the amount of boron to almost 23 wt % with a SSA of 1500 m^2/g . Isosteric heats of adsorption of ~10 KJ/mol were measured with these materials with a corresponding sorption capacity of 0.5 wt % at RT and 100 bar.

The results of similar experiments using different B-precursors and activation processes are summarized in Table 2-5. The B-precursors contained various inorganic salts (pore-forming additives) that were removed by water-washing after pyrolysis. For set A, the B content slowly decreases as the pyrolysis temperature is increased. The composition changes from BC_{11} at 600°C to BC_{13} and BC_{21} at 800° and 1100°C, respectively. As will

be discussed later, the evolution of the BC_x composition coincides with the development of a planar fused-ring structure and crystallinity. It is interesting to note that the composition becomes quite constant after 1500°C, with slightly more than 2 wt % B content, which is close to the reported maximum value of substitutional B content in the crystalline graphite structure obtained by high-temperature sublimation. The addition of external additives, such as $NaBH_4$, can significantly increase B content at a low temperature (600°–1000°C). However, after pyrolysis at 1500°C, the resulting BC_x materials also exhibit <3 mol % B content.

Table 2-5. A Summary of Porous BC_x Materials Prepared by B-Precursor Containing Inorganic Salts under Various Pyrolysis Conditions

Run No.	Pore-Forming Additives	Pyrolysis Temp. (°C)	B Content (wt %)		Surface Area (m ² /g)	Composition (BC_x)
			¹¹ B NMR	PGAA		
A-1	LiCl	600	7.7	7.7	780	BC_{11}
A-2	LiCl	800	6.4	6.0	528	BC_{13}
A-3	LiCl	1100	4.2	—	—	BC_{21}
A-4	LiCl	1400	3.5	3.7	—	BC_{25}
A-5	LiCl	1500	2.6	—	36	BC_{34}
A-6	LiCl	1800	2.2	2.0	—	BC_{40}
B-1	NaCl	600	6.5	—	634	BC_{13}
B-2	NaCl	900	5.2	—	—	BC_{17}
C-1	LiCl + $NaBH_4$	600	12.2	12.8	609	BC_6
C-2	LiCl + $NaBH_4$	800	10.4	9.2	—	BC_8

2.13.3.7 Templating BC_x and NC_x

APCI computational modeling results confirmed that B-substituted carbon would be effective as a hydrogen storage material by direct adsorption of hydrogen or as a hydrogen spillover receptor. Current methods of producing boron-substituted carbons have been moderately successful in increasing material surface area while incorporating high levels of boron substitution. However, a step-change increase in the surface might be realized with the application of templating methods to the existing B-precursor pyrolysis. Therefore, methods were developed to impregnate known precursors into porous silica materials and etch the silica with a minimal amount of boron loss. Researchers at NREL, Penn State, and APCI established methods to template BC_x on high-SSA carbons or silica zeolites. This templating reaction is based on previously developed thin-film BC_x synthesis procedures that use the stoichiometric reaction of benzene and boron trichloride to produce BC_3 (i.e., $2 BCl_3 + C_6H_6$ goes to $2 BC_3 + 6 HCl$) (Way et al. 1992). The generic formula BC_x is used for the resulting samples because non-stoichiometric conversion and the presence of the carbon template (in the case of activated carbon templates) ensures that the ultimate stoichiometry of the material is BC_x where x is >3. The reaction is performed in a chemical vapor furnace under flowing gas conditions. Typically, the BC_x material is chemical vapor deposited onto the template material substrate (e.g., Y-, β -, or MCM zeolite, activated carbon) at high temperatures (e.g., 900°C). If a zeolite template is used, the zeolite is etched away after BC_x deposition using a hydrofluoric acid etch, leaving behind a porous BC_x material with a geometric structure similar to the template material that was removed. Porous BC_x materials with boron content as high as 17 atomic percent (at. %) and SSAs ranging from

250 to 600 m²/g were synthesized with templating techniques. Isothermic heats of adsorption as high as 12 kJ/mol were observed for templated BC_x materials, demonstrating the viability of this technique to form sorbents with higher hydrogen binding energies.

2.13.3.8 Direct Assembly of B-Substituted Carbon

Boron substituted in SWNTs was synthesized either by arc discharge or pulsed laser chemical vapor synthesis. High-temperature arc synthesis of boron-carbon materials was studied by Penn State with electrode boron content ranging from 1 to 20 at. %. Raman scattering showed that boron-substituted nanotubes were produced for electrodes with less than 4 at. %, with lower nanotube fractions as B-content increased. Optical absorption shows a shift in the optical bands associated with transitions between valence and conduction bands, demonstrating that boron substituted into the sp² lattice lowered the Fermi energy, as desired. Inelastic neutron scattering at NIST of the rotational transitions of molecular hydrogen adsorbed on these nanotubes demonstrated enhanced binding for adsorption near the B-site at a magnitude consistent with that observed in studies on nanoporous BC_x produced by other methods.

NREL developed the first successful high-yield laser vaporization synthesis of high-quality boron-substituted single-walled carbon nanotubes (B-SWNTs). Boron was loaded into graphite targets in the form of elemental B or as nickel boride (NiB) and vaporized in a laser-oven apparatus in both Ar and N₂ atmospheres. While targets containing elemental B produced no or low yields of SWNTs, the NiB catalyst in N₂ produced SWNT bundles comparable in quality to the best pure carbon SWNTs produced from traditional Ni/Co catalysts. A variety of different samples were analyzed by TEM, Raman spectroscopy, XRD, NMR spectroscopy, and nanoprobe EELS. Using EELs, boron was found to be substitutionally incorporated in the SWNT lattice at content up to 1.8 at. %. The NiB catalyst was also used successfully to produce B-SWNTs by arc discharge.

2.13.3.9 B, N, and P Atom Substitution into Chemically Synthesized Graphene

Rice used solution-based chemistry to synthetically form substituted graphene materials. The general goal was to chemically form stable substituted graphene sheets with high substitution content, and then to use the graphene scaffolding processes Rice has developed for its optimized nanostructures work to form high-SSA materials with high substitution concentrations. The all-carbon and heteroatom-substituted synthetic graphenes were prepared using the procedures identified in the paper by Zhong and colleagues (2011). This included refluxing chloro-substituted organic reagents containing sp² carbon and chosen heteroatom precursors together with sodium in high-boiling point solvents, as shown in Figure 2-12. For the heteroatom-substituted synthetic graphenes, triisopropyl borate, triethylphosphite, and cyanuric chloride were used as the boron, phosphorous, and nitrogen sources, respectively. Alternatively, boron trichloride and phosphorous trichloride also could serve as boron and phosphorous sources, respectively. Two heteroatom precursors with different substitution elements can also be simultaneously added in the reaction system for the preparation of co-substituted products, such as boron/phosphorous and boron/nitrogen co-substituted synthetic graphenes. To remove residual salts and organic compounds completely, the filter cake is

washed, filtered, and dried. Initial efforts resulted in isosteric heats of adsorption of 8.6 kJ/mol for B-graphene with 5.4 at. % boron substitution; 8.3 kJ for P-graphene with 7.5 at. % phosphorous substitution, and 5.6 kJ for N-graphene with 13.5 at. % nitrogen doping. While the goal is to find routes to much higher substitution concentrations for boron and perhaps phosphorous, these initial results demonstrate that high (i.e., 25 at. %) sp^2 -coordinated substitutions can be achieved (e.g., with nitrogen), and the results confirm the original calculations that predicted that nitrogen substituted in carbon would not significantly increase hydrogen binding. As predicted, however, B substitution did increase hydrogen binding, and it appears that P does as well. These results also demonstrate the intrinsic issue of limited substitution for elements that appear to increase binding. Although the SSAs were still low, the hydrogen storage capacities of these materials were significantly higher than expected for typical activated carbon with similar SSAs.

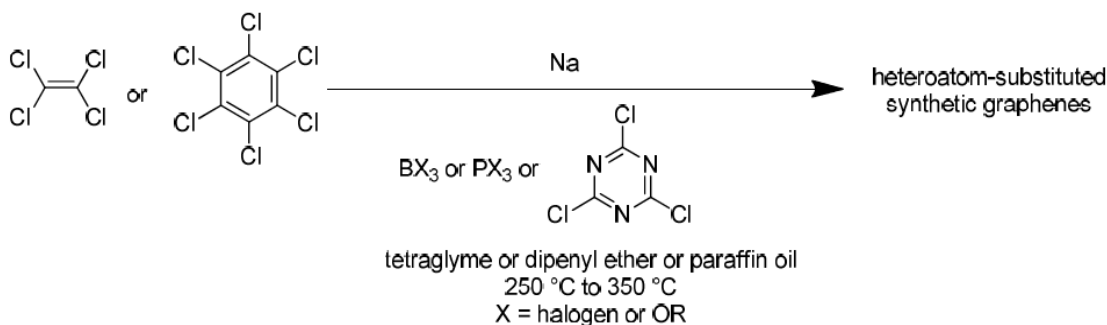


Figure 2-12. Schematic of bottom-up preparation of heteroatom-substituted synthetic graphenes by a solution-phase process. The all-carbon synthetic graphenes were prepared in the same manner, but with deletion of the boron-, phosphorous- and nitrogen-containing precursors.

2.13.3.10 Cross-Cutting Calculations for Substituted Materials

In general, the HSCoE explored many different materials and processes via calculations to efficiently identify viable paths to hydrogen storage materials that may be used to meet DOE targets. With regard to substituted materials, a few specific examples not discussed elsewhere in this report are summarized below.

Increased BC_x Binding from Curvature

Negative sheet curvature models of nanoporous carbons based on the Schwartzite structures (see Figure 2-13) were investigated by DFT under varying degrees of boron substitution, obtaining enhanced hydrogen binding energies of ~ 0.14 eV/mol within DFT. The combination of boron substitution, heptagonal carbon rings, negative Gaussian curvature, and pore size can induce these significant enhancements in hydrogen binding. The negative curvature induced by the heptagonal rings is important to activating the boron for increased hydrogen binding.

BC₃ as a Self-Catalyzing Spillover Material

Using DFT, APCI investigated the hydrogen storage properties of bulk BC₃. The minimum energy pathway to move H₂ molecules from the gas phase into the lattice through the edges of the layered, crystalline material was determined. In contrast to the large energy barriers for H₂ diffusion into crystalline graphite, APCI found that H₂ migration into bulk BC₃ is both thermodynamically and kinetically feasible. Unlike graphite, the c-axis spacing of the crystalline BC₃ can be expanded to accommodate H₂ molecules with only a modest barrier (~30 kJ/mol). Within the BC₃ lattice, H₂ will undergo dissociative chemisorption to form C-H bonds, which provides a chemical driving force for H₂ intercalation. The calculated H₂ chemisorption energies in bulk BC₃ based on the GGA suggest that the adsorption strength is modest, making the material a promising candidate for reversible hydrogen storage under near-ambient conditions.

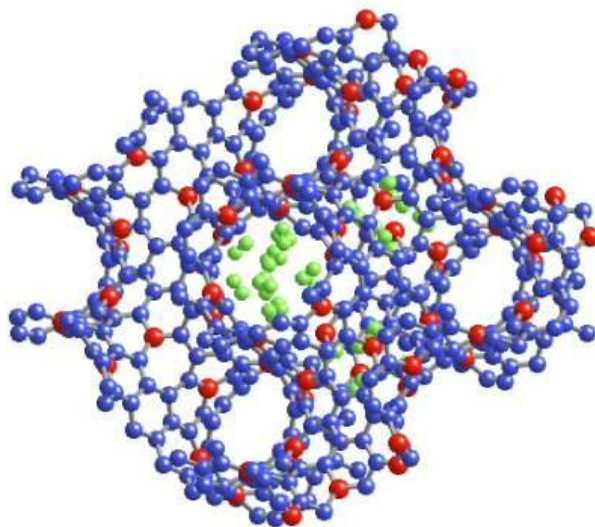


Figure 2-13. Example of a B-substituted structure (Schwartzite) with heptagonal carbon rings, negative Gaussian curvature, and small pore size that enhances hydrogen binding (blue is carbon, red is boron, and green is hydrogen)

Transition Metal Clustering with B Substitution

ORNL used *ab initio* spin density functional theory to investigate the energetics and kinetics of transition metal clustering on neutral, charged, and B-substituted fullerene surfaces. The formation energy and kinetics of sparsely dispersed zero-dimensional (0-D), compact single-layered two-dimensional (2-D), and clustered three-dimensional (3-D) transition-metal configurations were compared as a function of cluster size ($N \leq 12$). ORNL found that a Ti cluster's 0-D configuration is always less stable than that of 2-D and 3-D configurations, and 0-D to 2-D transformations involved in a single Ti diffusion process have a kinetic barrier of 0.7 eV. On the other hand, there exists a critical cluster size (N_C) of $N_C = 5$ (for Ti), below which 2-D layers are preferred to 3-D clusters. Hole or B substitution greatly enhances the Ti-fullerene interactions and lead to stronger dispersion of Ti atoms. Even so, for a moderate charge induced from substitution (less than seven holes), the critical size of Ti atoms on neutral C₆₀ surprisingly remains unchanged or only slightly increases to $N_C = 6$ with B substitution. However, the formation of 3-D clusters may be hindered by a high kinetic barrier related to the process of single Ti atoms climbing up a single Ti layer. This barrier is ~1 eV or even 1.47 eV for B-substituted C₆₀ surfaces, which is high enough to stabilize larger 2-D structures ($N \geq N_C$) at low temperatures.

2.13.4 Strong/Multiple Dihydrogen Interactions

2.13.4.1 Overview of First-Principles and Materials Design

To increase dihydrogen binding beyond that typically achieved with physisorption, more “chemical” type bonding must occur. In the case of dihydrogen, this means enhanced electron sharing between the gas molecule and the sorption material. This can only be achieved by creating structures in the material that are electronically out of equilibrium (i.e., reactive or frustrated). Unfortunately, this is relatively difficult and thus only a few approaches have been identified to work. As discussed above, sp^2 -coordinated boron sites substituted in a carbon lattice provide enhanced dihydrogen binding on the order of 10 to 15 kJ/mol. However, to increase the dihydrogen binding energy to >20 kJ/mol requires the use of materials with higher chemical potentials, such as metal-based materials. The HSCoE championed the use of coordinated metal centers to increase dihydrogen binding and to also enable multiple dihydrogen binding at a single adsorption site (Zhao et al. 2005). NREL’s seminal paper (Zhao et al. 2005) has been cited nearly 200 times, and theorists and experimentalists around the world have worked to iteratively design and synthesize new materials with coordinated metal centers. Furthermore, several of the metal-based materials designed by the HSCoE are able to bind dihydrogen in an optimum binding energy throughout their entire capacity range (Figure 2-14).

Recently, substantial amounts of work identified the unique properties of Ca for hydrogen storage (Ataca, Akturk, and Ciraci 2009; Kim, Sun, and Zhang 2009; Sun et al. 2009; Yoon et al. 2008). As discussed in more detail below, Ca coordinated in the correct manner may reversibly store more than 100 g/L and 10 wt % of hydrogen at ambient temperatures (Figure 2-14). This is substantially higher than liquid hydrogen and occurs at ambient temperature. Based on initial modeling from ANL, storage systems with more than 75% of the material capacities should be achievable under these conditions. Thus, these inexpensive materials that bind multiple hydrogen molecules per site could provide a reasonable path toward meeting DOE’s ultimate storage targets of 7.5 wt % and 70 g/L.

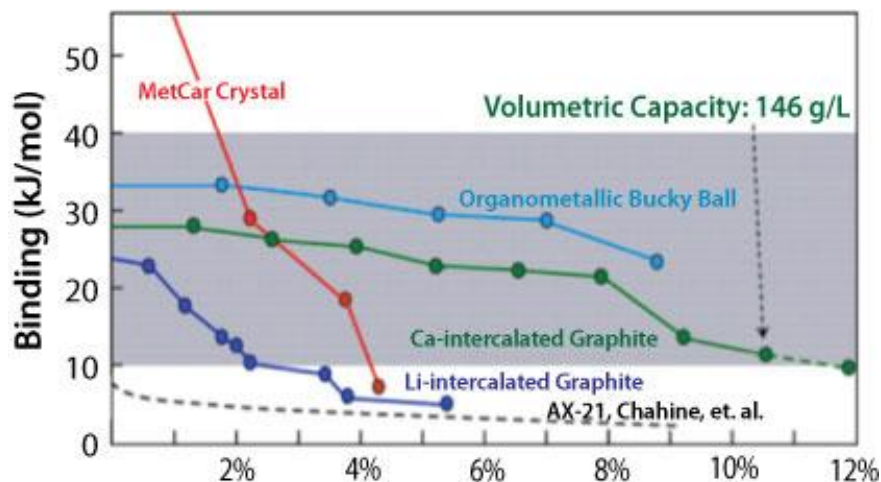


Figure 2-14. Examples of metal-based materials designed by the HSCoE that maintain optimum hydrogen binding energies (shaded area) throughout their entire H₂ capacity range

From the outset, the HSCoE strictly adhered to the criteria of synthesizing stable materials that have the potential to meet DOE hydrogen storage targets. Thus, the goal of the center's theorists was not only to identify new materials, but also to work with experimentalists to identify thermodynamically viable synthetic paths to form stable materials. A class of materials that can enhance dihydrogen binding was first identified by Kubas et al. (2007) and involved creating organometallic structures with transition metal centers that were able to coordinate a nearly intact H₂ ligand. Although initial work has demonstrated multiple H₂ adsorption to 5-D transition metal sites (Wang and Andrews 2002), the key findings since the inception of the HSCoE are that lightweight alkali, alkaline earth, and 3-D transition metals can be configured to enhance H₂ binding and perhaps lead to the binding of multiple (more than two) dihydrogen molecules to a single metal atom. As shown in Figure 2-14, materials containing a high density of metal sites that are structurally coordinated but electronically unsaturated may enable dihydrogen storage at ambient temperature. Interestingly, alkali and alkaline earth metal-based sorbents have small cohesive energies, and therefore, fewer tendencies to form metal clusters. Metal sites can be stabilized within framework materials (e.g., "exposed" metal sites in MOFs or Met-Cars) or on high-SSA supports with specific metal binding sites (e.g., boron-substituted sites in carbon materials). Metal clustering and reaction with other elements reduces or eliminates the enhanced H₂ capacities, and thus materials must be intelligently designed to stabilize (disperse) the metal atoms to maintain a high density of H₂ binding sites.

The main challenges associated with coordinated metal center approaches to hydrogen storage include being able to uniformly disperse these higher binding sites in such a way that they are accessible to the dihydrogen, are stable and do not degrade with time/refueling cycles, and provide relatively uniform dihydrogen binding throughout as much of the material storage capacity range as possible. This latter point is important from an engineering perspective so that the net available capacity can be maximized over as small a temperature and pressure range as possible, which reduces the overall system costs. Overall, the material systems that the HSCoE investigated fall into the following two general categories:

- Integration of metals into framework structures, e.g., Met-Cars or MOFs
- Coordination of metals to high-SSA supports, e.g., fullerenes or boron-doped activated carbon.

2.13.4.2 Effectiveness and Accuracy of Density Functional Theory for Hydrogen Adsorption

As discussed above, the use of transition metals for dihydrogen storage is well founded in experimental observation and basic electronic coordination chemistry. The key component developed by the HSCoE was the computational tools to predict accurately the coordination energies of dihydrogen with the different possible metal configurations. Initially, the HSCoE studied the well-known Kubas complex Cr(CO)₃(PH₃)₂, which is experimentally known to bind one dihydrogen with a binding energy of 80 kJ/mol. DFT calculations showed that only one dihydrogen was bound to the metal center with a calculated binding energy of 70 kJ/mol, closely matching the experimental value (Zhao et al. 2006). In general, DFT calculations have been widely used for modeling and

designing hydrogen storage materials. For strongly bonded systems, the accuracy of DFT has been well tested (Sun et al. 2010). For example, the cohesive energy of typical metal and semiconductor materials can be accurate to within 0.2 eV per atom (or 5%). When the systems involve primarily vdW interactions, however, the accuracy of DFT calculations quickly deteriorates because of the small magnitude of the interaction energy (which can be as small as 0.05 eV per atom). The DFT typically overestimates the vdW interactions in the LDA, but underestimates or even gives no binding in the GGA, which is due to the fundamental difference in their approximation of exchange-correlation effect.

For designed sorbents based on H₂ binding in between the vdW interaction and traditional chemical bonding (i.e., 0.15 to 0.50 eV/H₂), the accuracy of the DFT approach had to be determined by the HSCoE and others using the common approximations in the exchange-correlation functionals to estimate the interaction between the metal centers and dihydrogen. Initially, NREL selected four representative systems, namely Ti-ethylene (C₂H₄), Sc-cyclopentadienyl (C₅H₅), Ca-1,4-benzenedicarboxylate (BDC), and Li-1,4-BDC, which cover a wide range of sorbent materials proposed for high-capacity RT H₂ storage. Highly accurate calculations were performed at the MP2/cc-pVQZ level and further corrected the correlation energy at the CCSD(T)/cc-pVTZ level to obtain the dihydrogen binding energies on these systems. These accurate results were used to evaluate nine exchange-correlation functionals widely used in standard DFT calculations. The comparison (Table 2-6) indicates that the H₂ binding energy obtained with PBE and PW91 functionals are accurate to within a few hundredth of an eV/H₂, in the desired binding energy range for reversible hydrogen storage. These results demonstrate that DFT theory with the appropriate exchange-correlation assumptions can predict hydrogen storage properties of metal centers with accuracy.

Table 2-6. Comparison of the H₂ Binding Energies (in kJ/mol H₂) from the Nine Density Functionals with Accurate Benchmark Results

Method	Bench	LDA	PW91	PBE	BLYP	TPSS	B3LYP	B98	X3LYP	M05-2X
TiH ₂ (Et)(H ₂) ^A	34.6	100.4	38.0	36.3	22.1	27.4	25.4	27.5	28.1	36.7
TiH ₂ (Et)(H ₂) ^B	24.2	74.0	31.4	29.4	11.8	22.4	14.8	18.4	17.4	26.3
TiH ₂ (Et)(H ₂) ₂	33.5	73.1	36.6	34.8	20.7	27.4	23.6	26.1	26.3	34.9
TiH ₂ (Et)(H ₂) ₃	35.1	82.9	40.8	39.0	21.6	30.9	24.3	27.6	27.1	37.0
ScH ₂ (Cp)(H ₂) ^A	20.5	68.2	27.5	25.7	12.4	19.8	13.8	16.7	15.9	21.6
ScH ₂ (Cp)(H ₂) ^B	18.4	36.1	17.3	16.3	9.4	12.7	11.2	13.9	13.2	19.2
ScH ₂ (Cp)(H ₂) ₂	20.3	62.8	28.0	26.3	11.8	21.1	13.3	16.2	15.5	21.2
Ca(TPA)(H ₂) ₂ ^A	21.4	43.8	20.5	19.3	10.9	15.7	13.8	16.8	16.0	24.7
Ca(TPA)(H ₂) ₂ ^B	18.3	42.5	20.4	19.1	14.5	15.3	15.5	16.0	15.5	23.0
Li(TPA)(H ₂) ₂	15.4	25.1	14.3	13.0	7.6	10.7	9.3	11.8	11.1	15.1

2.13.4.3 Integration of Metals in Framework Structures

Metal-Organic Frameworks

As with the initial organometallic structures identified by Kubas (2007), the integration of metal centers into frameworks provides an excellent coordination environment for the metal that prevents agglomeration and migration of the metal. However, it is difficult to form structures in which the metals are electronically unsaturated and/or not sterically hindered, thus preventing hydrogen access. Organized framework materials offer one route to forming crystalline materials with integrated metal centers that are known to have enhanced H₂ binding sites. Numerous MOF materials have been synthesized that demonstrate isosteric heats of adsorption at low hydrogen coverage (between 5 and 10 kJ/mol), an effect that is attributed primarily to hydrogen metal centers interactions (Liu et al. 2008; Dinca et al. 2007; Liu et al. 2007; Dinca et al. 2006; Peterson et al. 2006; Prestipino et al. 2006). Within the HSCoE, NIST worked with groups around the world to study the metal-hydrogen interactions in MOFs using a suite of neutron-scattering tools. As stated above, several of the initial experimental studies demonstrated that exposed transition metal (TM) sites in framework materials have H₂ isosteric heats of adsorption of ~10 kJ/mol. This binding is significantly smaller than that observed in other metal-center hydrogen storage systems (Kubas 2001).

In collaboration with researchers at the University of Sydney, NIST investigated the nature of the unsaturated coordination sites in the Cu²⁺ carboxylate paddle-wheel building units in a HKUST-1 MOF. Powder neutron diffraction experiments were used to locate the hydrogen adsorption sites and conclusively verify that deuterium (D₂) initially binds to the Cu²⁺ metal ions in HKUST-1. The lower heats of adsorption (~5 kJ/mol) are correlated with hydrogen being associated more with the organic parts of the framework. The distance between the metal and the centroid of nuclear deuterium scattering (e.g., 2.39(1) Å for the Cu-based HKUST-1 MOF) is significantly reduced from that typically observed for vdW interactions. However, these hydrogen-metal distances are substantially larger (i.e., 1.7 to 1.9 Å) than those found in the well-known organometallic Kubas compounds where there is evidence for electron donation from the dihydrogen to transition metal and elongation of the H–H bond through back bonding. INS and first-principles computer simulations provide a detailed understanding of the local potential of para-hydrogen (*p*-H₂) adsorbed at the primary metal adsorption site. The form factors of the three main rotational peaks follow that expected for a free hydrogen molecule with a regular H–H intramolecular bond distance and provide evidence against a Kubas-type interaction. The form factors associated with the individual adsorption sites are characterized by differing Debye-Waller factors, reflecting the strength of the site-specific adsorption strengths. Three binding sites are progressively populated when the H₂ loading is less than 2.0 H₂:Cu, which is consistent with the result obtained from NIST's neutron powder diffraction experiments. The temperature dependence of the INS spectra reveal the relative binding enthalpies for H₂ at each site and compare well with the site-averaged volumetric adsorption values. Based on the calculated potentials using the DFT formalism and GGA functional, all of the features observed in the INS data were assigned for hydrogen adsorbed in HKUST-1. The orientational potential is slightly two-dimensional and dominated by a small Coulombic term, hence there is a tendency for the H₂ to lie in a plane perpendicular to the Cu-Cu bond. The in-plane rotation is almost free

and unhindered. The features observed at 9.1, 12.75, and 14.0 meV with increasing H₂ loading are due to rotational transitions from J = 0 to 1, M = ±1. The other features observed in the data are due to rotation-rotation or rotation-phonon excitations.

Another avenue was explored in a collaboration of two HSCoE partners, NIST and Caltech. Using neutron powder diffraction alongside isotherm measurements showed that H₂ adsorbed on the MOF-74 surface has a higher surface density at 77 K than that of solid H₂ at ≈ 4 K and zero pressure. These results revealed the shortest intermolecular D₂-D₂ distance observed in a physisorption-based material without the application of pressure. This high density can be attributed to the presence of coordinatively unsaturated Zn²⁺ centers that promote intermolecular deuterium distances of about 2.85 Å at 4 K. This observation, along with results from other systems with exposed metals that exhibit large surface adsorption densities, presents an avenue to increase the surface density of adsorbed hydrogen in this class of materials.

Ab initio calculations (see Figure 2-15) quantitatively account for the experimental findings described above, and further show that the splitting and occupation of the spin orbitals in MOF systems is why their binding energies for dihydrogen is smaller than expected for metal centers (Sun et al. 2007). However, these calculations also predict that if other transition metals are used (e.g., Sc, Ti, V, Cr, or Mn), the H₂ binding energy by the MOF metal centers can be tuned to between 10 and 50 kJ/mol. As yet, it remains unclear if standard framework materials can be designed with the metal in an appropriate state to enable back-donation.

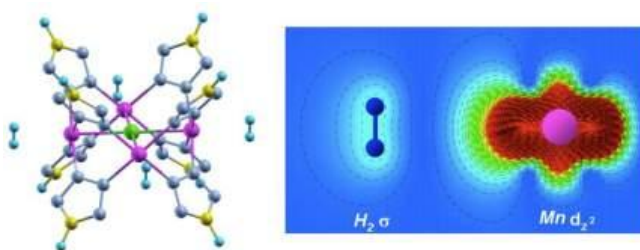


Figure 2-15. (Left) Simulated model for Mn-based MOF systems. Four H₂ molecules are adsorbed on the four Mn centers. (Right) Electron density plot of an anti-bonding state between the H₂ σ and Mn d_{z²} orbitals. These calculations quantitatively agree with experimentally measured binding energies and indicate that splitting and occupation of the spin orbitals reduces the binding.

Within the HSCoE, TAMU investigated ways to enhance H₂ uptake with framework materials by increasing the number of nearest-neighbor open metal sites of each H₂-hosting void in a 3-D framework and to align the open metal sites so that they could interact directly with the H₂ molecules inside the void. Based on this issue, different materials were synthesized (e.g., Cu-5,5'-methylene-di-isophthalate (mdip) MOFs termed PCN-12 and PCN-12') and characterized for their hydrogen-storage properties.

Metallo-carboranes and Macromolecules

In addition to materials such as MOFs, the HSCoE also performed limited investigations of other framework structures with well-defined metal centers. Again, clustering of metal atoms is a major issue associated with using metal centers for hydrogen storage. The most stable method to resolve this issue is to embed the metal atoms directly in structures. Structures like metallo-carboranes (Met-Cars; see Figure 2-16) and macromolecules (Figure 2-17) can be configured so that their metal centers are accessible to hydrogen molecules and sufficiently active to enhance adsorption. Met-Car molecules interact with each other strongly through their edges, which allow for the formation of rigid microporous crystals with appropriate pore sizes for H₂ adsorption. About 4 wt % H₂ can be strongly adsorbed at the metal sites in the Met-Car crystal shown in Figure 2-16, and as much as 3 wt % H₂ can be physisorbed. The total gravimetric and volumetric capacities are ~5–7 wt % and 40–50 kg/L, respectively. The biggest advantage of Met-Car crystals is their stability. Neither clustering of transition metal atoms nor collapsing of the frameworks occurs at extreme conditions. In addition, Met-Cars may be designed to be reversible dissociation hydrogen-storage materials (Zhao et al. 2006).

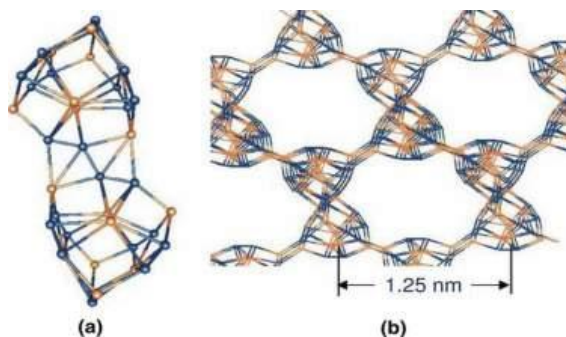


Figure 2-16. Structure of (a) a Met-Car dimer and (b) corresponding tetrahedral Met-Car crystal

Recently, oligocyclopentadienyl metal complexes were synthesized by Yu et al. (2006). Because cyclopentadienyl (Cp) rings are good supports for isolating transition metal atoms, Cp polymers functionalized with Mn atoms were predicted to make good hydrogen-storage materials with capacities predicted to be ~6.5 wt % and ~45 kg/m³ (Figure 2-17). Because a polymer structure is mechanically soft, clustering of the transition metal atoms on polymers may be an issue, especially when the polymers are small. However, if larger dendrimers are formed, the structural interlocking could stabilize the metal separation for efficient hydrogen storage. Similarly, ANL investigated integrating metals substitutionally into porous polymers using both replacement and direct *in situ* synthesis processes. These efforts were modeled after well-known metal-containing polyporphyrin materials, in which nitrogen-metal

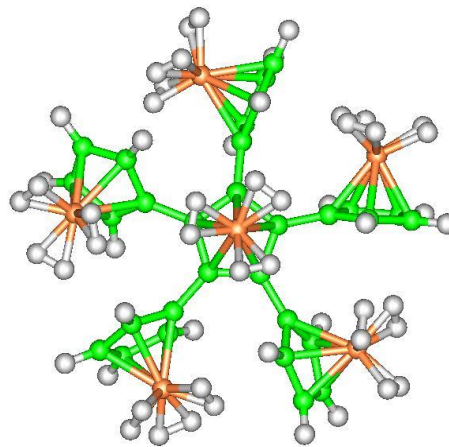


Figure 2-17. A Cp polymer decorated by Mn atoms (orange). Each Mn binds three H₂ molecules (white).

complexes form an integral component of the polymer structure. ANL performed this work and will continue developing these materials after the HSCoE ends as part of its continuing hydrogen-storage material development effort.

2.13.4.4 Coordination of Metals to High-Surface-Area Supports

Typically, metal centers in framework structures are sterically hindered and thus can adsorb one or at most two hydrogen molecules. To go beyond this limitation and enable adsorption of multiple hydrogen molecules to each metal site, single metal atoms must have additional access for the hydrogen molecules. However, this access must be balanced against the need to coordinate the metal atoms so that they are sufficiently immobile to prevent agglomeration and the formation of metal hydrides. Several groups outside of the HSCoE identified that metal integration with pure all-carbon supports can enhance dihydrogen binding (Ataca, Akturk, and Ciraci 2009; Sun et al. 2006; Yildirim and Ciraci 2005). The HSCoE explored this approach by investigating the effects of metal integration with several nanostructured all-carbon supports, including SWNTs, fullerenes, graphite, and graphene. In general, it is very difficult experimentally to integrate metals (both alkali and transition metals) with pure carbon supports and prevent metal agglomeration. Therefore, most of the experimental attempts performed by the HSCoE did not provide any definitive results nor confirm the theoretical predictions made by others outside the HSCoE. From these initial studies, it was clear that metal atoms must be bound to well-defined sites on a high-SSA substrate with precisely tuned energetics. However, initial work performed by NREL identified that alkali metal integration with nanostructured carbon materials induced hydrogenation of the carbon substrate and the formation of C-H bonds with substantially enhanced binding energies.

Metal Coordination to Fullerenes

Because of their commercial accessibility and well-controlled/understood properties, fullerenes (C_{60}) and SWNTs were initially used to investigate metal atom integration with pure carbons and their corresponding hydrogen-storage properties. Synthetic routes were identified to integrate Li, K, Na, Sc, Ti, Co, Cr, Ni, Fe, and other metals with the fullerenes. For example, K_6C_{60} is a well-known material (Andreoni, Giannozzi, and Parrinello 1995; Zhou et al. 1991). These materials were analyzed with NMR spectroscopy, electron paramagnetic spin resonance, Raman spectroscopy, TEM, EELS, and TPD, along with having their pore size, SSA, and hydrogen isotherm properties measured. In general, new reversible hydrogen adsorption sites consistent with hydrogen molecules bound with heats of adsorption significantly higher than physisorption were observed for many of the complexes. For example, TPD occurs at 235°, 230°, 180°, and 0°C for the Cr, Sc, Co, and Fe complexes, respectively. These desorption temperatures are below what is expected for chemisorption and therefore indicate that dihydrogen ligands are bound. In each of these cases, the total adsorption capacity is quite low.

In similar work, ORNL (Yoon et al. 2008) and others outside the HSCoE (Ataca, Akturk, and Ciraci 2009), identified that fullerenes (C_{60}) and equivalent graphene-based materials coated with calcium, respectively, may function as ideal molecular hydrogen attractors. Specifically, the resulting hydrogen uptake on $Ca_{32}C_{60}$ is predicted to be >8.4 wt % with a binding energy (i.e., 5 H_2 adsorbed at ~40 kJ/mol) that would allow for near-ambient adsorption. ORNL and NREL synthesized a series of Ca_xC_{60} (e.g., $x = 10, 32, \text{ or } 57$)

compounds either by Ca vapor deposition or by reacting C₆₀ in a solution of calcium in liquid ammonia. TPD and hydrogen pressure measurements indicated a moderate amount of low-temperature hydrogen sorption.

Solution-Phase Hydrogenation of Carbon Nanostructures

Nanostructured carbons can be hydrogenated by alkali metals via two distinct methods: the modified Birch reduction in ammonia (Borondics, Jakab, and Pekker 2007; Zhang et al. 2006; Zhang, Cao, and Chen 2003; Pekker et al. 2001) and the reaction with alkali metal naphthalides in tetrahydrofuran (THF) (Borondics, Jakab, and Pekker 2007; Borondics et al. 2005; Penicaud et al. 2004). In both cases, the reduced carbon materials undergo a limited hydrogenation via a reaction with methanol. In contrast, NREL discovered that significant amounts of hydrogen (~4 wt %) could be stored on reduced nanostructured carbon materials in the presence of cyclic ether solvents. The generation of a highly reactive nanostructured carbon radical anion is able to remove the acidic α -proton on THF, similar to the behavior observed for butyl lithium reagents (Bates, Kropskai, and Potter 1972; Carnahan and Closson 1972). The hydrogenation process is reversible, with the nanostructured carbon materials regenerated after dehydrogenation to 550°C as evidenced by Raman spectroscopy and TEM. The dehydrogenated materials can then be rehydrogenated to the same gravimetric level using the same solution-phase procedures developed by NREL.

Metal Intercalation in Graphite Compounds

To bridge the gap between theoretical predictions and experimental synthesis, the HSCoE worked to identify materials that could be easily designed and synthesized. For example, alkali metal intercalation in graphite produces well-known materials with well-established synthetic routes and hydrogen-storage properties (Goldman et al. 1989; Enoki et al. 1983; Watanabe et al. 1973). Dihydrogen molecules can be adsorbed directly in K-, Rb-, and Cs-intercalated graphite when the temperature is lower than 200 K. At temperatures >200 K, the hydrogen molecules dissociate into atomic hydrogen. The hydrogen concentration can be H₂/alkaline metal atom (Enoki et al. 1990). In general, the intercalated alkali metals are integrated as single metal atoms between the graphene planes, enabling sufficient space for physisorption of dihydrogen on the graphene surfaces and also inducing higher binding of dihydrogen because the metal-graphene coordination significantly reduces the propensity to form hydrides. These materials provided a model system that demonstrated how to achieve uniform isosteric heats of adsorption for the entire capacity of the material, and how alkali metal atoms, which like to form hydrides, can be sufficiently coordinated with a support to enable reversible dihydrogen storage.

To go beyond the limited capacities of the alkali metal-intercalated graphite materials, NREL investigated methods to intercalate metals and create large spaces for hydrogen adsorption. NREL identified that cointercalated graphite with Li and small organic molecules, such as benzene and tetrahydrofuran, could create stage 1 (intercalation between every layer of graphene) materials, with the interlayer graphene distance predicted to be ~7.7 Å (Figure 2-18). The increased space permits multiple H₂ species to be bound to Li cations with a predicted binding energy of 10~22 kJ/mol. Furthermore, in the interstitial area free of Li cations, the negative charge in the graphene sheets is

predicted to enhance the H₂ binding energy to ~9 kJ/mol through electrostatic attraction. To restrain nucleation of lithium hydrides, the Li array was limited to a Li₄(THF)C₇₂ structure, which is predicted to reversibly store ~3.4 wt % hydrogen (Zhao et al. 2008).

Figure 2-18 is a graphical representation of a designed co-intercalation graphite compound, in which Li and THF are co-intercalated to form Li₄(THF)C₇₂. Similar to the previously reported Li₁₂C₆₀ compound (Sun et al. 2006; Kohanoff, Andreoni, and Parrinello 1992), the intercalated Li atoms serve to stabilize dihydrogen species with binding energies that are enhanced relative to pure physisorption. The THF co-intercalant molecule plays two roles: it both prevents clustering and expands the graphite lattice to allow for H₂ adsorption. The Li₄(THF)C₇₂ co-intercalation compound has a reversible capacity of 3.4 wt % for H₂ coordinated with Li, resulting in enhanced binding energies of 9~22 kJ/mol H₂. The total hydrogen uptake capacity of the simple system is 5.7 wt %. This includes an additional 2.3 wt % of physisorbed H₂ that is not interacting directly with the Li atoms and is adsorbed with a binding energy of ~5 kJ/mol H₂.

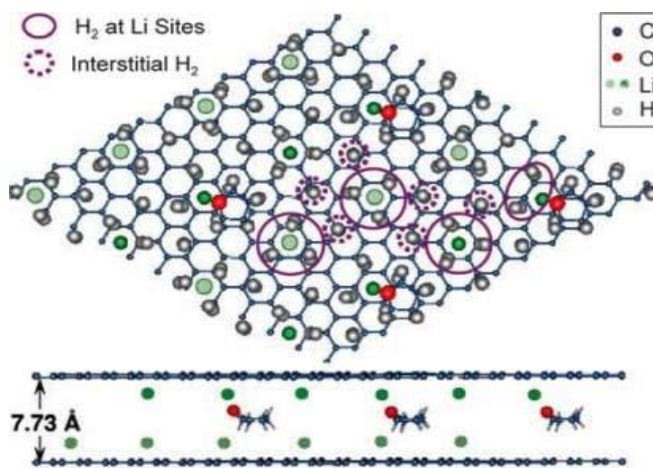


Figure 2-18. Design of a co-intercalated-graphite compound, in which Li and THF are the co-intercalation species

As mentioned above, the integration of single metal atoms with pure all-carbon materials has proven very challenging. Most materials synthesized to date are only marginally stable, and thus positive results have been limited. To improve metal coordination, and thus the stability of the metal atoms, higher-energy binding sites must be incorporated into the substrates. High-SSA carbon substrates with specific functional groups, including boron-substituted carbon materials, were developed and designed to provide well-defined reaction sites for metal atoms.

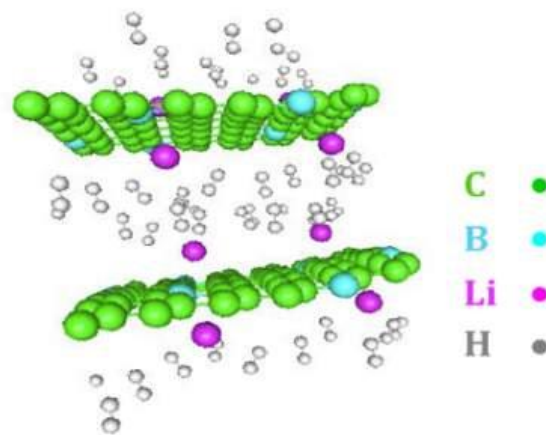


Figure 2-19. H₂ storage in Li-intercalated BC_x graphite

In addition to increasing the hydrogen binding energy, heterogeneous materials such as boron-substituted carbons can stabilize single metal atoms. For example, boron-substituted carbon materials with sp^2 -coordinated boron sites have the potential to stabilize Li atoms (Figure 2-19). As shown in Table 2-7, the addition of these new boron sites within the graphitic carbon materials leads to an increase in the non-clustering Li density. These NREL predictions also indicate that the B enhances charge transfer, and therefore enhances the overall hydrogen binding strength such that each Li atom may be able to store as many as three H_2 molecules. For a 1/18 Li density in the B-substituted graphite system, 4.98 wt % hydrogen molecules can be adsorbed with a binding energy of 6~19 kJ/mol (Figure 2-20). Alternatively, for a Li density of 1/9, the binding energy becomes smaller (5~14 kJ/mol), but the H_2 capacity goes as high as 7 wt %.

Table 2-7. Total energy (eV, in red) of metal-clustered structures relative to the metal-dispersed structures and nearest Li–Li distance (Å, in blue). It is demonstrated that Li-clustered structures become energetically more favorable at $Li_{10}C_{66}B_6$.

	$Li_4C_{66}B_6$	$Li_6C_{66}B_6$	$Li_8C_{66}B_6$	$Li_{10}C_{66}B_6$
Cluster	1.7/5.2	2.3/3.2	0.49/2.8	-0.26/2.4
Dispersed	0/7.4	0/6.1	0/5.7	0/5.1

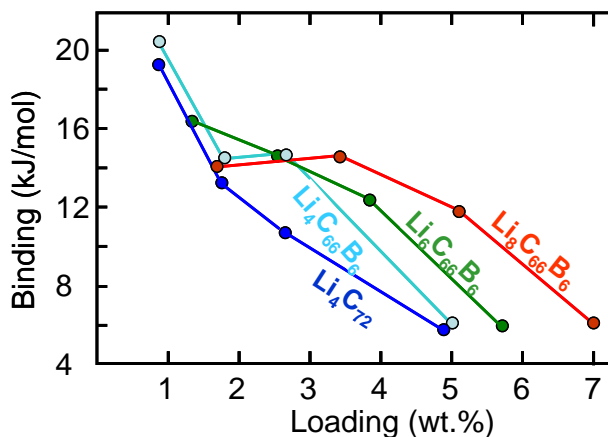


Figure 2-20. Binding energy vs. capacity. Hydrogen binding energy versus loading in intercalated graphite with and without B doping.

Metal Coordination to Functionalized Substrates

As discussed above, the HSCoE investigated a variety of methods to coordinate metal atoms to substrates and concluded that it is synthetically challenging to avoid metal agglomeration (clustering) in all carbon frameworks. The metal must be bound to well-defined sites on high-SSA substrates. Therefore, the HSCoE investigated synthetic methods for tailoring the surface chemistry of the substrates by incorporating functional groups on the surface that would coordinate transition metals. For example, phosphines ($-PR_2$), amines ($-NH_2$), and thioethers ($-SR$) have all been used to stabilize metals. The phosphine ligands are of particular interest as these ligands have been used in Kubas complexes that have been shown to reversibly bind dihydrogen. NREL and LLNL

developed reaction pathways to provide well-defined, site-specific binding of transition metal complexes to high-SSA supports. The metal binding sites were integrated into the skeletal network of the aerogels either through the addition of monomer(s) containing the organometallic ligand to the sol-gel reaction or through surface modification of the aerogel network. Anchoring of these complexes to the inner surfaces of a low-density, high-SSA framework was used to fabricate solid-state hydrogen sorbents. The aerogel architecture possesses a number of desirable structural features for the fabrication of these supports, including high SSAs, tunable porosities, and low mass densities. In addition, the flexibility of aerogel synthesis can be used to appropriately functionalize the inner surfaces of these materials for the specific ligands. An example of a procedure to form a hydrogen storage material using metal-stabilizing ligands integrated with aerogels is shown in Figure 2-21. Here, the stabilizing ligands (L) on the transition metal (M) must be easily displaced in the presence of H₂ or by external processing controls such as heat or UV light. Using these techniques, NREL and LLNL investigated the use of high-SSA aerogels as supports for organometallic species capable of reversibly storing H₂ molecules.

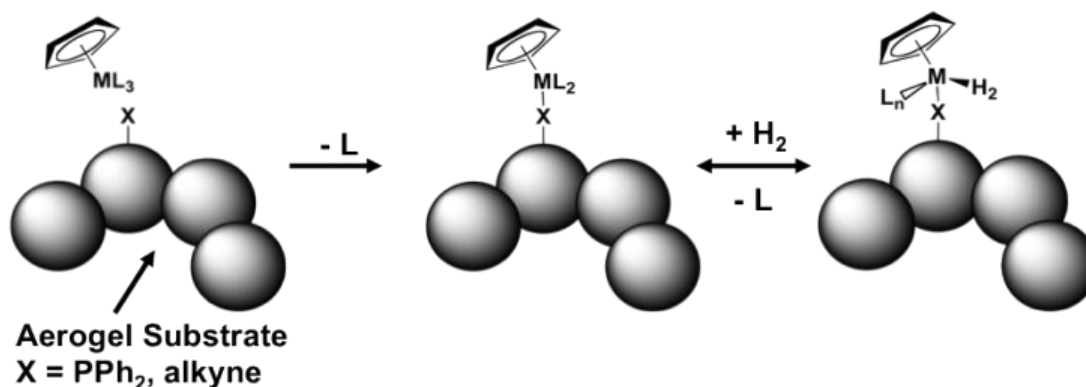


Figure 2-21. Concept for synthesizing transition metal-decorated aerogel supports

Similar to the aerogel work, NREL and Rensselaer Polytechnic Institute (RPI) identified that GO can stabilize metal centers for hydrogen storage (Wang et al. 2009). Here, the functionality of the GO material provides sites for the covalent attachment of TM atoms that have the potential to accommodate multiple H₂ molecules. This work was analogous to that reported by Hamaed and coauthors (2008), in which organometallic Ti fragments were coordinated to amorphous-silica via strong Ti-silanol bonds (i.e., ~400 kJ/mol). In the metal-decorated GO materials, oxygen functional groups are key in anchoring the metal atoms and enhancing the metal substrate binding. Zhang and coinvestigators reported that Ti atoms grafted on GO could bind multiple H₂ ligands with the desired binding energies (14–41 kJ/mol H₂) (Wang et al. 2009). NREL developed a successful reaction pathway to synthesize Ti-GO using a solution-phase chemistry process, which resulted in new enhanced H₂ binding sites.

In general, the HSCoE investigated a number of strategies to coordinate single metal atoms to substrates including gas-phase synthesis techniques. In addition to solution-phase chemistries, NREL developed novel synthetic gas-phase processes to create structures in which TM hydrides are partially coordinated on lightweight, highly porous,

activated carbon supports known to have oxygen functional groups. The synthetic processes involved organometallic precursors mixed with porous activated carbon and heated in flowing hydrogen. Non-toxic, non-flammable, and low-reactivity organometallic precursors containing Fe, Co, V, and Sc were used. The results of these investigations are provided in Section 3.0 (Results) of this report.

2.13.4.5 Unique Properties of Coordinated Ca Metal Centers

The HSCoE was the first to identify the unique properties of the inexpensive metal calcium. NREL applied its unique predictive metal- $x\text{H}_2$ theories to investigate the hydrogen-storage properties of groups I and II metals. Unlike Li, Na, and Mg, Ca can be coordinated to matrix materials in such a way that a pseudo 3-D band state forms, enabling substantial amounts of dihydrogen to be reversibly adsorbed (Kim, Sun, and Zhang 2009). For example, Ca-intercalated graphene, with the graphene layers separated sufficiently to allow dihydrogen molecules access to the Ca atoms, has the potential to have net hydrogen capacities in excess of 100 g/L and 10 wt %. In this case, the carbon-graphene layers stabilize the Ca atoms, and the Ca binding energy is relatively small, 50–90 kJ/mol. Furthermore, the Ca atoms adsorb dihydrogen at 20–40 kJ/mol. The Ca-C binding and charge transfer are sufficiently strong to prevent Ca clustering; they become weaker as more dihydrogens adsorb. The Ca- $x\text{H}_2$ binding is sufficient to store and release dihydrogen at densities much higher than liquid hydrogen, but at ambient temperatures and moderately low pressures (i.e., 4 to 30 bar). Even though the synthetic pathways remain a challenge, this set of work provides a breakthrough that clearly defines sorbent materials that could be used to meet DOE's ultimate storage targets.

In addition to the initial Ca-graphene work, NREL also found that graphitic B-C and some covalent organic framework (COF) and MOF materials stabilize open Ca centers. In the case of COFs, two Ca atoms are bound to benzene linkers at ~120 kJ/mol, which in turn will adsorb four dihydrogen molecules with an average binding energy of 15 kJ/mol. Although this particular material will have a hydrogen storage capacity of only ~44 g/L and 5.6 wt %, theorists and experimentalists have worked together to identify materials with viable synthetic pathways.

2.13.4.6 Coordinated Metal Centers for Storing Hydrogen

The use of coordinated metal centers for hydrogen storage is based on the unique properties of the TM d -orbitals. In simple metal atoms, the d -orbitals are either completely filled or very high in energy. In contrast, TM atoms usually have low-lying d -orbitals, which are partly occupied in most free TM atoms, and the energy differences between the occupied and empty d -orbitals are not large. This gives rise to unique properties (e.g., magnetic) of TM materials. For example, Kubas and others (see for example Kubas 2001) identified that the empty d -orbital(s) have a strong ability to accept external electrons because they are below the vacuum level. On the other hand, the occupied d -orbital(s) are ready to donate electrons. Consequently, the mechanism loosely termed “Kubas coordination” (Kubas 2001) can be described as two components of charge donation or nonclassical orbital hybridization (Figure 2-22). Here, the hydrogen molecule donates a fraction of electrons in its bonding state (σ) to the empty d -orbital of the TM atom, and the total energy is lowered because the two electrons in the hydrogen

molecule now occupy a lower orbital hybridized from σ and d^{empty} . This in turn pulls the anti-bonding H_2 state σ^* down to $\sigma^\#$, which helps the partial back-donation of an electron from a filled d -orbital (d^{fill}) to σ and further lowers the total energy. These two components of hybridization stretch the H-H bond, but the hydrogen molecule remains undissociated (i.e., dihydrogen). Quantitative decomposition of dihydrogen binding energy into the two components is possible within the charge decomposition analysis (Dapprich and Frenking 1995) or extended transition state analysis (Li and Ziegler 1996).

The key to dihydrogen binding is a localized empty orbital, which is below the vacuum level and has an affinity for the bonding electrons of a H_2 molecule. The lower the empty orbital, the more favorable is the formation of a dihydrogen complex. In general, the empty orbital does not have to be a TM d -orbital. For example, positive simple-metal ions can also bind dihydrogen (Lochan and Head-Gordon 2006), because the lower bonding orbital(s) is now empty. Without back-donation, the three-center, two-electron (3c-2e) coordination is already completed. Actually, the 3c-2e coordination is only rigorous when there is no back-donation, because back-donation involves more (than 2) electrons occupied in another orbital. Back-donation takes advantage of lowering of σ^* due to donation of σ charge, adding to the dihydrogen binding. But if the back-donation is too strong, eventually the H_2 molecule will split (dissociate) to form hydrides. The dihydrogen-dihydride transition depends on the energy levels of the occupied and empty d -orbitals and their separation. The higher the d -orbitals and the smaller the separation between the empty and occupied d -orbitals, the more easily the transition happens (Tomas, Lledos, and Jean 1998).

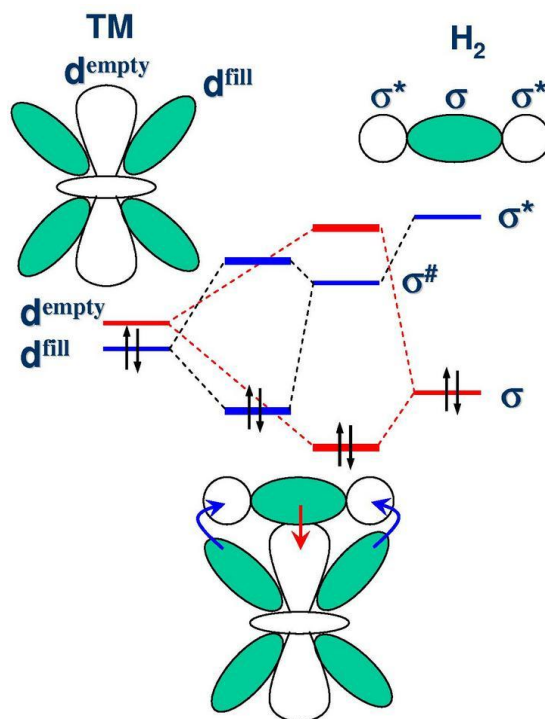


Figure 2-22. Mechanism for Kubas coordination. The shading (green) represents charge density. Donation and back donation are denoted in blue and red, respectively.

The above mechanism explains why simple metals only form hydrides: (1) simple metals do not have low-lying empty orbitals, and therefore do not satisfy the condition for 3c-2e coordination; and (2) simple metals have a very strong tendency to “back-donate” all of their valence electrons to hydrogen. For the TM elements close to the simple metals in the periodic table (e.g., Sc), hydride formation is also highly favorable. However, after using up all valence electrons to form hydrides, the TM atom still binds dihydrogen with its empty *d*-orbital(s) (Zhao et al. 2005). The TM atoms to the right of the periodic table bind dihydrogen more strongly, because they have sufficient valence electrons for back-donation, yet their valence electrons are not radical enough to split the H₂ molecule. In this case, the binding energy of dihydrogen could be larger than 100 kJ/mol, which is good for static observation of the dihydrogen identity, but too strong for reversible hydrogen storage at near RT.

Experimentally, multiple dihydrogens interacting with a TM center were observed in gas-phase cluster measurements nearly 20 years ago (see Bowers 1994 and the references therein). Here, H₂ binding energies ranging from 20 to 40 kJ/mol were observed for the five and six H₂ bound to Sc⁺ and Ti⁺ metal centers, respectively. This agrees very well with the theoretical calculations. Recently, an experimental group observed four H₂ bound to WH₄ via infrared spectroscopy (Wang and Yang 2008), also in good agreement with DFT calculations made by HSCoE. Very recently, Ti atoms have been successfully dispersed on an amorphous silica surface, using strong Ti-silanol bonds. On average each Ti center was found to bind 2.7 H₂ molecules with a binding energy of 22 kJ/mol H₂ (Hamaed, Trudeau, and Antonelli 2008).

2.13.5 Weak Chemisorption/Spillover

The HSCoE also investigated methodologies to store dissociated hydrogen molecules (e.g., hydrogen atoms). Unlike the work discussed previously to increase binding for dihydrogen, the key issue was actually developing ways to store dissociated hydrogen with binding energies substantially lower than what is typically observed for hydride formation. For example, initial work involving endohedral fullerenes indicates that appropriate energies can be achieved to reversibly hydrogenate and dehydrogenate these materials (Zhao et al. 2007). Additional development is required to fully demonstrate these type of materials experimentally and to investigate kinetics and capacities limits. Among the more promising material classes, the HSCoE demonstrated that catalyzed hydrogen molecule dissociation followed by “spillover” (Figure 2-23) onto lightweight receptor support materials enabled ambient-temperature storage with binding energies in the range of 10 to 25 kJ/mol. Although the phenomenon of spillover has been known for many decades, the HSCoE partners demonstrated that this material class could be used to store substantial (>30 g/L and >4 wt %) amounts of hydrogen at near-ambient temperature and nominal pressure. The HSCoE demonstrated spillover both experimentally and by thermodynamic principles as a process for ambient-temperature, reversible hydrogen storage. However, the materials have tended to be very sensitive to synthetic processing conditions, resulting in substantial irreproducibilities. Furthermore, the intrinsic nature of the spillover storage mechanisms makes hydrogen refill rates, material stability/durability, and intrinsic material costs challenging issues that must be adequately resolved. Nonetheless, once these issues are addressed, initial analyses

indicate that storage systems with more than 75% of the material capacities could be achieved. Because the potential spillover material storage limits are ~80 g/L and ~8 wt %, and ultimately fill rates, materials costs, and durability are tractable issues, this mechanism may provide a means to meet DOE's 2015 targets.

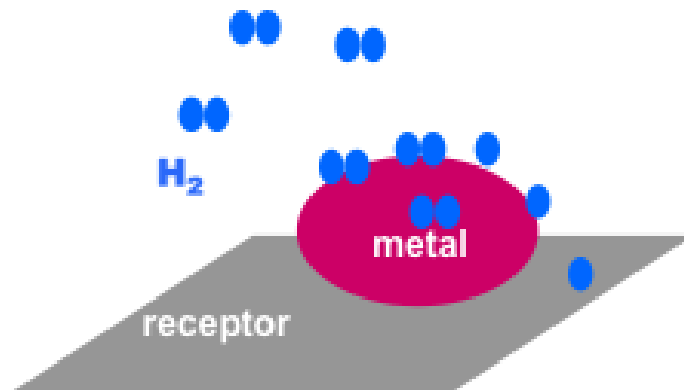


Figure 2-23. Conceptual diagram of hydrogen spillover processes. Reversible RT hydrogen storage on metal-doped carbon materials via a “spillover” mechanism involves a series of steps: (a) molecular H₂ dissociates on the metal catalyst particles; (b) atomic H migrates to the receptor; and (c) atomic H diffuses across the receptor surfaces.

Spillover is a process that dissociates dihydrogen onto a metal catalyst, followed by migration of hydrogen atoms onto the surface of a receptor material and subsequent diffusion away from the catalyst site, which leads to significant storage of hydrogen (see, for example, Li and Yang 2007; Lueking and Yang 2002). The concept of hydrogen spillover has its genesis in fundamental studies with heterogeneous metal catalysts, particularly with the type of systems used for chemical hydrogenation reactions (Conner and Falconer 1995). Within catalytic processes, the metal has the role of "activating" hydrogen by reversibly dissociating H₂ into metal-H atom (hydride) species on its surface. For example, it has been observed that by heating Pt dispersed on carbon at 623 K, Pt/Al₂O₃ at 473–573 K, Pd/C at 473 K, and Pt/WO₃, under hydrogen pressure, the amount of H₂ absorbed exceeds the known H₂-sorption capacity of the metal alone (Sermon and Bond 1974). In these seminal reports, the “excess quantity” of this hydrogen on the support is usually very small, amounting to only several atoms of H for every H that's bound to the metal. In addition, the role of spillover was recognized as essential to the activity and selectivity, formation of catalytic sites, and further enhancement of reaction rates. Several comprehensive reviews of hydrogen spillover in catalysis have been published (see, for example, Conner and Falconer 1995). Spillover is highly dependent on the metal catalysts, the support/receptor chemical composition, and the synergistic interaction between the two.

In the application of spillover for substantial hydrogen storage, graphitic or nano-structured carbon and framework materials are typically used as receptors and catalyst supports because of their high SSAs, which may enhance capacity. Hydrogen spillover is a multiple step process: (1) catalyzed hydrogen dissociation, (2) surface diffusion from the catalyst to a surface, (3) weak chemisorption of the dissociated hydrogen species to the receptor, and finally (4) diffusion along the receptor surfaces (Figure 2-23). The

equilibrium established for these competing processes determines the overall hydrogen sorption capacity of the material of interest. In contrast to straight physisorptive or chemisorptive processes, and because “large-scale” hydrogen spillover includes both of these plus the necessity of surface diffusion on the substrate, a dependence on surface chemical composition and structural features (e.g., pore structure, pore volume, surface substituents, catalyst size, catalyst dispersion, interface, diffusion pathway) affects hydrogen supply to the surface, the diffusion rate, and hence the total sorption capacity. The HSCoE hydrogen spillover efforts included investigations associated with catalyst deposition techniques; metal catalyst type; metal catalyst doping efficiencies/dispersion; chemical composition and structure of the support, substitutional doping of the support with boron and/or nitrogen, or altering the surface chemistry of the support; and the type of support (aerogels, template growth, MOFs) and generation of “bridges” between the metal and the receptor materials.

For spillover materials, an especially high level of care must be exercised in the measurement to correctly ascertain the amount of hydrogen uptake. The very high SSA and presence of highly reactive catalysts in the matrix are known to be prone to side reactions or impurity effects that can be easily misinterpreted as hydrogen storage. For example, significant uptake may be observed because of the reaction of hydrogen with weakly bound oxygen to form water or hydrocarbons. Similarly, impurities in the gas stream even at parts per million (ppm) levels can react with active components of the sample material and be detected as a false-positive hydrogen sorption process. Impurities may also deactivate (or passivate) the sample, impeding hydrogen uptake and resulting in a false-negative hydrogen capacity result when performing volumetric measurements. Another important difference between measuring spillover sorption versus the high-SSA physisorption is in the tolerance in system leakage. Because the kinetics of spillover are slow compared to the nearly instantaneous physisorption process, the tolerance in leakage for measuring spillover needs to be substantially lower, or false results may occur. Ultimately, as in any sorption process, significant differences observed in a material’s hydrogen storage capacity that is dependent on the method of measurement are a strong indication of systematic error within a system, secondary reactions, and/or impurity effects. Spillover demonstrates the importance and complexity of sorption measurements and how they are not turnkey procedures.

2.13.5.1 Spillover Thermodynamics

Rice, APCI, and NREL performed initial computations to identify potential bound hydrogen configurations on receptors that are thermodynamically stable compared to the energy of molecular H₂. As shown in Figure 2-24, on graphene surfaces, hydrogen atoms are thermodynamically stable with lower binding energies when stored in groups or clusters. The group of hydrogen atoms tends to form compact clusters, influenced by aromaticity rules and the pyramidalization strain compensation, so that the lowest-energy clusters consist of closed six-hydrogen rings. Evaluation of the Gibbs formation energy as a function of temperature and pressure indicates that the hydrogen-cluster formation has phase-nucleation dependencies, guided by nucleus barriers and corresponding critical cluster size. One important aspect of this analysis is that the calculated balance between the fluidic gas phase and the immobilized storage-phase indicates that spillover can store ~7.7 wt % hydrogen and the balance can be changed in either direction by changing

pressure and temperature not too far from ambient conditions. Thus, these analyses indicate that thermodynamically, spillover is a reasonably reversible ambient-temperature hydrogen-storage process.

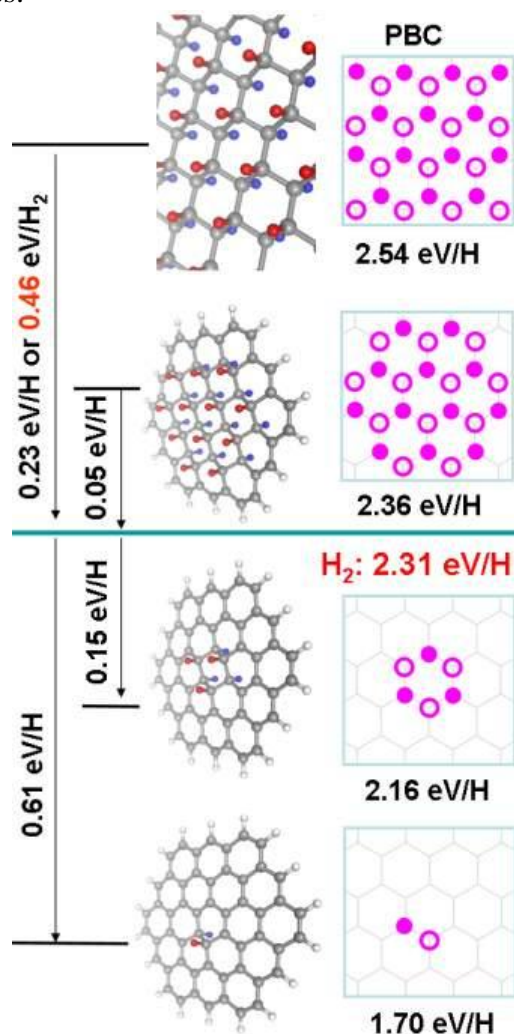


Figure 2-24. Average binding energy of the chemically absorbed hydrogen atom blocks (size of 2, 6, 24, ∞ of hydrogen atoms) on graphene, compared to the cohesive energy of the free hydrogen molecule, H_2

In general, spillover is a multiple-step process starting with the catalyzed dissociation of hydrogen and diffusion from the catalyst to the receptor. As shown in Figure 2-25, Rice within the HSCoE assessed the effect of hydride formation on the catalytic activity of metal clusters by calculating the chemical potential of H using Pd-hydride ($PdH_{0.75}$) (Singh, Ribas, and Yakobson 2009) and Ni-hydride (Ni_4H_{2n}) as model systems. Overall, the less expensive Ni behaves similarly to the Pd. The chemical potential for H and the onset of spillover is computed by calculating the binding energies of H_2 on a free metal catalyst as well as a graphene-supported metal catalyst.

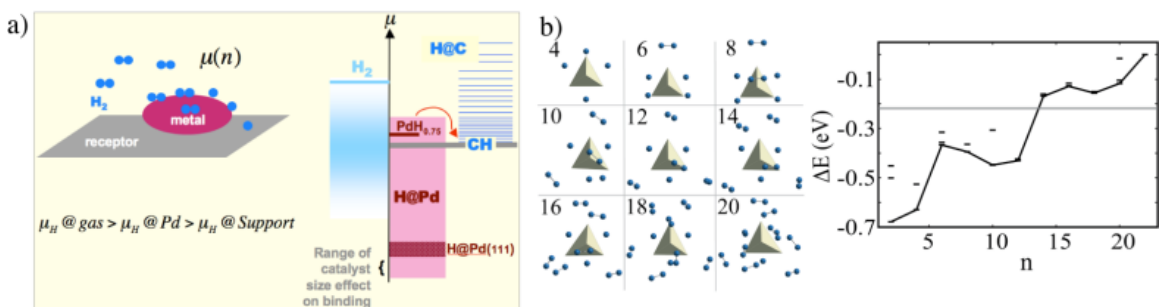


Figure 2-25. a) Left: Schematics of spillover process in real space. The inequality shows the range of chemical potential μ_H favorable for spillover. Right: model of spillover in energy space displays the relative energy (chemical potential) of H in different states. The gray, dark-red, and blue lines show the μ_H in fully hydrogenated graphene (CH), in metal hydride, and in the H_2 molecule, respectively. The pink and dark red blocks show the range of energies of H at the catalyst and at the Pd(111) surface with the H coverage varying from 0.25 to 1 mL. The family of thin dark blue lines corresponds to the energies of H bound to graphene. b) The optimized structure of Ni_4H_{2n} ($n = 2$ to 10). The plot of incremental energy E_{incr} vs. number of H atoms. The gray line shows the H binding energy in the fully hydrogenated phase. The E_{incr} crosses this line after the 6th H_2 molecule, indicating the thermodynamic onset of spillover.

The migration barrier for the diffusion of H from the metal catalysts to the H-graphene phase is calculated to be ~ 0.68 eV, which is kinetically feasible at ambient temperatures. Thermodynamic calculations show that the presence of the hydrogenated phase of graphene makes the spillover step from metal to receptor thermodynamically favorable. Under the right conditions, spillover from the catalysts to the receptor will occur before hydride formation, and thus spillover is not kinetically limited by the metal hydride properties.

NREL investigated the hydrogenation properties of carbon and other receptor materials in more detail to understand the issues involved. For example, the uniqueness of carbon materials lies in the multiple configurations of hybridization, i.e., sp , sp^2 , and sp^3 hybridization. The strong, topologically flexible sp^2 bonding configuration imparts to this light element a single-atom layered film structure, which can be wrapped up in nanoscale to form tubular and spherical shells with extraordinary mechanical properties. All of these materials have high SSA for gas sorption.

More interestingly, the sp^2 - sp^3 transition is quite straightforward because (1) the promotion energy for rehybridization $sp^{2+\delta}$ is almost a continuous function of $0 < \delta < 1$ (Park et al. 2003), and (2) no topological rearrangement is needed in such a transition. Figure 2-26 illustrates the mechanism of weak chemisorption of H atoms to carbon sorbents through the so-called $sp^{2+\delta}$ rehybridization. The advantage of this type of sorption is the tunable H binding energy. Basically, the degree of rehybridization, measured by δ , can be tuned by the curvature of the carbon shell. The larger the curvature, the bigger the value of δ and the larger the average H binding energy. This sorption mechanism also has serious disadvantages. *First*, strain accumulation with H loading usually makes H binding less and less favorable; therefore, the hydrogen capacity is not sufficiently high. *Second*, the kinetics of hydrogen charge/discharge is slow, even if

a catalyst is used. However, this mechanism is applicable to hydrogen storage via spillover (Li and Yang 2006; Lueking and Yang 2002).

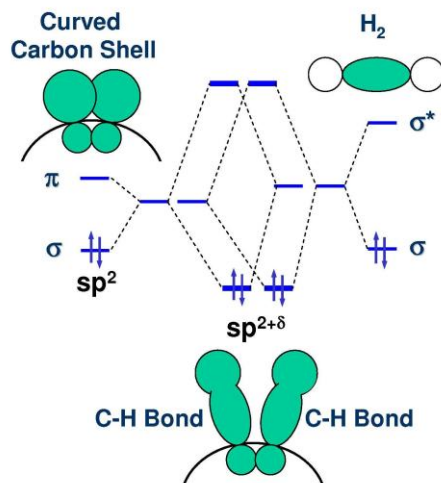


Figure 2-26. Weak C-H bonds formed through sp^2+d rehybridization

The binding behavior versus coverage directly affects the capacity and energy efficiency. There is typically no long-range correlation of hydrogen binding in sorbents. In the same functional core, the binding energy of hydrogen, especially hydrides, often changes dramatically with hydrogen loading, because hydrogenation gradually modifies the property of the sorbent building block. A general decreasing trend of hydrogen binding energy would be expected as shown by the straight lines in Figure 2-27. The cutoff number of H atoms adsorbed (C_1 , C_2 in Figure 2-27) determines the hydrogen capacity. By structurally modifying the sorbents, the binding energy can be adjusted to be a more flat line so that the binding energy of all the sequentially added hydrogen can be confined into the ideal range. As a result, the hydrogen capacity is simultaneously increased from C_1 to C_2 .

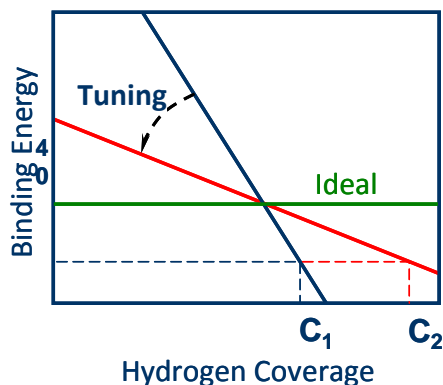


Figure 2-27. Schematic illustration of binding energy vs. hydrogen coverage in nanosorbents and the requirement for binding energy tuning

The coexistence of sp^2 and sp^3 domains in a partially hydrogenated carbon shell or sheet introduces a few key interactions. The first-order effect is the attraction of dangling π

bonds (single π electrons) created in the boundaries between the sp^2 and sp^3 domains. In any conditions, the dangling π bonds have to be paired up, which instantly excludes the odd number of unhydrogenated (naked) carbon atoms from the stable patterns. For example, in hydrogenation of carbon cages, a naked five-member ring is obviously forbidden. Concerning the reaction dynamics, in the early stage of hydrogenation, the energetically favorable sorption sites and the H hopping pathway are not arbitrary (Ferro, Marinelli, and Allouche 2003; Hornekaer et al. 2006; Zecho et al. 2002). When a small domain of hydrogenated carbon is formed, the structure of domain boundaries and its propagation should largely be determined by the attraction of the dangling π bonds.

Even the isolated π bonds (paired π electrons) are not sufficiently stable. In the second order, these π bonds attract each other through resonant effects (Chen and King 2005; Kertesz, Choi, and Yang 2005) such as aromaticity. In fact, this interaction could be strong enough to conform the domain shape. Table 2-8 shows the reaction heat associated with hydrogenation of ethane molecules, benzene molecules, and infinite graphene. The electronic resonant interaction is so strong that the energy is lowered by more than 1.0 eV per π -bond in benzene molecules (110 kJ/mol), and nearly 1.7 eV in graphene.

Table 2-8. Reaction Heat (kJ/mol H₂) of Hydrogenation of Small Hydrocarbon Molecules and Graphene Sheet

$C_2H_4+H_2 \rightarrow C_2H_6$	$C_6H_6+3H_2 \rightarrow C_6H_{12}$	Graphene+nH ₂ → Hydrocarbon sheet
200	90	40

Another famous example is the hydrogenated fullerene, C₆₀H₃₆. Haufler and colleagues (1990) proposed a structure with Th symmetry, in which the 12 naked carbon pairs form isolated π -bonds and are evenly distributed across the cage. Later it was found that a tetrahedral isomer (Taylor 1992), with four aromatic rings formed of the 12 π -bonds, is 3 eV lower in energy (Buehl, Thiel, and Schneider 1995). In this case, aromaticity lowers the energy by only 0.25 eV per π -bond. The possible reasons are: (1) the 12 π -bonds in the Th structure may not be as isolated as their geometry suggests, and (2) the tetrahedral structure may cause more strain.

The lattice mismatch between sp^2 and sp^3 domains causes substantial strain in a carbon sheet. If one defines a positive sign for one side and negative for the other, the interaction of sorption sites follows the rule that “opposites attract, and likes repel.” According to this rule, two-side hydrogenation favors a full coverage of all carbon atoms with H atoms. For example, if a hydrogen atom is simply added on top of each carbon atom alternatively on both sides of a graphene layer, one obtains a single-layer, diamondlike hydrocarbon. In this hydrocarbon sheet, the hydrogen capacity is ~7 wt % with an almost ideal binding energy of ~40 kJ/mol H₂ (Table 2-8). However, to apply such a simple concept for hydrogen storage is still a challenge. In reality, hydrogen atoms or molecules have to be added one by one, and the reaction has to experience complicated kinetics, which is due to all the aforementioned interactions (Stojkovic et al. 2003).

A carbon cage is different from a carbon sheet in two aspects. First, it has inherent strain resulting from the curvature. Second, it opens only the outer side to hydrogenation. In such a system, low coverage of H chemisorption actually releases the inherent strain if the hydrogenation follows a particular pattern. An example is linear hydrogenation of a CNT along the axial direction, in which hydrogen (Gulseren, Yildirim, and Ciraci 2002) or other chemisorbed species (Kudin, Scuseria, and Yakobson 2001) form axial lines dividing the CNT circumferentially into flat sp^2 facets. It is also found in $C_{60}H_x$ that strain relief is maximized at $x = 36$ (Yoshida et al. 1993). After the critical coverage is exceeded, hydrogen becomes exceptionally less favorable.

The HSCoE did not find sufficient results from which a general rule can be extracted to clarify all of these types of interaction and their effects on hydrogenation of carbon materials. This is an interesting direction—one that is important for future hydrogen-storage development work. Carbon materials offer an excellent scaffold for development of high-SSA material, and if pure carbon materials cannot meet the goals, at least they can serve as good backbone frameworks for further functionalization with, for example, metals.

2.13.5.2 Spillover Kinetics

From the initial thermodynamic calculations and the corresponding experimental evidence, the main step in the spillover process that is not well understood is that of H diffusion on the receptor. Again, diffusion on the metal catalyst and to the receptor can be understood within standard thermodynamic principles. These were important findings at the beginning of the HSCoE, providing an initial atomistic understanding of potential spillover mechanisms that helped guide experimental efforts along with focused efforts to better understand the kinetic mechanisms involved. Also, because in some cases H storage on the receptor may need to be in the form of clusters, calculations indicate that diffusion is thermodynamically possible as a localized front or group of hydrogen atoms. However, it is not clear how this can occur on an atom-by-atom basis.

NREL was the first to identify that barriers to migration are lowered sufficiently to enable spillover via structural and electronic features, and/or via quantum mechanical tunneling where H will diffuse before it desorbs. Based on calculations, NREL identified that H migration increases substantially via hopping between surfaces that are closely spaced (Figure 2-28) (Ciobanu and Zhao, forthcoming). This suggests that perhaps layered or corner structures may enable hydrogen atom diffusion via hopping. Similarly, calculations indicated that free holes lower the barrier energy of H atom diffusion due to the H strong negative potential behavior. In this case, the barrier drops for graphene from 1.04 eV H^0 to 0.60 eV for H^+ , and for MOFs from 1.52 eV H^0 to 0.52 eV for H^+ . Thus, doping, defects, or functionalizations that form holes may enhance hydrogen storage via spillover (Lee et al. 2010). Finally, ambient-temperature quantum tunneling lowers the diffusion barrier energy. These results provide development paths to creating higher capacity, higher-rate H-storage spillover materials that may be used to meet DOE system targets.

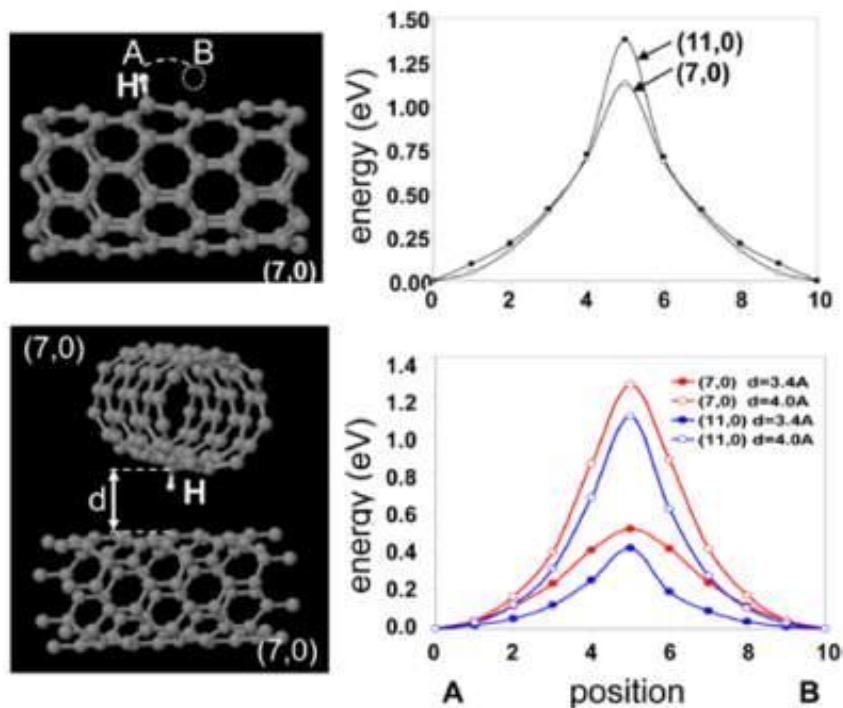


Figure 2-28. Initial calculations at NREL identified that, compared to migration along a surface, hopping between closely spaced surfaces substantially lowers the barrier for hydrogen diffusion.

2.13.5.3 Thermodynamic Calculations Validation

To validate many of the thermodynamic calculations, APCI modeled the well-known spillover phenomenon associated with hydrogen bronzes from metal oxides (eg., MoO_3 and WO_3) and metal sulfides (eg, ZnS and MoS_2). Ritter and coworkers applied solid-state NMR techniques to study the bonding properties, location, and mobility of hydrogen in H_xMoO_3 (Ritter, Muller-Warmuth, and Schollhorn 1985). They found that the activation energies for hydrogen diffusion are on the order of 15 to 30 kJ/mol and also concluded that hydrogen atoms reside on a line connecting the vertex sharing oxygen atoms within the $(\text{MoO}_6)_n$ layers. An atomic force microscopy study by Smith and Rohrer (1998) unraveled the evolution of the MoO_3 (010) surface during reduction in H_2 - N_2 mixtures at 700 K. The results demonstrate that MoO_3 intercalates H atoms during the gas-phase reactions, resulting in protonation, which in turn leads to precipitates of hydrogen molybdenum bronze. In an additional example, an increase in hydrogen storage capacity by spillover on CeO_2 in the presence of Pt catalysts was recently reported, and NMR studies indicated the presence of protonic hydrogen on the oxide surfaces (Mitchell et al. 2003). The hydrogen bronze complexes can be prepared most effectively via hydrogen spillover in the presence of Pt or Pd catalysts. The solid metal oxide compounds are generally semiconductors, but are transformed into metals (conductors) immediately on hydrogen bronze formation via hydrogen spillover.

APCI used a simple Pt cluster model to represent the Pt catalyst nanoparticles and examine H_2 dissociative chemisorption on the cluster until it was fully saturated by H

atoms (Chen et al. 2007). APCI showed that H₂ molecules can undergo sequential dissociative chemisorption of the selected Pt₆ cluster up to a Pt/H ratio of 1:4, at which point the cluster is fully saturated. The results indicate that the H₂ dissociative chemisorption is dictated by the charge transfer from the Pt cluster to H₂ molecules via 5d-1σ* orbital overlap. The charge transfer increases with the H coverage, revealing the role of the Pt clusters in hydrogenation/dehydrogenation processes as an electron reservoir. Using the insights gained by the catalyst cluster study, APCI performed extensive quantum-mechanical calculations to model the hydrogen spillover phenomenon that leads to the formation of H bronze in MoO₃ (Chen et al. 2008). The results indicate that spillover occurs on adsorption of H atoms originating from a Pt catalyst fully saturated with H atoms onto the MoO₃ (010) surface, followed by H diffusion in the lattice. For the first time, the detailed mechanisms of H-insertion into MoO₃ were unraveled. APCI showed that the H atoms can readily migrate from the Pt catalyst to the MoO₃ (010) surface, followed by protonation, to form strong covalent bonds with the terminal oxygen atoms. Subsequently, the protons were able to migrate into the lattice via low-energy-barrier pathways to form a hydrogen bronze. These results suggest that the H adsorption and migration are facilitated by the massive H-bonding network in the lattice, and that hydrogen bronze formation can occur at moderate temperatures. The calculated diffusion barriers were in quantitative agreement with data measured by NMR, and the predicted relative thermodynamic stability of adsorption sites was consistent with experimental observations. The study revealed that H atoms supplied locally by a Pt catalyst can flow nearly freely into the entire lattice, which is precisely the essence of the so-called spillover phenomenon.

DFT calculations were used to study the two main components of hydrogen spillover in α-MoO₃, which are the absorption and diffusion of atomic hydrogen (Sha et al. 2009). APCI first calculated the structure of bulk α-MoO₃. The optimized lattice parameters were in good agreement with the experimental values, and the calculated electronic structure of this material exhibits a typical semiconductor bandgap. On incorporation of H atoms at various concentrations into α-MoO₃, hydrogen molybdenum bronze materials, H_xMoO₃, were formed, and the crystalline lattices underwent significant relaxation near the absorption sites. Energetically, the most favorable binding sites were identified. The results indicate that the two most preferred absorption sites, the terminal and asymmetric oxygen atoms, interact with H atoms with nearly equal bond strength. Consequently, they may both be populated on H atom absorption, which is likely the reason why the precise locations of H atoms in the lattice vary in different experiments, depending on sample preparation.

Hydrogen absorption in α-MoO₃ results in an extensive hydrogen bonding network in the crystalline lattice. As a consequence, the hydrogen molybdenum bronze materials were all found to be metallic with the valence band widened across the Fermi level and into the conduction band, consistent with experimental observations. The Bader population analysis indicates that absorbed H atoms lose electron density, becoming protonic in nature. The charge transfer from hydrogen to the O atom, on which the H atom resides, gives rise to the reduction on the adjacent Mo atom and thus a weaker Mo-O bond.

To understand the mobility of the H atoms in the lattice, APCI performed calculations on H atom diffusion in bulk α -MoO₃ along a prescribed diffusion pathway. The results indicate that the protonic hydrogen diffuses with very small activation barriers, suggesting that these H atoms should be highly mobile at near-ambient temperatures. The calculated barrier heights lie well within the range of experimentally measured values. The high mobility of H atoms in the lattice, facilitated by the massive hydrogen bonding network, reflects the essence of the spillover mechanism in these materials. The study shows that hydrogen desorption to form H₂ molecules is an exothermic process for hydrogen bronzes with a H concentration higher than HMoO₃ and becomes endothermic at low H loadings.

2.13.5.4 Spillover via Physisorbed Atomic Hydrogen

The understanding generated by the study of spillover on metal oxides materials was used in subsequent APCI modeling of hydrogen spillover on carbon-based materials. To clearly describe the spillover processes, APCI selected three graphitic carbon materials representing both finite and extended systems (Chen et al. 2007). As before, the catalyst was modeled with a Pt cluster fully saturated by H atoms. The effect of support and bridge materials was neglected in the theoretical model. The hydrogen spillover processes were then broken into three steps. The first step involves H₂ dissociative chemisorption into H atoms on the Pt catalyst. In the second step, the Pt catalyst fully saturated by H atoms delivers H atoms to the graphitic surfaces. The migration of H atoms from the catalyst to the substrates may involve both chemisorption and physisorption processes. APCI's computational results indicate that the chemisorption process might be able to proceed readily at ambient conditions with small-to-moderate activation barriers. The calculated H chemisorptions strength was found to be curvature-dependent with higher adsorption energies associated with the carbon atoms of materials such as nanotubes with more pronounced curvature. With the minimum H desorption energy of approximately 2.4 eV from the fully saturated Pt cluster, APCI speculates that the physisorption process can only be induced by the support and/or bridge materials.

APCI's previous computational study on hydrogen spillover in MoO₃ suggests that this process in a massive H-bonding system can take place readily. The bridge materials used in Yang's experimental studies at the University of Michigan (Michigan) are composed of carbonized sugar (e.g., sucrose) molecules. Although the material is carbonized on heat treatment at 400°C for several hours, oxygen atoms left over in the form of oxygen-containing functional groups could still be relevant for hydrogen spillover. It is possible that those oxygen atoms (likely in the form of graphite oxides) provide a H-bonding network, similar to what was found in MoO₃, that allows H atoms on the Pt catalyst to migrate to the substrate. If these H atoms are "hot" on migration (i.e., they have a high kinetic energy), they will immediately form a bond with a carbon atom nearby. If they are sufficiently "cold," the H atoms can be physisorbed at least 2.5 Å above the graphitic surfaces, in which case H diffusion throughout the surfaces is energetically feasible. Of course, it remains a question how stable these physisorbed H atoms are on the carbon material surfaces and the degree to which H atoms recombine to form molecular hydrogen.

An *ab initio* molecular dynamics simulation of 60 H atoms physisorbed on C₆₀ at RT suggests that most of the H atoms will either form C-H bonds with the fullerene or recombine to form H₂ molecules, the latter of which does not contribute to the overall hydrogen storage capacity. In the final step of the hydrogen spillover process, APCI studied diffusion of a H atom chemisorbed on surfaces of the selected graphitic materials. Similar to the calculated chemisorption strength, the calculated diffusion barriers were also found to be curvature-dependent with a higher barrier associated with carbon atoms of higher-curvature SWNTs. The computational results suggest that it would be difficult for chemisorbed H atoms to move freely at moderate, near-ambient temperatures, because diffusion must require C-H bond dissociation, which requires substantial activation energy for all the materials investigated here. The implication here is that H diffusion in graphitic materials would not be energetically favorable if the H atom is chemisorbed, and APCI suggests that a possible mechanism for H atoms to spread out in the entire material is via physisorption.

In additional studies, APCI conducted extensive theoretical calculations using DFT by first mapping out the energy profile of hydrogenating one C atom on selected carbon materials and subsequently performing *ab initio* molecular dynamics simulations on an assembly of physisorbed H atoms on graphene and on fullerenes such as C₆₀ at RT (Sha et al. 2008). APCI also explored the influence of substrate type on hydrogen spillover capacity and on dehydrogenation by evaluating the average C-H bond strength. The results indicate that the energetic well depth of the C-H bond formation increases as the size of fullerenes decreases, and that kinetically, this reactive process is essentially barrierless. Hydrogenation of graphene requires an activation energy of ~0.2 eV, and a corresponding well depth of 0.76 eV. Hydrogenation of these carbon materials presents an energetically competitive process to H recombination to form H₂. APCI's *ab initio* molecular dynamics simulations suggest that both processes will occur simultaneously. In particular, the study indicates that the physisorbed H atoms in the selected carbon environments are only metastable and ultimately will either react with the carbon substrates to form C-H bonds or recombine to form H₂ molecules. The recombined H₂ molecule can of course interact again with the metal catalysts to regenerate H atoms in a cyclic hydrogen/physisorbed H atom/recombined hydrogen process. It appears that the H physisorption process provides a means for H atoms to diffuse from the sites near the metal catalyst particles to distant sites, which is a necessary component of the H spillover phenomenon.

The degree of inherent curvature of the external surfaces of fullerenes and the resulting effects of the bond-angle distortions of the carbon atoms in the fullerenes has a profound influence on the thermodynamics of C-H bond formation. The calculated reaction energies of forming H₂ molecules from the hydrogenated fullerene molecules as well as for graphene appear to be favorable. However, based on the calculated average C-H bond energies, APCI believes that it will be kinetically challenging to break moderately strong C-H bonds, and a carefully designed catalytic process would be necessary to facilitate the hydrogen desorption process.

2.13.5.5 Hydrogen Storage via Spillover

The HSCoE partners at Michigan pioneered storing substantial quantities of hydrogen at ambient temperature via spillover (Li and Yang 2007; Lueking and Yang 2007). These high, ambient-temperature hydrogen storage capacities were achieved using a variety of materials and catalysts, and some of the results have been experimentally reproduced by other scientists (Chen and Huang 2007; Dutta et al. 2007).

The HSCoE and others investigated the use of many different materials to understand how to increase capacities and adsorption rates. These materials include carbon nanofibers (Marella and Tomaselli 2006); activated carbon (Zielinski et al. 2005); graphite (Mitchell et al. 2003); SWNTs (F.H. Yang, Lachawiec, and R.T. Yang 2006); and MOF complexes (Li and Yang 2006). An overview of the types of systems investigated by HSCoE partners is shown in Table 2-9.

In addition to sorbents and catalysts, sample preparation to control structure, chemical composition of the receptor surfaces, and catalyst properties were also critical components in spillover material development. Thus, a variety of solution- and vapor-phase deposition techniques were investigated to achieve high metal dispersion and appropriate receptor properties for high-capacity spillover. In general, the most straightforward way to achieve spillover is by directly integrating metal catalysts with the receptor surfaces. High metal dispersion and intimate contact with the receptors are critical for effective spillover. The HSCoE partners developed a number of techniques to integrate 1–3 nm metal catalyst particles including direct mixing, incipient wetness impregnation technique, microwave-assisted deposition, magnetron sputtering, and microemulsion. However, in the case of some receptors such as MOFs, direct metal integration was not possible. In these cases, catalysts on supports were integrated with the receptor materials, and it was determined that the formation of “bridges” substantially improved spillover capacities. These bridges were typically formed by pyrolyzing sucrose that has been integrated with the catalyst supports and receptors where all the materials were mixed very well.

Table 2-9. Overview of the Different Sorbents and Catalysts Used by HSCoE Partners To Construct Spillover Materials for Hydrogen Storage

Sorbent	Catalysts, Metals	Catalysts, Deposition Techniques	Max Gravimetric (100 bar, ambient temperature)	Notes
Activated Carbons (ax-21, CM-Tec, maxsorb 20/30)	Pt, Ru, Pd, PdHg, Ceria, Ni, Pt-Ceria Core Shell	Solution Electroless: Microwave Processing, Sputter Deposition Microemulsion	~1.6%	Variation in performance dependent on catalyst dispersion support surface chemistry
Graphene Oxides	Pt, Ru, Pd, PdHg	Solution	NA Side reactions dominate	Considerable water formation with all catalysts
Carbon Aerogels	Pt, Ru, Pd, Ni	Solution, Microwave	NA	No enhancement observed
Metal-Organic Frameworks	Pt, Ru, Ni, Pd	Solution, Bridging	~4% with bridged materials	Maximum adsorption for spillover observed ~4 wt % (highly unstable materials)
Templated Carbons (silica spheres, commercial zeolites)	Pt, Ru, Pd	Solution Electroless: Microwave Processing, Sputter Deposition	~1.8% wt % for zeolites (>2000 m ² /g) ~1.2% for silica templates (<600 m ² /g)	Pt templated carbon (silica) showed max capacity enhancement. Pt TC from zeolites showed maximum capacity at ~2 wt %.
Single-Walled Carbon Nanohorns	Pt, Ca	Solution, Vapor phase	~1.5% wt %	Observed formation of C-H interaction with neutron scattering
Boron-Substituted Carbon Support (templated growth on activated carbon or zeolites)	Pt, Ru, Pd	Solution, Microwave, Sputter Deposition	~1.0 % wt % (160 bar)	15% enhancement over base materials

Spillover Receptors

The HSCoE focused a great deal of effort on understanding and improving spillover on carbon-based receptor materials. For example, a hydrogen spillover-induced increase of hydrogen storage capacity for activated carbon and SWNTs by factors of 2.9 and 1.6, respectively, was observed (Lachawiec, Qi, and Yang 2005). This difference may be consistent with the predictions discussed above that suggest that the higher-energy curved surfaces and/or the inability to populate both the inside and outside of the nanotube surfaces may decrease the amount of hydrogen that can be stored on the nanotubes. However, based on the unique processes involved with spillover, which has been described as “loosely adsorbed” hydrogen atoms on receptor surfaces (Zielinski et al. 2007), a number of other factors may also account for the differences between different receptors. Even minor deviations in sample preparation and treatment may lead to diminished or no spillover. For metal-carbon systems, the different factors that affect spillover include:

1. Highly dispersed metal nanoparticles (i.e., ~2 nm diameters) enhance spillover. As with synthesis of fuel cell catalyst materials, the Pt particle size is affected by

- the nucleation rate versus particle growth during catalyst deposition, and an aggregation can occur during the activation heating, or even from the exothermic nature of side reactions during sorption measurements.
2. It is speculated that in the case of highly dispersed Pt for example, the specific face, such as Pt(110), and high energy edges/steps are the most preferred for effective splitting of hydrogen.
 3. Improper activation and catalyst cleaning, as in the case where RuO₂ is formed, can lead to a large amount of water or other irreversible side reactions that adversely affect the spillover measurements.
 4. Ultrasonication can assist in creating more intimate contacts between the particles and the substrate during the impregnation of metal particles, however it can also oxidize the surface and collapse fine structures within the support.
 5. After reduction by H₂ at ~573 K, sample pretreatment by degassing at higher temperatures (e.g., 623 K) is needed to fully remove hydrogen and other molecules from the carbon surfaces.
 6. For catalyst-bridged MOFs, the MOF's quality and particle size are affected by the starting materials and the synthesis method. Nanosized MOFs are preferred because the nanosized MOFs have more external surface area and more contacts with the dissociation source.
 7. For MOFs, direct integration of the catalyst induces structural collapse and other issues, so mixing and bridging are necessary. Uniform mixing of the three components, Pt/C, sucrose, and MOF, is very important for hydrogen spillover, which is affected by the sample amounts, compatibility in the particle sizes, and the grinding time and intensity. Batch-to-batch mixing issues must be reduced to decrease the large storage capacity variability presently observed with these spillover materials. In addition, carbonization temperature (e.g., ~523 K) is important and dependent on the MOF. Temperatures that are too high will degrade the MOF structure due to the exothermic carbonization process for sucrose or glucose. It is also crucial to minimize the exposure of MOFs to ambient air. The moisture in the air causes hydrolysis of the MOFs.
 8. Prior to measurements and characterization, a high-degassing temperature (473 K) is needed to fully prepare the sample.

INS spectroscopy demonstrated spillover hydrogen on carbon sorbents (Mitchell et al. 2003). Similar neutron scattering observations were made for SWNH materials by the HSCoE partners at ORNL. Nanohorns are cone-shaped, atomic-layer-thick nanostructures that contain preferred hydrogen adsorption sites in their tips and have variable internal and interstitial pores that have been shown to contain hydrogen at liquid-hydrogen density or higher (see Figure 2-7). Nanohorns can be functionalized by tailoring their pores and by metal decoration and have unique adsorption sites for catalysts. Pt-nanohorns, in which the nanohorns were oxidized, were reported to have significantly higher hydrogen storage capacity at ambient temperature compared to oxidized nanohorns without Pt. The “nanoengineered pores” of nanohorns are distinct from other carbon materials, by both the unique nanostructure self-assembled during synthesis and the activated pores during oxidation.

One of the breakthrough developments made by the HSCoE was Michigan's use of carbonized bridges that enable good interconnection between different components and MOFs, which are used as receptors. Because of their variable building blocks, frameworks have very large SSAs, high porosities, uniform and adjustable pore sizes, and well-defined hydrogen occupation sites. These features make MOFs promising candidates for hydrogen storage, but frameworks typically decompose with direct catalyst integration. However, Michigan demonstrated that bridging materials can be used to effectively join catalysts with the frameworks to substantially increase hydrogen spillover capacities (i.e., greater than 4 wt % at ambient temperatures).

Spillover Adsorption and Desorption

To obtain a better understanding of the processes involved in spillover, deuterium isotope tracer and TPD studies were performed with Pt/C samples (Y.W. Li, F.H. Yang, and R.T. Yang 2007). A typical result is shown in Figure 2-29.

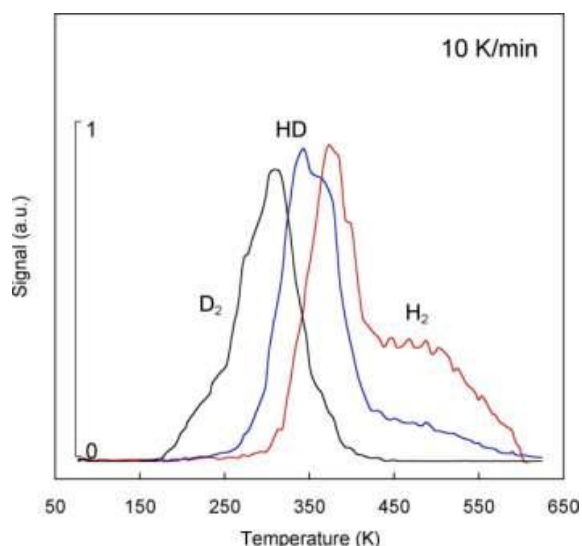


Figure 2-29. TPD result from 6 wt % Pt on templated carbon (3400 m²/g) after dosing with 0.4 atm H₂ followed by D₂ at 298 K for 5 min (followed by quench, gas phase removal, and TPD)

In these experiments, ~0.4 atm of H₂ was dosed first, followed by dosing with 0.4 atm D₂. The TPD results show clear desorption peaks of D₂, hydrogen deuteride (HD), and H₂, in the reversed sequence of dosing. Importantly, a large desorption peak of HD occurred. The results are direct evidence showing that (1) atomic species are formed during spillover storage to account for the formation of HD, and (2) the desorption step follows a reverse spillover process, i.e., atoms migrate back to the metal particle, on which to recombine and desorb as molecules. These results are consistent with the H₂ molecules undergoing dissociative chemisorption on interacting with a supported transition metal catalyst (e.g., nanoparticles of platinum); the generated H atoms migrating from the catalyst particles to the storage receptor materials; and the H atoms further diffusing across the receptor surfaces in a wave-front motion in which the first atoms on are the ones that move the furthest away from the catalysts. Furthermore, for the spillover process to occur to any significant extent, it is essential that the H atoms be

able to move from the vicinity of the catalyst particles to substrate sites far from where the catalysts reside. Within the HSCoE, active research efforts were made to understand the hydrogen spillover processes. These studies have suggested elements of the spillover mechanisms that can satisfactorily explain the observed large storage capacity (>4 wt.% of H₂) and facile hydrogen desorption kinetics from the carbon-based storage compounds at near-ambient temperatures (Mavrandonakis and Klopffer 2008). The key issues really revolve around the kinetics of atomic hydrogen diffusion on the receptor materials.

Spillover Kinetics

The kinetics of adsorption and desorption was measured as percent completion (or fractional completion) during each pressure-changing step when obtaining volumetric sorption properties. Figure 2-30 shows the adsorption and desorption kinetics using a Pt/AX-21 sample at various end pressures (5–100 atm) and 298 K. The results indicate that desorption rates are always higher than adsorption, and that the rates decreased with hydrogen loading. Although the adsorption rates are slow to reach full capacity at a given pressure, a large fraction of full capacity is achieved within a few minutes, indicating that if sufficient capacity can be achieved with spillover, then refueling rate targets may be met without reaching the full capacity of the sorbent. In addition, NREL demonstrated that by using higher initial pressures, the adsorption rates increased, and Michigan and NREL identified methods to increase adsorption rates by improving catalysts and receptor properties. In general, the desorption rates, which are faster than adsorption, are sufficient to meet the DOE fuel delivery rate targets.

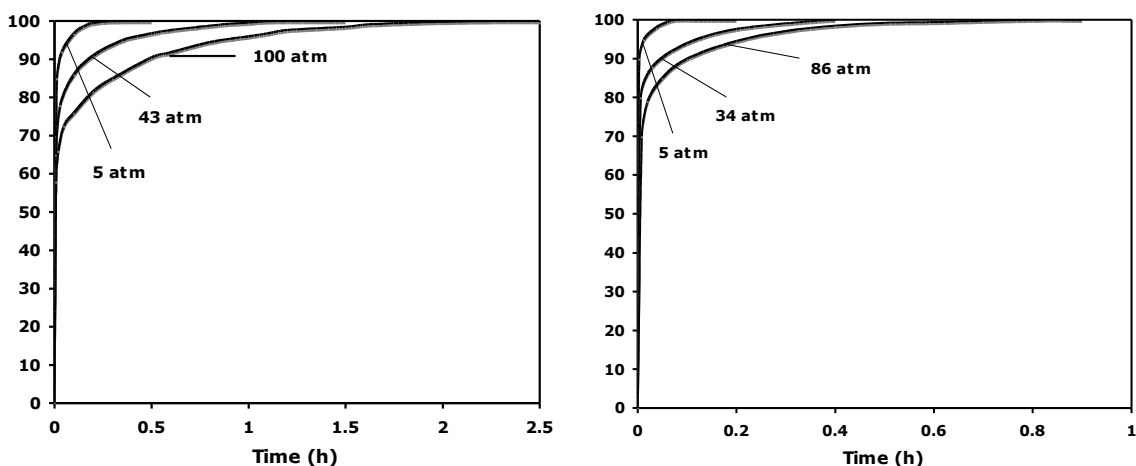


Figure 2-30. Rates of adsorption (a), and desorption (b) at different pressures using Pt/AX-21 samples (T = 298 K)

2.13.5.6 Other Weak Chemisorption Hydrogen Storage Materials

The HSCoE also investigated other methods and materials to form reversible ambient-temperature hydrogen-storage materials. As discussed in the Cross-Cutting Theory subsection that follows, direct metal integration into lightweight structures and/or materials such as endohedral fullerenes may catalyze molecular hydrogen dissociation and storage as atomic hydrogen. Furthermore, as discussed previously in this document, APCI identified that BC_x materials may also catalyze hydrogen dissociation and store atomic hydrogen. HSCoE partners performed some experiments investigating some of these novel materials, but focused development efforts were not performed. For example, NREL developed solution-phase hydrogenation of carbon nanostructures and demonstrated methods to reversibly adsorb and desorb the atomic hydrogen. The key to these materials is the reduction of the nanostructures by alkali metals. This reduction and subsequent hydrogenation can be accomplished via two distinct methods: a modified Birch reduction in liquid ammonia; and a reaction with alkali metal naphthalides in tetrahydrofuran. The extent of hydrogenation observed ranged from $C_{125}H$ (~0.8% w/w) to C_2H (~ 4.0% w/w), depending on the carbon source materials and alkali metal. The stability of the C-H interactions, as measured via thermal desorption, varied from ambient temperature to ~400°C depending on the materials and processes used.

2.13.6 Cross-Cutting Theory

As discussed throughout this document, first-principle models were used to design and predict the performance of hydrogen storage materials. The vast majority of these efforts were directly integrated with experimental efforts. However, predictive efforts easily outpace experimental ones, and several important theoretical findings stand alone and must be fully vetted by future focused experimental efforts. Some of the more important findings are discussed in this section. Table 2-10 provides an overview of the types of efforts performed by the HSCoE.

Table 2-10. Overview of Predictive Efforts for Designed Hydrogen Storage Materials

Optimized Nanostructures	Substituted Materials	Strong/Multiple H_2 Binding	Weak Chemisorption
Carbon nano-framework	B, Be-doped carbon cages, tubes	TM-, Li-, Ca-decorated carbon cages, tubes, graphene	Hydrogenated C_{60} , CNTs, metallofullerene
Porous carbon	B-doped porous carbon	TM, Li, Ca decorated MOF, COF, carbon nano-frameworks	Nanographene, nanographite
Carbon nanotubes	B-doped graphite, BC_x	TM carbide nanoparticles, Met-Car crystals	MOFs
Activated carbon (the effect of dangling bonds)	N-doped carbon	TM-decorated boron cages	Met-Car
Nanographene	F anion-intercalated graphite and N-doped graphite	Metallo-borane and carborane	Transition metal borides

Optimized Nanostructures	Substituted Materials	Strong/Multiple H ₂ Binding	Weak Chemisorption
Zeolites	Tetrathiafulvalene - tetracyanoquinodimethene (TTF-TCNQ)	Li, Ca-intercalated graphite and B-doped graphite	BC _x
		Li-dispersion in porous SiO ₂	Hydrogenation of hydrocarbon, BNH molecules
		Metal-decorated polymers, dendrimers	

2.13.6.1 Hydrogenation of Boron-Nitride Materials

In addition to performing detailed investigations of the different components involved with weak chemisorption of carbon-based receptor materials, NREL also looked at other systems including boron nitride (BN), Met-Cars, and macromolecules. BN is analogous to C material in that both have 1-D atomic chains, 2-D sheets or shells, and 3-D diamondlike structures via different types of hybridizations. The sp³ hybridization in BN crystals is similar to that in diamond, except that the B-N (C-C) bonds are polar (non-polar). Thus, the hybridizations in 1-D chains or 2-D sheets of BN differ more than the standard sp and sp² for carbon. To describe the origin of this difference, we first examine the electronic structures of BH₃ and NH₃ molecules, both of which are sp² coordinated. However, there is a hole state in BH₃, whereas the NH₃ has a lone electron pair. Therefore, a double bond in the BN sheets should contain a σ-bond and a nonclassical bond, rather than a σ-bond and a classical π-bond. For the same reason, each triple bond in a B-N chain has a σ component, a π component, and a nonclassical component (see Figure 2-31).

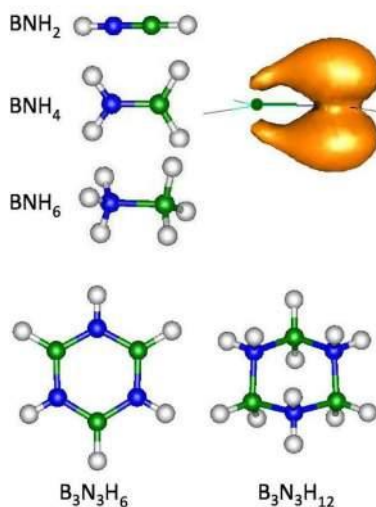


Figure 2-31. Atomic structure and charge contour of small boron-nitride molecules

The different nature of hybridization in BN and C systems should be reflected in their sp^2 - sp^3 transitions, as shown in Table 2-11 for the reaction heats of sequential hydrogenation of their small molecules. The sp - sp^2 transitions (shown by the first column in Table 2-11) in carbon and BN systems are very similar, but sp^2 - sp^3 transitions (the second column) are completely different. The difference originates from the fact that the rehybridization consumes, respectively, a classical π bond in the carbon system and a nonclassical bond in the BN system. Obviously, the nonclassical B-N bond is more stable than the C-C or B-N π bonds. This is also evidenced by the fact that transition metal atoms bind less strongly to $B_3N_3H_6$ than to benzene ring. The other distinguishing result is the reaction-heat differences of the sp^2 - sp^3 transitions in diatomic molecules and the aromatic rings. Because of the aromaticity, hydrogenation of benzene ring gives reaction heats that are 110 kJ/mol H_2 less than that of C_2H_4 . The difference is only 15.5 kJ/mol H_2 for the BN systems, indicating a much less pronounced resonant effect of the nonclassical bonds (at least in this particular case) than that of the delocalized π bonds. Obviously, hydrogen storage through hydrogenation of BN nanotubes is not feasible.

Table 2-11. Reaction Heat (kJ/mol H_2) of Hydrogenation of Small Hydrocarbon and Ammonia-Borane Molecules

$C_2H_2+H_2 \rightarrow C_2H_4$	$C_2H_4+H_2 \rightarrow C_2H_6$	$C_6H_6+3H_2 \rightarrow C_6H_{12}$
180	200	90
$BNH_2+H_2 \rightarrow BNH_4$	$BNH_4+H_2 \rightarrow BNH_6$	$B_3N_3H_6+3H_2 \rightarrow B_3N_3H_{12}$
168	12	-3.5

The intermolecular interaction in BN systems is stronger than that in hydrocarbon, which is due to the polarized B-N, B-H, and N-H bonds. For example, C_2H_6 is liquid with a low vaporization temperature, but BH_3NH_3 molecules form solids at ambient conditions. This renders the ammonia-borane a potential material for hydrogen storage. But it suffers from slow kinetics and irreversibility once larger BN molecules such as borazine ($B_3N_3H_6$) are formed.

2.13.6.2 Met-Cars

Most transition metals form metal carbides (Oyama, Keiffer, and Carbides 1992) through polar covalent bonds as a consequence of the moderate difference in electronegativity of transition metals and carbon. The covalent bonding nature in metal carbides is not as obvious as in the typical covalent crystals such as diamond. Both carbon and metals have large coordination numbers in transition metal carbides. For example, TiC has a rock salt structure in which each carbon or Ti atom has six nearest neighbors. In this sense, the TiC solid is similar to ionic crystals, and Ti is indeed less electronegative than C. On the other hand, if one does not distinguish the two types of atoms, the TiC structure is a simple cubic structure like pure metal, which favors higher coordination numbers. In fact, carbides formed with transition metals from the left side of periodic table are more ionic because these elements are more electropositive. Carbides formed with transition metals

from the right side are more metallic, due to the more valence electrons in these metals. This explains the decreasing melting point of transition metal carbides from the left to right in the periodic table (Oyama, Keiffer, and Carbides 1992).

The covalent bonding nature becomes clearer in small metal carbide clusters such as metallocarbohedrene (Met-Car, Ti_8C_{12}) in which carbon atoms appear as dicarbon units (Guo et al. 1992). The two carbon atoms in each dicarbon are connected with a triple bond in between and bonded covalently with Ti atoms from both sides (Figure 2-32). The C_2Ti_2 motif in Met-Cars resembles the C_2H_2 molecule. Here the transition metal atoms not only catalyze the hydrogenation of carbon atoms, but also weaken the H binding to the carbon atoms significantly. The interaction mechanism can be explained by Figure 2-32, in which the Ti atoms 1 and 1' are more reactive and can catalyze dissociation of H_2 molecules, which spill H atoms over to the dicarbon (2-2') in between. However, the C-H bonds so formed are much weaker than that in a free C_2H_4 molecule, because the triple carbon bond in Met-Cars is stabilized by the Ti atom 3 through Dewar coordination. Importantly, the hydrogen dissociation and recombination is highly reversible through the catalytic effect (Zhao et al. 2006).

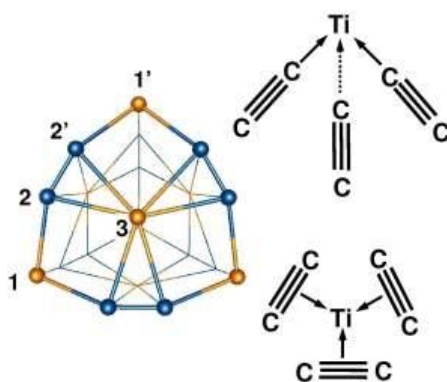


Figure 2-32. Bonding framework in a Ti_8C_{12} Met-Car molecule

2.13.6.3 Endohedral Fullerene

An unexpectedly interesting case of carbon hydrogenation affected by metal has been found in the endohedral metallofullerenes. With the increase of hydrogen coverage, hydrogenation of empty fullerenes usually is divided into two stages by a critical coverage (e.g., $x = 36$ for C_{60}H_x) at which the strain is optimized. The hydrogen binding is strong (~ 1.0 eV/ H_2 for C_{60}) before reaching this critical coverage and drops sharply after that. This is not so good for hydrogen-storage applications, which would prefer a flat linear binding behavior with intermediate values (~ 0.3 eV/ H_2) in a wide coverage range (see Figure 2-27). However, metal atoms encapsulated inside the fullerene cages generally weaken the H binding in the earlier stage and strengthen it in the later one (Figure 2-33), independent of the reaction pathways (Zhao et al. 2007). The charge transfer from the inside metal atoms stabilizes the outside carbon cage, and therefore H binding in the earlier stage is weakened. However, hydrogenation in the later stage becomes more favorable because it induces negative curvature at the naked carbon sites, which form chemical bonds with the encapsulated metal atoms. It is interesting that a few

hidden metal atoms can systematically affect such a complicated reaction by altering the patterns of hydrogen coverage on the surface of the fullerenes. For example, the inside metal atoms may also stabilize some special structures, e.g., the naked five-member rings, which are forbidden in hydrogenation of empty fullerenes.

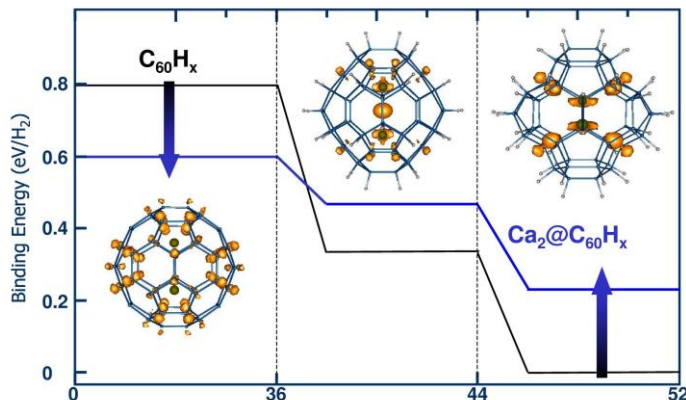


Figure 2-33. Energy of H binding to pure C_{60} (black curve) and Ca-encapsulated C_{60} (blue curve). When metal atoms are encapsulated, the charge transfer from the metal to the cage decreases and then increases again as H coverage increases, as shown by the insets, where the charge density is contributed by the four electrons just below the Fermi level.

2.14 References

Andreoni, W.; Giannozzi, P.; Parrinello, M. (1995). "Molecular Structure and Chemical Bonding in $K_3 C_{60}$ and $K_6 C_{60}$." *Phys. Rev. B* (51:4); pp. 2087–2097. <http://link.aps.org/doi/10.1103/PhysRevB.51.2087>.

Ataca, C.; Akturk, E.; Ciraci, S. (2009). "Hydrogen Storage of Calcium Atoms Adsorbed on Graphene: First-Principles Plane Wave Calculations." *Phys. Rev. B* (79:4); pp. 0414061-1–0414061-4. <http://link.aps.org/doi/10.1103/PhysRevB.79.041406>.

Bates, R.B.; Kroposki, L.M.; Potter, D.E. (1972). "Cycloreversions of Anions from Tetrahydrofurans. A Convenient Synthesis of Lithium Enolates of Aldehydes." *J. Org. Chem.* (37:4); pp. 560–562. <http://pubs.acs.org/doi/pdf/10.1021/jo00969a007>.

Baumann, T.F.; Worsley, M.A.; Han, T.Y.; Satcher, Jr., J.H. (2008). "High Surface Area Carbon Aerogel Monoliths with Hierarchical Porosity." *J. Non-Cryst. Solids* (354:29); pp. 3513–3515. <http://dx.doi.org/10.1016/j.jnoncrsol.2008.03.006>.

Behabtu, N.M., et al. (2010). "Spontaneous High-Concentration Dispersions and Liquid Crystals of Graphene." *Nat. Nanotechnol.* (5:6); pp. 406–411. <http://www.nature.com/nano/journal/v5/n6/full/nnano.2010.86.html>.

Bhatia, S.K.; Myers, A.L. (2006). "Optimum Conditions for Adsorptive Storage." *Langmuir* (22:4); pp. 1688–1700. <http://pubs.acs.org/doi/full/10.1021/la0523816>.

Borondics, F.; Bokor, M.; Matus, P.; Tompa, K.; Pekker, S.; Jakab, E. (2005). "Reductive Functionalization of Carbon Nanotubes." *Fuller. Nanotub. Car. N.* (13:S1); pp. 375–382. <http://dx.doi.org/10.1081/FST-200039375>.

Borondics, F.; Jakab, E.; Pekker, S. (2007). "Functionalization of Carbon Nanotubes via Dissolving Metal Reductions." *J. Nanosci. Nanotech.* (7:4–5); pp. 1551–1559. <http://dx.doi.org/10.1166/jnn.2007.339>.

Bowers, M.T. (1994). "Cluster Ions: Carbon, Met-Cars, and Sigma-Bond Activation." *Acc. Chem. Res.* (27:11); pp. 324–332. <http://dx.doi.org/10.1021/ar00047a002>.

Brown, C.M.; Liu, Y.; Yildirim, T.; Peterson, V.K.; Kepert, C.J. (2009). "Hydrogen Adsorption in HKUST-1: a Combined Inelastic Neutron Scattering and First-Principles Study." *Nanotechnology* (20:20); pp. 204025-1–204025-11. http://iopscience.iop.org/0957-4484/20/20/204025/pdf/0957-4484_20_20_204025.pdf.

Brown, C.M.; Yildirim, T.; Neumann, D.A.; Heben, M.J.; Gennett, T.; Dillon, A.C.; Alleman, J.L.; Fischer, J.E. (2000). "Quantum Rotation of Hydrogen in Nanotubes." *Chem. Phys. Lett.* (329:3–4); pp. 311–316. [http://dx.doi.org/10.1016/S0009-2614\(00\)01003-4](http://dx.doi.org/10.1016/S0009-2614(00)01003-4).

Buehl, M.; Thiel, W.; Schneider, U. (1995). "Magnetic Properties of C₆₀H₃₆ Isomers." *J. Am. Chem. Soc.* (117:16); pp. 4623–4627. <http://pubs.acs.org/doi/pdf/10.1021/ja00121a019>.

Cansado, I.P.P.; Goncalves, F.; Carrott, P.J.M.; Carrott, M. (2007). "High Micropore Activated Carbon Prepared from Polyetheretherketone." *Carbon* (45:12); pp. 2454–2455. <http://dx.doi.org/10.1016/j.carbon.2007.07.004>.

Carnahan, J.; Closson, W.D.J. (1972). "Reaction of Naphthalene Dianions with Tetrahydrofuran and Ethylene." *Org. Chem.* (37:26); pp. 4469–4471. <http://dx.doi.org/10.1021/jo00799a042>.

Carrington, A.; McLachlan, A.D. (1967). *Introduction to Magnetic Resonance with Applications to Chemistry and Chemical Physics*. New York: Harper & Row.

Chen, L.; Cooper, A.C.; Pez, G.P.; Cheng, H. (2008). "On the Mechanisms of Hydrogen Spillover in MoO₃." *J. Phys. Chem. C* (112:6); pp. 1755–1758. <http://pubs.acs.org/doi/full/10.1021/jp7119137>.

Chen, L.; Cooper, A.C.; Pez, G.P.; Cheng, H. (2007). "Density Functional Study of Sequential H₂ Dissociative Chemisorption on a Pt₆ Cluster." *J. Phys. Chem. C* (111:14); pp. 5514–5519. <http://pubs.acs.org/doi/full/10.1021/jp070181s>.

Chen, L.; Cooper, A.C.; Pez, G.P.; Cheng, H. (2007). "Mechanistic Study on Hydrogen Spillover onto Graphitic Carbon Materials." *J. Phys. Chem. C* (111:51); pp. 18995–19000. <http://pubs.acs.org/doi/full/10.1021/jp074920g>.

Chen, C.H.; Huang, C.C. (2007). "Hydrogen Storage by KOH Modified Multi-Walled Carbon Nanotubes." *Int. J. Hydrogen Energy* (32:2); pp. 237–246. <http://dx.doi.org/10.1016/j.ijhydene.2006.03.010>.

Chen, Z.F.; King, R.B. (2005). "Spherical Aromaticity: Recent Work on Fullerenes, Polyhedral Boranes, and Related Structures." *Chem. Rev.* (105:10); pp. 3613–3642. <http://pubs.acs.org/doi/full/10.1021/cr0300892>.

Cho, S.J.; Song, K.S.; Kim, J.W.; Kim T.H.; Choo, K. (2002). "Hydrogen Sorption in HCl-Treated Polyaniline and Polypyrrole: New Potential Hydrogen Storage Media." *Fuel Chemistry Division, 224th National Meeting of the American Chemical Society: August 18–22, 2002, Boston, Massachusetts*, Vol. 47; pp. 790–791.

Chung, T.C.M.; Jeong, Y.; Chen, Q.; Kleinhammes, A.; Wu, Y. (2008). "Synthesis of Microporous Boron-Substituted Carbon (B/C) Materials Using Polymeric Precursors for Hydrogen Physisorption." *J. Am. Chem. Soc.* (130:21); pp. 6668–6669. <http://pubs.acs.org/doi/full/10.1021/ja800071y>.

Ciobanu, C.V.; Zhao, Y. "Self-Mediated Hydrogen Migration in Pure Carbon Materials" (forthcoming).

Collins, D.J.; Zhou, H.-C. (2007). "Hydrogen Storage in Metal-Organic Frameworks." *J. Mater. Chem.* (17:30); pp. 3154–3160. <http://dx.doi.org/10.1039/b702858j>.

Conner, W.C.; Falconer, J.L. (1995). "Spillover in Heterogeneous Catalysis." *Chem. Rev.* (95:3); pp. 759–788. <http://dx.doi.org/10.1021/cr00035a014>.

Copley, J.R.D.; Neumann, D.A.; Kamitakahara, W.A. (1995). "Energy Distributions of Neutrons Scattered from Solid C₆₀ by the Beryllium Detector Method." *Can. J. Phys.* (73:11–12); pp. 763–771. <http://dx.doi.org/10.1139/p95-112>.

Dapprich, S.; Frenking, G. (1995). "Structure and Bonding of Transition Metal Dihydrogen Complexes [M(CO)₅(H₂)] (M = Cr, Mo, W)." *Angew. Chem., Int. Ed. Engl.* (34:3); pp. 354–357. <http://dx.doi.org/10.1002/anie.199503541>.

de Boer, J.H. (1968). *The Dynamical Character of Adsorption*, 2nd ed. Oxford, UK: Clarendon.

Dinca, M.; Dailly, A.; Liu, Y.; Brown, C.M.; Neumann, D.A.; Long, J.R. (2007). "Observation of Cu²⁺-H₂ Interactions in a Fully Desolvated Sodalite-Type Metal–Organic Framework." *Angew. Chem. Int. Ed.* (46:9); pp. 1419–1422. <http://dx.doi.org/10.1002/anie.200604362>.

Dinca, M.; Han, W.S.; Liu, Y.; Dailly, A.; Brown, C.M.; Long, J.R. (2006). "Hydrogen Storage in a Microporous Metal–Organic Framework with Exposed Mn²⁺ Coordination Sites." *J. Am. Chem. Soc.* (128:51); pp. 16876–16883. <http://dx.doi.org/10.1021/ja0656853>.

Dutta, G.; Waghmare, U.V.; Baidya, T.; Hegde, M.S. (2007). "Hydrogen Spillover on CeO₂/Pt: Enhanced Storage of Active Hydrogen." *Chem. Mat.* (19:26); pp. 6430–6436. <http://dx.doi.org/10.1021/cm071330m>.

- Eckert, J.; Nicol, J.M.; Howard, J.; Trouw, F.R. (1996). "Adsorption of Hydrogen in Ca-Exchanged Na-A Zeolites Probed by Inelastic Neutron Scattering Spectroscopy." *J. Phys. Chem.* (100:25); pp. 10646–10651. <http://dx.doi.org/10.1021/jp952982d>.
- Enoki, T.; Miyajima, S.; Sano, M.; Inokuchi, H. (1990). "Hydrogen–Alkali–Metal–Graphite Ternary Intercalation Compounds." *J. Mater. Res.* (5:2); pp. 435–466. <http://dx.doi.org/10.1557/JMR.1990.0435>.
- Enoki, T.; Sano, M.; Inokuchi, H. (1983). "Hydrogen in Aromatics. III. Chemisorption of Hydrogen in Graphite–Alkali Metal Intercalation Compounds." *J. Chem. Phys.* (78:4); pp. 2017–2029. <http://dx.doi.org/doi:10.1063/1.444949>.
- Ferro, Y.; Marinelli, F.; Allouche, A. (2003). "Density Functional Theory Investigation of the Diffusion and Recombination of H on a Graphite Surface." *Chem. Phys. Lett.* (368:5–6); pp. 609–615. [http://dx.doi.org/10.1016/S0009-2614\(02\)01908-5](http://dx.doi.org/10.1016/S0009-2614(02)01908-5).
- FitzGerald, S.A.; Yildirim, T.; Santodonato, L.J.; Neumann, D.A.; Copley, J.R.D.; Rush, J.J.; Trouw, F. (1999). "Quantum Dynamics of Interstitial H₂ in Solid C₆₀." *Phys. Rev. B.* (60:9); pp. 6439–6451. <http://link.aps.org/doi/10.1103/PhysRevB.60.6439>.
- Fricke, J.; Petricevic, R. (2002). "Carbon Aerogels," Chapter 4.10.2. Schüth, F.; Sing, K.S.W.; Weitkamp, J., eds. *Handbook of Porous Solids*, Weinheim, Germany: Wiley-VCH; pp. 2037–2062.
- Geohegan, D.B., et al. (2007). "In Situ Time-Resolved Measurements of Carbon Nanotube and Nanohorn Growth." *Phys. Status Solidi B* (244:11); pp. 3944–3949. <http://dx.doi.org/10.1002/pssb.200776204>.
- Ghosh, A.; Subrahmanyam, K.S.; Krishna, K.S.; Datta, S.; Govindaraj, A.; Pati, S.K.; Rao, C.N.R. (2008). "Uptake of H₂ and CO₂ by Graphene." *J. Phys. Chem. C* (112:40); pp. 15704–15707. <http://dx.doi.org/10.1021/jp805802w>.
- Goldmann, M.; Pilliere, H.; Beguin, F. (1989). "High Temperature Physintercalation into the 2nd Stage CsC₂₄." *Synthetic Met.* (34:1–3); pp. 59–65. [http://dx.doi.org/10.1016/0379-6779\(89\)90364-0](http://dx.doi.org/10.1016/0379-6779(89)90364-0).
- Gross, A.F.; Vajo, J.J.; Van Atta, S.L.; Olson, G.L. (2008). "Enhanced Hydrogen Storage Kinetics of LiBH₄ in Nanoporous Carbon Scaffolds." *J. Phys. Chem. C* (112:14); pp. 5651–5657. <http://dx.doi.org/10.1021/jp711066t>.
- Gulseren, O.; Yildirim, T.; Ciraci, S. (2002). "Metal Nanoring and Tube Formation on Carbon Nanotubes." *Phys. Rev. B* (66:4); pp. 045409-1–045409-5. <http://link.aps.org/doi/10.1103/PhysRevB.66.045409>.
- Guo, J.; Gui, B.; Xiang, S.X.; Bao, X.T.; Zhang, H.J.; Lua, A.C. (2008). "Preparation of Activated Carbons by Utilizing Solid Wastes from Palm Oil Processing Mills." *J. Porous Mat.* (15:5); pp. 535–540. <http://dx.doi.org/10.1007/s10934-007-9129-z>.
- Guo, K.B.C.; Kerns, P.; Castleman, A.W. (1992). "Ti₈C¹²⁺-Metallo-Carbohedrenes: A New Class of Molecular Clusters?" *Science* (255:5050); pp. 1411–1413. <http://www.sciencemag.org/cgi/reprint/255/5050/1411.pdf>.

- Hamaed, A.; Trudeau, M.; Antonelli, D. (2008). "H₂ Storage Materials (22KJ/mol) Using Organometallic Ti Fragments as σ -H₂ Binding Sites." *J. Am. Chem. Soc.* (130:22); pp. 6992–6999. <http://dx.doi.org/10.1021/ja710288g>.
- Haufler, R.E., et al. (1990). "Efficient Production of C₆₀ (Buckminsterfullerene), C₆₀H₃₆, and the Solvated Buckide Ion." *J. Phys. Chem.* (94:24); pp. 8634–8636. <http://dx.doi.org/10.1021/j100387a005>.
- Heremans, J.; Olk, C.H.; Morelli, D.T. (1994). "Magnetic Susceptibility of Carbon Structures." *Phys. Rev. B* (49:21); pp. 15122–15125. <http://link.aps.org/doi/10.1103/PhysRevB.49.15122>.
- Hornekaer, L.; Sljivancanin, Z.; Xu, W.; Otero, R.; Rauls, E.; Stensgaard, I.; Lægsgaard, E.; Hammer, B.; Besenbacher, F. (2006). "Metastable Structures and Recombination Pathways for Atomic Hydrogen on the Graphite (0001) Surface." *Phys. Rev. Lett.* (96:15); pp. 156104-1–156104-4. <http://link.aps.org/doi/10.1103/PhysRevLett.96.156104> .
- Hudson, J.L.; Casavant, M.J.; Tour, J.M. (2004). "Water-Soluble, Exfoliated, Nonroping Single-Wall Carbon Nanotubes." *J. Am. Chem. Soc.* (126:36); pp. 11158–11159. <http://dx.doi.org/10.1021/ja0467061>.
- Hummers, W.S.; Offeman, R.E. (1958). "Preparation of Graphitic Oxide." *J. Am. Chem. Soc.* (80:6); p. 1339. <http://dx.doi.org/10.1021/ja01539a017>.
- Jin, Z.; Lu, W.; O'Neill, K.J.; Parilla, P.A.; Simpson, L.J.; Kittrell, C.; Tour, J.M. (2011). "Nano-Engineered Spacing in Graphene Sheets for Hydrogen Storage." *Chem. Mater.* (23:4), pp. 923–925. <http://pubs.acs.org/doi/abs/10.1021/cm1025188>.
- Johnson, C.S.; Waugh, J.S. (1962). "Nuclear Relaxation in Adulterated Hydrogen." *J. Chem. Phys.* (36:9); pp. 2266–2272. <http://link.aip.org/link/JCPSA6/v36/i9/p2266/s1>.
- Kertesz, M.; Choi, C.H.; Yang, S.J. (2005). "Conjugated Polymers and Aromaticity." *Chem. Rev.* (105:10); pp. 3448–3481. <http://dx.doi.org/10.1021/cr990357p>.
- Kim, Y.-H.; Dillon, A.C.; Heben, M.J.; Zhang, S.B. (2005). "Hydrogen Storage in Novel Organometallic Buckyballs." *Phys. Rev. Lett.* (94:15); pp. 155504-1–155504-4. <http://link.aps.org/doi/10.1103/PhysRevLett.94.155504>.
- Kim, Y.-H., Zhao, Y.; Williamson, A.; Heben, M.J.; Zhang, S.B. (2006). "Nondissociative Adsorption of H₂ Molecules in Light-Element-Doped Fullerenes." *Phys. Rev. Lett.* (96:1); pp. 016102-1–016102-4. <http://link.aps.org/doi/10.1103/PhysRevLett.96.016102>.
- Kim, Y.-Y.; Sun, Y.Y.; Zhang, S.B. (2009). "Ab initio Calculations Predicting the Existence of an Oxidized Calcium Dihydrogen Complex to Store Molecular Hydrogen in Densities up to 100 g/L." *Phys. Rev. B* (79:11); pp. 115424-1–115424-5. <http://link.aps.org/doi/10.1103/PhysRevB.79.115424>.
- Kleinhammes, A.; Anderson, R.J.; Chen, Q.; Jeong, Y.; Chung, T.C.M.; Wu, Y. (2010). "Enhanced Binding Energy and Slow Kinetics of H₂ in Boron-Substituted Graphitic Carbon." *J. Phys. Chem. C* (114:32); pp. 13705–13708. <http://pubs.acs.org/doi/full/10.1021/jp102972c>

- Kohanoff, J.; Andreoni, W.; Parrinello, M. (1992). "A Possible New Highly Stable Fulleride Cluster: $\text{Li}_{12}\text{C}_{60}$." *Chem. Phys. Lett.* (198:5); pp. 472–477. [http://dx.doi.org/10.1016/0009-2614\(92\)80030-F](http://dx.doi.org/10.1016/0009-2614(92)80030-F).
- Kubas, G.J. (2007). "Fundamentals of H_2 Binding and Reactivity on Transition Metals Underlying Hydrogenase Function and H_2 Production and Storage." *Chem. Rev.* (107:10); pp. 4152–4205. <http://dx.doi.org/10.1021/cr050197j>.
- Kubas, G.J. (2001). "Metal–Dihydrogen and σ -Bond Coordination: the Consummate Extension of the Dewar–Chatt–Duncanson Model for Metal–Olefin π Bonding." *J. Organomet. Chem.* (635:1–2); pp. 37–68. [http://dx.doi.org/10.1016/S0022-328X\(01\)01066-X](http://dx.doi.org/10.1016/S0022-328X(01)01066-X).
- Kudin, K.N.; Scuseria, G.E.; Yakobson, B.I. (2001). " C_2F , BN, and C Nanoshell Elasticity From *ab initio* Computations." *Phys. Rev. B* (64:23); pp. 235406-1–235406-10. <http://link.aps.org/doi/10.1103/PhysRevB.64.235406>.
- Lachawiec, A.J.; Qi, G.S.; Yang, R.T. (2005). "Hydrogen Storage in Nanostructured Carbons by Spillover: Bridge-Building Enhancement." *Langmuir* (21:24); pp. 11418–11424. <http://dx.doi.org/10.1021/la051659r>.
- Lee, K.; Kim, Y-H.; Sun, Y.Y.; West, D.; Zhao, Y.; Chen, Z.; Zhang, S.B. (2010). "Hole Mediated Hydrogen Spillover Mechanism in Metal–Organic Frameworks," *Phys. Rev. Lett.* (104:23); pp. 236101–236104. <http://dx.doi.org/10.1103/PhysRevLett.104.236101>.
- Li, J.; Ziegler, T. (1996). "Periodic Trends and Ligand Effects in Transition Metal Dihydrogen Complexes: A Quasi-relativistic Density Functional Study." *Organometallics* (15:18); pp. 3844–3849. <http://dx.doi.org/10.1021/om950956w>.
- Li, Y.W.; Yang, F.H.; Yang, R.T. (2007). "Kinetics and Mechanistic Model for Hydrogen Spillover on Bridged Metal–Organic Frameworks." *J. Phys. Chem. C* (111:8); pp. 3405–3411. <http://dx.doi.org/10.1021/jp065367q>.
- Li, Y.W.; Yang, R.T. (2007). "Hydrogen Storage on Platinum Nanoparticles Doped on Superactivated Carbon." *J. Phys. Chem. C* (111:29); pp. 11086–11094. <http://dx.doi.org/10.1021/jp072867q>.
- Li, Y.W.; Yang, R.T. (2006). "Hydrogen Storage in Metal–Organic Frameworks by Bridged Hydrogen Spillover." *J. Am. Chem. Soc.* (128:25); pp. 8136–8137. <http://dx.doi.org/10.1021/ja061681m>.
- Liu, Y.; Brown, C.M.; Neumann, D.A.; Peterson, V.K.; Kepert, C.J. (2007). "Inelastic Neutron Scattering of H_2 Adsorbed in HKUST-1." *J. Alloys Compd.* (446/447); pp. 385–388. <http://dx.doi.org/10.1016/j.jallcom.2006.12.106>.
- Liu, Y.; Kabbour, H.; Brown, C.M.; Neumann, D.A.; Ahn, C.C. (2008). "Increasing the Density of Adsorbed Hydrogen with Coordinatively Unsaturated Metal Centers in Metal–Organic Frameworks." *Langmuir* (24:9); pp. 4772–4777. <http://dx.doi.org/10.1021/la703864a>.
- Lochan, R.C.; Head-Gordon, M. (2006). "Computational Studies of Molecular Hydrogen Binding Affinities: the Role of Dispersion Forces, Electrostatics, and Orbital

Interactions.” *Phys. Chem. Chem. Phys.* (8:12): pp. 1357–1370.
<http://dx.doi.org/10.1039/B515409J>.

Lomeda, J.R.; Doyle, C.D.; Kosynkin, D.V.; Hwang, W.F.; Tour, J.M.J. (2008). “Diazonium Functionalization of Surfactant-Wrapped Chemically Converted Graphene Sheets.” *J. Am. Chem. Soc.* (130:48); pp. 16201–16206.
<http://dx.doi.org/10.1021/ja806499w>.

Lueking, A.; Yang, R.T. (2002). “Hydrogen Spillover from a Metal Oxide Catalyst onto Carbon Nanotubes—Implications for Hydrogen Storage.” *J. Catal.* (206:1); pp. 165–168.
<http://dx.doi.org/10.1006/jcat.2001.3472>.

Marella, M.; Tomaselli, M. (2006). “Synthesis of Carbon Nanofibers and Measurements of Hydrogen Storage.” *Carbon* (44); pp. 1404–1413.
<http://dx.doi.org/10.1016/j.carbon.2005.11.020>.

Mavrandonakis, A.; Klopper, W. (2008). “Comment on ‘Kinetics and Mechanistic Model for Hydrogen Spillover on Bridged Metal-Organic Frameworks.’” *J. Phys. Chem. C* (112:8); pp. 3152–3154. <http://dx.doi.org/10.1021/jp074758h>.

McAllister, M.J., et al. (2007). “Single Sheet Functionalized Graphene by Oxidation and Thermal Expansion of Graphite.” *Chem. Mater.* (19:18); pp. 4396–4404.
<http://dx.doi.org/10.1021/cm0630800>.

McKeown, N.B., et al. (2006). “Towards Polymer-Based Hydrogen Storage Materials: Engineering Ultramicroporous Cavities within Polymers of Intrinsic Microporosity,” *Angew. Chem. Int. Ed.* (118:11); pp 1804–1807.
<http://dx.doi.org/10.1002/ange.200504241>.

Mitchell, P.C.H.; Ramirez-Cuesta, A.J.; Parker, S.F.; Tomkinson, J.; Thompsett, D. (2003). “Hydrogen Spillover on Carbon-Supported Metal Catalysts Studied by Inelastic Neutron Scattering. Surface Vibrational States and Hydrogen Riding Modes.” *J. Phys. Chem. B* (107:28); pp. 6838–6845. <http://dx.doi.org/10.1021/jp0277356>.

Mitchell, P.C.H.; Ramirez-Cuesta, A.J.; Parker, S.F.; Tomkinson, J. (2003). “Inelastic Neutron Scattering in Spectroscopic Studies of Hydrogen on Carbon-Supported Catalysts-Experimental Spectra and Computed Spectra of Model Systems.” *J. Mol. Struct.* (651–653); pp 781–785. [http://dx.doi.org/10.1016/S0022-2860\(03\)00124-8](http://dx.doi.org/10.1016/S0022-2860(03)00124-8).

Murata, K.; Kaneko, K.; Kanoh, H.; Kasuya, D.; Takahashi, K.; Kokai, F.; Yudasaka, M.; Iijima, S. (2002). “Adsorption Mechanism of Supercritical Hydrogen in Internal and Interstitial Nanospaces of Single-Wall Carbon Nanohorn Assembly.” *J. Phys. Chem. B* (106:43); pp. 11132–11138. <http://dx.doi.org/10.1021/jp020583u>.

Nielsen, M.J.P.M.; McTague, J.P.; Ellenson, W. (1977). *J. Phys., Coll. C* (38); pp. C4-10.

Nijkamp, A.G.; Raaymakers, J.E.M.J.; van Dillen, A.J.; de Jong, K.P. (2001). “Hydrogen Storage Using Physisorption – Materials Demands.” *Appl. Phys. A* (72:5); pp. 619–623.
<http://dx.doi.org/10.1007/s003390100847>.

- Novoselov, K.S.; Geim, A.K.; Morozov, S.V.; Jiang, D.; Zhang, Y.; Dubonos, S.V.; Grigorieva, I.V.; Firsov, A.A. (2004). "Electric Field Effect in Atomically Thin Carbon Films." *Science* (306); pp. 666–669. <http://dx.doi.org/10.1126/science.1102896>.
- Nyulasi, B.; Kovacs, A. (2006). "Theoretical Study of $F^-(H_2)_n$ and $Cl^-(H_2)_n$ ($n = 1-8$) Anion Complexes." *Chem. Phys. Lett.* (426:1-3); pp. 26–29. <http://dx.doi.org/10.1016/j.cplett.2006.05.083>.
- Oyama, S.T.; Keiffer, R. (1992). "Carbides, Survey." Howe-Grant, M.E., ed. *Kirk-Othmer Encyclopedia of Chemical Technology*, 3rd ed, Vol. 4, New York: John Wiley & Sons; pp. 476–482.
- Panella, B.; Hirscher, M.; Roth, S. (2005). "Hydrogen Adsorption in Different Carbon Nanostructures." *Carbon* (43:5696); pp. 2209–2214. <http://dx.doi.org/10.1016/j.carbon.2005.03.037>.
- Patchkovskii, S.; Tse, J.S.; Yurchenko, S.N.; Zhechkov, L.; Heine, T.; Seifert, G. (2005). "Graphene Nanostructures as Tunable Storage Media for Molecular Hydrogen." *Proc. Natl. Acad. Sci. USA* (102:30) pp. 10439–10444. <http://dx.doi.org/10.1073/pnas.0501030102>.
- Pekala, R.W. (1989). "Organic Aerogels from the Polycondensation of Resorcinol with Formaldehyde." *J. Mater. Sci.* (24:9); pp. 3221–3227. <http://dx.doi.org/10.1007/BF01139044>.
- Pekker, S.; Salvetat, J.-P.; Jakab, E.; Bonard, J.-M.; Forro, L. (2001). "Hydrogenation of Carbon Nanotubes and Graphite in Liquid Ammonia." *J. Phys. Chem. B* (105:33); pp. 7938–7943. <http://dx.doi.org/10.1021/jp010642o>.
- Penicaud, A.; Poulin, P.; Derre, A.; Anglaret, E.; Petit, P. (2004). "Spontaneous Dissolution of a Single-Wall Carbon Nanotube Salt." *J. Am. Chem. Soc.* (127:1); pp. 8–9. <http://dx.doi.org/10.1021/ja0443373>.
- Perdew, J.; Zunger, A. (1981). "Self-Interaction Correction to Density-Functional Approximations for Many-Electron Systems." *Phys. Rev. B* (23:10); pp. 5048–5079. <http://link.aps.org/doi/10.1103/PhysRevB.23.504>.
- Peterson, V.K.; Liu, Y.; Brown, C.M.; Kepert, C. (2006). "Neutron Powder Diffraction Study of D_2 Sorption in $Cu_3(1,3,5\text{-benzenetricarboxylate})_2$." *J. Am. Chem. Soc.* (128:49); pp. 15578–15579. <http://dx.doi.org/10.1021/ja0660857>.
- Prestipino, C., et al. (2006). "Local Structure of Framework Cu(II) in HKUST-1 Metallorganic Framework: Spectroscopic Characterization upon Activation and Interaction with Adsorbates." *Chem. Mater.* (18:5); pp. 1337–1346. <http://dx.doi.org/10.1021/cm052191g>.
- Puretzky, A.A.; Geohegan, D.B.; Styers-Barnett, D.; Rouleau, C.M.; Zhao, B.; Hu, H.; Cheng, M.D.; Lee, D.W.; Ivanov, I.N. (2008). "Cumulative and Continuous Laser Vaporization Synthesis of Single Wall Carbon Nanotubes and Nanohorns." *Appl. Phys. A* (93:4); pp. 849–855. <http://dx.doi.org/10.1007/s00339-008-4744-3>.

- Ritter, C.; Muller-Warmuth, W.; Schollhorn, R. (1985). "Structure and Motion of Hydrogen in Molybdenum Bronzes H_xMoO_3 as Studied by Nuclear Magnetic Resonance." *J. Chem. Phys.* (83:12); pp. 6130–6138. <http://link.aip.org/link/JCPSA6/v83/i12/p6130/s1>.
- Sakintuna, B.; Yurum, Y. (2005). "Templated Porous Carbons: A Review Article." *Ind. Eng. Chem. Res.* (44:9); pp. 2893–2902. <http://dx.doi.org/10.1021/ie049080w>.
- Schniepp, H.C., et al. (2006). "Functionalized Single Graphene Sheets Derived from Splitting Graphite Oxide." *J. Phys. Chem. B* (110:17); pp. 8535–8539. <http://dx.doi.org/10.1021/jp060936f>.
- Sermon, P.A.; Bond, G.C. (1974). "Hydrogen Spillover." *Catal. Rev.* (8:1); pp. 211–239. <http://dx.doi.org/10.1080/01614947408071861>.
- Sha, X.; Chen, L.; Cooper, A.C.; Pez, G.P.; Cheng, H. (2009). "Effect of C_{60} on the Photocatalytic Activity of TiO_2 Nanorods." *J. Phys. Chem. C* (113:31); pp. 11399–13905. <http://dx.doi.org/10.1021/jp902417j>.
- Sha, X.; Jackson, B. (2002). "First-Principles Study of the Structural and Energetic Properties of H Atoms on a Graphite (0 0 0 1) Surface." *Surf. Sci.* (496:3); pp. 318–330. [http://dx.doi.org/10.1016/S0039-6028\(01\)01602-8](http://dx.doi.org/10.1016/S0039-6028(01)01602-8).
- Sha, X.; Knippenberg, M.T.; Cooper, A.C.; Pez, G.P.; Cheng, H. (2008). "Dynamics of Hydrogen Spillover on Carbon-Based Materials." *J. Phys. Chem. C* (112:44); pp. 17465–17470. <http://dx.doi.org/10.1021/jp803495y>.
- Singh, A.K.; Ribas, M.A.; Yakobson, B.I. (2009). "H-Spillover through the Catalyst Saturation: An *Ab Initio* Thermodynamics Study." *ACS Nano* (3:7); pp. 1657–1662. <http://dx.doi.org/10.1021/nn9004044>.
- Slanina, Z.; Pulay, P.; Nagase, S. (2006). " H_2 , Ne, and N_2 Energies of Encapsulation into C_{60} Evaluated with the MPWB1K Functional." *J. Chem. Theory Comput.* (2:3); pp. 782–785. <http://dx.doi.org/10.1021/ct0503320>.
- Smith, A.P.; Benedek, R.; Trouw, F.R.; Minkof, M.; Yang, L.H. (1996). "Quasi-Two-Dimensional Quantum States of H_2 in Stage-2 Rb-Intercalated Graphite." *Phys. Rev. B* (53:15); pp. 10187–10199. <http://link.aps.org/doi/10.1103/PhysRevB.53.10187>.
- Smith, R.L.; Rohrer, G.S. (1998). "The Protonation of MoO_3 during the Partial Oxidation of Alcohols." *J. Catal.* (173:1); pp. 219–228. <http://dx.doi.org/10.1006/jcat.1997.1909>.
- Stalick, J.K.; Prince, E.; Santoro, A.; Schroder, I.G.; Rush, J.J. (1995). "Materials Science Applications of the New National Institute of Standards and Technology Powder Diffractometer." *Mater. Res. Soc. Symp. Proc.* (376); p. 101.
- Stankovich, S.; Dikin, D.A.; Dommett, G.H.B.; Kohlhaas, K.M.; Zimney, E.J.; Stach, E.A.; Piner, R.D.; Nguyen, S.T.; Ruoff, R.S. (2006). "Graphene-Based Composite Materials." *Nature* (442:7100); pp. 282–286. <http://dx.doi.org/10.1038/nature04969>.
- Stephens, R.D.; Gross, A.F.; Van Atta, S.L.; Vajo, J.J.; Pinkerton, F.E. (2009). "The Kinetic Enhancement of Hydrogen Cycling in $NaAlH_4$ by Melt Infusion into Nanoporous

- Carbon Aerogel.” *Nanotechnology* (20:20); pp. 204018-1–204018-6.
<http://dx.doi.org/10.1088/0957-4484/20/20/204018>.
- Stojkovic, D.; Zhang, P.; Lammert, P.E.; Crespi, V.H. (2003). “Collective Stabilization of Hydrogen Chemisorption on Graphenic Surfaces.” *Phys. Rev. B* (68:19); pp. 195406-1–195406-5. <http://link.aps.org/doi/10.1103/PhysRevB.68.195406>.
- Sun, Q.; Jena, P.; Wang, Q.; Marquez, M. (2006). “First-Principles Study of Hydrogen Storage on $\text{Li}_{12}\text{C}_{60}$.” *J. Am. Chem. Soc.* (128:30); pp. 9741–9745.
<http://dx.doi.org/10.1021/ja058330c>.
- Sun, Y.; Lee, K.; Kim, Y.-H.; Chen, W.; Chen, Z.; Zhang, S.B. (2010). “Accuracy of Density Functional Theory Methods for Weakly Bonded Systems: The Case of Dihydrogen Binding on Metal Centers.” *Phys. Rev. B* (82:7); pp. 073401-1–073401-4.
<http://link.aps.org/doi/10.1103/PhysRevB.82.073401>.
- Sun, Y.Y.; Kim, Y.-H.; Lee, K.; Zhang, S.B. (2008). “Accurate and Efficient Calculation of van der Waals Interactions Within Density Functional Theory by Local Atomic Potential Approach.” *J. Chem. Phys.* (129:15); pp. 154102-1–154102-8.
<http://link.aip.org/link/JCPSA6/v129/i15/p154102/s1>.
- Sun, Y.Y.; Lee, K.; Kim, Y.-H.; Zhang, S.B. (2009). “*Ab initio* Design of Ca-Decorated Organic Frameworks for High Capacity Molecular Hydrogen Storage with Enhanced Binding.” *Appl. Phys. Lett.* (95:3); pp. 33109-1–33109-3.
<http://link.aip.org/link/APPLAB/v95/i3/p033109/s1>.
- Sun, Y.Y.; Kim, Y.-H.; Zhang, S.-B. (2007). “Effect of Spin State on the Dihydrogen Binding Strength to Transition Metal Centers in Metal-Organic Frameworks.” *J. Am. Chem. Soc.* (129:42); pp. 12606–12607. <http://dx.doi.org/10.1021/ja0740061>.
- Sweany, R.L.; Ogden, J.S. (1997). “Infrared Characterization of Simple Adducts of Matrix-Isolated Cesium Fluoride and Sodium Chloride with Dihydrogen: Evidence of a Cation Interaction.” *Inorg. Chem.* (36:12); pp. 2523–2526.
<http://dx.doi.org/10.1021/ic960672j>.
- Tabony, J. (1980). “Nuclear Magnetic Resonance Studies of Molecules Physisorbed on Homogeneous Surfaces.” *Prog. Nucl. Magn. Reson. Spectrosc.* (14:1); pp. 1–26.
[http://dx.doi.org/10.1016/0079-6565\(80\)80001-X](http://dx.doi.org/10.1016/0079-6565(80)80001-X).
- Taylor, R.J. (1992). “Will Fullerene Compounds C_{78}X_6 Be Readily Formed?” *J. Chem. Soc., Perkin Trans. 2*; pp. 1667–1669. <http://dx.doi.org/10.1039/P29920001667>.
- Tomas, J.; Lledos, A.; Jean, Y. (1998). “A Theoretical Insight into the Ability of Group 6 ML_5 Metal Fragments to Break the H–H Bond.” *Organometallics* (17:23); pp. 4932–4939. <http://dx.doi.org/10.1021/om980308n>.
- Trewin, A.; Darling, G.R.; Cooper, A.I. (2008). “‘Naked’ Fluoride Binding Sites for Physisorptive Hydrogen Storage.” *New. J. Chem.* (32:1); pp. 17–20.
<http://dx.doi.org/10.1039/B714593D>.
- Wang, A. (2002). “Neon Matrix Infrared Spectrum of WH_6 : A Distorted Trigonal Prism Structure.” *J. Am. Chem. Soc.* (124:20); pp. 5636–5637.
<http://dx.doi.org/10.1021/ja020216w>.

- Wang, L.; Lee, K.; Sun, Y.-Y.; Lucking, M.; Chen, Z.; Zhao, J.J.; Zhang, S.B. (2009). "Graphene Oxide as an Ideal Substrate for Hydrogen Storage." *ACS Nano* (3:10); pp. 2995–3000. <http://dx.doi.org/10.1021/nn900667s>.
- Wang, X.; Andrews, L.; Infante, I.; Gagliardi, L. (2008). "Infrared Spectra of the $\text{WH}_4(\text{H}_2)_4$ Complex in Solid Hydrogen." *J. Am. Chem. Soc.* (130:6); 1972–1978. <http://dx.doi.org/10.1021/ja077322o>.
- Watanabe, K.; Kondow, T.; Soma, M.; Onishi, T.; Tamaru, K. (1973). "Molecular-Sieve Type Sorption on Alkali Graphite Intercalation Compounds." *Proc. R. Soc. Lond. A* (333:1592); pp. 51–67. <http://dx.doi.org/10.1098/rspa.1973.0047>.
- Watanabe, K.; Soma, M.; Onishi, T.; Tamaru, K. (1971). "Sorption of Molecular Hydrogen by Potassium Graphite." *Nature Physical Science* (233:43); pp. 160–161.
- Way, B.M.; Dahn, J.R.; Tiedje, T.; Myrtle, K.; Kasrai, M. (1992). "Preparation and Characterization of B_xC_{1-x} Thin Films with the Graphite Structure." *Phys. Rev. B* (46:3); pp. 1697–1702. <http://link.aps.org/doi/10.1103/PhysRevB.46.1697>.
- Wong-Foy, A.G.; Matzger, A.J.; Yaghi, O.M. (2006). "Exceptional H_2 Saturation Uptake in Microporous Metal-Organic Frameworks." *J. Am. Chem. Soc.* (128:11); pp. 3494–3495. <http://dx.doi.org/10.1021/ja058213h>.
- Yang, F.H.; Lachawiec, A.J.; Yang, R.T. (2006). "Adsorption of Spillover Hydrogen Atoms on Single-Wall Carbon Nanotubes." *J. Phys. Chem. B* (110:12); pp. 6236–6244. <http://dx.doi.org/10.1021/jp056461u>.
- Yang, Z.; Xia, Y.; Mokaya, R. (2007). "Enhanced Hydrogen Storage Capacity of High Surface Area Zeolite-like Carbon Materials." *J. Am. Chem. Soc.* (129:6); pp. 1673–1679. <http://dx.doi.org/10.1021/ja067149g>.
- Yildirim, T.; Ciraci, S. (2005). "Titanium-Decorated Carbon Nanotubes as a Potential High-Capacity Hydrogen Storage Medium." *Phys. Rev. Lett.* (94:17); pp. 175501-1–175501-4. <http://link.aps.org/doi/10.1103/PhysRevLett.94.175501>.
- Yoon, M.; Yang, S.Y.; Hicke, C.; Wang, E.G.; Geohegan, D.; Zhang, Z.Y. (2008). "Calcium as the Superior Coating Metal in Functionalization of Carbon Fullerenes for High-Capacity Hydrogen Storage." *Phys. Rev. Lett.* (100:20); pp. 206806-1–206806-4. <http://link.aps.org/doi/10.1103/PhysRevLett.100.206806>.
- Yoon, M.; Yang, S.; Wang, E.; Zhang, Z. (2007). "Charged Fullerenes as High-Capacity Hydrogen Storage Media." *Nano. Lett.* (7:9); pp. 2578–2583. <http://dx.doi.org/10.1021/nl070809a>.
- Yoshida, Z.I.; Dogane, I.; Ikehira, H.; Endo, T. (1993). "Investigation of Hydrogenation of C_{60} Using Theoretical Calculations." *Chem. Phys. Lett.* (201:5–6); pp. 481–484. [http://dx.doi.org/10.1016/0009-2614\(93\)85105-W](http://dx.doi.org/10.1016/0009-2614(93)85105-W).
- Yu, Y.; Bond, A.; Leonard, P.; Vollhardt, P.C.; Whitener, G.D. (2006). "Syntheses, Structures, and Reactivity of Radial Oligocyclopentadienyl Metal Complexes: Penta(ferrocenyl)cyclopentadienyl and Congeners." *Angew. Chem. Int. Ed.* (45:11); pp. 1794–1799. <http://dx.doi.org/10.1002/anie.200504047>.

Yuan, S.; Kirklin, S.; Dorney, B.; Liu, D.-J.; Yu, L. (2009). "Nanoporous Polymers Containing Stereocontorted Cores for Hydrogen Storage." *Macromolecules* (42:5); pp. 1554–1559. <http://dx.doi.org/10.1021/ma802394x> .

Zecho, T.; Guttler, A.; Sha, X.; Lemoine, D.; Jackson, B.; Kupperts, J. (2002). "Abstraction of D Chemisorbed on Graphite (0001) with Gaseous H Atoms." *Chem. Phys. Lett.* (366:1–2); pp. 188–195. [http://dx.doi.org/10.1016/S0009-2614\(02\)01573-7](http://dx.doi.org/10.1016/S0009-2614(02)01573-7).

Zhang, C.J.; Alavi, A. (2007). "Hydrogen Absorption in Bulk BC₃: A First-Principles Study." *J. Chem. Phys.* (127:21); pp. 214704-1–214704-7. <http://link.aip.org/link/JCPSA6/v127/i21/p214704/s1>.

Zhang, G.; Qi, P.; Wang, X.; Lu, Y.; Mann, D.; Li, X.; Dai, H. (2006). "Hydrogenation and Hydrocarbonation and Etching of Single-Walled Carbon Nanotubes." *J. Am. Chem. Soc.* (128:18); pp. 6026–6027. <http://dx.doi.org/10.1021/ja061324b>.

Zhang, X.; Cao, D.; Chen, J. (2003). "Hydrogen Adsorption Storage on Single-Walled Carbon Nanotube Arrays by a Combination of Classical Potential and Density Functional Theory." *J. Phys. Chem. B* (107:21); pp. 4942–4950. <http://dx.doi.org/10.1021/jp034110e>.

Zhao, Y.; Zhang, S.B.; Kim, Y.-H.; Heben, M.J. (2010). "Theory of Hydrogen Storage in Nanoscale Materials." Narlikar, A.V.; Fu, Y.Y., eds. *The Oxford Handbook of Nanoscience and Technology*, Vol. III, Oxford, UK: Oxford University Press, pp. 699–735.

Zhao, Y.; Kim, Y.-H.; Simpson, L.J.; Dillon, A.C.; Wei, S.-H.; Heben, M.J. (2008). "Opening Space for H₂ Storage: Cointercalation of Graphite with Lithium and Small Organic Molecules." *Phys. Rev. B* (78:14); pp. 144102-1–144102-5. <http://link.aps.org/doi/10.1103/PhysRevB.78.144102>.

Zhao, Y.; Heben, M.J.; Dillon, A.C.; Simpson, L.J.; Blackburn, J.L.; Dorn, H.C.; Zhang, S.B. (2007). "Nontrivial Tuning of the Hydrogen-Binding Energy to Fullerenes with Endohedral Metal Dopants." *J. Phys. Chem. C* (111:32); pp. 13275–13279. <http://dx.doi.org/10.1021/jp073482a>

Zhao, Y.; Dillon, A.C.; Kim, Y.-H.; Heben, M.J.; Zhang, S.B. (2006). "Self-Catalyzed Hydrogenation and Dihydrogen Adsorption on Titanium Carbide Nanoparticles." *Chem. Phys. Lett.* (425:4–6); pp. 273–277. <http://dx.doi.org/10.1016/j.cplett.2006.05.034>.

Zhao, Y.; Kim, Y.-H.; Dillon, A.C.; Heben, M.J.; Zhang, S.B. (2005). "Hydrogen Storage in Novel Organometallic Buckyballs." *Phys. Rev. Lett.* (94:15), 155504-1–155504-4. <http://link.aps.org/doi/10.1103/PhysRevLett.94.155504>.

Zhong, J.; Yao, J.; Kittrell, C.; Tour, J.M. (2011). "Bottom-Up Preparation of Synthetic Graphenes." *American Chemical Society NANO* (5); pp. 4112–4117.

Zhou, O., et al. (1991). "Structure and Bonding in Alkali-Metal-Doped C₆₀." *Nature* (351:6326); pp. 462–464. <http://dx.doi.org/10.1038/351462a0>.

Zielinski, M.; Wojcieszak, R.; Monteverdi, S.; Mercy, M.; Bettahar, M.M. (2005). "Hydrogen Storage on Nickel Catalysts Supported on Amorphous Activated Carbon." *Catal. Commun.* (6:12); pp. 777–783. <http://dx.doi.org/10.1016/j.catcom.2005.07.001>.

Zielinski, M.; Wojcieszak, R.; Monteverdi, S.; Mercy, M.; Bettahar, M.M. (2007). "Hydrogen Storage in Nickel Catalysts Supported on Activated Carbon." *Int. J. Hydrogen Energy* (32:8); pp. 1024–1032. <http://dx.doi.org/10.1016/j.ijhydene.2006.07.004>.

Zlotea, C.; Moretto, P.; Steriotis, T. (2009). "A Round Robin Characterisation of the Hydrogen Sorption Properties of a Carbon Based Material." *Int. J. Hydrogen Energy* (34:7); pp. 3044–3057. <http://dx.doi.org/10.1016/j.ijhydene.2009.01.079>.

Zuttel, A.; Sudan, P.; Mauron, P.; Wenger, P. (2004). "Model for the Hydrogen Adsorption on Carbon Nanostructures." *Appl. Phys. A* (78:7); pp. 941–946. <http://dx.doi.org/10.1007/s00339-003-2412-1>.

3.0 Results

3.1 Major Findings

The Hydrogen Sorption Center of Excellence (HSCoE) made substantial progress in developing sorbents for hydrogen storage. This included identifying numerous specific materials and entire material classes where development efforts either were not started or were ended, and where the HSCoE recommends that future efforts not be performed on these materials/classes. In addition, the HSCoE identified clear development paths for constructing sorbents that have the potential to meet the U.S. Department of Energy's (DOE's) revised 2015 and ultimate full-fleet targets for light-duty vehicles. The HSCoE recommends that development efforts for specific materials/classes be continued where there are viable routes for synthesizing sorbents that can be used to meet DOE's targets.

In general, the major findings for the HSCoE are aligned with the specific sorption mechanisms investigated. However, one of the more important conclusions of the center is related directly to the experimental measurements. During the past 5 years, the HSCoE has measured the hydrogen-storage properties of thousands of different sorbents from center partners and development groups around the world. The lack of consensus and the inability to validate storage capacity measurements stands out as a major problem that plagues the community. This problem is highlighted by the recent European Commission JRC report showing round-robin test results from the "Novel Efficient Solid Storage for Hydrogen" partners (Zlotea, Moretto, and Steriotis 2009), which found more than 100% deviation in capacities for the same relatively low-capacity sorption material. Reproducibility and measurement error problems tend to only get worse with higher-capacity laboratory-scale materials where only 50 to 100 mg may be available for measurement. To be fair, the results from a couple of the laboratories were similar, but interestingly, the agreement between the laboratories was different depending on the storage temperature of the measurements.

The HSCoE partners also had significant deviations between different partners, but the partners worked together to identify measurement differences and to work through the problems. This included working closely with the writing of DOE's *Recommended Best Practices for the Characterization of Storage Properties of Hydrogen Storage Materials* (DOE 2008), which provides a comprehensive and detailed set of methodologies for performing measurements. Paradoxically, implementation of, and the specific protocols used for, some of the methodologies still results in significant measurement differences, especially for high-capacity sorbents.

As shown in Figure 3-1, it is possible for two institutions that developed measurement systems completely independently to get the exact same isotherm for the same material. The HSCoE was fortunate to have three groups—the National Renewable Energy Laboratory (NREL), California Institute of Technology (Caltech), and the National Institute of Standards and Technology (NIST)—that had good agreement in hydrogen-storage-capacity isotherm results at different temperatures and pressures. The center worked together to help all the different groups develop protocols to accurately measure isotherms, but equipment and training limitations kept even a close group

such as the HSCoE partners from achieving complete agreement. In general, though, when partners worked together, hydrogen-storage-capacity measurements could be brought into close agreement for sorbents, and validation by specific laboratories is sufficient to ensure the competency of the results.

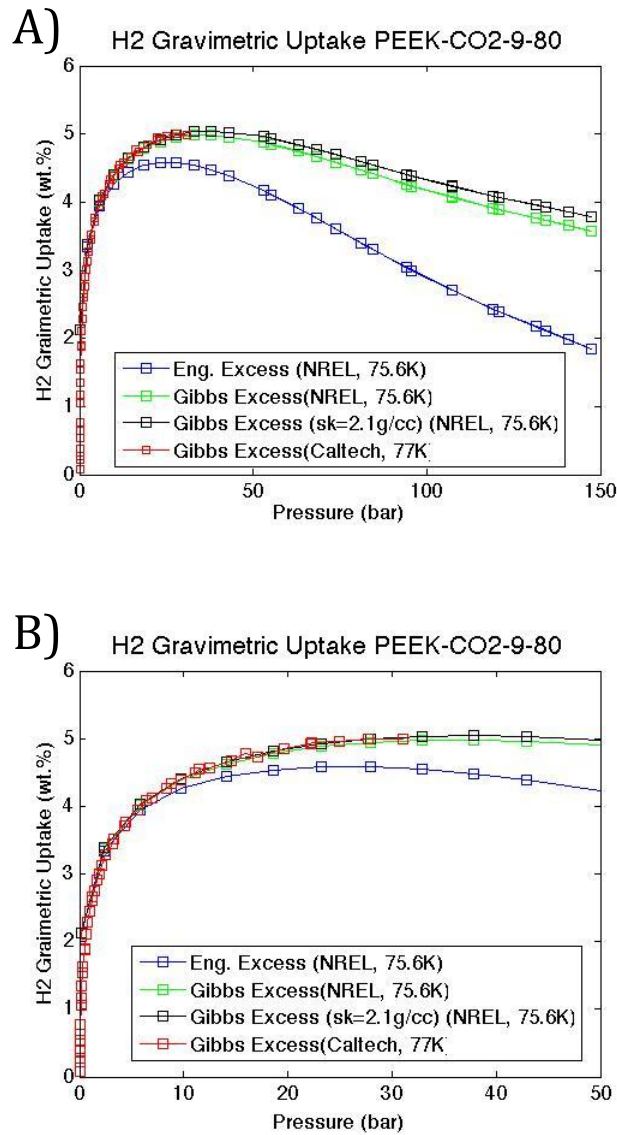


Figure 3-1. Excess H₂ gravimetric uptake isotherms ($\pm 0.1\%$ error) of a pyrolyzed PEEK material measured at NREL and Caltech. The agreement of the data from two different laboratories is exceptional, providing very good evidence of the outstanding hydrogen-storage properties of this sorbent. (A) Shows a full pressure range (0–150 bar) and (B) focuses on the lower-pressure region (0–50 bar). The estimated error of the excess H₂ gravimetric uptakes for the data from Caltech is $\pm 0.1\%$.

The important issue here is that the HSCoE, sorbent-development groups, and the hydrogen-storage community as a whole continue to waste valuable resources dealing with reports of exceptional hydrogen-storage results that ultimately in months or years turn out to be basic problems with measurements. As discussed below, one of the HSCoE recommendations directly addresses this issue by calling for sorbent standards and qualification practices to be implemented that go well beyond what can be accomplished with the Best Practices Document. The other reason for spotlighting this important measurement-reproducibility issue up front is that actual progress and major findings must be compared to validated results—not to unsubstantiated claims that ultimately cannot be reproduced. With this in mind, the HSCoE successfully advanced hydrogen-storage sorbents in a number of ways including improving nanostructures for optimal hydrogen storage and enhancing isosteric heats of adsorption along with capacities.

3.2 Optimized Nanostructures

In general, storage capacities for physisorption-based sorbents increase with higher specific surface areas SSAs and higher bulk densities. These are necessary requirements for high storage capacities, but other factors, including optimized pore sizes and enhanced binding energies for the entire capacity range, also play a role. The HSCoE focused efforts to improve all of these material properties independently and simultaneously. During the lifespan of the center, a tremendous amount of progress was made on increasing SSAs of materials using coordinated-framework and porous carbon materials. SSAs were increased by ~50%, gravimetric capacities were increased by ~40%, and volumetric capacities were increased by more than 100%.

The HSCoE pursued several synthetic routes to form optimized geometric materials using processes that include templating, graphene, aerogel, chemical, vapor, and/or pyrolysis. Even though most of these materials will require cryocompression, they have no significant heat-transport issues, can operate at moderate pressures, and may require the least engineering (compared to metal or chemical hydrides) to design and construct a storage system that could meet the DOE targets. Some of the center's accomplishments and findings related to optimized nanostructures for hydrogen storage follow.

3.2.1 Enhancing Physisorption Enthalpies Through Geometric Structures

The graphene layers in materials such as graphite and carbon nanotubes are one of the most ideal sorbents because they are lightweight, chemically resistive, strong, and have high thermal conductivity. However, the main issue is providing appropriate spacing (i.e., 0.7 to ~1.5 nm) between the graphene layers to maximize hydrogen storage. HSCoE partners, Rice University (Rice) and Caltech, investigated ways to prop open the graphene layers using intercalated scaffold molecules and alkali metals. Rice leveraged its extensive expertise with carbon nanotubes to form nanoribbons by exfoliating (Kosynkin 2009) graphite and integrating proppants such as aryl sulfonates, methyl dianiline, and t-butyl aniline (Lomeda 2008) to form graphene scaffolds. These graphene scaffolds effectively form idealized slit pores with the appropriate uniform spacing to provide hydrogen storage with a fairly uniform isosteric heat of adsorption over the entire capacity range. Using these methods the HSCoE constructed sorbents with SSAs as high as ~900 m²/g that have shown higher hydrogen-storage capacities than activated carbons

with similar SSAs. Ideally, graphene scaffolds could have SSAs $>2500 \text{ m}^2/\text{g}$ and maximum excess hydrogen-storage capacities $>7 \text{ wt } \%$ and 50 g/L at $\sim 80 \text{ K}$ and $\sim 40 \text{ bar}$. These graphene scaffolds can be formed into structural components including fibers and are projected to cost $\$1$ to $\$3/\text{kg}$ ($\$20$ to $\$70/\text{kg H}_2$). Furthermore, the graphene scaffolds functionalized with materials such as pyridine may be used to stabilize support alkali metals to electrostatically enhance hydrogen adsorption and enable higher-temperature storage. Although a significant amount of work is still required to synthesize scaffolded graphene sorbents that meet their potential in terms of capacities, these materials represent the “ideal” slit-pore geometry for optimal hydrogen storage in which almost all the hydrogen is sorbed with approximately the same isosteric heat of adsorption.

Isosteric heat, or the heat produced during the hydrogenation process, is an important parameter that must be considered when engineering hydrogen-storage systems. Material systems in which the isosteric heat decays with hydrogen loading create additional engineering challenge, because they will require different pressures and temperatures to load and unload the storage system.

To help understand this issue further and to provide insight with some of the graphene scaffolds being made by Rice, Caltech synthesized and evaluated stage 2 (i.e., two graphite layers with no guest material in between and alternating with an intercalated layer) alkali metal-intercalated graphites. Compared to typical activated carbons (Figure 3-2), these systems effectively maintain a constant isosteric heat for the entire capacity range (Figure 3-3). The isosteric heat in KC_{24^-} , RbC_{24^-} , and CsC_{24^-} -intercalated graphites are 9, 11, and 13 kJ/mol H_2 , respectively, and unlike most other physisorbents where the heats decay as a function of loading, the values from intercalated graphites are generally constant as a function of loading (Purewal 2010).

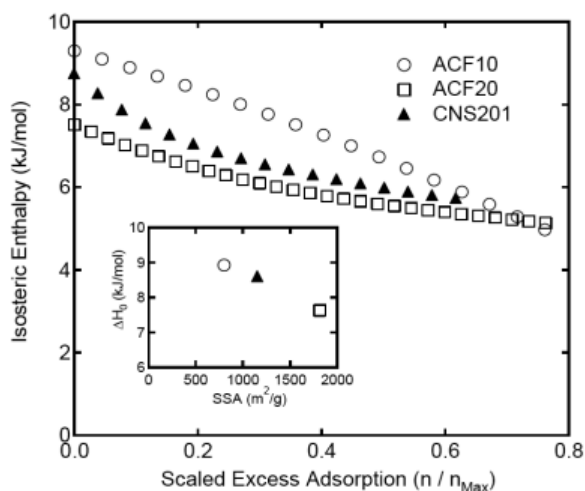


Figure 3-2. The H_2 isosteric enthalpy of adsorption for ACF10, ACF20, and CNS201 as a function of excess adsorption. Inset: the isosteric heat is plotted as a function of the fractional amount of adsorption (excess adsorption divided by the saturation adsorption amount at 77 K).

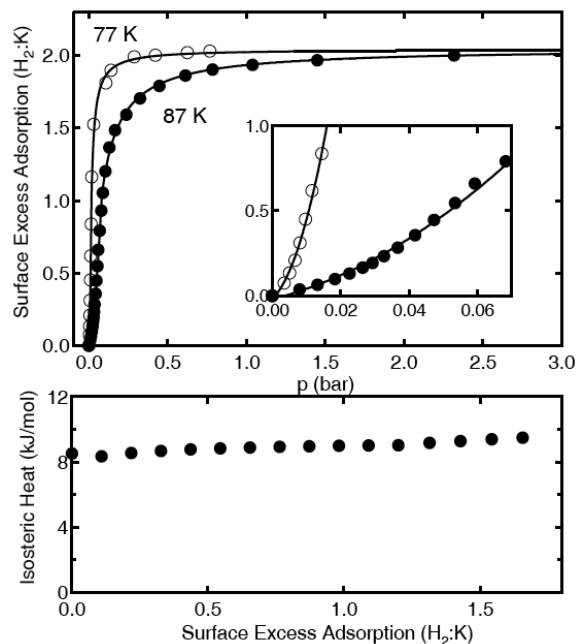


Figure 3-3. (Upper) 77 and 87 K isotherms of KC_{24} (K intercalated graphite) with a blowup of the low-pressure regime in the inset. (Lower) Plot of the isosteric enthalpy of adsorption demonstrating nearly constant sorption enthalpy values with loading.

The result from ACF10 is particularly important, because the near-single pore size in this material should provide a fairly constant heat of adsorption as a function of loading of ~ 5 kJ/mol. It should, but it does not. This result suggests that even in materials with uniform pore sizes, other effects or features may be important for hydrogen storage (e.g., edge, exterior surfaces, or surface functional groups). The alkali-intercalated graphite materials also demonstrate that higher isosteric heats of adsorption can be achieved with appropriate geometrical structures. However, as seen in Figure 3-3, the overall gravimetric hydrogen-storage capacity is substantially reduced (i.e., to ~ 2 wt % maximum excess adsorption at 77 K). This is because the higher heat of adsorption is being provided by the hydrogen molecule interacting with two graphene layers (instead of one), thus substantially decreasing the number of adsorption sites for other hydrogen molecules. Thus, while geometrical structures can provide higher heats of adsorption that enable a higher hydrogen capacity at higher temperatures, the overall maximum achievable capacity is substantially decreased. Specifically, the storage capacity of the alkali metal-intercalated graphite at 195 K is ~ 1.3 wt % or $\sim 65\%$ of the 2 wt % maximum excess at ~ 80 K. This is substantially higher than the 25% to 35% observed at ~ 195 K for typical single-walled physisorption materials (Richard, Bernard, and Chahine 2009), demonstrating that enhanced isosteric heats retain more of their hydrogen-storage capacities at higher temperatures. However, the ultimate storage capacities of typical high-SSA carbons at 195 K is ~ 2 wt %, so even though the retained component is less with lower binding energy, the increased SSA of typical activated carbons creates a higher overall capacity. These intercalated graphite results support the predictions of higher isosteric heats with narrower pore sizes in the range of 0.6 to 0.9 nm, the ability of intercalated graphite to monoatomically disperse alkali metals, and/or the potential enhanced heats of adsorption by electron donation to the lattice from the alkali atoms,

resulting in enhanced (10 to 15 kJ/mol) heats of adsorption. However, even if stage 1 (i.e., in which graphite layers and intercalated layers alternate) alkali metal or similar intercalated graphite materials could be made, effectively doubling or possibly tripling the capacities reported in Figure 3-3, the substantially smaller pore sizes needed to obtain the higher heats of adsorption result in capacities that are too low to be used to meet DOE 2015 targets.

The HSCoE work with intercalated and scaffolded graphite/graphene provided valuable insights into the effects of uniform pore distribution, geometrical structures providing enhanced isosteric heats of adsorption and thus higher retained capacities at higher temperatures, and potential methods to construct viable hydrogen-storage sorbents that may be used to meet DOE targets. In addition, this work clearly demonstrates that the only way to enhance isosteric heats of adsorption with geometrical structures requires multiple-wall adsorption effects that ultimately decrease the maximum excess capacity of the sorbent. It may be possible to attain higher capacities at temperatures approaching ambient with these geometrically enhanced heats, compared to that for typical physisorption materials, but the capacities for either will not be sufficient to meet DOE 2015 hydrogen-storage targets. Thus, the emphasis for future work to increase heats of adsorption must focus on enhanced binding to single surfaces and not on “geometrical structures” in which multiple-wall interactions are required. In effect, physisorption materials that have the largest gradients in isosteric heats as a function of loading probably have significant amounts of these sites that ultimately decrease the maximum attainable excess capacities, and thus should be reconfigured.

3.2.2 Increasing Specific Surface Area

As discussed previously, in general, storage capacities of physisorption-based materials increase with higher SSAs and higher bulk densities. Therefore, the HSCoE performed systematic experiments to determine viable methods to inexpensively increase the SSA of sorbents. Intrinsically, the solution-based synthesis processes associated with carbon aerogels and coordinated framework sorbents offer potentially inexpensive routes to high-SSA sorbent manufacturing. During the lifespan of the HSCoE, substantial progress was made on increasing SSAs and hydrogen-storage capacities of materials using coordinated framework and porous carbon materials. For example, sorbents were made with $>6000 \text{ m}^2/\text{g}$ Langmuir SSAs and excess hydrogen-storage capacities greater than 7 wt % and 35 g/L. This represents a 25%–50% increase in SSAs and storage capacities since the center’s inception, and has led to sorbents that may be used to meet DOE hydrogen-storage system targets.

3.2.2.1 Carbon Aerogels

Carbon aerogels (CAs) are a unique class of porous materials that possess a number of desirable structural features for the storage of hydrogen, including high SSAs ($>3000 \text{ m}^2/\text{g}$), continuous and tunable porosities, and variable densities. In addition, the flexibility associated with CA synthesis allows for the incorporation of modifiers or catalysts onto the surfaces of the carbon matrix in order to alter hydrogen sorption enthalpies in these materials. Since the properties of CAs can be systematically modified (i.e. surface chemistry, pore structure, amount/type of dopant), novel materials can be fabricated that exhibit enhanced hydrogen storage properties. Lawrence Livermore

National Laboratory (LLNL) within the HSCoE explored several approaches to synthesize new activated CA H₂ sorbents with Brunauer-Emmett-Teller (BET) SSAs in excess of 3200 m²/g (Baumann et al. 2008). These SSA values are the highest known for CAs and are comparable to those of the highest-SSA activated carbons. At 77 K, surface excess H₂ sorption of the CAs scales with BET SSA as high as ~2500 m²/g, yielding gravimetric densities as high as ~5 wt % H₂ (Kabbour et al. 2006). The SSA dependence for activated CAs with SSAs >3000 m²/g, however, is somewhat weaker, with these materials showing gravimetric densities of ~5.3 wt %. The weakened SSA dependence is due likely to the change in micropore structure that occurs at longer activation times; i.e., larger size structures that can produce higher SSAs ultimately do not add as much to hydrogen capacity. Nevertheless, the absolute value of 5.3 wt % is comparable to the highest values measured in other porous carbon systems. It is important to note that the surface excess hydrogen values are a measure of H₂ adsorbed on the surface of the CA only and do not account for free hydrogen gas in the pores of the CA. Therefore, total gravimetric hydrogen capacities (free and adsorbed) in these CA materials are higher than the surface excess values.

In addition to gravimetric capacity, volumetric capacity is an equally important consideration in the design of functional hydrogen sorbents. The bulk monolithic densities of the CA sorbents depend on the degree of activation, and, as a result, the volumetric capacity of these materials can range from 10 to 29 g H₂/L. Although these values are on par with those of other porous carbon materials, the volumetric capacities are still too low for practical storage systems, and pore-structure optimization (i.e., increased micropore volume) of the CA sorbents is required for increased hydrogen energy density. For example, as stated previously, further modification of the activation process should improve the micropore size distribution in the CA sorbents. The hydrogen-binding enthalpies measured for the activated CAs ranged from 6.7 to 6.2 kJ/mol, as would be expected for a carbon-based sorbent.

The key to commercial application of these materials will be increasing the volumetric hydrogen capacities in the activated CAs. Going forward, further modifications to both the aerogel framework and the activation process should yield CAs with increased volumetric capacities for hydrogen. These materials possess a number of other desirable qualities for use as hydrogen sorbents. For example, the CAs are prepared as robust and conformable monolithic structures, an important aspect both in terms of material handling and storage tank design. In addition, the thermal conductivity in these monolithic structures is greater than that of powder or granular sorbents. As a result, the CAs are expected to more efficiently manage the flow of heat in and out of the storage tank during charge/discharge cycles relative to beds of packed powders. Finally, the synthesis of these CA sorbents is relatively inexpensive and amenable to large-scale production. Recent cost analysis of resorcinol-formaldehyde aerogels have shown that these materials can be produced for less than \$2.00/kg, including the cost of raw materials, energy, manpower, equipment, and facilities (Carlson et al. 1995). From this analysis, the cost of materials, namely that of resorcinol, was determined to be the key cost driver in the manufacture of these materials. The overall cost of CA sorbents can be reduced significantly through the substitution of phenol for resorcinol in the sol-gel polymerization reaction. Although phenol is not as reactive as resorcinol in addition

reactions with formaldehyde, LLNL previously showed that phenol can indeed be used to prepare CA materials with textural properties similar to those prepared with resorcinol. When using phenol as the aromatic sol-gel precursor, the cost of the activated CAs is calculated to be less than \$0.60/kg. Therefore, these sorbent materials are viable candidates for the cryogenic storage of hydrogen in vehicular applications as well as other technologies, including stationary power generation or portable power sources. In general, CAs enable a very flexible format for tuning pore sizes and incorporating multiple components into a relatively inexpensive (less than \$12/kg H₂) sorbent. Although further optimization is required to help meet specific application targets, CAs are a scalable, commercially manufacturable route to making large quantities of hydrogen-storage sorbents.

3.2.2.2 Carbon Aerogel Scaffolds for Complex Hydrides

Among the various strategies investigated for the solid-state storage of hydrogen, the use of light-element complex hydrides, such as amides (i.e. NH₂⁻), borohydrides (BH₄⁻) and alanates (AlH₄⁻), offers a number of advantages, including high gravimetric and volumetric hydrogen capacities (Orimo et al. 2007). The thermodynamics and kinetics associated with reversible hydrogen storage in these systems, however, present significant obstacles to their use at reasonable operating temperatures and pressures. For example, decomposition of LiBH₄ to LiH, B, and 3/2 H₂ generates 13.6 wt % hydrogen (Zuttel et al. 2003). Yet, the enthalpy for this reaction is ~67 kJ/mol H₂ and, as a result, this system must be heated to temperatures greater than 400°C to produce an equilibrium H₂ pressure of 1 bar. In addition, the kinetics of both hydrogenation and dehydrogenation in these systems are quite slow. One approach to improve these reaction rates is through the incorporation of catalysts, such as Ti, into the light metal hydride system (Bogdanovic et al. 2000; Bogdanovic and Schwickardi 1997).

As an alternative, nanostructured hydrides have been shown to exhibit enhanced kinetics for reversible hydrogen storage relative to the bulk materials. The shorter diffusion distances for hydrogen as well as the other elements (e.g., Li, B) within the nanostructured hydride can lead to improved rates for both hydrogenation and dehydrogenation. This effect, however, is diminished after several cycles, which is due to coarsening of the material structure. To overcome this limitation, the center's efforts focused on the design of nanoporous materials that can act as scaffolds for nanostructured hydride materials. Incorporation of the metal hydride into a porous scaffolding material can potentially limit coarsening and, therefore, preserve the enhanced kinetics and improved cycling behavior of the nanostructured metal hydride. Previous work showed that the kinetics of hydrogen sorption in both chemical and complex hydrides can be improved through the use of nanoporous scaffold materials (Stephens et al. 2009; Gross et al. 2008; de Jongh et al. 2007; Yu et al. 2007; Zhang et al. 2007; Balde et al. 2006; Gutowska et al. 2005). Practical application of the scaffold approach, however, requires the design of porous solids with (1) small pore sizes (< 20 nm) to confine the nanostructured hydride, and (2) large accessible pore volumes (> 4 cm³/g) to minimize the gravimetric and volumetric capacity penalties associated with the use of the scaffold. In addition, these scaffold materials should be chemically inert, mechanically robust, and capable of managing thermal changes associated with the cycling of the incorporated metal hydride. LLNL worked with the Metal Hydride Center of Excellence (MHCoE) to

design and develop porous CA scaffolds. These efforts focused primarily on the design of porous carbon scaffolds for the mixed $\text{LiBH}_4/\text{MgH}_2$ system. This system was of particular interest in the MHCoe as an example of a destabilized metal hydride. Destabilization has been proposed as a means for overcoming the thermodynamic issues associated with using complex hydrides for reversible hydrogen storage at practical temperatures and pressures. The strategy involves the addition of a secondary component to a hydride system that forms an alloy or compound with the dehydrogenated products and, therefore, provides a lower energy pathway for H_2 sorption. In the case of $\text{LiBH}_4/\text{MgH}_2$, MgB_2 is formed in the dehydrogenated state, thus reducing the reaction enthalpy of the system (Vajo, Skeith, and Mertens 2005). LLNL's work on scaffold design was performed in collaboration with groups at HRL Laboratories and NIST. The majority of the efforts were directed toward fabrication and optimization of CA scaffold systems for LiBH_4 . Incorporation of metal hydrides into the scaffold and evaluation of the kinetics and cycling performance of these composites were performed at HRL. Characterization of the CA scaffolds and the metal hydride/scaffold composites using neutron scattering was performed at NIST.

The pore structure within CAs is largely determined by the sol-gel reaction chemistry. Several factors of the sol-gel polymerization reaction have a significant impact on network formation in these materials. For example, the amount and type of polymerization catalyst used in the sol-gel reaction influences the nucleation, growth, and interconnectivity of the primary particles that comprise the aerogel framework. The morphology and spatial arrangement of these particles, in turn, determines the textural properties of the CA. Using this flexibility, LLNL prepared a series of CA scaffolds to determine the extent to which the different structural aspects of the scaffold (e.g., pore diameter, interconnectivity, microporosity, surface chemistry) influence the kinetics of hydrogen exchange in LiBH_4 . The first-generation scaffolds possessed extremely large pore volumes ($\sim 3 \text{ cm}^3/\text{g}$), but also contained larger-diameter pores and broader pore-size distributions. Typically, CAs with large pore volumes also have larger pore diameters. The LiBH_4 composites prepared using these scaffolds exhibited $>8 \text{ wt } \%$ H_2 desorption and showed a decrease in hydrogen desorption temperature relative to bulk LiBH_4 (Figure 3-4, blue curve). Although these initial results were promising, reversibility of the metal hydride in the composite was poor, indicating that the average pore size of the scaffold was not sufficiently small to alter the kinetics during cycling. Through modification of the sol-gel formulation, specifically the amount of catalyst, a second series of CA scaffolds with smaller average pore sizes ($<10 \text{ nm}$) and narrower pore-size distributions were prepared. The resulting materials did not possess the large pore volumes of the first-generation scaffolds, but they allowed LBNL to investigate the influence of smaller pore sizes on the cycling of the LiBH_4 . Composites with LiBH_4 using these scaffolds did show a more significant decrease in H_2 desorption temperature when compared to the larger-pore materials. For example, the LiBH_4 composite prepared with a CA with an average pore size of 4 nm had a mid-point temperature of dehydrogenation of $\sim 357^\circ\text{C}$, compared to 453°C for bulk LiBH_4 (Figure 3-4, red curve). These results indicate that confinement of nanostructured LiBH_4 within the scaffold reduces the activation energy for dehydrogenation, the extent of which is likely correlated with the pore size of the scaffold. These materials, however, desorbed significantly less H_2 than the first-generation materials, a consequence of the smaller pore volumes of the scaffolds

(<1 cm³/g). To increase the pore volume in these small-pore scaffolds, LBNL further modified the sol-gel reaction through the addition of anionic surfactants to the sol-gel reaction (Worsley, Satcher, and Baumann 2010). These structure-directing agents influence the growth and organization of the primary particles that comprise the aerogel framework, yielding materials with smaller average pore size and larger pore volumes. The surfactants are then removed from the aerogel during the carbonization step. With this approach, scaffolds with average pore sizes of ~15 nm and pore volumes >2.5 cm³/g were prepared. This set of materials presented a significant step forward in terms of increasing pore volume in the scaffolds while maintaining smaller average pore sizes. The H₂ desorption temperatures observed for LiBH₄ composites prepared with these materials (~380°C) was in the range that would be expected for scaffolds with an average pore size of ~15 nm.

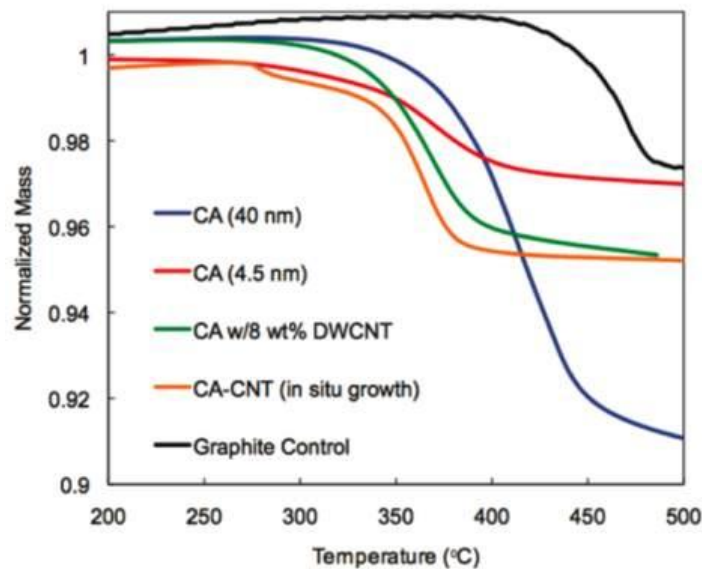


Figure 3-4. Representative thermal gravimetric analysis data for LiBH₄ incorporated into various CA scaffolds showing the influence of pore size and carbon nanotubes on the dehydrogenation reaction. The black curve is LiBH₄ mixed with nonporous graphite. The weight losses indicate dehydrogenation and scale with LiBH₄ loading.

Further structural refinement of these scaffolds presents a challenging trade-off in terms of porosity and mechanical properties. Increasing the pore volume in these scaffolds while maintaining small pore sizes requires that the walls defining the pore structure be very thin. The thickness of the wall structure, in turn, determines the mechanical integrity of the material. This aspect of scaffold design is an important consideration, as these materials need to have sufficient mechanical strength to withstand the stresses associated with infiltration and cycling of the metal hydride. As an illustration of this point, researchers prepared and tested two CA scaffolds with extremely large internal mesopore volumes. The first material had a pore volume of 4.6 cm³/g and an average pore size of ~15 nm, whereas the second material had a pore volume of 5.6 cm³/g and an average pore size of ~30 nm. Using their respective pore size and volumes and assuming a cylinder-

shaped pore geometry, an average wall thickness could then be estimated for these materials. The material with 30-nm pores had an estimated wall thickness of ~ 1.23 nm, and the scaffold with 15-nm pores had even thinner walls at ~ 0.78 nm. These values are much smaller than those calculated for the other CAs (2 to 3 nm) that had been tested as scaffolds for LiBH_4 . Not surprisingly, monolithic samples of both materials swelled and then broke apart during infiltration with molten LiBH_4 , indicating that the wall structures in these materials were not sufficiently thick to handle the wetting process. Based on these results, it is clear that viable scaffold candidates will need to be engineered with average wall thicknesses greater than 1.5 nm to exhibit the necessary mechanical integrity. Efforts in this area should continue to focus on the fabrication of new robust scaffold materials with optimal pore structures.

In addition to possessing the requisite porosity and mechanical properties, scaffold materials should also be capable of managing thermal changes associated with the cycling of the incorporated metal hydride. As described above, complex hydrides typically require high temperatures to produce a reasonable equilibrium pressure of hydrogen. Moreover, rehydrogenation of the complex hydride, if performed on a short time scale, can generate significant heat loads. Therefore, the framework of the scaffold should be designed to optimize thermal transport in the composite system. The thermal conductivity of CAs is reduced relative to an equivalent non-porous carbon, which is due mainly to the disordered nature of the CA skeleton that restricts phonon propagation in these materials. Because the thermal conductivity in CAs is dependent on the interconnectivity of the carbon framework, thermal conductivity in CAs typically scales with density (scaling factor of ~ 2.2) and can range from ~ 0.1 to 2 W/m K (Lu et al. 1993). One approach to improve the thermal transport properties of these materials is to prepare CA composites with a second material that exhibits superior thermal conductivity, such as carbon nanotubes (CNTs). CNTs possess high thermal conductivities (>1500 W/m K) and, based on their extremely high aspect ratios (100 to 1000), only small volume fractions (~ 0.01) are needed to create a percolation network within the CA scaffold. Additionally, CNTs can serve as reinforcing filler in the CA framework and may provide additional mechanical integrity to scaffolds with thinner wall structures. Our interest in CA-CNT composites as scaffolds is also related to the fact that CNTs and other graphitic structures have been reported to influence the rate of hydrogen exchange in complex hydrides, such as LiBH_4 and NaAlH_4 (Berseth et al. 2009; Fang et al. 2008). These reports contend that the interaction of the hydride with an electronegative surface, such as that of a carbon fullerene or nanotube, disrupts the bonding structure of the hydride and, as a result, provides lower-energy pathways for hydrogen exchange. Therefore, the incorporation of CNTs into the aerogel structure may provide multiple benefits in scaffold design in terms of thermal management, mechanical strength, and sorption kinetics.

In the course of this work, LLNL developed three different approaches to synthesizing CNT/CA scaffolds, with each yielding a distinct structural motif. The first approach involved the dispersion of low levels of double-walled CNTs (DWNT) into the walls of the CA structure. These materials were synthesized through the addition of the DWNTs to the sol-gel polymerization reaction. Because CAs are typically prepared in water, one

of the main challenges with this approach was efficient dispersion of the nanotubes in the reaction media to ensure uniform distribution within the aerogel framework. To address this issue, anionic surfactants were used to stabilize dispersions of the DWNT in the sol-gel reaction. With this approach, researchers synthesized a series of monolithic CA composites containing 1 to 8 wt % DWNT (up to 1.3 vol %) homogeneously distributed throughout the carbon network (Worsley, Satcher, and Baumann 2008). Although these composite scaffolds exhibited large pore volumes ($>2.5 \text{ cm}^3/\text{g}$), the aerogels also had rather large average pore sizes ($>30 \text{ nm}$). Interestingly, the incorporated DWNTs appear to reinforce the aerogel framework and limit the volumetric shrinkage that occurs during the carbonization process, leading to composites with lower densities and larger average pore sizes than would be expected based on the reaction formulation. These materials also exhibited enhanced thermal and electrical transport properties relative to the undoped CAs of equivalent density (Worsley, Satcher, and Baumann 2009). For example, the thermal conductivity of a CA composite containing 1 vol % DWNT was improved by a factor of two (0.072 vs. 0.036 W/m K) compared to that of a pristine CA of equivalent density. This approach, although promising, was limited in the amount of CNT that could be incorporated into the aerogel framework. Nevertheless, these materials were tested as scaffolds, and composites prepared with LiBH_4 showed a significant decrease in the dehydrogenation temperature (Figure 3-4). This observation was surprising considering the large average pore size of the scaffold and may indicate that the presence of the incorporated DWNTs in the walls of the scaffold, even at these low loading levels, is influencing the dehydrogenation process.

Based on these promising results, a second approach was developed that allowed for increased CNT loadings into the scaffold structure. For this process, highly purified single-walled CNTs (SWNT) were used, as these nanotubes can be readily suspended in water with sonication and do not require surfactants for dispersion. Unlike the first-generation CA-CNT composites, these materials comprise mostly SWNTs (up to 60 wt %), with the sol-gel-derived carbon serving as a “nanoglue” to crosslink randomly oriented bundles of SWNTs (Worsley et al. 2009a). The use of the carbon nanoglue allows bulk transport properties (i.e., thermal conductivity) to be maintained in the monolithic structures, even at low densities ($<10 \text{ mg}/\text{cm}^3$). These CNT foams are the stiffest low-density nanoporous solids reported and exhibit elastic behavior to strains as large as $\sim 80\%$. These results indicate that CNT incorporation can potentially be used to enhance the mechanical properties of the scaffolds. Because the skeletal network is defined by the large aspect ratio of the CNT bundles, these scaffolds possessed relatively large pore volumes and very large average pore sizes ($>50 \text{ nm}$). Therefore, these foams were not expected to influence the dehydrogenation rates through pore confinement of the metal hydride. These scaffolds were used, however, to examine the influence of higher CNT loadings on sorption kinetics. As with the previous generation of CA-CNT scaffolds, composites prepared with LiBH_4 using these scaffolds exhibited lower dehydrogenation temperatures ($\sim 360^\circ\text{C}$)—more than would be expected based on the pore size of the scaffold. Despite the large increase in CNT content in the scaffold, however, researchers did not observe a significant reduction in dehydrogenation temperature for these composites relative to those prepared with the first-generation CNT scaffolds. The observation may be attributed to the amount of accessible CNT SSA in

each type of scaffold. In the scaffolds with high CNT loading, the carbon nanoglue used to prepare the foam partially coats the surfaces of the CNT bundles, thus reducing the potential SSA available for interaction with the metal hydride. By contrast, the CNTs in the first-generation CA-CNT scaffolds are initially coated with a surfactant that is subsequently removed during the carbonization step, exposing the full SSA of the incorporated CNTs. Therefore, despite the large difference in CNT loading levels, the overall accessible SSA of CNTs in the two types of scaffold may not differ significantly, thus explaining the similarities in the dehydrogenation temperatures of the incorporated LiBH_4 .

To enhance the interaction between the CNTs and the incorporated metal hydride within the scaffold architecture, LLNL developed a third approach that involves the direct growth of CNTs on the inner surfaces of metal-loaded CAs using chemical vapor deposition. The nanotubes are grown within the free pore space of the aerogel and are not coated by sol-gel carbon, ensuring accessibility of metal hydride to the CNT surfaces. LLNL demonstrated the utility of this approach through the growth of multi-walled CNTs on metal-loaded CAs prepared by the ion-exchange method (Fe-loaded) (Steiner et al. 2007) and the impregnation/reduction method (Ni-loaded). An additional benefit of these systems is that the CNT catalysts, such as Ni, are also catalysts for hydrogen exchange in metal hydrides and, therefore, their presence in the scaffold may influence the kinetics of hydrogen sorption as well. Initial tests with LiBH_4 composites prepared with these materials showed an additional decrease in hydrogen-desorption temperature relative to LiBH_4 composites prepared with the other CNT-CA scaffolds (Figure 3-4, orange line). The extent to which the improved kinetics can be attributed to the increase in accessible CNT SSA or to the presence of the Ni nanoparticles was not determined. Nevertheless, this design approach appears promising and efforts should focus on optimizing both the CVD growth process as well as the overall pore structure of the scaffold.

Although pore size clearly influences dehydrogenation kinetics of hydrides, other aspects of the scaffold structure may play an important role in this process as well, such as surface texture/composition, micropore content, and pore connectivity. Efforts should continue to focus on how these structural features affect dehydrogenation rates of LiBH_4 . For example, thermal activation should be used to examine how microporosity influences hydrogen sorption. Thermal activation of CA scaffolds increases the total micropore volume in these materials without significantly changing the average mesopore size. The ability to tune the micropore content in these materials may provide some insight into the role that micropores play in this process. To study the effects of surface chemistry, thermal treatments should be used to modify the amount and type of edge site terminations (i.e. oxygen groups, free radicals) within the scaffold. Finally, the effects of pore morphology should be examined through the preparation of templated carbon materials that possess hexagonally ordered pore structures (Jun et al. 2000). While the average pore dimensions in these materials are similar to those of CA scaffolds, the arrangement of the pores, as ordered one-dimensional channels, is quite different from the disordered and tortuous mesoporous networks of traditional CAs. Therefore, comparison of the ordered porous carbons to the CAs as scaffolds may provide additional

information regarding the extent to which pore connectivity influences hydrogen desorption.

Increasing the functionality of the scaffold should be done through the incorporation of destabilizing agents or catalysts into the scaffold framework. Similar to dispersing graphitic structures, such as CNTs, into the scaffold to act as dehydrogenation catalysts for complex hydrides, LLNL can homogeneously coat the inner surfaces of CA scaffold structures with potential destabilizing agents. For example, LLNL developed a solution-based method that allows coating of the ligaments of carbon scaffolds with a uniform layer of TiO_2 without sacrificing a significant portion of the free pore volume in the scaffold (Worsley et al. 2009b). Recent work has shown that TiO_2 can serve as a destabilizing agent for LiBH_4 , with the formation of LiTiO_2 as the destabilized intermediate (Yu, Grant, and Walker 2008). This approach should be optimized to control the coating thickness so that the correct stoichiometry of LiBH_4 to TiO_2 exists in the composite structure.

Methods for controlling the surface chemistry of CAs need to be developed to improve the wetting behavior of other destabilizing entities, such as Mg, in these materials. As described earlier, one of the main goals in this effort is to design a scaffold structure that can accommodate the mixed $\text{LiBH}_4/\text{MgH}_2$ system. Magnesium metal, however, does not adequately wet the inner surfaces of these porous carbon structures to achieve the necessary loading levels for the mixed hydride system. In addition, a portion of the magnesium that does wet the CA is readily oxidized to MgO through reaction with surface oxygen groups. One approach developed in the MHCoe to increase the amount of Mg metal incorporated into CA scaffolds involves the deposition of metallic wetting layers (i.e., Ni or Cu) onto the surfaces of the scaffold (Gross et al. 2009). Alternatively, the decomposition of organomagnesium compounds within the pores of the scaffold has also been used for the incorporation of Mg into CAs (Zhang et al. 2009). Although both strategies have shown some promise for Mg incorporation, neither approach has afforded sufficiently high Mg loading levels in the scaffold. Therefore, LLNL needs to investigate methods for preparing scaffolds with surface coatings that are both inert and have improved wetting characteristics of the scaffold for magnesium metal. One route that could be investigated is the use of metal carbide or carbonitride coatings on the scaffold surfaces (Worsley et al. 2009c). Titanium carbide surfaces have been shown to exhibit better wetting compatibility with Mg than pure carbon surfaces (Levi, Bamberger, and Kaplan 1999). These coatings can be formed in scaffold structures through the heating of the TiO_2 -coated CAs to 1400°C under an argon atmosphere, leading to the carbothermal reduction of the TiO_2 film to TiC (or TiCN, if performed under N_2). These materials need to be investigated as substrates for loading with Mg metal.

LLNL's work within the HSCoe, as well as the other work within the MHCoe, has clearly demonstrated that porous scaffolds can be used to influence the kinetics of hydrogen desorption in complex hydrides. Several structural aspects of the scaffold appear to play a role in the improved kinetics. For example, the effect can be correlated, in part, to the average pore size of the scaffold, with smaller pores having a larger effect on the rate of dehydrogenation. Other textural properties of the scaffold, however, may

also influence the hydrogen-exchange process such as micropore content and surface chemistry. In addition, the incorporation of modifiers, such as CNTs, into the scaffold structure appears to have a notable effect on hydrogen desorption. Although the mechanism of this interaction is not yet fully understood, the presence of the nanotubes in the walls and/or pores of the scaffold decreases the temperature of hydrogen desorption for LiBH_4 , even in scaffold architectures with larger average pore sizes. LLNL needs to develop methods to further refine the structures of these CA-CNT nanocomposites and to incorporate other modifiers into the scaffold, specifically destabilizing agents such as Mg metal. Additional work is needed to identify the important mechanistic aspects of the observed kinetic effects in both the small-pore scaffolds and the CNT-CA composites. Further optimization of the aerogel architecture is also required for the design of robust scaffolds that can accommodate larger weight fractions of the complex hydride. Based on the progress made in this area, scaffolds present a promising option for improving the kinetics of hydrogen exchange in complex hydride systems.

3.2.2.3 Frameworks

In the past decade, interest has escalated in the study of framework materials based on their fascinating structures and intriguing application potential. Their exceptionally high SSAs, uniform and tunable pore sizes, and well-defined adsorbate interaction sites make them suitable for hydrogen storage. Various strategies to increase the hydrogen capacity of frameworks, such as using optimal pore sizes for hydrogen molecules, increasing SSA and pore volume, utilizing catenation, and introducing coordinatively unsaturated metal centers (CUMCs) have been widely explored to increase the hydrogen uptake. Inelastic neutron scattering (INS) and neutron powder diffraction as well as computational studies suggest that the choice of both metal centers and ligands can play an important role in tailoring the gas-framework interactions. Additionally, those ligands containing phenyl rings have proven favorable for hydrogen adsorption. Frameworks with outstanding SSAs and excellent gravimetric hydrogen-storage capacities have been reported (Long and Yaghi 2009) for reasonable pressures (i.e., 30 to 50 bar) and cryogenic temperatures (i.e., 77 K). Increasing the weak interaction between hydrogen molecules and frameworks and eliminating pore sizes greater than ~ 2 nm were the major focus of the HSCoE's efforts.

Initially, Dr. Omar Yaghi's group at the University of California, Los Angeles (formally at the University of Michigan) was part of the HSCoE. During this participation, UCLA synthesized metal-organic frameworks (MOFs) such as MOF-177, which at the time had the highest specific SSA ($\sim 5900 \text{ m}^2/\text{g}$, Langmuir) and gravimetric hydrogen-storage capacity ($\sim 6.8 \text{ wt } \%$) of any known material. UCLA has subsequently gone on to make several more materials with higher SSAs and gravimetric capacities approaching $8 \text{ wt } \%$. (Furukawa 2010) After Dr Yaghi left the HSCoE in 2007, Dr. Hangcai Zhou at Texas A&M University (TAMU) joined to continue development of framework materials. TAMU focused on preparing and evaluating frameworks with catenation isomer pairs, nanoscopic cages based on double-bond-coupled di-isophthalate linkers, stability by incorporating mesocavities with microwindows, and CUMCs.

Catenated Frameworks

TAMU used catenation, the intergrowth of two or more identical frameworks, as an alternative way to form MOFs with less meso- and macroporosity. TAMU determined that catenation can lead to a 41% improvement of apparent Langmuir surface area (3800 m²/g catenation versus 2700 m²/g noncatenation), a 67% increase in excess gravimetric hydrogen uptake (6.7 versus 4 wt %) at 77 K and ~50 bar, and a 160% increase in volumetric hydrogen uptake (9.19 versus 3.49 kg/m³) in the catenation isomer pair called PCN-6/PCN-6'. INS spectroscopy studies revealed that the first sites occupied by H₂ are the open Cu centers of the paddlewheel units in both PCN-6 and PCN-6'. However, PCN-6 contains three specific H₂-binding Cu sites, whereas PCN-6' has only one. At high hydrogen loadings, the interaction between H₂ molecules and the organic linkers is stronger in catenated PCN-6 than that in noncatenated PCN-6'. This stronger interaction resulted in more effective hydrogen binding sites in catenated PCN-6. This work demonstrates that, in the correct framework, catenation can substantially increase capacities and the bulk density of the sorbent. However, frameworks with even higher bulk densities need to be developed to meet DOE hydrogen-storage targets.

Double-Bond-Coupled Di-Isophthalate Linkers

To better understand the role framework linkers play in hydrogen storage, TAMU studied double-bond-coupled di-isophthalate linkers in place of the phenyl rings typically used for hydrogen adsorption. To do this, TAMU synthesized MOFs containing nanoscopic cages based on two predesigned double-bond-coupled bis(isophthalate) ligands: azobenzene-3,3',5,5'-tetracarboxylate (abtc) and transstilbene-3,3',5,5'-tetracarboxylate (sbtc). Solvothermal reactions of Cu(NO₃)₂ with H₄abtc or H₄sbtc give rise to isostructural PCN-10 and PCN-11, respectively. In these frameworks, two copper atoms are linked by four bridging carboxylates to form a paddlewheel secondary building unit (SBU) and become coordinatively unsaturated on removal of the axial water ligands. Every 12 ligands connect 6 paddlewheel SBUs to form an octahedral cage with 8 triangular openings of 8.13 × 9.26 Å² and about 900 Å³ of space, providing an accessible interior surface for gas storage. Every 8 octahedral cages connect to each other through vertex sharing to form an elongated cuboctahedral cage. Each cuboctahedral cage connects 6 other cuboctahedral cages and 6 octahedral cages, leading to an extended NbO-type 3-D network with two types of oval-shaped channels. One type has an open window size of 8.13 × 9.26 Å² on the [0, 15, 13] plane, and the other is 8.13 × 8.13 Å² viewed from the c axis.

The enduring porosity of PCN-10 and PCN-11 is confirmed by gas-adsorption studies. The N₂ adsorption isotherms of the activated samples exhibit type-I sorption behavior with a BET surface area of 1407 or 1931 m²/g and a total pore volume of 0.67 or 0.91 mL/g for PCN-10 or PCN-11, respectively. In particular, both contain nanoscopic cages that are particularly suitable for gas storage. The maximum excess adsorption at 77 K occurs around 20 bar and reaches values of 4.33% (33.2 g/L) and 5.05% (37.8 g/L) for PCN-10 and PCN-11, respectively. Gas-adsorption experiments suggest that MOFs containing C=C double bonds are more favorable than those with N=N double bonds in retaining enduring porosity after thermal activation, although the N=N double bond has slightly higher H₂ affinity.

“Close-Packing” Alignment of Open Metal Sites

Many efforts have been devoted to the enhancement of hydrogen affinity in frameworks to increase hydrogen-storage capacities. In addition to the framework interpenetration and constructing optimally sized pores for hydrogen storage, another approach uses the higher affinities of the metals in the framework materials. However, as discussed previously, these coordinated metals are often sterically hindered from hydrogen adsorption. Thus TAMU developed frameworks that enhance H₂ uptake by strengthening the MOF-H₂ interaction via increasing the number of nearest-neighbor open metal sites of each H₂-hosting void in a 3-D framework and by aligning the open metal sites so that they interact directly with the guests (H₂ molecules) inside the void. To do this, TAMU designed a ligand using 5,5'-methylene-di-isophthalate (mdip) and two Cu-mdip to form frameworks labeled PCN-12 and PCN-12' (see Figure 3-5).

PCN-12 adopts a dicopper paddlewheel motif as its SBU (see Figure 3-5). The paddlewheel occupies the 12 vertices of a cuboctahedron, whereas 24 isophthalate motifs span all 24 edges. As expected, at the 12 corners of the cuboctahedron are 12 open copper-coordination sites pointing toward the center of the cage. Each square face is connected to another square face of a neighboring cuboctahedron through four mdip bridges. Every cuboctahedron connects to six others in three orthogonal directions to form a 3-D net. However, in PCN-12' every mdip ligand has C_{2v} symmetry. Each of the six paddlewheels connects three mdip ligands in a trigonal-prismatic fashion with paddlewheel units occupying all corners of the “prism” and the three mdip ligands residing on the three sides. Evidently, the open metal coordination sites point away from the cavity of the polyhedron.

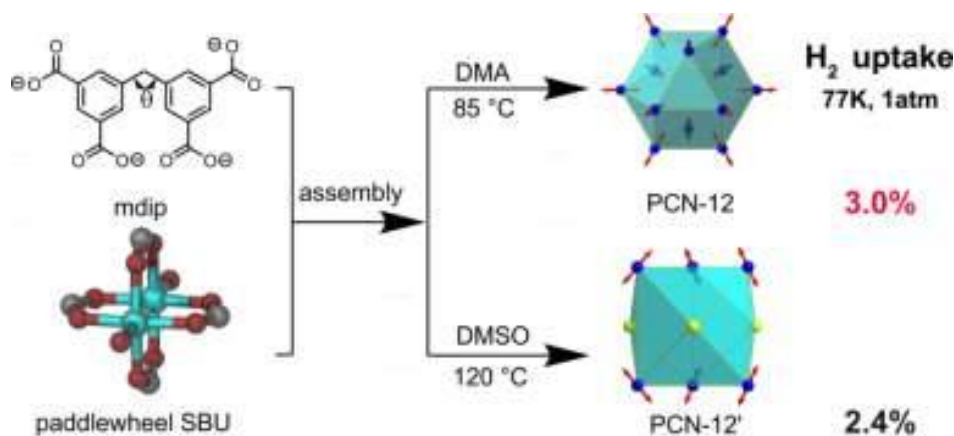


Figure 3-5. Schematic of TAMU's PCN-12 and 12' materials. Small adjustments enable metal centers to be more open and accessible for hydrogen storage.

The BET surface area and pore volume of PCN-12 are 1943 m² g⁻¹ and 0.94 mLg⁻¹, respectively, whereas those for PCN-12' are 1577 m² g⁻¹ and 0.73 mLg⁻¹, respectively. The hydrogen-adsorption isotherm of PCN-12' shows a 2.40 wt % (20.4 gL⁻¹) hydrogen uptake at 77 K and 1 bar, which is comparable to those of other MOFs containing cuboctahedral cages. However, PCN-12 exhibits an exceedingly high hydrogen uptake of 3.05 wt % (23.2 gL⁻¹) under the same conditions. This high hydrogen uptake of PCN-12, compared to PCN-12', can be ascribed to both the formation of cuboctahedral cages and

the alignment of open metal sites within each cage of the open copper sites in PCN-12, strengthening the H₂-framework interaction. To our knowledge, PCN-12 possesses the highest hydrogen uptake reported for a MOF at 1 bar and 77 K. As polymorphs of each other, PCN-12 and PCN-12' have not only the same formula after solvate removal, but also the same atom-to-atom connectivity. However, the gravimetric hydrogen uptake of PCN-12 is 27% higher than that of PCN-12' at 77 K and 1 bar. These remarkable improvements can be attributed mainly to the “close-packing” strategy, namely, the formation of cuboctahedral cages and the unique alignment of open metal sites in each cuboctahedral cage in PCN-12. This strategy may have general implications in the search for a practical adsorptive hydrogen-storage material for fuel-cell-driven cars.

Mesocavities and Microwindows

TAMU also investigated other methods to increase hydrogen-storage capacities of framework materials including increasing the aromaticity of the organic linkers, which lead to relatively higher initial isosteric heats of adsorption (i.e., 8.6 kJ/mol); the use of lanthanide, which has a larger coordination sphere and more flexible coordination geometry that, among other things, may help with selective adsorption of H₂; 3-D interdigitated (also known as inclined interpenetration) frameworks constructed from 2-D sheets to create structures with sorption hysteresis; and frameworks with the incorporation of mesocavities and microwindows. For the latter, polyhedron-based frameworks may lead to higher stability and porosity if the sizes of the open windows of the polyhedra are limited. A (3,24)-connected network was achieved by connecting the 24 edges of a cuboctahedron (or the 24 corners of a rhombicuboctahedron) with a linker having C₃ symmetry. On the basis of this connection mode, an isorecticular series of MOFs can be obtained by changing the size of the linker while keeping the cuboctahedron building units unchanged. TAMU developed a strategy for stabilizing frameworks with high SSAs by introducing mesocavities with microwindows into the MOFs based on this (3,24)-connected network. The nanoscopic hexatopic carboxylate ligands designed for this purpose are 5,5',5''-benzene-1,3,5-triyltris(1-ethynyl-2-isophthalate) (btei) and 5,5',5''-(4,4',4''-nitriyltris(benzene-4,1-diyl)tris(ethyne-2,1-

diyl))triiisophthalate (ntei), and solvothermal reactions of H₆btei and H₆ntei with copper salts yielding four MOFs: PCN-61, PCN-66, PCN-68, and PCN-69 (Figure 3-6).

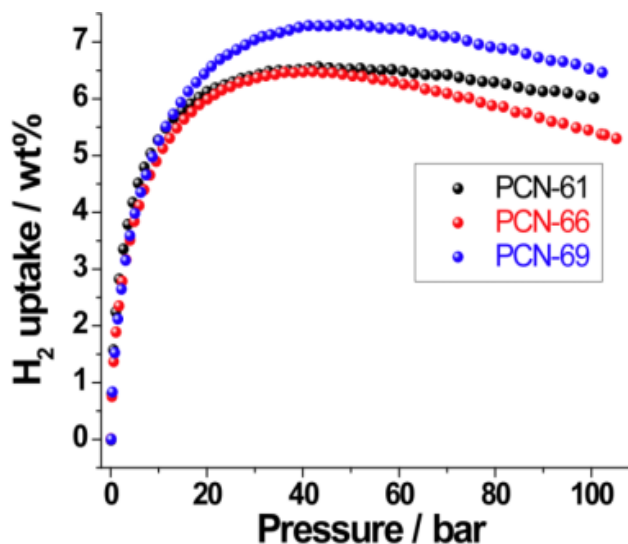


Figure 3-6. Isotherms of PCN materials made by TAMU. Note that the data labeled PCN-69 in this graph actually correlate to PCN-68. The data were measured by Dailly and coworkers at General Motors.

As expected, PCN-61 and PCN-66 are isostructural. The three isophthalate moieties in bte of PCN-61 are linked through the copper paddlewheel clusters to form the cuboctahedral SBUs, which are covalently linked through the 5-positions of the isophthalate moieties to form a (3,24)-connected network. The 3-D framework can be viewed as the packing of three types of polyhedron: a cuboctahedron (13 Å), a truncated tetrahedron (T-Td, 15 Å), and a truncated octahedron (T-Oh, 23 Å). Each truncated triangular face of a T-Td or T-Oh is fully occupied by one ligand. Each cuboctahedron shares its eight triangular faces with eight T-Tds and its six square faces with six T-Ohs. It is evident that increasing the size of the central part of the ligand can further enlarge the size of the T-Oh, which is accompanied by a mild increase in the size of the T-Td and no change in the size of the cuboctahedron. Accordingly, for PCN-66, the diameters are 13 Å for cuboctahedron, 16 Å for the T-Td, and 26 Å for the T-Oh.

From the crystal structure, it is evident that the sizes of the cavities within the two MOFs range from microporous (cuboctahedron and T-Td) to mesoporous (T-Oh). This hierarchical porous structure is reflected in the N₂ sorption isotherms collected at 77 K. The hybrid porous structures exhibit reversible pseudo-type-I isotherms with a small step before the plateau appears, as is typical in MOFs with both micro- and mesopores. With the BET model, an activated PCN-61 sample was estimated to have a SSA of 3000 m² g⁻¹, and the Langmuir surface area was 3500 m² g⁻¹ assuming monolayer coverage. For PCN-66, in which the larger ligand was used, there was a remarkable increase in SSA (BET, 4000 m² g⁻¹ and Langmuir, 4600 m² g⁻¹), which supports TAMU's hypothesis that the expansion of the ligand leads to increased SSA. The use of even larger hexatopic carboxylate ligands in PCN-68 and PCN-69 led to even higher SSAs of 6033 m²/g Langmuir (5109 m²/g BET) and 6268 m²/g (3866 m²/g BET), respectively. To the best of the TAMU research team's knowledge, PCN-69 possesses the highest Langmuir surface area reported to date for MOFs based on paddlewheel clusters. These materials also had good maximum excess hydrogen-storage capacities with PCN-69 having the highest at 7.2 wt % (Figure 3-6).

Although additional work needs to be performed to increase the SSAs and capacities of these materials further, TAMU has demonstrated several methodologies for increasing the hydrogen-storage capacities of framework materials. These efforts have led to development of novel frameworks with some of the highest SSAs and hydrogen capacities reported to date. Another focus of the HSCoE and TAMU was to make framework materials with good bulk densities and thus high volumetric excess capacities. TAMU demonstrated that cantenation is a viable route to improving volumetric capacities, but a substantial amount of additional development will be needed to attain framework materials with exceptional volumetric capacities (i.e., 30 to 50 g/L at 77 K). Ultimately, it should be possible to create frameworks with high bulk densities and perhaps with higher heats of adsorption to enhance volumetric capacities and capacities at higher temperatures.

3.2.3 Increasing Volumetric Capacity

As discussed previously, volumetric capacity scales with gravimetric capacity through material density. Simultaneously increasing volumetric and gravimetric capacity requires increasing both SSA and material “bulk” density, which means pores of just the right size need to be used. Specifically, the pores must be large enough to allow single-wall interaction of all the surfaces with dihydrogen. In addition, capillary or equivalent effects may also play a role in enhanced capacities of microporous materials. Thus, ideally, depending on the specific pore geometry, pores should be at least twice the kinetic diameter of hydrogen molecules (i.e., ~0.3 nm), and to allow an extra layer of hydrogen to go between those sorbed on the walls, perhaps larger than three times the kinetic diameter. This suggests that optimal pore sizes for hydrogen storage is somewhere between 0.7 and 1.5 nm, again depending upon the pore geometry. In the case of “slit pores” (e.g., graphene sheets), the interplane distance should be ~0.9 nm. However, in the case of cylindrical or spherical pores, the diameters should be a little bigger to enable enough access for hydrogen molecules over the entire surface. The main point here is that optimal pore sizes lead to higher bulk densities and thus higher volumetric capacities. As shown in Figure 2-3, if bulk densities greater 1 g/L can be achieved with 6 to 7 wt % hydrogen-storage materials, then volumetric capacities surpassing those of liquid hydrogen (i.e., 70 g/L) could be achieved at a much higher temperature than 20 K (i.e., ~80 K). This will dramatically reduce system and delivery costs.

In addition to the techniques discussed above involving graphite, carbon aerogels, and framework materials, the HSCoE members synthesized new high-SSA physisorption materials with optimal uniform pore size using a variety of scalable/inexpensive processes, such as zeolite templated carbons, controlled activation/pyrolyzation of polymers and bulk carbons, and synthesis of porous polymers. For example, Argonne National Laboratory (ANL) in conjunction with the University of Chicago (UC) worked on developing polymers with intrinsic porosity (Figure 3-7). Porous polymers with greater than 1800 m²/g BET SSAs have been synthesized. Unlike heterogeneous pore-size materials (e.g., activated carbon), ANL’s polymer materials with small (i.e., less than 1 nm) uniform pore sizes can be compressed to form materials with ~1.4 g/mL bulk densities without significant loss of gravimetric hydrogen-storage capacity. If these materials had gravimetric capacities and SSAs similar to activated carbons, their volumetric capacities would be more than three times higher and could exceed the DOE 2015 volumetric hydrogen-storage target of 40 g/L. The porous polymers synthesized by ANL/UC are also very flexible chemically, enabling substituted elements including metals to be incorporated uniformly in the polymer crystal structure. ANL/UC has demonstrated that porphyrin-type structures can be integrated into the polymer structures, where the Fe atoms are open for hydrogen exposure. Many other routes to increasing SSA and hydrogen capacities are being investigated by ANL/UC with the focus on using the intrinsic advantages of porous polymers to control pore sizes and compositions.

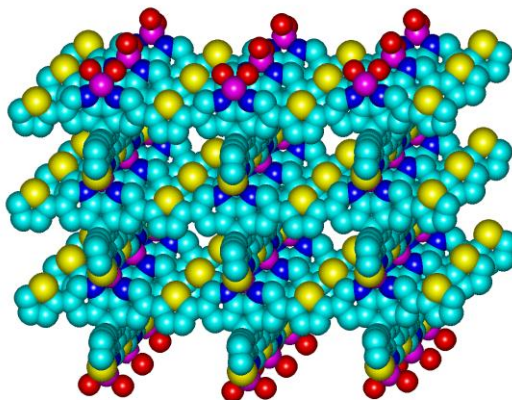


Figure 3-7. Schematic of one of ANL/UC's porous polymers in which the conductive backbone has been incorporated with different elements

Activation is one method that might be applicable to increasing the SSA and optimizing the pore diameters of the new polymers being developed by ANL/UC. In general activation processing has been used to synthesize a number of different sorbents, including, and from within the HSCoE, materials from corncobs and commercial polymers such as polyetheretherketone (PEEK). Prior to the HSCoE, numerous carbon materials were activated with potassium hydroxide (KOH) and high-temperature CO₂ processes to form some of the best commercially available sorbents. However, these sorbents were not optimized for hydrogen storage. Thus, the HSCoE investigated methods to improve the activation processing to form sorbents optimized for hydrogen storage. This included an effort at the University of Missouri-Columbia (Missouri) that uses similar KOH (e.g., ~800°C) and CO₂ processing with pyrolyzed corncobs as starting materials to form sorbents with SSAs >3000 m²/g, pore sizes of 0.5 to 3 nm, and hydrogen-storage capacities between 5 and 6 wt %. This project began during the latter period of the HSCoE in 2009, and therefore substantial additional work must be performed to optimize hydrogen-storage capacities and properties. Missouri continued to develop sorbents after the HSCoE ended, and focused on creating more SSA and better controlling pore uniformity. This work demonstrates how inexpensive sources of carbon can be used to form high-capacity sorbents for hydrogen storage.

As a complement to the polymer work by ANL/UC, Duke investigated the use of vapor-based activation processes involving CO₂ and water to systematically control pore formation in polymer materials such as PEEK (Cansado et al. 2007). This method is simple, potentially inexpensive, robust, and does not require the removal of any template or the use of any dangerous chemicals. It relies on selective oxidization of the PEEK structure to create well-defined pores. Subsequent work was performed by Duke and the HSCoE to appropriately characterize this method, explore its versatility, and determine the best hydrogen-storage properties possible. Using CO₂ or H₂O activation of PEEK, Duke synthesized sorbents with >3000 m²/g SSAs and pores <2 nm in size. As shown in Figure 3-1, even non-optimized activated PEEK has very good hydrogen-storage properties. The main feature to note with this material is that even though the excess gravimetric capacities (>5 wt % at 77 K) and SSAs (>3100 m²/g) are similar to AX-21 and other “superactivated” commercial carbon sorbents at the same temperatures and

pressures, based on the the smaller pore sizes, bulk densities greater than 0.7 g/ml can be achieved, enabling excess volumetric capacities greater than 35 g/L—more than double that of AX-21.

A series of experiments were performed in which the PEEK polymer precursors were systematically graphitized and then activated under a CO₂ or H₂O environment at elevated temperature. One notable outcome is that the excess gravimetric capacities of some of these materials outperform other materials with higher SSAs. Surface area is a key factor involved in H₂ storage; however, in the case of these PEEK-derived materials, it is obvious that other factors contribute significantly to their H₂ sorption profiles. For example, PEEK-CO₂-9-80 has a larger H₂ gravimetric uptake compared to AX-21 at the same temperature and pressure.

Additionally, high-pressure excess H₂ adsorption isotherms were achieved for PEEK-CO₂-9-80 (Figure 3-1). As stated previously, this material has an extremely large SSA (3103 m²/g), which is particularly beneficial for achieving large excess H₂ gravimetric uptake values. Furthermore, this material has a large cumulative pore volume (>1 cm³) and small pore diameters (predominantly ≤3 nm). Both of these characteristics are ideal for creating a material optimized for H₂ storage. As such, this material demonstrates an exceptionally large gravimetric uptake, reaching ~5 wt % at 77 K and 20 bar (Figure 3-1). Furthermore, this corresponds to a H₂ volumetric uptake of ~35 g/L using the unaltered porous carbon density of ~0.7 g/ml. However, it should be noted that on compression of 15 metric tons, the density of this material was effectively raised to ~1 g/ml, which corresponds to a H₂ volumetric uptake of ~50 g/L. Further work needs to be done to fully characterize these products, but it is obvious that these materials possess outstanding H₂ volumetric adsorption capacities.

Both the PEEK and corncob materials demonstrate good (i.e., greater than 5 wt % at 77 K) excess gravimetric capacities and bulk densities using starting materials and processes that are inexpensive and scalable to form sorbents with the desired controlled microstructure needed for high storage capacities.

Creating optimal geometric structures in which all sorption sites are accessible to hydrogen requires the careful design of materials and processes. This issue is the same regardless of the sorption mechanism employed, but does require that the structures be optimized for the desired type and conditions of the hydrogen storage. Templating is a technique employed by the HSCoE to enable systematic investigations of how specific structures and compositions affect hydrogen-storage properties. Templating involves the vapor- or chemical-phase deposition of a partial or full layer of material onto a porous structure. If, for example, carbon is coated onto a zeolite template, the zeolite template can be removed via chemical or vapor processing, leaving behind a porous carbon material that mimics the geometric structure of the removed zeolite template. Zeolites can be synthesized with just the right pore sizes that are uniform throughout. However, the aluminum and silicon in the zeolites are too heavy to meet DOE hydrogen-storage standards, so these materials must ultimately be removed. This type of process has been used to make highly porous carbon materials (i.e., with SSAs >3500 m²/g) with pores that are nearly identical to the zeolite, resulting in materials with ~7 wt % hydrogen-storage

capacities (Yang 2007) NREL and Pennsylvania State University (Penn State) have used this technique to make novel lightweight hydrogen-storage materials with optimal compositions and pore structures that mimic the chosen template. This technique accelerates development by increasing the synthesis rate of appropriate materials in which all of the higher hydrogen binding sites of the heterogeneous surfaces are accessible. Within the HSCoE, most of the templating work was associated with synthesis of boron-substituted carbons, which will be discussed later in this report.

To understand the potential effects that may have been attributed to templated carbon material results reported by Yang and coauthors (2007), NREL worked directly with Dr. Mokaya with sample exchanges to provide some analysis. Unfortunately, initial modeling could not account for the anomalously high capacities. The result of these investigations indicates that any substantial hydrogen-storage capacity increase reported for templated carbons is probably not due to any significant enhancement from optimal pore sizes or unique carbon coordination within the materials. Clearly, the effects of contact-angle issues need to be investigated further to see if there is a substantial difference between the nitrogen used to measure SSA and the hydrogen, and if the dangling ends of the surfaces interact with the hydrogen in unique ways.

In general, the HSCoE focused most of its efforts from the outset on creating high-SSA sorbents with optimal and uniform pore sizes. Whether the work involved frameworks, activated carbons, polymers, nanotube scaffolds, or intercalated graphite, the goals remained the same. This focused set of efforts succeeded. The HSCoE created materials with extremely high SSAs ($>6200 \text{ m}^2/\text{g}$ Langmuir) and gravimetric capacities ($\sim 8 \text{ wt } \%$) at 77 K, high bulk densities in the range of 0.7 to 1.4 g/ml, and, in a few cases, materials with both good SSAs and bulk densities. This latter set of results is ultimately where DOE and the greater scientific community need to be with all sorbent materials. In the best case where the best SSAs and best bulk densities via optimal pore sizes can be combined, it may ultimately be possible synthesize physisorption materials with $>7 \text{ wt } \%$ and $>50 \text{ g/L}$ capacities at $\sim 80 \text{ K}$ and $\sim 40 \text{ bar}$. It may be possible to meet DOE 2010 hydrogen-storage targets with presently demonstrated sorbents at $\sim 80 \text{ K}$ storage temperatures. In addition, although present projections for sorbents are a little low to meet DOE 2015 targets at $\sim 80 \text{ K}$, it's worth noting that sorbent capacities can easily be increased by $\sim 30\%$ (i.e., $>9 \text{ wt } \%$ and $>65 \text{ g/L}$) using storage temperatures at $\sim 50 \text{ K}$. With that in mind, there are clear paths forward for sorbent-based hydrogen-storage systems to meet DOE 2015 capacity targets. These increased capacities need to be balanced with system costs and efficiency. However, storage-system costs will be significantly lower at the 20 bar needed for 50 K storage compared to the 350 or 700 bar pressures needed for ambient-temperature storage. Even though physisorption-based sorbents will require cryocompression, they have no significant heat-transport issues, can operate at moderate pressures, and may require the least engineering (compared to metal or chemical hydrides) to design and construct a system that could meet the DOE 2015 targets.

3.2.4 Go/No-Go Decision for Nanotube-Based Storage at Ambient Temperature

As part of the DOE's continuing effort to identify and develop on-board hydrogen storage materials, a decision was made regarding the future research and development activities of pure carbon nanotubes within the Fuel Cell Technologies Program in October 2006. To aid with this decision, the HSCoE provided a brief report on the state of SWNT hydrogen-storage properties (DOE 2006). A summary of that report is provided here for completeness.

Soon after the simultaneous discovery of carbon SWNTs in 1991 (Iijima 1991) their application as a hydrogen-storage material was investigated based on their promising structure and lightweight-materials characteristics. Several initial hydrogen-capacity measurements on SWNTs suggested hydrogen uptake of well over 6 wt % at RT (see for example Ding 2001). However, other research suggested near-zero hydrogen uptake at near-ambient conditions. Although uncertainties still remain with several of the published results, the HSCoE verified that hydrogen-uptake measurements of ~3 wt % with pure carbon SWNTs are reproducibly achieved at liquid nitrogen temperatures (~77 K) and ~20 bar pressure, and that ~0.5 wt % is reproducibly achieved at RT and ~70 bar pressure. Although other published work by very reputable researchers suggest that 5 to 6 wt % hydrogen uptake can be achieved at 77 K (Poirer et al. 2004; Pradhan et al. 2002), no verified result indicates that pure SWNTs can store 6 wt % hydrogen at ambient temperature, even at 100 bar. The verified hydrogen-storage results with pure carbon SWNTs do not significantly exceed the physisorption of hydrogen on planar graphite with a binding energy of ~5 kJ/mol. This low binding energy is sufficient to store dihydrogen on SWNT surfaces at 77 K, but a binding energy of ~15 to 20 kJ/mol will be required to store >6 wt % dihydrogen at room temperature (RT) and moderate pressure. Furthermore, although SWNTs show higher hydrogen-storage capacities compared to other porous carbon materials on a SSA basis (as measured with nitrogen BET), reproducible processing has not demonstrated the ability of SWNTs to achieve even half of the theoretical maximum SSA of ~2600 m²/g.

Even if higher SSAs can be achieved (via routes involving SWNT scaffolds or other nanostructured materials such as single-walled nanohorns) to enable higher dihydrogen storage capacities, higher binding energies will be required to obtain substantial (>6 wt %) uptake at RT. Although binding energies can be increased with dopants and atom/cluster decoration (discussed below), the only conjectured route to increase binding energies of pure carbon SWNTs is through substantially increased curvature (Cheng et al. 2005). This may be achieved with SWNT diameters of 4 to 5 Å. However, stability and available SSA issues may ultimately limit this route to increased hydrogen storage, even if the materials can be made. Attempts to measure significantly enhanced heats of adsorption with small diameter SWNTs were not successful.

Based on systematic development and testing within the HSCoE and a thorough review of the literature, it was concluded that pure undoped carbon SWNTs did not, and probably cannot, meet the 6 wt % hydrogen-storage goal (on a materials basis) at RT,

even at moderate pressures (<100 bar). That said, it was also concluded that technically viable pathway exists via substitution, metal center integration, and spillover to create materials with greater than 6 wt % hydrogen uptake at RT in which SWNTs are a major constituent. Furthermore, there are clear technical paths where pure carbon SWNTs via scaffolding, metal decoration, and/or boron substitution can provide substantial hydrogen storage at cryogenic temperatures.

Ultimately, a “No-Go” decision was effectively made for pure SWNTs providing ambient-temperature hydrogen storage. Development efforts continued with SWNTs for cryocompressed storage and as components in other storage processes. However, resources were directed toward more fully developing the next-generation materials that were predicted to have improved performance. The investment made by DOE in SWNT research was used for further advances in hydrogen storage and also in other applications relevant to the DOE Office of Energy Efficiency and Renewable Energy such as fuel cells, batteries, solar cells, and ultracapacitors. The go/no-go decision focused on the capabilities of pure SWNTs for ambient-temperature hydrogen storage and was taken in the context that no known material meets all DOE targets for on-vehicle hydrogen storage. Thus, development activities continued on other sorbent-based materials.

3.3 Substituted Materials

3.3.1 First-Principles Materials Design

To enhance dihydrogen adsorption, the HSCoE studied the effects of integrating lightweight elements with chemically stable carbon sorbents using a number of different approaches including endohedral Li and F, and substitution of N, B, and Be, as shown in Table 3-1. For Li, although the volume of the cage is slightly increased, which is consistent with electron transfer from Li to the cage, there is no significant increase in the adsorption energy, $E_a = 0.07$ eV/H₂. The situation is even worse for F, in which the electron transfer reverses its direction and the adsorption energy decreases to $E_a = 0.04$ eV/H₂. Substitutional nitrogen also has no advantage for H₂ adsorption. Here, $E_a = 0.06$ eV/ H₂ and there is no sign that charge transfer takes place between N and H₂.

Table 3-1. Adsorption Energy (in eV units) of H₂ for Doped C₃₆. Endo- and Sub-Strand for Endohedral and Substitutional Doping, Respectively

Pristine	Endo-Li	Endo-Li	Sub-N	Sub-B	Sub-Be
0.07	0.07	0.04	0.06	0.39	0.65

In contrast, H₂ binds to substitutional B or Be with significantly larger local density approximation (LDA) binding energies of 0.39 and 0.65 eV/ H₂, respectively. Highly accurate quantum-mechanical calculations predict 0.2±0.05 eV/H₂ adsorption energy for C₃₅B-H₂. Although this value is about 0.2 eV/ H₂ smaller than that of LDA, it is still significantly larger than the van der Waals (vdW) energy of about 0.04 eV/ H₂.

To understand the enhanced adsorption of H₂ in doped fullerenes, we calculated the site-decomposed local density of states (LDOS) for B and Be. Figure 3-8a and b show the LDOS for the initial configurations in which the H₂ molecules are unbound and

Figure 3-8c and d show the final configurations in which the H₂ molecules are bound. For unbound C₃₅B-H₂ (Figure 3-8a), the doubly occupied H₂ σ state shows a single peak about 5 eV below the Fermi level, E_f , whereas the B p_z -like state shows two peaks about 1 and 3 eV above E_f . The presence of this doublet is the result of a strong hybridization of B p_z state with carbon π -states. For bound C₃₅B-H₂ (Figure 3-8c), the H₂ σ state spreads out with two main peaks about 10 eV below E_f , whereas the B p_z states move to higher energies outside the energy range of Figure 3-8. These level shifts are consistent with the notion that H₂ binds to B through an electronic hybridization. A similar hybridization is also seen for C₃₅Be-H₂ in Figure 3-8b and d. Because of a larger separation of the Be p_z state in Figure 3-8b, the magnitude of the shift of the H₂ σ level (about 3 eV) is smaller than that of B. By comparing Figure 3-8e and f, one sees that the Be-H₂ coupling perturbs the carbon host states less than the B-H₂ coupling.

In contrast, no such hybridization was observed between H₂ and the other substitutional and endohedral impurities studied. This is understandable because in endohedral doping with species such as Li and F, there is no localized empty impurity state on the fullerene that would allow hybridization with the H₂ σ state. In the case of substitutional N, the p_z -like N lone pair is already doubly occupied. Hybridization with the low-lying H₂ σ state would increase its energy and is therefore not favored. In other words, the presence of a highly localized empty p_z orbital is essential for the non-dissociative adsorption of H₂ to doped fullerenes.

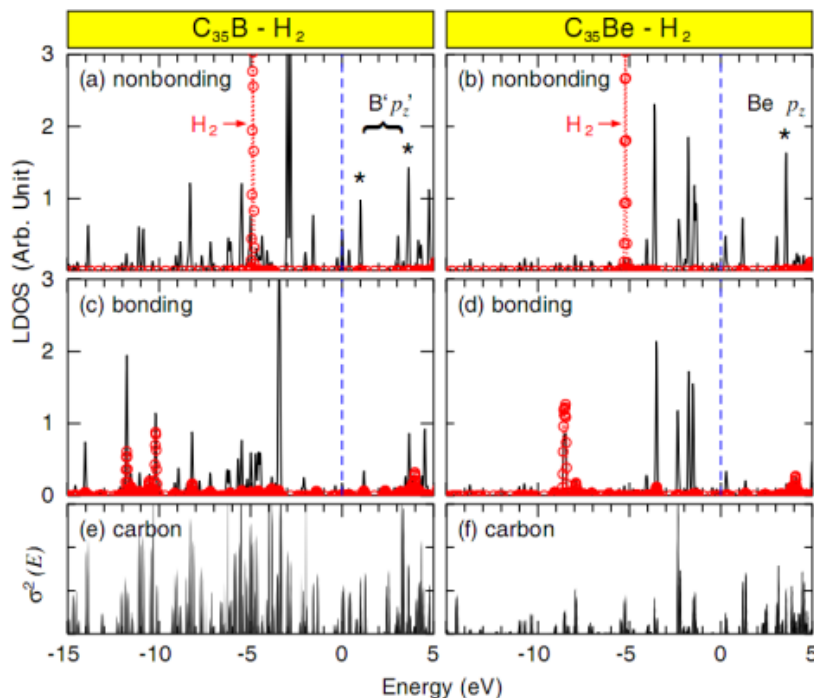


Figure 3-8. (a)–(d): The calculated local density of states (LDOS) for B (Be) in C₃₅B(Be)-H₂. The LDOS for B (Be) are solid lines, whereas the LDOS for H₂ are open circles. **(e) and (f):** The square changes of the carbon states caused by H₂ sorption, namely $\sigma^2 = [\delta\text{LDOS}(\text{carbon})]^2$ between the non-bonding and bonding states.

3.3.1 Synthesis and Hydrogen Storage Results of B-Substituted Carbons

Several techniques were used by the HSCoE to form high-SSA and high-boron-content porous carbon materials. For example, Penn State formed porosity in B-containing precursors; NREL formed B-substituted SWNTs in gas-phase synthesis; Penn State, Air Products and Chemicals Inc. (APCI), and NREL deposited ultrathin BC_x layers in templates; and Missouri used B ion-beam implantation. Contrary to literature reports (Marchand 1971), all attempts by the HSCoE partners to use boron oxide in physical contact with graphene materials at high temperatures did not produce any significant boron-substituted carbons with the correct coordination. Similarly, initial attempts to form SP^2 -coordinated B substituted in carbons with ion beam implantation was not successful. These ion-beam implantation experiments began in 2009 and continued beyond the center with the project at the Missouri.

3.3.1.1 Pyrolysis Synthesis of BC_x

Penn State pyrolyzed B-containing precursors such as poly(diethynylphenylborane chloride or benzene-1,4-bis(ethynylborondichloride) (Chung et al. 2008) in facile thermal transformations to form a BC_x fused ring structure in which inert LiCl or NaCl salts served as the pore-forming templates (removed after pyrolysis by water-washing) to produce porous BC_x morphologies (e.g., Figure 3-9).

The resulting porous structure in the BC_x material essentially mirrors the structure of the impregnated inorganic

aggregates in the matrix. The basic idea is that B has similar atomic size to C, and that B forms a strong tri-valence bonding structure with C. Therefore, it is possible that B can be effectively substituted in the C (graphene) structure without significantly distorting its planar structure. In fact, some existing organoborane compounds (e.g., triethylboron) have similar B-substituted, fused-ring structures. The key concept here was to design suitable B-precursors that can be thermally transformed into a fused-ring structure without losing the B and C elements. At

the same time, the precursors must create a microporous structure with high SSA in the resulting BC_x material. It is highly desirable to have strong acidic B moieties (i.e., electron deficiency) in the resulting BC_x that engage in p-electron delocalization in the

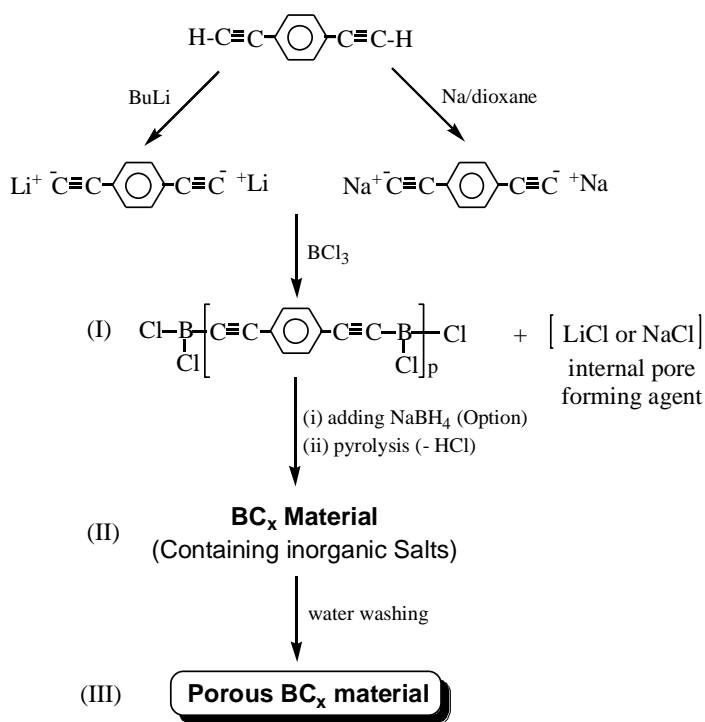


Figure 3-9. Example of a B-precursor synthesis route using poly(diethynylphenylborane) chloride for preparing porous BC_x materials

fused-ring structures and serve as p-type internal dopants to activate the surfaces and increase the H₂ binding energy. This material was 7.7% B, which is only slightly less than the 8.4% B/C ratio in the starting B-precursor.

Similarly, substitutional boron was incorporated by the Penn State team into high-SSA microporous carbons by pyrolysis of a blend of microporous-forming polymer precursor (polyfurfuryl alcohol) and boron-containing organic precursor (tetraethylammonium borohydride). The as-prepared pyrolyzed sample had 1%–5% of boron incorporated. However, activation with CO₂ selectively removed carbon, increasing the amount of boron to almost 23% with a SSA of 1500 m²/g. The isosteric heat of adsorption of the sample was ~10 kJ/mol with a sorption capacity of 0.5 wt % at RT and 100 bar. As discussed above, INS measurements of these BC₅ materials exhibit similar characteristics compared to a similarly prepared carbon material, but the hydrogen is more apparently rotationally hindered through the entire adsorption range in BC₅ than for the pure carbon. However, desorption studies with temperature indicate that both materials retain similar amounts of hydrogen between 60 and 85 K, indicating a lack of strong adsorption sites.

BC_x Molecular Structures

The molecular structure of the BC_x materials during pyrolysis was monitored by a combination of solid-state ¹¹B MAS-NMR (magic angle spinning nuclear magnetic resonance), X-ray diffraction, and transmission electron spectroscopy (TEM). Figure 3-10 shows the ¹¹B MAS-NMR spectra of several resulting porous BC_x materials that were prepared by pyrolysis of a B-precursor containing *in situ*-formed LiCl salts at various temperatures, followed by water-washing to remove all LiCl additives. After pyrolysis at 600°C, the resulting porous BC₁₁ (run A-1) shows one distinctive broad chemical shift centered at 10 ppm, corresponding to trivalent B moieties that involve some p-electron delocalization in the C fused rings. There is a minor peak centered at 0 ppm, which may be associated with a few B moieties located at the edge area of the porous BC₁₁ structure. During water-washing, the remaining B-Cl groups should change to B-OH groups. As the pyrolysis temperature increases from 600° to 800°C, the major trivalent B peak slowly moves upfield, indicating a gradual increase of electron density at B and better p-electron conjugation in the BC₁₃ material (run A-2). On the other hand, the edge-area B moieties sharply decrease in intensity. At 1100°C, only a trivalent B peak at 8 ppm was observed in BC₂₁ (run A-3). Evidently, the BC_x fused-ring structure increases in size as the pyrolysis temperature increases, and most of B moieties become the substitutional trivalent species inside the BC_x structure. After further annealing the sample at higher temperatures (1500°C), the BC_x material appears to graphitize on a larger scale, with a single B chemical shift abruptly moving upfield to –5 ppm in the BC₂₈ material (run A-5), which indicates that B is highly involved in p-electron delocalization to form very weak acidic (or even basic) B moieties.

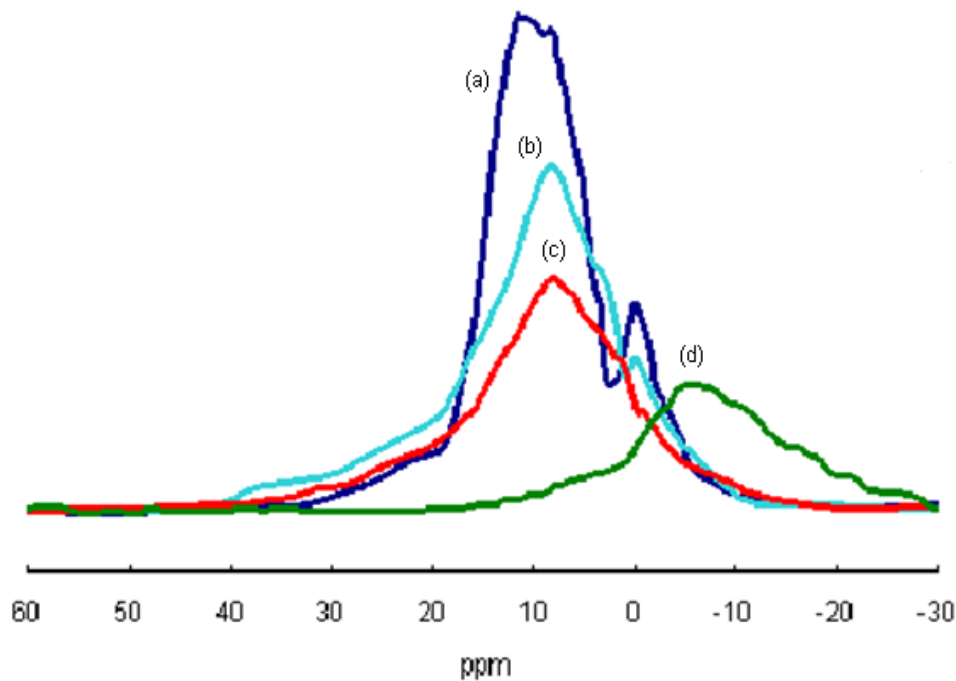


Figure 3-10. Solid-state ^{11}B MAS-NMR spectra of BC_x materials prepared from pyrolysis of a B-precursor (with LiCl salts) at (a) 600°C (run A-1), (b) 800°C (run A-2), (c) 1100°C (run A-3), and (d) 1500°C (run A-5).

Table 3-2 summarizes the X-ray crystallite parameters of interlayer spacing (d), crystallite size (L_c), and crystallite width (L_a). Generally speaking, the d -spacing decreases with heat-treatment temperature, whereas both L_c and L_a increase with temperature. The BC_{11} sample (run A-1) is almost completely amorphous, and the BC_x material gradually shows small-order domains as the pyrolysis temperature increases to 1400°C (run A-4), with two broad (100) and (101) peaks. It is interesting to note that a small amount of boron carbide (B_4C) was also observed at 1500°C (run A-5). The B content in the BC_x material at 1500°C was dramatically reduced to 2.6 wt %, which is close to the maximum B-solubility level in the graphitic structure. Evidently, at this temperature, some small crystallites were formed with a short-range order structure, which ejects excess B in the form of B_4C from the matrix. However, both crystallite size and crystallite width remain relatively small even after pyrolysis at 1800°C, which may be associated with the co-existence of inorganic salts (impurities) that limit the expansion of crystallite domains and prevent the long-range order. The final BC_x materials basically resemble the disordered (non-graphitizable) carbons. However, it is interesting to note that the d -spacing of run A-6 is 0.339 nm—very close to 0.335 nm in ideal graphite. Despite the relatively low pyrolysis temperature at 1800°C, the highly short-range ordering may be associated with having B in the precursor, which enhances the graphitization process.

Table 3-2. Lattice Parameters of BC_x Materials Measured by X-Ray Diffraction Patterns

Run No.	Pyrolysis Temp. (°C)	Composition (BC _x)	d-Spacing (nm)	La (nm)	Lc (nm)
A-1	600	BC ₁₁	-	-	-
A-2	800	BC ₁₃	0.367	3.70	1.10
A-3	1100	BC ₂₁	0.356	3.73	1.23
A-4	1400	BC ₂₅	0.353	4.87	1.61
A-5	1500	BC ₂₈	0.347	5.04	1.64
A-6	1800	BC ₄₀	0.339	6.04	2.77

High-resolution TEM provides direct observation of microstructures. Figure 3-11 compares two TEM images of BC₁₁ (run A-1) and BC₄₀ (run A-6) materials. The BC₁₁ material, prepared at 600°C, displays fingerprint patterns with short and curved fringes, and randomly oriented fringes between fingerprint patterns. On the other hand, randomly oriented stacks of several layers, with extended, straight, and parallel organized fringes, were observed in the BC₄₀ material prepared at 1800°C. The stack thickness (Lc; crystallite size) is about 2–3 nm, and the stack length (crystallite width) is in the range of 5–7 nm—consistent with the X-ray results (Table 3-2). It is interesting to note that the TEM image for the BC₆ material (run C-1), using the B-precursor (I) containing both *in situ*-formed LiCl and the externally added NaBH₄ salts, shows a completely random configuration (no fingerprint patterns) with short and curved fringes. Evidently, the additional NaBH₄ salts were mixed well with the B-precursor (I), providing an additional B source. Although these salts don't interfere in the carbonization process of converting the B-precursor (I) into BC_x material, their presence in the matrix does effectively prevent any development of a local ordering structure by maintaining a high edge area.

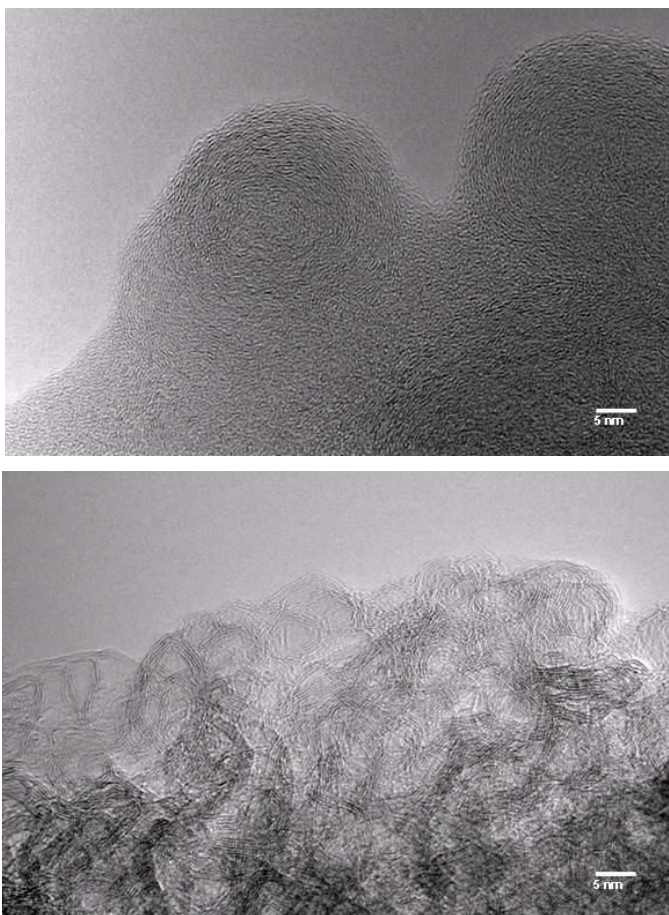


Figure 3-11. TE images of (top) BC₁₁ (run A-1) and (bottom) BC₄₀ (run A-6)

As illustrated in Figure 3-12, the chemical structure of BC_x changes from a disordered (less π -conjugated) state—with a boron-puckered configuration at $600^\circ\text{--}800^\circ\text{C}$ —to an ordered (highly π -conjugated) state—with a planar and multiple-layered configuration at 1500°C . The resulting planar graphitic layers can accommodate only a reduced amount (<3%) of B content that is consistent with the previous observation.

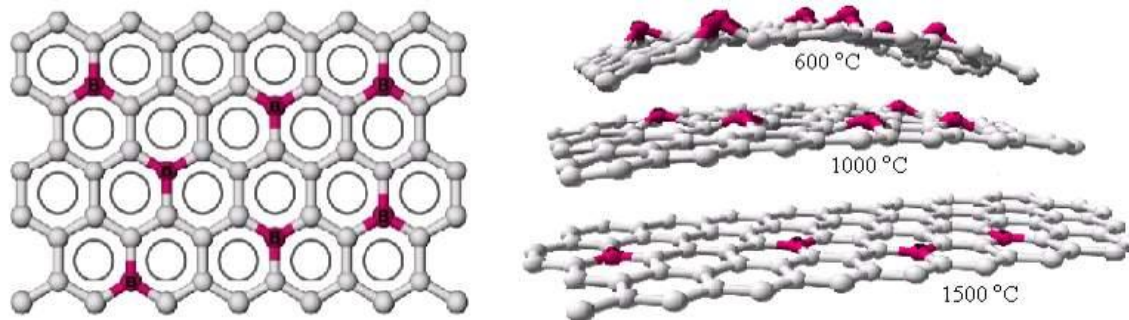


Figure 3-12. Schematics of BC_x materials: (left) top view and (right) side view

BC_x Properties

Penn State performed specific experiments to understand how pyrolysis temperature and inorganic salts affect BC_x morphology. The inorganic additives serve as the pore-forming templates, and are removed after pyrolysis, so the pore structure also reveals the distribution of inorganic salts in the BC_x matrix during pyrolysis. Figure 3-13 shows scanning electron microscopy (SEM) images of three BC_x materials, including BC_{11} (run A-1), BC_{40} (run A-6), and one control sample that was prepared by pyrolysis (600°C) of a low-molecular-weight pure B-precursor (I) containing no inorganic salts. Despite very different pyrolysis temperatures (600° vs. 1800°C), both the BC_{11} and BC_{40} materials show similar macro-phase morphology with many continuous micron-width channels (Figure 3-13a and b). However, a completely dense BC_x material (Figure 3-13c), with almost no SSA, was observed from the same B-precursor that did not contain the LiCl salts or other additives, such as NaCl and NaBH_4 . These macro-porous structures are clearly the result of LiCl aggregates in the matrix, which may be formed (phase-separated from BC_x) during pyrolysis.

Figure 3-14 shows a high-resolution, field-emission SEM image of the same BC_{11} sample (Figure 3-13a). Both micropores and mesopores clearly exist in the BC_{11} matrix. However, the resolution does not allow for the determination of pore size and distribution. The specific pore sizes and pore size distributions in the BC_x materials were examined by a BET surface-area analyzer using N_2 and CO_2 gases.

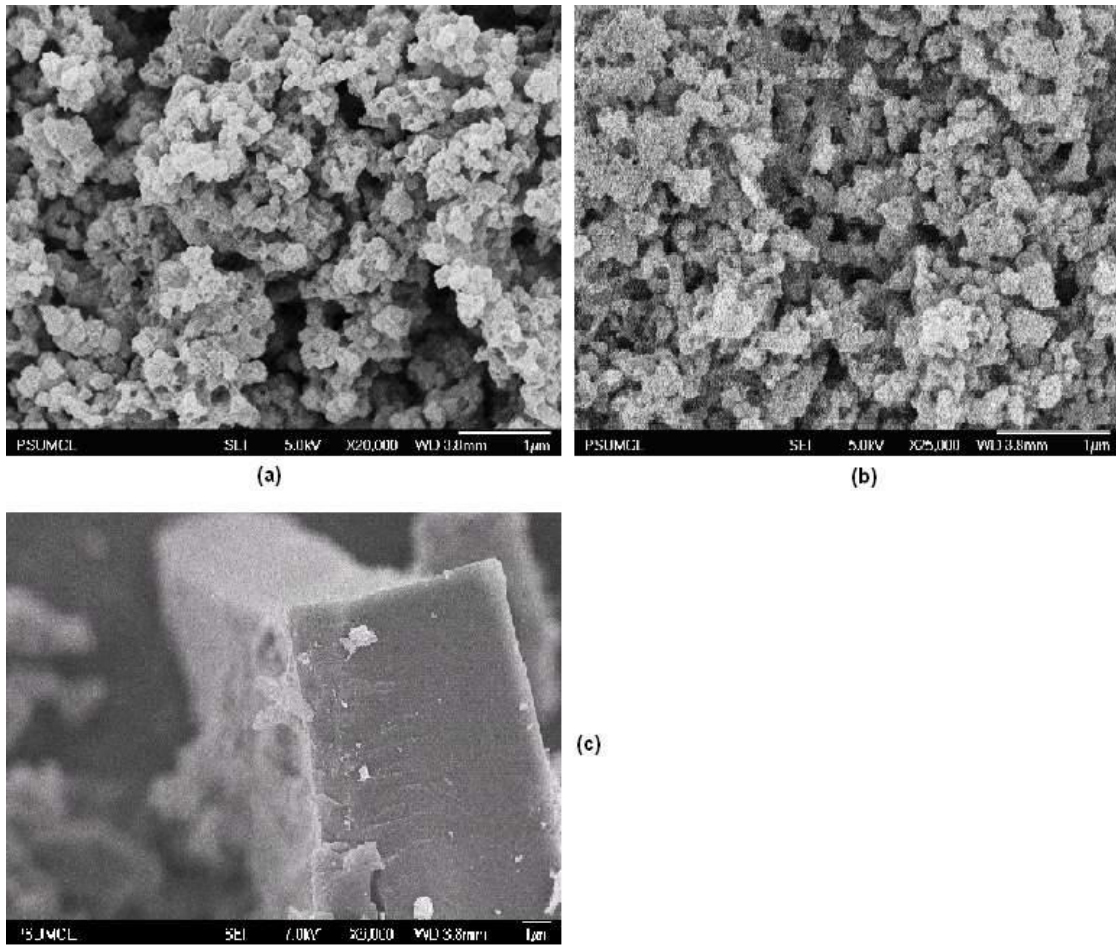


Figure 3-13. SEM images of BC_x materials obtained after pyrolysis of B-precursors (with LiCl) at (a) 600°C (run A-1) and (b) 1800°C (run A-6), and (c) B-precursor (without LiCl) at 600°C

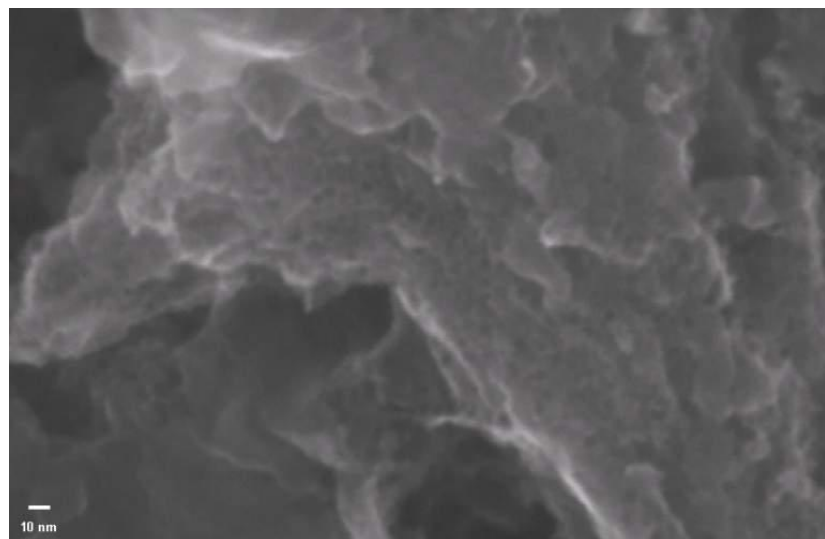


Figure 3-14. SEM image of BC₁₁ materials (run A-1)

Figure 3-15 compares four pore-size distribution curves of BC₁₁ (run A-1), BC₁₃ (run A-2), BC₁₃ (run B-1), and BC₁₇ (run B-2), prepared by pyrolysis of the B-precursor (I) containing LiCl or NaCl salts under various pyrolysis temperatures. Table 3-3 summarizes their SSAs and micropore volumes that were calculated from adsorption isotherms of N₂ (77 K) and CO₂ (273 K). It is interesting to note that the SSAs measured by CO₂ sorption consistently show higher values than those measured by N₂, especially in the B-1 and B-2 samples. Because the CO₂ measurement is capable of covering the extremely small pores (between 3.2 and 3.6 Å), the B-1 and B-2 samples prepared by NaCl impregnation may contain smaller pores. The A-1 and A-2 materials, which are obtained from B-precursors (I) with LiCl salts at 600° and 800°C, respectively, each contain micropores (with pore diameter centered at 1.2 nm) and mesopores (with pore diameter centered at 3.75 nm), but with very different proportions. The significant shift of the micropore-dominated A-1 sample (83 vol % micropores in Figure 3-15a) to the mesopore-dominated A-2 sample (87 vol % mesopores in Figure 3-15b) implies some local LiCl agglomeration after pyrolysis, beyond its melting temperature at 605°C. As expected, the BET surface area also reduces from 780 to 528 m²/g. The same general trend was also observed in B-1 and B-2 pair that was prepared at 600° and 900°C, respectively. It is interesting to see that the BC₁₃ material in Figure 3-15c, prepared in run B-1 with NaCl additives, consists mainly of micropores, and that the B-2 sample maintained more than half of its micropores, even after heating at a significantly higher temperature. The NaCl salts, having a higher melting temperature (800°C), remain in a well-dispersed phase in the BC_x matrix at 600°C. Clearly, the combination of additives and pyrolysis temperature offers a unique tool (templates) to control BC_x morphology.

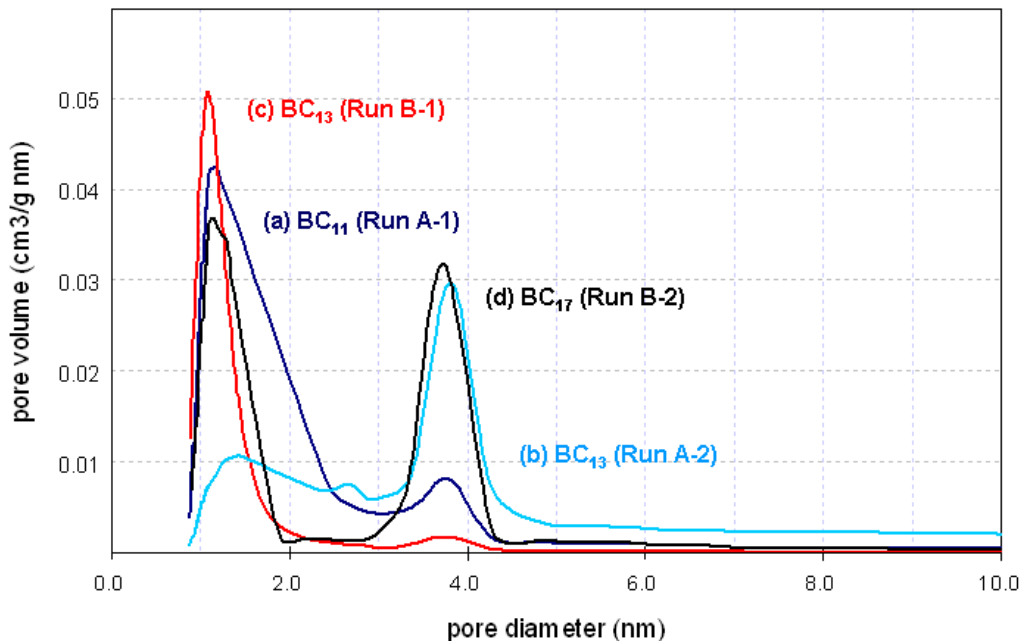


Figure 3-15. Pore size distribution of (a) BC₁₁ (run A-1), (b) BC₁₃ (run A-2), (c) BC₁₃ (run B-1), and (d) BC₁₇ (run B-2)

Table 3-3. Summary of Specific Surface Area and Pore Volume of Four BC_x Materials

Sample	N ₂ sorption at 77K			CO ₂ sorption at 273K	
	Surface area ^a (m ² /g)	Micropore volume ^b (cm ³ /g)	Desorption cumulative pore volume ^b (cm ³ /g)	Surface area ^c (m ² /g)	Micropore volume ^c (cm ³ /g)
A-1	780	0.38	0.43	873	0.33
A-2	528	0.10	0.29	569	0.16
B-1	634	0.34	0.34	828	0.32
B-2	405	0.16	0.29	762	0.25

- a. Calculated by BET equation
- b. Estimated by BJH method
- c. Estimated by D-R method

Figure 3-16 shows an X-ray diffraction (XRD) pattern of the impregnated LiCl during the pyrolysis of B-precursor (I), which provides direct evidence of a LiCl agglomeration at a high pyrolysis temperature. At temperatures <400°C, the dispersed LiCl molecules show no diffraction peak. As the pyrolysis temperature increases to >450°C, several sharp diffraction peaks appear that are associated with the LiCl crystals in hydrated (exposed in air) and anhydrous forms. Evidently, the dispersed LiCl molecules start to flow below the melting point (605°C) of LiCl crystal, and aggregate progressively into bigger particles. It is important to note that the *in situ*-formed LiCl molecules in B-precursor (I) were used for convenience as the internal pore-forming additives to prepare various porous structures in the BC_x material; they can be removed completely by water-washing. The resulting pore structure in BC_x is the mirror image of the impregnated LiCl aggregates in the matrix.

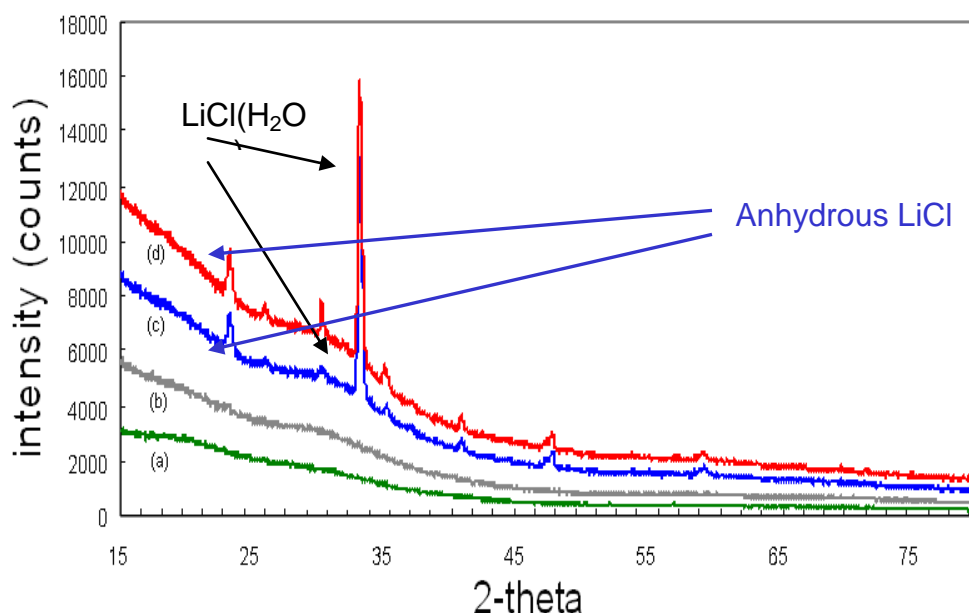


Figure 3-16. X-ray diffraction patterns of LiCl salts in B-precursor after pyrolysis at various temperatures: (a) 150°C, (b) 400°C, (c) 450°C, and (d) 600°C

Both gravimetric and volumetric hydrogen-adsorption measurements were performed under various temperatures and pressure conditions for different BC_x sorbents made from pyrolysis. Figure 3-17 shows hydrogen adsorption of BC₁₁ (run A-1) and BC₆ (run C-1) at 77 and 293 K, respectively. The BC₁₁ material, with a SSA of 780 m²/g, had ~0.37 wt % hydrogen adsorption at ambient temperature and 80 bars pressure. This same material has ~3 wt % hydrogen uptake at 77 K and 50 bar. Both of these values are substantially higher than porous carbon materials with similar SSAs. The BC₆ material with more boron and lower SSA (i.e., 609 m²/g) has 0.54 wt % and 3.8 wt % hydrogen adsorption at 273 and 77 K, respectively. Despite the reduction of SSA, the overall hydrogen-adsorption capacity increases. This suggests that the substituted B elements enhance adsorption by increasing the surface energy for binding hydrogen. The quantitative H₂ binding energy on the BC₁₁ and BC₆ materials was estimated by adsorption isotherms (at 77 and 87 K) under low hydrogen pressure (<1 bar). The volume adsorbed at different pressures was converted to heats of adsorption by using the Clausius-Clapeyron equation. The measured isosteric heat of adsorption at low coverage for BC₁₁ (run A-1) and BC₆ (run C-1) is 12.47 and 20 kJ/mol, respectively. Both samples maintain quite high adsorption energy levels (>10 kJ/mol) to higher surface coverage. They are significantly higher than those observed in pure carbon materials (i.e., 4 to 5 kJ/mole).

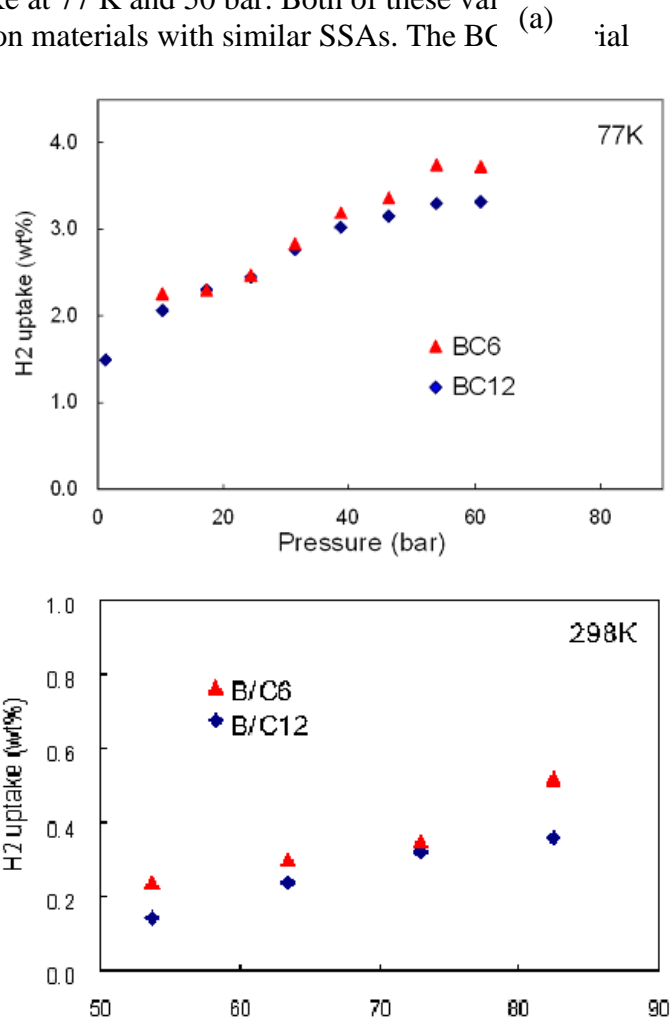


Figure 3-17. Hydrogen adsorption vs. H₂ pressure for two porous (BC₆ and BC₁₂) materials at (a) 77 and (b) 293 K

Nuclear Magnetic Resonance Study of B-Substituted Pyrolyzed Carbons

B-doped disordered graphitic carbon was evaluated for hydrogen storage using ¹H nuclear magnetic resonance (NMR). The B/C material was prepared by the polyaddition adduct of phenyldiacetylene and BCl₃. After initial polymerization at 60°C, the sample was carbonized at 800°C to produce a dense disordered graphitic carbon material with a BET surface area of 54 m²/g. The sample is a powder of packed grains of several micrometers. The boron content was 1.5 wt % as determined by ¹¹B NMR, which was confirmed by prompt Gamma-ray activation analysis. NMR with *in situ* high-pressure hydrogen loading is very sensitive for selectively detecting hydrogen molecules confined

in nanopores. Calibration of the intensity in terms of H_2 mass or number of H_2 molecules was achieved by placing a capillary of known volume inside the sapphire sample tube. The spectral line associated with free H_2 gas in the capillary was used as the intensity standard, and the number of molecules associated with this peak was calculated using the ideal gas law.

Figure 3-18 shows the 1H NMR spectrum of the B/C sample exposed to H_2 gas at 10 MPa at RT, demonstrating the appearance of three distinct peaks. Peak A at 7.70 ppm (relative to tetramethylsilane, TMS) arises from H_2 gas in the capillary. Peaks B and C (5.87 ppm and -1.36 ppm, respectively) are shifted upfield from the capillary peak, indicating that they arise from H_2 molecules in close proximity to the graphitic basal plane of the sample. Because they have distinct chemical shifts, they must arise from hydrogen molecules in two different types of confined regions with different average proximity to the surface. Furthermore, 2-D NMR experiments confirm that the molecules associated with each peak do not exchange on the NMR time scale used here (3 ms). Figure 3-19 shows the individual RT isotherms for peaks A, B, and C. Peaks A and B have linear isotherms, suggesting both are related to non-adsorbing H_2 gas molecules. Peak B is thus assigned to the hydrogen gas residing in the void space between the micron-sized grains of the B/C sample. The isotherm for peak C is non-linear, and is thus assigned to the H_2 molecules adsorbed to the sample surface at RT. A Langmuir fit to the isotherm of peak C yields a binding energy of 9.2 kJ/mol, a significantly higher binding energy than that of typical graphitic carbon materials (i.e., ~ 4 kJ/mol).

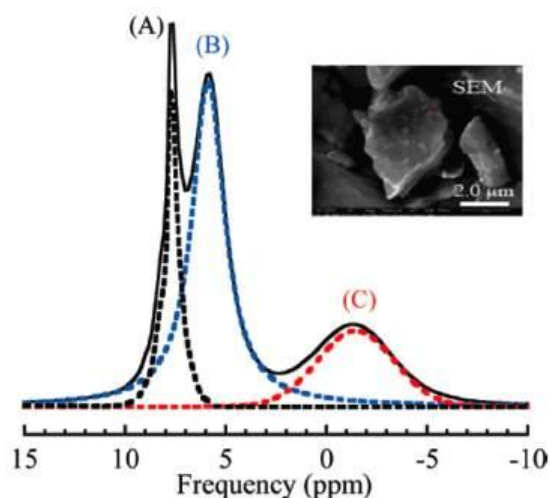


Figure 3-18. 1H NMR of boron-substituted graphitic carbon exposed to H_2 gas at 295 K and 10 MPa. The thick continuous line is the spectrum, and the dashed lines are the three components used to fit the spectrum: (A) H_2 in capillary, (B) H_2 in large voids, (C) H_2 in nanopores. Inset: SEM image of sample granule.

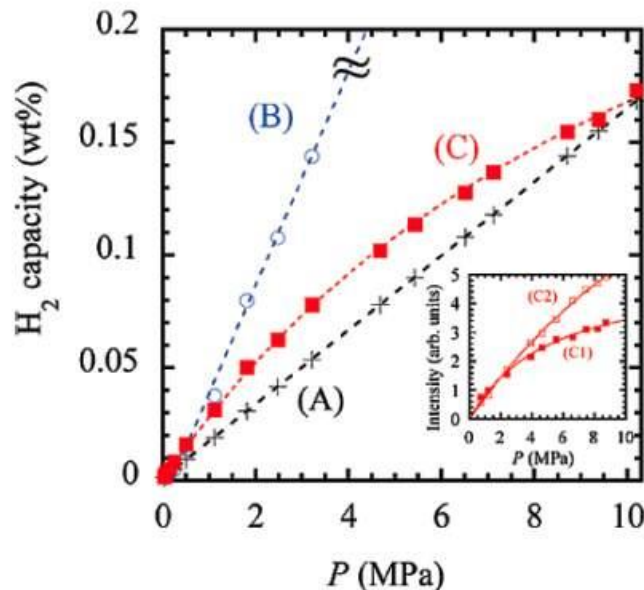


Figure 3-19. RT isotherms based on the intensities of lines (A), (B), and (C) in Figure 3-18. The inset shows the isotherms of the two components of peak C, identified by T_1 measurements. C1 is associated with the long- T_1 component, and C2 is associated with the short- T_1 component. The lines are fits with Langmuir isotherms.

Spin-lattice relaxation time, T_1 , measurements and temperature-dependent hydrogen charging experiments were performed to further explore the unique binding site associated with peak C. The saturation recovery of nuclear magnetization, $M(t)$, for peak C contains two components, a short T_1 and a long T_1 . The isotherm for the long T_1 component is dominated by adsorbed H_2 and has a Langmuir-fit binding energy of 11.4 kJ/mol, suggesting that the pore size associated with this component is most likely on the order of 1 nm or smaller. Two temperature-dependent charging measurements demonstrated that hydrogen diffusion dominates the charging kinetics of the binding site associated with peak C. In the first experiment, the sample was first charged at 7.5 MPa at RT, and the temperature was then dropped to 100 K. Then, as the H_2 pressure was incrementally reduced at a constant T of 100 K, the intensity of peak C did not change. In the second experiment, the sample was first cooled from RT under dynamic vacuum to 100 K; the sample was then exposed to 10 MPa H_2 at 100 K. Under these conditions, peak C does not appear over a period of 10 h. These experiments clearly demonstrate that H_2 molecules can only access (through adsorption or desorption) the micropores associated with peak C very slowly at a temperature of 100 K, indicating an activated diffusion process.

Templating of BCx onto High-Surface-Area Carbons and Zeolites

Some of the highest-SSA carbons ever reported were prepared by templating methods, such as the use of furfuryl alcohol in zeolite NaY (Nishihara et al. 2009). Furfuryl alcohol is a model carbonization precursor because it is inexpensive, readily available, stable at RT, can be polymerized with gentle heating, has incorporated oxygen that aids in the carbonization process, and is small and flexible enough to penetrate and fill the pores of a zeolite. However, zeolite NaY with ~ 7.4 Å diameter pores is a bit too small for some of

the boron-containing precursors (e.g., Penn State's precursor, $\text{Cl}_2\text{B-C}_2\text{-Ph-C}_2\text{-BCl}_2$, is about 7.6 Å) used for templating. In these cases, zeolites with larger pore sizes were used, such as commercially available mesoporous silicas of the MCM-type (e.g., hexagonal MCM-41 with pore diameters ranging from 15–25 Å). In other cases, zeolites such as MCM-48 were used because they have smaller pore variations, while allowing pore filling from all directions based on their interconnecting pore structure. Templated carbons from these systems have been produced (Lin et al. 2006) with SSAs of $>1200 \text{ m}^2/\text{g}$. Several groups used boron-containing precursors to form templated BC_x materials by depositing BC_x materials on templates such as zeolites followed by removal of the template with hydrofluoric acid washes or an equivalent. Solvents, thermal processes, proper polymerization, heating rates, and template removal techniques are all very important in the synthesis of high-porosity, high-boron-content templated BC_x sorbents.

BC_x Templated Materials from BCl_3 /Benzene Reaction

Figure 3-20 shows TEM images of BC_x deposited onto a high-SSA carbon support, CM-Tec. The highly porous open structure can be observed in the CM-Tec parent material (left figure). For the BC_x -coated material (right figure), a turbostratic graphite-like overlayer is seen coating the CM-Tec parent material. XRD on a thin film of the BC_x material, deposited onto a quartz witness slide, indicates that the material is somewhat graphitic, but highly disordered (i.e., turbostratic), with a larger than usual d spacing for the graphite planes.

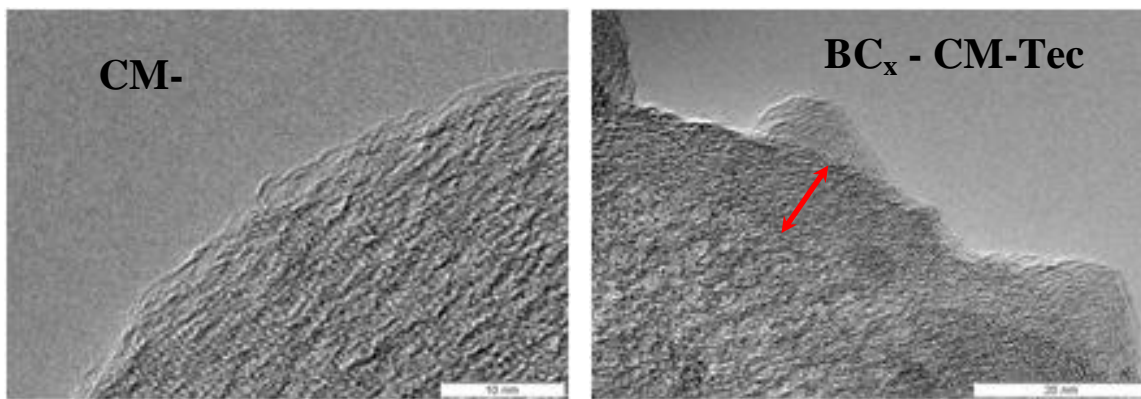


Figure 3-20. TEM images of CM-Tec parent material (left) and BC_x deposited onto CM-Tec (right). Red arrow in right figure denotes the turbostratic overlayer of deposited BC_x .

Other boron-carbon sources were used for producing BC_x at NREL, with the most successful results from a triethylboron (TEB) precursor. This molecule was delivered by an inert carrier gas, either by bubbling the carrier gas through a hexane solution of TEB or through the pure TEB liquid. Of note, TEB has no halogen-containing by-products, which may help to avoid poisoning of the B sites in the produced material. TEB can be used to template BC_x directly onto a template, or it can be pyrolyzed directly (i.e., with no substrate) to produce a BC_6 material (13 at % B). Figure 3-21 shows the high-SSA, porous material derived from direct pyrolysis of TEB.

The boron content and SSA of the BC_x-templated materials varied significantly depending on the duration of templating. Boron content was measured by X-ray photo-electron spectroscopy (XPS) and varied from ~4% (BC₂₅) to ~15% (BC₇). The SSA decreased as a function of boron content. For example, when using CM-Tec as a template (2950 m²/g starting SSA), the SSA varied from ~1650 m²/g (BC₂₅) to 250 m²/g (BC₈).

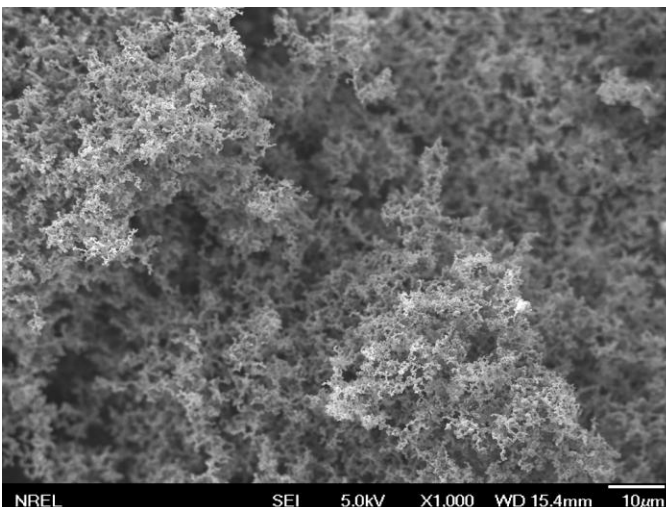


Figure 3-21. High-surface-area, porous BC6 material produced by direct pyrolysis of triethylboron at 900°C

Two interesting phenomena were observed for the hydrogen-storage properties of this templated material, as shown in Figure 3-22. Volumetric hydrogen sorption measurements demonstrated that the 77-K, 2-bar capacity decreased as the boron content increased. However, the reduction in capacity was not as dramatic as expected for such a dramatic reduction in SSA. For example, the BC₈ sample, with only ~250 m²/g SSA, stored ~1.35 wt % H₂, which is nearly five times the capacity that would be expected for a typical activated carbon with similar SSA. Conversely, hydrogen-storage capacities measured by temperature-programmed desorption (TPD) actually *increased* as the boron content increased. The BC₈ sample material stored two orders of magnitude more hydrogen than the parent CM-Tec material (0.2 wt % versus 0.02 wt %, respectively), as measured by TPD. For these measurements, the sample is charged with hydrogen (1 bar) at RT and then cooled to 77 K, where the hydrogen overpressure is removed and the sample chamber is evacuated to a base pressure of ~3 x 10⁻⁸ torr. Hydrogen is then desorbed from the sample while measuring the effluent with a mass spectrometer. This dramatic increase may be due, at least in part, to a reduction in the kinetics of hydrogen diffusion and/or desorption in the BC_x samples (Figure 3-23). For identical charging and desorption conditions, the hydrogen desorbs much slower on the BC_x-templated sample. The origins for the slow kinetics are not known and need to be investigated further.

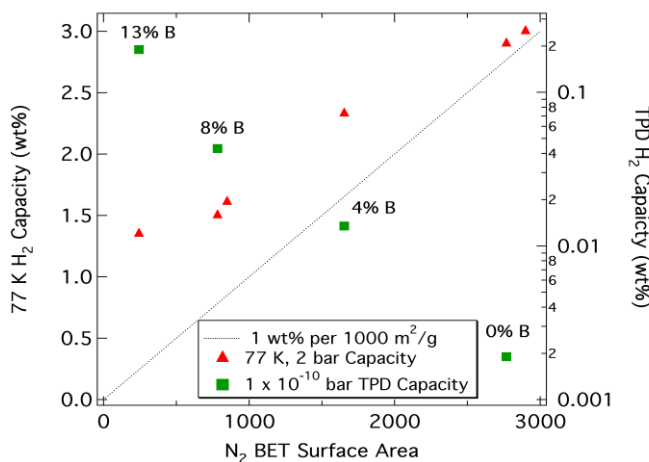


Figure 3-22. Sieverts capacity at 77 K and 2 bar, and TPD capacity, as a function of nitrogen BET surface area for a variety of BC_x-templated activated carbons. CM-Tec is the parent activated carbon material for all samples.

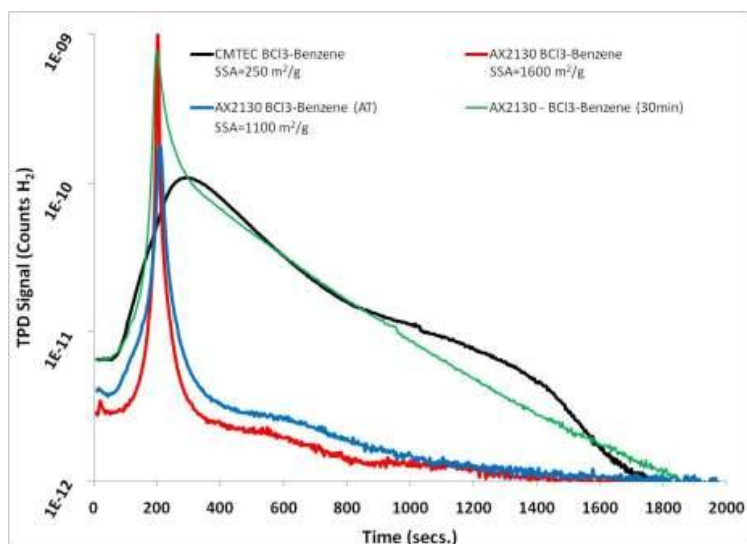
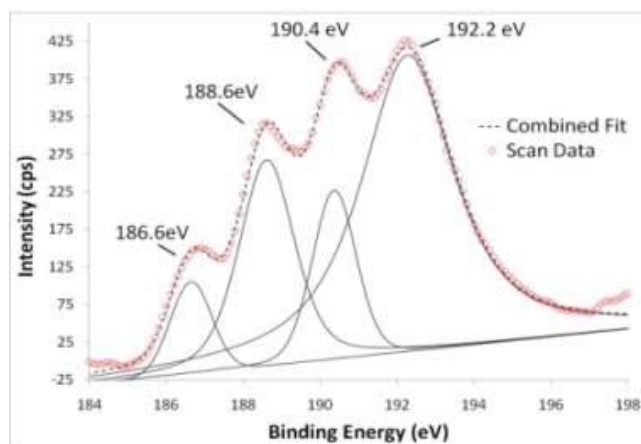


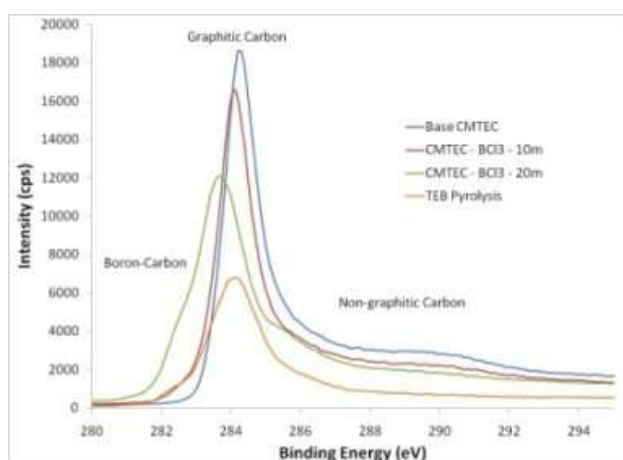
Figure 3-23. Representative example of hydrogen temperature-programmed desorption for a templated BC_x sorbent. The hydrogen desorption from templated BC_x materials with higher B concentration is much slower than from materials with less B.

X-Ray Photoelectron Spectroscopy

XPS was used to investigate the state of boron incorporation into the graphitic lattice. The boron 1s and carbon 1s spectra are useful in determining the exact state of boron binding. Figure 3-24 shows the high-resolution B 1s spectrum and the associated boron binding energies. The four main peaks are attributable to boron carbide, elemental boron, sp² boron, and boron oxide. Although other states of boron binding are possible, and in fact likely, the figure demonstrates the complexity of binding in the carbon-boron deposited material. The goal of the borontrichloride-benzene deposition is to maximize the atomic percent of boron incorporation into the sp² state, or more precisely the boron incorporated into the graphitic lattice. These are the sites theoretically predicted to have higher binding energy for hydrogen (10–12 kJ/mol). As Figure 3-24a indicates, the boron oxide is the dominant constituent form of boron, with sp² boron being the second largest composition. By using the entire four binding energies to calculate the atomic composition, a value 12.6% can be found. However, using only the sp² bonded boron reduces the atomic percent to 4.5%. Another indication of the incorporation of boron into the graphitic carbon lattice is in the carbon 1s spectrum shown in Figure 3-24b. In this spectrum, the base CM-Tec carbon peak is shifted from 284.5 eV, the recognized value for graphitic carbon, to 283 eV with an associated shoulder at 282 eV. The shift to lower binding energies and the shoulder in the spectrum is attributed to the boron-carbon binding sites. The exact nature of the sites is indeterminate however, as the influence of numerous states of boron-carbon binding convolute the separation between the distinct binding energies.



(a)



(b)

Figure 3-24. B and C XPS of templated BC_x materials

Nuclear Magnetic Resonance Spectroscopy

¹¹B and ¹³C NMR of BC_x powder samples provided by NREL are consistent with boron incorporated in a planar structure. The ¹³C magic angle spinning (MAS) spectrum indicates that carbon is sp² bonded. ¹¹B static and MAS spectra are also consistent with boron in a planar geometry (Figure 3-25). The static ¹¹B spectrum appears to be determined by an axially symmetric anisotropic chemical shift tensor consistent with sp² bonded trigonal boron. The MAS spectrum is broad (2.2 kHz) with the width likely caused by second-order quadrupole interaction. The ¹³C MAS spectrum probed over a large chemical shift range (inset, Figure 3-25a) shows only one line, indicating that the spectrum represents only one carbon bonding configuration. The isotropic chemical shift at 128 ppm (TMS) corresponds to the expected value for aromatic carbon. As seen in Figure 3-25b, the spectrum is unusually broad for a MAS spectrum spun at 9.7 kHz, indicating a large isotropic chemical shift distribution that possibly is due to disorder on the atomic scale.

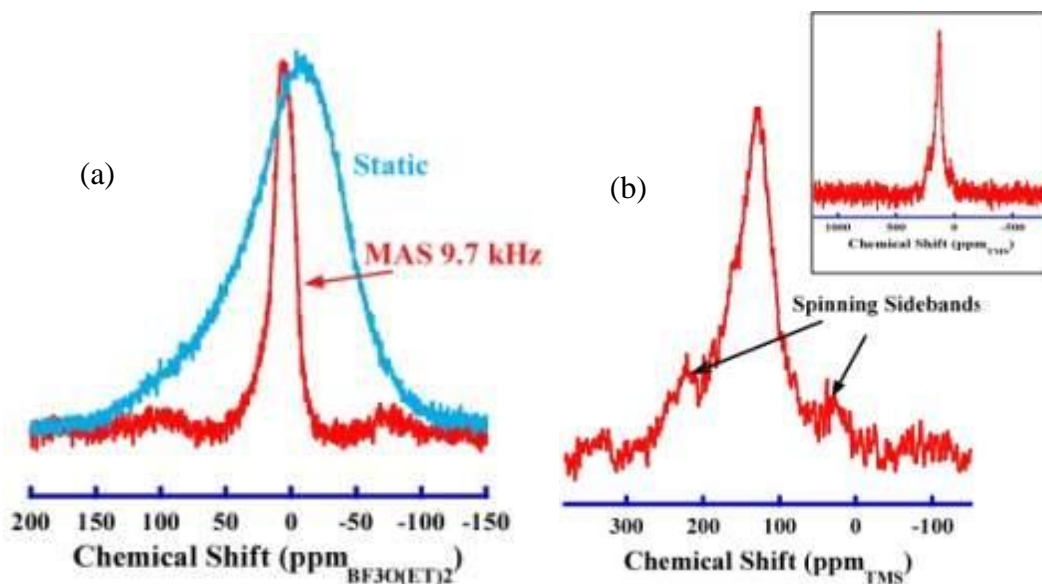


Figure 3-25. (a) Static and magic angle spinning (MAS) ^{13}C NMR spectra of BC_5 powder. (b) Static and MAS ^{11}B NMR spectra of BC_5 powder.

Templated BC_x Using B-Containing Precursors

APCI investigated the use of the B-containing precursors used by Penn State as templating agents. Initially, APCI attempted to use Zeolite NaY. Zeolite NaY has a limiting pore diameter of 7.4 Å, whereas the minimum vdW cross-section distance of the Penn State precursor ($\text{Cl}_2\text{B}-\text{C}_2-\text{Ph}-\text{C}_2-\text{BCl}_2$) is about 7.6 Å, with a long-axis distance of 16.5 Å. Thus, these precursors could not be used to template BC_x on zeolite NaY. Although moving to larger pore sizes brings with it more limitations to the attainable SSA and pore volumes of the ideal products, it became apparent that using commercially available mesoporous silicas of the Mobil Crystalline Material (MCM) type (e.g., hexagonal MCM-41 with pore diameters ranging from 15–25 Å) represented an excellent starting point for concept development. It is conceivable that the analogous MCM-48 could also be used as a template for smaller pore variations, while allowing pore filling from all directions based on the inter-connecting pore structure. It is helpful to note that templated carbons from these systems have also been produced (Lin et al. 2006), offering the expectation for SSAs of 1200 m²/g or higher. These silicas are thermally resilient and can be dried at very high temperatures.

Based on the selection of the Penn State BC_x precursors (Chung et al. 2008) and the desire to use microporous structured materials, it was important to select precursors that are smaller in order to allow impregnation into the template and provide the greatest boron content based on the boron-to-carbon ratio (B/C). This distills the choice to two obvious candidates, (1) and (2), as shown in Figure 3-26.

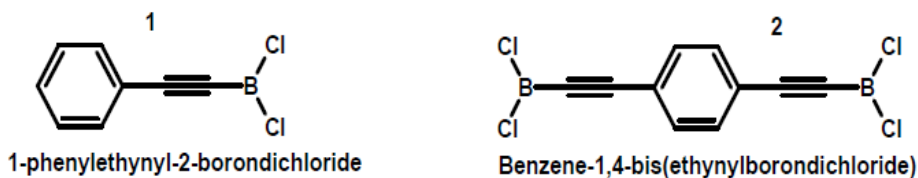


Figure 3-26. Diagrams of boron-containing precursors used to form porous boron-substituted carbon materials

Penn State represents the only group to have reported a successful preparation of these materials by lithiation followed by condensation with boron trichloride. Other groups that indicated this to be problematic reported the preparation of this material class via the more selective condensation between the boron trihalide and the corresponding alkynylstannane (Parks, von H. Spence, and Piers 1995). The first step of the sequence is selection of a solvent. Following the strategy of the Penn State group, APCI initially attempted to avoid ether solvents, as there was a general concern that they may incorporate oxygen into the BC_x product. Although convenient for their lack of reactivity, alkane solvents do not afford solubility of the aryl alkyne precursors. Because benzene and toluene afford suitable solubility, toluene was initially used for the relative toxicological safety. Ether solvents gave variable results in terms of oxygen incorporation into the carbonized product. Tetrahydrofuran (THF) presented several challenges as it tends to polymerize in an acidic environment, thus giving rise to significant amounts of oxygen in the carbonized product. Stabilizer-free ethyl ether was found to be beneficial in producing added solubility, while at the same time it could be completely removed from the substrate before carbonization, thus avoiding oxygen incorporation. It was also suggested that dimethyl ether, despite the challenges of handling at RT, might also be a suitable solvent for the reactions.

Lithiation of the alkyne can be performed with lithium hydride, which is convenient for separation methods; however, the convenience of commercial 2.5M butyllithium in hexanes, as used by the Penn State group, was the reason for its selection as the base. With toluene as a solvent, the lithiated alkynes were highly insoluble. With ether as a solvent, phenylethynyllithium and the monolithium diacetylene derivative were soluble, but the dilithiated diacetylide derivative was insoluble. Because of the volumetric bulk imposed by the insoluble organometallics, it was imperative to introduce extensive dilution of nearly 1%–2% by weight alkyne precursor in solvent, which was required to accomplish efficient mixing and transfer of the slurries. In the case of both solvents, deuteration experiments and subsequent analysis by Grand Canonical Monte Carlo (GCMC) simulation indicated quantitative conversion of the alkyne to the fully lithiated products with no evidence of addition of the alkyllithium to the alkyne. The slurries of the alkynyllithium compounds were stable at RT. The alkynyllithium must then be reacted with a boron trihalide to provide the BC_x precursors (1) and (2). The Penn State group employed the strategy of adding the boron trihalide to the alkynyllithium slurry at ice temperatures based on convenience of the addition. This order of addition, however, is not conducive to the preparation of (1) and (2), but rather the tetrahedral coordinated borate ion product, because the reaction is expected to be very rapid (Wakefield 1988). Instead, APCI opted to employ techniques to slowly add the alkynyllithium slurry to a cold solution of the boron trihalide. At this point of the reaction, there appeared to be a

delineation in the solvent that one should use in order to obtain (1) and (2). The APCI researchers discovered that the strict use of toluene gave rise to products (1) and (2), which were stable only in solution for periods of only 24–48 h as observed by NMR. The decomposition invariably produced sticky, tarlike polymers that were insoluble in all solvents but strong acids, indicating cleavage of boron-carbon bonds leading to destructive depolymerization, which is known for many poly(organoboranes) (Midland et al. 1975). It is theorized that the polymer byproduct is the result of haloboration polymerization of the multivalent products (1) and (2).

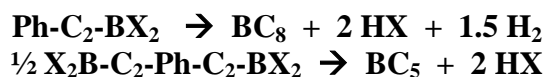
There are a number of methods for performing templating of carbons; however, because APCI decided to work with solutions of relatively sensitive substrates (1) and (2), the options become limited. These solutions are only suitable to absorption impregnation into the templates. This means that the template must be evacuated of all gases to facilitate filling of the pores with solution. Intuitively, it seems reasonable to expect the arylalkynylboron halides to be selectively absorbed into the pores over dissolution in the employed solvents. The degassed solutions of compounds (1) and (2) are introduced to the template and stirred until the precursor is absorbed, as determined by infrared (IR) or NMR analysis of the liquid phase. Indeed, the signals for the precursors subside within 24–48 h, as long as an excess of free volume inside the template is provided. By calculation, APCI attempted to provide at least a threefold excess of free volume in the MCM-41 to incorporate the precursor with a possibly coordinated solvent.

Once the absorption of the precursor was confirmed analytically, the impregnated MCM-41 was washed with a small amount of solvent to prevent particle-coating effects. Powder XRD data for the treated template was obtained to confirm filling of the pores, as observed by the loss of the reflections indicating regulated pore structure. This is not evidence that the pores were completely filled with the precursor alone, because they undoubtedly included solvent. Although better templating results were obtained by this method when ethyl ether was used as a solvent, APCI discovered a second method of performing the reaction condensation directly on the template that allowed use of the toluene solvent; APCI refers to this concept as “on-template” synthesis. This was accomplished by preparing the alkynyllithium intermediate as a slurry in toluene. Although the solubilities of the lithiated derivatives are quite low in toluene, they are significant enough to be detected by NMR in solution. The MCM-41 template was added to the slurry of alkynyllithium and stirred vigorously. At RT, a 5% stoichiometric excess of BCl_3 per equivalent of alkynyllithium was added all at once and allowed to stir. Monitoring of the reaction was conducted by ^{11}B -NMR. All of the BCl_3 was consumed within 18 h, giving rise to a deep-purple solid. The solvent can be easily removed under reduced pressure, exposing the purple solid. Because the preparation is performed in toluene, it is likely that the product polymerizes inside the template, so stability of the precursor is of little concern. It is important to point out that the on-template synthesis of BC_x differs from the direct templating method in that it does not incorporate a purification step to remove undesirable byproducts, including LiCl . It is possible that the LiCl may aid in the development of additional porosity as shown by the Penn State group.

Once the precursor has been impregnated into the template, it must be polymerized in to fix it into place and avoid sublimation or being otherwise ejected from the pore. The Penn State group reported that heating the precursors (1) and (2) to 350°C effectively dries and hardens the material. In ACPI's experience, polymerization of the precursors occurs readily without heating when toluene is used as the solvent. However, when ether is used as the stabilizing solvent, volatilization of the precursor with ether generally precedes polymerization in a thermally based process. It appears that the stabilizing mechanism employed affords excessive protection against polymerization.

From the literature (Midland et al. 1975), neutral and acidic environments support hydroboration and haloboration additions across unsaturated systems, and bases tend to coordinate the boron center causing rehybridization and loss of reactivity. Based on this information, it was postulated that a protic acid may catalyze the haloboration polymerization that is needed to fix the precursor in place. Indeed, ACPI discovered that catalytic amounts of HCl caused nearly instantaneous polymerization of the precursors in solution. It is important to minimize the quantity of protic acid, as there is the possibility it may liberate BCl₃, causing undesirable boron loss. The polymers were insoluble in all solvents except strong protic acids. The on-template preparations should not intuitively require acid-catalyzed polymerization if they were prepared in the absence of ether. However, ACPI did find that acid treatment of these intermediates assisted in obtaining better carbonization yields.

Carbonization of the precursor was accomplished by thermolysis in the absence of air and moisture (e.g., under a purge of argon or high vacuum). During the carbonization process, it is desirable to eliminate hydrogen halide from the precursor or polymerized precursor to obtain a thoroughly inorganic BC_x. As shown in the schemes below, the stoichiometry of the dialkynyl precursor ideally suits a perfect condensation to BC_x, with no halogen or hydrogen remaining, because the mono alkynyl compound leaves an excess of hydrogen (not to indicate that elemental hydrogen is the actual by-product), opening the viability for boron migration and elimination chemistry (facilitating loss of boron):



It would be ideal to have a condensation reaction in which no bound hydrogen remains, as it can facilitate rearrangements that allow boron loss as volatile small molecules in the heating process. ACPI was able to confirm the stages of various thermal processes in the carbonization by thermal gravimetric analysis (TGA) and TGA-IR analysis of precursor (1), PhC₂BCl₂. It was evident that the etherate of the precursor becomes volatile and produces very low yields upon heating as the unpolymerized material. The value of proper polymerization is also clear, as it dramatically improves the net yield of the carbonized product. Identical results were obtained for the dialkynyl precursor (2), Cl₂BC₂PhC₂BCl₂.

Another differentiation in yield was observed by varying the heating rate. Higher heating rates gave greater net yields, which indicate that faster heating rates kinetically advance

the elimination of HCl over rearrangement chemistry, creating larger volatile by-products of carbon and boron. A comparison of the various TGA data clearly showed the stages where solvent and volatile materials are removed up to 150°C, which is followed by the chemical condensation zone up to ca. 400°C, a temperature at which most of the XH elimination chemistry and bond rearrangement will take place. Because many of the BC_x materials covered in this study are high melting pitches, heating them to 600°C and holding for a time (~4 h) is sufficient to anneal the carbonized product and provide graphitic BC_x.

The direct carbonization of the precursors (1) and (2) or their related polymers at 600°C consistently produced boron-containing products of a graphitic nature. The SEM/TEM analyses were very useful in screening for porosity on the scale expected for MCM-41. Electron dispersive spectroscopy (EDS) was also useful in discerning purity and screening for boron. Although it is usually not suitable to evaluate light elements such as boron, APCI pioneered methods incorporating low incident beam energies (~5 kV) to obtain information about boron. Although none of the EDS results were quantitative and elemental analysis was required to get such values, APCI researchers observed that a small (non-resolvable) shoulder or tail on the carbon peak of such EDS is coincident with boron values of at least 3% or as compared to elemental analysis.

The most successful structural templating attempts were accomplished by the on-template preparations discussed previously. The result was a quantitative preparation of a porous solid with mixed morphology from that of literature MCM-41 templating and that of the salt-leaching templating employed by Penn State. With production of materials with SSAs approaching 600 m²/g, this method represents one of APCI's more promising methods.

The final step of the templating process is the selective removal of the template. Zeolite and mesoporous silica templates are routinely removed with either concentrated aqueous hydrogen fluoride (HF) or concentrated aqueous hydroxide. Some of the earliest work with BC_x materials confirmed expectations that conditions sufficient to etch a zeolite or porous silica with these reagents also completely compromises the boron content of the resulting material.

APCI used a different approach by leveraging its experience and capabilities with anhydrous HF (aHF). Researchers discovered that aHF can instantaneously convert silica to volatile SiF₄ at temperatures (-78°C) near the melting point of HF and preserve some of the boron content of templated BC_x, as long as the HF is removed below -50°C and the residual water by-product HF adduct is removed under high vacuum between -50° and 0°C. Although the study was incomplete, there were indications that the HF compromises only about half of the boron content in the material during this process.

Templated BC_x enhanced H₂ storage (per unit SSA)

As shown in Figure 3-27, the resulting porous BC_x materials had substantially higher hydrogen adsorption on a per SSA basis compared to pure carbon materials. In general, maximum excess gravimetric hydrogen-adsorption capacities of ~3 wt % are observed at 77 K for materials with 600 to 800 m²/g SSAs. In addition, ~65% of the 77 K capacity is retained with some porous BC_x materials at ~200 K. This compares to 25% to 30% with pure carbon materials at the same temperature.

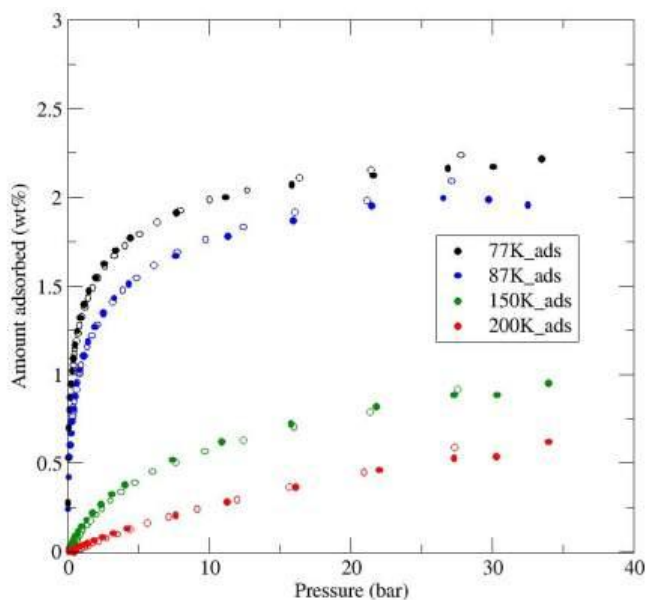


Figure 3-27. Representative example of hydrogen adsorption (solids) and desorption (open) excess gravimetric isotherms of porous BC_x sorbents. Because this material SSAs of only 600 to 800 m²/g, the maximum excess hydrogen adsorption of ~2.3 wt % at 77 K is much higher than what is typically observed for pure carbon sorbents (i.e., 1.2 to 1.6 wt %).

Calculations and experimental measurements both show that stronger dihydrogen binding between 10 and 15 kJ/mol (Chung et al. 2008) occurs when B is substituted with sp² coordination with carbons (see Figure 3-28). This is sufficient to substantially increase the storage temperature compared to typical cryo-compressed materials, and potentially enable BC₃-like materials to be used to meet DOE hydrogen storage capacity targets at 150 to 250 K temperatures if sufficient SSAs can be obtained. Any significant storage temperature increase toward ambient significantly reduces weight and costs, thus making it easier to meet DOE system targets.

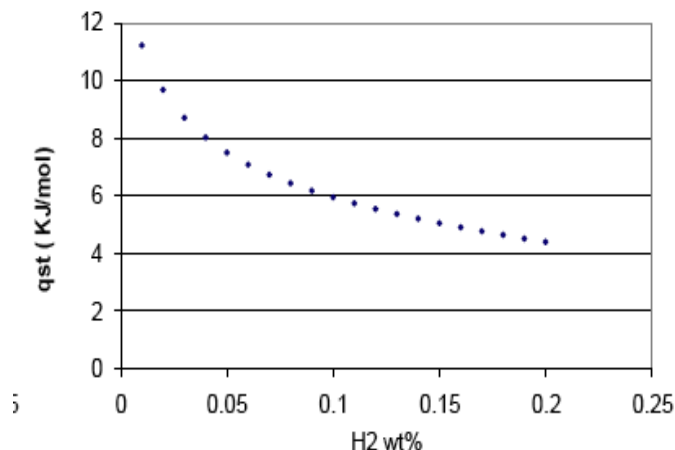


Figure 3-28. Representative example of the hydrogen isosteric heat of adsorption for a porous templated BC_x sorbent

Neutron Spectroscopy of BC_x Materials

Non-destructive prompt-gamma activation analysis (PGAA) determines the bulk elemental composition of synthesized samples. Small-angle neutron scattering (SANS) and inelastic neutron-scattering (INS) measurements on nanoporous carbons provide insights into the morphology of the pore structure and how hydrogen is adsorbed into these materials. With the low hydrogen loadings on nanoporous carbon derived from blends of polyfurfuryl alcohol and polyethylene glycol produced by the Penn State group, there is a clear splitting of the 14.7 meV, indicating a relatively strong interaction of adsorbed hydrogen with the carbon material. Until 0.8 wt % hydrogen loading, the split feature is very clear, however, at 1.6 wt % hydrogen loading, the spectrum begins to narrow and centers around 14.7 meV. At the largest loading of 4.2 wt %, the rotational transition peak exhibits one peak with a much smaller full-width at half-maximum of ~1.46 meV. This transition from a split feature in the rotational transition peak to an apparent single peak suggests that the local environment of the adsorbed hydrogen molecules has changed dramatically between 0.8 and 1.6 wt % loading. The split feature observed at low coverage indicates that the rotation of hydrogen molecules adsorbed in the NPC sample is strongly hindered because of the adsorption of hydrogen molecules in nanopores smaller than 1 nm. The INS peak character change between 0.8 and 1.6 wt % indicates that hydrogen molecules continue to be adsorbed in larger pores with lower curvature of the graphitic walls, and the rotation of hydrogen molecules is much less hindered.

Approximately one gram of BC₈ material was produced by templated reaction of benzene and BCl₃ on CM-Tec activated carbon at NREL. The resulting BC₈ carbon had a SSA of ~250 m²/g and a sieverts hydrogen-storage capacity of ~1.5 wt %. A thorough INS comparison of the templated BC₈ material to the CM-Tec control was performed. For a routine INS collection, each sample was loaded with hydrogen at 50 K and cooled to 4 K for measurement of the spectrum. The BC₅ sample was loaded up to 1.5 wt % and the CM-Tec sample was loaded up to 6 wt %. The focus is to obtain the para-ortho transition spectra around 14.7 meV. Shifts and splittings imply a difference in orientational

potential and hence binding enthalpies. At low loadings, both samples showed a split ortho-para peak around 14.7 meV (~13 and 15 meV). At higher loadings, this changed to a single peak centered at 14.7 meV. Another peak appeared at ~30 meV, which is either a $J=1 \rightarrow 2$ peak or multiple $J=0 \rightarrow 1$ transition. At low loading, the BC_8 and CM-Tec look the same, indicating the H_2 is in similar environments. NREL also performed a degas experiment for both carbons. For this experiment, after loading with hydrogen, the sample was heated to a particular temperature and pumped for a short amount of time to establish a $\sim 10^{-5}$ torr base pressure. The sample was then cooled back to 4 K to measure the INS spectrum of the hydrogen remaining on the sample after the degas step. The peak intensities of the hydrogen measured following each degas step are plotted in Figure 3-29. Two trends are apparent. For one, hydrogen is lost from the CM-Tec sample much more rapidly after degassing to relatively low temperatures (< 55 K). For example, after degassing to ~ 40 K, the CM-Tec sample lost $\sim 55\%$ of the hydrogen stored at 30 K, whereas the BC_8 sample lost only $\sim 30\%$. After 55 K, the rates of H_2 loss as a function of degas temperature appear equivocal. However, >55 K, the BC_8 material retains a slightly higher residual H_2 capacity. These observations could indicate sites within the BC_8 material with higher binding enthalpy than the sites within the CM-Tec base material. Such sites would retain H_2 better as the sample is degassed, which is in accordance with other reports within the center for higher isosteric heats of adsorption (as high as 12 kJ/mol) for BC_x -templated materials at low loading.

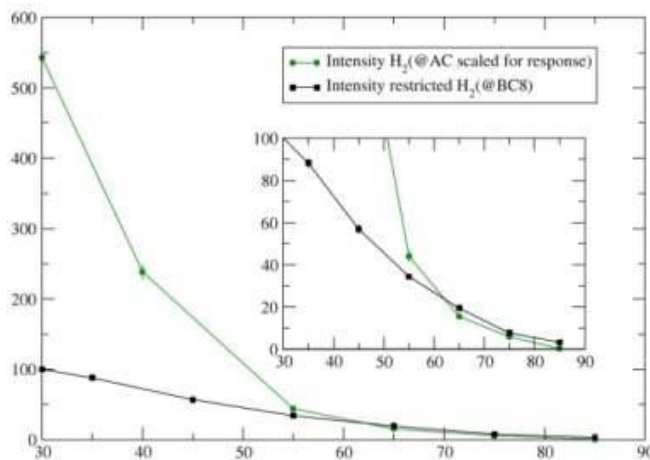


Figure 3-29. INS measurement of the intensity of hydrogen remaining on the sample as a function of temperature. The data show that the B-containing samples hold hydrogen to a greater extent at temperatures below ~ 65 K.

Boron-Substituted Nanotubes

A series of INS investigations was performed on hydrogen adsorbed on purified SWNT bundles (Figure 3-30), both with and without boron substitution (≤ 1 at %, Figure 3-31). Samples of both types were generated by arc- and laser-production methods. At H_2 coverages $\leq 3 H_2/B$, a clear splitting was observed for the $J = 1, m = 0$ and $J = 1, m = \pm 1$ sublevels in all arc-produced samples (Figure 3-32). In contrast, the spectra from the laser-produced materials exhibit one broad peak (Figure 3-33), which may contain different peaks resulting from the splitting of $J=1$ sublevels. Further increases in H_2

coverage resulted in adsorption at lower binding energy sites. No distinct signature of an enhanced boron-hydrogen interaction was observed. However, the overall line width of the rotation transition peak from a laser-produced sample was substantially smaller than that from all arc-prepared samples. This difference might imply that some of the splitting features of the H₂ rotation transition peak might not be due to the intrinsic features of SWNTs. These observations call into question the previous assignment in the literature of hydrogen adsorption at the groove sites as the origin of the splitting of the rotational transition for arc-produced samples.

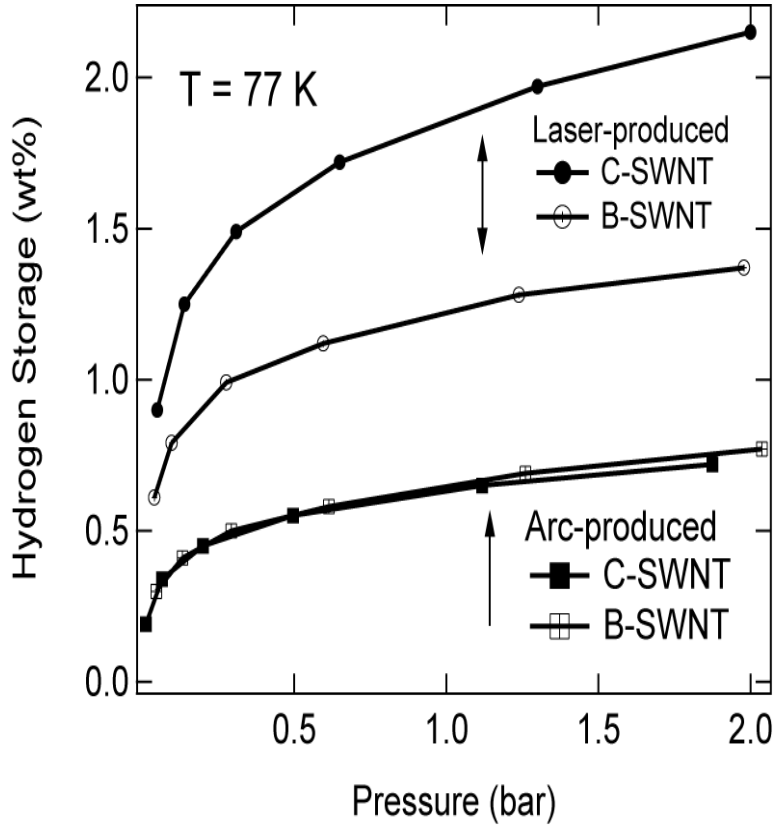


Figure 3-30. Isotherm comparison of volumetric hydrogen storage capacities of laser-produced and arc-produced C-SWNTs and B-SWNTs

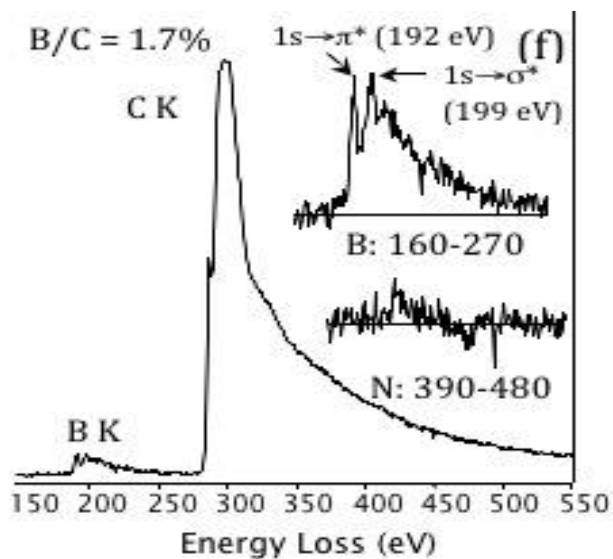


Figure 3-31. EELS spectrum for boron-doped SWNTs prepared by laser vaporization; laser target contained 11% NiB catalyst

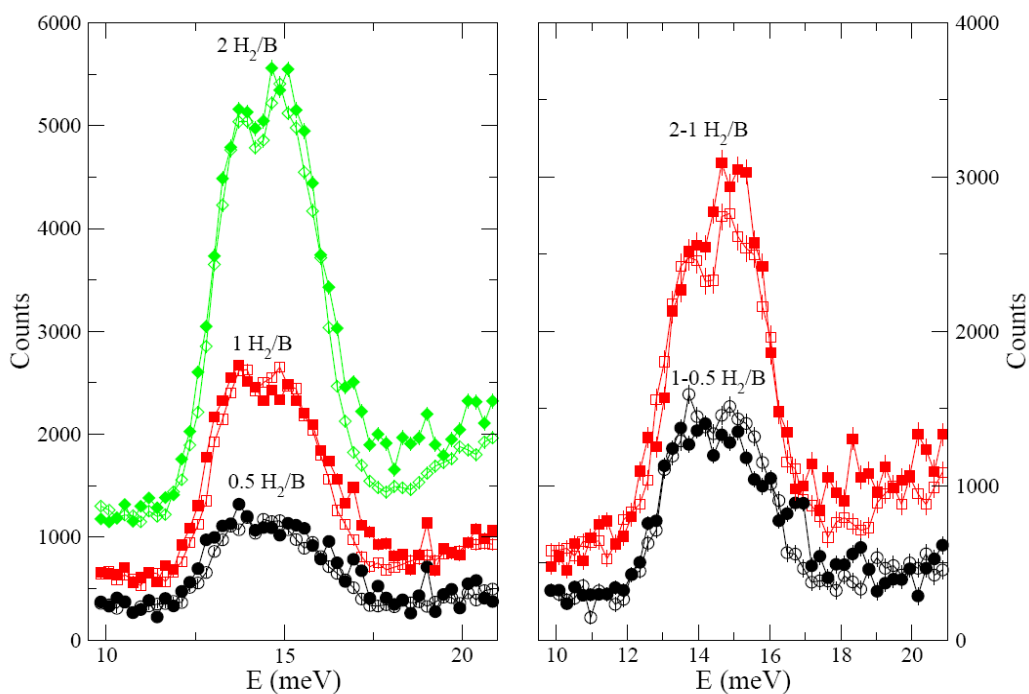


Figure 3-32. Neutron spectra for arc-produced C-SWNTs (open symbols) and B-SWNTs (filled symbols). A mass fraction of 0.1% is equivalent to a 1 H₂:B atomic ratio of the B-SWNT samples. Right panel displays the different spectra.

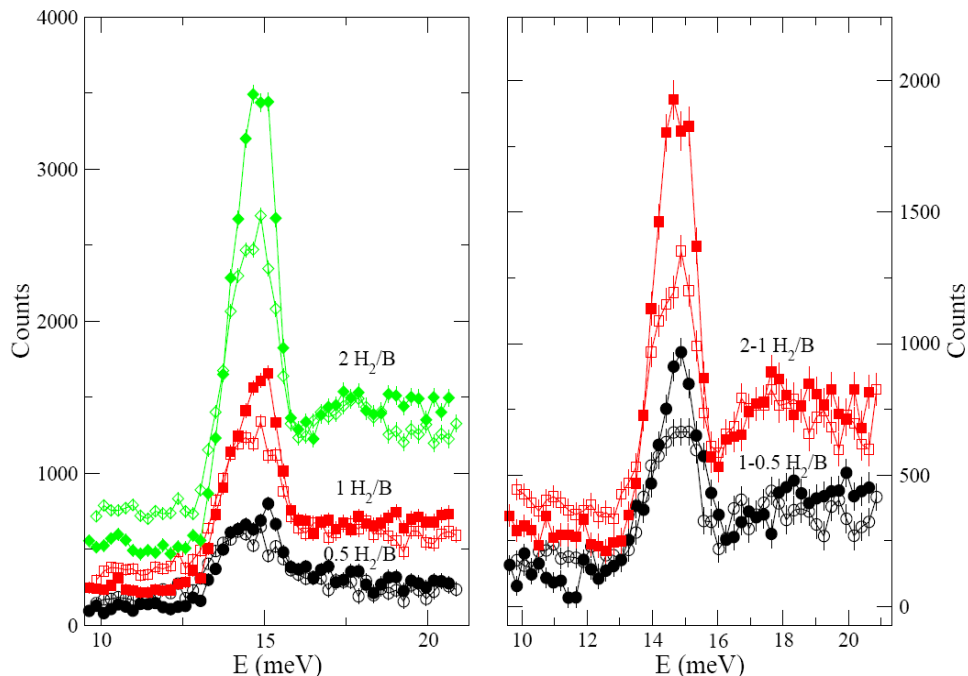


Figure 3-33. Comparison of neutron spectra for laser-produced C-SWNT (open symbols) and B-SWNTs (filled symbols). Data are labeled for H₂:B atomic ratios of the B-SWNT samples with the equivalence of 0.2% mass fraction being equivalent to 1 H₂. Right panel displays the different spectra between 0.5 H₂:B and 1 H₂:B and 1 H₂:B and 2 H₂:B.

Nanoprobe electron energy loss spectroscopy (EELS) measurements were employed to determine the local B content and B bonding geometry in B-SWNT bundles and to identify which growth parameters permitted the incorporation of B into the SWNT lattice. The B-SWNT composition and bonding information were obtained by insuring that the EELS probe only examined clean bundles that were well separated from other non-nanotube fractions in the sample. The EELS data for a sample prepared from a target containing 11% NiB catalyst show that the amount of B incorporated into the nanotubes increases as the concentration of NiB is increased in the target. Integration of the EELS spectrum yields a B/C ratio of 1.7 at %, whereas the range of the B/C ratio from bundle to bundle was ~0.8–1.8 at %. The most striking features are the sharp, well-defined $1s \rightarrow \pi^*$ and $1s \rightarrow \sigma^*$ resonances, which confirm the achievement of true substitutional doping of B into the SWNT lattice. Although a sharp B $1s \rightarrow \pi^*$ resonance at ~192 eV is typically used as evidence for incorporation of B into a nanotube lattice, it is often not appreciated nor discussed that other impurities may give rise to such a peak. For example, this peak is observed for hexagonal boron nitride (h-BN), highly crystalline boron carbide (B₄C), and for the NiB catalyst particles. One must also consider that the $1s \rightarrow \pi^*$ peak for boron oxide at 194 eV is very close to the $1s \rightarrow \pi^*$ signal for sp² bonded B at 192 eV. Thus, it is critical that nanoprobe EELS measurements are performed on very clean, well-formed SWNT bundles.

3.3.2 Other Benefits of Heterogeneous Sorbents

In addition to direct substitution, initial efforts identified that materials with intercalated and/or absorbed ions may enhance dihydrogen binding. For example, anions with high charge/volume ratio (e.g., fluoride) can donate electron density to s^* -orbitals of dihydrogen. Similarly, other intercalated species (e.g., alkali and alkaline metals, anions) may induce charge interactions to improve hydrogen adsorption enthalpies. Some of these effects may have been observed in the alkali metal intercalated graphite materials discussed previously that produced the higher and uniform binding energies due to multiwall interactions. In some cases, it is theorized that molecular dopants complexed with nanostructures can generate sufficient electric fields to enhance H_2 storage. Finally, some of these substituted or functionalized materials may improve sorption of other elements/molecules for different hydrogen mechanisms associated with back-donation and/or spillover.

Following Zhang and Alavi (2007), APCI used DFT-LDA (density functional theory-local density approximation) calculations to identify that it is energetically possible to move H_2 molecules into bulk BC_3 through the edge planes. Given an equilibrated initial position for the H_2 molecule of about 3.5 Å away from the edge, researchers gradually moved the molecule toward the slit pore so that they passed through the edge and ended in a location between two B atoms of adjacent BC_3 layers in the middle of the selected unit cell. The LDA calculations suggest that H_2 diffusion into the slit pore of BC_3 is facile, and the intercalated H_2 will undergo spontaneous dissociation to form covalent bonds with C atoms. These C-H bonds might be sufficiently labile to allow the H atoms to diffuse throughout the lattice in a thermally activated process, which would make BC_3 a highly promising hydrogen-storage material with good capacity and facile desorption kinetics. In particular, BC_3 might be an ideal media to store hydrogen via hydrogen spillover. It should be more efficient than the materials that have been used as hydrogen spillover substrates to date, because it would require no metal catalyst to promote the release of storage hydrogen by the dissociation of molecular H_2 .

In addition to optimizing geometric structures to improve storage properties, the HSCoE pioneered the use of multiple-element materials to improve dihydrogen binding. In good agreement with theoretical models, substituted with an sp^2 structure in carbon enhances hydrogen binding to ~11 kJ/mol. The main issues remaining include the need to substantially increase the B concentration while maintaining a high SSA. The HSCoE identified several synthetic techniques to address these issues, including pyrolysis of BC precursor materials, templating of BC_3 , and chemical replacement processes. In addition to B enhancing dihydrogen binding and thus storage capacity at near-ambient temperatures, B and N have also been used to stabilize single metal centers and metal clusters on high-SSA materials (Zhao et al. 2005). Thus, substituted or heterogeneous materials provide a number of benefits for hydrogen sorbents and should continue to be developed in future sorbent projects.

Other Systems Beyond B-Substituted Carbons

Rice used solution-based chemistry to synthetically form substituted graphene materials. The general goal was to chemically form stable substituted graphene sheets with high substitution content, and then to use the graphene scaffolding processes that Rice has

developed for its optimized nanostructures work to form high-SSA materials with high substitution concentrations. All-carbon and heteroatom-substituted synthetic graphenes were prepared using the procedures identified in the paper by Zhong and colleagues (2011). This included refluxing chloro-substituted organic reagents containing sp^2 carbon and chosen heteroatom precursors together with sodium in high-boiling solvents, as shown in Figure 3-34. For the heteroatom-substituted synthetic graphenes, triisopropyl borate, triethylphosphite, and cyanuric chloride were used as the boron, phosphorous, and nitrogen sources, respectively. Alternatively, boron trichloride and phosphorous trichloride could serve as boron and phosphorous sources, respectively. Two heteroatom precursors with different substitution elements can also be simultaneously added in the reaction system for the preparation of co-substituted products, such as boron/phosphorous and boron/nitrogen co-substituted synthetic graphenes. To remove residual salts and organic compounds completely, the filter cake is washed, filtered, and dried. High-resolution EELS was used to determine the substitutional incorporation level and spatial distribution of B, N, and P atoms, as shown in Figure 3-34.

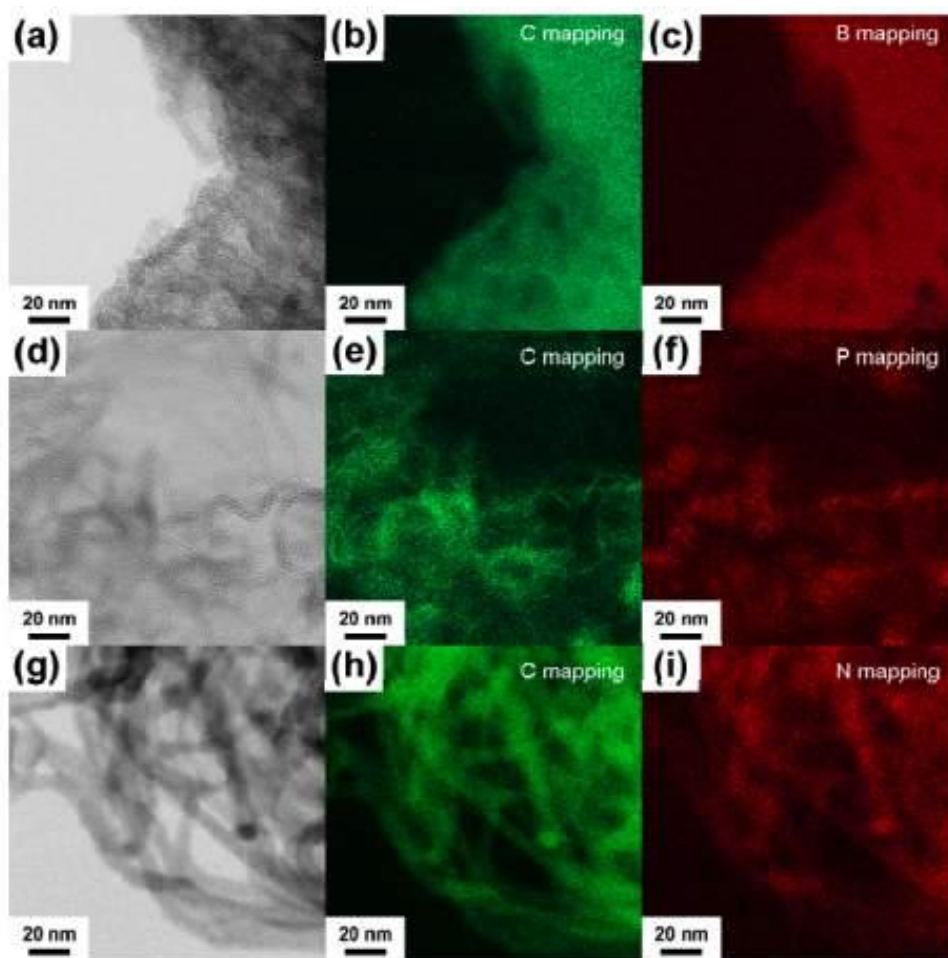


Figure 3-34. Elemental mapping of C, B, N, and P in substituted graphene structures using EELS.

Initial efforts resulted in isosteric heats of adsorption of 8.6 kJ/mol for B-graphene with 5.4 at % boron substitution; 8.3 kJ for P-graphene with 7.5 at % phosphorous substitution, and 5.6 kJ for N-graphene with 13.5 at % nitrogen doping. Although the goal is to find routes toward much higher substitution concentrations for boron and perhaps phosphorous, these initial results demonstrate that high (i.e., 25 at %) sp^2 -coordinated substitutions can be achieved (e.g., with nitrogen). The results also confirm predictions from the original calculations that nitrogen substituted in carbon would not significantly increase hydrogen binding. However, as predicted, B substitution did increase hydrogen binding, and it appears that P does as well. These results also demonstrate the intrinsic issue of limited substitution for elements that appear to increase binding. Even though the SSAs are still low, the hydrogen-storage capacities of these materials were significantly higher than expected for typical activated carbon with similar SSAs (Figure 3-35).

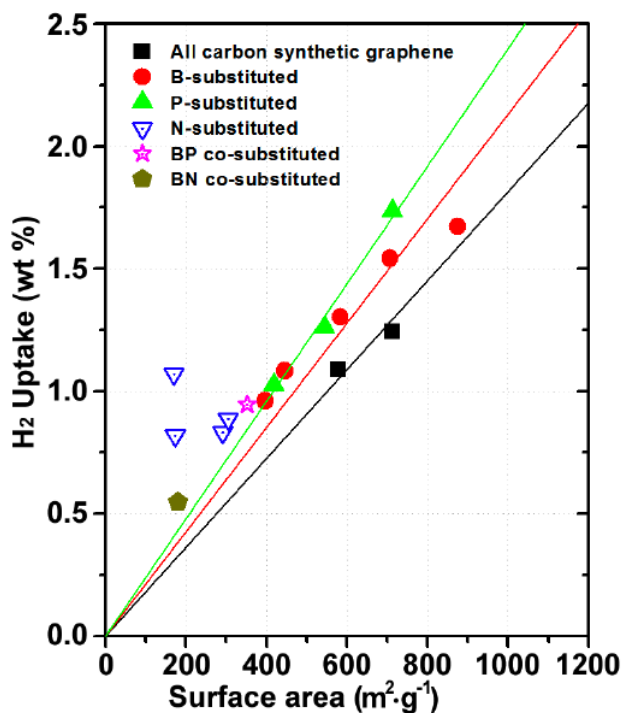


Figure 3-35. SSA measurements from nitrogen BET at 77 K vs. hydrogen uptake at 77 K and 2 bar. The data for all-carbon and substituted synthetic graphenes are indicated by the different colored symbols, as shown in the legend. The solid lines with the matching colors are the linear fits and extrapolations obtained from the sample data.

Fluoride-Intercalated Graphite

To ascertain if partially fluorinated graphites are capable of adsorbing H₂, APCI synthesized a number of first- and second-stage fluoride samples of graphite intercalation compounds (GICs) and subsequently measured H₂ isotherms and derived the isosteric heats of adsorption. Graphite fluoroborates, C_xBF₄, were synthesized by exposing crystalline graphite powder (Timrex SFG6, dried at 900°C under argon) to a mixture of F₂ and BF₃ at RT (Brusilovsky et al. 1988; Rosenthal, Mallouk, and Bartlett 1984). C_xBF₄ was then heated to 150°C under vacuum, partially removing BF₃ from the lattice to form

$C_xF(BF_4)_y$ (Nikonorov 1979). The partial decomposition of the C_xBF_4 was designed to yield a mixed GIC that contained both naked fluoride anions and residual BF_4 , which could function as a “spacer” to sustain adequate interlayer spacing for the adsorption of H_2 . Hydrogen isotherms on a number of $C_xF_y(BF_4)_{1-y}$ ($x=8-26$, $y=0.1-0.7$) samples were generated at pressures up to 1500 psia using differential-pressure volumetric adsorption (Zielinski et al. 2007). The isosteric heat of adsorption (heat of adsorption at equal H_2 coverage) revealed that partially fluorinated graphite can adsorb hydrogen at near-ambient temperatures with an enthalpy as large as *ca.* -12 kJ/mol H_2 . Although this heat of adsorption is lower than those predicted by the molecular dynamics (MD) simulations performed at low H_2 loadings, the average enthalpy is higher than those reported for non-intercalated carbon materials such as graphite (Pace and Siebert 1959) (*ca.* -4 kJ/mol H_2 at 20 K and H_2 coverage of <0.9 mmol/g) or activated carbon (Benard and Chahine 2001) [$-(6.5-5.0)$ kJ/mol H_2 at 77–273 K and H_2 coverage of 0–12 mmol/g]. The measured H_2 storage capacity of the GIC at near-ambient temperatures and the heat of adsorption are comparable to MOF incorporating coordinatively unsaturated transition metals (TMs) (Ma et al. 2007; Dinca et al. 2006) despite the extremely large difference in SSAs.

Besides the well-known LDA overbinding (Perdew et al. 1992), the gap between the calculated energies at low loading and the experimental heat of adsorption is likely due to the presence of residual BF_4 in the as-prepared GIC, which dilutes the gravimetric hydrogen density and adsorption enthalpy. After measuring isotherms on a large number of $C_xF_y(BF_4)_{1-y}$ samples, researchers found the isosteric heat of adsorption to be very sensitive to both the C:F ratio and the amount of residual BF_4 . These variables likely affect the semi-ionic/covalent nature of the C-F bonds and accessibility of H_2 to the intercalated fluoride ions. It is apparent from the SSAs and H_2 uptake that only a fraction of the fluoride ions in the samples are accessible to H_2 .

NC_5

Through predictive computational modeling, APCI identified a nitrogen-doped GIC of formula $(C_6N_2)_n^{2n+} 2nF^-$ with strong H_2-F^- interactions. To quantify the adsorption energy at hydrogen loadings relevant to meeting the 2010 DOE hydrogen storage system targets, researchers performed MD simulations at 300 K of 7.4 wt % hydrogen adsorption in porous $(C_6N_2)_n^{2n+} 2nF^-$. The MD simulation showed several interesting phenomena, including a large lattice expansion upon H_2 adsorption and F^- interaction with carbon, leading to non-planarity of the nitrogen-doped graphene sheets. A calculated average H_2 adsorption energy of -20 kJ/mol H_2 at 7.4 wt % H_2 loading was determined by the MD simulation. This very high hydrogen adsorption energy from the MD simulation of the solid-state material is important for establishing the viability of reversible hydrogen adsorption at near-ambient temperatures.

The experimental efforts toward hydrogen-adsorption testing of nitrogen-doped GICs began with the synthesis of nitrogen-doped carbons as a starting material for the N-doped graphite fluoride intercalation complex. Using procedures from the literature, nitrogen-doped carbon materials were synthesized by chemical vapor deposition (CVD) from acetonitrile (CH_3CN) on alumina-supported Ni catalysts at 800°C.

The experiments explored the use of unsupported nickel nanoparticles (100–3000 nm) as catalysts. Argon was purged through a tube as it was heated to 400°C. After the tube was

equilibrated at 400°C, 100% H₂ was introduced into the tube and allowed to reduce any oxide impurities on the Ni catalyst for 1 h. The H₂ was then shut off, and Ar was used to purge the tube while it heated to 900°C. After reaching 900°C, the Ar flow was redirected through a sparger containing acetonitrile. The CVD process at 900°C was performed for 5–6 h.

The elemental analysis of the resulting carbon fibers resulted in stoichiometries of C₂₅N to C₄₀N, which is consistent with literature reports for materials made at 800°–900°C. Increasing the acetonitrile vapor concentration in the reactor through heating the sparger and increasing the reaction pressure gave better yields, but drastically reduced the nitrogen incorporation. This may be due to the effects of annealing the fibers in hydrogen at high temperature. H₂ is likely present during the pyrolysis of CH₃CN, and could decompose C_xN through formation of HCN. Increasing the vapor concentration of acetonitrile adversely affects the N incorporation by also increasing the concentration of hydrogen in the reactor. Using the 100-nm Ni catalyst at lower temperatures improved the N-doping, but yields were still extremely low.

TEM and EELS analysis of the synthesized nitrogen-doped carbon fiber materials (elemental analysis formula, C₁₉N) were performed. The TEM images showed that C_xN fibers (diameter ~0.3 microns) were composed of smaller entwined graphite-like ribbons with diameters/widths of approximately 5 nm. The graphene-sheet interlayer spacing in this material was between 3 and 4 Å, as expected for a graphitic fiber. The ribbon morphology leads to the potential for a high-SSA material. The EELS spectra indicate that the variety of different morphology fibers in the C_xN mix all contain carbon atoms that are “C₆₀-like” (ie., sp² hybridization with some degree of sp³ character) and doped nitrogen atoms that have some sp² character.

Nitrogen-doped carbon nanofibers (elemental formula C₃₀N) were subjected to the same BF₃/F₂ treatment protocol to produce the type of intercalation compounds used for regular graphite. A weight increase of ~20% was observed, which was below the 31% expected for second-stage C₁₆BF₄ and the 47% required for first-stage C₈BF₄. Subtracting the 10% weight of Ni in the C_xN fibers (remaining from the CVD synthesis procedure), and assuming that the BF₃/F₂ did not chemically react with Ni, the weight increase was still only 22.6%. Despite the low BF₄⁻ concentration, TEM/EELS was used to analyze this intercalated C₃₀N material. Graphitic lattice fringes were observed after intercalation and appear to be spaced ~12 Å apart, consistent with a second-stage C₁₆BF₄ material. EELS spectra suggest that the incorporation of B and F was uniform throughout the material. However, the low concentration of N made the EELS detection difficult for the nitrogen atoms in the sample. These data provided encouraging information that these smaller graphitic domains intercalate in a manner similar to bulk flake graphite. However, because of the limited amount of nitrogen in the host material, no additional intercalation work was performed.

An alternative approach to creating nitrogen-rich carbon materials is the uncatalyzed CVD reaction of pyridine and chlorine at 700°C. This was suggested in the literature to result in a “turbostratic” graphitic material with the formula C₅N. APCI performed

several reactions following the literature conditions to yield hundred of milligrams of material. XRD analysis revealed the flaky product to be largely amorphous. A broad 002 reflection indicated that the layers were poorly ordered along the c-axis direction.

Approximately 700 mg of C₅N was ground to a powder in a mortar and pestle under acetone to reduce static charge. The powder was dried in a vacuum oven for 3 days before it was loaded into a reactor in the glove box. The C₅N powder was exposed to a 2:1 molar ratio of BF₃/F₂ mixture at RT for 4 days with constant mild agitation. The reactor was evacuated for 3 h to remove any adsorbed gas. The sample did not visibly increase in volume, but showed a 5% increase in mass. XRD and other analyses suggested that no intercalation resulted from the reaction.

3.4 Strong/Multiple Dihydrogen Interactions

To increase the heat of adsorption of dihydrogen (and enhance H₂ binding) beyond typical physisorption phenomena requires arranging atoms in specific configurations within a high-SSA material so that the H₂-substrate interactions are energetically more favorable/stable. The HSCoE leveraged first-principle calculations to guide experiments and rationally design and synthesize sorbents that strongly bind multiple dihydrogen ligands. Dihydrogen ligands may be bound to a single metal atom with binding energies in a desirable range for vehicular hydrogen storage. The synthesis of materials that have open, isolated metal sites exhibiting moderate H₂ heats of adsorption, with interactions potentially similar to those observed in Kubas-type complexes (Kubas 2007), were explored and optimized by HSCoE members. Metal clustering and reaction with other elements reduce or eliminate the enhanced capacities, and thus materials must be designed to stabilize the metal atoms in the correct configuration. The calculations used to make these initial predictions are in good agreement with experimental results that have observed adsorption of two or more dihydrogen molecules. Furthermore, similar calculations have identified that calcium (Ca) has unique hydrogen-storage properties that could produce carbon-based materials with >10 wt % and 100 g/L H₂ capacities. A few other first-row TMs are also good candidates for hydrogen-storage materials. However, based on work performed by the center, it is imperative that calculations and synthetic expertise be used to identify new energetically stable materials and viable synthetic routes. The key issues include balancing the reactivity of the hydrogen sorption sites with their stability and hydrogen capacity of the material. The HSCoE rationally designed and developed scalable and reproducible methods to synthesize lightweight, high-SSA materials with coordinated but electronically unsaturated metal centers. The methods used and major findings are outlined below.

3.4.1 Frameworks

Metal centers in MOFs or equivalent materials bind dihydrogen in the 10–15 kJ/mol range, which is sufficient for near-ambient temperature (150 to 220 K) storage. The main issue with these types of materials is that a high number of the binding sites must be uniformly dispersed and accessible to significantly enhance dihydrogen adsorption properties/capacities. The main issue with framework materials is that the high SSAs often obtained are mutually exclusive with the high density of metal centers that provide the higher-energy binding sites. Furthermore, the open-pore structures often needed to attain high SSAs make the structures less stable with low crystal densities that reduce volumetric capacities. Thus, to increase the binding energy for most of their capacity range, framework materials must be designed with densely packed metal centers that are open for hydrogen adsorption. This is especially critical because the metal centers in framework materials will typically be able to adsorb only a single hydrogen molecule.

MOFs exhibiting stronger binding interactions are needed to facilitate H₂ adsorption at higher temperatures. In collaboration with Dr. Long's group at the University of California, Berkeley, researchers at NIST used neutron powder diffraction to demonstrate that the highest maximum isosteric heat of adsorption (10.1 kJ/mol) ever observed for a MOF was directly related to H₂ binding at coordinatively unsaturated Mn²⁺ centers within the 1,3,5-benzenetristetrazolate (BTT) framework shown in Figure 3-36 (Dinca et al. 2006). This type of metal:H₂ interaction also held true for other subsequent MOFs characterized in the HSCoE with CUMCs of different metal ions (Sumida et al. 2010; Liu et al. 2008; Dinca et al. 2007; Peterson et al. 2006). In addition, Sun, Kim, and Zhang (2007) speculated that the binding of the hydrogen in the Mn-BTT MOF could be assigned to Kubas interaction. Here, Sun and coauthors summarized the four key factors that affect the orbital interactions between a TM center in a MOF and a dihydrogen molecule as follows: “(1) the separation of the H₂ σ level and the TM d levels which decreases when the atomic number increases; (2) the splitting of the spin-up and spin-down d levels which is reflected by the magnetic moment of the TM center; (3) the position of the most responsive d levels to the approaching H₂ which is determined by the crystal field splitting of the d orbitals according to the local symmetry of the TM center; and (4) the occupancy of the responsive d levels which is determined by the number of valence electrons and the oxidation states.” An explanation of the abnormally small H₂ binding energy experimentally measured in the Mn-BTT MOF system (10.1 kJ/mol) was attributed to the spin-polarization argument. Specifically, the splitting and occupation of the spin orbitals accounted for the weak Mn:H₂ binding. Based on this argument, the trend for the calculated H₂ binding energies in different TM-based MOF systems became clear (binding energies per H₂: Sc > Ti > V > Cr > Mn). It was also found that the binding energy of the TM:H₂ interaction could be tuned to a range of about 10 to 50 kJ/mol depending on the TM (Sun, Kim, and Zhang 2007).

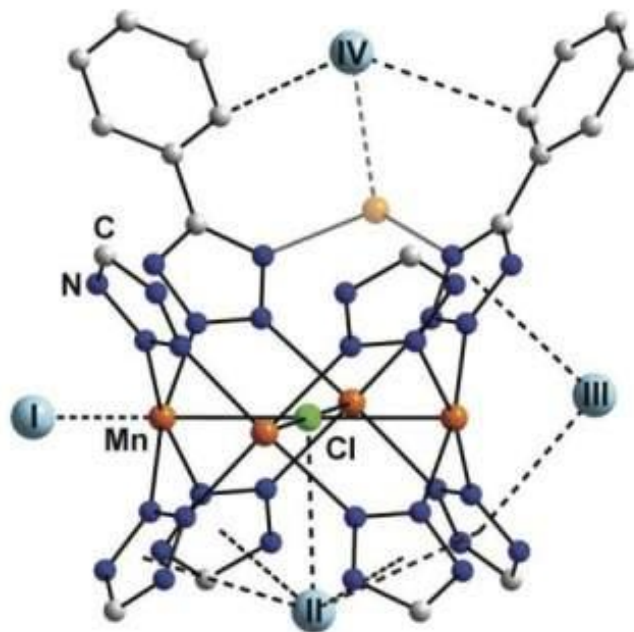


Figure 3-36. Simulated model for Mn-based MOF systems. Four deuterium (D₂) molecules are adsorbed on the four Mn centers. Light blue spheres represent D₂ centroids, and the orange spheres show the position of a partially occupied, extra framework Mn²⁺ ion site. Sites are labeled I to IV in order of the observed adsorption sites.

Using INS, NIST studied a series of BTT-MOFs with different TMs (Mn, Fe, and Cu) (Figure 3-37) synthesized by Long and Yaghi (2009) to show that the primary H₂ adsorption sites were at the metal sites, and that these sites had the highest adsorption enthalpies. Furthermore, NIST showed that the H₂ adsorption strength (Fe²⁺ > Mn²⁺ > Cu²⁺) strongly correlated with the metal-H₂ distance (Fe²⁺ < Mn²⁺ < Cu²⁺). However, these data did not correlate with the metal ion radius, and the data contradicted predictions made by Zhou, Wu, and Yildirim (2008), suggesting that there were strong correlations between the metal ion radius, metal-H₂ distance, and H₂ binding strength. In NIST's calculations, the H₂ binding energies derived from first-principles calculations followed the same trend as the experimental isosteric heats of adsorption for H₂ for a series of 2,5-dihydroxyterephthalate MOFs, confirming that the major interaction between the H₂ and the open metals was an electrostatic Coulomb attraction. Subsequent work needs to be performed to see if spin-polarization effects are fully accounted for in the observed behavior above (Sun, Kim, and Zhang 2007).

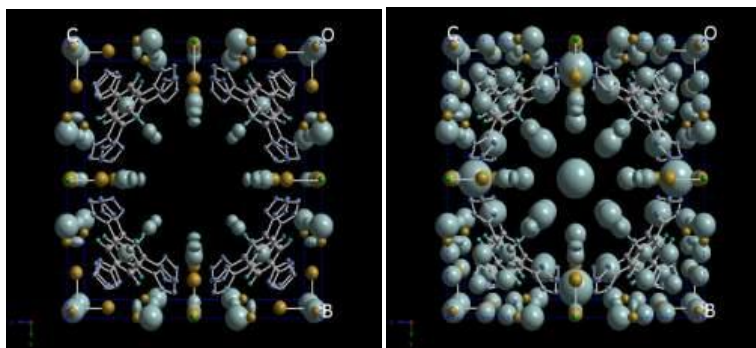


Figure 3-37. Diagrams of the Fe, Mn, and Cu MOF materials made by the University of California at Berkeley that were used by NIST to measure the hydrogen interactions with the metal centers. NIST performed INS that identified that the H₂ adsorption strength was strongest for Fe²⁺ > Mn²⁺ > Cu²⁺, which correlates to the metal-H₂ distance: Fe²⁺ < Mn²⁺ < Cu²⁺ (i.e., 2.17 < 2.27 < 2.47 Å, respectively). However, this does not correlate to the metal ionic radius (i.e., Mn²⁺ > Fe²⁺ > Cu²⁺). NIST also found that the Fe²⁺ site catalyzes hydrogen conversion to para-H₂ (completely at low loading, partially at high loading).

Although these efforts demonstrate significant progress, the low surface packing density (SPD) of many carbon materials at technically relevant temperatures has limited their adsorption capabilities. For example, if H₂ in MOF-177, with a SSA of 4500 m²/g (see Chae et al. 2004), had a similar hydrogen surface density to that of hydrogen in activated carbons, its excess adsorption would reach ~9.0 wt % rather than 7.5 wt % at 77 K. A collaborative HSCoE study of MOF-74 using neutron powder diffraction alongside isotherm measurements showed that H₂ adsorbed on the MOF-74 surface has a higher SPD at 77 K than that of solid H₂ at 4 K and zero pressure. The results revealed the shortest intermolecular D₂-D₂ distance observed in a physisorption-based material without the application of pressure (Figure 3-38). Part of this high density can be attributed to the presence of coordinatively unsaturated Zn²⁺ centers that promote intermolecular deuterium distances of about 2.85 Å at 4 K. This observation, along with results from other systems with CUMCs that exhibit large SPDs, presents an avenue to increase the surface density of adsorbed hydrogen in this class of materials (Liu et al. 2008).

The first evidence for CUMC-H₂ interactions (Prestipino et al. 2006) came from low-temperature IR spectra of a nanostructured MOF, Cu₃(1,3,5-benzenetricarboxylate)₂ (HKUST-1) (Chui et al. 1999). This revealed at least three distinct binding sites with induced red shifts in the vibrational-mode frequencies attributed to site-specific binding energies ranging from 2.5 to 4 kJ mol⁻¹, with the molecule undergoing relatively free rotation. Powder neutron diffraction experiments located the hydrogen adsorption sites and conclusively verified that initially D₂ binds to the unsaturated coordination sites of the Cu²⁺ carboxylate paddle-wheel building units (Peterson et al. 2006), followed by filling of the small cages before the Cu²⁺ site is fully saturated (Liu et al. 2007; Peterson et al. 2006). Filling of the larger pores followed along with some structural rearrangement of the dihydrogen molecules in the smaller pore. The distance between the metal and the centroid of nuclear deuterium scattering is 2.39(1) Å, a much-reduced distance from that typical of vdW interactions. This interaction should also be compared to the range of M-H distances from *ca.* 1.7 to 1.9 Å found in the well-known organometallic Kubas

compounds, in which evidence exists for electron donation from the dihydrogen to the TM and elongation of the H–H bond through back bonding (Kubas 2007).

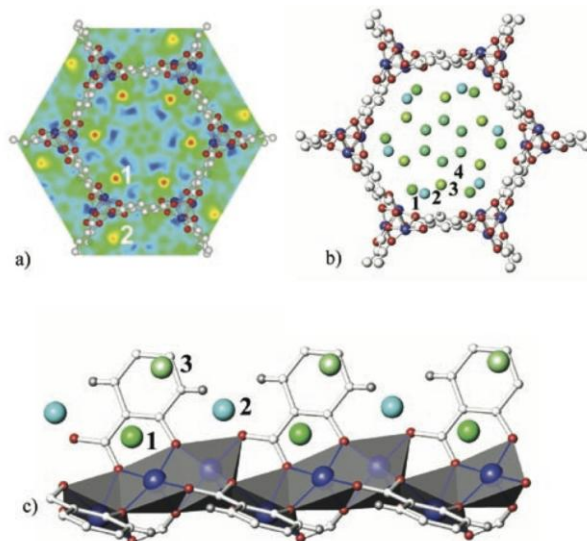


Figure 3-38. D₂ Adsorption Sites in MOF-74 at a loading of 4.2 D₂:Zn. (a) Suppositions of Fourier difference map together with the crystal structure of MOF-74 projected down the *c*-axis. The red-yellow regions indicate the high scattering regions of the first two adsorption sites. (b) The four D₂ adsorption sites identified by neutron powder diffraction (labeled 1–4, spheres of green and light blue). (c) The first three D₂ adsorption sites are shown with the first site directly interacting with the Zn²⁺ ions (blue balls) at a distance of 2.6 Å.

To address this issue further, INS and first-principles computer simulations were used to gain additional insight into the framework structure of HKUST-1 and to provide a detailed understanding of the local potential of para-hydrogen (*p*-H₂) adsorbed at the primary metal adsorption site (Figure 3-39). The form factors of the three main rotational peaks follow that expected for a free hydrogen molecule with a regular H–H intramolecular bond distance and provides evidence against a Kubas-type interaction. The form factors associated with the individual adsorption sites are characterized by differing Debye-Waller factors reflecting the strength of the site-specific adsorption strengths. Based on the calculated potentials using the DFT formalism and generalized gradient approximation (GGA) functional, all the features observed in the INS data were assigned to hydrogen adsorbed in HKUST-1 (Table 3-4). The orientational potential was found to be slightly two-dimensional and dominated by a small Coulombic term, hence there was a tendency for the H₂ to lie in a plane perpendicular to the Cu–Cu bond. The in-plane rotation was almost free and unhindered. The features observed at 9.1, 12.75, and 14.0 meV with increasing H₂ loading are due to rotational transitions from *J* = 0 to 1, *M* = ±1. The other features observed in the data are due to rotation-rotation or rotation-phonon excitations.

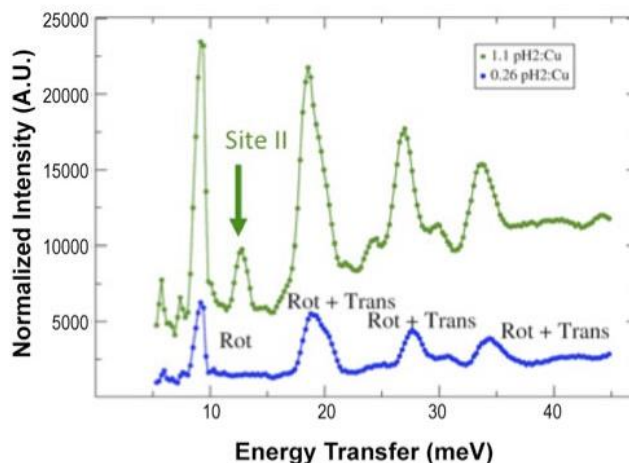


Figure 3-39. Different INS spectra of p -H₂ loaded HKUST-1 and the bare substrate measured on FANS. The displayed spectra result from p -H₂ scattering only, and peaks of significant intensity are labeled as either rotations (Rot) or a combination of rotation and transition (Trans). Ratios of p -H₂ to copper are 0.26 (blue circles, adsorption at Cu site only) and 1.1 (green circles, adsorption at Cu site and second site).

Table 3-4. Orientational potential obtained from GGA calculations and the corresponding rotational levels. The calculated classical harmonic H₂ phonons for a fixed H₂ orientation perpendicular to the Cu-Cu bond are $\omega(x') = 9.56$ meV, $\omega(y') = 13.44$ meV, and $\omega(z') = 22.87$ meV. The coupling of phonons with rotational transitions explains the observed INS spectra.

H ₂ rotational levels for an orientational potential:			
$V(\Omega) = V_0 + \sum_{lm} A_{lm} Y_{lm}(\Omega)$			
$V_0 = -53.3$ meV $A_{20} = 82.0$ meV $A_{22} = 0.2$ meV $A_{40} = 3.0$ meV $A_{60} = 1.0$ meV			
State #	Energy (meV)	$E_i - E_0$ (meV)	Major JM
0	-61.47	0	J=0, M=0
1	-51.85	9.61	J=1, M=+/-1
2	-51.71	9.76	J=1, M=-/+1
3	-25.39	36.08	J=2, M=+/-2
4	-25.39	36.08	J=2, M=-/+2
5	-24.20	37.27	J=1, M=0

The TAMU research team viewed the implementation of CUMCs into porous MOFs as one of the most promising ways to improve the affinities to hydrogen. As stated above, recent theoretical calculations suggest that the H₂-open metal center interactions may be tuned by varying the metal types (Sun et al. 2007). Using these concepts, TAMU focused on evaluating the different CUMCs' affinities to hydrogen molecules and attempted to design porous MOFs with high hydrogen-adsorption capacities, especially at near-ambient temperatures. Three isostructural porous MOFs were prepared and designated as PCN-9 (Co), PCN-9 (Fe), and PCN-9 (Mn), respectively.

These compounds all adopt the square-planar $M_4(\mu_4-O)$ ($M = Co, Fe, Mn$) SBU, with the μ_4-O residing at the center of the square of four M atoms. All four of the M atoms in the SBU are in the same plane and coordinate five oxygen atoms with square-pyramidal geometry. These compounds contain two types of cages: one is a truncated octahedral cage defined by six $M_4(\mu_4-O)$ SBUs at the corners and eight TATB (4,4',4''-s-triazine-2,4,6-triyltribenzoate) ligands on the faces, and the other is a cuboctahedral cage enclosed by eight truncated octahedral cages occupying the vertices of the cube. Every cuboctahedral cage connects eight truncated octahedral cages via facesharing, and each truncated octahedral cage links six cuboctahedral cages to form a (8,3)-net framework. Two such (8,3)-nets are mutually interpenetrated due to the π - π interactions of the TATB ligand pairs, with the second being generated through translation along [110]. The staggered TATB ligand pairs resulting from strong π - π interactions lead to the truncated octahedral cages of one set framework enclosed by the cuboctahedral cages of the other set framework with triangular face-sharing. This closes the windows of the truncated octahedral cages and also reduces the size of the opening of the cuboctahedral cages, resulting in $\sim 5 \times 5 \text{ \AA}^2$ square pores with all entatic metal centers open toward channels ready for gas substrates to bind. To test the permanent porosities of the three porous MOFs, N_2 sorption isotherms were measured at 77 K. All of them exhibit type-I sorption behavior, as expected for microporous materials. Derived from the N_2 sorption data, the BET surface areas are $1064 \text{ m}^2/\text{g}$ (Langmuir surface area, $1355 \text{ m}^2/\text{g}$), $682 \text{ m}^2/\text{g}$ (Langmuir surface area, $848 \text{ m}^2/\text{g}$), and $836 \text{ m}^2/\text{g}$ (Langmuir surface area, $1057 \text{ m}^2/\text{g}$) for PCN-9 (Co), PCN-9 (Fe), and PCN-9 (Mn), respectively. H_2 sorption measurements at 77 K were also carried out to check their hydrogen-storage performances. At 77 K and 760 torr, the hydrogen uptake capacity of PCN-9 (Co) is 1.53 wt %; PCN-9 (Fe) can adsorb 1.06 wt % hydrogen, whereas PCN-9 (Mn) can uptake 1.26 wt % hydrogen. The H_2 affinities of the three porous MOFs have been estimated by isosteric heats of adsorption (Q_{st}). PCN-9 (Co) has a Q_{st} of 10.1 kJ/mol, PCN-9 (Mn) has a Q_{st} of 8.7 kJ/mol, and PCN-9 (Fe) has a relatively lower Q_{st} of 6.4 kJ/mol. These results revealed that the entatic Co center possesses a higher hydrogen affinity compared to the entatic Fe and Mn centers, indicating that the implementation of open Co centers into porous MOFs may be a promising way to enhance hydrogen adsorption enthalpies for near-ambient temperature hydrogen-storage application.

Alternatively, PCN-12 adopts a dicopper paddlewheel motif as its SBU (Figure 3-40). The paddlewheel SBU occupies the 12 vertices of a cuboctahedron, whereas 24 isophthalate motifs span all 24 edges. As expected, at the 12 corners of the cuboctahedron, there are 12 open copper-coordination sites pointing toward the center of the cage. Each square face is connected to another square face of a neighboring cuboctahedron through four methylenediisophthalic (mdip) bridges. Every cuboctahedron connects to six others in three orthogonal directions to form a 3-D net. However, in PCN-12', every mdip ligand has C_{2v} symmetry. Each of the six paddlewheels connects three mdip ligands in a trigonal-prismatic fashion with paddlewheel units occupying all corners of the "prism" and the three mdip ligands residing on the three sides. Evidently, the open metal coordination sites point away from the cavity of the polyhedron.

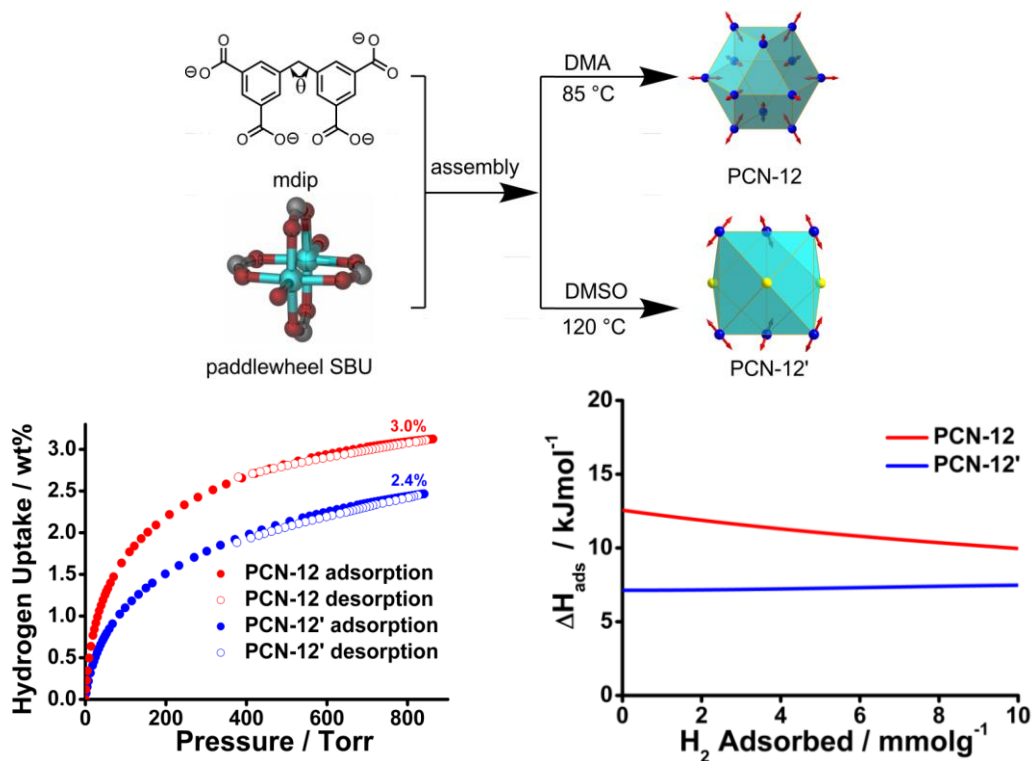


Figure 3-40. The synthesis and open metal site alignment (top), hydrogen uptake (bottom, left), and heat of adsorption (bottom, right) of the two MOF polymorphs: PCN-12 and PCN-12'

The nitrogen adsorption isotherms reveal that both PCN-12 and PCN-12' exhibit typical type-I adsorption behavior. The Langmuir surface area, BET surface area, and pore volume of PCN-12 are $2425 \text{ m}^2 \text{ g}^{-1}$, $1943 \text{ m}^2 \text{ g}^{-1}$, and 0.94 mLg^{-1} , respectively, whereas those for PCN-12' are $1962 \text{ m}^2 \text{ g}^{-1}$, $1577 \text{ m}^2 \text{ g}^{-1}$, and 0.73 mLg^{-1} , respectively. The hydrogen-adsorption isotherm of PCN-12' shows a 2.40 wt % (20.4 gL^{-1}) hydrogen uptake at 77 K and 1 atm, comparable to those of other MOFs containing cuboctahedral cages. However, PCN-12 exhibits an exceedingly high hydrogen uptake of 3.05 wt % (23.2 gL^{-1}) under the same conditions. This high hydrogen uptake of PCN-12, compared to PCN-12', can be ascribed to both the formation of cuboctahedral cages and the alignment of open metal sites within each cage of the open copper sites in PCN-12, strengthening the H_2 -framework interaction. As polymorphs of each other, PCN-12 and PCN-12' have not only the same formula after solvate removal, but also the same atom-to-atom connectivity. However, the gravimetric hydrogen uptake of PCN-12 is 27% higher than that of PCN-12' at 77 K and 1 bar (Figure 3-40). The reason behind these remarkable improvements can be attributed mainly to the “closepacking” strategy, namely, the formation of cuboctahedral cages and the unique alignment of open metal sites in each cuboctahedral cage in PCN-12. In addition, the heat of adsorption of PCN-12' is 7.13 kJ/mol at lower coverage. However, the H_2 -adsorption heat of PCN-12 can reach as high as 12.5 kJ/mol at low coverage, higher than those of other PCN-based

MOFs (Figure 3-40). This strategy may have general implications in the search for a practical adsorptive hydrogen-storage materials that could meet the DOE targets.

In this work, TAMU developed different framework materials with the specific goal of forming structures with open metal center frameworks that have higher binding energies. TAMU focused on using isostructural porous MOFs with Co, Fe, and Mn metal centers. The SSAs of the synthesized MOFs ranged from ~800 to 1100 m²/g, with the hydrogen capacities ranging from ~1 to 1.5 wt % at 77 K, and the isosteric heats of adsorption ranging from ~6 to 10 kJ/mol. However, the H₂-adsorption heat of PCN-12 reached as high as 12.5 kJ/mol at low coverage, higher than those of other PCN-based MOFs. These results demonstrate the difficulty of creating framework materials with a high density of metal adsorption sites and high SSA. Currently, only 1 H₂ is able to bind to the transition-metal site in the MOFs studied to date.

3.4.2 Coordination of Metals to High-Surface-Area Supports

In general, metal centers in framework structures are sterically hindered and thus can adsorb only one or at most two hydrogen molecules. To go beyond this limit and enable adsorption of multiple hydrogen molecules to each metal site, the single metal atoms must have more access for the hydrogen. Theoretical studies predicted that Kubas like interactions between transition metal (TM) centers and coordinated H₂ could fall within a desirable binding energy range that may enable substantial ambient H₂ storage (Yildirim and Ciraci 2005; Zhao et al. 2005). Such predictions are consistent with recent experimental studies using metal-organic frameworks (MOFs) with under-coordinated TMs (see preceding section), (Wang et al. 2009).

As will be detailed in the sections that follow, attempts to anchor TMs directly onto pure all-carbon nanostructures, similar to structures predicted by researchers outside of the HSCoE, have been very successful (Sun et al. 2006; Yildirim and Ciraci 2005). This is due partially to the fact that it is synthetically challenging to avoid metal agglomeration (clustering) in pure all-carbon frameworks. The metal must be bound to well-defined sites on high-SSA substrates with precisely tuned energetics. If this is not the case, an irreversible formation of a bulk metal hydride will occur. For example, Sun and coauthors (2006) simulated Li-coated C₆₀ and found that 12 Li atoms were spontaneously dispersed on the surface of a C₆₀ fullerene, which was due to the significant charge transfer from Li to the C₆₀ substrate. It was found that each Li ion could bind as many as 5 H₂ molecules with an average binding energy of only 7 kJ/mol H₂. A serious shortcoming of this simulation is that the formation of lithium hydride (LiH) was neglected, and once LiH clusters began to nucleate, bulk LiH cluster formation would be unavoidable and the material would lose its capability to reversibly store hydrogen. To avoid metal agglomeration and the irreversible formation of metal hydrides, Hamaed and colleagues (2008) used an organometallic precursor to successfully graft Ti onto the inner surface of mesoporous silica. Although this work demonstrated the feasibility of individually dispersing Ti and the capability of binding multi-H₂ by dispersed Ti, mesoporous silica has a relatively small surface-to-volume ratio and may be too heavy for practical hydrogen storage. Inspired by these recent experimental results, Wang and colleagues (2009) proposed combining the graphite oxide (GO) technique with Ti

anchoring to overcome the current synthesis bottleneck for practical storage materials. Similar to silica, GO contained ample hydroxyl groups, which are the active sites for anchoring Ti atoms. These theoretical studies, including initial NREL studies, initiated many subsequent experimental investigations into strong H₂ binding to metals on both pure all-carbon and functionalized supports.

3.4.1.1 Metal Coordination on Pure Carbon Supports

Zhao and coauthors identified a novel class of theoretically predicted nanostructured materials that could revolutionize hydrogen storage (Zhao et al. 2005). The theoretical calculations indicate that by complexing a fullerene such as C₆₀ with a TM or alkali metal, dihydrogen ligands could then be bound to the TM with binding energies between ~30 and 40 kJ/mol. This energy is within the ideal range for onboard vehicular storage. For example, in the optimized structures, the TM shares charge with all of the carbon atoms in a fullerene pentagon through Dewar coordination. The chemistry of C₆₀ is generally olefinic (i.e., the metal is coordinated to the fullerene through two carbon atoms contributing two electrons to the bonding). Thus, the above synthesis of fullerene-metal-H₂ complexes, where the metal is coordinating with five carbon atoms, was not expected to be straightforward. However, the calculations described above, together with others that have recently appeared, indicate that non-olefinic metallofullerene complexes are stable (Gagliardi and Pyykko 2004). Because the synthesis of these complexes is relatively unexplored and there are no guiding precedents, it has been necessary to discover the bonding preferences of the fullerene system and to open new synthetic pathways to the desired complexes. Rational synthetic methods to experimentally demonstrate fivefold coordination between a fullerene and a TM were explored.

Metal/C₆₀ Sample Preparation

Based on their commercial accessibility along with their well-controlled and understood properties, fullerenes (C₆₀) were initially used to investigate metal atom integration with pure carbons and their corresponding hydrogen-storage properties. Synthetic routes were identified to integrate Li, K, Na, Sc, Ti, Co, Cr, Ni, Fe, and other metals with the fullerenes. For example, K₆C₆₀ is a well-known material (Andreoni, Giannozzi, and Parrinello 1995; Zhou et al. 1991). For the Sc and Fe complexes, C₆₀ was used to make the reactive fulleride complex K₆C₆₀. Fullerenes and a slight excess of potassium were sealed under argon in a tube that was heated for approximately four days at 250°C. Both solid-state ¹³C NMR and Raman spectroscopy were employed to determine that the K₆C₆₀ complex was in fact synthesized. The K₆C₆₀ product was then reacted in nitrogen at -78°C with cyclopentadienyl-iron-dicarbonyl-iodide in THF to form the Fe complex. In a similar reaction, K₆C₆₀ was reacted with scandium-trifluoromethanesulfonate in THF to form the Sc complex. The Cr complex was formed by reacting C₆₀ directly with chromium-tricarbonyl-trimethylnitrile. The Co complex was formed by decomposing dicobalt-hexacarbonyl with ultraviolet photolysis on C₆₀. Finally, the Li(C₆₀) complex was formed by dissolving an excess amount of lithium and C₆₀ in liquid ammonia at -78°C. The ammonia was then pumped off while keeping the reaction flask submerged in a dry ice bath. Using this approach, the reaction does not go to completion, and a Li(C₆₀) compound with unknown Li:C₆₀ stoichiometry and excess Li metal is formed. If the reaction is allowed to warm to RT before removing the ammonia, the reaction goes to completion and compounds with known stoichiometries are formed. In all cases,

commercially available C_{60} (Aldrich) and an excess of the metal reactant were employed. Also, the recovered products were dried in an inert atmosphere. All of the products were stored in a glove box and transferred to sealed ampoules for both structural and H_2 capacity characterization. These materials were analyzed with NMR, electron paramagnetic spin resonance (EPR), Raman spectroscopy, TEM, EELS, and TPD, along with having their pore sizes, SSAs, and hydrogen-isotherm properties measured.

Analysis

It was difficult to dissolve the various new complexes in any organic solvent, making solid-state NMR necessary. For these studies, a BRUKER AVANCE 200 spectrometer operating at 200 MHz was employed. Solid-state ^{13}C NMR spectroscopy under fast MAS was required to obtain high-resolution spectra of the aforementioned complexes. EPR was performed on a BRUKER ELEXSYS 500 spectrometer. Raman spectroscopy was performed using the 2.54 eV (488 nm) excitation line of an Ar-ion laser. The excitation power was limited to 3 mW to ensure that the complexes did not decompose. The spectrometer collection slit was adjusted to 3 mm so that spectra were obtained by averaging three 60-s scans with a resolution of $\sim 10\text{ cm}^{-1}$. The nanoprobe EELS was performed on a state-of-the-art 2004 FEI, Tecnai F20 UT transmission electron microscope (Field Emission, 200 kV, Ultra Twin lens) with point-to-point resolution of 0.16 nm. The new hydrogen binding sites were analyzed with TPD spectroscopy. The samples were first degassed to 130°C in a vacuum of $\sim 10^{-8}$ torr. RT H_2 exposures for ~ 5 min at 500 torr were employed to probe the hydrogen adsorption. New hydrogen adsorption sites consistent with dihydrogen molecules bound to the surface with a binding energy significantly higher than that anticipated for physisorption were observed for all five complexes. The samples were also all tested to show that the hydrogen adsorption /desorption was reversible.

Structural Characterization of the Five New Metal C_{60} Complexes

Figure 3-41 displays the ^{13}C solid-state NMR spectra of each of the new organometallic C_{60} complexes (Li, Fe, Sc, Co, and Cr). Asterisks denote MAS side bands. In the spectrum of the Fe complex, the peak for the polyethylene cap on the NMR rotor is labeled. Also in the case of the Sc complex, a small amount of residual THF was detected, and the peaks are labeled accordingly. The NMR spectrum of the $Li(C_{60})$ complex (excess Li metal present) is similar but not identical to spectra previously reported for either Li_6C_{60} or $Li_{15}C_{60}$ (Tomaselli et al. 2001). This can most likely be attributed to the formation of a different $Li(C_{60})$ species. In addition, some NH_3 remains coordinated in the $Li(C_{60})$ complex, as ammonia was observed when the sample was degassed in the TPD hydrogen-desorption studies.

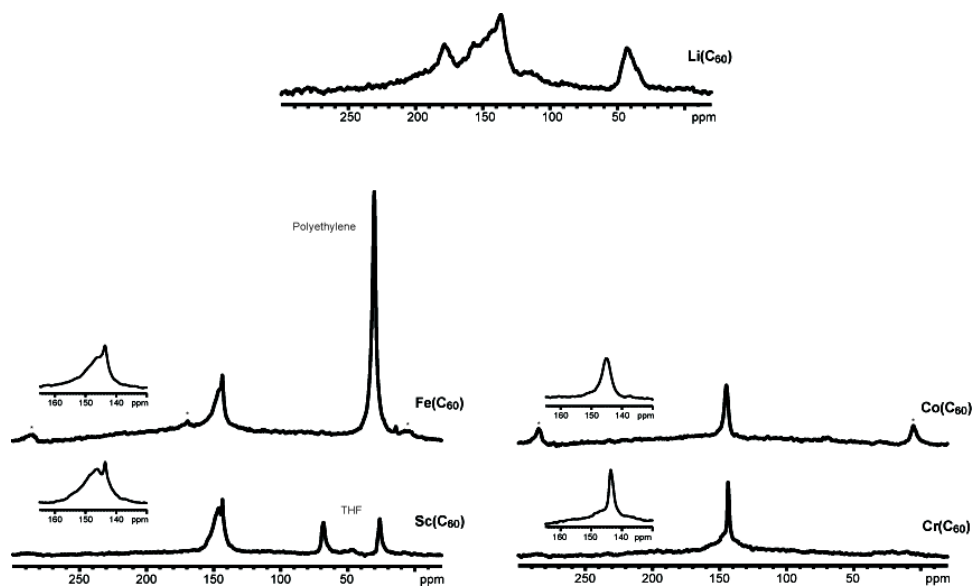


Figure 3-41. Solid-state ^{13}C NMR spectra of the fullerene compounds in which C_{60} interacts with Li, Fe, Sc, Co, and Cr

In the NMR spectrum of the Fe complex, the sharp peak at 143.7 ppm is attributed to residual unreacted C_{60} (Figure 3-41). The shift of the broad peak to higher ppm is consistent with C_{60} coordinated with an iron atom. Furthermore, by performing multiple solid-state NMR experiments of the Fe complex, it has been confirmed that only the aforementioned peaks, displayed in the insets for clarity, may be attributed to the new Fe complex. EPR was performed and has revealed the presence of Fe^{3+} in the sample, indicating stable $17 e^-$ species. Nanoprobe EELS was performed and revealed an iron content of 1.0–1.5 at %. Also, after extensive TEM analysis, no metal clusters were observed. The new data suggest that chain structures of $\text{C}_{60}\text{-Fe-C}_{60}\text{-Fe-C}_{60}\text{-}$ were formed. The ^{13}C solid-state NMR spectrum of the Sc complex is nearly identical to that of the Fe complex. Because the reactions were also similar, it was speculated that $\text{C}_{60}\text{-Sc-C}_{60}\text{-Sc-C}_{60}\text{-}$ chain structures were also formed. The formation of these chain structures may serve as a high-SSA porous network with multiple hydrogen adsorption sites. To better elucidate the precise structure of the $\text{Fe}(\text{C}_{60})$ complex, high-resolution transmission electron microscopy (HRTEM) and energy dispersive x-ray (EDX) spectroscopy were performed with a field emission microscope. As shown in Figure 3-42, the study revealed areas in the sample, circled in pink, that were consistent with small quantities of oxidized iron with the phase being Fe_2O_3 . The sample had been exposed to air, as the complex was not found to be air sensitive during hydrogen-adsorption studies. However, it is not surprising that small amounts of residual iron were oxidized immediately. More importantly, regions of C_{60} molecules, circled in yellow, containing $\sim 1.0\text{--}1.5$ at % iron were also observed (Figure 3-42). The fact that such low levels of iron were stable against oxidation definitively confirms that the iron is complexed to the C_{60} molecules. Furthermore, the detection of 1.0–1.5 at % iron is consistent with the formation of $\text{C}_{60}\text{-Fe-C}_{60}\text{-Fe-C}_{60}\text{-}$ chain structures. From the HRTEM image in Figure 3-42, some ordering in the C_{60} chainlike structures was detected.

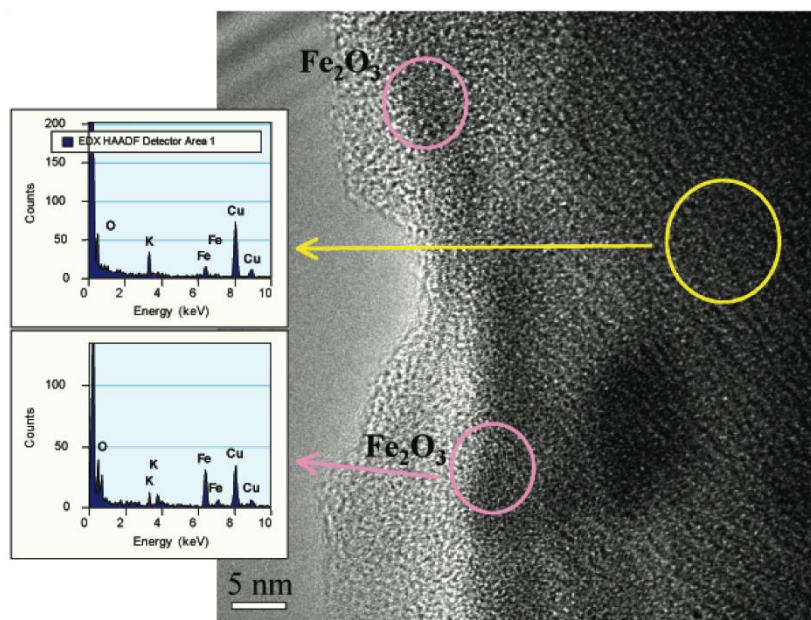


Figure 3-42. HRTEM and EDX analysis of the Fe(C₆₀) compound

XRD measurements were performed on the powdered Fe(C₆₀) sample. Figure 3-43 displays the XRD pattern for the Fe(C₆₀) sample. Several very broad features are observed that could be consistent with either disordered C₆₀ or the disordered fulleride (used as a reactive precursor in the initial reaction). However, these broad features could also be consistent with disordered C₆₀-Fe-C₆₀-Fe-C₆₀-chain structures. Furthermore, the sharper feature occurring at low angle is consistent with a crystalline d-spacing of ~13.3 Å. This d-spacing is not consistent with the face centered cubic (FCC) packing of either C₆₀ or the fulleride and suggests that a new packing of C₆₀ is observed and may be attributed to Fe(C₆₀) chainlike structures. The broad features in the XRD pattern of Figure 3-43 are also similar to features previously reported for SWNTs. In the case of SWNTs, features are detected with XRD because the nanotubes pack into crystalline bundles. The features are broad because the bundles are highly disordered, i.e., there is slippage along the axis of the tubes such that the graphitic structures are not perfectly aligned. Collectively, these data may suggest that the C₆₀-Fe-C₆₀-Fe-C₆₀-chain structures pack in loosely ordered bundles similar to SWNTs. It is possible that the 13.3 Å d-spacing represents the interstitial spacing between the chains. Figure 3-44 displays a cartoon representation of Fe(C₆₀) chains with an interstitial spacing of ~1.3 nm. (Note that based on the XRD data in Figure 3-43, the degree of alignment is not expected to be this high.) It has been proposed that SWNTs that are atomically doped with metals are still a promising hydrogen-storage material. The Fe(C₆₀) chain structures are very similar in structure to SWNTs doped with atomic metal. Optimization of these porous Fe(C₆₀) frameworks and production of these materials at higher yields may lead to ideal hydrogen-storage materials.

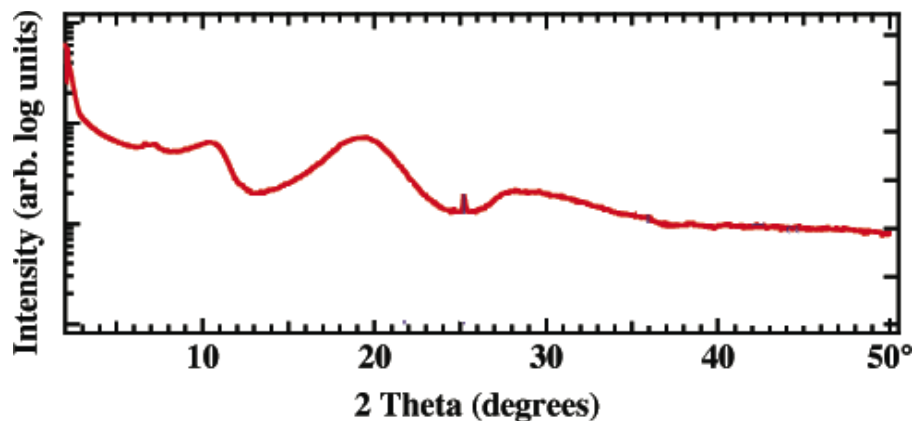


Figure 3-43. XRD pattern of the Fe(C₆₀) compound

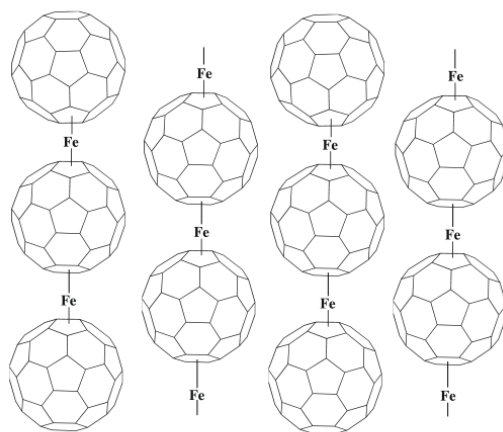


Figure 3-44. Cartoon representation of Fe(C₆₀) chains

The NMR spectrum of the Co complex exhibits a peak at ~144 ppm that is slightly broader than that expected for pure C₆₀ (Figure 3-41). TEM studies indicate that this reaction led to the formation of cobalt nanoparticles in intimate contact with the carbon species. Although this is not indicative of true complex formation, there must be some degree of charge transfer between the cobalt nanoparticles and the fullerenes that results in both the broader NMR peak and the new hydrogen-adsorption sites (discussed in the following section). Finally, the NMR spectrum of the Cr complex has a sharp peak at 143.7 ppm that was again attributed to residual C₆₀ (Figure 3-41). The broad shoulder at a slightly higher chemical shift indicates, however, that a new complex was formed at approximately 10% yield. Because Cr(CO)₃ arene complexes are very stable, formation of a (η⁶-C₆)Cr(CO)₃ complex at low yields most likely occurred.

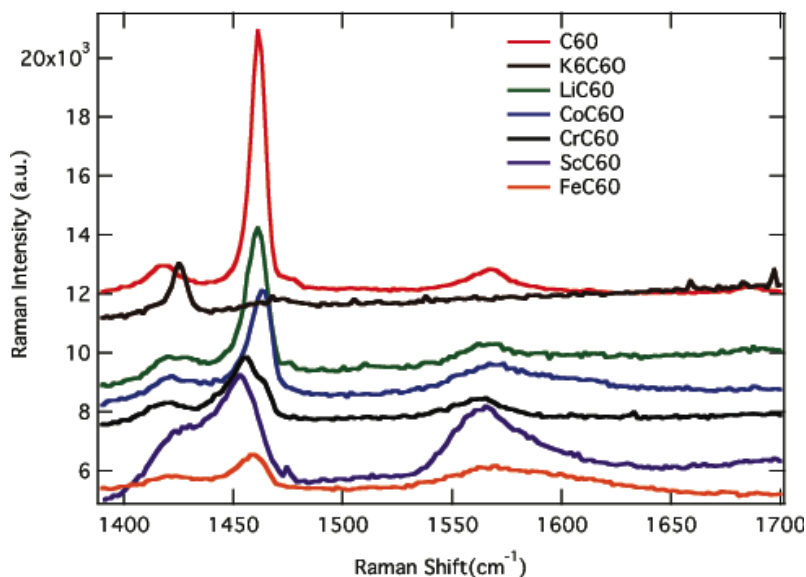


Figure 3-45. Raman spectra of pure C_{60} , K_6C_{60} , and all of the metal fullerene products (Li, Co, Cr, Sc, and Fe)

Figure 3-45 displays the Raman spectra of pure C_{60} , the K_6C_{60} reactive precursor, and all of the reaction products (Li, Co, Cr, Sc, and Fe). Pure C_{60} has a sharp major feature at 1461 cm^{-1} with minor lines appearing at 1418 and 1569 cm^{-1} . The feature at 1425 cm^{-1} is characteristic of the K_6C_{60} fulleride, indicating an anionic form of C_{60}^{6-} has been formed. The main line at 1461 cm^{-1} is reduced in intensity relative to the other features for the Li and Co complexes. This is also consistent with charge transfer from the Li or Co to form anionic C_{60} . Similar spectra for various forms of Li_xC_{60} have been reported (Roding, Wagberg, and Sundqvist 2005). It is interesting to note that the spectra of the Cr, Sc, and Fe complexes are significantly different from that of C_{60} . In each of these cases, true organometallic complexes (as opposed to metal salts) are formed. It is also interesting to note that the presence of the Cr complex appears to quench the major C_{60} Raman line. Fullerenes are still present in this material as evidenced by the solid-state NMR in Figure 3-41.

Characterization of the New Hydrogen-Adsorption Sites

Figure 3-46 displays TPD desorption spectra of the Cr, Sc, Co, and Fe complexes. All samples were degassed to 130°C and exposed to 500 torr hydrogen at RT. All samples display hydrogen desorption peaks at temperatures that are significantly above what is expected for physisorbed hydrogen on the samples. The peak desorption temperatures occur at 235° , 230° , 180° , and 0°C for the Cr, Sc, Co, and Fe complexes, respectively. These temperatures are lower than would be expected for chemisorptions, and therefore indicate that dihydrogen ligands are bound. In each of these cases, the total adsorption capacity is quite low. The TPD hydrogen capacities are 0.004, 0.002, 0.001, and 0.001 wt % for the Cr, Sc, Co, and Fe complexes, respectively. Thus the Cr, Sc, Co, and Fe complexes are each stabilizing significantly less than one hydrogen molecule per each TM/ C_{60} complex. For each of the TM fullerene complexes, the hydrogen adsorption/desorption process was found to be completely reversible.

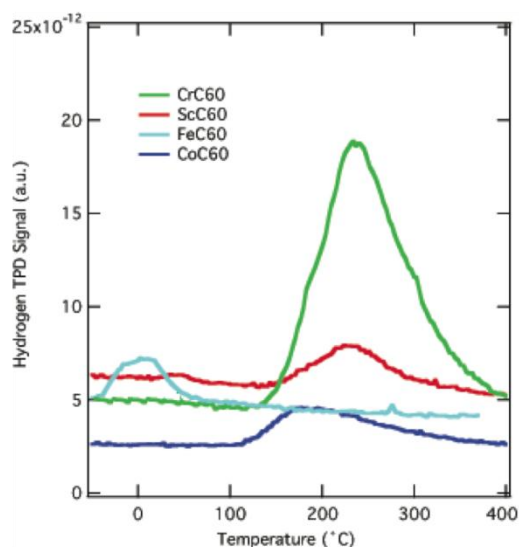


Figure 3-46. Hydrogen TPD spectra of the metal fullerene complexes in which C_{60} is interacting with Cr, Sc, Fe, or Co. The samples were degassed to 130°C and exposed to hydrogen at RT and 500 torr for ~5 min.

Figure 3-47 displays the TPD spectrum of the $\text{Li}(C_{60})$ complex (excess Li metal present). For comparison, the spectra of the Cr, Sc, Co, and Fe complexes are also plotted. However, the peaks that are observed in Figure 3-46 are not visible in Figure 3-47, as the hydrogen-storage capacity of the Li complex is more than two orders of magnitude greater than any of the other TM complexes. Again, all the samples were degassed to 130°C and exposed to 500 torr hydrogen at RT. The Li complex has a hydrogen-storage capacity of 0.47 wt % (TPD). Because an excess amount of Li was observed and the hydrogen evolution temperature was $>200^{\circ}\text{C}$, it is likely that lithium hydride was forming due to the excess Li. Therefore, the number of Li atoms coordinated to each C_{60} was not determined. Interestingly, the $\text{Fe}(C_{60})$ and $\text{Cr}(C_{60})$ compounds had reversible hydrogen capacities of 0.5 wt % at 77 K and 2 bar (sieverts). Pure C_{60} adsorbs negligible hydrogen under the same conditions, and the other compounds explored here had a reversible capacity of only 0.1–0.2 wt % at 77 K and 2 bar (sieverts).

Because the initial $\text{Li}(C_{60})$ compound (excess Li metal present) had a capacity of ~0.5 wt % following a RT exposure to hydrogen at 500 torr, the researchers established a method to control this reaction such that the compound could be studied in greater detail. A series of Li_xC_{60} compounds were made with varying Li stoichiometries. Initially, the compound was synthesized by dissolving Li and C_{60} in liquid ammonia in dry ice. The ammonia was then pumped off while maintaining the reaction at -78°C , and the reaction did not go to completion. Thus an unknown $\text{Li}(C_{60})$ compound was formed. If the reaction is allowed to warm to RT before removing the ammonia, the reaction goes to completion and compounds with known stoichiometries are formed.

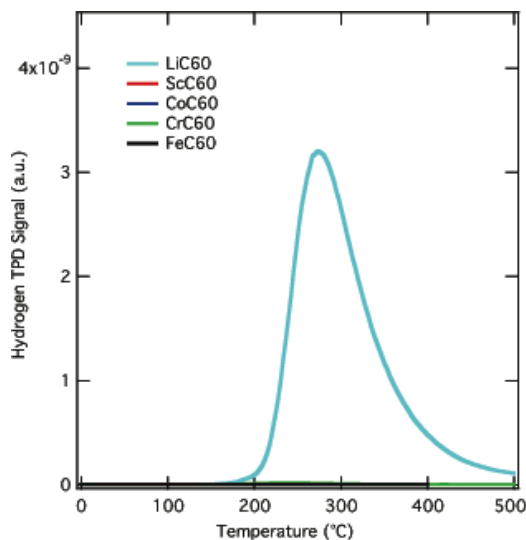


Figure 3-47. TPD spectra revealing that the hydrogen-adsorption capacity of the $\text{Li}(\text{C}_{60})$ complex (excess Li metal present) is more than two orders of magnitude greater than that of the Sc, Co, Cr, and Fe complexes.

A reaction was carried out in which the stoichiometric quantities corresponded to $\text{Li}_{12}\text{C}_{60}$. Figure 3-48 displays the ^{13}C NMR spectra of the $\text{Li}_{12}\text{C}_{60}$ compound (top) and the $\text{Li}(\text{C}_{60})$ compound (bottom). In the spectrum of the $\text{Li}(\text{C}_{60})$ compound (excess Li metal present), the feature at ~ 40 ppm indicates the presence of sp^3 -hybridized carbon. This feature is almost completely absent in the spectrum of the $\text{Li}_{12}\text{C}_{60}$ compound. The $\text{Li}_{12}\text{C}_{60}$ compound had a reduced hydrogen-storage capacity of only ~ 0.1 wt % following a RT exposure to hydrogen at 500 torr (TPD). This may possibly be due to the loss in sp^3 hybridization /polymerization and the corresponding breakdown in a porous framework. Alternately, the $\text{Li}_{12}\text{C}_{60}$ species has more Li bound to the fullerene cage than the $\text{Li}(\text{C}_{60})$ species, and it is possible that the larger Li loading actually leads to a loss in capacity and hydrogen binding sites. As stated above, a series of Li_xC_{60} compounds (where $x = 8, 12, 16, 20,$ or 34) were synthesized and extensive structural and adsorption characterization data were collected by NREL in an effort to make a direct comparison with the reported theoretical work by Sun and coauthors (2006). The $\text{Li}_{12}\text{C}_{60}$ compound stored ~ 0.2 wt % hydrogen at 77 K and 2 bar. The binding energy for this site was found to be ~ 6 kJ/mol, in good agreement with theoretical calculations performed by Sun and colleagues (2006), whereas the capacity was well below the calculated value of 9 wt %. This finding is due possibly to the idealized $\text{Li}_{12}\text{C}_{60}$ structure not being achieved, and perhaps also to an overestimate of the amount of dihydrogen molecules affected by the lithium loading. Therefore, research efforts involving the use of pure-carbon frameworks were discontinued.

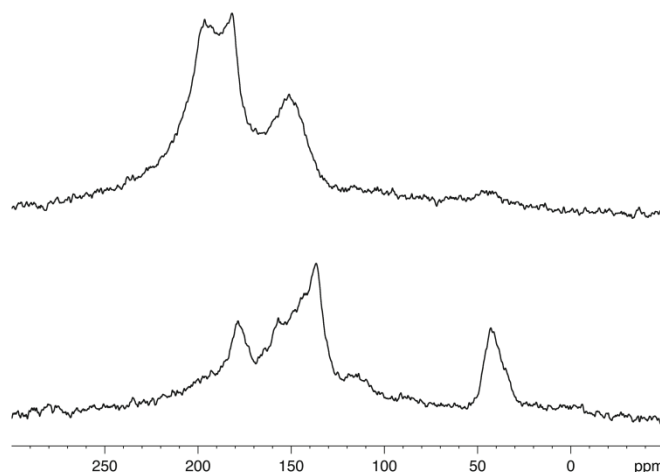


Figure 3-48. Solid-state ^{13}C NMR spectra of $\text{Li}_{12}\text{C}_{60}$ (top) and $\text{Li}(\text{C}_{60})$ (excess Li metal present, bottom).

Calcium-Decorated Nanohorns

In similar work, Oak Ridge National Laboratory (ORNL) identified that fullerenes (C_{60}) and single-walled carbon nanohorns (SWNHs) coated with calcium may function as ideal molecular hydrogen attractors (Yoon et al. 2008). Specifically, the resulting hydrogen uptake on $\text{Ca}_{32}\text{C}_{60}$ was predicted to be >8.4 wt % with a binding energy that would allow for near-ambient desorption (i.e., 5 H_2 adsorbed at ~ 40 kJ/mol). In the simulations of these Ca-coated carbon nanostructures, Ca atoms were observed to form a monolayer coating on the outside surface of the carbon cage, allowing for optimum accessibility for the hydrogen molecules. This strong metal: substrate interaction occurs because Ca atoms can transfer significantly more of their valence electrons to the carbon substrate than can TM atoms and other simple metals, such as Be or Mg. This mechanism of enhanced charge transfer is critical for stabilizing the Ca coating on the carbon nanostructure through (1) enhanced Ca-substrate Coulomb attraction and (2) Ca-Ca Coulomb repulsion. It was also found that *d*-orbitals of Ca atoms play an active role in coordinating with both the carbon substrate and dihydrogen molecules. All these effects are desirable for hydrogen storage, but this research neglected the formation of metal hydrides, which is especially difficult to avoid in a high-density Ca coating.

To address uniform activation of SWNHs and coating with Ca by dry, physical vapor deposition (PVD) methods, ORNL researchers developed new approaches using pulsed gas injection, fluidization, and laser vaporization at low pressures. In addition, they developed an apparatus for fluidization, suspension, and coating of large quantities of powder with radiant-heating capabilities. These PVD methods efficiently deposit reactive metal sites on substrates with minimal loss in surface area. Metal decoration with Ca was shown to result in smooth nanoparticle-free coatings and anomalously high storage, in agreement with the proposed mechanism of polarization induced by high local electric fields resulting from the alkaline-earth metal “doping” of C by decoration (Yoon et al. 2008). Hydrogen-adsorption isotherm measurements were performed at 77 K and 0.9 atm to compare the Ca-decorated oxidized SWNHs (o-SWNHs) with the undecorated o-

SWNHs. The isotherms were reversible, indicating that Ca-decorated o-SWNHs might be promising materials for enhancing hydrogen-storage capacities.

In an attempt to synthesize a Ca-coated fullerene material, NREL synthesized a series of Ca_xC_{60} (e.g., $x = 10, 32, \text{ or } 57$) compounds by using C_{60} in a solution of calcium containing liquid ammonia. TPD and 2-bar hydrogen-pressure measurements indicated a moderate amount of low-temperature hydrogen desorbed at ~ 100 K, consistent with physisorbed hydrogen for the $\text{Ca}_{32}\text{C}_{60}$ material. In addition, the formation of calcium hydride was observed, resulting in a capacity of 1.04 wt % for $\text{Ca}_{32}\text{C}_{60}$ following RT charging during synthesis. Based on the solid-state MAS ^{13}C NMR spectrum for $\text{Ca}_{32}\text{C}_{60}$, the theoretical chemical structure for $\text{Ca}_{32}\text{C}_{60}$ was not made and may be the reason why the theoretical capacity and binding energy were not achieved. A substantial amount of additional work is needed to improve the synthesis to prevent agglomeration and enable the maximum capacities to be obtained.

3.4.2.2 Solution-Phase Hydrogenation of Carbon Nanostructures

NREL investigated the mechanism for the chemical hydrogenation (i.e., strong binding) of high-SSA carbon-based materials through various routes in an effort to develop more reproducible and lower-temperature hydrogen-desorption processes. One approach unique to NREL uses a solution-based sodium naphthalide reduction process to chemically reduce carbon materials in THF. These reactive intermediates then adsorb hydrogen from their surrounding chemical environment, thus forming a hydrogenated carbon material. Both high-SSA activated carbons (ACs) and SWNTs were employed. NREL demonstrated the reproducible generation of hydrogenated SWNT materials containing ~ 5 wt % hydrogen (Figure 3-49). The SWNT samples were reversibly hydrogenated using the same chemical reduction processes. These same processes were applied to AC materials, which demonstrated ~ 4 wt % hydrogen desorption. TPD studies showed that the hydrogen-desorption temperatures ranged from 250° to 550°C for both the hydrogenated SWNT and AC nanostructures (Figure 3-49). Although initial results using alkali metal (e.g., Li, Na, K) reduced SWNTs were promising, reproducible processing remained a significant issue. In addition to being oxygen and moisture sensitive, attaching a consistent molar amount of TMs to the carbon matrix was difficult. Variability for metal reduction appeared to be related to the amount of oxygen and intercalated acid that was left from the purification processes. Thus, methodologies were developed to standardize the purification process and reduce the level of residuals. In general, the Na-SWNT material demonstrated the most reproducible and highest hydrogen-storage behavior. The additional water observed with the Li-SWNTs and K-SWNTs accounted for their marked difference in hydrogen-storage properties compared to the Na-SWNTs.

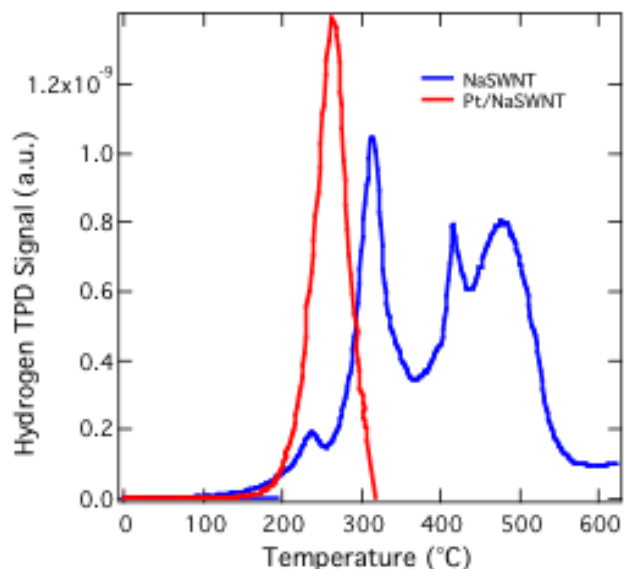


Figure 3-49. Representative TPD spectra for hydrogenated SWNT (Na-SWNT, blue) and Pt-AC/SWNT (Pt/Na-SWNT, red) samples. The addition of a Pt-AC catalyst material lowered desorption temperature by nearly 75°C and enabled reversible RT H₂ loading of the material. The Pt-AC/SWNT mixture was first degassed to 300°C and then exposed to ~500 torr of H₂ gas at RT.

NREL furthered its understanding of the hydrogenation of high-SSA carbon nanostructures via Fourier transform infrared (FTIR) spectroscopy. FTIR spectroscopy was chosen as a reasonable method to study C-H bonds on small quantities of reduced hydrogenated SWNT materials under inert atmospheres. The samples were dried thoroughly and monitored until all THF was degassed to exclude its C-H vibrations from THF. Figure 3-50 shows the FTIR spectrum of a Na_xSWNT-H_y sample. The simple spectrum of the reduced SWNT material indicates that the hydrogen is arranged on the tube in a symmetric, ordered fashion, as compared with the more complex spectrum observed for the methanol product, which is consistent with a random distribution of hydrogen on the tube backbone. This simple spectrum is consistent with recent theoretical predictions and experimental observations on SWNTs hydrogenated using polyaminines. This study found that ortho addition of hydrogen in zigzag lines parallel to the tube axis, as depicted schematically in Figure 3-50, is favored energetically compared to random distributions of isolated H atoms or isolated pairs of adjacent H atoms. This geometry introduces a corrugated shape to the surface of the tube, with the hydrogenated carbons taking on a pyramidal geometry and distorting out of the plane, and the intervening sp² carbons projecting below the original plane, to relieve strain. Thus there is a driving force for addition of hydrogen to the SWNTs in this preferred geometry, and step-wise addition of individual H atoms, which occurs here by means of a chemical reaction, can facilitate formation of this structure.

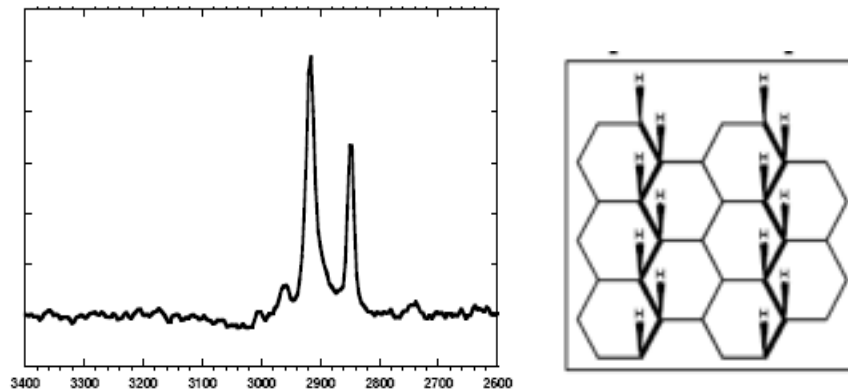


Figure 3-50. FTIR spectrum of a reduced SWNT material (left) and theoretical representation of C-H bonds on a nanotube surface (right)

A significant decrease in the hydrogen-desorption temperature for hydrogenated carbon materials was achieved via a TM catalyst (Figure 3-49). Mixtures of hydrogenated Pt-AC and SWNTs decreased the hydrogen-desorption temperature by nearly 75°C and enabled reversible RT H₂ loading. The ratio of Pt-AC to SWNTs was varied from 1:10 to 10:1 to optimize the hydrogen uptake. After an initial degas to 300°C and exposure to ~500 torr H₂ at RT, a material containing Pt-AC and SWNTs (1:9) stored 1.5 wt % hydrogen reversibly on the carbon matrix.

3.4.2.3 Metal Intercalation in Graphite Compounds

Using solution-phase chemistry techniques similar to those described above, metals can be intercalated in graphite. A proper balance of competing considerations can lead to the formation of remarkable hydrogen-storage materials through cointercalation processes. The balance is achieved through the selection of the right metal species, the right molecular species, and the optimum metal density. The NREL team focused on Li metal because it is lightweight and exhibits the best binding energy with H₂ among all of the alkali metals (Lochan and Head-Gordon 2006), whereas non-alkali metals (e.g., alkaline earth metal or TMs) are extremely difficult to fully disperse. Among the potential intercalating molecules, including N₂, NH₃, and C₆₀, tetrahydrofuran (THF) was chosen because this species can expand the interlayer distance between graphite plains ideally while being low weight. To maximize the hydrogen capacity, researchers determined the maximum metal density at which the Li cations remain homogeneously dispersed throughout the whole material system.

Demonstration of the experimental synthesis of the Li-THF co-intercalation system was easily achieved by employing rapid, RT reactions to form the co-intercalation compounds. Briefly, the alkali metal naphthalide was reacted with graphite in THF. TPD was employed to confirm co-intercalation of THF. A dimethyltetrahydrofuran system was also explored for comparison, and it was found with TPD that only the Li intercalated (i.e., co-intercalation was not observed). The XRD spectrum in 3-51 shows that Li-THF co-intercalates into graphite to form stage 1 compounds. The formation of a stage 1 compound indicates that the intercalation species are present between each of the graphite layers. If a stage 2 compound had formed, the intercalation species would be

observed in every other layer of the graphite (Shioyama 2000). Volumetric studies were employed to examine the hydrogen-adsorption properties of the Li-THF co-intercalated graphite, and the results were compared to the Li-intercalated graphite. Hydrogen-adsorption capacities at both RT and 77 K, with an overpressure of 2 bar, were obtained following no degas and degassing to 100° and 250°C. The results are tabulated in Table 3-5. Under all conditions, the Li-THF co-intercalated graphite was observed to adsorb more hydrogen than the Li-intercalated graphite. This confirms the theoretical prediction that the THF co-intercalation species is necessary to both prevent clustering and expand the graphite lattice allowing for H₂ adsorption, but overall H₂ capacities were still low. A maximum hydrogen capacity of 0.52 wt % was observed for the Li-THF co-intercalated graphite at 77 K, 2 bar following degassing to 250°C (Table 3-5). The XRD data in Figure 3-51, however, reveal that a significant fraction of the graphite is not intercalated by the Li-THF co-intercalants.

The synthetic method and co-intercalant species were refined in an attempt to create accessible metal sites for increasing H₂ capacities. Additional efforts explored the degas temperature of these graphite compounds to ensure that the metal sites were accessible. The H₂ capacities of these newly synthesized graphite co-intercalation compounds were still not consistent with the theoretical results. No H₂ binding to the Li atoms was observed, possibly due to a high density of intercalated THF or NH₃ (i.e., metal sites were not accessible). Therefore, work on Li-THF co-intercalation graphite systems was discontinued at this point.

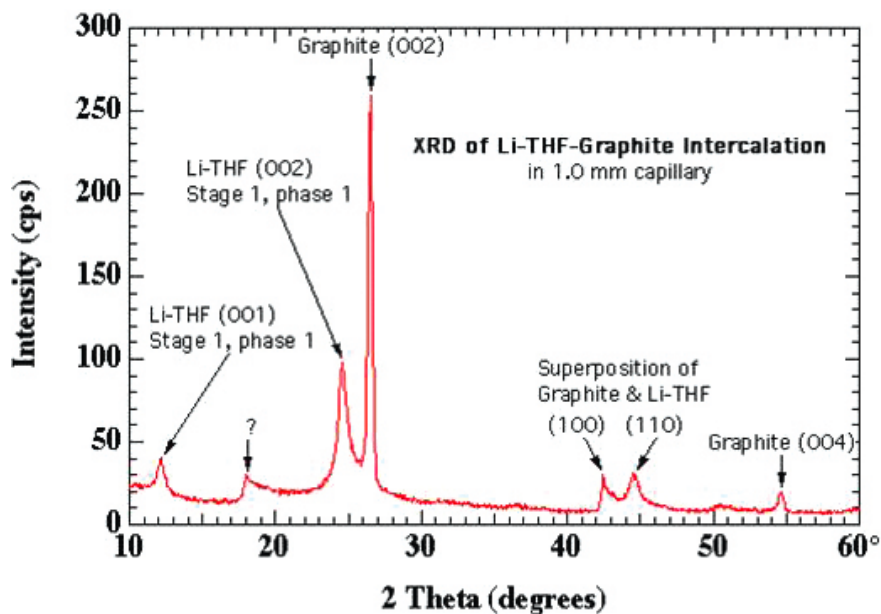


Figure 3-51. XRD spectrum of Li-THF co-intercalation in graphite

Table 3-5. Volumetric Hydrogen Adsorption Capacities at 2 Bar for Both RT and 77 K, Following No Degas and Degassing to 100° and 250°C for Li-THF Co-Intercalated and Li-Intercalated Graphite

Sample 2 bar volumetric	RT Degas		100 °C degas		250 °C degas	
	Wt% H ₂ @ RT	Wt% H ₂ @ 77 K	Wt% H ₂ @ RT	Wt% H ₂ @ 77 K	Wt% H ₂ @ RT	Wt% H ₂ @ 77 K
Li / THF	0.08	0.34	0.04	0.42	0.06	0.52
Li	0.003	0.02	Negligible	0.02	0.005	0.02

3.4.3 Metal Coordination to Functionalized Substrates

The integration of single metal atoms with pure all-carbon materials has proven very challenging. This is consistent with predictions made by NREL and others, including the seminal paper in this area (Zhao 2005). Most materials synthesized to date are only marginally stable, and thus positive results have been limited. To improve the coordination, and thus stability of the metal atoms, higher-energy binding metal sites need to be used. This can be accomplished by using functionalized materials such as activated carbons that are known to have exposed oxygen-containing functional groups on the surface. By using these types of functionalized activated carbons, NREL was able to integrate a series of TMs (V, Sc, Co, and Fe) with the activated carbon via vapor phase processing techniques and demonstrate the reversible storage of two hydrogen molecules. In this case, the results suggested that the metal atoms were coordinated and fixed to the oxygenated, activated carbon surfaces. The metals did not agglomerate, and hydrogen molecules reversibly adsorbed to the metal sites in qualitative agreement with theoretical predictions.

Integrating Li with similar types of oxygenated, activated carbons using solution-phase reduction chemistries was not sufficient to stabilize all the Li metal atoms and did not prevent metal-hydride formation. Thus, NREL investigated solution-phase Li integration with boron-substituted activated carbon (BC_x) materials. The formation of lithium hydride in this material was limited during the solution-phase synthesis in to maintain high site density and dispersion of Li metal atoms on the BC₆ material. As shown in Figure 3-52, TPD measurements demonstrate the reversible desorption of hydrogen at ~50°C following RT hydrogen exposure. Hydrogen-desorption temperatures increased from -120°C (for the parent BC_x material) to 50°C by the addition of Li. These TPD measurements are consistent with the NREL team's theoretical predictions that substituted boron provides well-defined metal binding sites. In addition, high-pressure hydrogen adsorption measurements on the lithiated BC₆ material at 100 bar and 30°C were ~1.5 times greater than the parent BC₆ material. Interestingly, the SSA of the Li-BC₆ material was only ~5 m²/g. Surprisingly, the H₂ adsorption sites in the lithiated BC₆ were stable in O₂ and H₂O. The Li-BC₆ materials were able to withstand diverse handling and processing conditions. TPD measurements revealed the reversible desorption of H₂ following exposure to O₂ and H₂O. The H₂ binding sites were highly versatile and robust under ambient conditions. Both XPS and TEM were performed on the Li-BC₆ materials after exposure to O₂ and H₂O, and suggested significant chemical and structural modifications relative to the parent BC₆ material (Figure 3-53). The shift in the C 1s spectrum for the Li-BC₆ material relative to both the parent BC₆ and CM-Tec AC

materials indicated possible enhanced substrate interaction in the presence of Li, whereas the XPS spectra for O 1s (529.3 eV) and Li 1s (52.6 eV) suggested the presence of Li₂O. These results, as well as a detailed structural understanding of the new H₂ binding sites, point to the importance of the metal/substrate interactions in enhancing the binding of H₂.

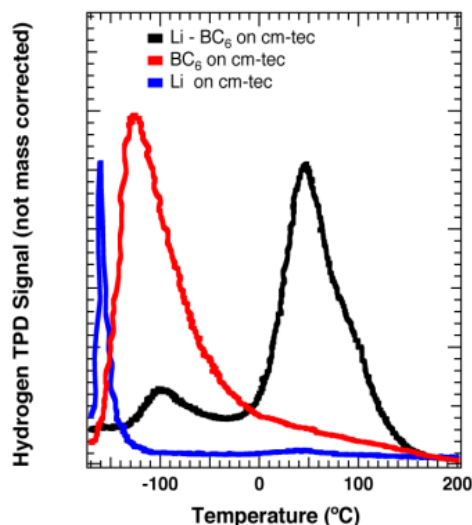


Figure 3-52. TPD for Li-BC₆ (black), BC₆ (red), and Li on AC (blue). Samples were degassed to 300°C prior to a 500-torr, RT H₂ dose.

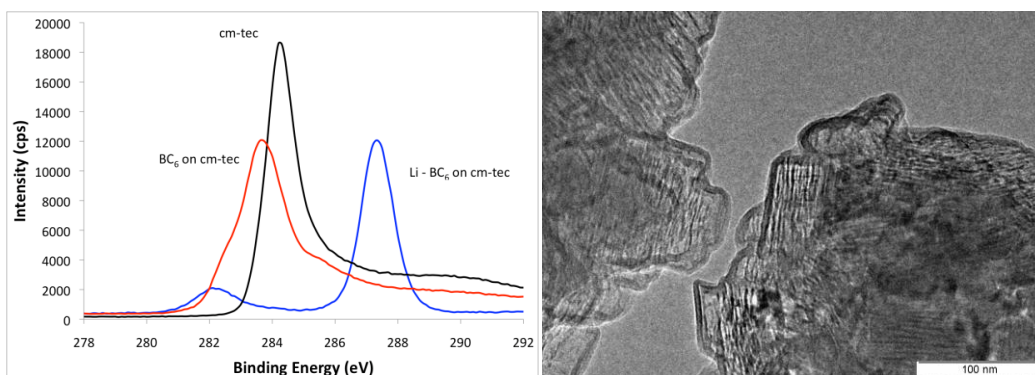


Figure 3-53. XPS of C 1s spectra for CM-Tec AC (black), BC₆ on CM-Tec AC (red), and Li-BC₆ on CM-Tec AC (blue). Right: High-resolution TEM of Li-BC₆ material.

3.4.3.1 Metal-Phosphine Coordination

Although additional work with boron- and nitrogen-substituted carbons needs to be performed in the future to fully characterize metal coordination for hydrogen storage, the HSCoE investigated other pathways for metal stabilization. This work included direct investigation of oxygen and other functional groups to stabilize single-metal atoms on well-defined surfaces. NREL theorists and experimentalists worked with LLNL to form open Ni metal centers via a novel Ni(BF₄)₂ (PPh₂)₂-SiO₂ aerogel process. These materials were prepared through the co-gelation of (CH₃O)₄Si and (EtO)₃SiCH₂CH₂PPh₂ in methanol, followed by drying of the gel in supercritical CO₂. The Ph₂P-SiO₂ aerogel exhibited a high BET SSA (~750 m²/g) and a low bulk density (< 0.1 g/cm³). The presence of the phosphine groups in the aerogel was confirmed by ³¹P NMR. The

reaction pathways outlined in Figure 3-54 were successfully developed and guided by several NREL theoretical calculations reported by NREL (Zhao et al. 2005). Here, the binding energies for consecutive adsorption of additional H₂ species to a CpM complex, where Cp = cyclopentadiene ring and M = Sc to Ni, were calculated. In several cases, the calculated H₂ binding energies for the TM complexes were ideal for on-board H₂ storage (~0.3 eV/H₂). The CpM complexes can be considered as basic building blocks for larger metal complexes and, therefore, were used to guide the synthetic efforts shown in Figure 3-54. Calculations performed at NREL indicated that the presence of the bulky stabilizing ligands sterically hindered the adsorption of H₂. Therefore, metal complexes must not only be electronically unsaturated to bind H₂ ligands, but must also be coordinatively unsaturated (i.e., ligands are easily displaced).

After careful consideration of the theoretical calculations discussed above, a well-defined, high-SSA, phosphine-functionalized SiO₂ aerogel was successfully decorated with four different Ni complexes. The phosphine groups on the SiO₂ aerogel provided specific binding sites for the Ni complexes to avoid metal clustering. The ligands on the Ni metal centers were easily displaced, leaving behind metal sites that were both coordinatively and electronically unsaturated. TPD measurements showed two new H₂ binding sites in a Ni-decorated inorganic aerogel with enhanced binding energies (Figure 3-55). For these materials, 1 H₂/Ni at ~25 kJ/mol was experimentally measured, which is in good agreement with theoretical predictions. On scaling up the synthesis of these Ni-supported aerogel materials, the new H₂ binding sites were not reliably reproduced and metal agglomeration was not avoided, i.e., 2–5-nm metal particles were observed (Figure 3-56). The H₂ binding sites with enhanced binding energies were unique to the Ni system, as no new H₂ sites were observed for a Fe-supported aerogel material, even after using similar reaction conditions (e.g., metal oxidation state +2 and counterion BF₄).

Even though this work demonstrated that one could indeed incorporate organometallic ligands into an aerogel framework, this particular system was down-selected based on reproducibility issues with metal complex formation in the aerogel and the low stability of the silica microstructure during solution-phase metal loading. Nevertheless, the NREL team believes that this concept still holds promise for the design of new sorbent materials, and that new strategies can be employed to facilitate metal coordination and enhance the stability of these materials. For example, the metal species can be incorporated into the functionalized aerogel through vapor-phase techniques, such as atomic layer deposition, to improve uniformity of loading and minimize stress on the aerogel microstructure. In addition, the mechanical integrity of the support can be enhanced through the use of composite aerogel structures, those comprising both carbon and metal oxide. This work demonstrates the ability of the HSCoE to work together to identify viable materials and synthetic paths to form coordinated metal centers that reversibly adsorb multiple hydrogen molecules and have the potential to meet DOE targets.

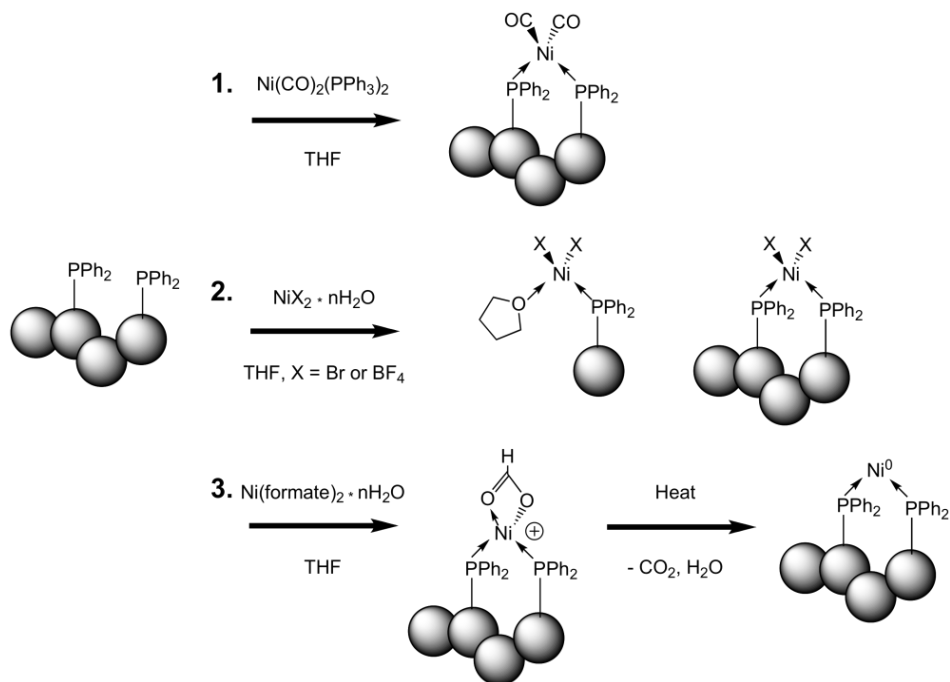


Figure 3-54. Reaction pathways to reactive Ni intermediates with reactive ligands that are easily displaced.

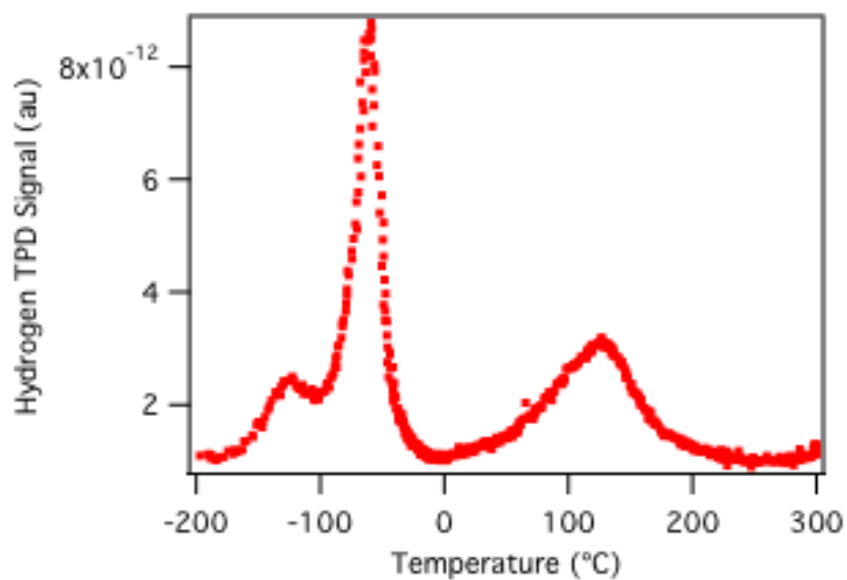


Figure 3-55. Hydrogen TPD data for a $\text{Ni}(\text{BF}_4)_2\text{-PPh}_2\text{-SiO}_2$ aerogel. The sample was degassed to 300°C prior to a RT 500-torr H_2 .

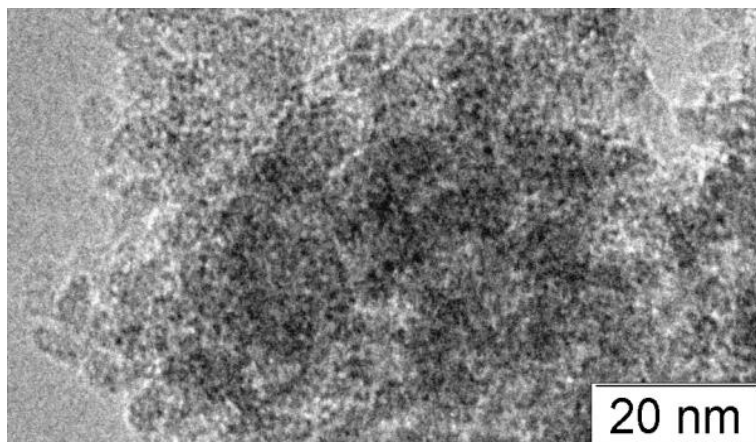


Figure 3-56. TEM micrograph of Ni nanoparticles (dark spots, 2–5 nm) on a functionalized SiO₂ aerogel

3.4.3.2 Metal-Graphene Oxide

GO can be a potential substrate to covalently anchor TM atoms that are undercoordinated and well exposed to accommodate multiple H₂ (Wang et al. 2009). GO substrate materials possess high surface-to-volume ratio, are lightweight, and provide anchor points for TM atoms that prevent metal cluster formation. Oxygen is the key in anchoring undercoordinated titanium and enhancing the TM substrate binding, as has been experimentally demonstrated on mesoporous silica (Hamaed, Trudeau, and Antonelli 2008). Hamaed and coauthors demonstrated that Ti dispersed on amorphous-silica internal surfaces are coordinated via strong Ti-silanol bonds (i.e., ~ 400 kJ/mol). However, each Ti atom still has sufficient reactivity to adsorb multiple dihydrogen molecules (2.7 H₂ at 22 kJ/mol). Wang and coauthors (2009) reported that Ti atoms grafted on GO could bind multiple H₂ ligands with the desired binding energies (Figure 3-57, 14–41 kJ/mol H₂). The estimated theoretical gravimetric and volumetric densities were 4.9 wt % and 64 g/L, respectively. The experimental results reported by Hamaed and colleagues (2008) confirm the basic premise of NREL's original work that an open metal site can store more than two H₂ molecules with energies appropriate for reversible hydrogen storage at ambient temperatures.

In a similar approach, NREL identified that GO has potential as a substrate to covalently anchor TM atoms that are undercoordinated and well exposed to accommodate multiple H₂. NREL developed a successful reaction pathway to synthesize Ti-GO materials by employing theoretical calculations to guide experimental investigations. As shown in Figure 3-58, organometallic Ti fragments were successfully deposited on degassed GO sheets using solution-phase chemistry processes and methodologies similar to those of Hamaed and colleagues (2008). The Ti-GO materials were isolated in an inert atmosphere and then exposed to 500 torr of H₂. TPD measurements demonstrated an enhanced H₂ binding site (i.e., desorption occurred at ~220 K), which resulted from the removal of one benzyl fragment. Future work must include additional studies to see if the additional supporting benzyl fragments can be removed to enable multiple dihydrogen adsorption.

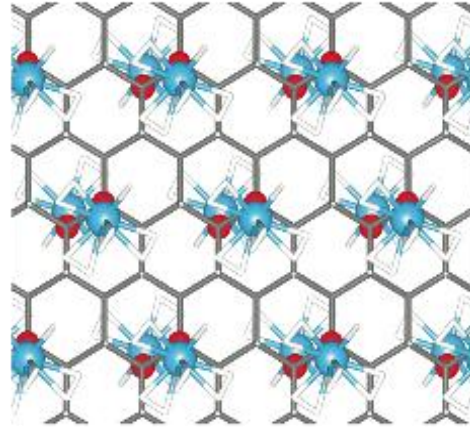


Figure 3-57. H₂ binding to Ti fragments on graphene oxide (Ti, blue; oxygen, red)

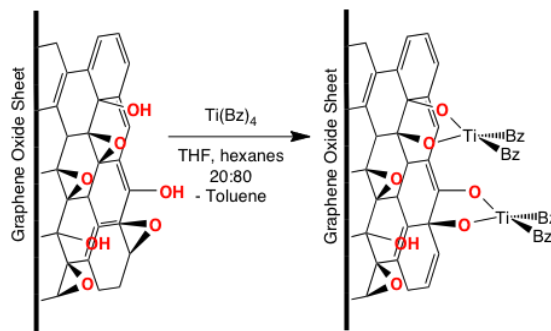


Figure 3-58. Schematic representation of the grafting of benzyl Ti fragments onto GO substrates

3.4.4 Strong/Multiple Dihydrogen Interactions: Conclusions

The HSCoE has championed the use of lightweight metals (i.e., first-row TMs and groups I and II elements) to enhance the binding of dihydrogen on matrix materials and, perhaps more importantly, to provide the ability to create sorption sites that can store more than one dihydrogen molecule per metal site. Since the publication of the seminal work in this area (Zhao 2005), which has been cited nearly 200 times, theorists and experimentalists have worked closely within the HSCoE to iteratively design and synthesize new materials with coordinated metal centers. Designs of new sorbents have adhered to the criteria of synthesizing stable materials that have the potential to meet DOE hydrogen-storage targets. For example, NREL has identified new material classes for hydrogen sorbents, such as Li_xSiO₂ (Figure 3-59). Whereas Li is light, cheap, and easy to disperse, Li-intercalation in carbon materials is extremely difficult to use for controlling the density of homogeneously dispersed Li and/or to co-intercalate because of the high mobility of Li.

To solve these issues, NREL investigated Li dispersion in porous SiO₂, which exists in various forms such as silica aerogels. The silica interacts very strongly with Li atoms by forming Li-O bonds. To mimic the porous material, the tubular form of SiO₂ was used (Figure 3-59). Such a nanotube is chemically stable with a wide bandgap. Therefore, Li-

intercalation is initially expected to be unfavorable. However, when Li atoms are loaded in this system with an external electric field, they induce defects, which are energetically favorable. The LiSiO_2 nanotube can bind dihydrogen in both the outer and inner surfaces. All the hydrogen molecules are bound to the Li centers. Neither the oxygen nor the silicon sites enhance hydrogen binding. With each Li binding, one H_2 binds to the inner surface at ~ 19 kJ/mol and one to the outer surface at ~ 30 kJ/mol. The smaller binding energy in the inner surface may be due to the relatively small pore size. In this structure, the total capacity of dihydrogen is 3 wt %.

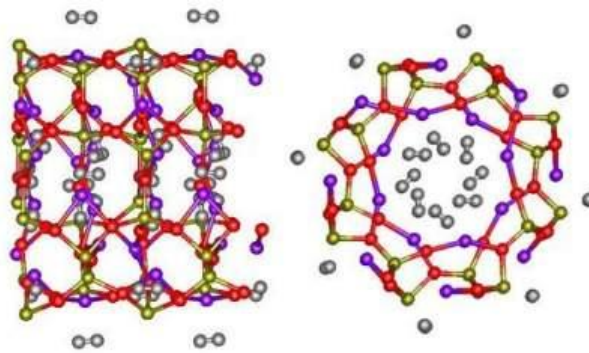


Figure 3-59. H_2 binding in a LiSiO_2 nanotube viewed toward the wall (left) and along the axial direction (right). Gold, red, purple, and grey balls denote, respectively, Si, O, Li, and H atoms.

The main issue here is the identification of a model system that can be synthesized with known processes to demonstrate the specific properties needed for enhanced hydrogen-storage capacities at higher temperatures. Thus, theorists not only identified new materials, but also worked with experimentalists to identify thermodynamically viable synthetic paths to form stable materials. In addition, the calculations used to identify these novel materials have been validated with all known 3-D metal- H_2 experimental results. Thus, there is good agreement for both the binding energy and the number of dihydrogens being stored between the theory and the known experimental results. Based on the successes of the Ni-silica aerogel and Ti-silanol work, the NREL team has fully validated the designed-material approach to forming strong dihydrogen adsorption with open metal centers. This work is applicable to most metals (e.g., Li, Na, Mg, Ca, Sc, Ti, V, Mn, Co) and matrix materials. In addition to oxygen and phosphorous functional groups, boron and nitrogen substituted in carbon materials also help stabilize metal centers for hydrogen storage. Finally, while most of these efforts focused on stable hydrogen sorption to single metal sites, the HSCoE also identified processes and materials in which metals induce stronger hydrogen sorption to the support materials, another potential storage route. The key future efforts must focus on materials/process optimization to increase the number of viable binding sites and ultimately the overall storage capacities.

3.4.4.1 Practical Paths Forward for Sorbent Materials

The DOE year 2015 system target for volumetric density is 81 g/L. Such a target raises an important fundamental question: *Can molecular hydrogen be stored more densely than that in liquid form?* The most practical high-pressure tank can store up to 39 g/L of hydrogen gas at RT and 700 bar. In comparison, at the extremely low temperature of 20 K, liquid hydrogen can be as dense as 70 g/L. The specific density of an adsorbed H_2 monolayer on porous SWNTs has been estimated at 64 g/L at its maximum, which is less than that of liquid hydrogen and the DOE target. In such estimations, the vdW intermolecule distance (typically 3.5 Å or larger) is usually assumed. Therefore, the packing

density in liquid H₂ is understandably modest. The HSCoE was the first to identify the special properties of inexpensive Ca. NREL applied its unique predictive M-xH₂ theories to investigate the hydrogen-storage properties of groups I and II metals. Unlike Li, Na, and Mg, Ca can be coordinated to matrix materials in such a way that a pseudo 3-D band state forms, enabling substantial amounts of dihydrogen to be reversibly adsorbed to the metal atom. Based on first-principles calculations, the NREL team predicted that when calcium or magnesium are oxidized, there exists a stable Ca(Mg)-dihydrogen complex that holds up to eight H₂ molecules. The resulting Ca(H₂)₈ cluster (Figure 3-60) has a record-high theoretical hydrogen content compared to other hydrogen-metal clusters such as WH₁₂ and MoH₁₂. For practical hydrogen storage, Ca-intercalated nanoporous materials were proposed. Calculations show that Ca-intercalated pillared graphite (Figure 3-60) can hold reversibly more than 70 g/L of H₂. Such high volumetric density can be achieved because the strong Ca-H₂ interaction assures a smaller H₂ intermolecule distance (2.7 Å or smaller).

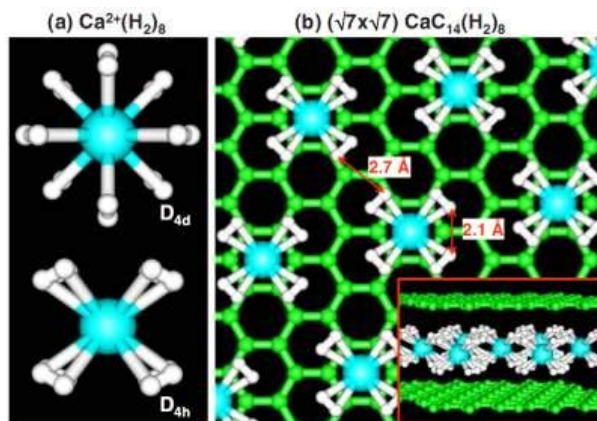


Figure 3-60. Atomic structures of (a) H₂-loaded Ca(H₂)₈ complexes with the D_{4d} and D_{4h} symmetries, and (b) Ca(H₂)₈-intercalated graphite in a $\sqrt{7}\times\sqrt{7}$ pattern. Inset shows the side view. Green, blue, and white atoms are C, Ca, and H, respectively.

Even though the synthetic pathways remain a challenge, this set of work provides a breakthrough that clearly defines sorbent materials that could be used to meet DOE's ultimate storage targets. In addition to the initial Ca-graphene work, NREL also found that both covalent-organic framework (COF) and MOF materials stabilize open Ca centers. In the case of COFs, the Zn₄O clusters typically found in MOFs were replaced by the much lighter C₄Si clusters, and two of the C atoms in the organic linkers by B atoms, as illustrated in Figure 3-61. The design of the resulting COF- α followed two criteria: (1) the electron counting rule should be satisfied so that no half-filled dangling bonds exist; and (2) strain in the system should be minimized. Using valence four Si and C atoms in the tetrahedral clusters, and replacing C by B in the organic linkers, satisfied the first criterion. Silicon at the center of the tetrahedral cluster serves to reduce the strain and therefore satisfies the second criterion.

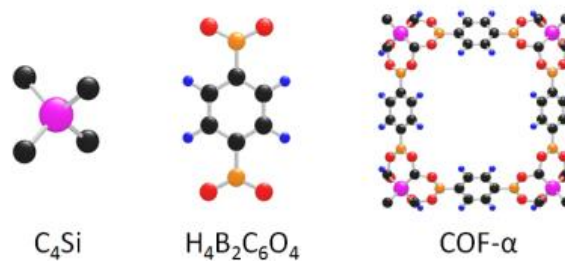


Figure 3-61. Building blocks and structure of COF- α (viewed along the [001] direction)

The COF design was inspired by the recent synthesis of COFs, in which strong bonds between B, C, and O atoms were used to form the rigid porous structures (Cote et al. 2005). Calculations further showed that each benzene linker in the COF- α can bind two

Ca (~120 kJ/mol), and each Ca can also hold four H₂ (15 kJ/mol). Although this particular COF material has a hydrogen-storage capacity of only ~44 g/L and 5.6 wt %, the theorists and experimentalists have worked together to identify materials with viable synthetic pathways.

3.4.5 Strong/Multiple Dihydrogen Interaction No-Go Decisions

Two of the main material areas investigated by NREL were considered carefully and discontinued (No-Go decision): (1) tractable solution-phase reactions involving organometallic Sc complexes and (2) reducible fulvalene-based MOF linkers.

3.4.5.1 Tractable Solution-Phase Reactions Involving Organometallic Sc Complexes

Initially, the scheme for the chemical synthesis of CpScH₂(H₂)₄ employing tractable reactions (shown in Figure 3-62) was unsuccessful based on the difficulty in isolating the Cl-bridged scandium precursor. A second reaction pathway was designed as shown in Figure 3-63 to attempt to make a simple organometallic Sc complex with multiple dihydrogen ligands bound to the first-row TM atom. The reaction of (C₅Me₄H)Sc(CH₂C₆H₄NMe₂)₂ (**2**) with H₂ in toluene at 80°C appears to cleave the Sc-C bonds to form *o*-CH₃C₆H₄NMe₂ ligands that remain coordinated to the Sc metal center through the amino group to give (C₅Me₄H)Sc(NMe₂C₆H₄CH₃)₂ (**3**). NMR measurements did not detect any hydride or dihydrogen ligands. Calculations performed subsequently at NREL on the Sc complexes **2** and **3** indicated that H₂ will not add in the presence of the bulky *o*-CH₃C₆H₄NMe₂ ligands (i.e., sterically hindering), but will add to form hydride and dihydrogen ligands if smaller amine ligands are used or one of the *o*-CH₃C₆H₄NMe₂ ligands is removed. Thus, theory was employed systematically to guide experimental progress.

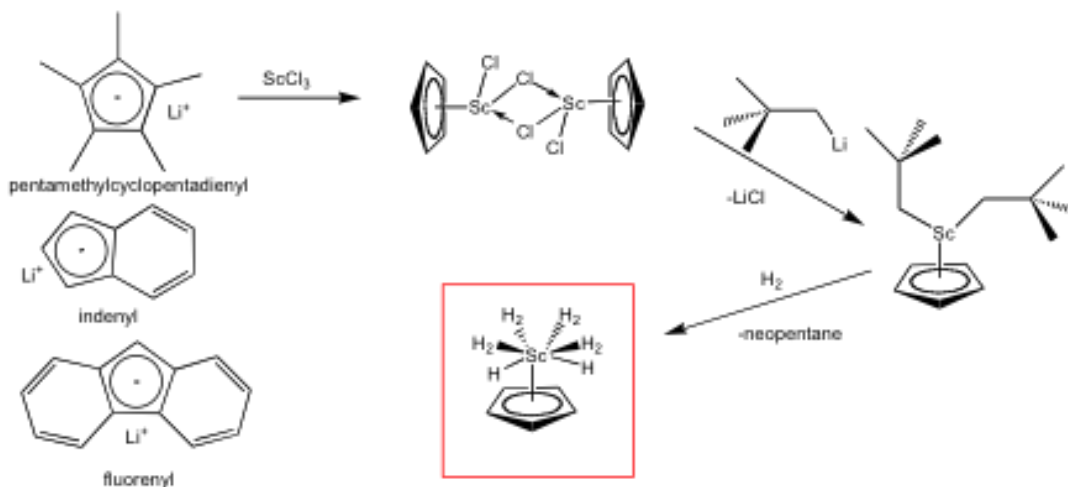


Figure 3-62. Schematic of the tractable reaction for the synthesis of CpScH₂(H₂)₄

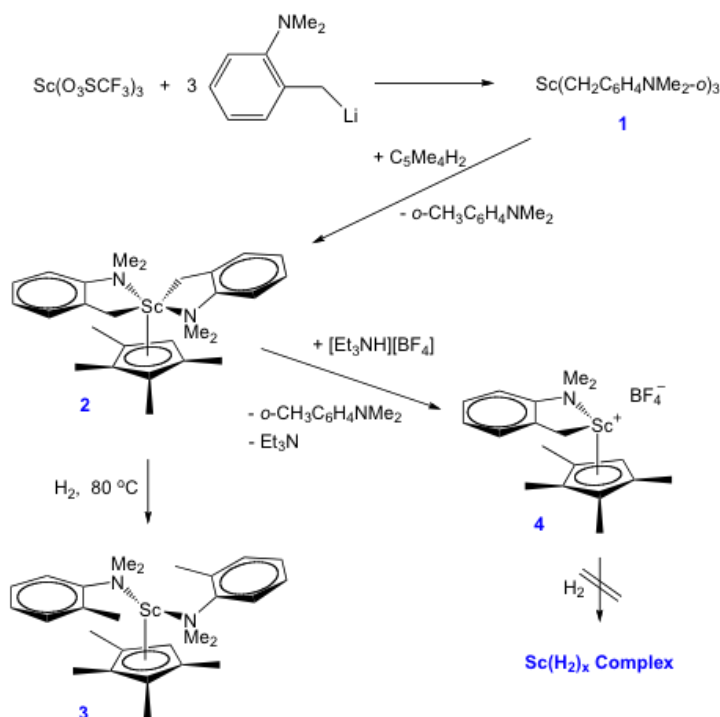


Figure 3-63. Reaction pathway for the synthesis of a Sc metal complex with multiple dihydrogen ligands

Alternatively, the reaction of the Sc metal center with a fluorinated borate salt is expected to yield a weakly coordinated complex, thus opening a site for the coordination of H_2 ligands. The reaction of $[\text{Et}_3\text{NH}^+][\text{BF}_4^-]$ with $(\text{C}_5\text{Me}_4\text{H})\text{Sc}(\text{CH}_2\text{C}_6\text{H}_4\text{NMe}_2)_2$ (**2**) was examined. Here, the borate salt protonates one of the aminobenzyl ligands to release *o*- $\text{CH}_3\text{C}_6\text{H}_4\text{NMe}_2$ yielding a Sc product (**4**) with a weakly coordinated $[\text{BF}_4^-]$ ligand. The reaction, carried out in toluene, produces a soluble Sc-containing product whose NMR spectrum shows a strong $[\text{C}_5\text{Me}_4\text{H}]$ resonance and a triplet at 0.76 ppm, which may be the remaining benzyl $-\text{CH}_2-$ group, split by the weakly coordinated F atoms. Several attempts at reacting (**4**) with hydrogen produced undesirable insoluble products, namely the electronically stable bridging Sc-H-Sc hydride complex. The aminobenzyl ligands were not easily displaced from the Sc metal center by H_2 . In addition, calculations at NREL indicated that the presence of the bulky aminobenzyl ligands hindered the adsorption of H_2 (i.e., sterically hindering). Metal complexes must be coordinatively and electronically unsaturated to bind H_2 ligands, therefore, tractable reactions involving organometallic Sc complexes were no longer pursued.

3.4.5.2 Reducible Fulvalene-Based MOF Linkers

Another strategy for avoiding metal agglomeration and enhancing H_2 binding is to bind metals to well-defined sites on high-SSA MOFs. The incorporation of reducible units into MOFs will improve the MOF's stability and provide sites for enhanced H_2 binding even without the addition of TMs. There is a significant need for more stable reducible MOF linkers (e.g., Cp linkers) because of the instability of the small arene-based linkers typically found in MOFs when exposed to reducing environments. Three new fulvalene-

based biscalboxylic acid and bispyridine MOF linkers (Figure 3-64) were successfully synthesized and isolated. The new compounds were confirmed via ^1H NMR.

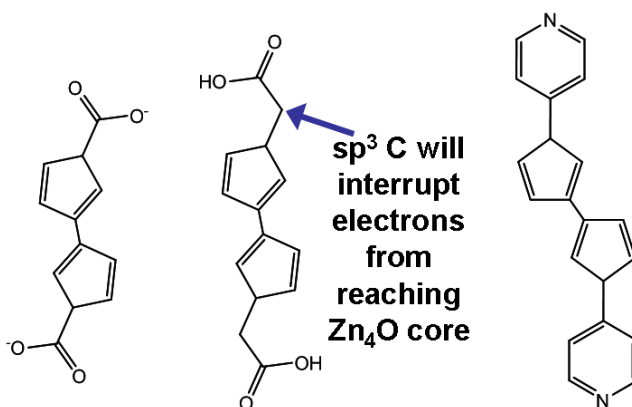


Figure 3-64. Chemical structures for three new fulvalene-based MOF linkers

The novel fulvalene-based linkers proved to lack stability under the Zn₄O MOF synthesis conditions. In each of the three cases, the high temperatures used in the MOF synthesis proved to be the catalyst for the presumed polymerization of these organic linkers. Therefore, a no-go decision on the solution-phase synthesis of fulvalene-based MOF linkers was made.

3.5 Weak Chemisorption/Spillover

This effort focused on the development of new RT sorbents based on a weak chemisorption process, i.e., a hydrogenation mechanism, which could meet the DOE 2010 targets for on-board vehicle hydrogen storage. As discussed previously, several hydrogenation mechanisms were investigated, but the vast majority of the work involved hydrogen spillover. By definition, hydrogen spillover is a process of dissociating dihydrogen onto a metal catalyst, followed by migration of the hydrogen atoms onto the surface of a receptor material and subsequent diffusion away from the catalyst site, which leads to chemisorption of hydrogen. As discussed previously, hydrogen spillover is a well-known and effectively proven phenomenon in heterogeneous catalysis. Thus, the issue is not whether spillover exists, but rather, what level of storage capacity can be achieved. The efficiency of spillover is highly dependent on the metal, the support chemical composition, and the synergistic interaction between the two.

In the application of spillover to hydrogen storage, graphitic or nanostructured carbon, and framework materials in some cases, are typically used as supports, because their high SSA and/or pore volume are conducive to enhancing hydrogen capacity. Hydrogen spillover is a multiple-step process: catalyzed hydrogen dissociation, surface diffusion from the catalyst to a surface, weak chemisorption of the dissociated hydrogen species to the support, and finally recombination followed by desorption of any mobile hydrogen species from the support. The equilibrium established for these competing processes is what determines the overall hydrogen sorption capacity and kinetics. To exploit spillover for hydrogen storage, the key questions include whether spillover is reversible at ambient

temperature, if the desorption rates at ambient temperature are fast enough for automotive applications, and how to develop materials to enhance reversible capacity and kinetics.

The spillover development work occurred across several laboratories and involved focused efforts not only to establish capacity/kinetic limits, but also to establish the mechanism of spillover to enable optimizing it for transportation-related hydrogen-storage applications. As the work proceeded beyond materials development and testing, the following empirical guidelines were used:

1. What is the status for capacity, kinetics, thermodynamics and reproducibility of spillover within the literature?
2. What is a realistic expectation of empirical limits for capacity/kinetics/cycle life for this type of process?
3. How can we better incorporate modeling to assist in explanation/validation of experimental results?
4. How can we improve the quality of hydrogen-capacity measurement processes within the literature?
5. What type of characterization techniques are essential to confirm enhanced sorption capacity if/when observed?

In contrast to straight physisorptive or chemisorptive processes, “large-scale” hydrogen spillover includes both physisorption and chemisorption *plus* the necessity of surface diffusion on the substrate, and a dependence on surface chemical composition and structural features (e.g., pore structure, pore volume, surface substituent(s), catalyst size, catalyst dispersion, interface, diffusion pathway). All of these factors will affect the total sorption capacity. The HSCoE attempts to validate and improve overall uptake via hydrogen spillover included investigation of: catalyst deposition techniques; metal catalyst type; metal catalyst doping efficiencies/dispersion; chemical composition and structure of the support, substitutional doping of the support with boron and/or nitrogen, or altering the surface chemistry of the support; and type of support (aerogels, template growth, MOFs), generation of “bridges” between the metal and the support that can further enhance spillover capacity.

Specifically, within spillover, a range of sorbent hydrogen receptors were investigated whereby spillover was catalyzed using transition and/or noble metals (e.g., Pt, Ru, Pd, Rh, Ni, PdHg) as the H₂ dissociation site. The receptors included superactivated carbons (AX-21, Maxsorb, CM-Tec), MOFs, templated growth carbon materials, nitrogen and b-doped CVD materials, silica spheres, and zeolites. A wide range of catalyst deposition methods were used and further developed to achieve high metal dispersion that, in some cases, showed significant spillover enhancements by as much as a factor of three compared to the starting materials. As for many other HSCoE research activities, this work was performed in conjunction with theorists.

Major accomplishments of the spillover work include:

1. Experimentally confirming spillover mechanism through the use of isotopic labeling
2. Achieving a gravimetric sorption limit at ~4% w/w RT adsorption on bridged MOFs
3. Enhancing kinetics through effective binding of catalysts within templated carbon materials or doped carbon receptors
4. Enhancing volumetric adsorption on zeolite materials
5. Using heterogeneous substrates for enhanced hydrogen binding energies
6. Establishing the importance of receptor chemistry (oxygen content/specific chromophores) on reversibility of hydrogen storage.

3.5.1 Spillover Storage on Metal-doped Superactivated Carbon

The most effective way to achieve spillover with a significant hydrogen sorption beyond the base material adsorption level on carbon is by direct doping of metal onto the receptor. The crucial factor for spillover on a metal-doped carbon is metal dispersion and particle size; a high metal dispersion is necessary for effective spillover, but agglomeration of the catalyst can lead to no enhancement at all (de Leon, Grange, and Delmon 1997; Chen, Falconer, and Chang 1991; Glugla, Bailey, and Falconer 1989). A number of techniques can be used for direct doping: Michigan used an incipient wetness impregnation technique, whereas NREL developed a variety of vapor- and solution-phase processing techniques. Missteps can be made easily, and each misstep will lead to reduced or no spillover, so the key steps are summarized below. Doping of Pt on AX-21 is used as an example. By following this procedure, Pt metal particles 1–3 nm in sizes are obtained, and the volumetric results shown in Figure 3-65 are achieved.

- Measure 200 mg dry AX-21 or Maxsorb (dried at 393 K). Add acetone until all particles are completely dissolved in a very dilute slurry (~20–100 mL). (*A more dilute solution increases metal dispersion and hence enhances spillover.*) After drying, minimize the amount of time the sample is exposed to air/humidity.
- Dissolve 26 mg H_2PtCl_6 (Aldrich, 99.9%) in at least 20 mg acetone and add at a consistent dropwise rate over at least 10 min while stirring vigorously. (*Using an overly concentrated Pt precursor solution and/or faster mixing will lead to poor and uneven metal dispersion and substantially less spillover.*) Stir vigorously for at least 10 min after the last drop has been added.
- Sonicate (100 W, 42 kHz) the solution for 1 h and then evaporate the excess liquid in an oven at 333 K. (*Allowing the solution to fully dry will lead to lowered enhancement.*)
- Dry the sample further in a quartz tube under He flow at 393 K for 2 h. Change the flow to H_2 and raise the temperature to 573K at 1 K/min and hold for at least 2 h. (*Holding for long times ensures complete reduction of Pt, but holding too long causes the platinum to migrate on the surface and agglomerate.*) Switch the flow to He to purge. (*Purge for at least 4 h and cool at a rate no faster than*

1 K/min, otherwise Pt will react vigorously with air during sample transfer, leading to poor metal dispersion.)

- Transfer the sample to the measurement system using a degas procedure of 623 K and a heating rate of no more than 5 K/min under vacuum for 8 h. (*Degassing at only 573 K is not adequate, because chemisorbed hydrogen attached during H₂ reduction will remain on the carbon surface.*)
- In H₂ measurement, the leak rate that is acceptable for physisorption measurement is not acceptable for spillover measurement, and allowing large dead spaces (in sample or reservoir cells) will lead to large errors.

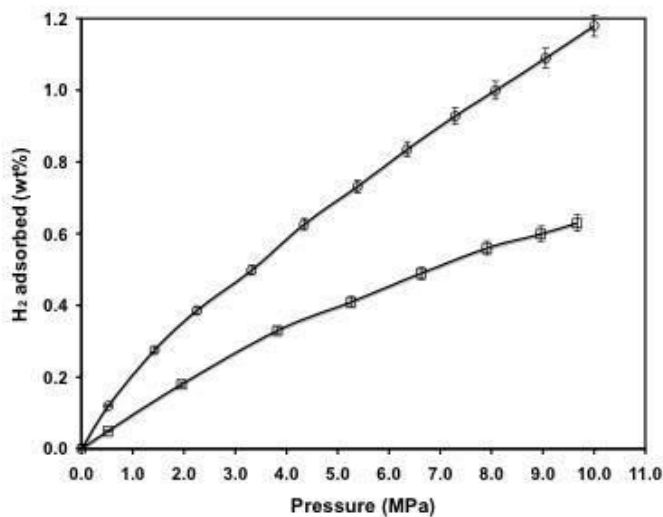


Figure 3-65. Typical and consistent results on hydrogen isotherms at 298 K on 6 wt % Pt/AX-21 are shown.

The detailed design and construction of a volumetric system for high-pressure measurements have been described elsewhere, and the Best Practices document developed by the HSCoE is essential (DOE 2008). The correction for He adsorption has also been described in detail (Pajonk 2000), although not all laboratories use this correction.

To obtain a better understanding of the processes involved in spillover, a deuterium isotope tracer in conjunction with TPD studies was performed on a Pt/carbon sample. The Pt/C sample was subjected to sequential dosing of H₂ and D₂ at 298 K, followed by quenching in liquid N₂, evacuation of excess gasses, and TPD. Representative results shown in Figure 3-66 demonstrate that, effectively, the spillover process is sequential with the first hydrogen adsorbed being the last desorbed or removed. In this case, H₂ was dosed first for 5 min at 298 K, followed by dosing with D₂ for 5 min. The TPD results show clear desorption peaks of D₂, HD, and H₂ in the reverse sequence of dosing (Sermon and Bond 1974). The results are direct evidence that (1) atomic species are formed during the spillover processes, as shown by the HD formation, and (2) desorption follows a reverse spillover process where atoms migrate back to the metal particle, on which to recombine and desorb as molecules.

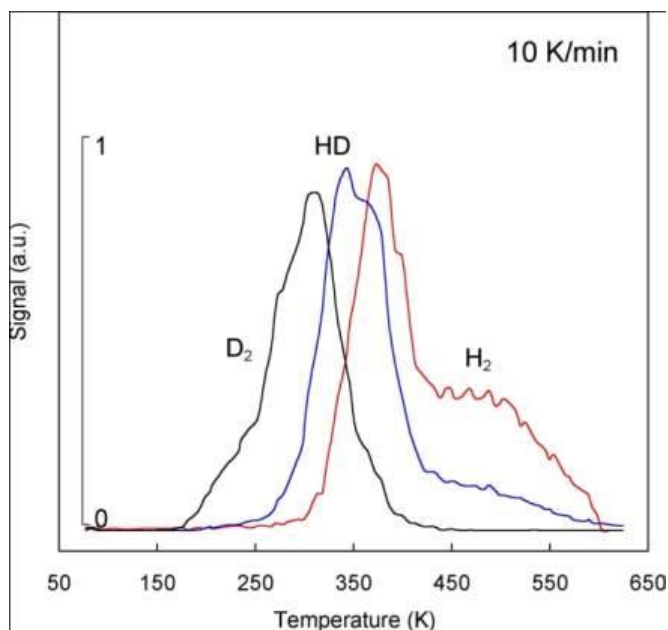


Figure 3-66. TPD result for 6 wt % Pt on carbon (3400 m²/g) after dosing with 0.4 atm H₂ followed by D₂ at 298 K for 5 min (followed by quench, gas-phase removal, and TPD).

The kinetics and mechanism of hydrogen spillover were also investigated (Glugla, Bailey, and Falconer 1989; Conner and Falconer 1995). It was found that hydrogen molecules were dissociated rapidly on metal sites and then diffused slowly away from them to the receptor. Surface diffusion of hydrogen atoms has been proposed to be the rate-determining step in hydrogen spillover. To better model the system, a full and complete surface characterization will be needed. Thus, by assuming that the surface diffusivity was not dependent on surface concentration, a phenomenological equilibrium isotherm equation was derived for spillover systems (Glugla, Bailey, and Falconer 1989; Hodnett and Delmon 1986). All of the constants involved could, in principle, be measured independently. At very high pressures, the adsorption amount will approach a constant (corresponding to saturation adsorption capacity). The apparent heats of adsorption (ΔH_{ads}), as calculated from the temperature dependence of the isotherms via the Claysius-Clayperon equation, were 23.3 kJ/mol (at 0.020 wt %), 16.6 kJ/mol (at 0.025 wt %), and 15.1 kJ/mol (at 0.031 wt %).

Direct or indirect catalyst integration is determined as one evaluates materials stability issues and need. In general, the catalyst size, dispersion, and type can all affect the efficiency and thus capacity of spillover (deLeon, Grange, and Delmon 1997; Chen, Falconer, and Chang 1991; Glugla, Bailey, and Falconer 1989). Spillover results vary substantially with the materials, processes, and treatments used, but there are a number of techniques for direct catalyst integration. Figure 3-67 shows typical spillover results where Pt directly integrated with the AX-21 activated carbon material had substantially higher ambient-temperature capacities compared to the base carbon material. HSCoE optimization efforts investigated the use of different catalysts and different porous carbons to find the materials with the highest capacities. To date, the highest activated carbon capacities have been observed with a EMC-2 zeolite templated carbon (developed at

Mulhouse University, France) with an initial BET SSA of 3839 m²/g and nanoparticle Ru catalysts (see Figure 3-68) (Teichner 1990). The storage capacities depended on the catalyst material (i.e., Ru > Pt > Ni) and dispersion. The apparent isostatic heats of adsorption (ΔH_{ads}) for the catalyst-activated carbon spillover materials were measured in the range of 15 to 23 kJ/mol.

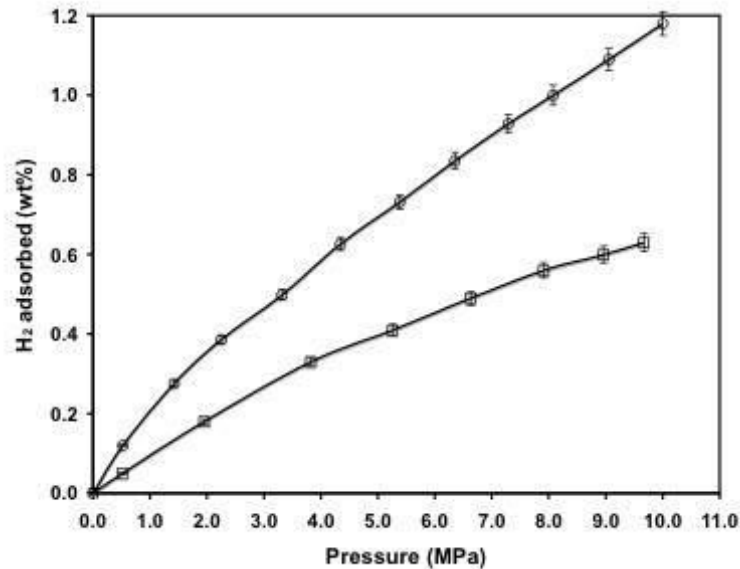


Figure 3-67. High-pressure hydrogen isotherms at 298 K on 6 wt % Pt/AX-21 (O, upper curve) by direct integration technique (error bars are based on 1 σ of 4 separately prepared samples). Undoped AX-21 (□, lower curve).

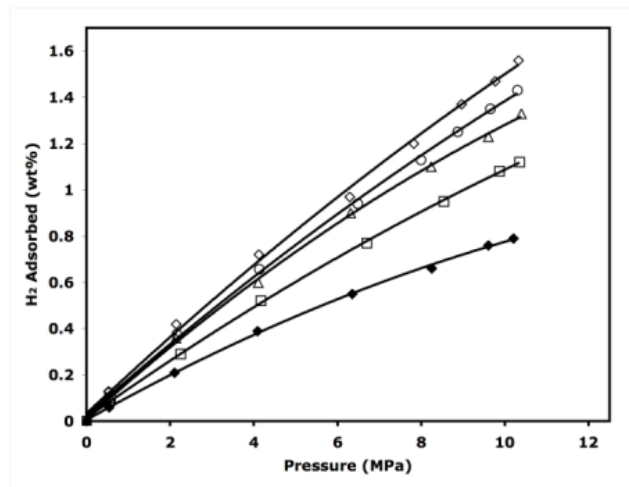


Figure 3-68. H₂ isotherms at 298 K on templated carbon (TC) and 6 wt % metal catalysts. All materials were H₂-reduced at 300°C except Ru/TC-T, which was thermally reduced (in N₂) at 900°C (1 h). BET SSAs for each sample were (m²/g): Ru/TC-T = 2090 (open diamonds); Ru/TC = 3004 (open circles); Pt/TC = 3120 (open triangles); Ni/TC = 3091 (open squares); TC = 3839 (closed diamonds).

As shown in Figure 3-69, the spillover desorption rates are typically higher than those of adsorption, and the rates decrease with hydrogen loading. Work by the HSCoE identified several factors that can increase adsorption rates, including using higher pressures during the initial loading step, integration of trace amounts of gasses such as water and methane, (Robell, Ballou, and Boudhart 1964) and chemical modification of the catalysts, dispersion of the catalysts particles, and the chemical composition of the receptor surface. Ultimately, the HSCoE demonstrated that depending on the capacity needed, it may be possible to meet the DOE 2015 refill rate target of ~3 min by going to only 80% to 90% of the maximum excess capacity, but at a high step pressure. In general, desorption rates are more than sufficient to meet DOE’s fuel supply rates, and can be accelerated with just the waste heat from the fuel cell heating chamber, i.e., 80°C.

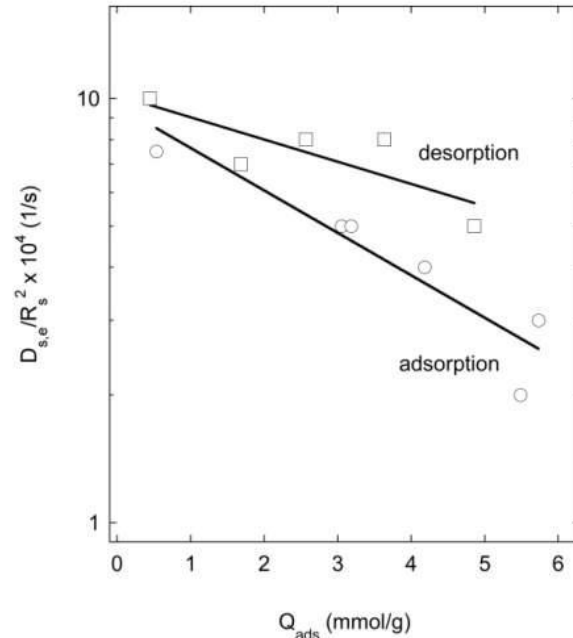


Figure 3-69. Representative diffusion time constants for H spillover on Pt/TC at 298 K

3.5.2 Irreversible Chemical Reactions

Systematic investigations of the effects of different surface oxygen groups on spillover led to the discovery of the formation of side-reaction products on some sorbent materials. In general, any given high-SSA, carbon-based sorbent has a number of different surface moieties involving oxygen, hydroxides, hydrogen, and other elements. To a significant extent, the effects of many of these are removed during the material synthesis and “activation” processes, which usually involve high-temperature exposure to flowing hydrogen for several hours. However, in some cases, the oxygen groups remain sufficiently active that they produce irreversible chemical reactions to form secondary reaction products, especially water or methane. Also, if direct monitoring of the effluent is not performed regularly, these secondary reactions can be interpreted as substantial hydrogen-storage capacities. These side reactions can also occur through the reduction of metal-surface oxides to hydrides, again possibly leading to erroneous results. However, because they are irreversible, the capacities are actually substantially lower. Careful and diligent monitoring of desorption isotherms for hysteresis, or multiple cycles of adsorption/desorption of hydrogen, can easily identify that these secondary reactions are occurring (see Figure 3-70).

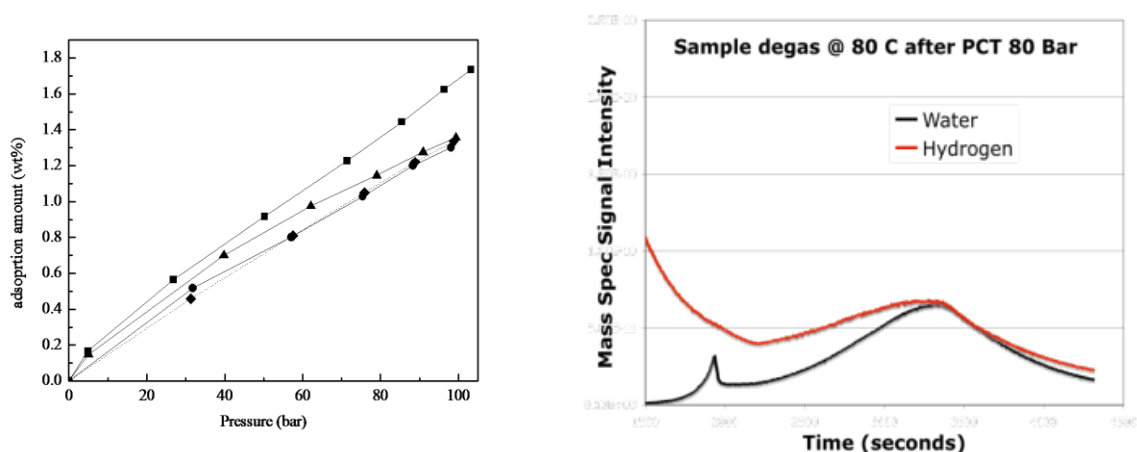


Figure 3-70. The graph on the left illustrates how an adsorption curve can be affected by side reactions. The squares illustrate the first adsorption cycle of a highly oxidized carbon-receptor-pt catalyst, and the triangles, diamonds, and circles show the next cycles with drastically reduced sorption capacities. This is a direct effect of water formation. The curve on the right illustrates a TPD after a typical high-pressure hydrogen adsorption. This illustrates how easily one can identify the formation of water.

3.5.3 High-Capacity Experimental Spillover Results

To increase spillover capacities beyond that which has been observed with activated carbons, the HSCoE investigated several routes. They included the use of substituted materials, physical mixtures of catalyst- and non-catalyst-containing materials, “bridged” structures, pore structures, and catalyst size/dispersion. In general, it is not always possible to integrate appropriate catalysts with a potential receptor material. In the case of some framework materials, the metal catalysts bind too strongly and destroy the structure. In the case of graphene, the binding is so low that the catalysts are too mobile and agglomerate quickly. One method to overcome some of these deficiencies is to physically mix potential receptor materials with materials that contain catalysts (e.g., Pt-activated carbon). If the receptor materials are significantly better as spillover receptor materials, then significant capacity enhancements are observed. These types of physical mixtures have been used to demonstrate significant spillover in SWNTs, other activated and templated carbons, zeolites, and framework materials.

To improve the diffusion capabilities beyond that achieved with physical mixtures, the HSCoE developed a “bridging technique” in which sucrose was mixed with the catalyst and receptor components, followed by a low-temperature (e.g., 200° to 300°C) bake to carbonize the sucrose. NREL has determined that pyrolyzed sucrose is an excellent spillover material in and of itself. However, when combined with Pt/AC catalyst material and framework materials, spillover capacities in excess of 4 wt % at ambient temperature have been demonstrated and validated (see Figure 3-71) (Wang et al. 2009).

Subsequent work demonstrated that spillover effects continue well past 100 bar, so these results with the bridged IRMOF8 material indicate that spillover well past 4 wt % should be achievable if higher pressures are applied.

These results were validated by other groups around the world and by DOE's validation laboratory, Southwest Research Institute. Although the use of the bridge material and the specific features of IRMOF8 must be studied and understood in greater detail, this work developed a simple and effective technique to build spillover materials with secondary receptor materials that have substantially higher capacities. The bridge-building process appears to be receptor specific, and optimization and/or use of other receptors may yield even greater hydrogen-storage capacities.

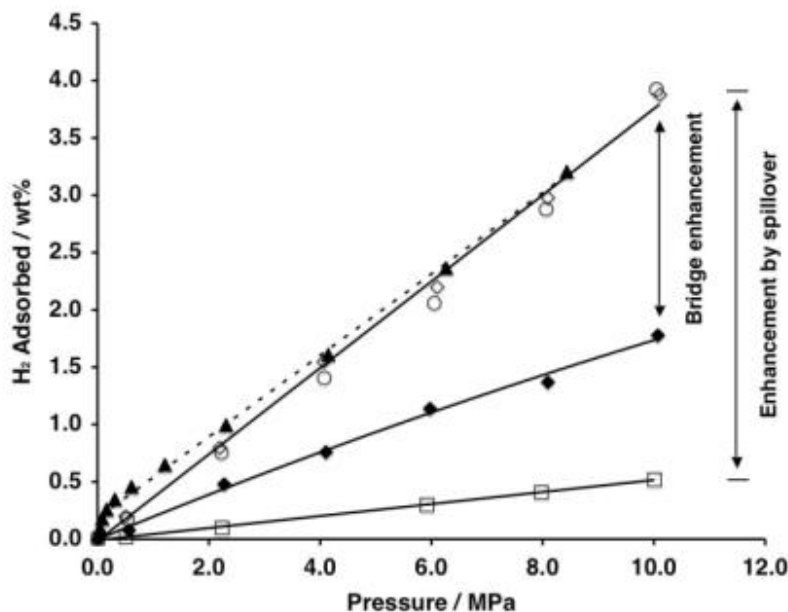


Figure 3-71. High-pressure hydrogen isotherms at 298 K for pure IRMOF-8 (\square), Pt/AC, and IRMOF-8 physical mixture (1:9 weight ratio) (solid diamonds), and for a bridged sample of Pt/AC-bridges-IRMOF-8: first adsorption (solid triangles), desorption (open diamonds), and second adsorption (open circles).

These strong effects of bridging materials on spillover were discovered soon after the discovery of the spillover phenomenon (Wang, Yang, and Yang 2009; Olson et al. 2010). Specifics of the strategy developed to form carbon bridges between the spillover catalyst source (such as Pt/AC) and MOF particles, using sugar as the precursor for carbon bridges, are described below. Some common pitfalls in the synthesis of the bridged material are also discussed.

Synthesis of IRMOF-8

Care must be taken in synthesizing smaller materials for bridging, because large crystals are incompatible with the small Pt/AC sizes. The sizes of the IRMOF-8 and IRMOF-1 crystals were in the range of 100–200 nm, which are comparable to those of the Pt/AC catalyst. The synthesis procedure is as follows:

1. $\text{Zn}(\text{NO}_3)_2 \cdot 6\text{H}_2\text{O}$ (1.19 g, 4 mmol, must be freshly opened) and 2,6-naphthalenedicarboxylic acid (0.43 g, 2 mmol) were dissolved in 40 ml of dimethylformamide (DMF) during vigorous stirring at RT.
2. Three drops of H_2O_2 aqueous solution (30 wt %) were added to the solution. Triethylamine (2.3 mL) was slowly added dropwise to the above solution under vigorous agitation for 1 h (one drop/30 s) to deprotonate the acid to initiate polymerization.
3. The white product was collected by repeated filtering, thorough washing with DMF for three times. The sample was degassed first at RT for 6 h, then heated to 180°C at a heating rate of 1°C/min, and held at that temperature for 12 h under degassing in vacuum. (*The boiling point of DMF is 153°C.*)

The specific steps for preparation of the bridged samples and sample pretreatment for isotherm measurements include:

1. IRMOF-8 (200 mg), 10% Pt/AC catalyst (25 mg), and sucrose (33.2 mg) were ground together for 1 h. (*Very gentle “grinding” with mortar and pestle to achieve uniform mixing; ball-milling may destroy the structure due to high energy; particle size compatibility is important.*)
2. This mixture was transferred to a quartz boat that was placed in a tubular reactor. The mixture was heated in flowing helium (100 mL/min) at a heating rate of 1°C/min to 200°C and held at this temperature for 3 h. (*The sample was piled in the quartz boat, not spread as a layer. The melting point of sucrose is 186°C.*)
3. Subsequently the temperature was increased at 1°C/min to 250°C and held for 12 h. The material was cooled to RT at 1°C/min in flowing helium. (*Higher temperatures could destroy the structure of MOFs.*)
4. The samples were stored in vacuum before being moved into the sample holder for high-pressure measurements. (*Use of a vacuum helps to avoid or minimize the decomposition of MOFs that could result from exposure to ambient air.*)
5. Approximately 200 mg of sample was used for isotherm measurement. Prior to measurements, the samples were degassed in vacuum at 200°C for 24 h. Pretreatment at lower temperatures would not be adequate to activate the catalyst.

3.5.4 Spillover on Boron-Substituted Carbon Materials

Following Zhang and Alavi (2007), APCI performed DFT-LDA calculations to examine whether it is energetically possible to move H_2 molecules into bulk BC_3 through the edge planes. Based on these calculations, APCI found that the overall activation barrier for H_2 migration and dissociative chemisorption in bulk BC_3 is quite modest (~30 kJ/mol). Thus, it is expected that H_2 diffusion through the slit pore into the bulk BC_3 lattice would be facile at near-ambient conditions. This is in sharp contrast to the analogous process in graphite, in which H_2 diffusion from the gas phase into the bulk is known to be very

difficult (Mitchell et al. 2003). Within the BC_3 lattice, the H_2 molecule is partially activated on arrival at the transition state, as evidenced by the elongated H-H bond distance. This quasi-dissociated state is maintained as the H_2 molecule continues its migration toward the center of the unit cell, where the H-H bond is abruptly ruptured to form the C-H bonds. The relaxation of the C atom where H is chemisorbed is relatively modest, and the neighboring B atom moves out of the BC_3 plane toward the opposite direction of the absorbed H. The lattice relaxation on H absorption in BC_3 is significantly smaller than that for graphite, in which the C atom that forms a bond with H is puckered out the plane by several tenths of an angstrom (Sha and Jackson 2002). These results suggest that H_2 diffusion into the slit pore of BC_3 is facile, and the intercalated H_2 will undergo spontaneous dissociation to form covalent bonds with C atoms. These C-H bonds might be sufficiently labile to allow the H atoms to diffuse throughout the lattice in a thermally activated process, which would make BC_3 a highly promising hydrogen-storage material with good capacity and facile desorption kinetics.

In particular, BC_3 would be an ideal media to store hydrogen via hydrogen spillover. It should be more efficient than the materials that have been used as hydrogen spillover substrates to date, because it would require no metal catalyst to promote the release of storage hydrogen by the dissociation of molecular H_2 . Thus, a critical issue is related to the reliability of the LDA calculations, because LDA is known to overestimate binding energies. Furthermore, because the intercalation of H_2 into the BC_3 lattice leads to H-H bond dissociation and C-H bond formation, generalized gradient approximation (GGA) should be a more appropriate method to describe the energetics. In contrast to the exothermic process predicted by the LDA calculation, this process was found to be moderately endothermic by ~ 46 kJ/mol. The calculated energy barrier of *ca.* 60 kJ/mol is also higher than the value obtained with LDA. Nevertheless, both the GGA-calculated thermochemistry and the activation barrier are modest, suggesting that H_2 diffusion into bulk BC_3 and the subsequent dissociative chemisorption near the edge could be facile at near-ambient conditions.

Some of the best results occurred with B-doped carbon materials synthesized on an activated carbon template. Specifically, B-doped-carbon on activated carbon with a SSA of only $750\text{ m}^2/\text{g}$ was coated with 8% w/w ruthenium particles 2–5 nm in size (see Figure 3-72). A hydrogen-adsorption transient occurred at every step, with greatly improved kinetics such that the maximum adsorption was achieved approximately 25 times faster than for similar carbon materials (10 min versus 4–6 h). Finally, although the total adsorption of 1.2%–1.5% w/w was only comparable to other state-of-the-art materials, the surface area of this new material was only one-fifth that of typical spillover sorbents. Future efforts need to focus on increasing the surface area of the templated B-doped materials in an attempt to improve on these extremely promising results.

Based on APCI's calculations, the HsCOE investigated the use of boron-substituted materials for spillover. At the very least, boron substitution may help stabilize catalyst particles for use in weak-chemisorption hydrogen storage. Although issues with SSA and B concentrations must be resolved, initial evaluations indicate that BC_x materials with a

Ru catalyst provide highly reproducible and reversible spillover that is 20% to 30% above the base material (Figure 3-72).

In general, the capacities of even the non-Ru-containing materials are substantially higher on a per-SSA basis (i.e., 750 m²/g) compared to activated carbons. The higher capacity observed with Ru catalysts, although modest, is well above detection limits, and unlike other materials used for spillover, this Ru/BC_x material is extremely durable, providing identical repeated performance even after multiple air exposures. The other main issue observed with the BC_x material is the substantial enhancement in kinetics where adsorption occurred within minutes, even at the highest pressures. The ruthenium catalyst deposited onto boron-substituted activated carbon material has shown preliminary results indicating weak chemisorption phenomena (spillover).

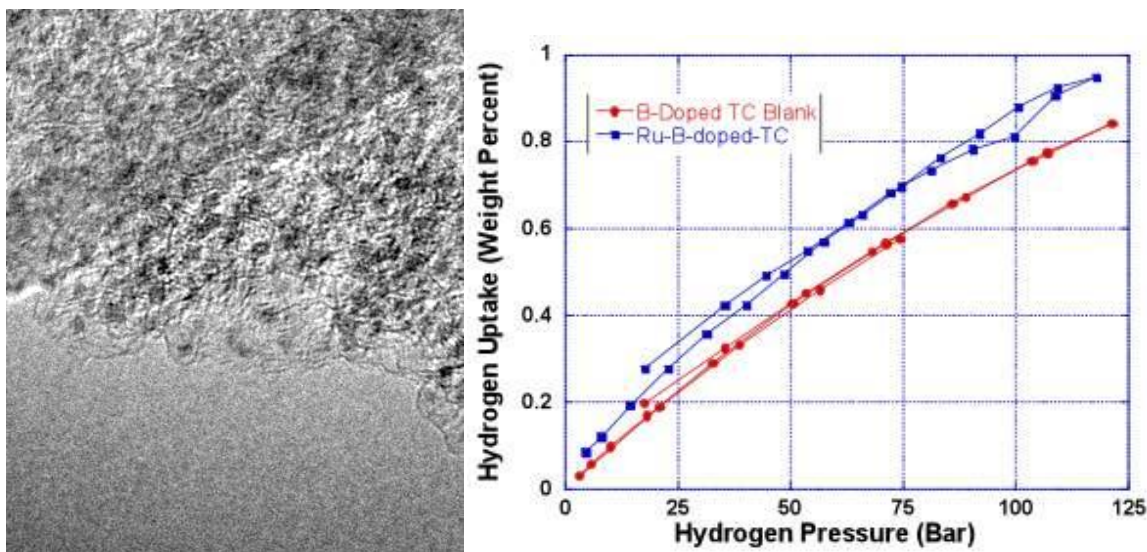


Figure 3-72. TEM image of Ru catalyst on BC_x sorbents (left) and ambient-temperature isotherm data (right) of BC_x and Ru catalyst on BC_x sorbents. These results demonstrate the enhanced reversible hydrogen-storage capacity of the BC_x sorbent with a Ru catalyst, consistent with a spillover mechanism. Each hydrogen pressure step in the isotherm required only ~10 min to equilibrate, substantially shorter than for carbons. Also note that these data have not been corrected for He adsorption during calibration.

Overall, the HSCoE demonstrated that substantial increases in hydrogen-storage capacity can be achieved at ambient temperatures with weak-chemisorption processes such as spillover. Although a significant amount of work is still required to develop highly reproducible and robust materials that have the high capacities demonstrated by the HSCoE with less durable materials, the clear indication is that weak chemisorption is a viable path for on-vehicle refuelable hydrogen storage.

3.5.5 Accelerated Sample Activation Process

NREL developed a new catalyst deposition process that reduces the time to prepare samples for measurement of hydrogen storage from several days to 5 min. This process is very reproducible and provides more uniform dispersion of catalysts within the samples. Using this new technique, NREL measured hydrogen storage via the spillover process consistent with results first published by another HSCoE member, the University of Michigan. The process focused on a new, simple microwave-activation process developed at NREL. Using this process, NREL demonstrated materials that at low pressure had a RT capacity that doubled previous in-house results. Specifically, the NREL team observed a capacity of 0.2 wt. % at 2 bar on platinum-activated carbon samples as compared to an unactivated sample, which had a capacity of only 0.02 wt % (see Figure 3-73). These materials appeared to demonstrate significantly increased adsorption kinetics for the spillover transients; they reached 83% of full capacity in 5 min at 42 bar. For context, Michigan had previously reported the highest low-pressure spillover result on an activated carbon with a value of 0.08 wt. %. The NREL result more than doubled this previous capacity. Also, Michigan previously reported that an 83% capacity was achievable in 20 min. NREL's result improves that by a factor of four. Thus, NREL developed processes that drastically reduced the deposition times and uniformly deposited catalysts with particle sizes to >1 nm with several different metals (e.g., Pt, Pd, Ru) on different types of receptor materials.

The significance of this accomplishment is that, based on the new enhanced kinetics, it should be possible to charge a spillover sample that could reach the theoretical limit of 6.6 wt. % in 5 min, ~100 bar, at RT. Thus, the new results indicate that the spillover process may meet the 2010 gravimetric targets and approach the 2010 rate targets. In addition, assuming a realistic density of the carbon material of 1 g/cm³, it would be possible to exceed the 2010 volumetric targets with a value of 0.06 kg H₂/L for the system.

3.5.6 Synergistic Spillover with Core Shell Materials

NREL also developed a platinum-ceria catalyst to help validate hydrogen spillover and storage (see Figures 3-74 and 3-75). Spillover is the result of dissociating hydrogen with a metal catalyst to form hydrogen atoms that consequently “spill” onto the surface of a receptor material, where they are stored at ambient temperature. The viability of this technology relies on reproducible synthesis, long-term stability, and improved material costs.

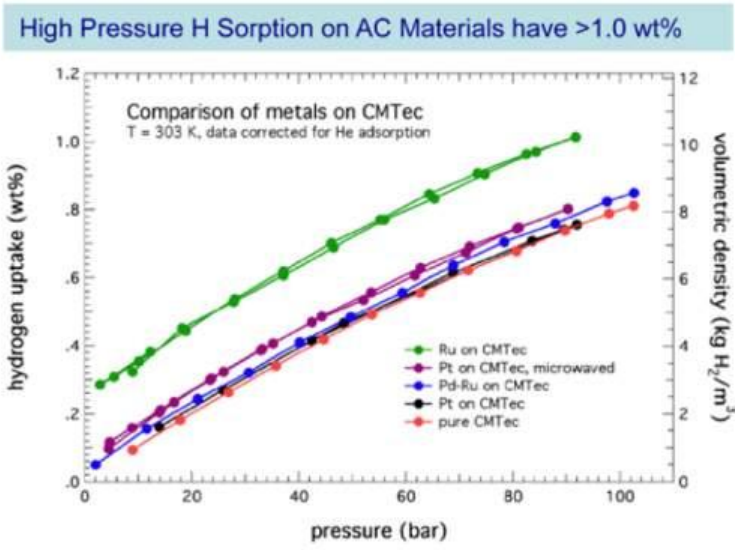
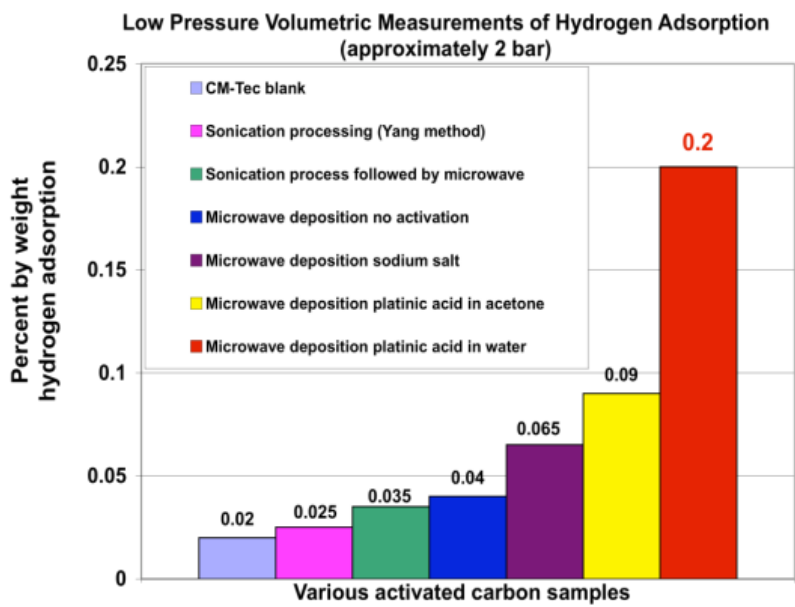


Figure 3-73. Hydrogen spillover results indicate that improved catalyst processing enhances capacity (top). Irreproducibility in the processing often results in limited hydrogen spillover. However, with appropriate processing, hydrogen spillover (e.g., Ru on CM-Tec data) is observed (bottom).

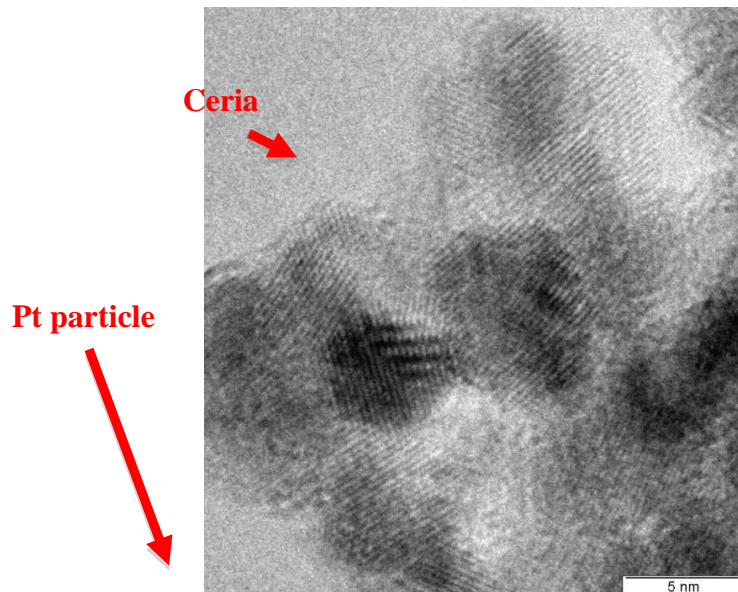


Figure 3-74. TEM image of the core-shell platinum-ceria catalyst that improved hydrogen spillover for storage

NREL achieved reproducible spillover results using a platinum-ceria catalyst on activated carbon with no loss of hydrogen-storage capacity after multiple cycles at both high and low pressures. Initial tests indicated that a 20% platinum-ceria-loaded activated carbon material provides ~1 wt % hydrogen storage at ~120 bar and RT (see Figure 3-75). This is comparable with platinum-activated carbon, despite the substantial decrease in SSA resulting from incorporating ceria and the reduction in total platinum content by a factor of eight.

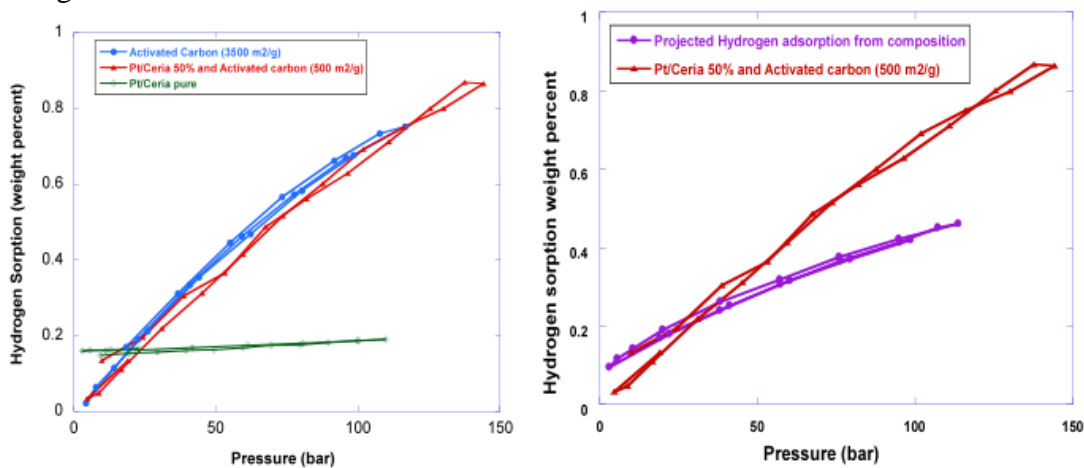


Figure 3-75. Pt-Ceria core shell materials mixed with an MSC-30 activated carbon matrix. Typically, the isolated core-shell nanoparticles were on the order of 3–5 nm. The hydrogen-sorption properties of the resultant materials were evaluated via low- to high-pressure volumetric adsorption at RT from 1–140 bar. The total gravimetric hydrogen adsorption is almost double that expected from the mixture if there were no synergistic/catalytic effect. Improving the catalyst/receptor interface appears to enhance spillover.

The platinum-ceria catalyst is a known spillover material used in various catalytic processes. The ceria helps stabilize the encapsulated ~2-nm platinum particles on the carbon matrix, inhibiting the catalyst agglomeration during repeated cycles. The ripening or coarsening of the catalyst, as known in fuel cell applications, will otherwise reduce the spillover capacities. The ceria also allows the spillover hydrogen to travel to the carbon receptor.

Using these materials, NREL established the validity of using a bridge to improve hydrogen-storage rate and capacity. Although these sorption rates were very slow, about 10 h to reach saturation, they did demonstrate the possibility of enhancing spillover and bridging of the catalyst to the sorbent matrix with the goal of improving durability. By encasing platinum with ceria, platinum or other metal catalysts are stabilized, which improves the reproducibility of the materials and enables direct integration with less-stable materials. Because the metal materials are partially coordinated with the oxides, core-shell catalyst materials prevent the metal particles from agglomerating, which reduces performance. Furthermore, core-shell materials are less mobile on the receptor surfaces compared with pure metals; thus, again the performance will not degrade. Both accomplishments will lead to substantially improving the durability and enhancing the lifetime of the spillover material for reversible hydrogen storage. The stability offered by these core-shell materials enables using fewer metals and potentially enables the use of inexpensive catalysts such as nickel. Both accomplishments would reduce catalyst material costs.

3.5.7 Spillover on Ru-Activated Carbon Matrix via Pyrolysis

NREL demonstrated ~1.6% w/w reversible hydrogen adsorption using a ruthenium-activated carbon system (with SSA less than 2500 m²/g) at 160 bar and RT (see Figure 3-76). On a 3000 m²/g material, the rates of desorption of this activated carbon system meet DOE targets. Additional work is needed to optimize the loading/synthetic conditions for this set of materials. To do so, NREL developed new processing that directly pyrolyzes ruthenium acetylacetonate in the presence of activated carbon. The resulting ruthenium metal particles are ~2–3 nm in diameter, but are heterogeneously distributed throughout the matrix. Future work will need to improve dispersion and distribute the catalyst particles uniformly.

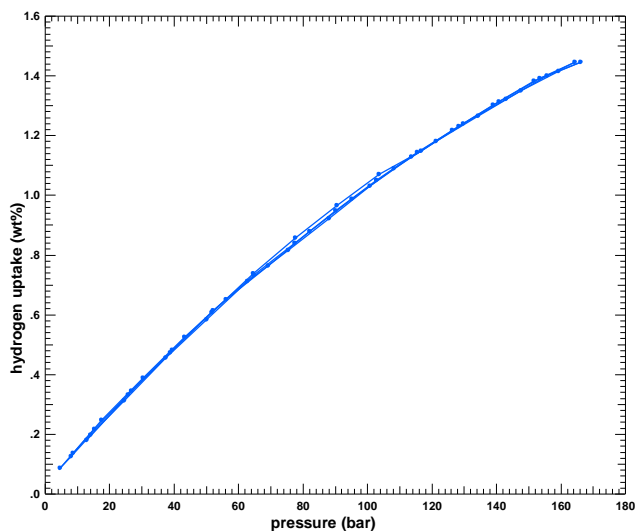


Figure 3-76. Hydrogen spillover capacity of a ruthenium-activated carbon material made via pyrolysis of Ru(acac) in the presence of activated carbon

3.5.8 Spillover of Hydrogen on Pt/Carbon from Pyrolyzed Sucrose Templated on Silica Sphere Templates

For these materials, NREL used materials that were originally developed with thoughts of application to PEM fuel cell systems. NREL found that some of the silica-templated materials had the correct pore distribution and platinum content for possible spillover applications. Porous silica particles are synthesized from tetraethylorthosilicate (TEOS, Purum >98%) silica precursors. The procedure is well outlined in the literature (Olson et al. 2010). Specifically, the NREL team found that the materials that worked best were those processed as follows: the silica is infused with a carbon precursor (sucrose), dried in a vacuum oven at 100°C for 30 min, and then heat-treated at 150°C for 1 h. This material is then saturated dropwise using a platinum precursor and pyrolyzed in N₂ atmosphere for 4 h at 800°C. To remove the silica template powder, after pyrolysis, the sample was soaked in 6 M KOH solution for 4 days, filtered, washed with DI water, and oven-dried at 120°C. The resulting material is shown in Figure 3-77.

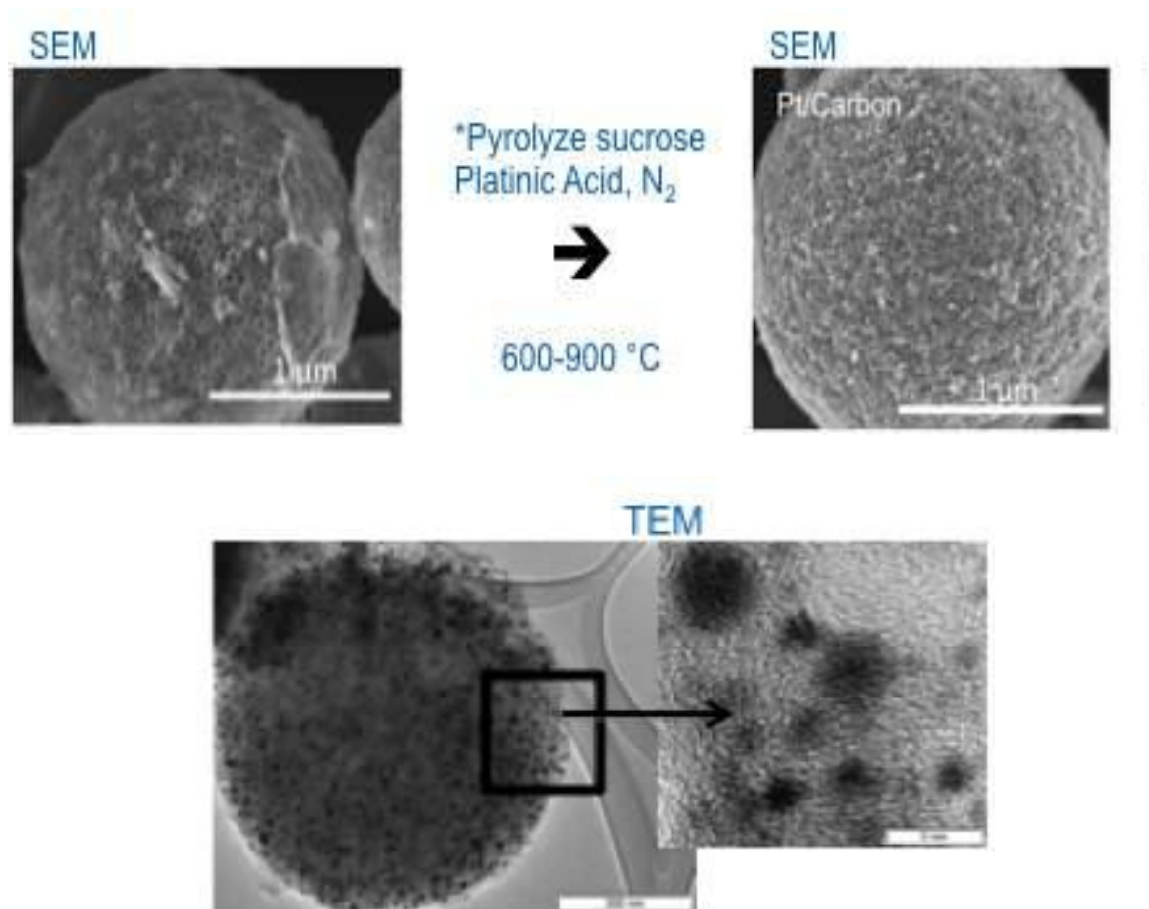


Figure 3-77. Microscopic images of silica-templated carbon matrix of ~600 m²/g prepared according to literature procedures. The platinum-doping level was ~10 wt %. The hydrogen-sorption properties of the material were unique and successful.

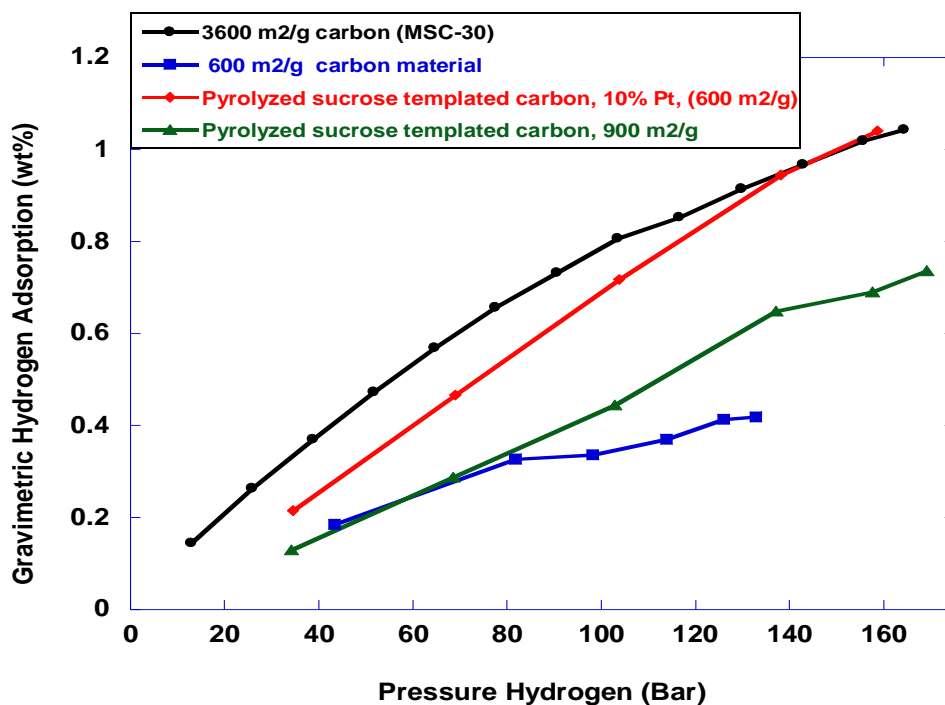


Figure 3-78. Volumetric hydrogen-adsorption isotherms that compare the sorption properties of: (a) black line is a 3600 m²/g activated carbon blank (MSC-30 an ax-21 like material); (b) blue line is a 600 m²/g carbon matrix blank; (c) green line is the 900 m²/gram silica-templated carbon matrix blank; (d) red line illustrates the hydrogen sorption properties of the Pt-carbon silica-templated matrix.

The hydrogen-sorption capacity of the platinum-decorated, silica-templated materials increased >50% from the base templated material with no metal and almost tripled the typical sorption expected for a substrate with a 600 m²/g BET surface area (see Figure 3-78). In summary, the achievements include:

- Excellent kinetics: <5 min to saturation
- First Pt-catalyst-based carbon substrate with spillover enhancement of hydrogen adsorption that was observed at NREL.
- Adsorption of hydrogen was still increasing approximately linearly at 150 bar.
- Minimal irreversibility. Multiple cycles were conducted with no loss of sorption capacity or water/methane formation.
- Unexpected capacity on “small” surface area, 600 m²/g
- Possibility of “hidden” pore structure; aptly positioned catalyst particles at optimal pores led to the “enhanced” adsorption.

3.5.9 Effects of Gaseous Impurities in H₂ and Carbon Surface Oxygen Groups on Spillover Storage

Michigan showed an apparent significant increase in spillover by adsorbing an impurity that is commonly found in H₂ such as CH₄. The results illustrate the significant errors related to using the Benson-Boudart method (for estimating the metal dispersion of supported metals) when spillover occurs, particularly that enhanced by gas impurities.

To investigate the effect of methane molecules on the spillover of hydrogen from the Pt surface to the AX-21 carbon surface, CH₄ was presorbed at predetermined pressures before H₂ isotherms were measured, as described previously. The results are shown in Figure 3-79 and Table 3-6. Figure 3-79 shows the effect of methane on hydrogen adsorption. The adsorption capacity of H₂ on Pt/AX-21 varied with the initial pressure of methane. Pre-sorbing with methane in the range of 5.0×10^{-4} to 3.4×10^{-3} atm resulted in significantly increased adsorption of H₂. From Figure 3-79 and Table 3-6, it is seen that the spillover-adsorption amount of H₂ reached the highest value when the initial pressure of methane was at 1.2×10^{-3} atm. At 1.2×10^{-3} atm of methane, the equilibrium adsorption amount of H₂ at 1 atm increased to 8.81 cm³/g standard temperature and pressure (STP) from 4.78 cm³/g STP without methane, i.e., nearly doubled.

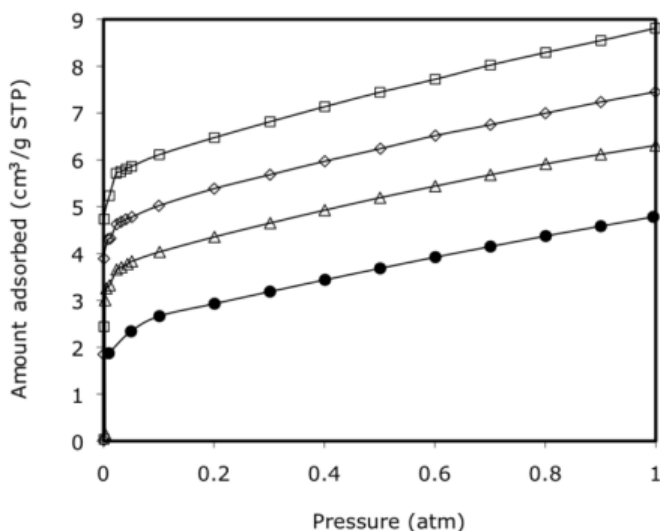


Figure 3-79. Adsorption isotherm of H₂ on Pt/AX-21 at 298 K with presorbed CH₄ at P(CH₄) = 0 (●), 5.0×10^{-4} (◇), 1.2×10^{-3} (□), and 3.4×10^{-3} atm (△). The three presorbed CH₄ points fall essentially on the origin, which is due to the large Y-axis scale.

Table 3-6. Results of CH₄ and H₂ Adsorption on Pt/AX-21

Initial Pressure of CH ₄ (atm)	Saturation Amount of CH ₄ (cm ³ /g, STP) ^a	Saturation Amount of H ₂ (cm ³ /g, STP) ^b	Chemisorption Amount of H ₂ (cm ³ /g, STP) ^c	Platinum Dispersion (%)
0	-	4.78	2.52	73
5.0×10^{-4}	1.5×10^{-2}	7.45	4.92	143
1.2×10^{-3}	3.7×10^{-2}	8.81	5.93	173
3.4×10^{-3}	15×10^{-2}	6.03	3.92×10^{-2}	114

^a The saturation amount of CH₄ was obtained at the corresponding initial pressure of CH₄.

^b The saturation amount of H₂ was obtained at 1.0 atm of H₂.

^c The chemisorption amount of H₂ adsorption was obtained at the equilibrium pressure of H₂ extrapolated to zero.

From the adsorbed amount of hydrogen extrapolated to zero pressure, the dispersion of Pt metal on AX-21 can be calculated according to the method of Benson-Boudart. The adsorption of pure hydrogen on AX-21 was by physical adsorption, because the adsorption capacity at zero pressure by extrapolating the isotherm was $\sim 0 \text{ cm}^3/\text{g}$ at STP (see Figure 3-80). The chemisorption amount at zero pressure on Pt/AX-21 was $2.52 \text{ cm}^3 \text{ STP/g}$ (see Figure 3-80 and Table 3-6). Using the assumption of one H per surface Pt atom, the dispersion using pure H_2 was 73%. However, the dispersion exceeded 100% when H_2 contained a small amount of CH_4 (see Table 3-6). At $1.2 \times 10^{-3} \text{ atm}$ of CH_4 , the dispersion reached 173% because of the enhanced spillover from the CH_4 bridges. Likewise, the dispersion reached 143% and 114% when the initial pressures of methane were at 5.0×10^{-4} and $3.4 \times 10^{-3} \text{ atm}$, respectively. At still higher pressures of CH_4 , competitive adsorption between H and CH_4 occurs, i.e., competition for the most energetic sites, as is the case in all binary mixture adsorption. Such was the case for CH_4 at $3.4 \times 10^{-3} \text{ atm}$. For the pure AX-21, neither hydrogen spillover nor the promotion effect of CH_4 on hydrogen adsorption was found (see Figure 3-80).

For H_2 storage, high-pressure isotherms were also measured, and the results are shown in Figure 3-80. Figure 3-80 shows that the capacity of pure hydrogen on Pt/AX-21 was 1.20 wt % at 25°C and 100 atm, which is the same with Michigan's previous work. The effect of methane on the H_2 storage at high pressures was similar to that at $< 1 \text{ atm}$. The greatest H_2 storage on Pt/AX-21 appeared at $5.0 \times 10^{-3} \text{ atm}$ of the initial CH_4 pressure. Increasing or decreasing the initial pressure of methane caused the adsorption amounts of hydrogen to decrease. When the pressure of methane was at $5.0 \times 10^{-3} \text{ atm}$, the H_2 storage reached 1.38 wt %, which was $\sim 15\%$ higher than that of pure H_2 adsorption. Taking the area per surface carbon atom as 8.2 \AA^2 , 0.21 H atom was adsorbed per C atom at 100 atm without CH_4 impurity. By preadsorbing CH_4 , the density increased to 0.24 H/C.

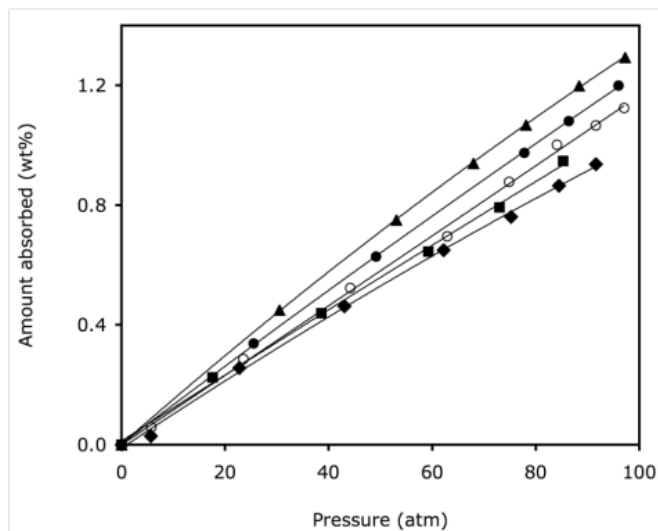


Figure 3-80. Adsorption isotherm of H_2 on Pt/AX-21 at 298K with presorbed CH_4 at $P(\text{CH}_4)=0$ (O), 1.0×10^{-3} (●), 5.0×10^{-3} (▲), 1.0×10^{-2} (■), and 0.1 atm (◆) (Wang and Yang 2008).

One of the factors determining the spillover-storage amounts is the surface chemistry of the receptor. NREL and Michigan found that doping carbon by heteroatoms including oxygen had strong effects. One may expect, therefore, that a receptor exhibiting stronger interaction with hydrogen molecules or atoms would be favorable for hydrogen adsorption. In a hydrogen-spillover system, the presence of oxygen groups (as will be shown for molecular orbital calculations) leads to stronger adsorption for the spilled-over hydrogen, thus an enhanced storage capacity could be expected on an oxygen-modified carbon receptor. However, the effect of oxygen in carbons on hydrogen storage via spillover has not been reported.

Carbon materials with oxygen groups can be obtained by oxygen doping or direct synthesis. Compared with boron or nitrogen doping, addition of surface oxygen groups to a carbon receptor is an easy process. As for direct synthesis, graphite oxide is a well-known carbon material with abundant oxygen groups. Since the first report in 1855 on the synthesis of graphite oxide by oxidizing graphite with $\text{KClO}_3/\text{HNO}_3$, graphite oxide has been prepared through various routes and studied by many authors. By considering these aspects, the Michigan team prepared two different carbons of super-activated carbon (AX-21) and graphite oxide doped with Pd metals, and investigated the effects of surface oxygen in these carbons on hydrogen storage via spillover.

The following three doped carbons were first prepared (using NaBH_4 as the reducing agent): 10 wt % Pd doped on AX-21 (Pd/AX-21); 10 wt % Pd doped on oxygen-modified AX-21 (Pd/AX-21-O); and 10 wt % Pd doped on graphite oxide (Pd/graphite oxide). Elemental analysis by XPS (O/(C+O): w/w) indicated oxygen content in Pd/AX-21-O was about 13 wt %, whereas in the graphite oxide it was approximately 40 wt %.

High-pressure hydrogen isotherms at 298 K for plain AX-21, Pd/AX-21, and Pd/AX-21-O samples are shown in Figure 3-81. In Figure 3-81, AX-21 exhibited a hydrogen-storage capacity of 0.61 wt % at 298 K and 10 MPa, which is in agreement with previous results. By doping 10 wt % Pd on AX-21 sample, the hydrogen uptakes on Pd/AX-21 and Pd/AX-21-O at 10 MPa were enhanced to 0.98 and 1.15 wt %, respectively. It can be seen that both Pd/AX-21 and Pd/AX-21-O samples exhibited much higher hydrogen-adsorption capacities than the plain AX-21 sample. The enhanced hydrogen-storage capacity cannot be attributed to the differences in SSA, because the doped samples have, in fact, lower SSAs than plain AX-21, as is evident from nitrogen-adsorption results. The enhancement in hydrogen storage was due to the spillover of atomic hydrogen from metal particles to AX-21. The enhancement of hydrogen storage by metal-doped carbon materials has been observed. It is significant that Pd/AX-21-O had a higher storage capacity than Pd/AX-21. Normalized by the BET SSA, the Pd/AX-21-O adsorbed 22% more hydrogen than Pd/AX-21. The surface oxygen groups on Pd/AX-21-O were responsible for this enhanced capacity. The enhancement is much stronger for graphite oxide. For the $1000 \text{ m}^2/\text{g}$ SSA of Pd/graphite oxide, the amount of spillover storage is 1.4 wt %. The result is significant for meeting the DOE targets.

An effective way to add oxygen functional groups on carbon surfaces is by O₂ plasma treatment. A templated carbon (TC) was thus treated with glow-discharge plasma, and designated as TC-Plasma. The pressure in the plasma cell was adjusted to the range of 100–200 Pa, and the glow-discharge plasma was generated by applying 5000 V to the electrodes using a DC high-voltage generator with oxygen as the plasma-forming gas. Details are described elsewhere (Wang, Yang, and Yang 2010).

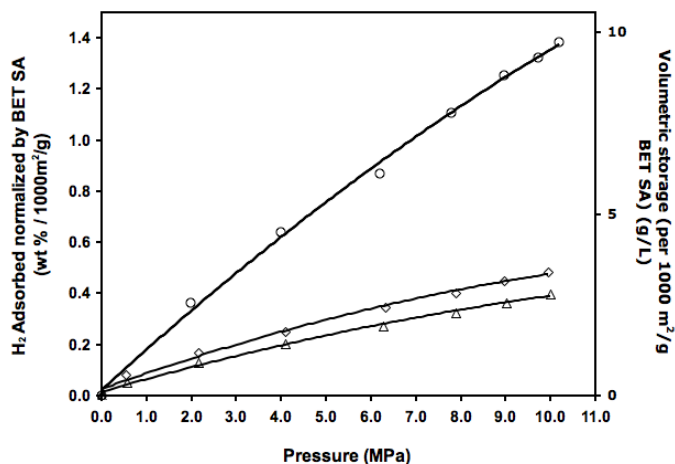


Figure 3-81. High-pressure hydrogen isotherms at 298 K for 10% Pd/graphite oxide (○), 10% Pd/AX-21-O (◇), and 10% Pd/AX-21 (△), normalized by the BET SSA. The BET SSAs are: 2466 m²/g for Pd/AX-21 and 2362 m²/g for Pd/AX-21-O, and 687 m²/g for Pd/graphite oxide (Wang et al. 2009).

It is shown that the enhancement is greater by oxygen plasma treatment compared to air oxidation, because different surface groups were formed. The surface groups were determined by XPS. Oxygen plasma treatment generated mainly semiquinone (C=O) groups, whereas air oxidation formed mainly hydroxyl (C-OH) groups. Experimental heats of adsorption, XPS analyses, and ab initio molecular orbital calculations showed that the binding energies between the spilled-over hydrogen and different groups followed the order lactone > semiquinone > carboxyl > basal plane. Thus, the H₂ storage capacity at 298 K and 10 MPa was increased from 1.17 wt % (without O₂ treatment) to 1.74 wt % on Pt-doped templated carbon that was pretreated with O₂ plasma. However, there was a decrease in storage capacity during the first three adsorption/desorption cycles (at 298 K and 10 MPa). The results are shown in Figures 3-82 and Table 3-7. The capacity decreased from 1.74 to 1.30 wt % and remained unchanged after three cycles. XPS results showed that this decrease was caused by the very strong (and irreversible) binding of the spilled-over hydrogen with the lactone groups (HO-C=O). Nonetheless, the main groups of semiquinone remain functional as receptor sites upon cycling, and the 1.32 wt % storage capacity is among the highest reversible capacities reported in the literature.

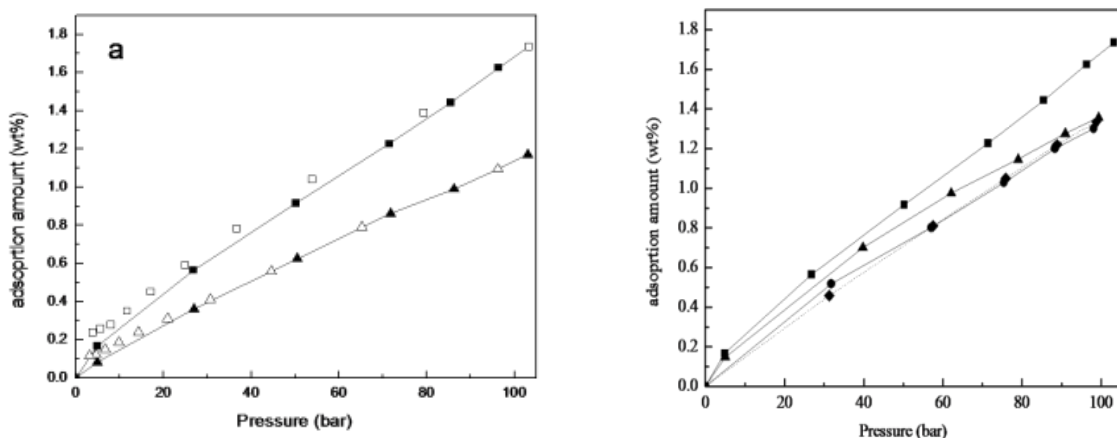


Figure 3-82. (Left) High-pressure hydrogen isotherms at 298 K for 6 wt % Pt doped on various carbons. Adsorption (■) and desorption (□) on Pt/TC-O (via O₂ plasma); adsorption (▲) and desorption (Δ) on Pt/TC (not oxidized). (Right) Cyclic adsorption/desorption of H₂ on 6 wt % Pt/TC-plasma: first cycle (■), 1.75 wt % at 100 atm; second cycle (▲), 1.36 wt %; third cycle (●), 1.32 wt %; and fourth cycle (◆), 1.32 wt % (Wang, Yang, and Yang 2010).

Table 3-7. XPS Relative Subpeak Area of C_{1s} of the Untreated and Oxygen Plasma-Treated Carbon (Wang, Yang, and Yang 2010)

S.A. and XPS (C _{1s} Rel. Area)	TC	TC Plasma	Pt/TC Plasma 4th cycle
BET S.A., m ² /g	3554	3110	
C-C (284.6eV)	89.43%	65.08%	67.53%
C-OH (286.1eV) Hydroxyl	4.61%	5.72%	6.37%
C=O (287.6eV) Semiquinone	3.77%	25.76%	25.13%
-O-C=O (289.6eV) Lactone	2.19%	3.44%	0.97%

3.5.10 Catalysts for Increasing the Rates of Spillover

To increase the rates of spillover, Michigan explored the doping of metal salts to study possible catalytic effects of, for example, TiF_3 on hydrogen spillover on Pt-doped carbon. By doping 2 wt % TiF_3 , the rates for both adsorption and desorption were significantly increased. The results are summarized in Figure 3-83. The rates were monitored at different steps with pressure increasing or decreasing. Figure 3-83 shows only one such step, but the results for other steps were similar. The H_2 isotherms on the Pt/Maxsorb and metal salt-doped samples were similar, with slight decreases in the amounts adsorbed caused by the slightly lower BET SSAs on TiF_3 doping. The rates were expressed in terms of fractional completion versus time on each pressure-increase step. Here, Pt-Maxsorb- TiF_3 (473 K) denotes that the doped sample was heat-treated at 473 K, whereas the other sample was heat-treated at 673 K. XPS results indicated that C-F bonds were formed in the sample and that the sample heat-treated at 673K had more C-F bonds, and consequently stronger catalytic effects.

Two other species demonstrated enhanced kinetics and spillover results comparable to Pt-AC materials. NREL synthesized catalysts via microwave processing for deposition of metals and for use in defined pore structures within templated materials. As shown in Figure 3-84, NREL demonstrated the ability to improve Ru-CM-Tec adsorption rates by increasing the single-step hydrogen overpressure from 10 bar: 5 min, 65% and 30 min, 90% of saturation, to 42-bar step: 5 min, 83% and 12 min, 90% of saturation. In the case of templated carbon materials, the saturation was obtained almost instantaneously (~3 min), and the mechanism of this process suggests a different pathway than occurs in classic spillover results.

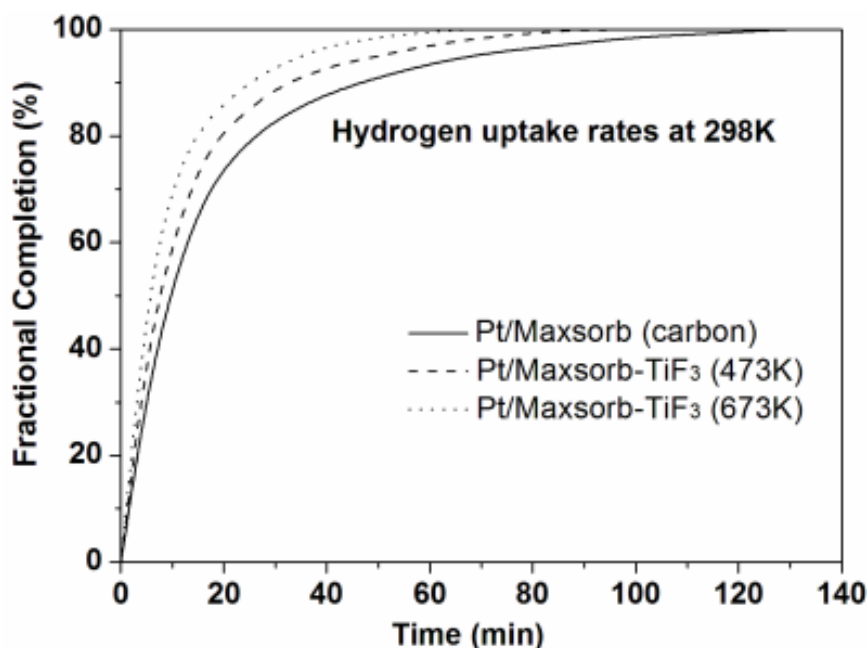


Figure 3-83. Hydrogen desorption rates on Pt/Maxsorb, Pt/Maxsorb- TiF_3 -A, and Pt/Maxsorb- TiF_3 -B at 298 K. Pressure step: (a) 77.7–52.8 atm for Pt/Maxsorb; (b) 78.1–53.1 atm for Pt/Maxsorb- TiF_3 -A; (c) 77.9–52.9 atm for Pt/Maxsorb- TiF_3 -B.

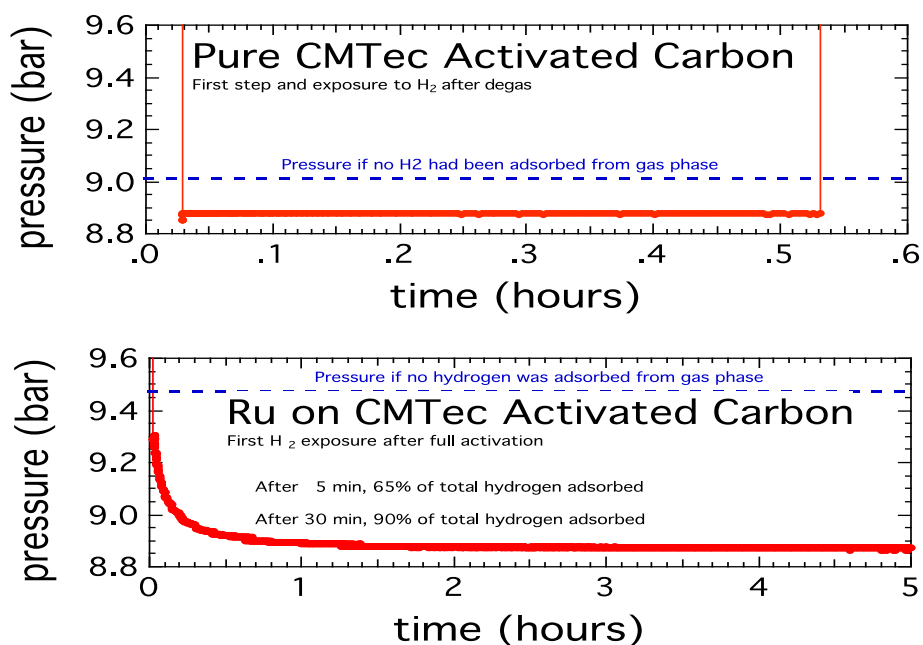


Figure 3-84. These results illustrate the change in hydrogen-sorption behavior from a receptor only (pure CM-Tec) to a Ru-decorated CM-Tec material. The significance of this accomplishment is that based on the new enhanced kinetics, it should be possible to charge a spillover sample so that it could reach the theoretical limit and be saturated at 6.6 wt % in 5 min, at ~100 bar and RT. Thus, the new results indicate that the spillover process may meet the DOE 2010 gravimetric targets and approach the 2010 rate targets. Additionally, assuming a realistic density of the carbon material of 1 g/cm³, it would be possible to exceed the 2010 volumetric targets with a system value of 0.06 kg H₂/L.

3.5.11 Spillover to Zeolites—Toward DOE Volumetric Targets

Zeolites are promising sorbents for achieving high-volumetric storage capacities. This is based on their high bulk densities—two to three times higher than for carbons and MOFs—plus the high densities of cation sites on a variety of zeolites.

Hydrogen-adsorption properties of low-silica type-X zeolites (LSX, Si/Al = 1) (Yang 2003) containing alkali or alkali-earth metal cations (Li⁺, Ca²⁺, and Mg²⁺) were studied in this project. Li-LSX is used commercially for air separation (Yang 2003). The HSCoE found that the hydrogen-adsorption capacities of LSX zeolites at 77 K are determined mainly by the porosity of the zeolite, whereas at 298 K, the storage capacities depend on both the H₂-cation interactions and the porosity. Among the three exchanged zeolites, Li-LSX had the highest H₂ capacity of 1.5 wt % at 77 K and 1 atm, and Ca-LSX had the highest capacity of 0.50 wt % at 298 K and 10 MPa.

Hydrogen storage in LSX zeolites via spillover was also investigated (Wang and Yang 2010). Three methods, including bridge building with a catalyst, metal doping via incipient wetness impregnation, and metal doping via CVD, were employed to induce hydrogen spillover and enhance the storage capacities. The storage capacities were increased to 0.96–1.2 wt % on the Pt-doped zeolites at 298 K and 10 MPa. The

differences between the three methods were compared and discussed. (Wang and Yang 2010) In addition, 5 and 10 wt % Ni were doped on a Ca-LSX zeolite. The 10 wt % Ni-doped Ca-LSX zeolite showed a storage capacity of 1.15 wt % at 100 atm and 298 K. The important volumetric-storage capacities of these zeolites were also estimated based on the densities of the densified zeolites. A density of 21 g/L was obtained for Pt-doped Ca-LSX, and 20 g/L was obtained for Ni-doped Ca-LSX, both at 298 K and 10 MPa. The high volumetric capacities were obtained because of the high densities of zeolites.

LSX

In the LSX study, 5 wt % Pt was doped on Ca-LSX zeolite by CVD of the platinum precursor (trimethyl) methylcyclopentadienyl platinum (IV) and subsequent reduction in a hydrogen atmosphere. The TEM image of CVD-Pt/Ca-LSX showed nanosized Pt (~1–3 nm) was well dispersed on the particles of LSX. The hydrogen-adsorption isotherm at 298 K (Figure 3-85) showed that CVD-Pt/Ca-LSX had a storage capacity of 1.20 wt % at 10 MPa, enhanced by a factor of 2.4 compared with that of plain Ca-LSX (0.5 wt %). Reversibility was evaluated by measuring the desorption branch down to 1 atm. The desorption branch nearly followed the adsorption branch, although there appeared to be a slight hysteresis. The second adsorption isotherm was in agreement with the first one. These results indicated that hydrogen adsorption in the CVD-Pt/Ca-LSX was reversible at 298 K.

In another procedure, 5 wt % Ni was doped on Ca-LSX by incipient wetness impregnation of an aqueous solution of $\text{Ni}(\text{NO}_3)_2 \cdot 6\text{H}_2\text{O}$ and subsequent reduction in a hydrogen atmosphere at 723 K. The TEM image showed that black Ni particles (4–10 nm in size) were dispersed on the LSX zeolites. The loading amount of Ni on Ca-LSX was further increased from 5 to 10 wt % to increase the dissociation sites. As shown in

Figure 3-86, the 10 wt % Ni/Ca-LSX had a storage capacity of 1.15 wt %. Although the loading amount of Ni was doubled, the storage capacity increased only slightly. The volumetric-storage capacity of Ni/Ca-LSX was estimated to be 20 g/L (Figure 3-86) based on the pellet density of 1.7 g/cm^3 . This indicates that Ni/Ca-LSX is a promising sorbent for onboard hydrogen storage.

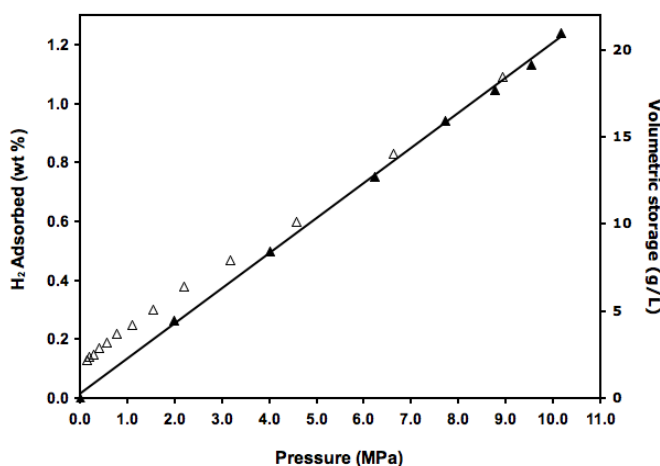


Figure 3-85. High-pressure hydrogen isotherms on CVD-Pt/Li-LSX. Adsorption (▲); desorption (△) at 298 K and 10 MPa (Wang and Yang 2010).

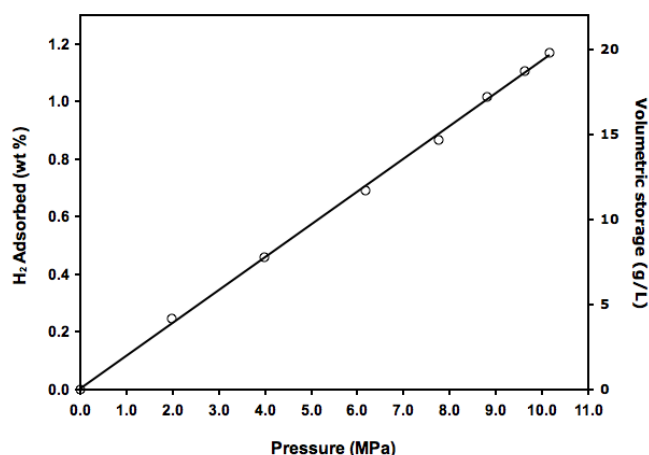


Figure 3-86. High-pressure hydrogen isotherms on 10 wt % Ni/Ca-LSX (O) at 298 K and 10 MPa (Wang and Yang 2010)

3.6 Summary of Development Efforts and Results

A summary of the different sorbent classes and specific materials investigated by the HSCoE is provided in the following tables.

Table 3-8. Summary of Hydrogen Storage Properties for Systems Developed and Investigated for van der Waals-Based, High-Specific-Surface-Area Sorbents

System	Partner(s) Involved	Predicted Capacity (wt %) ^a	Predicted ΔH (kJ/mol H ₂) ^a	Observed ΔH (kJ/mol H ₂)	Maximum Reported Hydrogen Capacity	Status
Pure carbon single-wall nanotubes (SWNTs)	NREL, Rice, Duke, APCI, NIST, UNC	5–10	16–46	19.6	0.01 wt % (223 K, 0 bar) ⁿ 3 wt % (77 K, 20 bar)	Discontinued; predicted reversible capacity not observed.
Fe-decorated carbon multi-walled nanotubes (MWNTs)	NREL	Not predicted	Not predicted	50	0.04 wt % (273 K, 0 bar) ⁿ	No longer considered; high reversible capacity not achieved.
Co-decorated SWNTs	NREL	Not predicted	Not predicted	27.9	0.01 wt % (223 K, 0 bar) ⁿ	No longer considered; high reversible capacity not achieved.
Small-diameter, cut SWNTs	APCI	7	8–18	8–11	1.5 wt % (77 K, 1 atm) ⁿ 0.5 wt % (298 K, 115 bar) ⁿ	Discontinued; high adsorption enthalpy not achieved.

System	Partner(s) Involved	Predicted Capacity (wt %) ^a	Predicted ΔH (kJ/mol H ₂) ^a	Observed ΔH (kJ/mol H ₂)	Maximum Reported Hydrogen Capacity	Status
Undoped activated carbon aerogels	LLNL, Caltech	6+	Not predicted	~6 kJ/mol	5.3 wt % (77 K and 30 bar) ^m 0.8 wt % at RT and 100 bar	Reached maximum capacity that was below DOE target. Additional tuning needed.
Double-walled carbon nanotubes (DWNTs)	Duke	Not predicted	Not predicted	Not measured	0.11 wt % (77K, 2 bar) ⁿ	Reported improvement in DWNTs not observed in measurements.
Pyrolyzed PEEK	Duke	Not predicted	Not predicted	Not measured	5.2 wt % and >35 g/L (77K, 20 bar) ^m	Excellent bulk density due to small uniform pore sizes
Pyrolyzed corncobs	Missouri	Not predicted	Not predicted	4–8	>5 wt % and >30 g/L (77K, 20 bar) ^m	Good bulk density due to small uniform pore sizes
Porous organic polymers	ANL	Not predicted	Not predicted	4–15	>3 wt % and >20 g/L (77 K, 30 bar) ^m	Must increase specific surface area (SSA), good bulk density
Scaffolded graphene	Rice	Not predicted	Not predicted	Not measured	>3 wt % (77K and 20 bar) ^m	Further optimization required
Alkali metal-intercalated graphite	Caltech	~4	4–15	4–13	1.5 wt % (77K and 3 bar) ^m	Model system, will not meet DOE targets
Templated carbon	NREL	4–8	7–8 wt %	4–10	~5 wt % (77K and 40 bar) ^m	Further optimization required
Frame-works	TAMU, UCLA	4–15	7–8 wt %	4–12	>7 wt % and >20 g/L (77K, 20 bar) ^m	Must increase bulk density to improve vol. capacities
Pyrolyzed conducting polymers	Penn	Not predicted	Not predicted	Not measured	<1 wt % (77K) ⁿ	Discontinued due to lack of performance
Nanotube scaffolds	Rice	4–8	6–8 wt %	Not measured	Not measured	Theoretical design of materials

- a. Predicted storage capacities and ΔH are based on first-principles models with an accurate accounting of probable reversible hydrogen-storage capacity for idealized conditions. The idealized conditions (e.g., pressure and temperature) will depend on several factors including the ΔH and entropy of the storage materials/system.
- m. Maximum excess adsorption quantities
- n. Not a maximum excess adsorption quantity, just a directly measured value at the temperature and pressure provided.

Table 3-9. Summary of Hydrogen Storage Properties for Systems Developed and Investigated for Substituted Sorbents

System	Partner(s) Involved	Predicted Capacity (wt %) ^a	Predicted ΔH (kJ/mol H ₂) ^a	Observed ΔH (kJ/mol H ₂)	Maximum Reported Hydrogen Capacity	Status
B-substituted SWNTs produced from B-containing graphite target	NREL, NIST	4 (capacity for 10 kJ/mol -H ₂)	10	4	2 wt % (77 K, 20 bar) ⁿ	Discontinued; at 1.8 at %, maximum boron loading was too low.
Li-, N-, O-, Na-substituted carbon	NREL	~7 wt	4	Not measured	Not measured	These substituted elements do not increase binding compared to just pure C.
Lithium-doped SWNTs	APCI	Not predicted	Not predicted	6.5–10.5	0.7 wt.% (77 K, 1 bar) ⁿ	Discontinued; small observed capacity.
F-intercalated carbons	APCI	1–8	4–24 (for range of 1–8 wt %)	8–14	0.24 wt % at 298 K, 100 bar) ⁿ	Discontinued; small observed capacity.
Pyrolyzed B-C precursors	Penn State	6–8	10–15	~11	2–3 wt % (77 K, 20 bar) ^m	Must increase SSA and B concentration.
Templated BC _x	NREL, Penn State, APCI	6–8	10–15	~11	2–3 wt % (77 K, 20 bar) ^m	Must increase SSA and B concentration.
B-, N-, P-substituted graphene	Rice	Not predicted	Not predicted	Not measured	1–2 wt % (77 K, 2 bar) ⁿ	Must increase SSA and B concentration.
Substituted porous organic polymers	ANL	Not predicted	Not predicted	Not measured		No significant enhancement
B ion implantation	Missouri	Not predicted	Not predicted	4–8		No significant enhancement

a. Predicted storage capacities and ΔH are based on first-principles models with an accurate accounting of probable reversible hydrogen-storage capacity for idealized conditions. The idealized conditions (e.g., pressure and temperature) will depend on several factors including the ΔH and entropy of the storage materials/system.

m. Maximum excess adsorption quantities

n. Not a maximum excess adsorption quantity, just a directly measured value at the temperature and pressure provided.

Table 3-10. Summary of Hydrogen-Storage Properties for Systems Developed and Investigated for Strong/Multiple Dihydrogen Binding-Based Sorbents

System	Partner(s) Involved	Predicted Capacity (wt %) ^a	Predicted ΔH (kJ/mol H ₂) ^a	Observed ΔH (kJ/mol H ₂)	Maximum Reported Hydrogen Capacity (wt %)	Comments
Fe-(C ₆₀)	NREL	3.5	60	4	0.5 (77 K, 2 bar) ⁿ 1 (77 K, 85 bar)	Discontinued; theoretical capacity/structure not observed.
Li ₁₂ (C ₆₀)	NREL	9	6	6	0.2 (77 K, 2 bar) ⁿ 0.1 (RT, 500 torr) [*]	Discontinued; reversible capacity not observed due to LiH formation.
Na-(C ₆₀)	NREL	-	-	-	1 (RT, 500 torr) [*]	No longer considered due to high H ₂ desorption temperature.
Ca ₃₂ (C ₆₀)	ORNL, NREL	8.4	20	6	0.25 (77 K, 2 bar) ⁿ 1.1 (RT, 500 torr) [*]	Discontinued; high reversible capacity not observed due to CaH formation.
K ₆ (C ₆₀)	NREL	-	-	-	0.004 (RT, 2 bar) ⁿ 0.06 (77 K, 2 bar) ⁿ	Discontinued due to high desorption temperature and low capacity.
Sc-(C ₆₀)	NREL	-	-	-	0.02 (RT, 2 bar) 0.04 (77 K, 2 bar) ⁿ	Discontinued due to high desorption temperature and low capacity.
Cr-(C ₆₀)	NREL	-	-	-	0.02 (RT, 2 bar) ⁿ 0.5 (77 K, 2 bar) ⁿ	Discontinued due to high desorption temperature and low capacity.

System	Partner(s) Involved	Predicted Capacity (wt %) ^a	Predicted ΔH (kJ/mol H ₂) ^a	Observed ΔH (kJ/mol H ₂)	Maximum Reported Hydrogen Capacity (wt %)	Comments
Co-(C ₆₀)	NREL	-	-	-	0.01 (RT, 2 bar) ⁿ 0.12 (77 K, 2 bar) ⁿ	Discontinued due to high desorption temperature and low capacity.
Met-Car (Ti ₈ C ₁₂ , Zr ₈ C ₁₂)	NREL, Penn State	3.7–6.1	15–60	-	-	Discontinued due to air sensitivity of the sample.
HKUST-1 MOF	NIST, U Sydney, A.U.	~4	-	6.6	3.26 (77 K, 30 bar) ⁿ	H ₂ binding strength weak
PCN-12 MOF	TAMU	-	-	12.5	3.0 (77 K, 1 bar) ⁿ	Highest reported isosteric heat of adsorption (at low coverage)
PCN-12' MOF	TAMU	-	-	7.13	2.4 (77 K, 1 bar) ⁿ	H ₂ binding strength weak
PCN-9 MOF (Co)	TAMU	-	-	10.1	1.53 (77 K, 1 bar) ⁿ	H ₂ binding strength weak
PCN-9 MOF (Fe)	TAMU	-	-	6.4	1.06 (77 K, 1 bar) ⁿ	H ₂ binding strength weak
PCN-9 MOF (Mn)	TAMU	-	-	8.7	1.26 (77 K, 1 bar) ⁿ	H ₂ binding strength weak
Fe-BTT MOF	NIST, U.C. Berkeley	-	-	11.9	3.7 (77 K, 15 bar) ^m 0.51 (298 K, 100 bar) ⁿ	Isosteric heat of adsorption is directly related to H ₂ binding at coordinatively unsaturated Fe ²⁺ centers within the framework (at low coverage).
Mn-BTT MOF	NIST, U.C. Berkeley	-	-	10.1	5.1 (77 K, 30 bar) ^m 0.95 (298 K, 90 bar) ⁿ	Isosteric heat of adsorption is directly related to H ₂ binding at coordinatively unsaturated Mn ²⁺ centers within the framework (at low coverage).

System	Partner(s) Involved	Predicted Capacity (wt %) ^a	Predicted ΔH (kJ/mol H ₂) ^a	Observed ΔH (kJ/mol H ₂)	Maximum Reported Hydrogen Capacity (wt %)	Comments
Cu-BTT MOF	NIST, U.C. Berkeley	-	-	9.4	4.2 (77 K, 30 bar) ^m 0.48 (298 K, 85 bar) ⁿ	Isosteric heat of adsorption is directly related to H ₂ binding at coordinatively unsaturated Cu ²⁺ centers within the framework (at low coverage).
MOF-74 (Zn)	NIST, Caltech	-	-	8.8	2.8 (77 K, 30 bar) ^m	Extremely high SPD, H ₂ binding strength too weak (at low coverage)
Prussian blue analogues	NIST, U.C. Berkeley	-	-	7.4	1.8 (77 K, 1 bar) ⁿ	Low SSA and H ₂ binding strength
Nickel metal complexes on functionalized inorganic aerogel supports	NREL, LLNL	-	-	20.5 (at low coverage)	0.29 (77 K, 2 bar) ⁿ	On scaling up the synthesis of the Ni-supported aerogel materials, the new H ₂ binding sites were not reliably reproduced and metal agglomeration was not avoided.
Organometallic scandium complex with multiple dihydrogen ligands	NREL	~9	~29	-	-	Sc sites were not coordinatively and electronically unsaturated in materials synthesized.
Li/THF graphite-intercalation compounds	NREL	5.7	9 BTT 22	-	0.52 (77 K, 2 bar) ⁿ 0.06 (RT, 2 bar)	Discontinued; theoretical capacity /structure not observed.
Na/THF graphite intercalation compounds	NREL	-	-	-	0.06 (77 K, 2 bar) ⁿ 0.05 (RT, 2 bar) ⁿ	Discontinued due to low capacity

System	Partner(s) Involved	Predicted Capacity (wt %) ^a	Predicted ΔH (kJ/mol H ₂) ^a	Observed ΔH (kJ/mol H ₂)	Maximum Reported Hydrogen Capacity (wt %)	Comments
Li/BC ₈ on CM-Tec activated carbon	NREL	-	-	~20	0.27 (77 K, 2 bar) ⁿ 0.22 (RT, 2 bar) ⁿ 0.52 (RT, 100 bar) ⁿ	TPD measurements revealed reversible desorption of H ₂ at <50°C following RT H ₂ exposure.
Hydrogenated SWNTs (sodium reduced)	NREL	-	-	-	1.5 (RT, 500 torr) [*]	H ₂ was reversibly loaded onto carbon matrix, but desorption temperature was too high (200°C).
Organometallic Ti fragments on GO sheets	NREL/RPI	4.9	14 BTT 41	-	-	TPD measurements revealed evidence for new enhanced H ₂ binding sites, low H ₂ capacity.
Ca on COF-5	NREL/RPI	5.6	~15	-	0.84 (77 K, 2 bar) ⁿ	TPD measurements did not reveal enhanced H ₂ binding sites; loss of SSA due to strong interaction with NH ₃ prevented access to H ₂ binding sites.
2.7 H ₂ -Ti-Amor-silica (T)	NREL	2.4 H ₂ /Ti	31		2.7 H ₂ /Ti	Theory agrees with experiment
CaC ₁₄ (H ₂) ₈ (T)	NREL	>10 wt % and >100 g/L	20 BTT 40			Proof of unique Ca properties for RT storage

* Temperature-programmed desorption measurement

- a. Predicted storage capacities and ΔH are based on first-principles models with an accurate accounting of probable reversible hydrogen-storage capacity for idealized conditions. The idealized conditions (e.g., pressure and temperature) will depend on several factors including the ΔH and entropy of the storage materials/system.
- m. Maximum excess adsorption quantities
- n. Not a maximum excess adsorption quantity, just a directly measured value at the temperature and pressure provided.

Table 3-11. Summary of Hydrogen Storage Properties for Systems Developed and Investigated for Weak Chemisorption Materials

System	Partner(s) Involved	Predicted Capacity	Predicted ΔH (kJ/mol H ₂)	Observed ΔH (kJ/mol H ₂)	Maximum Reported Hydrogen Capacity ⁿ	Status
Ti-6Al-4V-decorated SWNTs	NREL	Not predicted	Not predicted	Not measured	3.76 wt % (77 K, 85 bar)	No longer considered; high desorption temperature.
Pd-doped nanofibers	NIST, ORNL	Not predicted	Not predicted	Not measured	Not Measured	Did not observe much spillover H using neutrons.
NaAlH ₄ -doped AX-21	Michigan	Not predicted	Not predicted	Not measured	<1% (298 K, 100 atm)	No longer considered; H ₂ amount too low.
Pt-NaAlH ₄ -doped AX-21	Michigan	Not predicted	Not predicted	Not measured	1% (298 K, 100 atm)	No longer considered; H ₂ amount too low.
LiCl-doped MOF-177	Michigan	Not predicted	Not predicted	Not measured	-	Lower than undoped MOF
Pt-bridged MCM-41 (mesoporous silica, BET~1200)	Michigan	Not predicted	Not predicted	Not measured	0.65% (298 K, 100 atm)	No longer considered; H ₂ amount too low.
Pt-bridged COF-1	Michigan	Not predicted	Not predicted	Not measured	0.7% (298 K, 100 atm)	No longer considered; H ₂ amount too low.
Hg-Pd codoped AX-21	Michigan	Not predicted	Not predicted	Not measured	Not measured	Adding Hg decreased spillover compared to Pd alone.
Pt-doped activated carbon fibers (Osaka Gas)	Michigan	Not predicted	Not predicted	Not measured	Not measured	No longer considered; H ₂ amount too low.
Pd-doped on MOF-177	Michigan	Not predicted	Not predicted	Not measured	Not measured	Succeeded in reducing Pd <200°C, but H ₂ amount too low.
Pt-bridged ZIF-8	Michigan	Not predicted	Not predicted	Not measured	0.95% (298 K, 100at m)	Although ZIF-8 is the only H ₂ O-stable MOF, capacity is too low to continue.

System	Partner(s) Involved	Predicted Capacity	Predicted ΔH (kJ/mol H ₂)	Observed ΔH (kJ/mol H ₂)	Maximum Reported Hydrogen Capacity ⁿ	Status
Pt-bridged MIL-53	Michigan	Not predicted	Not predicted	Not measured	0.92% (298 K, 100 atm)	No longer considered; H ₂ amount too low.
Pt-doped on N-doped carbon	Michigan	Not predicted	Not predicted	Not measured	Not measured	No longer considered; H ₂ amount too low.
Hopping spillover kinetics	NREL	8 wt %, 70 g/L	10–30	Not measured	Not measured	Predicted method to increase rates and capacities.
Hole-assisted kinetics	NREL	8 wt %, 70 g/L	10–30	Not measured	Not measured	Predicted method to increase rates and capacities
Ru-, Pt-, Pd-C spillover	Michigan, NREL	8 wt %, 70 g/L	10–30	10–30	1–3 wt % (298 K, >100 bar) ⁿ	Capacities continue to improve with improved catalyst, surface treatments, and higher pressure.
Pt-, Ru-, Pd-bridged MOF	Michigan, NREL	8 wt %, 70 g/L	10–30	10–30	>4 wt % (298 K, >100 bar) ⁿ	Needs improved stability
Pd-Hg graphite oxide	NCSR Demokritos, Greece	Not predicted	Not predicted	Not Measured	<0.15 wt% irreversible	Substantial irreversible H storage
Pt-SWNHs	ORNL	Not predicted	Not predicted	Not measured	~1.5 wt % (298 K, 100 bar) ⁿ	Observed formation of C-H interaction with neutron scattering
Ru-BC _x	NREL	8 wt %, 70 g/L	10–30	10–30	>1 wt % (298 K, >100 bar) ⁿ	Needs improvement

n. Unless specifically stated, the material capacities listed are not a maximum excess adsorption quantity, just a directly measured value at the temperature and pressure provided.

3.7 References

- Andreoni, W.; Giannozzi, P.; Parrinello, M. (1995). "Molecular Structure and Chemical Bonding in K_3C_{60} and K_6C_{60} ." *Phys. Rev. B* (51:4); pp. 2087–2097. <http://link.aps.org/doi/10.1103/PhysRevB.51.2087>.
- Balde, C.P.; Hereijgers, B.P.C.; Bitter, J.H.; de Jong, K.P. (2006). "Facilitated Hydrogen Storage in $NaAlH_4$ Supported on Carbon Nanofibers." *Angew. Chem. Int. Ed.* (45:21); pp. 3501–3503. [10.1002/anie.200504202](http://dx.doi.org/10.1002/anie.200504202).
- Baumann, T.F.; Worsley, M.A.; Han, T.Y.; Satcher, Jr., J.H. (2008). "High Surface Area Carbon Aerogel Monoliths with Hierarchical Porosity." *J. Non-Cryst. Solids* (354:29); pp. 3513–3515. <http://dx.doi.org/10.1016/j.jnoncrysol.2008.03.006>.
- Benard, P.; Chahine, R. (2001). "Determination of the Adsorption Isotherms of Hydrogen on Activated Carbons above the Critical Temperature of the Adsorbate over Wide Temperature and Pressure Ranges." *Langmuir* (17:6); pp. 1950–1955. <http://dx.doi.org/10.1021/la001381x>
- Berseth, P.A.; Harter, A.G.; Zidan, R.; Blomqvist, A.; Araujo, C.M.; Scheicher, R.H.; Ahuja, R.; Jena, P. (2009). "Carbon Nanomaterials as Catalysts for Hydrogen Uptake and Release in $NaAlH_4$." *Nano Lett.* (9:4); pp. 1501–1505. <http://dx.doi.org/10.1021/nl803498e>.
- Bogdanovic, B.; Brand, R.A.; Marjanovic, A.; Schwickardi, M.; Tolle, J. (2000). "Metal-Doped Sodium Aluminium Hydrides as Potential New Hydrogen Storage Materials." *J. Alloy. Compd.* (302:1–2); pp. 36–58. [http://dx.doi.org/10.1016/S0925-8388\(99\)00663-5](http://dx.doi.org/10.1016/S0925-8388(99)00663-5).
- Bogdanovic, B.; Schwickardi, M. (1997). "Ti-Doped Alkali Metal Aluminium Hydrides as Potential Novel Reversible Hydrogen Storage Materials." *J. Alloy. Compd.* (253); pp. 1–9. [http://dx.doi.org/10.1016/S0925-8388\(96\)03049-6](http://dx.doi.org/10.1016/S0925-8388(96)03049-6).
- Brown, H.C.; Kramer, G.W.; Levy, A.B.; Midland, M. (1975). *Organic Syntheses via Boranes*. New York: John Wiley and Sons.
- Brusilovsky, D.; Selig, H.; Vaknin, D.; Ohana, I.; Davidov, D. (1988). "Graphite Compound with BF_3/F_2 : Conductivity and its Relation to Charge Transfer." *Synthetic Met.* (23:1–4); pp. 377–384. [http://dx.doi.org/10.1016/0379-6779\(88\)90510-3](http://dx.doi.org/10.1016/0379-6779(88)90510-3).
- Cansado, I.P.P.; Goncalves, F.; Carrott, P.J.M.; Carrott, M. (2007). "High Micropore Activated Carbon Prepared from Polyetheretherketone." *Carbon* (45:12); pp. 2454–2455. <http://dx.doi.org/10.1016/j.carbon.2007.07.004>.
- Carlson, G.; Lewis, D.; McKinley, K.; Richardson, J.; Tillotson, T. (1995). "Aerogel Commercialization: Technology, Markets and Costs." *J. Non-Cryst. Solids* (186); pp. 372–379. [http://dx.doi.org/10.1016/0022-3093\(95\)00069-0](http://dx.doi.org/10.1016/0022-3093(95)00069-0).

- Chae, H.C.; Siberio-Perez, D.Y.; Kim, J.; Go, Y.B.; Eddaoudi, M.; Matzger, A.J.; O’Keeffe, M.; Yaghi, O.M. (2004). “A Route to High Surface Area, Porosity and Inclusion of Large Molecules in Crystals.” *Nature* (427:6974); pp. 523–527. <http://dx.doi.org/doi:10.1038/nature02311>.
- Chen, B.S.; Falconer, J.L.; Chang, L. (1991). “Formation and Decomposition of Methoxy Species on a Ni/Al₂O₃ Catalyst.” *J. Catal.* (127:2); pp. 732–743. [http://dx.doi.org/10.1016/0021-9517\(91\)90195-A](http://dx.doi.org/10.1016/0021-9517(91)90195-A).
- Cheng, H.; Cooper, A.C.; Pez, G.P.; Kostov, M.K.; Piotrowski, P.; Stuart, S.J. (2005). “Molecular Dynamics Simulations on the Effects of Diameter and Chirality on Hydrogen Adsorption in Single Walled Carbon Nanotubes,” *J. Phys. Chem. B* (109:9); pp. 3780–3786.
- Chui, S.S.Y.; Lo, S.M.F.; Charmant, J.P.H.; Orpen, A.G.; Williams, I.D. (1999). “A Chemically Functionalizable Nanoporous Material [Cu₃(TMA)₂(H₂O)₃]_n.” *Science* (283:5405); pp. 1148–1150. <http://dx.doi.org/10.1126/science.283.5405.1148>.
- Chung, T.C.M.; Jeong, Y.; Chen, Q.; Kleinhammes, A.; Wu, Y. (2008). “Synthesis of Microporous Boron-Substituted Carbon (B/C) Materials Using Polymeric Precursors for Hydrogen Physisorption.” *J. Am. Chem. Soc.* (130:21); pp. 6668–6669. <http://dx.doi.org/10.1021/ja800071y>.
- Conner, W.C.; Falconer, J.L. (1995). “Spillover in Heterogeneous Catalysis.” *Chem. Rev.* (95:3); pp. 759–788. <http://dx.doi.org/10.1021/cr00035a014>.
- Cote, A.P.; Benin, A.I.; Ockwig, N.W.; O’Keeffe, M.; Matzger, A.J.; Yaghi, O.M. (2005). “Porous, Crystalline, Covalent Organic Frameworks.” *Science* (310:5751); pp. 1166–1170. <http://dx.doi.org/10.1126/science.1120411>.
- de Jongh, P.E.; Wagemans, R.W.P.; Eggenhuijen, T.M.; Dauvillier, B.S.; Radstake, P.B.; Meeldijk, J.D.; Geus, J.W.; de Jong, K.P. (2007). “The Preparation of Carbon-Supported Magnesium Nanoparticles Using Melt Infiltration.” *Chem. Mater.* (19:24); pp. 6052–6057. <http://dx.doi.org/10.1021/cm702205v>.
- de Leon, S.A.G.; Grange, P.; Delmon, B. (1997). “Characterization by Temperature-Programmed Reduction of Non-Conventional Catalysts for Hydrotreatment.” *Catal. Lett.* (47:1); pp. 51–55. <http://dx.doi.org/10.1023/A:1019099309001>.
- Dinca, M.; Dailly, A.; Liu, Y.; Brown, C.M.; Neumann, D.A.; Long, J.R. (2007). “Observation of Cu²⁺–H₂ Interactions in a Fully Desolvated Sodalite-Type Metal–Organic Framework.” *Angew. Chem. Int. Ed.* (46:9); pp. 1419–1422. <http://dx.doi.org/10.1002/anie.200604362>.
- Dinca, M.; Dailly, A.; Liu, Y.; Brown, C.M.; Neumann, D.A.; Long, J.R. (2006). “Hydrogen Storage in a Microporous Metal–Organic Framework with Exposed

Mn²⁺ Coordination Sites.” *J. Am. Chem. Soc.* (128:51); pp. 16876–16883.
<http://dx.doi.org/10.1021/ja0656853>.

Ding, R.G.; Lu, G.Q.; Yan, Z.F.; Wilson, M.A. (2001). “Recent Advances in the Preparation and Utilization of Carbon Nanotubes for Hydrogen Storage.” *J. of Nanoscience & Nanotechnology* (1:1); pp. 7–30.

DOE (2006). Go/No-Go Decision: Pure, Undoped Single Walled Carbon Nanotubes for Vehicular Hydrogen Storage U.S. Department of Energy (DOE) Hydrogen Program.
www.hydrogen.energy.gov/pdfs/go_no_go_nanotubes.pdf.

DOE (2008). *Recommended Best Practices for the Characterization of Storage Properties of Hydrogen Storage Materials*.
www.eere.energy.gov/hydrogenandfuelcells/pdfs/bestpractices_h2_storage_materials.pdf

Fang, Z.Z.; Kang, X.; Wang, P.; Cheng, H. (2008). “Improved Reversible Dehydrogenation of Lithium Borohydride by Milling with As-Prepared Single-Walled Carbon Nanotubes.” *J. Phys. Chem. C* (112:43); pp. 17023–17029.
<http://dx.doi.org/10.1021/jp803916k>.

Furukawa, H., et al. (2010). “Ultrahigh Porosity in Metal-Organic Frameworks,” *Science*, (329:5990); pp. 424–428. <http://dx.doi.org/10.1126/science.1192160>.

Gagliardi, L.; Pyykko, P. (2004). “How Many Hydrogen Atoms Can Be Bound to a Metal? Predicted MH₁₂Species.” *J. Am. Chem. Soc.* (126:46); pp. 15014–15015.
<http://dx.doi.org/10.1021/ja0459911>.

Glugla, P.G.; Bailey, K.M.; Falconer, J.L. (1989). “Activated Formation of a H-CO Complex on Ni/Al₂O₃ Catalysts.” *J. Catal.* (115:1); pp. 24–33.
[http://dx.doi.org/10.1016/0021-9517\(89\)90004-3](http://dx.doi.org/10.1016/0021-9517(89)90004-3).

Gross, A.F.; Ahn, C.C.; Van Atta, S.L.; Liu, P.; Vajo, J.J. (2009). “Fabrication and Hydrogen Sorption Behaviour of Nanoparticulate MgH₂ Incorporated in a Porous Carbon Host.” *Nanotechnology* (20:20); pp. 204005-1–204005-6. <http://dx.doi.org/10.1088/0957-4484/20/20/204005>.

Gross, A.F.; Vajo, J.J.; Van Atta, S.L.; Olson, G.L. (2008). “Enhanced Hydrogen Storage Kinetics of LiBH₄ in Nanoporous Carbon Scaffolds.” *J. Phys. Chem. C* (112:14); pp. 5651–5657. <http://dx.doi.org/10.1021/jp711066t>.

Gutowska, A., et al. (2005). “Nanoscaffold Mediates Hydrogen Release and the Reactivity of Ammonia Borane.” *Angew. Chem. Int. Ed.* (44:23); pp. 3578–3582.
<http://dx.doi.org/10.1002/anie.200462602>.

Hamaed, A.; Trudeau, M.; Antonelli, D. (2008). “H₂ Storage Materials (22KJ/mol) Using Organometallic Ti Fragments as σ -H₂ Binding Sites.” *J. Am. Chem. Soc.* (130:22); pp. 6992–6999. <http://dx.doi.org/10.1021/ja710288g>.

Hodnett, B.K.; Delmon, B. (1986). "Synergy in Catalytic Reactions Involving Hydrogen: Possible Role of Surface-Mobile Species," Chapter 2. Cerveny, L., ed. *Studies in Surface Science and Catalysis*, Vol. 27, Amsterdam: Elsevier; pp. 53–78.

Iijima, S. (1991). "Helical Microtubules of Graphitic Carbon," *Nature* (354); pp. 56–58. <http://dx.doi.org/10.1038/354056a0>.

Jun, S.S.; Joo, H.; Ryoo, R.; Kruk, M.; Jaroniec, M.; Liu, Z.; Ohsuna, T.; Terasaki, O. (2000). "Synthesis of New, Nanoporous Carbon with Hexagonally Ordered Mesostructure." *J. Am. Chem. Soc.* (122:43); pp. 10712–10713. <http://dx.doi.org/10.1021/ja002261e>.

Kabbour, H.; Baumann, T.F.; Satcher, J.H.; Saulnier, A.; Ahn, C.C. (2006). "Toward New Candidates for Hydrogen Storage: High-Surface-Area Carbon Aerogels." *Chem. Mater.* (18:26); pp. 6085–6087. <http://dx.doi.org/10.1021/cm062329a>.

Kosynkin, D.V.; Higginbotham, A.L.; Sinitskii, A.; Lomeda, J.R.; Dimiev, A.; Price, B.K.; Tour, J.M. (2009). "Longitudinal Unzipping of Carbon Nanotubes to Form Graphene Nanoribbons," *Nature* (458); p. 872–876. <http://dx.doi.org/10.1038/nature07872>.

Kubas, G. (2007). "Fundamentals of H₂ Binding and Reactivity on Transition Metals Underlying Hydrogenase Function and H₂ Production and Storage." *Chem. Rev.* (107:10); pp. 4152–4205. <http://dx.doi.org/10.1021/cr050197j>.

Levi, G.; Bamberger, M.; Kaplan, W.D. (1999). "Wetting of Porous Titanium Carbonitride by Al–Mg–Si Alloys." *Acta Mater.* (47:14); pp. 3927–3934. [http://dx.doi.org/10.1016/S1359-6454\(99\)00198-6](http://dx.doi.org/10.1016/S1359-6454(99)00198-6).

Lin, C.F.; Zhang, X.; Lin, H.; Wang, N.; Li, J.B.; Yang, X.Z. (2006). "Synthesis of Ordered Mesoporous Carbon Using MCM-41 Mesoporous Silica as Template." *Adv. Mater. Res.* (11–12); pp. 543–546. <http://dx.doi.org/10.4028/www.scientific.net/AMR.11-12.543>.

Liu, Y.; Brown, C.M.; Neumann, D.A.; Peterson, V.K.; Kepert, C.J. (2007). "Inelastic Neutron Scattering of H₂ Adsorbed in HKUST-1." *J. Alloy. Compd.* (446–447); pp. 385–388. <http://dx.doi.org/10.1016/j.jallcom.2006.12.106>.

Liu, Y.; Kabbour, H.; Brown, C.M.; Neumann, D.A.; Ahn, C.C. (2008). "Increasing the Density of Adsorbed Hydrogen with Coordinatively Unsaturated Metal Centers in Metal–Organic Frameworks." *Langmuir* (24:9); pp. 4772–4777. <http://dx.doi.org/10.1021/la703864a>.

Lochan, R.C.; Head-Gordon, M. (2006). "Computational Studies of Molecular Hydrogen Binding Affinities: the Role of Dispersion Forces, Electrostatics, and Orbital Interactions." *Phys. Chem. Chem. Phys.* (8:12); pp. 1357–1370. <http://dx.doi.org/10.1039/B515409J>.

- Lomeda, J.R.; Doyle, C.D.; Kosynkin, D.V.; Hwang, W.-H.; Tour, J.M. (2008). "Diazonium Functionalization of Surfactant-Wrapped Chemically Converted Graphene Sheets," *J. Am. Chem. Soc.* (130:48); pp. 16201–16206. <http://dx.doi.org/10.1021/ja806499w>.
- Long, J.R.; Yaghi, O.M. (2009). "The Pervasive Chemistry of Metal-Organic Frameworks." *Chem. Soc. Rev.* (38:5); pp. 1213–1214. <http://dx.doi.org/10.1039/b903811f>.
- Lu, X.P.; Nilsson, O.; Fricke, J.; Pekala, R.W. (1993). "Thermal and Electrical Conductivity of Monolithic Carbon Aerogels." *J. Appl. Phys.* (73:2); pp. 581–584. <http://link.aip.org/link/JAPIAU/v73/i2/p581/s1>.
- Ma, S.; Sun, D.; Ambrogio, M.; Fillinger, J.A.; Parkin, S.; Zhou, H.-C. (2007). "Framework-Catenation Isomerism in Metal–Organic Frameworks and Its Impact on Hydrogen Uptake." *J. Am. Chem. Soc.* (129:7); pp. 1858–1859. <http://dx.doi.org/10.1021/ja067435s>.
- Marchand A. (1971). "Electronic Properties of Doped Carbon." Walker P.L., ed. *Chemistry and Physics of Carbon*, Vol. 7, New York: Marcel Dekker; pp. 155–188.
- Mitchell, P.C.H.; Ramirez-Cuesta, A.J.; Parker, S.F.; Tomkinson, J.; Thompsett, D. (2003). "Hydrogen Spillover on Carbon-Supported Metal Catalysts Studied by Inelastic Neutron Scattering. Surface Vibrational States and Hydrogen Riding Modes." *J. Phys. Chem. B* (107:28); pp. 6838–6845. <http://dx.doi.org/10.1021/jp0277356>.
- Nikonorov, Y.I. (1979). "Catalytic Effect of Boron Trifluoride on Graphite Oxidation by Fluorine." *Kinetika i Kataliz* (20:6); p. 1598.
- Nishihara, H., et al. (2009). "High-Pressure Hydrogen Storage in Zeolite-Templated Carbon." *J. Phys. Chem. C* (113:8); pp. 3189–3196. <http://dx.doi.org/10.1021/jp808890x>.
- Olson, T.S.; Pylypenko, S.; Atanassov, P.; Asazawa, K.; Yamada, K.; Tanaka, H. (2010). "Anion-Exchange Membrane Fuel Cells: Dual-Site Mechanism of Oxygen Reduction Reaction in Alkaline Media on Cobalt-Polypyrrole Electrocatalyst," *Phys. Chem C.*, (114:11); pp. 5049–5059. <http://dx.doi.org/10.1021/jp910572g>.
- Orimo, S.; Nakamori, Y.; Eliseo, J.R.; Zuttel, A.; Jensen, C.M. (2007). "Complex Hydrides for Hydrogen Storage." *Chem. Rev.* (107:10); pp. 4111–4132. <http://dx.doi.org/10.1021/cr0501846>.
- Pace, E.L.; Siebert, A.R. (1959). "Heat of Adsorption of Parahydrogen and Orthodeuterium on Graphon." *J. Phys. Chem.* (63:9); pp. 1398–1400. <http://dx.doi.org/10.1021/j150579a014>.
- Pajonk, G.M. (2000). "Contribution of Spillover Effects to Heterogeneous Catalysis." *Appl. Catal. A-Gen.* (202:2); pp. 157–169. [http://dx.doi.org/10.1016/S0926-860X\(00\)00522-6](http://dx.doi.org/10.1016/S0926-860X(00)00522-6).

Parks, D.J.; von H. Spence, R.E.; Piers, W.E. (1995). "Bis(pentafluorophenyl)borane: Synthesis, Properties, and Hydroboration Chemistry of a Highly Electrophilic Borane Reagent." *Angew. Chem. Int. Ed.* (34:7); pp. 809–811.
<http://dx.doi.org/10.1002/anie.199508091>.

Perdew, J.P.; Chevary, J.A.; Vosko, S.H.; Jackson, K.A.; Pederson, M.R.; Singh, D.J.; Fiolhais, C. (1992). "Atoms, Molecules, Solids, and Surfaces: Applications of the Generalized Gradient Approximation for Exchange and Correlation." *Phys. Rev. B* (46:11); pp. 6671–6687. <http://link.aps.org/doi/10.1103/PhysRevB.46.6671>.

Peterson, V.K.; Liu, Y.; Brown, C.M.; Kepert, C. (2006). "Neutron Powder Diffraction Study of D₂ Sorption in Cu₃(1,3,5-benzenetricarboxylate)₂." *J. Am. Chem. Soc.* (128:49); pp. 15578–15579. <http://dx.doi.org/10.1021/ja0660857>.

Poirer E.; Chahine, R.; Bénard, P.; Cossement, D.; Lafi, L.; Mélançon, E.; Bose, T.K.; Désilets, S. (2004). "Storage of Hydrogen on Single-Walled Carbon Nanotubes and Other Carbon Structures," *Appl. Phys. A* (78:7); pp. 961–967. <http://dx.doi.org/10.1007/s00339-003-2415-y>.

Pradhan, B. K.; Harutyunyan, A.R.; Stojkovic, D.; Grossman, J.C.; Zhang, P.; Cole, M.W.; Crespi, V.; Goto, H.; Fujiwara, J.; Eklund, P.C. (2002). "Large Cryogenic Storage of Hydrogen in Carbon Nanotubes at Low Pressures." *J. Mater. Res.* (17:9); pp. 2209–2216.

Prestipino, C., et al. (2006). "Local Structure of Framework Cu(II) in HKUST-1 Metallorganic Framework: Spectroscopic Characterization upon Activation and Interaction with Adsorbates." *Chem. Mater.* (18:5); pp. 1337–1346.
<http://dx.doi.org/10.1021/cm052191g>.

Purewal, J. (2010). *Hydrogen Adsorption by Alkali Metal Graphite Intercalation Compounds*. Ph.D. Thesis. Pasadena: California Institute of Technology.

Richard, M.A.; Bernard, P.; Chahine, R. (2009). "Gas Adsorption Process in Activated Carbon over a Wide Temperature Range above the Critical Point. Part 1: Modified Dubinin-Astakhov Model." *Adsorption* (15:1); pp. 43–51.
<http://dx.doi.org/10.1007/s10450-009-9149>.

Robell, A.J.; Ballou, E.V.; Boudart, M.J. (1964). "Surface Diffusion of Hydrogen on Carbon." *J. Phys. Chem.* (68:10); pp. 2748–2753. <http://dx.doi.org/10.1021/j100792a003>

Roding, R.; Wagberg, T.; Sundqvist, B. (2005). "Structural Properties of the Polymeric Compounds Li_xNa_(4-x)C₆₀." *Chem. Phys. Lett.* (413:1–3); pp. 157–161.
<http://dx.doi.org/10.1016/j.cplett.2005.07.068>.

Rosenthal, G.L.; Mallouk, T.E.; Bartlett, N. (1984). "Intercalation of Graphite by Silicon Tetrafluoride and Fluorine to Yield a Second-Stage Salt C₂₄SiF₅." *Synthetic Met.* (9:4); pp. 433–440. [http://dx.doi.org/10.1016/0379-6779\(84\)90023-7](http://dx.doi.org/10.1016/0379-6779(84)90023-7).

Sermon, P.A.; Bond, G.C. (1974). "Hydrogen Spillover." *Catal. Rev.* (8:1); pp. 211–239. <http://dx.doi.org/10.1080/01614947408071861>.

Sha, X.W.; Jackson, B. (2002). "First-Principles Study of the Structural and Energetic Properties of H Atoms on a Graphite (0 0 0 1) Surface." *Surf. Sci.* (496:3); pp. 318–330. [http://dx.doi.org/10.1016/S0039-6028\(01\)01602-8](http://dx.doi.org/10.1016/S0039-6028(01)01602-8).

Shioyama, H. (2000). "The Interactions of Two Chemical Species in the Interlayer Spacing of Graphite." *Synthetic Met.* (114:1); pp. 1–15. [http://dx.doi.org/10.1016/S0379-6779\(00\)00222-8](http://dx.doi.org/10.1016/S0379-6779(00)00222-8).

Steiner, S.A.; Baumann, T.F.; Kong, J.; Satcher, J.H.; Dresselhaus, M.S. (2007). "Iron-Doped Carbon Aerogels: Novel Porous Substrates for Direct Growth of Carbon Nanotubes." *Langmuir* (23:9); pp. 5161–5166. <http://dx.doi.org/10.1021/la063643m>.

Stephens, R.D.; Gross, A.F.; Van Atta, S.L.; Vajo, J.J.; Pinkerton, F.E. (2009). "The Kinetic Enhancement of Hydrogen Cycling in NaAlH₄ by Melt Infusion into Nanoporous Carbon Aerogel." *Nanotechnology* (20:20); pp. 204018-1–204018-6. <http://dx.doi.org/10.1088/0957-4484/20/20/204018>.

Sumida, K., et al. (2010). "Hydrogen Storage and Carbon Dioxide Capture in an Iron-Based Sodalite-Type Metal–Organic Framework (Fe-BTT) Discovered via High-Throughput Methods." *Chem. Sci.* (1:2); pp. 184–191. <http://dx.doi.org/10.1039/C0SC00179A>.

Sun, Q.; Jena, P.; Wang, Q.; Marquez, M. (2006). "First-Principles Study of Hydrogen Storage on Li₁₂C₆₀." *J. Am. Chem. Soc.* (128:30); pp. 9741–9745. <http://dx.doi.org/10.1021/ja058330c>.

Sun, Y.Y.; Kim, Y.H.; Zhang, S.B. (2007). "Effect of Spin State on the Dihydrogen Binding Strength to Transition Metal Centers in Metal-Organic Frameworks." *J. Am. Chem. Soc.* (129:42); pp. 12606–12607. <http://dx.doi.org/10.1021/ja0740061>.

Teichner, S.J. (1990). "Recent Studies in Hydrogen and Oxygen Spillover and Their Impact on Catalysis." *Appl. Catal.* (62:1); pp. 1–10. [http://dx.doi.org/10.1016/S0166-9834\(00\)82232-0](http://dx.doi.org/10.1016/S0166-9834(00)82232-0).

Tomaselli, M.; Meier, B.H.; Ricco, M.; Shiroka, T.; Sartori, A. (2001). "NMR Evidence for sp³ Carbon in the Low-Temperature Phase of Li_xC₆₀." *Phys Rev. B* (63:11); 113405-1–113405-4. <http://link.aps.org/doi/10.1103/PhysRevB.63.113405>.

Vajo, J.J.; Skeith, S.L.; Mertens, F. (2005). "Reversible Storage of Hydrogen in Destabilized LiBH₄." *J. Phys. Chem. B* (109:9); pp. 3719–3722. <http://dx.doi.org/10.1021/jp040769o>.

Wakefield, B.J. (1988). *Organolithium Methods*. New York: Academic Press.

Wang, Y.H.; Yang, R.T. (2008). "Increased Hydrogen Spillover by Gaseous Impurity: the Benson-Boudart Method for Dispersion Revisited." *J. Catal.* (260:1); pp. 198–201. <http://dx.doi.org/10.1016/j.jcat.2008.09.013>.

Wang, L.; Lee, K.; Sun, Y.-Y.; Lucking, M.; Chen, Z.; Zhao, J.J.; Zhang, S B. (2009). "Graphene Oxide as an Ideal Substrate for Hydrogen Storage." *ACS Nano* (3:10), pp. 2995–3000. <http://dx.doi.org/10.1021/nn900667s>.

Wang, L.F.; Yang, F.H.; Yang, R.T. (2009). "Hydrogen Storage Properties of B- and N-Doped Microporous Carbon," *AIChE J.* (55); pp. 1823–1833. <http://dx.doi.org/10.1002/aic.11851>.

Wang, L.F.; Yang, F.H.; Yang, R.T.; Miller, M.A. (2009). "Effect of Surface Oxygen Groups in Carbons on Hydrogen Storage by Spillover," *Ind. Eng. Chem. Res.* (48:6); pp. 2920–2926. <http://dx.doi.org/10.1021/ie8014507>.

Wang, L.F.; Yang, R.T. (2010). "Hydrogen Storage Properties of Low-Silica Type X Zeolites," *Ind. Eng. Chem. Res.* (49:8); pp. 3634–3641. <http://dx.doi.org/10.1021/ie1003152>.

Wang, Z.; Yang, F.H.; Yang, R.T. (2010). "Enhanced Hydrogen Spillover on Carbon Surfaces Modified by Oxygen Plasma," *J. Phys. Chem. C*; (114:3); pp. 1601–1609. <http://dx.doi.org/10.1021/jp909480d>.

Worsley, M.A.; Satcher, J.H.; Baumann, T.F. (2010). "Influence of Sodium Dodecylbenzene Sulfonate on the Structure and Properties of Carbon Aerogels." *J. Non-Cryst. Solids* (356:3); pp. 172–174. <http://dx.doi.org/10.1016/j.jnoncrysol.2009.12.008>.

Worsley, M.A.; Kucheyev, S.O.; Hamza, A.V.; Satcher, Jr. J.H.; Baumann, T.F. (2009a). "Mechanically Robust and Electrically Conductive Carbon Nanotube Foams." *Appl. Phys. Lett.* (94:7); pp. 073115-1–073115-3. <http://link.aip.org/link/APPLAB/v94/i7/p073115/s1>.

Worsley, M.A.; Kuntz, J.D.; Cervantes, O.; Han, T.Y.; Gash, A.E.; Satcher J.H.; Baumann, T.F. (2009b). "Route to High Surface Area TiO₂/C and TiCN/C Composites." *J. Mater. Chem.* (19:38); pp. 7146–7150. <http://dx.doi.org/10.1039/B911994A>.

Worsley, M.A.; Kuntz, J.D.; Pauzauskie, P.J.; Cervantes, O.; Zaug, J.M.; Gash, A.E.; Satcher, J.H.; Baumann, T.F. (2009c). "High Surface Area Carbon Nanotube-Supported Titanium Carbonitride Aerogels." *J. Mater. Chem.* (19:31); pp. 5503–5506. <http://dx.doi.org/10.1039/B908284K>.

Worsley, M.A.; Satcher, J.H.; Baumann, T.F. (2009). "Enhanced Thermal Transport in Carbon Aerogel Nanocomposites Containing Double-Walled Carbon Nanotubes." *J. Appl. Phys.* (105:8); pp. 084316-1–084316-4. <http://link.aip.org/link/JAPIAU/v105/i8/p084316/s1>.

Worsley, M.A.; Satcher, Jr. J.H.; Baumann, T.F. (2008). "Synthesis and Characterization of Monolithic Carbon Aerogel Nanocomposites Containing Double-Walled Carbon Nanotubes." *Langmuir* (24:17); pp. 9763–9766. <http://dx.doi.org/10.1021/la8011684>.

Yang, Z.; Xia, Y.; Mokaya, R. (2007). "Enhanced Hydrogen Storage Capacity of High Surface Area Zeolite-like Carbon Materials." *J. Am. Chem. Soc.* (129:6); pp. 1673–1679. <http://dx.doi.org/10.1021/ja067149g>.

Yang, R.T. (2003). *Adsorbents: Fundamentals and Applications*. Wiley, Hoboken, NJ. Chapter 7.

Yildirim, T.; Ciraci, S. (2005). "Titanium-Decorated Carbon Nanotubes as a Potential High-Capacity Hydrogen Storage Medium." *Phys. Rev. Lett.* (94:17); pp. 175501-1–175501-4. <http://link.aps.org/doi/10.1103/PhysRevLett.94.175501>.

Yoon, M.; Yang, S.Y.; Hicke, C.; Wang, E.G.; Geohegan, D.; Zhang, Z.Y. (2008). "Calcium as the Superior Coating Metal in Functionalization of Carbon Fullerenes for High-Capacity Hydrogen Storage." *Phys. Rev. Lett.* (100:20); pp. 206806-1–206806-4. <http://link.aps.org/doi/10.1103/PhysRevLett.100.206806>.

Yu, X.B.; Grant, D.M.; Walker, G.S. (2008). "Low-Temperature Dehydrogenation of LiBH_4 through Destabilization with TiO_2 ." *J. Phys. Chem. C* (112:29); pp. 11059–11062. <http://dx.doi.org/10.1021/jp800602d>.

Yu, X.B.; Wu, Z.; Chen, Q.R.; Li, Z.L.; Weng, B.C.; Huang, T.S. (2007). "Improved Hydrogen Storage Properties of LiBH_4 Destabilized by Carbon." *Appl. Phys. Lett.* (90:3); pp. 034106-1–034106-3. <http://link.aip.org/link/APPLAB/v90/i3/p034106/s1>.

Zhang, C.J.; Alavi, A. (2007). "Hydrogen Absorption in Bulk BC_3 : A First-Principles Study." *J. Chem. Phys.* (127:21); pp. 214704-1–214704-7. <http://link.aip.org/link/JCPSA6/v127/i21/p214704/s1>.

Zhang, S.; Gross, A.F.; Van Atta, S.L.; Lopez, M.; Liu, P.; Ahn, C.C.; Vajo, J.J.; Jensen, C.M. (2009). "The Synthesis and Hydrogen Storage Properties of a MgH_2 Incorporated Carbon Aerogel Scaffold." *Nanotechnology* (20:20); pp. 204027-1–204027-6. <http://dx.doi.org/10.1088/0957-4484/20/20/204027>.

Zhang, Y.; Zhang, W.S.; Wang, A.Q.; Sun, L.X.; Fan, M.Q.; Chu, H.L.; Sun, J.C.; Zhang, T. (2007). "LiBH₄ Nanoparticles Supported by Disordered Mesoporous Carbon: Hydrogen Storage Performances and Destabilization Mechanisms." *Int. J. Hydrogen Energy* (32:16); pp. 3976–3980. <http://dx.doi.org/10.1016/j.ijhydene.2007.04.010>.

Zhao, Y.; Kim, Y.-H.; Dillon, A.C.; Heben, M.J.; Zhang, S.B. (2005). "Hydrogen Storage in Novel Organometallic Buckyballs." *Phys. Rev. Lett.* (94:15); pp. 155504-1–155504-4. <http://link.aps.org/doi/10.1103/PhysRevLett.94.155504>.

Zhong, J.; Yao, J.; Kittrell, C.; Tour, J.M. (2011). "Bottom-Up Preparation of Synthetic Graphenes." *American Chemical Society NANO* (5); pp. 4112-4117.

Zhou, O., et al. (1991). "Structure and Bonding in Alkali-Metal-Doped C₆₀." *Nature* (351:6326); pp. 462-464. <http://dx.doi.org/10.1038/351462a0>.

Zhou, W.; Wu H.; Yildirim, T. (2008). "Enhanced H₂ Adsorption in Isostructural Metal-Organic Frameworks with Open Metal Sites: Strong Dependence of the Binding Strength on Metal Ions." *J. Am. Chem. Soc.* (130:46); pp. 15268-15269. <http://dx.doi.org/10.1021/ja807023q>.

Zielinski, J.M.; Coe, C.G.; Nickel, R.J.; Romeo, A.M.; Cooper, A.C.; Pez, G.P. (2007). "High Pressure Sorption Isotherms via Differential Pressure Measurements." *Adsorption* (13:1); pp. 1-17. <http://dx.doi.org/10.1007/s10450-007-9005-9>.

Zlotea, C.; Moretto, P.; Steriotis, T. (2009). "A Round Robin Characterisation of the Hydrogen Sorption Properties of a Carbon Based Material." *Int. J. Hydrogen Energy* (34:7); pp. 3044-3057. <http://dx.doi.org/10.1016/j.ijhydene.2009.01.079>.

Zuttel, A.; Wenger, P.; Rentsch, S.; Sudan, P.; Mauron, P.; Emmenegger, C. (2003). "LiBH₄ a New Hydrogen Storage Material." *J. Power Sources* (118:1-2); pp. 1-7. [http://dx.doi.org/10.1016/S0378-7753\(03\)00054-5](http://dx.doi.org/10.1016/S0378-7753(03)00054-5).

4.0 Major Technical Accomplishments of Center

During its 5 years of operation, the Hydrogen Sorption Center of Excellence (HSCoE) improved sorbent properties to the point that they could be used to meet U.S. Department of Energy (DOE) on-vehicle hydrogen-storage-system targets. Specific accomplishments are described in the following.

1. Designed and developed reversible sorbents via ambient temperature hydrogenation/storage techniques (weak chemisorption) that demonstrated >4 wt % storage capacities with isosteric heats of adsorption between 10 and 30 kJ/mol.

The HSCoE pioneered the development of materials that have relatively low chemical binding of hydrogen, potentially allowing efficient, reversible on-vehicle refueling. This class of materials enables hydrogen-storage-system designs with more than 75% of the volumetric and gravimetric capacities of the materials and substantially reduces system costs and complexity. Hydrogen spillover has been observed on numerous materials for decades. However, prior to the HSCoE, spillover was observed at the ~0.01 wt % level. The HSCoE demonstrated much higher capacities experimentally and developed a substantially improved thermodynamic and kinetic understanding of the processes involved, where the models were validated with known spillover materials, e.g. “hydrogen bronze.” The main issues researchers probed included improving capacities, stability, and charging (refueling) rates.

Calculations indicate that 7–8 wt % (50–60 g/L) capacities at ambient temperature are possible. Hydrogenation experiments have demonstrated 7.5 wt % on carbon samples, albeit these specific results used chemical processes rather than “spillover” to hydrogenate the carbon. First-principles calculations indicate that spillover is thermodynamically viable, with binding in agreement with observed measurements. An improved understanding of spillover kinetics is needed to enable the design of materials with higher capacities and sorption rates that can meet DOE 2015 targets.

In general, weak chemisorption-based hydrogen storage may be able to meet DOE targets if kinetics and stability issues can be appropriately balanced with the thermodynamics needed to create the optimal isosteric heats of adsorption (i.e., 10 to 30 kJ/mol). The kinetics and thermodynamics depend on the functional groups and/or electronic properties on the surface of the receptor materials, which must be appropriately adjusted to be stable over repeated reversible hydrogen loading/discharge cycles. Charging rates, pressures, and receptor materials compositions can all be adjusted to achieve the desired hydrogen-storage properties. Although additional development and optimization work needs to be done, the principles of high-capacity, weak chemisorption-based hydrogen storage have been demonstrated, and the higher storage capacities measured to date have been validated in separate synthesis and measurement laboratories. However, reproducibility and stability remain major issues.

2. Developed new materials that increased the gravimetric (~50%, e.g., from ~5 to >7 wt % at 77 K) and volumetric (~150%, e.g., from ~15 to >35 g/L at 77 K) hydrogen-storage capacities by physisorption onto sorbents with high specific surface area (SSA) by optimizing pore sizes (0.7 to 1.5 nm) to increase SSA and packing density.

The HSCoE partners synthesized new high-SSA physisorption materials with optimized uniform pore sizes using a variety of scalable/inexpensive processes including aerogels, pyrolyzed carbons, templated carbons, and metal-organic frameworks. These optimized pore-structured sorbents can be used to construct hydrogen-storage systems that meet DOE 2015 delivered capacity targets of 5.5 wt % and 40 g/L if appropriate storage temperatures (i.e., 50 to 80 K) and pressures (i.e., 10 to 100 bar) are used. The decreased pressures, compared to high-pressure 350–700-bar storage systems, enabled by relatively inexpensive carbon-based sorbents could substantially reduce tank and balance-of-plant costs.

3. Discovered and demonstrated coordinated, unsaturated metal centers as a new class of hydrogen-storage materials that could meet DOE's targets. Several material systems were demonstrated, and specific synthetic paths based on known materials were identified.

This class of materials includes systems that use low-cost elements/materials that have the potential to meet DOE's ultimate capacity targets, with uniform isosteric heats of adsorption in the range of 15 to 30 kJ/mol for almost the entire capacity. Thus, this class of materials offers the potential to far exceed capacity and energy efficiency capabilities of any other on-vehicle refueling material-based and/or high-pressure storage system.

The HSCoE explored strong multiple binding, discovering and championing an entire new class of viable materials that uses lightweight (e.g., 3-D electron, alkali, and alkali earth metals) metal centers to enhance H₂ isosteric heats of adsorption and enable multiple H₂ binding on each metal site. The pioneering work done by the HSCoE partners spurred on substantial R&D efforts and resulted in hundreds of publications. To meet DOE targets, the HSCoE team leveraged known materials to develop and optimize routes to stabilize multiple hydrogen molecules on a metal atom that exhibit moderate H₂ binding energies. Individual transition metal atoms have been experimentally observed to adsorb 1–7 H₂ molecules with appropriate binding energies, and the theoretical predictions are in quantitative agreement with all known experimental results involving 3-D metals. The key has been and continues to be stably coordinating the metal atoms so that the H₂ molecules can reversibly adsorb/desorb in a hydrogen-storage system.

4. Designed and developed substitutional materials with enhanced dihydrogen binding energy to increase capacities at near ambient temperatures on a per-SSA basis.

By substituting one element into that of another single element structure, materials with enhanced hydrogen isosteric heats of adsorption (e.g., ~11 kJ/mol for B-substituted

carbon, compared to ~5 kJ/mol for pure carbon) can be created to increase capacities at near ambient (e.g., ~200 K) temperatures. Thus, substituted materials have the potential to meet DOE's 2015 hydrogen storage system capacity targets. Increasing storage temperatures to near ambient helps decrease system costs by reducing the amount of insulation, tank, and balance-of-plant costs.

HSCoE researchers created high-SSA B-C material using several different scalable and inexpensive methods. In complete agreement with theoretical calculations, the HSCoE found that these substituted materials required the B to be electronically frustrated with the correct coordination in the carbon lattice (i.e., sp^2 coordination) to increase H_2 binding (e.g., ~11 kJ/mol) and capacities at temperatures approaching ambient. Neutron spectroscopy data showed, for the first time, a large rotational splitting indicative of enhanced H_2 interactions in a B-substituted carbon. Diffuse reflectance infrared Fourier transform spectroscopy measurements showed reversible hydrogen interaction with the B:C material. Future efforts must focus on increasing simultaneously both the boron concentration and SSAs of these substituted materials

5. Developed unique measurement capabilities to accurately and reliably characterize hydrogen-storage properties of small laboratory-scale (1–100 mg) samples to enhance high throughput and rapid screening analysis (isotherms, SSA, pore size distribution, isosteric heats of adsorption, temperature-programmed desorption, nuclear magnetic resonance).

Accurate hydrogen storage property measurements have been a major problem in the community for decades. This has partly been due to only having small quantities of the most novel “laboratory scale materials” to characterize. The Center's investment in developing protocols and measurements capable of providing accurate results from small amounts of sample have substantially enhanced throughput by eliminating the need to develop larger scale synthetic methods or repeating synthesis processes numerous times to make enough material.

6. Confirmed that standard physisorption-based dihydrogen adsorption scales with SSA. To date, no validated experimental evidence exists that any substantial capacity enhancements occur as a result of geometric configurations.

At the outset of the HSCoE's activities, numerous publications had reported extraordinary results for high-SSA materials, in which the enhanced capacities were potentially a result of novel geometries or structures within the material. In general, heats of adsorption can be increased with multiple wall-interactions, but this ultimately reduces capacities. The center did not validate any single-element material or any materials with unexceptional electronic states that have substantially higher hydrogen-storage capacities beyond that expected based on the SSA and specific storage conditions. For example, at one time carbon nanotubes were thought to possibly have unique hydrogen-storage properties, but after a dedicated, focused effort, the HSCoE made a No-Go decision on using carbon nanotubes as an ambient-temperature, hydrogen-storage material. The emphasis here is that even though the heats of adsorption can be increased, the overall

capacity cannot be significantly increased based on geometrical structures alone. Ultimately, if appropriately arrayed, carbon nanotubes may still provide excellent hydrogen storage at cryogenic temperatures.

7. Performed hundreds of systematic investigations, in which the ultimate conclusion for dozens of specific materials and/or processes were that they should not be investigated further for vehicular hydrogen-storage applications.

Identification of paths, processes, and/or materials that should no longer be investigated provides DOE and the hydrogen-storage community with valuable information that can be used to better define and identify future efforts.

5.0 Recommendations

5.1 Review of Go/No-Go Decisions

As mentioned previously, the focused development efforts of the Hydrogen Sorption Center of Excellence (HSCoE) identified a substantial number of materials/material classes that should not be investigated further based on a number of considerations, including detailed selection criteria developed specifically for sorption materials. Based on the nature of the HSCoE's development of hydrogen-storage mechanisms (rather than specific materials), the exact number of materials down-selected is difficult to identify. Through these efforts, the HSCoE was able to quickly pinpoint the few selected material classes and their required properties and stress them for present and future development. For example, regardless of the specific elements used, a pure physisorption material needs to have a specific surface area of more than 2000 to 3000 m²/g (depending on storage temperature used). This requirement alone eliminates hundreds of elements and materials that are just too heavy to be able to meet this requirement if only a van der Waals adsorption of hydrogen is used. Thus, the HSCoE eliminated most alumina silica-based zeolites from further consideration basically at the outset.

Furthermore, through calculations and a limited number of specific experimental investigations, it became clear that only correctly coordinated boron substituted in graphitic carbon is a viable route to improve hydrogen storage for substituted carbon materials, and thus the use of other lightweight elements received little to no additional investigation. In terms of carbon materials, this eliminated the need to perform experimental investigations on hundreds of potential element/process combinations for this material class. Similarly, from the outset, the HSCoE continually evaluated different sorbents to identify the material classes and their corresponding properties that received focused development based on their potential ability to meet U.S. Department of Energy (DOE) hydrogen-storage targets.

The HSCoE formally reviewed all partner projects at the end of Phase I (approximately 18 months after the start in fiscal year [FY] 2005) and redirected projects and specific development efforts based on the progress made and the potential future development capabilities needed. At that time, recommendations were made where subsequently the University of California, Los Angeles, pursued independent development and left the HSCoE, the project at the University of Pennsylvania was stopped based on the lack of any evidence that conducting polymers could provide substantial hydrogen storage at ambient conditions, and most of the carbon-nanotube work was redirected to develop other sorbents. This latter redirection of carbon-nanotube efforts followed an intensive ~18-month effort by several HSCoE partners to reproduce literature results with independent validation of measurements. A formal [go/no-go decision](#) (DOE 2006) for single-walled carbon nanotube (SWNT) sorbents for ambient-temperature hydrogen storage was provided to DOE. This formal no-go decision did not preclude development for cryo-compressed storage, nor the use of SWNTs in other structures or for doped materials.

In FY 2009, the HSCoE formally evaluated the status of sorbents that could meet DOE hydrogen-storage targets and wrote a report for the DOE Office of Energy Efficiency and Renewable Energy Fuel Cell Technologies Program. This HSCoE project deliverable, the [*Hydrogen Sorption Center of Excellence \(HSCoE\) Materials Go/No-Go Recommendation Document*](#), is available on the DOE website (HSCoE 2009). It provides an overview of the work performed by the HSCoE through November 2009; specific recommendations to DOE for materials development efforts that should, and should not, be continued; and a list of key research priorities remaining to be resolved. The center identified clear development paths for constructing sorbent materials that have the potential to meet DOE's revised 2015 and ultimate full-fleet targets (DOE 2009) for light-duty vehicles. The center recommended that development efforts for specific materials/classes be continued where viable routes existed for synthesizing sorbents that could be used to meet DOE's targets. This document is provided in Appendix C.

5.2 Materials/Systems/Classes Recommended for Continued R&D

Because this sorbents go/no-go recommendation was made within the last year, substantial amounts of the recommendations remain pertinent, feeding directly into the recommendations that follow here. At this point in time, which is the formal completion of the HSCoE's research, a specific set of recommendations are as follows:

Overall recommendation: The HSCoE recommends that development efforts for specific material classes be continued where viable routes exist for synthesizing sorbents that can be used to meet the appropriate set of targets. The specific selection criteria for future efforts should focus on the DOE 2015 and the ultimate full-fleet hydrogen storage targets. The focus has been, and should remain, on capacity, kinetics, thermodynamics, and costs. The HSCoE recommends these focus areas because the majority of the other DOE 2015 and ultimate targets for sorbents will be more of a systems-engineering issue than an intrinsic material property issue.

Even when hydrogen binding energies are substantially increased to enable near-ambient-temperature storage, these binding energies (typically 10 to 25 kJ/mol) and the associated entropies of hydrogen should not be an issue. They are low enough that the relatively small amount of heat generated during refueling should be easily removed with the typical sorption material's intrinsic thermal conductivity properties and/or appropriately designed integration of thermal conductivity materials in condensed "pelletized" materials. In addition, because most sorbent materials will likely operate at moderate pressures (i.e., 10 to 100 bar), delivery rates and system pressures should not be significant issues.

In general, a range of temperatures and pressures can be used as long as the materials and systems can be constructed to meet the DOE targets. However, the closer to ambient conditions the system operates, the less expensive the system costs. This must be traded against overall system performance, which includes the potential need for added heat

removal. This need for balance leads to four specific recommendations related to materials, system, and classes.

1. Develop materials for hydrogen storage by weak chemisorption. Ambient-temperature storage via catalytic hydrogen dissociation and transfer to high-SSA receptor materials (e.g., spillover) demonstrates 10 to 30 kJ/mol reversible hydrogen binding energies, which enable ambient-temperature storage. Furthermore, because the binding energies for spillover are much lower than for typical metal or chemical hydrides, thermal management issues for heat removal during refueling and delivery rate issues should be moderate, and thus should not significantly impact the overall storage system. Thus, the center recommends that spillover or equivalent materials continue to be developed for hydrogen storage.

Although some of the processes involved have been demonstrated experimentally and by thermodynamic principles, additional development is needed to further understand and improve atomic hydrogen transport on the receptor material (for uptake/refill and discharge kinetics) and to improve the performance reproducibility and effectiveness of the synthetic processes. Once these issues are addressed, initial analyses indicate that because spillover enables ambient-temperature storage, systems with more than 75% of the material capacities can be achieved using basic pressurized (~100 bar) tanks.

Initial analysis indicates that excess material storage capacities of more than 7 wt % should be possible with spillover. In addition, because spillover should be applicable to materials with more than 1 g/ml bulk density, storage systems with more than 50 g/L and more than 5.5 wt % capacities should be achievable at ambient temperature and ~100 bar. Thus, with inexpensive, carbon-based materials and the development of inexpensive, highly dispersed catalysts (e.g., nanoparticle Ni), spillover materials should be usable in systems that meet DOE's 2015 targets.

2. Develop materials for multiple-dihydrogen storage on designed sites. Although substantial efforts will be needed to form the novel structures, development of multiple-dihydrogen adsorption on designed sites should be continued because the resulting structures could meet DOE ultimate targets—making it one of the few solutions identified with this potential.

Multiple-dihydrogen adsorption on designed sites provides a reasonable path toward meeting DOE's ultimate full-fleet targets (DOE 2009), with the provision that this may require substantial development efforts. Several inexpensive material systems have been predicted that may be used to meet these targets at near-ambient temperature. One prediction includes the use of inexpensive Ca with inexpensive carbon supports to form materials that may be able to store hydrogen at ambient temperature with twice the gravimetric and volumetric densities of liquid hydrogen. Such a structure, if it is possible to synthesize and stabilize, would be a tremendous breakthrough. Meeting DOE's ultimate targets will enable hydrogen to become a viable energy carrier for transportation and other important renewable energy applications.

3. Develop substituted/heterogeneous materials with demonstrated hydrogen binding energies in the range of 10–25 kJ/mol. The center recommends that researchers develop substituted/heterogeneous materials that can be used to enhance dihydrogen isosteric heats of adsorption in the range of 10–25 kJ/mol. These materials will enable near-ambient-temperature (150–250 K) hydrogen storage. Development efforts should focus on creating materials with the appropriate chemical and electronic structures, sufficient composition, and high SSAs. These materials could potentially decrease system hardware costs and constraints and may be used to meet DOE’s 2015 hydrogen storage system targets (40 g H₂/L; 5.5 wt %).

For single-element materials such as carbon, only a few elements (e.g., boron substituted in sp² coordination) substantially enhance dihydrogen binding. However, other heterogeneous systems (e.g., certain MOFs) have demonstrated enhanced dihydrogen binding. In general, the principle is well established; the main issues include access and creating enough high-binding-energy sites to substantially increase capacities. In addition, these heterogeneous materials also demonstrate substantial stabilization of single metal centers and other absorbed species that improve hydrogen storage.

4. Limit development of materials in which the storage mechanism is physisorption to only those with optimized structures. The center recommends that present and future development be performed only on a select set of materials in which the primary storage mechanism is physisorption. To meet the DOE 2015 targets, the only physisorption materials that should be considered for development are those that can have SSAs greater than ~3,000 m²/g, optimized uniform pore sizes in the range of ~0.7 to ~1.5 nm, and excess material hydrogen storage capacities greater than 50 g/L and 7 wt % at cryogenic temperatures (~80–200 K) and moderate pressures (less than 100 bar).

- Although it may be possible to meet the DOE 2015 system targets with high-SSA materials, isosteric heats of adsorption between 10 and 25 kJ/mol will be required to increase storage temperatures to greater than 200 K to significantly improve system capacity and/or costs. Furthermore, near-ambient temperatures will probably be required to meet DOE’s ultimate full-fleet storage targets (DOE 2009). Such targets can be met in a number of ways, including developing specific heterogeneous materials, coordinated but unsaturated metal centers, and weak hydrogenation processes such as spillover.

With currently demonstrated bulk-material packing densities and hydrogen storage properties, sorbents will substantially decrease the volume and pressure now used for high-pressure (350 to 700 bar) compressed tanks, and thus could significantly reduce overall system costs. Future selection criteria should focus further on identifying materials that can be used to meet DOE’s ultimate targets. In addition to the specific performance issues for each material class discussed previously, developing material synthetic processes and pathways that are scalable, inexpensive, and reproducible—and producing materials that can meet the DOE system cost targets—remains a challenge that must be pursued aggressively in all cases.

Again, in general, the main issues for sorbents are the relatively low dihydrogen binding energies, which directly affect storage temperature. This adversely impacts system costs, volumetric capacity, and available gravimetric capacity. Thus, the main focus of future applied development efforts must be on enhancing and/or optimizing hydrogen binding energies. This focus will require balancing improved hydrogen storage system costs and capacities with perhaps adversely affected material-contamination sensitivity, durability, refill rates, and materials' cost issues.

5.3 Suggestions for New Materials Systems To Be Investigated

As discussed previously, the HSCoE identified several material classes that include numerous material systems with the potential to meet DOE 2015 and even ultimate hydrogen storage targets and therefore should be investigated further. The main emphasis for developing new sorbents should be placed on performing systematic investigations with model systems within the material classes the HSCoE has recommended for further development. For example, within the multiple-dihydrogen adsorption class of materials, the Ca-graphene and equivalent systems have been identified as having very good storage capacities and viable synthetic routes. Thus, the HSCoE suggests that future efforts focus on developing sorbents that use the unique properties of coordinated Ca atoms. Similar examples of material systems exist within all the material classes recommended for further investigation. Thus, the main focus for sorbents should be on developing new material systems within the heterogeneous/substitution, multiple dihydrogen adsorption sites, and weak chemisorption material classes.

Based on the work performed by the HSCoE, additional heterogeneous/substitution systems that do not involve carbon should be investigated to determine their potential to meet DOE targets. That said, the HSCoE did not identify any other systems with a clear path to meet these goals, and thus any future efforts must be pursued only after a reasonable route has been identified. Similarly, new multiple dihydrogen or weak chemisorption materials should be developed only after clear paths have been identified to synthesize sorbents that can meet DOE 2015 hydrogen-storage targets, and all experimental evidence is validated.

Finally, improved computational developments are needed to be able to more accurately predict stable material synthesis, as well as the actual pressure- and temperature-dependent hydrogen-storage capacities of designed sorbents.

5.4 Identification of Remaining Issues for Recommended Systems

Each material system and material class has individual and unique challenges that cannot be adequately summarized here (but are discussed in the body of the report). However, sorbents as a whole have common issues that must be adequately addressed. These include the need to:

1. Develop robust, reproducible, and scalable synthetic methods that create materials in which all adsorption sites are accessible to the hydrogen. Whether for high-SSA physisorption materials, weak-chemisorption spillover materials, or other sorption materials, the main issue has been and remains development of improved synthetic methods to create the materials that have been designed for optimum hydrogen storage. Although substantial progress has been made, clear improvements are needed with synthetic processes to form the requisite materials that can be used reproducibly and be scaled up for commercial manufacturing.

2. Improve computational methods to more accurately predict the ability to synthesize designed materials and hydrogen storage capacity as a function of temperature and pressure. In general, HSCoE theorists and experimentalists worked very closely together to design materials that have good hydrogen storage properties and that can be synthesized. However, to advance these efforts further will require that each step and precursor in a process be accurately modeled (as compared to just the end state) so that viable routes to designed materials can be quickly identified computationally before the experiments are performed.

In addition, presently there are no good computational platforms that accurately predict a material capacity as a function of pressure and temperature. Models based on grand canonical Monte Carlo simulation use non-first-principle and/or empirical force fields that require calibration and thus tend to lack the required accuracy for predicting capacities.

3. Develop a better understanding of atomic hydrogen transport on receptor materials. Clearly, the main issue with weak chemisorption is a fundamental lack of understanding of how hydrogen atoms diffuse along the receptor materials. Eliminating this deficiency is critical to ultimately predicting the full potential of and designing optimized spillover materials.

4. Develop a better understanding of metal center coordination and its effect on hydrogen adsorption. Although a rudimentary first-principles understanding exists, a more robust and predictive set of computational tools is needed to enable designing coordinated metal centers that are more stable to environmental contaminants and other degradation mechanisms (i.e., cluster formation), while at the same time are optimized for storing the maximum number of hydrogen molecules.

5. Develop materials in concert with designs for hydrogen storage systems. Development efforts should continue on optimizing the materials needed for specific storage systems. Based on the successes achieved since the center's inception, researchers have created sorbents that have the potential to meet DOE's revised 2010 targets, assuming that storage systems are optimized for the material being used. If sorbents are to be used to meet DOE's 2015 and ultimate targets, it will be even more imperative that storage systems be optimized for the new sorbent materials with higher binding energies and other substantially different but critical performance characteristics. For example, compared to compressed (350 to 700 bar) or cryo-compressed hydrogen storage technologies, which have demonstrated material packing densities and storage properties,

the main benefits of sorption materials include substantial (twofold) reductions in volume, reductions in pressure (~20-fold), and a fourfold or more increase in storage temperature. All of these benefits substantially improve system costs, resonance times for boil-off, and resolution of engineering-design issues. However, capacity and other performance characteristics must be balanced against system costs and overall well-to-tank and in-tank efficiencies.

6. Develop sorbent material measurements standards and certifications. In conjunction with DOE's *Recommended Best Practices for the Characterization of Storage Properties of Hydrogen Storage Materials* (DOE 2008), specific standards, mechanisms for measurement qualifications, and certifications need to be developed with regard to hydrogen storage capacity and some material property measurements. As with standards, qualifications, and certificates that are available for measuring SSAs in highly porous materials, a similar set needs to be developed to ensure that hydrogen storage capacities, isosteric heats of adsorption, and even sub-nanometer pore size distributions are being measured accurately and calculated and reported uniformly.

The cornerstone of materials development is the accurate determination of material properties and performance. For decades, claims of spectacular results that ultimately turned out to be erroneous have plagued the gas-storage community, resulting in loss of valuable time and resources. As interest in hydrogen storage ramps up, the number of publications and results—and the desire to publish/report outstanding results quickly—increases commensurately. This rush to publish results that push the envelope is often at odds with performing detailed measurements that ensure that all of the hydrogen storage metrics being published are rigorously validated. In addition, presently there are no national or international established standards, procedures, or certifications that provide independent qualification of measurement systems and procedures. Thus, the HSCoE recommends that planning and implementation of useful standards and certifications be performed to help the community accelerate materials development and to minimize wasting limited resources on efforts that ultimately serve only to resolve poor measurements.

5.5 Identification of Systems Recommended for No Further Investigation

A complete list of materials and processes recommended for no further R&D has been assembled by the HSCoE. Specific details are provided in the Section 3.6 of this report. Because sorbent materials are arranged more by a specific mechanism than by a system, down-selections can only occur with a given material/process. Thus, in general, future sorbent development should follow the recommendations provided in this document and minimize repeating work that has already been done. Again, only a select few elements and materials will be able to be used in sorbents to meet DOE hydrogen-storage system targets. The key is arranging those elements and materials for optimal hydrogen storage. Thus, future development should eliminate any materials that cannot be used to meet DOE 2015 targets. For sorbents specifically, capacity and cost targets must be fully addressed. This indicates that many of the high-specific-surface-area (SSA) materials

(e.g., many MOFs) that have good gravimetric capacities but poor bulk densities and cannot meet DOE volumetric-capacity targets, even using crystal densities, should be eliminated from further investigation. This will free up resources to focus on MOFs and other materials that are more stable with higher bulk densities and thus higher volumetric capacities and minimize wasting efforts developing inappropriate materials.

5.6 Recommended Storage Options and Material Systems for Early Market Applications

In general, DOE has not defined criteria for early market hydrogen- storage applications, and the HSCoE did not develop sorbents optimized for any application except light-duty vehicles. That said, in general, sorbents provide unique engineering solutions that will be of benefit to many early market applications. For example, optimized high-SSA materials in slightly modified compressed and cryo-compressed tanks will provide substantial improvements over present storage systems for forklifts, buses, and other high-use, short-term storage, transportation, and portable power applications. The main benefits of sorbents, including ease of engineering and enhanced volumetric capacities compared to high-pressure hydrogen, make them ideal to reduce the volume and increase the capacity of the storage systems for buses and forklifts.

5.7 References

DOE (2006). Go/No-Go Decision: Pure, Undoped Single Walled Carbon Nanotubes for Vehicular Hydrogen Storage U.S. Department of Energy (DOE) Hydrogen Program. www.hydrogen.energy.gov/pdfs/go_no_go_nanotubes.pdf.

DOE (2008). *Recommended Best Practices for the Characterization of Storage Properties of Hydrogen Storage Materials*. www.eere.energy.gov/hydrogenandfuelcells/pdfs/bestpractices_h2_storage_materials.pdf

DOE (2009). Targets for Onboard Hydrogen Storage Systems for Light-Duty Vehicles. www.eere.energy.gov/hydrogenandfuelcells/storage/pdfs/targets_onboard_hydro_storage_explanation.pdf.

HSCoE (2009). Hydrogen Sorption Center of Excellence (HSCoE) Materials Go/No-Go Recommendation. www.eere.energy.gov/hydrogenandfuelcells/pdfs/hscoe_recommendation_feb_10.pdf.

6.0 Lessons Learned from the Center Approach

The HSCoE approach opened up collaborations in ways that could not have been attained with any other format. Central to this is the knowledge that the complexity of the problems encountered required skills and talents of multidisciplinary investigators. Efforts based on material classes enabled focus-area experts to work closely together to solve difficult problems. Further, the synthesis of optimized materials required integration of complementary approaches, including joint synthesis, measurement, and structural-characterization facilities, that enabled comprehensive capabilities for all partners. Beyond this, such collaborative work enabled unified support for wider (non-center) researchers. Such collaborations accelerate R&D efforts by months or even years. The center joined partners together in a precompetitive environment. Similarly, it established research directions based on broad expertise and capabilities. This in turn enabled rapid/flexible response to new development. Also important, this team approach allowed fast validation of results.

From an institutional standpoint, consistent funding spanning 5 or more years encourages the focus on the longer-term efforts that are needed to solve complex and difficult problems. Given this span, it becomes incumbent upon participants to make sure that the R&D momentum is retained in detailed knowledge, which assures that past funding is not wasted. The core knowledge gained should be retained within government systems to enable work with all stakeholders and partners throughout the world. The HSCoE's focus on on-board refueling was the most challenging approach possible, but it was clearly needed, because otherwise a migration to easier goals (e.g., off-board regeneration and higher-pressure storage) would have been too tempting.

The joint non-disclosure agreement (NDA) was absolutely essential to success, enabling the openness needed to develop the close working relationships that led to success. Even with the NDA, it took a while to become comfortable with each other and to work as a concerted group. However, once this was achieved and people trusted each other, the HSCoE was able to use resources efficiently, perform joint feasibility analyses for material development selection, and engineer center-wide materials deliverables.

6.1 Lessons Applicable to All R&D Efforts

The joint NDS and direct interaction between partners were key contributors to success. For efficient use of resources, feasibility analyses should be performed for materials-development selection, engineering center materials deliverables, and scale-up. In general, cost analyses must be an integral part of the decision process for all future efforts. Materials design via modeling is an effective tool that must be incorporated in all materials- and process-development activities.

Furthermore, high-throughput combinatorial methods should be incorporated for materials optimization. However, because not all materials discovered can benefit from combinatorial methods, this should not be a requirement for all future materials-development efforts. In general, durability (and thus reactivity) studies should be part of any materials-development effort for materials selected as “promising” and being

considered for engineering evaluations. For the engineering center to develop systems that can meet the DOE 2015 targets, continued new materials (and thus material scale-up) must be integrated into the effort. Thus, materials-synthesis groups must work closely with the engineering center to ensure efficient use of limited resources in this type of activity. Thus, material quantities and qualities may need to be adjusted based on delivery and testing requirements. Markets that can support the initial high cost of new storage systems should be included as part of DOE's overall plan. As such, those involved in materials-development efforts should take these other potential applications into consideration in their development plans.

7.0 Conclusions

At the inception of the Hydrogen Sorption Center of Excellence (HSCoE), the required hydrogen-storage performance criteria and a number of other factors were used to quickly identify potential development materials and sorption mechanisms that could be used to meet U.S. Department of Energy (DOE) targets. Thus, from the outset, the center quickly eliminated entire classes of materials and processes that received no further development effort. Instead, the center focused activities on developing novel scalable synthetic processes to form high-surface-area, lightweight materials with optimum pore structures and compositions that had the potential to be used to meet DOE's 2015 and even DOE's ultimate full-fleet on-vehicle refueling system targets. The HSCoE is the only materials center that focused exclusively on solving the very difficult challenges of developing materials only for on-vehicle refueling and storage. Based on the intrinsic low isosteric heats of adsorption associated with sorbents, typically system capacity and costs are the main issues that must be resolved, and thus the center focused most of its efforts on improving these factors.

To accelerate development to the maximum, the HSCoE quickly identified focused efforts and directed specific partners and capabilities toward solving the most challenging problems. These focused development efforts included optimizing structures, substitution/heterogeneous materials, strong/multiple H₂ binding, weak chemisorption, and cross-cutting theory. Also, substantial efforts were performed in improving sorbent measurements to provide accurate characterization of the most important properties needed for developing materials. These measurement development efforts included improving accuracies to accelerate development so that laboratory-scale samples could be quickly characterized without the need for scaling up.

The HSCoE's organization, evaluation processes, and accelerated development efforts were used to continually identify promising new materials/processes as well as sorbents that did not make the cut and received no additional development. For example, at the outset of the HSCoE, a great deal of literature reported that materials such as carbon nanotubes and pyrolyzed conducting polymers could provide high-capacity ambient-temperature hydrogen storage based on their unique structures. Thus, the HSCoE initially established significant activities to reproduce the results and resolve the exact capabilities of these different materials. The center determined that even though isosteric heats of adsorption may be increased, no significant gravimetric capacity improvements can be attained simply by improved geometrical structures for physisorption-based hydrogen storage beyond that expected based on material properties such as SSA. This was a critical finding for the center that led to [no-go decisions on carbon nanotubes](#) (DOE 2006) and conducting polymers for ambient-temperature hydrogen storage.

Ultimately, measurement calibration and control is at the heart of many of the erroneous results reported in the literature. For sorbents, the relatively light, low-density materials used, as well as the relatively low binding with hydrogen, can easily lead to inaccurate measurements. Thus, the center identified measurement standards, qualification, and certification as potential efforts that should be supported in the future. Measurement issues aside, the HSCoE did develop novel sorbents with improved capacities that can be

used to meet DOE 2010 hydrogen storage system targets. Furthermore, the HSCoE developed and identified materials that may be able to be used to meet DOE 2015 and ultimate targets. In general, physisorption-based sorbents will need lower temperatures to meet DOE 2015 targets, and thus overall hydrogen energy efficiencies, system and hydrogen costs, and dormancy times must be balanced against capacities to engineer an appropriate system.

The HSCoE identified that increasing the isosteric heat of adsorption of sorbents for hydrogen, beyond that typically observed for physisorption, lowers system engineering constraints and costs. Thus, the HSCoE identified that properly structured heterogeneous materials such as boron-substituted carbon can substantially increase hydrogen storage capacities at near-ambient temperatures (i.e., ~220 K). The main issue here is developing materials with enough accessible sorption sites that the overall capacities at near-ambient temperatures can meet DOE targets. However, heterogeneous materials also help improve other sorbents including stabilizing coordinated metals and weak chemisorption. To increase heats of adsorption beyond what substituted/heterogeneous materials can do, the center identified coordinated but electronically unsaturated metals and weak chemisorption of hydrogen as two viable mechanisms that enable ambient-temperature hydrogen storage.

The center championed the development of weak chemisorption (spillover) for large-capacity ambient-temperature hydrogen storage. The center developed several new materials and catalyst processes that improved capacity and charging rates. An improved understanding of surface functionalization, catalyst size, and dispersion enhanced the sorption processes involved. The center also began investigating the barriers to migration based on structural and electronic features to provide development paths to create high-capacity, high-rate H storage spillover materials that meet DOE targets. These factors, along with decreasing processing times, increasing scalability, and improved kinetic performance, accelerated the materials-development activities, enabling the HSCoE to identify viable paths forward to create weak chemisorption materials that have the potential to be used to meet DOE 2015 hydrogen storage system targets.

The successful marriage of theory and experiment was most evident in the HSCoE's design of feasible materials based on multiple hydrogen storage per sorption site. From the center's outset, the ability to synthesize, the stability, and the DOE targets were selection criteria for the design of new materials. This along with interesting results reported in the literature led to the HSCoE championing the development of extremely novel sorbents. Such sorbents directly address the volumetric issues associated with ambient-temperature storage with high-specific-surface-area materials, while maintaining most of the advantages of sorbents to create materials that can meet even DOE's ultimate targets. For example, the HSCoE identified new inexpensive materials that use unique properties of Ca with highly viable synthetic routes. These revolutionary new materials could reversibly store hydrogen at twice the volumetric capacities (i.e., >100 g/L and >10 wt %) of liquid hydrogen, but at ambient temperature (i.e., ~300 K higher).

Sorbent materials, which will be refilled on-vehicle, enable the potential for substantially higher refueling efficiencies (and thus lower costs), because storage-material transport

and regeneration will not be needed. Thus, the center believes that the on-vehicle refueling capability of sorbent materials is a tremendous advantage that should be exploited for hydrogen storage. However, to fully leverage this advantage, it is imperative that discovery and development efforts focus on reducing material and system costs. This cost reduction can be achieved by improving material storage capacities at near-ambient temperatures. Furthermore, any future efforts must also investigate the material properties related to hydrogen-storage systems so that thermal conductivity, heat dissipation, refill and discharge rates, durability, and other engineering issues can be quantified fully.

At the time of the HSCoE's inception, the required hydrogen storage performance criteria used to identify potential development materials were strict. Based on this and a number of other factors, a substantial amount of materials have been down-selected that should not be developed further. However, a limited number of viable routes exist to synthesize sorbent materials that can likely be used to meet DOE's 2015 and even DOE's ultimate full-fleet on-board system targets.

Sorbent materials, which will be refilled on-vehicle, enable the potential for substantially higher refueling efficiencies (and thus lower costs) because storage-material transport and regeneration will not be needed. Thus, the center believes that the on-vehicle refueling capability of sorbent materials is a tremendous advantage that should be exploited for hydrogen storage. However, to fully exploit this advantage, it is imperative that development efforts focus on reducing material and system costs. This cost reduction can be achieved by improving material-storage capacities at near-ambient temperatures. Furthermore, any future efforts must also investigate the material properties related to hydrogen-storage systems so that thermal conductivity, heat dissipation, refill and discharge rates, durability, and other engineering issues can be fully quantified

7.1 References

DOE (2006). Go/No-Go Decision: Pure, Undoped Single Walled Carbon Nanotubes for Vehicular Hydrogen Storage U.S. Department of Energy (DOE) Hydrogen Program. www.hydrogen.energy.gov/pdfs/go_no_go_nanotubes.pdf.

Appendix A: Hydrogen Sorption Center of Excellence Bibliography

During the 5-year lifetime of the Hydrogen Sorption Center of Excellence, research conducted by the center partners generated hundreds of journal articles, dissertations, and patent applications. These publications are listed below. Also listed are the people who worked in the center and their awards and special accomplishments.

A.1 Publications

2005 and Earlier

Centrone, A.; Siberio-Pérez, D.Y.; Millward, A.R.; Yaghi, O.M.; Matzger, A.J.; Zerbi, G. "Raman Spectra of Hydrogen and Deuterium Adsorbed on a Metal-Organic Framework," *Chem. Phys. Lett.*; Vol. 411, **2005**; pp. 16-519.

Cheng, H.; Cooper, A.C.; Pez, G.P.; Kostov, M.K.; Piotrowski, P.; Stuart, S.J. "Molecular Dynamics Simulations on the Effects of Diameter and Chirality on Hydrogen Adsorption in Single Walled Carbon Nanotubes," *J. Phys. Chem. B*; Vol. 109, **2005**; pp. 3780-3786.

Cote, A.P.; Benin, A.I.; Ockwig, N.W.; O'Keeffe, M.; Matzger, A.J.; Yaghi, O.M. "Porous, Crystalline, Covalent Organic Frameworks," *Science*; Vol. 310 (5751), **2005**; pp. 1166-1170.

Dillon, A.C.; Blackburn, J.L.; Parilla, P.A.; Zhao, Y.; Kim, Y.-H.; Zhang, S.B.; Mahan, A.H.; Alleman, J.L.; Jones, K.M.; Gilbert, K.E.H.; Heben, M.J. "Discovering the Mechanism of H₂ Adsorption on Aromatic Carbon Nanostructures to Develop Adsorbents for Vehicular Applications," *Mat. Res. Soc. Symp. Proc.*; Vol. 837, **2005**; pp. 117-123.

Dillon, A.C.; Jones, K.M.; Bekkedahl, T.A.; Kiang, C.H.; Bethune, D.S.; Heben, M.J. "Storage of Hydrogen in Single-Walled Carbon Nanotubes," *Nature*; Vol. 386 (6623) **1997**; pp. 377-379.

Dillon, A.C.; Parilla, P.A.; Alleman, J.L.; Gennett, T.; Jones, K.M.; Heben, M.J. "Systematic Inclusion of Defects in Pure Carbon Single-Wall Nanotubes and Their Effect on the Raman D-Band," *Chem. Phys. Lett.*; Vol. 401, **2005**; pp. 522-528.

Dillon, A.C.; Parilla, P.A.; Alleman, J.L.; Mahan, A.H.; Gilbert, K.E.H.; Jones, K.M.; Heben, M.J. "Enhancing Hydrogen Adsorption by Metal Incorporation in Carbon Multiwall Nanotubes Produced by Continuous Hot-Wire Chemical Vapor Deposition," *Mat. Res. Soc. Symp. Proc.*; Vol. 801, **2004**; p. 167.

Dillon, A.C.; Yudasaka, M.; Dresselhaus, M.S. "Employing Raman to Qualitatively Evaluate the Purity of Carbon Single-Wall Nanotube Materials," *J. Nanosci. and Nanotech.*; Vol. 407, **2004**; p. 691.

Fu, R.; Baumann, T.F.; Cronin, S.; Dresselhaus, G.; Dresselhaus, M.S.; Satcher, J.H. "Formation of Graphitic Structures in Cobalt- and Nickel-Doped Carbon Aerogels," *Langmuir*; Vol. 21, **2005**; p. 2647.

- Gilbert, K.E.H. *Purification and Gas Adsorption Studies of Single-Walled Carbon Nanotubes*, Ph.D. Dissertation. Golden, CO: Department of Chemical Engineering, Colorado School of Mines, **2005**.
- Haas, M.K.; Zielinski, J.M.; Dantsin, G.; Coe, C.G.; Pez, G.P.; Cooper, A.C. "Tailoring Singlewalled Carbon Nanotubes for Hydrogen Storage," *J. Mater. Res.*; Vol. 20, **2005**; p. 3214.
- Lachawiec, A.J.; Qi, G.S.; Yang, R.T. "Hydrogen Storage in Nanostructured Carbons by Spillover: Bridge Building Enhancement," *Langmuir*; Vol. 21, **2005**; p. 11418.
- Landi, B.J.; Raffaele, R.P.; Heben, M.J.; Alleman, J.L.; VanDerveer, W.; Gennett, T. "Development and Characterization of Single Wall Carbon Nanotube–Nafion Composite Actuators," *Mater. Sci. Eng. B*; Vol. 116 (3), **2005**; pp. 359-362.
- Lui, P.; Lee, S.-H.; Yan, Y.; Gennett, T.; Landi, B.J.; Dillon, A.C.; Heben, M.J. "Electrochemical Transformation of SWNT/Nafion Composites," *Electrochem. Solid-State Lett.*; Vol. 7 (11), **2004**; p. A421.
- Moudrakovski, I.L.; Ratcliffe, C.I.; Ripmeester, J.A.; Wang, L.-Q.; Exarhos, G.J.; Baumann, T.F.; Satcher, J.H. "Nuclear Magnetic Resonance Studies of Resorcinol-Formaldehyde Aerogels," *J. Phys. Chem. B*; Vol. 109, **2005**; p. 11215.
- Parilla, P.A.; Dillon, A.C.; Parkinson, B.A.; Jones, K.M.; Alleman, J.L.; Riker, G.; Ginley, D.S.; Heben, M.J. "Formation of Nanooctahedra in Molybdenum Disulfide and Molybdenum Diselenide Using Pulsed Laser Vaporization," *J. Phys. Chem. B*; Vol. 108, **2004**; p. 6197.
- Puretzky, A.A.; Styers-Barnett, D.; Rouleau, C.M.; Hu, H.; Zhao, B.; Ivanov, I.N.; Geohegan, D.B. "Cumulative and Continuous Laser Vaporization Synthesis of Single Wall Carbon Nanotubes and Nanohorns," *Appl. Phys. A*; Vol. 93 (4), **2003**; pp. 849-855.
- Rosi, N.L.; Eckert, J.; Eddaoudi, M.; Vodak, D.T.; Kim, J.; O'Keeffe, M.; Yaghi, O.M. "Hydrogen Storage in Microporous Metal-Organic Frameworks," *Science*; Vol. 300 (5622), **2003**; pp. 1127-1129.
- Rowsell, J.L.C.; Spencer, E.C.; Eckert, J.; Howard, J.A.K.; Yaghi, O.M. "Gas Adsorption Sites in a Large-Pore Metal-Organic Framework," *Science*; Vol. 309 (5739) **2005**; pp. 1350-1354.
- Rowsell, J.L.C.; Yaghi, O.M. "Strategies for Hydrogen Storage in Metal-Organic Frameworks," *Angew. Chem. Int. Ed.*; Vol. 44 (30), **2005**; pp. 4670-4679.
- Sadana, A.K.; Liang, F.; Brinson, B.; Arepalli, S.; Farhat, S.; Hauge, R.H.; Smalley, R.E.; Billups, W.E. "Functionalization and Extraction of Large Fullerenes and Carbon-Coated Metal Formed During the Synthesis of Single Wall Carbon Nanotubes by Laser Oven, Direct Current Arc, and High-Pressure Carbon Monoxide Production Methods," *J. Phys. Chem. B*; Vol. 109, **2005**; p. 4416.
- Sha, X.; Cooper, A.C.; Bailey III, W.H.; Cheng, H. "Revisiting Hydrogen Storage in Bulk BC3," *J. Phys. Chem. C*; Vol. 115, 2010; p. 3260.
- Wagg, L.M.; Hornyak, G.L.; Grigorian, L.; Dillon, A.C.; Jones, K.M.; Blackburn, J.; Parilla P.A.; Heben, M.J. "Experimental Gibbs Free Energy Considerations in the

Nucleation and Growth of Single-Walled Carbon Nanotubes,” *J. Phys. Chem. B*; Vol. 109, **2005**; pp. 10435-10440.

Wang, Y.H.; Kim, M.J.; Shan, H.W.; Kittrell, C.; Fan, H.; Ericson, L.M.; Hwang, W.F.; Arepalli, S.; Hauge, R.H.; Smalley, R.E. “Continued Growth of Single-Walled Carbon Nanotubes,” *Nano Lett.*; Vol. 5 (6), **2005**; pp. 997-1002.

Xu, Y.Q.; Peng, H.Q.; Hauge, R.H.; Smalley, R.E. “Controlled Multistep Purification of Single-Walled Carbon Nanotubes.” *Nano Lett.*; Vol. 5, **2005**; p. 163.

Yildirim, T.; Ciraci, S. “Titanium-Decorated Carbon Nanotubes as a Potential High-Capacity Hydrogen Storage Medium,” *Phys. Rev. Lett.*; Vol. 94, **2005**; p. 175501.

Yildirim, T.; Hartman, M.R. “Direct Observation of Hydrogen Adsorption Sites and Nano-Cage Formation in Metal-Organic Frameworks (MOF),” *Phys. Rev. Lett.*; Vol. 95, **2005**; p. 215504.

Yildirim, T.; Iniguez, J.; Ciraci, S. “Molecular and Dissociative Adsorption of Multiple Hydrogen Molecules on Transition Metal Decorated C₆₀,” *Phys. Rev. B*; Vol. 72, **2005**; p. 153403.

Zhao, Y.; Kim, Y.-H.; Dillon, A.C.; Heben, M.J.; Zhang, S.B. “Interaction of Hydrogen with Carbon Based Molecules Through Transition Metal Atoms,” *Mat. Res. Soc. Proc.*; Vol. 19 (4), **2004**.

Zhao, Y.; Kim, Y.-H.; Dillon, A.C.; Heben, M.J.; Zhang, S.B. “Towards 9 wt%, Reversible, Room Temperature Hydrogen Adsorbents: Hydrogen Saturated Organometallic Bucky Balls,” *Phys. Rev. Lett.*; Vol. 94 (15), **2005**; p. 155504.

Ziegler, K.J.; Gu, Z.N.; Peng, H.Q.; Flor, E.L.; Hauge, R.H.; Smalley, R.E. “Controlled Oxidative Cutting of SWNTs,” *J. Am. Chem. Soc.*; Vol. 127 (5), **2005**; pp. 1541-1547.

Ziegler, K.J.; Gu, Z.N.; Shaver, J.; Chen, Z.Y.; Flor, E.L.; Schmidt, D.J.; Chan, C.; Hauge, R.H.; Smalley, R.E. “Cutting Single-Walled Carbon Nanotubes,” *Nanotechnology*; Vol. 16 (7), **2005**; pp. S539-S544.

2006

Ajayan, P.M.; Yakobson, B.I. “Oxygen Breaks into Carbon World,” *Nature*; Vol. 441, **2006**; pp. 818-819.

Blackburn, J.L.; Engtrakul, C.; McDonald, T.; Dillon, A.C.; Heben, M.J. “Effects of Surfactant and Boron Doping on the BWF Feature in the Raman Spectrum of Single-Wall Carbon Nanotube Aqueous Dispersions,” *J. Phys. Chem.*; Vol. 110, **2006**; p. 25551.

Blackburn, J.L.; Yan, Y.; Engtrakul, C.; Parilla, P.A.; Jones, K.; Gennett, T.; Dillon, A.C.; Heben, M.J. “Synthesis and Characterization of Boron-Doped Single-Wall Carbon Nanotubes Produced by the Laser Vaporization Technique,” *Chem. Mater.*; Vol. 18 (10), **2006**; p. 2558.

Chen, Z.Y.; Ziegler, K.J.; Shaver, J.; Hauge, R.H.; Smalley, R.E. “Cutting of SWNTs by Ozonolysis,” *J. Phys. Chem. B*; Vol. 110 (24), **2006**; pp. 11624-11627.

- Dailly, A.; Vajo, J.J.; Ahn, C.C. "Saturation of Hydrogen Sorption in Zn Benzenedicarboxylate and Zn Naphthalenedicarboxylate," *J. Phys. Chem. B*; Vol. 110, **2006**; p. 1099.
- Dillon, A.C.; Mahan, A.H.; Deshpande, R.; Alleman, J.L.; Blackburn, J.L.; Parilla, P.A.; Heben, M.J.; Engtrakul, C.; Gilbert, K.E.H.; Jones, K.M.; To, R.; Lee, S.H.; Lehman, J.H. "Hot-Wire Chemical Vapor Synthesis for a Variety of Nano-Materials with Novel Applications," *Thin Solid Films*; Vol. 501 (1-2), **2006**; pp. 216-220.
- Dillon, A.C.; Nelson, B.P.; Zhao, Y.; Kim, Y.-H.; Tracy, C.E.; Zhang, S.B. "Importance of Turning to Renewable Energy Resources with Hydrogen as a Promising Candidate and On-Board Storage a Critical Barrier," *Mat. Res. Soc. Symp. Proc.*; Vol. 895, **2006**; pp. 115-122.
- Dinca, M.; Han, W.S.; Liu, Y.; Dailly, A.; Brown, C.M.; Long, J.R. "Hydrogen Storage in a Microporous Metal-Organic Framework with Exposed Mn²⁺ Coordination Sites," *J. Am. Chem. Soc.*; Vol. 128 (51), **2006**; p. 16876.
- Hartman, M.R.; Peterson, V.K.; Liu, Y.; Kaye, S.S.; Long, J.R. "Neutron Diffraction and Neutron Vibrational Spectroscopy Studies of Hydrogen Adsorption in the Prussian Blue Analogue Cu₃[Co(CN)₆]₂," *Chem. Mater.*; Vol. 18, **2006**; p. 3221.
- Kabbour, H.; Baumann, T.F.; Satcher, J.H.; Saulnier, A.; Ahn, C.C. "Toward New Candidates for Hydrogen Storage: High-Surface-Area Carbon Aerogels," *Chem. Mater.*; Vol. 18 (26), **2006**; p. 6085.
- Kim, Y.-H.; Zhao, Y.; Williamson, A.; Heben, M.J.; Zhang, S.B. "Non-Dissociative Adsorption of H₂ Molecules in Light-Element Doped Fullerenes," *Phys. Rev. Lett.*; Vol. 96, **2006**; p. 016102.
- Knippenberg, M.T.; Stuart, S.J.; Cooper, A.C.; Pez, G.P.; Cheng, H. "Physical Adsorption Strength in Open Systems," *J. Phys. Chem. B*; Vol. 110, **2006**; p. 22957.
- Li, Y.W.; Yang, R.T. "Hydrogen Storage in Low Silica Type X Zeolites," *J. Phys. Chem. B*; Vol. 110, **2006**; p. 17175.
- Li, Y.W.; Yang, R.T. "Hydrogen Storage in Metal-Organic Frameworks by Bridged Hydrogen Spillover," *J. Am. Chem. Soc.*; Vol. 128, **2006**; p. 8136.
- Li, Y.W.; Yang, R.T. "Significant Enhancement of Hydrogen Storage Capacity in Metal-Organic Frameworks via Spillover," *J. Am. Chem. Soc.*; Vol. 128, **2006**; p. 726.
- Lu, C.; Liu, J. "Controlling the Diameter of Carbon Nanotubes in Chemical Vapor Deposition Method by Carbon Feeding," *J. Phys. Chem. B*; Vol. 110 (41), **2006**; pp. 20254-20257.
- Neumann, D.A. "Neutron Scattering and Hydrogenous Materials," *Materials Today*; Vol. 9 (1-2), **2006**; p. 34.
- Peterson, V. K.; Liu, Y.; Brown, C.M.; Kepert, C. "Neutron Powder Diffraction Study of D₂ Sorption in Cu₃(1,3,5-benzenetricarboxylate)₂," *J. Am. Chem. Soc.*; Vol. 128, **2006**; p. 15578.

- Price, B.K.; Tour, J.M. "Functionalization of Single-Walled Carbon Nanotubes On Water," *J. Am Chem. Soc.*; Vol. 128, **2006**; pp. 12899-12904.
- Smalley, R.E.; Li, Y.; Moore, V.C.; Price, B.K.; Colorado, R.; Schmidt, H.K.; Hauge, R.H.; Barron, A.R.; Tour, J.M. "Single Wall Carbon Nanotube Amplification: En Route to a Type-Specific Growth Mechanism," *J. Am. Chem. Soc.*; Vol. 128, **2006**; pp. 15824-15829.
- Stephenson, J.J.; Hudson, J.L.; Azad, S.; Tour, J.M. "Individualized SWNTs from Bulk Material Using 96% Sulfuric Acid as Solvent," *Chem. Mater.*; Vol. 18, **2006**; pp. 374-377.
- Stephenson, J.J.; Sadana, A.K.; Higginbotham, A.L.; Tour, J.M. "Highly Functionalized and Soluble Multi-Walled Carbon Nanotubes by Reductive Alkylation and Arylation: The Billups Reaction," *Chem. Mater.*; Vol. 18, **2006**; pp. 4658-4661.
- Venancio, E.C.; Wang, P.C.; MacDiarmid, A.G. "The Azanes: A Class of Material Incorporating Nano/Micro Self-Assembled Hollow Spheres Obtained by Aqueous Oxidative Polymerization of Aniline," *Synth. Met.*; Vol. 156 (5-6), **2006**; pp. 357-369.
- Xu, Y.Q.; Flor, E.; Kim, M.J.; Hamadani, B.; Schmidt, H.; Smalley, R.E.; Hauge, R.H. "Vertical Array Growth of Small Diameter Single-Walled Carbon Nanotubes," *J. Am. Chem. Soc.*; Vol. 128 (20), **2006**; pp. 6560-6561.
- Xu, Y.Q.; Flor, E.; Schmidt, H.; Smalley, R.E.; Hauge, R.H. "Effect of Atomic Hydrogen and Active Carbon Species in the 1mm Vertically Aligned Single-Walled Carbon Nanotubes Growth," *Appl. Phys. Lett.*; Vol. 89 (12), **2006**; pp.123116-123116-3.
- Yang, F.H.; Lachawiec, A.J.; Yang, R.T. "Adsorption of Spillover Hydrogen Atoms on Single-Wall Carbon Nanotubes," *J. Phys. Chem. B*; Vol. 110, **2006**; p. 6236.
- Zhao, Y.; Dillon, A.C.; Kim, Y.-H.; Heben, M.J.; Zhang, S.B. "Self-Catalyzed Hydrogenation and Dihydrogen Adsorption on Titanium Carbide Nanoparticles," *Chem. Phys. Lett.*; Vol. 425, **2006**; p. 273.

2007

- Bénard, P.; Chahine, R.; Chandonia, P.A.; Cossement, D.; Dorval-Douville, G.; Lafi, L.; Poirier, E.; Blackburn, J.L.; Curtis, C.; Dillon, A.C.; Gennett, T.; Heben, M.J.; Kim, Y.-H.; Parilla, P.A.; Simpson, L.J.; Whitney, E.S.; Zhang, S.B.; Zhao, Y. "Hydrogen Storage in Carbon-Based Materials," Final report for Task C1 for the International Energy Agency Hydrogen Implementing Agreement; Task 17, Final Report, **2007**.
- Brown, C.M.; Liu, Y.; Hu, H.; Rols, S.; Poretzky, A.A.; Zhou, B.; Rouleau, C.M.; Styers-Barnett, D.; Neumann, D.A.; Geohegan, D.B. "Inelastic Neutron Scattering as a Probe of the States of Hydrogen in Carbon Materials," Carbon 2007 Proceedings, Seattle, Washington; **2007**.
- Chen, L.; Cooper, A.C.; Pez, G.P.; Cheng, H. "Density Functional Study of Sequential H₂ Dissociative Chemisorption on a Pt₆ Cluster," *J. Phys. Chem. C*; Vol. 111, **2007**; p. 5514.
- Chen, L.; Cooper, A.C.; Pez, G.P.; Cheng, H. "Mechanistic Study on Hydrogen Spillover onto Graphitic Carbon Materials," *J. Phys. Chem. C*; Vol. 111, **2007**; p. 18995.

- Chen, L.; Cooper, A.C.; Pez, G.P.; Cheng, H. "Sequential Chemisorption of H₂ on a Pt₆ Cluster," *J. Phys. Chem. C*; Vol. 111, **2007**; p. 5514.
- Cheng, H.; Cooper, A.C.; Pez, G.P.; Kostov, M.K.; Knippenberg, M.T.; Piotrowski, P.; Stuart, S.J. "Molecular Dynamics Simulations of Hydrogen Adsorption in Finite and Infinite Bundles of Single Walled Carbon Nanotubes," Sokalski, W.A., ed. *Molecular Materials with Specific Interactions: Modeling and Design*. New York: Springer, **2007**; p. 469.
- Cheng, M-D.; Lee, D-W.; Zhao, B.; Hu, H.; Styers-Barnett, D.J.; Puzos, A.A.; DePaoli, D.W.; Geohegan, D.B.; Ford, E.A.; Angelini, P. "Formation Studies and Controlled Production of Carbon Nanohorns Using Continuous In Situ Characterization Techniques," *Nanotechnology*; Vol. 18, **2007**; p. 185604.
- Collins, D.J.; Zhou, H.-C. "Hydrogen Storage in Metal-Organic Frameworks." *J. Mater. Chem.*; Vol. 17, **2007**; p. 3154.
- Dillon, A.C.; Whitney, E.; Engtrakul, C.; Curtis, C.J.; O'Neill, K.J.; Parilla, P.A.; Simpson, L.J.; Heben, M.J.; Zhao, Y.; Kim, Y-H.; Zhang, S.B. "Novel Organometallic Fullerene Complexes for Vehicular Hydrogen Storage," *Phys. Status Solidi B*; Vol. 244, **2007**; pp. 4319-4322.
- Dinca, M.; Dailly, A.; Liu, Y.; Brown, C.M.; Neumann, D.A.; Long, J.R. "Observation of CuII-H₂ Interactions in a Fully-Desolvated, Sodalite-Type Metal-Organic Frameworks," *Ang. Chem. Int. Ed.*; Vol. 46, **2007**; p. 1419.
- Ding, F.; Lin, Y.; Krasnov, P.; Yakobson, B.I. "Nanotube Derived Carbon Foam for Hydrogen Storage," *J. Chem. Phys.*; Vol. 127, **2007**; p. 164703.
- El-Kaderi, H.M.; Hunt, J.R.; Mendoza-Cortes, J.L.; Cote, A.P.; Taylor, R.E.; O'Keeffe, M.; Yaghi, O.M. "Designed synthesis of 3D covalent organic frameworks," *Science*; Vol. 316 (5822), **2007**; pp. 268-272.
- Geohegan, D.B.; Puzos, A.A.; Styers-Barnett, D.; Hu, H.; Zhao, B.; Cui, H.; Rouleau, C.M.; Eres, G.; Jackson, J.J.; Wood, R.F.; Pannala, S.; Wells, J. "In Situ Time-Resolved Measurements of Carbon Nanotube and Nanohorn Growth," *Phys. Status Solidi B*; Vol. 244 (11), **2007**; p. 3994.
- Hu, H.; Zhao, B.; Puzos, A.A.; Rouleau, C.M.; Styers-Barnett, D.; Geohegan, D.B.; Brown, C.M.; Liu, Y.; Zhou, W.; Kabbour, H.; Neumann, D.A.; Ahn, C. "Tailoring of Single Walled Carbon Nanohorns for Hydrogen Storage and Catalyst Supports," Carbon 2007 Proceedings, Seattle, Washington; **2007**.
- Krasnov, P.; Ding, F.; Singh, A.K.; Yakobson, B. I. "Clustering of Sc on SWNT and Reduction of Hydrogen Uptake: Ab-Initio All-Electron Calculations," *J. Phys. Chem. C*; Vol. 111 (49), **2007**; pp. 17977-17980.
- Larsson, P.; Larsson, J.A.; Ahuja, R.; Ding, F.; Yakobson, B.I.; Duan, H.; Rosén, A.; Bolton, K. "Calculating Carbon Nanotube-Catalyst Adhesion Strengths," *Phys. Rev. B*; Vol. 75, **2007**; p. 115419.
- Li, Y.; Yang, R.T. "Gas Adsorption and Storage in Metal-Organic Framework MOF-177," *Langmuir*; Vol. 23, **2007**; p. 12937.

- Li, Y.; Yang, R.T. "Hydrogen Storage on Platinum Nanoparticles Doped on Super-Activated Carbon," *J. Phys. Chem. C*; Vol. 111, **2007**; p. 11086.
- Li, Y.; Yang, R.T.; Liu, C.J.; Wang, Z. "Hydrogen Storage on Carbon Doped with Platinum Nanoparticles Using Plasma Reduction," *Ind. Eng. Chem. Res.*; Vol. 46, **2007**; p. 8277.
- Li, Y.W.; Yang, F.H.; Yang, R.T. "Kinetics and Mechanistic Model for Hydrogen Spillover on Bridged Metal-Organic Frameworks," *J. Phys. Chem. C*; Vol. 111, **2007**; p. 3405.
- Liu, Y.; Brown, C.M.; Baumann, T.F.; Neumann, D.A. "Applications of Neutron Scattering Techniques to Hydrogen Storage Materials," Proceedings of the American Nuclear Society Annual Meeting, December **2007**.
- Liu, Y.; Brown, C.M.; Blackburn, J.L.; Neumann, D.A.; Gennett, T.; Simpson, L.J.; Parilla, P.A.; Dillon, A.C.; Heben, M.J. "Inelastic Neutron Scattering of H₂ Adsorbed on Boron Substituted SWNTs," *J. Alloys Compd.*, Vols. 446-447, **2007**; pp. 368-372.
- Liu, Y.; Brown, C.M.; Neumann, D.A.; Peterson, V.K.; Kepert, C. "Inelastic Neutron Scattering of H₂ Adsorbed in HKUST-1," *J. Alloys Compd.*; Vols. 446-447, **2007**; pp. 385-388.
- Ma, S.; Sun, D.; Ambrogio, M.; Fillinger, J.A.; Parkin, S.; Zhou, H.-C. "Framework-Catenation Isomerism in Metal-Organic Frameworks and its Impact on Hydrogen Uptake," *J. Am. Chem. Soc.*; Vol. 129, **2007**; p. 1858.
- Ma, S.; Sun, D.; Wang, X.-S.; Zhou, H.-C. "A Mesh-Adjustable Molecular Sieve for General Use in Gas Separation," *Angew. Chem. Int. Ed.*; Vol. 46, **2007**; p. 2458.
- Ma, S.; Wang, X.-S.; Collier, C.D.; Manis, E.S.; Zhou, H.-C. "Ultramicroporous Metal-Organic Framework Based on 9,10-Anthracenedicarboxylate for Selective Gas Adsorption," *Inorg. Chem.*; Vol. 46, **2007**; p. 8499.
- Ma, S.; Wang, X.-S.; Manis, E.S.; Collier, C.D.; Zhou, H.-C. "Metal-Organic Framework Based on a Trinickel Secondary Building Unit Exhibiting Gas-Adsorption Hysteresis," *Inorg. Chem.*; Vol. 46, **2007**; p. 3432.
- Peterson, V.K.; Liu, Y.; Brown, C.M.; Kepert, C.J. "Structural Characterization of D₂ in Cu₃(1,3,5-benzenetricarboxylate)₂ Using Neutron Powder Diffraction," *Mater. Sci. Forum*; Vols. 561-565, **2007**; p. 1601.
- Qi, H.; Qian, C.; Liu, J. "Synthesis of Double-Walled Carbon Nanotubes Using Iron Disilicide as Catalyst," *Nano Lett.*; Vol. 7 (8), **2007**; pp. 2417-2421.
- Qi, H.; Yuan, D.; Liu, J. "Two-Stage Growth of Single-Walled Carbon Nanotubes," *J. Phys. Chem. C*; Vol. 111 (17), **2007**; pp. 6158-6160.
- Stephenson, J.J.; Hudson, J.L.; Leonard, A.D.; Price, B.P.; Tour, J.M. "Repetitive Functionalization of Water-Soluble Single-Walled Carbon Nanotubes," *Chem. Mater.*; Vol. 19, **2007**; pp. 3491-3498.

Sun, Y.Y.; Kim, Y.-H.; Zhang, S.B. "Effect of Spin State on the Dihydrogen Binding Strength to Transition Metal Centers in Metal-organic Frameworks," *J. Am. Chem. Soc.*; Vol. 129, **2007**; p. 12606.

Weck, P.F.; Kim, E.; Balakrishnan, N.; Cheng, H.; Yakobson, B.I. "Designing Carbon Nanoframeworks Tailored for Hydrogen Storage," *Chem. Phys. Lett.*; Vol. 439, **2007**; pp. 354-359.

Yoon, M.; Yang, S.; Wang, E.; Zhang, Z. "Charged Fullerenes as High-Capacity Hydrogen Storage Media," *Nano Lett.*; Vol. 7, **2007**; p. 2578.

Yuan, D.; Liu, J. "Purification of Semiconducting Carbon Nanotubes," *Small*; Vol. 3 (3), **2007**; pp. 366-367.

Zhao, Y.; Heben, M.J.; Dillon, A.C.; Simpson, L.J.; Blackburn, J.L.; Dorn, H.C.; Zhang, S.B. "Nontrivial Tuning of Hydrogen Binding Energy to Fullerenes with Endohedral Metal Dopants," *J. Phys. Chem. C*; Vol. 111, **2007**; p. 13275.

Zielinski, J.M.; Coe, C.G.; Nickel, R.J.; Romeo, A.M.; Cooper, A.C.; Pez, G.P. "Accurate Hydrogen Sorption Measurements via Differential Pressure Analyses," *Adsorption*; Vol. 13 (1), **2007**.

Zielinski, J.M.; McKeon, P.; Kimak, M.F. "A Simple Technique for the Measurement of H₂ Sorption Capacities," *Ind. Eng. Chem. Res.*; Vol. 46, **2007**; p. 329.

2008

Baumann, T.F.; Worsley, M.A.; Han, T.Y.; Satcher, J.H. "High Surface Area Carbon Aerogel Monoliths with Hierarchical Porosity," *J. Non-Cryst. Solids*; Vol. 354, **2008**; p. 3513.

Blackburn, J.L.; Parilla, P.A.; Gennett, T.; Hurst, K.E.; Dillon, A.C.; Heben, M.J. "Measurement of the Reversible Hydrogen Storage Capacity of Milligram Ti-6Al-4V Alloy Samples with Temperature Programmed Desorption and Volumetric Techniques," *J. Alloys Compd.*; Vol. 454 (1-2), **2008**; pp. 483-490.

Bo, W.; Cote, A.P.; Furukawa, H.; O'Keeffe, M.; Yaghi, O.M. "Colossal Cages in Zeolitic Imidazolate Frameworks as Selective Carbon Dioxide Reservoirs," *Nature*; Vol. 453, **2008**; pp. 207-211.

Brown, C.M.; Liu, Y.; Kabbour, H.; Neumann, D.A.; Ahn, C.C. "Denser than Solid Hydrogen: Improving Hydrogen Storage," Cappelletti, R.L., ed. *2008 NIST Center for Neutron Research Accomplishments and Opportunities*. NIST Special Publication 1089. Washington, D.C.: U.S. Government Printing Office, **2008**; pp. 30-31.

Brown, C.M.; Liu, Y.; Neumann, D.A. "Neutron Powder Diffraction of Metal-Organic Frameworks for Hydrogen Storage," *PRAMANA J. Phys.*; Vol. 71, **2008**; p. 755.

Burket, C.L.; Rajagopalan, R.; Foley, H.C. "Overcoming the Barrier to Graphitization in a Polymer-Derived Nanoporous Carbon," *Carbon*; Vol. 46, **2008**; p. 501.

Chen, L.; Cooper, A.C.; Pez, G.P.; Cheng, H. "On the Mechanisms of Hydrogen Spillover in MoO₃," *J. Phys. Chem. C*; Vol. 112, **2008**; p. 1755.

- Chen, L.; Pez, G.P.; Cooper, A.C.; Cheng, H. "A Mechanistic Study of Hydrogen Spillover in MoO₃ and Carbon-Based Graphitic Materials," *J. Phys.: Condens. Matter*; Vol. 20, **2008**; p. 064223.
- Cheng, H.; Chen, L.; Cooper, A.C.; Sha, X.; Pez, G.P. "Hydrogen Spillover in the Context of Hydrogen Storage Using Solid-State Materials," *Energy Environ. Sci.*; Vol. 1, **2008**; pp. 338-335.
- Chung, T.C.M.; Jeong, Y.; Chen, Q.; Kleinhammes, A.; Yue, W. "Synthesis of Boron-Substituted Carbon (B/C) Materials Using Polymeric Precursors and Evaluation for Hydrogen Physisorption," *J. Am. Chem. Soc.*; Vol. 130 (21), **2008**; p. 6668.
- Collins, C.S.; Sun, D.; Liu, W.; Zuo, J.-L.; Zhou, H.-C. "Reaction-Condition-Controlled Formation of Secondary-Building-Units in Three Cadmium Metal-Organic Frameworks with an Orthogonal Tetrakis(Tetrazolate) Ligand," *J. Mol. Struct.*; Vol. 890, **2008**; p. 163.
- Collins, D.J.; Zhou, H.-C. "Nano/Microporous Materials: Hydrogen Storage Materials," Lukehart, C.M.; Scott, R.A. eds. *Nanomaterials: Inorganic and Bioinorganic Perspectives*. New York: Wiley, **2008**; pp. 535-542.
- Ding, F.; Lin, Y.; Yakobson, B.I. "Hydrogen Storage on Graphene as a Phase Nucleation Process," *Phys. Rev. B*; Vol. 78, **2008**; p. 041402-R.
- Furukawa, H.; Kim, J.; Ockwig, N.W.; O'Keeffe, M.; Yaghi, O.M. "Control of Vertex Geometry, Structure Dimensionality, Functionality, and Pore-Metrics in the Reticular Synthesis of Crystalline Metal-Organic Frameworks and Polyhedra," *J. Am. Chem. Soc.*; Vol. 130, **2008**; pp. 11650-11661.
- Hess, N.J.; Hartman, M.R.; Brown, C.M.; Mamontov, E.; Karkamkar, A.; Heldebrant, D.J.; Daemen, L.L.; Autrey, T. "Quasielastic Neutron Scattering Experiments of Orthorhombic Ammonia Borane," *Chem. Phys. Lett.*; Vol. 259, **2008**; p. 85.
- King, J.S.; Wittstock, A.; Biener, J.; Kucheyev, S.O.; Wang, Y.M.; Baumann, T.F.; Giri, S.K.; Hamza, A.V.; Baeumer, M.; Bent, S.F. "Ultra-Low Loading Pt Nanocatalysts Prepared by Atomic Layer Deposition on Carbon Aerogels," *Nano Lett.*; Vol. 8, **2008**; p. 2405.
- Lachawiec, A.J.; DiRaimondo, T.R.; Yang, R.T. "A Robust Volumetric Apparatus and Method for Measuring High-Pressure Hydrogen Storage Properties of Nanostructured Materials," *Rev. Sci. Instr.*; Vol. 79, **2008**; p. 063906.
- Lachawiec, A.J.; Yang, R.T. "Isotope Tracer Study of Hydrogen Spillover on Carbon-Based Adsorbents for Hydrogen Storage," *Langmuir*; Vol. 24, **2008**; p. 6159.
- Li, Y.W.; Yang, R.T. "Hydrogen Storage in Metal-Organic Frameworks and a Covalent-Organic Framework," *AIChE Journal*; Vol. 54, **2008**; p. 269.
- Lin, C.K.; Yang, Z.Z.; Xu, T.; Zhao, Y.Z. "An In Situ Electrical Study on Primary Hydrogen Spillover from Nanocatalysts to Amorphous Carbon Support," *Appl. Phys. Lett.*; Vol. 93, **2008**; p. 233110.
- Lin, Y.; Ding, F.; Yakobson, B.I. "Hydrogen Storage by Spillover on Graphene as a Phase Nucleation Process," *Phys. Rev. B*; Vol. 78, **2008**; p. 041402-R.

Liu, S.; Bremer, M.; Lovaasen, J.; Caruso, A.N.; O'Neill, K.; Simpson, L.; Parilla, P.A.; Heben, M.J.; Schulz, D.L. "Structural and Magnetic Studies of Two-Dimensional Solvent-Free Manganese(II) Complexes Prepared via Ligand Exchange Reaction Under Solvothermal Conditions," *Inorg. Chem.*; Vol. 47 (5), **2008**; pp. 1568-1575.

Liu, X.M.; Romero, H.E.; Gutierrez, H.R.; Adu, K.; Eklund, P.C. "Transparent Boron-Doped Carbon Nanotube Films," *Nano Lett.*; Vol. 8, **2008**; p. 2613.

Liu, Y.; Brown, C.M.; Neumann, D.A.; Kabbour, H.; Ahn, C.C. "Hydrogen Adsorption in MOF-74 Studied by Inelastic Neutron Scattering," in *Life Cycle Analysis for New Energy Conversion and Storage Systems*; Fthenakis, V.M.; Dillon, A.C.; Savage, N., Eds.; *Mater. Res. Soc. Symp. Proc.*; Volume 1041E, Warrendale, PA, **2008**; p. 1040-R2_03.

Liu, Y.; Her, J.-H.; Dailly, A.; Ramirez-Cuesta, A.J.; Neumann, D.A.; Brown, C.M. "A Reversible Structural Transition of MIL-53 with Temperature Hysteresis," *J. Am. Chem. Soc.*; Vol. 130, **2008**; p. 11813.

Liu, Y.; Kabbour, H.; Brown, C.M.; Neumann, D.A.; Ahn, C.C. "Increasing the Density of Adsorbed Hydrogen with Coordinatively Unsaturated Metal Centers in Metal-Organic Frameworks," *Langmuir*; Vol. 24, **2008**; p. 4772.

Lomeda, J.R.; Doyle, C.D.; Kosynkin, D.V.; Hwang, W.-F.; Tour, J.M. "Diazonium Functionalization of Surfactant-Wrapped Chemically Converted Graphene Sheets," *J. Am. Chem. Soc.*; Vol. 130, **2008**; p. 16201.

Luo, J.; Xu, H.; Liu, Y.; Zhou, Y.; Daemen, L.L.; Brown, C.M.; Timofeeva, T.V.; Ma, S.; Zhou, H.-C. "Hydrogen Adsorption in a Highly Stable Porous Rare-Earth Metal-Organic Framework: Sorption Properties and Neutron Diffraction Studies," *J. Am. Chem. Soc.*; Vol. 130, **2008**; p. 9626.

Ma, S.; Sun, D.; Simmons, J.M.; Collier, C.D.; Yuan, D.; Zhou, H.-C. "Metal-Organic Framework from an Anthracene Derivative Containing Nanoscopic Cages Exhibiting High Methane Uptake," *J. Am. Chem. Soc.*; Vol. 130, **2008**; p. 1012.

Ma, S.-Q.; Eckert, J.; Forster, P.; Yoon, J.; Chang, J.-S.; Collier, C.; Parise, J.; Zhou, H.-C. "Further Investigation of the Effect of Framework Catenation on Hydrogen Uptake in Metal-Organic Frameworks," *J. Am. Chem. Soc.*; Vol. 130, **2008**; p. 15896.

Ma, S.-Q.; Wang, X.-S.; Yuan, D.-Q.; Zhou, H.-C. "A Coordinatively Linked, Doubly Interpenetrated, Yb Metal-Organic Framework Demonstrating High Thermal Stability and Uncommon Gas-Adsorption Selectivity," *Angew. Chem. Int. Ed.*; Vol. 47, **2008**; p. 4130.

Pupysheva, O.V.; Farajian, A.A.; Yakobson, B.I. "Fullerene Nanocage Capacity for Hydrogen Storage," *Nano Lett.*; Vol. 8, **2008**; p. 767.

Sha, X.; Knippenberg, M.T.; Cooper, A.C.; Pez, G.P.; Cheng, H. "Dynamics of Hydrogen Spillover on Carbon-Based Materials," *J. Phys. Chem. C*; Vol. 112 (44), **2008**; pp. 17465-17470.

- Wang, L.F.; Yang, R.T. "Hydrogen Storage Properties of Carbons Doped with Ruthenium, Platinum, and Nickel Nanoparticles," *J. Phys. Chem. C.*; Vol. 112, **2008**; 12486.
- Wang, L.F.; Yang, R.T. "New Sorbents for Hydrogen Storage by Hydrogen Spillover – A Review," *Energy Environ. Sci.*; Vol. 1, **2008**; p. 268.
- Wang, X.-S.; Ma, S.-Q.; Forster, P.M.; Yuan, D.-Q.; Eckert, J.; López, J.J.; Murphy, B.J.; Parise, J.B.; Zhou, H.-C. "Enhancing H₂ Uptake by 'Close-Packing' Alignment of Open Copper Sites in Metal-Organic Frameworks," *Angew. Chem. Int. Ed.*; Vol. 47, **2008**; p. 7263.
- Wang, X.-S.; Ma, S.-Q.; Rauch, K.; Simmons, J.M.; Yuan, D.-Q.; Wang, X.-P.; Yildirim, T.; Cole, W.C.; Lopez, J.J.; De Meijere, A.; Zhou, H.-C. "Metal-Organic Frameworks Based on Double-Bond-Coupled Di-Isophthalate Linkers with High Hydrogen and Methane Uptakes," *Chem. Mater.*; Vol. 20, **2008**; p. 3145.
- Wang, Y.H.; Yang, R.T. "Increased Hydrogen Spillover by Gaseous Impurity - Benson-Boudart Method for Dispersion Revisited," *J. Catalysis*; Vol. 260, **2008**; p. 198.
- Worsley, M.A.; Satcher, J.H.; Baumann, T.F. "Synthesis and Characterization of Monolithic Carbon Aerogel Nanocomposites Containing Double-Walled Carbon Nanotubes," *Langmuir*; Vol. 24, **2008**, 24; p. 9763.
- Yang, S.; Yoon, M.; Wang, E.; Zhang, Z. "Energetics and Kinetics of Ti Clustering on Neutral and Charged C-60 Surfaces," *J. Chem. Phys.*; Vol. 129, **2008**; p. 134707.
- Yang, S.; Yoon, M.; Zhang, Z.; Wang, E. "Electron Transfer and Localization in Endohedral Metallofullerenes," *Phys. Rev. B*; Vol. 78, **2008**; p. 115435.
- Yang, Y.; Schalch, J.; Liu, Y.; Her, J.-H.; Simmons, J.; Brown, C.M.; Webley, P.A.; Chaffee, A.L. "Hydrogen Storage on Ordered Microporous Carbon Molecular Sieves Containing Dispersed Platinum Nanoparticles," in *American Chemical Society National Meeting, Philadelphia, ACS Division of Fuel Chemistry, Preprints*; Vol. 53 (2), **2008**.
- Yoon, M.; Yang, S.; Hicke, C.; Wang, E.; Geohegan, D.; Zhang, Z. "Calcium as a Superior Coating Metal in Functionalization of Carbon Fullerenes for High-Capacity Hydrogen Storage," *Phys. Rev. Lett.*; Vol. 100, **2008**; p. 206806.
- Yuan, Y.; Cabasso, I.; Liu, H. "Surface Morphology of Nanostructured Polymer-Based Activated Carbons," *J. Phys. Chem. B*; Vol. 112, **2008**; p. 1364.
- Zhao, D.; Yuan, D.-Q.; Zhou, H.-C. "The Current Status of Hydrogen Storage in Metal-Organic Frameworks," *Energy Environ. Sci.*; Vol. 1, **2008**; p. 222.
- Zhao, Y.; Kim, Y.-H.; Simpson, L.J.; Dillon, A.C.; Wei, S.-H.; Heben, M.J. "Opening Space for H₂ Storage: Cointercalation of Graphite with Metal and Small Organic Molecules," *Phys. Rev. B*; Vol. 78, **2008**; p. 144102.
- Zhao, Y.; Lusk, M.T.; Dillon, A.C.; Heben, M.J.; Zhang, S.B. "Boron-Based Organometallic Nanostructure: Hydrogen-Storage Properties and Structure Stability," *Nano Lett.*; Vol. 9, **2008**; 157-161.

2009

- Biener, J.; Wittstock, A.; Baumann, T.F.; Weissmüller, J.; Bäumer, M.; Hamza, A.V. "Surface Chemistry in Nanoporous Materials," *Materials*; Vol. 2, **2009**; p. 2404.
- Brown, C.M.; Zhou, W.; Liu, Y.; Wu, H.; Yildirim, T.; Peterson, V.K.; Kepert, C. "Toward an Improved Understanding of Hydrogen Interactions with Coordinated Metals," in *2009 NIST Center for Neutron Research Accomplishments and Opportunities, NIST Special Publication 1105*; R. L. Cappelletti, Ed.; U.S. Government Printing Office, Washington, D.C., **2009**; pp. 30-31.
- Brown, C.M.; Liu, Y.; Yildirim, T.; Peterson, V.K.; Kepert, C.J. "Hydrogen Adsorption in HKUST-1: A Combined Inelastic Neutron Scattering and First-Principles Study," *Nanotechnology*; Vol. 20, **2009**; p. 204025.
- Cheng, H.; Sha, X.; Chen, L.; Cooper, A.C.; Foo, M.-L.; Lau, G.C.; Bailey III, W.H.; Pez, G.P. "An Enhanced Hydrogen Adsorption Enthalpy for Fluoride Intercalated Graphite Compounds," *J. Am. Chem. Soc.*; Vol. 131, **2009**; p. 17732.
- Chung, T.C.M.; Jeong, Y.; Kleinhammes, A.; Wu, Y. "Synthesis of Micro-Porous Boron-Substituted Carbon (B/C) Materials Using Polymeric Precursors for Hydrogen Physisorption," *ECS Transactions*; Vol. 19 (10), **2009**; pp. 57-66.
- Contescu, C.I.; Brown, C.M.; Liu, Y.; Bhat, V.V.; Gallego, C. "Detection of Hydrogen Spillover in Palladium-Modified Activated Carbon Fibers During Hydrogen Adsorption," *J. Phys. Chem.*; Vol. 113, **2009**; p. 5886.
- Doonan, C.J.; Morris, W.; Furukawa, H.; Yaghi, O.M. "Isorecticular Metalation of Metal-Organic Frameworks," *J. Am. Chem. Soc.*; Vol. 131, **2009**; pp. 9492-9493.
- Firlej, L.; Roszak, S.; Kuchta, B.; Pfeifer, P.; Wexler, C. "Enhanced Hydrogen Adsorption in Boron Substituted Carbon Nanospaces," *Virtual Journal of Nanoscale Science and Technology*; Vol. 20, **2009**; p. 19.
- Firlej, L.; Roszak, S.; Kuchta, B.; Pfeifer, P.; Wexler, C. "Enhanced Hydrogen Adsorption in Boron Substituted Carbon Nanospaces," *J. Chem. Phys.*; Vol. 131, **2009**; p. 164702.
- Her, J.-H.; Zhou, W.; Stavila, V.; Brown, C.M.; Udovic, T.J. "Crystal Structure of Na₂B₁₂H₁₂ and the Role of Cation Size on the Structural Behavior of the Alkali-Metal Dodecahydro-Closo-Dodecacaborates," *American Chemical Society National Meeting, Washington D.C., ACS Division of Fuel Chemistry, Preprints*; Vol. 54 (2), **2009**.
- Her, J.-H.; Zhou, W.; Stavila, V.; Brown, C.M.; Udovic, T.J. "The Role of Cation Size on the Structural Behavior of the Alkali-Metal Dodecahydro-Closo-Dodecacaborates," *J. Phys. Chem. C*; Vol. 113, **2009**; p. 11187.
- Kim, Y.-H.; Sun, Y.Y.; Zhang, S.B. "Ab Initio Calculations Predicting the Existence of an Oxidized Calcium Dihydrogen Complex to Store Molecular Hydrogen Densities up to 100 g/L," *Phys. Rev. B*; Vol. 79, **2009**; p. 115424.
- Kim, Y.-H.; Sun, Y.Y.; Choi, W.I.; Kang, J.; Zhang, S.B. "Enhanced Dihydrogen Adsorption in Symmetry-Lowered Metal-Porphyrin-Containing Frameworks," *Phys. Chem. Chem. Phys.*; Vol. 11 (48), **2009**; p. 11400-3.

- Kishore, S; Narehood, D.G.; Goto, H.; Adair, J.H.; Nelson, J.A.; Gutiérrez, H.R.; Sokol, P.E.; Eklund, P.C. "X-Ray Diffraction and H-Storage in Ultra-Small Palladium Particles," *Int. J. Hydrogen Energy*; Vol. 34 (2), **2009**; pp. 952-960.
- Kosynkin, D.V.; Higginbotham, A.L.; Sinitskii, A.; Lomeda, J.R.; Dimiev, A.; Price, B.K.; Tour, J.M. "Longitudinal Unzipping of Carbon Nanotubes to Form Graphene Nanoribbons," *Nature*; Vol. 458, **2009**; pp. 872-876.
- Kuchta, B.; Firlej, L.; Pfeifer, P.; Wexler, C. "Numerical Estimation of Hydrogen Storage Limits in Carbon Based Nanospaces," *Carbon*; Vol. 47, **2009**; pp. 223-231.
- Kuppler, R.J.; Timmons, D.J.; Fang, Q.-R.; Li, J.-R.; Makal, T.A.; Young, M.D.; Yuan, D.; Zhao, D.; Zhuang, W.; Zhou, H.-C. "Potential Applications of Metal-Organic Frameworks" *Coord. Chem. Rev.*; Vol. 253 (23-24), **2009**; pp. 3042-3066.
- Lachawiec, A.J.; Yang, R.T. "Reverse Spillover of Hydrogen on Carbon-Based Nanomaterials: Evidence of Recombination Using Isotopic Exchange," *J. Phys. Chem. C*; Vol. 113, **2009**; p. 13933.
- Leonard, A.D.; Tour, J.M.; et al. "Nanoengineered Carbon Scaffolds for Hydrogen Storage," *J. Am. Chem. Soc.*; Vol. 131 (2), **2009**; pp. 723-728.
- Li, J.-L.; Timmons, D.; Zhou, H.-C. "Interconversion Between Molecular Polyhedra and Metal-Organic Frameworks," *J. Am. Chem. Soc.*; Vol. 131, **2009**; p. 6368.
- Li, J.-R.; Kuppler, R.J.; Zhou, H.-C. "Selective Gas Adsorption and Separation in Metal-Organic Frameworks," *Chem. Soc. Rev.*; Vol. 38, **2009**; pp. 1477-1504.
- Li, J.-R.; Zhou, H.-C. "Metal-Organic Hendecahedra Assembled from Dimetal-Paddlewheel Nodes and Mixtures of Ditopic Linkers with 120 and 90° Bend-Angles," *Angew. Chem. Int. Ed.*; Vol. 48, **2009**; pp. 8465-8468.
- Li, Y.; Zhou, Z.; Shen, P.; Zhang, S.B.; Chen, Z. "Computational Studies on Hydrogen Storage in Aluminum Nitride Nanowires/Tubes," *Nanotechnology*; Vol. 20, **2009**; p. 215701.
- Lin, X.; Telepeni, I.; Blake, A.J.; Dailly, A.; Brown, C.M.; Simmons, J.; Zoppi, M.; Walker, G.S.; Thomas, K.M.; Mays, T.J.; Hubberstey, P.; Champness, N.R.; Schroder, M. "High Capacity Hydrogen Adsorption in Cu(II) Tetracarboxylate Framework Materials: The Role of Pore Size, Ligand Functionalization, and Exposed Metal Sites," *J. Am. Chem. Soc.*; Vol. 131, **2009**; p. 2159.
- Ma, S.-Q.; Simmons, J. M.; Sun, D.-F.; Yuan, D.-Q.; Zhou, H.-C. "Porous Metal-Organic Frameworks Based on an Anthracene Derivative: Syntheses, Structure Analysis and Hydrogen Sorption Studies," *Inorg. Chem.*; Vol. 48, **2009**; p. 5263.
- Ma, S.-Q.; Simmons, J.M.; Yuan, D.-Q.; Li, J.-R.; Weng, W.; Liu, D.-J.; Zhou, H.-C. "A Nanotubular Metal-Organic Framework with Permanent Porosity: Structure Analysis and Gas Sorption Studies," *Chem. Commun.*; **2009**; pp. 4049-4051.
- Ma, S.-Q.; Sun, D.-F.; Forster, P.M.; Yuan, D.-Q.; Zhuang, W.-J.; Chen, Y.-S.; Parise, J.; Zhou, H.-C. "A Three-Dimensional Porous Metal-Organic Framework Constructed from Two-Dimensional Sheets via Interdigitation Exhibiting Dynamic Features," *Inorg. Chem.*; Vol. 48, **2009**; p. 4616.

- Ma, S.-Q.; Sun, D.-F.; Yuan, D.-Q.; Wang, X.-S.; Zhou, H.-C. "Preparation and Gas Adsorption Studies of Three Mesh-Adjustable Molecular Sieves with a Common Structure," *J. Am. Chem. Soc.*; Vol. 131, **2009**; p. 6445.
- Ma, S.-Q.; Yuan, D.-Q.; Chang, J.-S.; Zhou, H.-C. "Investigation of Gas Adsorption Performances and H₂ Affinities of Porous Metal-Organic Frameworks with Different Entatic Metal Centers," *Inorg. Chem.*; Vol. 48, **2009**; p. 5398.
- Ma, S.-Q.; Yuan, D.-Q.; Wang, X.-S.; Zhou, H.-C. "Microporous Lanthanide Metal-Organic Frameworks Containing Coordinatively Linked Interpenetration: Syntheses, Gas, Adsorption Studies, Thermal Stability Analysis, and Photoluminescence Investigation," *Inorg. Chem.*; Vol. 48, **2009**; p. 2072.
- Ma, S.; Collier, C.; Zhou, H.-C. "Design and Construction of Metal-Organic Frameworks for Hydrogen Storage and Selective Gas Adsorption," Chen, L.; Hong, M.-C., eds. *Design and Construction of Coordination Polymers*. New York: Wiley, **2009**; pp. 353-373.
- McNicholas, T.P.; Ding, L.; Yuan, D.; Liu, J. "Density Enhancement of Aligned Single-Walled Carbon Nanotube Thin Films on Quartz Substrates by Sulfur-Assisted Synthesis," *Nano Lett.*; Vol. 9, **2009**; pp. 3646-3650.
- Narehood, D.G.; Kishore, S.; Goto, H.; Adair, J.H.; Nelson, J.A.; Gutierrez, H.R.; Eklund, P.C. "X-Ray Diffraction and H-Storage in Ultra-Small Palladium Particles," *Int. J. Hydrogen Energy*; Vol. 34, **2009**; p. 952.
- Pfeifer, P.; Wexler, C.; Suppes, G.; Hawthorne, F.; Jalisatgi, S.; Lee, M.; Robertson, D. "Multiply Surface-Functionalized Nanoporous Carbon for Vehicular Hydrogen Storage," *DOE Hydrogen Program 2009 Annual Progress Report*.
- Purewal, J.; Kieth, J.B.; Ahn, C.C.; Fultz, B.; Brown, C.M.; Tyagi, M. "Adsorption and Melting of Hydrogen in Potassium-Intercalated Graphite," *Phys. Rev. B*; Vol. 79, **2009**; p. 054305.
- Purewal, J.J.; Kabbour, H.; Vajo, J.J.; Ahn, C.C.; Fultz, B. "Pore Size Distribution and Supercritical Hydrogen Adsorption in Activated Carbon Fibers," *Nanotechnology*; Vol. 20, **2009**; p. 204012.
- Qiaowei, L.; Wenyu, Z.; Miljanic, O.S.; Chi-Hau, S.; Yan-Li, Z.; Lihua, L.; "Docking in Metal-Organic Frameworks," *Science*; Vol. 325 (5942), **2009**; pp. 855-859.
- Scott, T.A.; Ooro, B.A.; Collins, D.J.; Shatruk, M.; Yakovenko, A.; Dunbar, K.R.; Zhou, H.-C. "After 118 Years, the Isolation of Two Common Radical Anion Reductants as Simple, Stable Solids," *Chem. Commun.*; **2009**; pp. 65-67.
- Sha, X.; Chen, L.; Cooper, A.C.; Pez, G.P.; Cheng, H. "Hydrogen Absorption and Diffusion in Bulk α -MoO₃," *J. Phys. Chem. C*; Vol. 113 (26), **2009**; pp. 11399-11407.
- Singh, A.K.; Ribas, M.A.; Yakobson, B.I. "H-Spillover through the Catalyst Saturation: An Ab Initio Thermodynamics Study," *Am. Chem. Soc. Nano*; Vol. 3, **2009**; p. 1657.
- Sun, Y.Y.; Lee, K.; Kim, Y.-H.; Zhang, S.B. "Ab Initio Design of Ca-Decorated Organic Frameworks for High Capacity Molecular Hydrogen Storage with Enhanced Binding," *Appl. Phys. Lett.*; Vol. 95, **2009**; p. 033109.

- Tranchemontagne, D.J.; Mendoza-Cortes, J.L.; O’Keeffe, M.; Yaghi, O.M. “Secondary Building Units, Nets and Bonding in the Chemistry of Metal-Organic Frameworks,” *Chem. Soc. Rev.*; Vol. 38, **2009**; pp. 1257-1283.
- Wang, L.F.; Yang, F.H.; Yang, R.T. “Hydrogen Storage Properties of B- and N-Doped Microporous Carbon,” *AIChE J.*; Vol. 55, **2009**; p. 1823.
- Wang, L.F.; Yang, F.H.; Yang, R.T.; Miller, M.A. “Effect of Surface Oxygen Groups in Carbons on Hydrogen Storage by Spillover,” *Ind. Eng. Chem. Res.*; Vol. 48, **2009**; p. 2920.
- Wang, L.; Lee, K.; Sun, Y.-Y.; Lucking, M.; Chen, Z.; Zhao, J.; Zhang, S.B. “Graphene Oxide as an Ideal Substrate for Hydrogen Storage,” *J. Am. Chem. Soc. Nano*; Vol. 3, **2009**; pp. 2995-3000.
- Wang, L.; Zhao, J.; Zhou, Z.; Zhang, S.B.; Chen, Z. “First-Principles Study of Molecular Hydrogen Dissociation on Doped Al₁₂X (X= B, Al, C, Si, P, Mg, Ca) Clusters,” *J. Comp. Chem.*; Vol. 30, **2009**; p. 2509.
- Wang, L.F.; Yang, R.T. “Hydrogen Storage Properties of N-Doped Microporous Carbon,” *J. Phys. Chem. C*; Vol. 113, **2009**; p. 21883.
- Wang, X.-S.; Ma, S.; Yuan, D.; Yoon, J.; Hwang, Y.; Chang, J.-S.; Wang, X.; Jørgensen, M.; Chen, Y.-S.; Zhou, H.-C. “A Large-Surface-Area Boracite-Network-Topology Porous MOF Constructed from Conjugated Ligand Exhibiting High Hydrogen Uptake Capacity,” *Inorg. Chem.*; Vol. 48, **2009**; pp. 7519-7521.
- Worsley, M.A.; Kucheyev, S.O.; Kuntz, J.D.; Hamza, A.V.; Satcher, J.H.; Baumann, T.F. “Stiff and Electrically Conductive Composites of Carbon Nanotubes, Aerogels, and Polymers,” *J. Mater. Chem.*; Vol. 19, **2009**; p. 3370.
- Worsley, M.A.; Kucheyev, S.O.; Satcher, J.H.; Baumann, T.F. “Mechanically Robust and Electrically Conductive Carbon Nanotube Foams,” *Appl. Phys. Lett.*; Vol. 94, **2009**; p. 073115.
- Worsley, M.A.; Kuntz, J.D.; Cervantes, O.; Han, T.Y.; Gash, A.E.; Satcher, J.H.; Baumann, T.F. “Route to High Surface Area TiO₂/C and TiCN/C Composites,” *J. Mater. Chem.*; Vol. 19, **2009**; p. 7146.
- Worsley, M.A.; Kuntz, J.D.; Pauzauskie, P.J.; Cervantes, O.; Zaug, J.M.; Gash, A.E.; Satcher, J.H.; Baumann, T.F. “High Surface Area Carbon Nanotube-Supported Titanium Carbonitride Aerogels,” *J. Mater. Chem.*; Vol. 19, **2009**; pp. 5503-5506.
- Worsley, M.A.; Satcher, J.H.; Baumann, T.F. “Enhanced Thermal Transport in Carbon Aerogel Nanocomposites Containing Double-Walled Carbon Nanotubes,” *J. Appl. Phys.*; Vol. 105, **2009**; p. 084316.
- Yang, R.T.; Wang, Y.H. “Catalyzed Hydrogen Spillover for Hydrogen Storage,” *J. Am. Chem. Soc.*; Vol. 131, **2009**; p. 4224.
- Yoon, M.; Yang, S.; Zhang, Z. “Interaction Between Hydrogen Molecules and Metallofullerenes,” *J. Chem. Phys.*; Vol. 131, **2009**; p. 064707.

Yuan, S.; Kirklin, S.; Dorney, B.; Liu, D.-J.; Yu, L. "Nanoporous Polymers Containing Stereo-Contorted Cores for Hydrogen Storage," *Macromolecules*; Vol. 42 (5), **2009**; pp. 1554-1559.

Zhang, C.-G.; Zhang, R.; Wang, Z.-X.; Zhou, Z.; Zhang, S.B.; Chen, Z. "Ti-Substituted Boranes as Hydrogen Storage Materials: A Computational Quest for the Ideal Combination of Stable Electronic Structure and Optimal Hydrogen Uptake," *Chem. Eur. J.*; Vol. 15, **2009**; pp. 5910-5919.

Zhang, Z.; Sun, Z.; Yao, J.; Kosynkin, D.V.; Tour, J.M. "Transforming Carbon Nanotube Devices into Nanoribbon Devices," *J. Am. Chem. Soc.*; Vol. 131, **2009**; pp. 13460-13463.

Zhao, D.; Yuan, D.-Q.; Sun, D.-F.; Zhou, H.-C. "Stabilization of Metal-Organic Frameworks with High Surface Areas by the Incorporation of Mesocavities with Microwindows," *J. Am. Chem. Soc.*; Vol. 131 (26), **2009**; pp. 9186-9188.

2010

Anderson, R.J.; McNicholas, T.P.; Kleinhammes, A.; Wang, A.; Liu, J.; Wu, Y. "NMR Methods for Characterizing the Pore Structures and Hydrogen Storage Properties of Microporous Carbons," *J. Am. Chem. Soc.*; Vol. 132 (25), **2010**; pp. 8618-8626.

Chen, H.; Yang, R.T. "Catalytic Effects of TiF₃ on Hydrogen Spillover on Pt/Carbon for Hydrogen Storage," *Langmuir*; Vol. 26 (19), 2010; pp. 15394-15398.

Choi, W.I.; Jhi, S.-H.; Kim, K.; Kim, Y.-H. "Divacancy-Nitrogen-Assisted Transition Metal Dispersion And Hydrogen Adsorption in Defective Graphenes: A First-Principles Study," *Phys. Rev. B*; Vol. 81, **2010**; p. 085441.

Collins, D.J.; Ma, S.; Zhou, H.-C. "Hydrogen and Methane Storage in Metal Organic Frameworks," MacGillivray, L., ed. *Metal-Organic Frameworks: Design and Application*. New York: Wiley, **2010**; pp. 249-266.

Fang, Q.-R.; Makal, T.A.; Young, M.D.; Zhou, H.-C. "Recent Advances in the Study of Mesoporous Metal-Organic Frameworks," *Comments on Inorganic Chemistry*; Vol. 31, **2010**; pp. 165-195.

Fang, Q.; Sculley, J.; Zhu, G.; Zhou, H.-C. "Porous Metal-Organic Frameworks," *Comprehensive Nanoscience and Technology*. New York: Elsevier Academic Press, **2010**.

Furukawa, H.; Ko, N.; Go, Y.B.; Aratani, N.; Choi, S.B.; Choi, E.; Yazaydin, A.Ö.; Snurr, R.Q.; O'Keeffe, M.; Kim, J.; Yaghi, O.M. "Ultra-high Porosity in Metal-Organic Frameworks," *Science*; Vol. 329 (5990), **2010**; pp. 424-428.

Han, Z.-B.; Zhang, G.-X.; Zeng, M.-H.; Yuan, D.-Q.; Fang, Q.-R.; Li, J.-R.; Ribas, J.; Zhou, H.-C. "Unprecedented Marriage of a Cationic Pentanuclear Cluster and a 2D Polymeric Anionic Layer Based on a Flexible Tripodal Ligand and a Cu(II) Ion," *Inorg. Chem.*; Vol. 49, **2010**; p. 769.

He, H.Y.; Yuan, D.Q.; Ma, H.Q.; Sun, D.F.; Zhang, G.Q.; Zhou, H.-C. "Control over Interpenetration in Lanthanide–Organic Frameworks: Synthetic Strategy and Gas-Adsorption Properties," *Inorg. Chem.*; Vol. 49, **2010**; pp. 7605-7607.

Jin, Z.; Sun, Z.Z.; Simpson, L.J.; O'Neill, K.J.; Parilla, P.A.; Li, Y.; Stadie, N.P.; Ahn, C.C.; Kittrell, C.; Tour, J. M. "Solution-Phase Synthesis of Heteroatom-Substituted Carbon Scaffolds for Hydrogen Storage," *J. Am. Chem. Soc.*; Vol. 132 (43), **2010**; pp. 15246-15251.

Kleinhammes, A.; Anderson, R.J.; Chen, Q.; Jeong, Y.; Chung, T.C.M.; Wu, Y. "Enhanced Binding Energy and Slow Kinetics of H₂ in Boron-Substituted Graphitic Carbon," *J. Phys. Chem. C*; Vol. 114 (32), **2010**; pp. 13705-13708.

Kuchta, B.; Firlej, L.; Cepel, R.; Pfeifer, P.; Wexler, C. "Structural and Energetic Factors in Designing a Nanoporous Sorbent for Hydrogen Storage," *Colloids and Surfaces A: Physicochem. Eng. Aspects*; Vol. 357, **2010**; pp. 61-66.

Kuchta, B.; Firlej, L.; Roszak, Sz.; Pfeifer, P.; Wexler, C. "Influence of Structural Heterogeneity of Nano-Porous Sorbent Walls on Hydrogen Storage," *Applied Surf. Sci.*; Vol. 256 (17), **2010**; pp. 5270-5274.

Lee, K.; Kim, Y.-H.; Sun, Y.Y.; West, D.; Zhao, Y.; Chen, Z.; Zhang, S.B. "Hole Mediated Hydrogen Spillover Mechanism in Metal-Organic Frameworks," *Phys. Rev. Lett.*; Vol. 104, **2010**; pp. 236101–236104.

Li, J.-R.; Zhou, H.-C. "Bridging-Ligand-Substitution Strategy for the Preparation of Metal-Organic Polyhedra," *Nature Chem.*; Vol. 2, **2010**; pp. 893-898.

Liu, D.-J.; Yuan, S.; Goenaga, G.; Yang, J.; White, D.; Mason, A. "Exploring Applications of Nanomaterials for Fuel Cell and Hydrogen Storage," *Proc. Am. Chem. Soc., Div. Fuel Chem.*; Vol. 55 (1), **2010**.

Lu, W.; Yuan, D.; Zhao, D.; Schilling, C. I.; Plietzsch, O.; Muller, T.; Brase, S.; Guenther, J.; Blumel, J.; Krishna, R.; Li, Z.; Zhou, H.C. "Porous Polymer Networks: Synthesis, Porosity, and Applications in Gas Storage/Separation," *Chem. Mater.*; Vol. 22, **2010**; pp. 5964-5972.

Ma, S.; Zhou, H.-C. "Gas Storage in Porous Metal-Organic Frameworks for Clean Energy Applications," *Chem. Comm.*; Vol. 46, **2010**; pp. 44-53.

McNicholas, T.P.; Wang, A.; O'Neill, K.; Anderson, R.J.; Stadie, N.P.; Kleinhammes, A.; Parilla, P.; Simpson, L.; Ahn, C.C.; Wang, Y.; Wu, Y.; Liu, J. "H₂ Storage in Microporous Carbons from PEEK Precursors," *J. Phys. Chem. C*; Vol. 114 (32), **2010**; pp. 13902-13908.

Purewal, J. *Hydrogen Adsorption by Alkali Metal Graphite Intercalation Compounds*. Ph.D. Thesis. Pasadena, California: California Institute of Technology, **2010**.

Sha, X.; Cooper, A.C.; Bailey III, W.H.; Cheng, H. "Revisiting Hydrogen Storage in Bulk BC₃," *J. Phys. Chem. C*; Vol. 114, **2010**; p. 3260.

Shao, L.H.; Biener, J.; Kramer, D.; Viswanath, R.N.; Baumann, T.F.; Hamza, A.V.; Weissmuller, J. "Electrocapillary Maximum and Potential of Zero Charge of Carbon Aerogels," *Phys. Chem. Chem. Phys.*; Vol. 12, **2010**; p. 7580.

- Singh, A.K.; Sadrzadeh, A.; Yakobson, B.I. "Metallacarboranes: Toward Promising Hydrogen Storage Metal-Organic Frameworks," *J. Am. Chem. Soc.*; Vol. 132, **2010**; pp. 14126-14129.
- Stuckert, N.R.; Wang, L.F.; Yang, R.T. "Characteristics of Hydrogen Storage by Spillover on Pt-doped Carbon and Catalyst-Bridged Metal Organic Framework," *Langmuir*; Vol. 26, **2010**; p. 11963.
- Sumida, K.; Horike, S.; Kaye, S.S.; Herm, Z.R.; Queen, W.L.; Brown, C.M.; Grandjean, F.; Long, G.J.; Dailly, A.; Long, J.R. "Hydrogen Storage and Carbon Dioxide Capture in an Iron-Based Sodalite-Type Metal-Organic Framework (Fe-BTT) Discovered via High-Throughput Methods," *Chem. Sci.*; Vol. 1, **2010**; pp. 184-191.
- Sun, D.; Ma, S.; Simmons, J.M.; Li, J.-R.; Yuan, D.; Zhou, H.-C. "An Unusual Case of Symmetry-Preserving Isomerism," *Chem. Comm.*; Vol. 46, **2010**; pp. 1329-1331.
- Wang, L.F.; Yang, R.T. "Hydrogen Storage on Carbon-Based Adsorbents and Storage at Ambient Temperature by Hydrogen Spillover," *Catalysis Reviews – Sci. & Eng.*; Vol. 54(4), **2010**; pp. 411-461.
- Wang, L.F.; Yang, R.T. "Hydrogen Storage Properties of Low-Silica Type X Zeolites," *Ind. Eng. Chem. Res.*; Vol. 49 (8), **2010**; pp. 3634-3641.
- Wang, Z.; Yang, F.H.; Yang, R.T. "Enhanced Hydrogen Spillover on Carbon Surfaces Modified by Oxygen Plasma," *J. Phys. Chem. C*; Vol. 114, **2010**; p. 1601.
- Wang, Z.; Yang, R.T. "Enhanced Hydrogen Storage on Pt-Doped Carbon by Plasma Reduction," *J. Phys. Chem. C*; Vol. 114, **2010**; p. 5956.
- Wexler, C.; Olsen, R.; Pfeifer, P.; Kuctha, B.; Firlej, L.; Roszak, S. "Numerical Analysis of Hydrogen Storage in Carbon Nanopores," *Int. J. Mod. Phys. B*; Vol. 24 (25-26), **2010**; pp. 5152-5162.
- Worsley, M.A.; Kuntz, J.D.; Satcher, J.H.; Baumann, T.F. "Synthesis and Characterization of Monolithic, High Surface Area SiO₂/C and SiC/C Composites," *J. Mat. Chem.*; Vol. 20, **2010**; p. 4840.
- Worsley, M.A.; Pauzauskie, P.J.; Olson, T.Y.; Satcher, J.H.; Baumann, T.F. "Synthesis of Graphene Aerogels with High Electrical Conductivity," *J. Am. Chem. Soc.*; Vol. 132, **2010**; p. 14067.
- Worsley, M.A.; Satcher, J.H.; Baumann, T.F. "Influence of Sodium Dodecylbenzene Sulfonate on the Structure and Properties of Carbon Aerogels," *J. Non-Cryst. Solids*; Vol. 356, **2010**; p. 172.
- Worsley, M.A.; Stadermann, M.; Wang, Y.M.; Satcher, J.H.; Baumann, T.F. "High Surface Area Carbon Aerogels as Porous Substrates for Direct Growth of Carbon Nanotubes," *Chem. Comm.*; Vol. 46, **2010**; p. 9253.
- Wu, H.; Simmons, J. M.; Liu, Y.; Brown, C.; Wang, X.-S.; Ma, S.; Peterson, V.; Southon, P.; Kepert, C.; Zhou, H.-C.; Yildirim, T.; Zhou, W. "Metal-Organic Frameworks with Exceptionally High Methane Uptake: Where and How is Methane Stored?" *Chemistry – A European Journal*; Vol. 16 (17), **2010**; pp. 5205-5214.

Xia, J.; Yuan, S.; Wang, Z.; Kirklin, S.; Dorney, B.; Liu D.-J.; Yu, L. "Nanoporous Polyporphyrin as Adsorbent for Hydrogen Storage," *Macromolecules*; Vol. 43, **2010**; pp. 3325-3330.

Yang, R.; Li, L.; Xiong, Y.; Li, J.-R.; Zhou, H.-C.; Su, C.-Y. "Two Robust Porous Metal–Organic Frameworks Sustained by Distinct Catenation: Selective Gas Sorption and Single-Crystal-to-Single-Crystal Guest Exchange," *Chem.-Asian J.*; Vol. 5, **2010**; pp. 2358-2368.

Yuan, D.; Zhao, D.; Sun, D.; Zhou, H.-C. "An Isoreticular Series of Metal-Organic Frameworks with Dendritic Hexa-Carboxylate Ligands and Exceptionally High Gas Uptake Capacity," *Angew. Chem. Int. Ed.*; Vol. 49, **2010**; pp. 5357-5361.

Yuan, S.; Dorney, B.; White, D.; Kirklin, S.; Zapol, P.; Yu L.; Liu, D.-J. "Microporous Polyphenylenes with Tunable Pore Size for Hydrogen Storage," *Chem. Comm.*; Vol. 46, **2010**; pp. 4547-4549.

Zhao, D.; Yuan, D.; Krishna, R.; Van Baten, J. M.; Zhou, H.C. "Thermosensitive Gating Effect and Selective Gas Adsorption in a Porous Coordination Nanocage," *Chem. Comm.*; Vol. 46, **2010**; pp. 7352-7354.

Zhao, D.; Yuan, D.; Yakovenko, A.; Zhou, H.-C. "A NbO-Type Metal-Organic Framework Derived from a Polyyne-Coupled Di-Isophthalate Linker Formed In Situ," *Chem. Comm.*; Vol. 46, **2010**; pp. 4196-4198.

Zhao, Y.; Kim, Y.-H.; Zhang, S.B.; Heben, M.J. "Theory of Hydrogen Storage in Nanoscale Materials," *The Oxford Handbook of Nanoscience and Technology, Frontiers and Advances*. Vol. 3. London: Oxford University Press, **2010**; pp. 700-736.

Zhao, Y.; Xu, Q.; Simpson, L.J.; Dillon, A.C. "Prediction of Diamond-Like, Metallic Boron Structures," *Chem. Phys. Lett.*; Vol. 496 (4-6), **2010**; pp. 280-283.

Zhuang, W.J.; Ma, S.; Wang, X.-S.; Yuan, D.; Li, J.-R.; Zhao, D.; Zhou, H.-C. "Introduction of Cavities up to 4 nm into a Hierarchically-Assembled Metal-Organic Framework Using an Angular, Tetratopic Ligand," *Chem. Comm.*; Vol. 46, **2010**; pp. 5223-5225.

2011

Biener, J.; Stadermann, M.; Suss, M.; Worsley, M.A.; Biener, M.M.; Rose, K.A.; Baumann, T.F. "Advanced Carbon Aerogels for Energy Applications," *Energy Environ. Sci.*; Vol. 4, **2011**; p. 656.

Ding, F.; Yakobson, B.I. "Challenges in Hydrogen Adsorptions: from Physisorption to Chemisorption" *Frontiers of Physics* Vol. 6 (2), **2011**; pp. 142-150

Han, T.Y.; Worsley, M.A.; Baumann, T.F.; Satcher, J.H. "Synthesis of ZnO-Coated Activated Carbon Aerogel by Simple Sol-Gel Route," *J. Mat. Chem.*; Vol. 21, **2011**; p. 330.

Liu, X.; Peaslee, D.; Jost, C.Z.; Baumann, T.F.; Majzoub, E.H. "Systematic Pore-Size Effects of Nanoconfinement of LiBH₄: Elimination of Diborane Release and Tunable Behavior of Hydrogen Storage Applications," *Chem. Mat.*; Vol. 23, **2011**; p. 1331.

- Lu, W.; Yuan, D.; Zhao, D.; Zhou, H.-C. "Highly Stable Porous Polymer Networks with Exceptionally High Gas-Uptake Capacities," *Advanced Materials*; online, **2011**.
- Makal, T. A.; Yuan, D.; Zhao, D.; Zhou, H.-C. "Metal-Organic Frameworks," *The Chemistry of Nanostructured Materials*, Vol. II. Yang, P.; Ed. World Scientific: Singapore, **2011**; pp. 37-64.
- Olsen, R.J.; Firlej, L.; Kuchta, B.; Taub, H.; Pfeifer, P.; Wexler, C. "Sub-Nanometer Characterization of Activated Carbon by Inelastic Neutron Scattering," *Carbon*; Vol. 49 (5), **2011**; pp. 1663-1671.
- Peterson, V.K.; Brown, C.M.; Liu, Y.; Kepert, C. "Structural Study of D₂ within the Trimodal Pore System of a Metal Organic Framework," *J. Phys. Chem. C*; Vol. 115 (17), **2011**; pp. 8851-8857.
- Singh, A.K.; Lu, J.; Aga, R.S.; Yakobson, B.I. "Hydrogen Storage Capacity of Carbon-Foams: Grand Canonical Monte Carlo Simulations," *J. Chem. Phys. C*; Vol. 115, **2011**; pp. 2476-2482.
- Sumida, K.; Her, J.-H.; Dinca, M.; Murray, L.J.; Schloss, J.M.; Pierce, C.J.; Thompson, B.A.; FitzGerald, S.A.; Brown, C.M.; Long, J.R. "Neutron Scattering and Spectroscopic Studies of Hydrogen Adsorption in Cr₃(BTC)₂ - A Metal-Organic Framework with Exposed Cr²⁺ Sites," *J. Phys. Chem. C*; Vol. 115 (16), **2011**; pp. 8414-8421.
- Sun, Y.Y.; Kim, Y.-H.; Lee, K.; West, D.; Zhang, S.B. "Altering the Spin State of Transition Metal Centers in Metal-Organic Frameworks by Molecular Hydrogen Adsorption: A First-Principles Study," *Phys. Chem. Chem. Phys.*; Vol. 13, **2011**; pp. 5042-5046.
- Worsley, M.A.; Olson, T.Y.; Lee, J.R.I.; Willey, T.M.; Nielsen, M. H.; Roberts, S.K.; Pauzuskie, P.J.; Biener, J.; Satcher, J.H.; Baumann, T. F. "High Surface Area, sp²-Cross-Linked Three-Dimensional Graphene Monoliths," *J. Phys. Chem. Lett.*; Vol. 2, **2011**; p. 921.
- Yang, Y.; Brown, C.M.; Zhao, C.; Chaffee, A.L.; Nick, B.; Zhao, D.; Webley, P.A.; Schalch, J.; Simmons, J.M.; Liu, Y.; Her, J.-H.; Buckley, C.E.; Sheppard, D.A. "Micro-Channel Development and Hydrogen Adsorption Properties in Templated Microporous Carbons Containing Platinum Nanoparticles," *Carbon*; Vol. 49 (4), **2011**; pp. 1305-1317.
- Yuan, D.; Zhao, D.; Timmons, D. J.; Zhou, H.-C. "A Stepwise Transition from Microporosity to Mesoporosity in Metal-Organic Frameworks by Thermal Treatment," *Chem. Sci.*; Vol. 2, **2011**; pp. 103-106.
- Yuan, S.; White, D.; Mason, A.; Liu, D.-J. "Porous Organic Polymers Containing Carborane for Hydrogen Storage," *Int. J. of Mater. Research*; online, **2011**.
- Zhao, D.; Timmons, D.J.; Yuan, D.Q.; Zhou, H.C. "Tune the Topology and Functionality of Metal-Organic Frameworks by Ligand Design," *Accounts Chem. Res.*; Vol. 44, **2011**; pp. 123-133.
- Zhong, J.; Yao, J.; Kittrell, C.; Tour, J.M. "Bottom-Up Preparation of Synthetic Graphenes." *American Chemical Society NANO* (5), **2011**; pp. 4112-4117.

To Be Published

Anderson, R.J.; McNicholas, T.P.; Kleinhammes, A.; Wang, A.; Liu, J.; Wu, Y. “NMR Methods for Characterizing the Pore Structures and Hydrogen Storage Properties of Microporous Carbons,” submitted to *J. Am. Chem. Soc.*

Argonne, U. of Chicago, U. of North Carolina, “Investigation on hydrogen-polymer interaction in nanospace using high pressure NMR method,” under preparation.

Ciobanu, C.V.; Zhao, Y. “Self-Mediated Hydrogen Migration in Pure Carbon Materials,” in preparation.

Engtrakul, C.; Blackburn, J.L.; Bult, J.B.; O’Neill, K.J.; Barker, J.G.; Parilla, P.A.; Gennett, T.; Simpson, L.J. “Synthesis of Novel Lithiated BC₆ Materials with Enhanced H₂ Binding Sites,” in preparation.

Gennett, T.; Engtrakul, C.; Curtis, C.; Ellis, J.E.; Blackburn, J.; Dillon, A.C.; Simpson, L.; Jones, K.; Parilla, P.; Heben, M.J. “Hydrogenation Mechanism for the Reaction of Single-Walled Carbon Nanotubes with Tetrahydrofuran,” submitted to *J. Am. Chem. Soc.*

Goenaga, G.A.; Yuan, S.; Liu, L.; Liu, D.-J. “Cobalt-containing Porous Organic Polymer (POP) as Precursor of New Electrode Catalyst for Oxygen Reduction Reaction,” to be submitted.

Kim, Y.-H.; Sun, Y.Y.; Choi, W.I.; Kang, J.; Zhang, S.B. “Symmetry-Assisted Hydrogen Adsorption And Control On Transition Metal Incorporated Porphyrins,” *Phys. Rev. Lett.*; under review.

Kraus, M.; Ilavsky, J.; Beckner, M.; Wexler, C.; Pfeifer, P. “Average Structural Units of Activated and Non-Activated Nanoporous Carbons from USAXS Measurements,” *J. Appl. Crystallog.*; in preparation.

Lee, K.; Lucking, M.; Sun, Y.Y.; Chen, Z.; Zhang, S. “Structural Stability and Hydrogen Storage Properties of Ti Anchored on Silica,” *Nano Lett.*; in preparation.

Leimkuehler, E.; Tekeei, A.; Gordon, M.; Burrell, J.; Sawyer, B.; Romanos, J.; Pfeifer, P.; Suppes, G.J. “Highly Nanoporous Activated Carbon Process Characterization,” submitted to *Ind. Eng. Chem. Res.*

Liu, Y., et al. “Studying Hydrogen Spillover on Pt-Single-Walled Carbon Nanohorns Using Inelastic Neutron Scattering and High Pressure Gas Adsorption Experiments,” in preparation.

Liu, Y.; Brown, C.M.; Neumann, D.A.; Geohegan, D.B.; Puzos, A.A.; Rouleau, C.M.; Hu, H.; Styers-Barnett, D.; Yakobson, B.I.; Krasnov, P.O. “Studying Hydrogen Spillover on Pt-decorated Single-Walled Carbon Nanohorns Using Inelastic Neutron Scattering and High Pressure Gas Adsorption Experiments,” to be submitted.

Rajagopalan, R.; Foley, H. “A Simple Approach to Synthesize Nanoporous Carbons with High Heats of Adsorption for Hydrogen,” in preparation.

Singh, A.K.; Yakobson, B.I. “Effect of Catalyst Anchors on their Binding and Spillover,” in preparation.

Sun, D.; Ma, S.; Simmons, J.M.; Li, J.-R.; Yuan, D.; Zhou, H.-C. “Comparative Evaluation of Carbon-Foams Hydrogen Storage Capacity through Monte-Carlo Simulations,” in preparation.

Yoon, M.; Scheffler, M. “High-Capacity Hydrogen Storage in Metal-Free Organic Molecular Crystals,” submitted to *Phys. Rev. Lett.* April 5, 2011.

Yuan, S.; White, D.; Mason, A.; Repogle, B.; Yu, L.; Liu, D.-J. “Improving Hydrogen Adsorption Enthalpy through Coordinatively Unsaturated Cobalt in Porous Polymer,” to be submitted.

Zhao, Y., et al. “Energetics of Hydrogenation of Single-Walled Carbon Nanotubes,” in preparation.

Zhao, Y.; Dillon, A.C. “Rich Chemistry and Structure Rule of sp^2 and sp^3 Boron,” in preparation.

A.2 People Who Worked in the Hydrogen Sorption Center of Excellence

- **Air Products and Chemicals Inc. (APCI)**, led by Alan Cooper, Hansong Cheng, and Guido Pez (retired).
 - Charles Coe, John Zielinski, Maw-Lin Foo, Liang Chen (Professor at Ningbo Institute of Materials Technology and Engineering, Chinese Academy of Science, Ningbo, China), Michael Kimak, Garret Lau, Xianwei Sha, Donald Fowler, Wade Bailey
- **Argonne National Laboratory (ANL)**, led by Di-Jia Liu and Yuping Lu, University of Chicago.
 - Shengwen Yuan, Desiree White, Alex Mason, Briana Repogle, Peter Zapol, Brian Dorney, Scott Kirklin, Suhas Niyogi
 - University of Chicago: Jiangbin Xia, Zhuo Wang
- **California Institute of Technology (Caltech)**, led by Channing Ahn.
 - Dr. Anne Dailly (Staff General Motors Research and Development), Dr. Houria Kabbour (staff CNRS Unité de Catalyse et de Chimie du Solide, Lille, France), Angelique Saulnier, Dr. Justin Purewal, Dr. Michael Winterrose, Nicholas Stadie, Dr. Justin Purewal, Dr. Michael Winterrose (Staff at Lincoln Laboratories, Lexington, MA)
- **Duke University**, led by Jie Liu.
 - Hang Qi, Chenguang Lu, Thomas P. McNicholas, Anmiao Wang
- **Lawrence Livermore National Laboratory (LLNL)**, led by Ted Baumann and Joseph Satcher.
 - Marcus Worsley (postdoc converted to staff), Julie Herberg
- **University of Michigan (Michigan)**, led by Ralph T. Yang.
 - Hao Chen, Thomas R. DiRaimondo, Anthony J. Lachawiec, Jr. (Senior Engineer, Intel Research Center in Oregon), Yingwei Li (Professor of

Chemistry, South China University of Science and Technology), Nick Stuckert, Lifeng Wang, Yuhe Wang (Professor of Chemistry, Harbin Normal University, China)

- **University of Missouri-Columbia (Missouri)**, led by Peter Pfeifer.
 - C. Wexler, R. Olsen, B. Kuctha, L. Firlej, S. Roszak, R. Cepel, J. Burrell, M. Kraus, M. Beckner, G. Suppes
- **National Institute of Standards and Technology (NIST)**, led by Dan Neumann and Craig Brown.
 - Jae-Hyuk (G.E. Global Research in New York), Yun Liu (converted to staff at NIST), Matthew Hudson, Wendy Queen
- **National Renewable Energy Laboratory (NREL)**, led by Lin Simpson, Michael Heben, Anne Dillon, Thomas Gennett, Phillip Parilla, Jeffrey Blackburn, Chaiwat Engtrakul, Yufeng Zhao, Shengbai Zhang, and Katherine Hurst.
 - C.J. Curtis, M. Davis, T. Elko-Hansen, K.M. Jones, Y-H. Kim, K.J. O'Neill, J.D. Rocha, E. Whitney, R. Deshpande
- **Oak Ridge National Laboratory (ORNL)**, led by Dave Geohegan, Mina Yoon, and Alexander A. Puretzky.
 - M. Yoon (postdoc hired as staff at Oak Ridge Natl. Lab, and Univ. Tennessee), Yang, Shenyan, Hicke, Christian, Wang, Enge, Zhang, Zhenyu, A.A. Puretzky, D. Styers-Barnett, H. Hu, B. Zhao, H. Cui, C.M. Rouleau, G. Eres, J.J. Jackson, R.F. Wood, S. Pannala, J.C. Wells, D.W. DePaoli, D.-W. Lee, M.-D. Cheng, I.N. Ivanov
- **Pennsylvania State University (Penn State)**, led by Peter C. Eklund (deceased), Michael Chung, Henry Foley, and Vincent Crespi.
 - R. Rajagopalan, Z. C. Zhang, W. Chen, X.M. Liu, H.E. Romero, K. Adu
- **Rice University (Rice)**, led by James Tour, Carter Kittrell, and Richard E. Smalley (deceased).
 - Ashley D. Leonard, Jared L. Hudson, Hua Fan, Richard Booker, S. Chakraborty, E. Billups, H.K. Schmidt, M. Pasquali, J.J. Stephenson, J.L. Hudson, B.P. Price
- **Rice University**, led by Boris Yakobson and Robert Hauge.
 - Feng Ding (Hong Kong Polytechnic University, Professor), Yu Lin (Schlumberger Inc., Houston, Senior Project Leader), Pavel Krasnov (Krasnoyarsk State University, Russia, Associate Professor), Abhishek Singh (Indian Institute of Science, Bangalore, Professor), Morgana Ribas (Cookson Electronics R&D Centre, Bangalore, Team Leader)
- **Texas A&M University (TAMU)**, led by Hongcai Zhou (formerly of Miami University-Ohio).
 - Andrey Yakovenko, Trevor Makal, Jinhee Park, Julian Sculley, Zhangwen Wei, Yang Yang Liu, Muwei Zhang, Dawei Feng, Kyle Denk, Dr.

Wenjuan Zhuang, Dr. Jian-Rong Li, Dr. Weigang Lu, Dr. Da-Qiang Yuan, Dr. Zhiyong Wang, Dr. Mario Wriedt, Dr. Shengqian Ma (Director's Postdoctoral Fellowship, Argonne National Laboratory, 2008-2010, Assistant Professor, University of South Florida, 2010-present), Dr. David J. Collins (Assistant Professor in the Chemistry Department at SUNY Cortland, 2008-present), Dr. Dan Zhao (Postdoctoral Fellowship, Argonne National Laboratory, 2010-present), Dr. Xi-sen Wang, Dr. Yanxiong Ke (Professor at the East China University of Science and Technology, 2005-present), Dr. Daofeng Sun (Professor at Shandong University, China, 2007-present), Dr. Mark Young, Dr. Xiaodan Guo, Dr. Zhengbo Han

- **University of North Carolina, Chapel Hill (UNC)**, led by Yue Wu and Alfred Kleinhammes.
 - Robert J. Anderson (University of Hawaii John A. Burns School of Medicine, Magnetic Resonance Research Center), Shenghua Mao
- **University of Pennsylvania (Penn)**, led by Alan G. MacDiarmid (deceased), Pen-Cheng Wang, and E.C. Venancio.
- **Former Partner: Michigan/University of California, Los Angeles (UCLA)**, led by Omar Yaghi.
 - A.J. Matzger, A. Centrone, D.Y. Siberio-Pérez, A.R. Millward

A.3 Awards and Special Accomplishments

- **Channing Ahn**
 - Member Expert, International Energy Agency Task 22, “Fundamental and Applied Hydrogen Storage Materials Development,” 2006–2011
- **Craig Brown**
 - The Presidential Early Career Award for Scientists and Engineers
 - Dept. of Commerce Silver Medal
 - Neutron Scattering Society of America 2010 Science Prize
- **Brian Dorney**
 - Outstanding thesis award, Kettering University, based on hydrogen storage research
- **David Geohegan**
 - Fellow of the American Physical Society
- **Michael Heben**
 - Endowed Academic Chair, University of Toledo
 - Interviewed on Lehrer Report
- **Jae-Huyk Her**
 - Young Scientist Travel Award July 2009, American Crystallographic Association, Toronto, ON, Canada
 - Winner of 2009 Sigma-Xi (NIST Chapter) “Materials” Postdoctoral Poster Prize
- **Matthew Hudson**

- Winner of 2011 Sigma-Xi (NIST Chapter) Postdoctoral Poster Prize
- **Yun Liu**
 - Winner of 2008 Sigma-Xi (NIST Chapter) “Materials” Postdoctoral Poster Prize
- **Dan Neumann**
 - Fellow of the American Physical Society
 - Fellow of the Neutron Scattering Society of America
- **Morgana Ribas**
 - Roberto Roca Foundation Fellowship
- **Lin Simpson and the HSCoE**
 - U.S. Department of Energy Hydrogen Program Special Recognition Award
- **Desiree White**
 - Outstanding thesis award, Kettering University and NSF fellow, based on hydrogen storage research
- **Yue Wu**
 - Fellow of the American Physical Society, 2010
- **Boris I. Yakobson**
 - U.S. Department of Energy R&D Award, 2008
 - Nanotech Briefs Nano 50 Innovator Award, 2008
- **Ralph Yang**
 - U.S. Department of Energy Hydrogen Program Special Recognition Award
- **S. Yuan, B. Dorney, S. Kirklin, D. White, J. Xia, Z. Wang, L. Yu, and D.-J. Liu**
 - “Porous Organic Polymers (POPs) for Hydrogen Storage,” Poster Prize at 1st International Conference on Materials for Energy, Karlsruhe, Germany, July 4-8, 2010
- **Shengbai Zhang**
 - Endowed Academic Chair, Rensselaer Polytechnic Institute
- **Hongcai Zhou**
 - Air Products Faculty Excellence Award
 - Scientific Advisory Committee for H2Can, the NSERC Hydrogen Canada Strategic Research Network, 2008-2013

A.4 Patents, Patent Applications, and Records of Invention

Bagzis, L.; Appleby, J.; Pez, G.P.; Cooper, A.C. "Method of Delivering a Reversible Hydrogen Storage Fuel to a Mobile or Stationary Fuel Source," U.S. Patent Application No. 20050013767; January **2005**.

Baumann, T.F.; Worsley, M.A.; Satcher, J.H. "Carbon Nanotube-Filled Activated Carbon Aerogels," Patent Disclosure.

Baumann, T.F.; Worsley, M.A.; Satcher, J.H. "High Surface Area Carbon Foams as Adsorbents for Fuel Gases," Patent Application filed June **2009**.

Biener, J.; Baumann, T.F.; Shao, L.; Weissmueller, J. "Nanoporous Carbon Actuator and Methods of Use Thereof," U.S. Patent Application No. 20100230298; September **2010**.

Cooper, A.C.; Cheng, H.; Pez, G.P.; "Hydrogen Storage Utilizing Carbon Nanotube Materials," U.S. Patent Application No. 20050118091; June **2005**.

Dillon, A.C.; Heben, M.J.; Gennett, T.; Parilla, P.A. "Metal-Doped Single-Walled Carbon Nanotubes and Production Thereof," PCT Patent WO 03/085178; **2008**.

Ecklund, P.C. "Boron-Doped Single-Walled Nanotubes (SWCNT)," U.S. Patent Application No. 20100219383; September **2010**.

Ecklund, P.C., et al. "Hydrogen Storage Material Based on Platelets and/or a Multilayered Core/Shell Structure," U.S. Patent No. 7,288,325; October **2007**.

Farha, O.K.; Hupp, J.T. "Activation of Porous MOF Materials," U.S. Patent Application No. 20110144367; June **2011**.

Farha, O.K.; Hupp, J.T. "Purification of Metal-Organic Framework Materials," U.S. Patent Application No. 20100267951; October **2010**.

Farha, O.K.; Hupp, J.T. "Tetratopic Phenyl Compounds, Related Metal-Organic Framework Materials and Post-Assembly Elaboration," U.S. Patent Application No. 20100170395; July **2010**.

Gennett, T.; Raffaele, R.P.; Landi, B.J.; Heben, M.J. "Carbon Nanotube-Polymer Composite Actuators," U.S. Patent No. 7,361,430; April **2008**.

Geohegan, D.B., et al. "Transparent Conductive Nano-Composites," U.S. Patent No. 7,923,922; April **2011**.

Geohegan, D.B.; Ivanov, I.N.; Poretzky, A.A. "Fabrication of High Thermal Conductivity Arrays of Carbon Nanotubes and Their Composites," U.S. Patent Application No. 20060279191; December **2006**.

Geohegan, D.B.; Ivanov, I.N.; Poretzky, A.A.; Jesse, S.; Hu, B. "Transparent Conductive Nano-Composites," U.S. Patent Application No. 20080191606; August **2008**.

Geohegan, D.B.; Seals, R.D.; Poretzky, A.A.; Fan, X. "Nanorods and Other Materials from Condensed Phase Conversion and Growth Instead of From Vapor," U.S. Patent Application No. 20060111005; May **2006**.

Grigorian, L.; Hornyak, L.; Dillon, A.C.; Heben, M.J. "Continuous Growth of Single-Wall Carbon Nanotubes Using Chemical Vapor Deposition," U.S. Patent No. 7,431,965; October **2008**.

Hauge, R.H.; Xu, Y.-Q.; Peng, H.; Smalley, R.E. "Multi-Step Purification of Single-Wall Carbon Nanotubes," U.S. Patent No. 7,670,583; March **2010**.

Hesse, M.; Mueller, U.; Yaghi, O.M. "Shaped Bodies Containing Metal-Organic Frameworks," U.S. Patent Application No. 20090155588; June **2009**.

Hwang, W.-F.; Chen, Z.; Tour, J.M. "Short, Functionalized, Soluble Carbon Nanotubes, Methods of Making Same, and Polymer Composites Made Therefrom," U.S. Patent Application No. 20090215953; August **2009**.

Hwang, W.-F.; Tour, J.M.; Chen, Z.; Hauge, R.H.; Kobashi, K. "Copolymerization and Copolymers of Aromatic Polymers with Carbon Nanotubes and Products Made Therefrom," U.S. Patent Application No. 20070118937; May **2007**.

Ivanov, I.N.; Geohegan, D.B. "Carbon Nanotube Temperature and Pressure Sensors," U.S. Patent Application No. 20110051775; March **2011**.

Jesse, S.; Geohegan, D.B.; Guillorn, M. "SEM Technique for Imaging and Measuring Electronic Transport in Nanocomposites Based on Electric Field Induced Contrast," U.S. Patent Application No. 20070164218; July **2007**.

Kittrell, W.C.; Wang, Y.; Kim, M.J.; Hauge, R.H. "Fibers Comprised of Epitaxially Grown Single-Wall Carbon Nanotubes, and a Method for Added Catalyst and Continuous Growth at the Tip," U.S. Patent No. 7,727,504; June **2010**.

Lee, R.; Fitch, F.R.; Tamhankar, S.S. "Methods for Hydrogen Storage and Refrigeration," U.S. Patent No. 7,976,620; July **2011**.

Margrave, J.L., et al. "Sidewall Derivatized Carbon Nanotubes," U.S. Patent No. 7,780,939; August **2010**.

Müller, U.; Lippert, G.; Schubert, O.; Hesse, M.; Hess, R.; Stoesser, M.; Yaghi, O.M. "Process for preparing an organometallic framework material," U.S. Patent Application No. 20050154222; July **2005**.

Müller, U.; Metelkina, O.; Hesse, M.; Stoesser, M.; Haas, P.; Yaghi, O.M. "Process for the Alkoxylation of Monools in the Presence of Metallo-Organic Framework Materials," U.S. Patent Application No. 20060135824; July **2006**.

Müller, U.; Metelkina, O.; Hesse, M.; Stoesser, M.; Haas, P.; Yaghi, O.M. "Process for the Alkoxylation of Monools in the Presence of Metallo-Organic Framework Materials," U.S. Patent Application No. 20050004404; January **2005**.

Müller, U.; Harth, K.; Hölzle, M.; Hesse, M.; Lobree, L.; Harder, W.; Yaghi, O.M.; Eddaoudi, M. "Method of Storing, Uptaking, Releasing of Gases by Novel Framework Materials," U.S. Patent No. 6,929,679; August **2005**.

Müller, U.; Hesse, M.; Heß, R.; Senk, R.; Hölzle, M.; Yaghi, O.M. "Gas Storage System," U.S. Patent No. 7,309,380; December **2007**.

Müller, U.; Hesse, M.; Pütter, H.; Yaghi, O.M. “Metal-Organic Framework Materials for Gaseous Hydrocarbon Storage,” U.S. Patent Application No. 20060185388; August **2006**.

Müller, U.; Hesse, M.; Pütter, H.; Yaghi, O.M. “Metal-Organic Framework Materials for Gaseous Hydrocarbon Storage,” U.S. Patent No. 7,343,747; March **2008**.

Müller, U.; Lippert, G.; Schubert, O.; Hesse, M.; Hess, R.; Stoesser, M.; Yaghi, O.M. “Process for Preparing an Organometallic Framework Material,” U.S. Patent No. 7,411,081; August **2008**.

Müller, U.; Lobree, L.; Hesse, M.; Yaghi, O.M.; Eddaoudi, M. “Process for the Epoxidation of an Organic Compound with Oxygen or an Oxygen-Delivering Compounds Using Catalysts Containing Metal-Organic Framework Materials,” U.S. Patent No. 6,624,318; September **2003**.

Pez, G.P.; Cheng, H.; Cooper, A.C.; Foo, M.-L. “Hydrogen Storage with Graphite Anion Intercalation Compounds,” U.S. Patent Application No. 20080175780; July **2008**.

Pez, G.P.; Cheng, H.; Cooper, A.C.; Foo, M.-L. “Hydrogen Storage with Graphite Anion Intercalation Compounds,” U.S. Patent Application No. 20080175780; July **2008**.

Pez, G.P.; Cooper, A.C.; Scott, A.R. “Autothermal Hydrogen Storage and Delivery Systems,” U.S. Patent Application No. 20080260630; October **2008**.

Pez, G.P.; Scott, A.R.; Cooper, A.C.; Cheng, H. “Hydrogen Storage by Reversible Hydrogenation of Pi-Conjugated Substrates,” U.S. Patent Application No. 20050002857; January **2005**.

Pez, G.P.; Scott, A.R.; Cooper, A.C.; Cheng, H. “Hydrogen Storage by Reversible Hydrogenation of Pi-Conjugated Substrates,” U.S. Patent Application No. 20040223907; November **2004**.

Pez, G.P.; Scott, A.R.; Cooper, A.C.; Cheng, H. “Hydrogen Storage by Reversible Hydrogenation of Pi-Conjugated Substrates,” U.S. Patent No. 7,429,372; September **2008**.

Pez, G.P.; Scott, A.R.; Cooper, A.C.; Cheng, H. “Hydrogen Storage by Reversible Hydrogenation of Pi-Conjugated Substrates,” U.S. Patent No. 7,351,395; April **2008**.

Pez, G.P.; Scott, A.R.; Cooper, A.C.; Cheng, H. “Hydrogen Storage by Reversible Hydrogenation of Pi-Conjugated Substrates,” U.S. Patent No. 7,101,530; September **2006**.

Pfeifer, P.; Suppes, G.J.; Shah, P.; Burrell, J.W. “High Surface Area Carbon and Process for its Production,” U.S. Patent Application No. 20080207442; August **2008**.

Smalley, R.E., et al. “Amplification of Carbon Nanotubes Via Seeded-Growth Methods,” U.S. Patent Application No. 20080213162; September **2008**.

Smalley, R.E., et al. “Array of Fullerene Nanotubes,” U.S. Patent No. 7,632,569; December **2009**.

Smalley, R.E., et al. “Continuous Fiber of Fullerene Nanotubes,” U.S. Patent No. 7,655,302; February **2010**.

Strano, M.S., et al. "Methods for Selective Functionalization and Separation of Carbon Nanotubes," U.S. Patent No. 7,887,774; February **2011**.

Strano, M.S.; Ursey, M.; Barone, P.; Dyke, C.A.; Tour, J.M.; Carter Kittrell, W.; Hauge, R.H. "Methods for Selective Functionalization and Separation of Carbon Nanotubes," U.S. Patent Application No. 20100028247; February **2010**.

Tour, J.M.; Bahr, J.L.; Yang, J. "Process for Derivatizing Carbon Nanotubes with Diazonium Species and Compositions Thereof," U.S. Patent Application No. 20090301896; August **2007**.

Tour, J.M.; Dyke, C.A. "Thermal Treatment of Functionalized Carbon Nanotubes in Solution to Effect Their Functionalization," U.S. Patent Application No. 20070071667; March **2007**.

Tour, J.M.; Dyke, C.A.; Stephenson, J.J.; Yakobson, B.I. "Interaction of Microwaves with Carbon Nanotubes to Facilitate Modification," U.S. Patent Application No. 20080169061; July **2008**.

Tour, J.M.; Hudson, J.L.; Dyke, C.A.; Stephenson, J.J. "Functionalization of Carbon Nanotubes in Acidic Media," U.S. Patent Application No. 20070280876; March **2005**.

Tour, J.M.; Hudson, J.L.; Krishnamoorti, R.; Yurekli, K.; Mitchell, C.A. "Polymerization Initiated at Sidewalls of Carbon Nanotubes," U.S. Patent No. 7,879,940; February **2011**.

Tour, J.M.; Stewart, M.P. "Functionalized, Hydrogen-Passivated Silicon Surfaces," U.S. Patent Application No. 20090269593; October **2009**.

Tour, J.M.; Stewart, M.P. "Method of Making a Molecule-Surface Interface," U.S. Patent Application No. 20070249180; October **2007**.

Tour, J.M.; Stewart, M.P. "Method of Making a Molecule-Surface Interface," U.S. Patent No. 7,527,831; May **2009**.

Worsley, M.A.; Biener, A.J.; Satcher, J.H.; Baumann, T.F. "Graphene-Doped Carbon Aerogels," Patent Application filed September **2010**.

Worsley, M.A.; Han, T.Y.; Kuntz, J.D.; Cervantes, O.; Gash, A.E.; Baumann, T.F.; Satcher, J.H. "High Surface Area, Electrically Conductive Nanocarbon-Supported Metal Oxides," U.S. Patent Application No. 20100190639; July **2010**.

Worsley, M.A.; Baumann, T.F.; Kuntz, J.D.; Satcher, J.H.; Hamza, A.V. "Mechanically Stiff, Electrically Conductive Composites of Polymers and Carbon Nanotubes," U.S. Patent Application No. 20110024698; February **2011**.

Worsley, M.A.; Baumann, T.F.; Satcher, J.H.; Hamza, A.V. "Mechanically Robust, Electrically Conductive Ultralow-Density Carbon Nanotube-Based Aerogels," U.S. Patent Application No. 20100187484; July **2010**.

Worsley, M.A.; Kuntz, J.D.; Cervantes, O.; Han, T.Y.; Gash, A.E.; Satcher, J.H.; Baumann, T.F. "High Surface Area, Electrically Conductive Nanocarbon-Supported Metal Oxides," Patent Application filed November **2009**.

Worsley, M.A.; Kuntz, J.D.; Satcher, J.H.; Baumann, T.F. "High-Surface Area Titanium Carbonitride-Coated Carbon Aerogel," Patent Disclosure.

Worsley, M.A.; Kuntz, J.D.; Satcher, J.H.; Baumann, T.F. "High-Surface Area, Conductive Ultralow-Density Titanium Carbonitride-Decorated Carbon Nanotube Foam," Patent Disclosure.

Yaghi, O.M.; Chen, B. "High Gas Adsorption in a Microporous Metal-Organic Framework with Open-Metal Sites," U.S. Patent Application No. 20060252641; November **2006**.

Yaghi, O.M.; Chen, B. "High Gas Adsorption Metal-Organic Framework," U.S. Patent No. 7,662,746; February **2010**.

Yaghi, O.M.; Cote, A.P.; El-Kaderi, H.M.; Hunt, J.R. "Crystalline 3D- and 2D Covalent Organic Frameworks," U.S. Patent Application No. 20100143693; June **2010**.

Yaghi, O.M.; Eddaoudi, M.; Li, H.; Kim, J.; Rosi, N. "Isorecticular Metal-Organic Frameworks, Process for Forming the Same, and Systematic Design of Pore Size and Functionality Therein, with Application for Gas Storage," U.S. Patent No. 6,930,193; August **2005**.

Yaghi, O.M.; Eddaoudi, M.; Li, H.; Kim, J.; Rosi, N. "Isorecticular Metal-Organic Frameworks, Process for Forming the Same, and Systematic Design of Pore Size and Functionality Therein, with Application for Gas Storage," U.S. Patent Application No. 20050192175; September **2005**.

Yaghi, O.M.; Furukawa, H.; Wang, B. "Preparation of Functionalized Zeolitic Frameworks," U.S. Patent Application No. 20100186588; July **2010**.

Yaghi, O.M.; Hayashi, H.; Banerjee, R.; Park, K.S.; Wang, B.; Cote, A.P. "Preparation of Functionalized Zeolitic Frameworks," U.S. Patent Application No. 20070202038; August **2007**.

Yaghi, O.M.; Matzger, A.J.; Benin, A. "Covalently Linked Organic Frameworks and Polyhedra," U.S. Patent Application No. 20060154807; July **2006**.

Yaghi, O.M.; Matzger, A.J.; Benin, A.; Cote, A.P. "Covalently Linked Organic Frameworks and Polyhedra," U.S. Patent No. 7,582,798; September **2009**.

Yaghi, O.M.; Matzger, A.J.; Rowsell, J.L.C. "Implementation of a Strategy for Achieving Extraordinary Levels of Surface Area and Porosity in Crystals," U.S. Patent No. 7,652,132; January **2010**.

Yaghi, O.M.; Sudik, A. "Metal-Organic Polyhedra," U.S. Patent Application No. 20050124819; June **2005**.

Yakobson, B.I.; Avramov, P.V.; Margrave, J.L.; Mickelson, E.T.; Hauge, R.H.; Boul, P.J.; Huffman, C.B.; Smalley, R.E. "High-Yield Method of Endohedrally Encapsulating Species Inside Fluorinated Fullerene Nanocages," U.S. Patent No. 7,252,812 B2; August **2007**.

Yang, R.T.; Li, Y.; Lachawiec, A.J. "Enhancing Hydrogen Spillover and Storage," U.S. Patent Application No. 20100019196; January **2010**.

Yang, R.T.; Li, Y.; Qi, G.S.; Lachawiec, A.J. “Chemical Bridges for Enhancing Hydrogen Storage by Spillover and Methods for Forming the Same,” U.S. Patent Application No. 20070082816; April **2007**.

Yang, R.T.; Li, Y.W.; Lachawiec, A.J.; Qi, G. “Chemical Bridges for Enhancing Hydrogen Storage by Spillover and Methods for Forming the Same,” U.S. Patent Application No. 11/442,898; May **2006**.

Yu, L.; Liu, D.-J.; Yuan, S.; Yang, J. “Porous Polymeric Materials for Hydrogen Storage,” U.S. Patent Application No. AC08J9228FI; June **2008**.

Yu, L.; Liu, D.-J.; Yuan, S.; Yang, J. “Porous Polymeric Materials for Hydrogen Storage,” U.S. Patent Application No. 20090023828; January **2009**.

Zhou, H-C; et al. “Porous Materials Containing Built-In Single-Molecule Traps for Small Molecule Capture,” (TAMUS 3321) Patent Disclosure.

Zhou, H-C; et al. “Preparation and Applications of Porous Polymer Networks,” (TAMUS 3320) Patent Disclosure.

Ziegler, K.J.; Schmidt; D.J.; Hauge; R.H.; Smalley; R.E. “Length-Based Liquid-Liquid Extraction of Carbon Nanotubes Using a Phase Transfer Catalyst,” U.S. Patent No. 7,578,941; August **2009**.

Appendix B: Updated Table (June 2009) of DOE Targets

Technical System Targets: On Board Hydrogen Storage for Light Duty Vehicles							
Storage Parameter	Units	2010	2015	Ultimate			
System net Gravimetric ^a	kWh/kg (kg H ₂ /kg system)	1.5 (0.045)	1.8 (0.055)	2.5 (0.075)			
System Volumetric Capacity: Usable energy density from H ₂ (net useful energy/max system volume)	kWh/L (kg H ₂ /L system)	0.9 (0.028)	1.3 (0.040)	2.3 (0.070)			
Storage system cost ^b (& fuel cost) ^c	\$/kWh net (\$/kg H ₂) \$/gge at pump	4* (133) 2-3	2* (67) 2-3	TBD 2-3			
Durability/Operability <ul style="list-style-type: none"> Operating ambient temperature^d Min/max delivery temperature Cycle life (1/4 tank to full)^e Cycle life variation^f Min delivery pressure from storage system; FC= fuel cell, ICE= internal combustion engine Max delivery pressure from storage system^g 	°C °C Cycles % of mean (min) at % confidence Atm (abs) Atm (abs)	-30/50 (sun) -40/85 1000 90/90 4FC/35 ICE 100	-40/60 (sun) -40/85 1500 99/90 3FC/35 ICE 100	-40/60 (sun) -40/85 1500 99/90 3FC/35 ICE 100			
Charging/discharging Rates <ul style="list-style-type: none"> System fill time (for 5-kg H₂) Minimum full flow rate Start time to full flow (-20°C)^h Start time to full flow (20°C)^h Transient response 10%-90% and 90% -0%ⁱ 	min (Kg H ₂ /min) (g/s)/kW s s s	4.2 min (1.2 kg/min) 0.02 5 15 0.75	3.3 min (1.5 kg/min) 0.02 5 15 0.75	2.5 min (2.0 kg/min) 0.02 5 15 0.75			
Fuel Purity (H ₂ from storage) ^j	% H ₂	99.99 (dry basis)					
Environmental Health & Safety <ul style="list-style-type: none"> Permeation & leakage^k Toxicity Safety Loss of useable H₂^l 	Scc/h - - (g/h)/kg H ₂ stored	Meets or exceeds applicable standards <table border="1"> <tr> <td>0.1</td> <td>0.05</td> <td>0.05</td> </tr> </table>			0.1	0.05	0.05
0.1	0.05	0.05					

*The storage system costs are currently under review and will be changed at a future date.

Note: Above targets are based on the lower heating value of hydrogen; targets are for a complete system, including tank, material, valves, regulators, piping, mounting brackets, insulation, added cooling capacity, and/or other balance-of-plant components. Unless otherwise indicated, all targets are for both internal combustion engine and for fuel cell use, based on

the low likelihood of power-plant specific fuel being commercially viable. Also note that while efficiency is not a specified target, systems must be energy efficient. For reversible systems, greater than 90% energy efficiency for the energy delivered to the power plant from the on-board storage system is required. For systems generated off-board, the energy content of the hydrogen delivered to the automotive power plant should be greater than 60% of the total energy input to the process, including the input energy of hydrogen and any other fuel streams for generating process heat and electrical energy.

Useful constants: 0.2778kWh/MJ, ~33.3kWh/gal gasoline equivalent.

- ^a Generally the ‘full’ mass (including hydrogen) is used, for systems that gain weight, the highest mass during discharge is used.
- ^b 2003 US\$; total cost includes any component replacement if needed over 15 years or 150,000 mile life.
- ^c 2005 US\$; includes off-board costs such as liquefaction, compression, regeneration, etc; 2015 target based on H₂ production cost of \$2 to \$3/gasoline gallon equivalent untaxed, independent of production pathway.
- ^d Stated ambient temperature plus full solar load. No allowable performance degradation from –20C to 40C. Allowable degradation outside these limits is TBD.
- ^e Equivalent to 200,000; 300,000; and 300,000 miles respectively (current gasoline tank spec).
- ^f All targets must be achieved at end of life.
- ^g For delivery *to* the storage system, in the near term, the forecourt should be capable of delivering 10,000 psi (700 bar) compressed hydrogen, liquid hydrogen, or chilled hydrogen (35 to 77K) and up to 5,000 psi (350 bar). In the long term, it is anticipated that delivery pressures will be reduced to between 50 and 150 atm for solid state storage systems, based on today’s knowledge of sodium alanates.
- ^h Flow must initiate within 25% of target time.
- ⁱ At operating temperature.
- ^j The storage system will not provide any purification, but will receive incoming hydrogen at the purity levels required for the fuel cell. For fuel cell systems, purity meets SAE J2719, Information Report on the Development of a Hydrogen Quality Guideline in Fuel Cell Vehicles. Examples include: total non-particulates, 100 ppm; H₂O, 5 ppm; total hydrocarbons (C₁ basis), 2 ppm; O₂, 5 ppm; He, N₂, Ar combined, 100 ppm; CO₂, 1 ppm; CO, 0.2 ppm; total S, 0.004 ppm; formaldehyde (HCHO), 0.01 ppm; formic acid (HCOOH), 0.2 ppm; NH₃, 0.1 ppm; total halogenates, 0.05 ppm; maximum particle size, <10 μm, particulate concentration, <1 μg/L H₂. These are subject to change. See Appendix on Hydrogen Quality in the DOE EERE Hydrogen Fuel Cells and Infrastructure Technologies Program Multiyear Research, Development and Demonstration Plan (www.eere.energy.gov/hydrogenandfuelcells/myppp) to be updated as fuel purity analyses progress. Note that some storage technologies may produce contaminants for which effects are unknown; these will be addressed as more information becomes available.
- ^k Total hydrogen lost into the environment as H₂; relates to hydrogen accumulation in enclosed spaces. Storage system must comply with CSA/HGV2 standards for vehicular tanks. This includes any coating or enclosure that incorporates the envelope of the storage system.
- ^l Total hydrogen lost from the storage system, including leaked or vented hydrogen; relates to loss of range.

Appendix C: HSCoE Materials Go/No-Go Recommendation Document (September 2009)

In FY 2009, the HSCoE formally evaluated the status of sorbents that could meet the U.S. Department of Energy (DOE's) hydrogen-storage targets and wrote a report for the DOE Office of Energy Efficiency and Renewable Energy Fuel Cell Technologies Program. This HSCoE project deliverable, the *Hydrogen Sorption Center of Excellence (HSCoE) Materials Go/No-Go Recommendation Document*, comprises Appendix C and begins on the following page.



U.S. Department of Energy
Office of Energy Efficiency and Renewable Energy
Fuel Cell Technologies Program
Hydrogen Sorption Center of Excellence (HSCoE)

Materials Go/No-Go Recommendation Document

November 30, 2009

Fiscal Year 2009 Project Deliverable on Materials Recommendations

Lin Simpson
Director, HSCoE
National Renewable Energy Laboratory¹
Golden, CO

¹ NREL is a national laboratory operated by the Alliance for Sustainable Energy, LLC, for the United States Department of Energy under contract DE-AC36-08GO28308.

Acknowledgements

For this document, we thank and acknowledge the contributions of our colleagues at the Hydrogen Sorption Center of Excellence (HSCoE) partner institutions listed below. We also thank Dr. Sunita Satyapal (DOE), Dr. Carole Read (DOE), Dr. George Thomas (Sandia-retired), Dr. Sara Dillich (DOE), Dr. David Thorn (LANL), and Mr. Jesse Adams (DOE) for their input to the document and guidance of the HSCoE.

National Renewable Energy Laboratory, **Lin Simpson (Primary Contact)**

Anne Dillon, Philip Parilla, Thomas Gennett, Yufeng Zhao, Jeff Blackburn, and Chaiwat Engtrakul, Michael Heben (now at University of Toledo), Shengbai Zhang (now at Rensselaer Polytechnic Institute)

1617 Cole Blvd.

Golden, CO 80401

Phone 303-384-6625; fax 303-384-6655

E-mail *lin.simpson@nrel.gov*

Partners:

Air Products and Chemicals Inc., Alan Cooper and Guido Pez (retired)

Argonne National Laboratory (ANL), Di-Jia Liu and Yuping Lu, U. of Chicago

California Institute of Technology (Caltech), Channing Ahn

Duke University, Jie Liu

Lawrence Livermore National Laboratory (LLNL), Ted Baumann and Joe Satcher

National Institute of Standards and Technology (NIST), Dan Neumann and Craig Brown

Oak Ridge National Laboratory (ORNL), Dave Geohegan

Pennsylvania State University, Peter C. Eklund (deceased), Michael Chung, Henry Foley, and Vincent Crespi

Rice University, James Tour, Carter Kittrell, and Richard E. Smalley (deceased)

Rice University, Boris Yakobson and Robert Hauge

Texas A&M University (TAMU), Hongcai Zhou (formerly of Miami University-Ohio)

University of Michigan (UM), Ralph T. Yang

University of Missouri-Columbia (UMC), Peter Pfeifer

University of North Carolina, Chapel Hill (UNC), Yue Wu and Alfred Kleinhammes

University of Pennsylvania, Alan G. MacDiarmid (deceased), Pen-Cheng Wang

Former Partner: UM/University of California, Los Angeles (UCLA), Omar Yaghi

DOE Points of Contact:

DOE Technology Development Manager: Carole Read

E-mail: *Carole.Read@ee.doe.gov*

DOE Project Officer: Jesse Adams

E-mail: *Jesse.Adams@go.doe.gov*

Table of Contents

Acknowledgements	2
Table of Contents	3
EXECUTIVE SUMMARY	4
INTRODUCTION.....	8
APPROACH AND RESEARCH ACTIVITIES	12
Engineered Nanospaces.....	13
Substitution	14
Strong/Multiple Dihydrogen Binding	15
Weak Chemisorption/Spillover	15
SELECTION CRITERIA	16
Cryogenic Sorbents (nominally 77K storage)	17
Substituted Materials	17
Strong Binding/Multiple H ₂ Metal Centers.....	17
Weak Chemisorption/Spillover	18
RESULTS AND DISCUSSION	18
Optimizing Structures.....	18
Increasing Dihydrogen Binding Energy	21
Optimizing Weak Chemisorption	24
RECOMMENDATIONS FOR FUTURE RESEARCH DIRECTION	25
Recommendation 1 – Develop only a select set of materials in which the primary storage mechanism is physisorption.....	25
Recommendation 2 – Develop substituted/heterogeneous materials that have demonstrated hydrogen binding energies in the range 10 – 25 kJ/mol.....	26
Recommendation 3 – Develop materials for hydrogen storage by spillover.....	26
Recommendation 4 – Develop materials for multiple dihydrogen storage on designated sites.....	27
Recommendation 5 - Develop materials in concert with designs for hydrogen storage systems.....	27
Conclusion	27
REFERENCES AND SELECTED PUBLICATIONS ON MATERIALS INVESTIGATED BY THE HSCoE.....	31
APPENDICES.....	34
Appendix I: Updated Table (June 2009) of DOE On-Board Hydrogen Storage System Targets for Light-Duty Vehicles.....	34
Appendix II: Recommended Down-Selected Materials by Class.....	36

EXECUTIVE SUMMARY

The DOE Hydrogen Sorption Center of Excellence (the Center) was formed in FY2005² to research and develop hydrogen storage materials mainly for the application of light-duty vehicles. However, sorbent materials may find use in other hydrogen storage applications such as stationary power generation, portable power, back-up power, and niche, early-market vehicles. For transportation applications, sorbent materials offer tremendous advantages. These include fast hydrogen fill-up and discharge rates, nominal thermal management requirements during refueling, ease of engineering, ability to provide required pressures, and favorable system energy efficiencies (which affect costs). In addition, use of sorbent materials may significantly reduce the volume and weight of storage systems compared to 350- and 700-bar high-pressure tanks.

When the Center was established, the main issue for sorbent materials revolved around the relatively low binding energies with hydrogen, and thus the need to use cryogenic temperatures (e.g., 77K, -193°C, liquid nitrogen temperature at 1 bar). The Center's critical goals included the original FY2010³ hydrogen storage system targets: net available capacity of 45 g/L and 6 wt%, and system cost of \$133/kg H₂. From the outset during proposal formulation, Center partners were chosen to provide the specific expertise and capabilities necessary to develop sorbent materials that could be used to meet the DOE hydrogen storage system targets. The virtual Center includes development activities at more than 20 different institutions throughout the United States, and direct collaborations with institutions around the world.

This document provides: an overview of the work performed by the DOE-funded Center; specific recommendations to DOE for materials development efforts that should, and should not, be continued; and a list of key research priorities remaining to be resolved. The Center is led by the National Renewable Energy Laboratory (NREL), with partners at other U.S. national laboratories and universities, and at Air Products and Chemicals, Inc (our corporate partner). To ensure that the development activities were performed as efficiently as possible, the Center formed four complementary, focused research clusters based on one of four different sorption-based hydrogen storage mechanisms. By focusing on specific mechanisms, the Center leveraged appropriate materials and synthetic capabilities and expertise of the different partners to create: optimized pore size and high specific surface-area materials; heterogeneous materials with enhanced dihydrogen binding; materials with coordinated metal centers; and spillover or chemisorbed hydrogen materials.

Since the Center's inception, substantial progress has been made in developing sorption hydrogen storage materials. This progress includes down-selecting of numerous specific materials, but more importantly, entire material classes. Thus, the Center recommends that no further development efforts be performed on these materials/classes.

² Awarded from the FY2003 EERE Hydrogen Storage Grand Challenge Solicitation, Funding Opportunity Announcement DE-PS36-03GO93013, September 2003.

³ Note that in FY2009, DOE revised the hydrogen storage system targets for light-duty vehicles (see Appendix I). Thus, all DOE targets discussed in the remainder of this document will reference the revised DOE hydrogen storage system targets.

In addition, the Center has identified clear development paths for constructing sorbent materials that have the potential to meet DOE's revised 2015 and Ultimate Full-Fleet targets for light-duty vehicles (see Table ES-1). The Center recommends that development efforts for specific materials/classes be continued where there are viable routes for synthesizing sorbents that can be used to meet DOE's targets.

For example, after substantial efforts, it has become clear that only certain materials will meet the DOE 2015 targets. Specifically, among the materials that rely only on relatively weak physisorption where cryogenic (e.g., <100K) temperatures will be required, only those materials with very high specific-surface areas (>3,000 m²/g) and optimized pore sizes in the range of ~0.7 to 1.2 nm have the potential to achieve at least the 50 g/L (bulk density) and 7 wt% excess material capacities that will be needed to meet the DOE 2015 targets. Thus, the Center recommends that physisorption-based materials that do not have these attributes be down-selected and not pursued in future development efforts. As demonstrated by this example, by investigating a specific class of materials, the Center is able to select materials based on their specific characteristics for a given hydrogen storage mechanism, thus enabling the elimination of dozens of materials with limited or no effort. However, the Center recommends that physisorption materials with the requisite attributes be investigated further for hydrogen storage systems.

Improving sorbent properties for hydrogen storage beyond that attained with weak physisorption materials will require substantial increases in binding energy that improves capacities at higher temperatures, towards ambient. In the select few cases where binding energies can be increased, the stringent specific surface area and pore size distribution criteria applied to weak physisorbents will be different, even though material optimization will still be important. Since its inception, the Center has investigated several methodologies and material systems to increase the intrinsic binding energy of dihydrogen molecules or H₂. Based on these efforts, numerous materials have been down-selected, and a select few materials/material classes have been identified with the potential to be used to meet DOE system targets. For example, almost all lightweight elements (e.g., Li, N, O, and F) substituted in a carbon matrix do not significantly increase dihydrogen binding. Only beryllium (Be) and boron (B) will substantially increase dihydrogen binding energy when substituted in carbon in the appropriate coordination.

Similarly, metal centers in metal-organic frameworks (MOFs) or equivalent materials bind dihydrogen in the 10–15 kJ/mol range, which is sufficient for near-ambient temperature (150 to 220K) storage. The main issue with all of these types of materials is the need for a high number of these binding sites to be uniformly dispersed and accessible in order to have the enhanced dihydrogen adsorption properties available for a significant fraction of the material storage capacity. Thus, the Center recommends that future efforts should only develop these types of materials with demonstrated higher binding energy sites, and the focus should be on creating materials with the appropriate chemical/electronic structures, sufficient composition, and specific-surface areas needed for these materials to meet, at a minimum, DOE's 2015 targets.

In addition to higher dihydrogen binding, the ability to adsorb multiple-dihydrogens on designed sites will probably be required to meet DOE's Ultimate targets. Several inexpensive material systems and synthetic pathways (e.g., Calcium [Ca] integrated with graphene and other

framework materials) have been identified that may be used to meet DOE's Ultimate targets. Such systems and pathways, however, will require substantial applied development efforts to achieve the breakthroughs necessary to form the novel structures that have enhanced dihydrogen binding for the entire capacity range. Even so, the basic principles of forming multiple-dihydrogen bonding on these sites with 15 to 40 kJ/mol binding energies have been demonstrated experimentally. Because these sites have higher binding energies, development efforts will most likely require airless and dry processing, and material stability and contamination issues will have to be fully addressed. However, the potential to store H₂ at ambient temperature and nominal pressures between 10 and 50 bar with theoretical densities greater than twice that of liquid hydrogen make these development efforts highly promising.

The Center has also investigated methodologies to store dissociated hydrogen molecules (e.g., hydrogen atoms). Unlike the work discussed previously to increase binding for dihydrogen, the key issue was actually developing ways to store dissociated hydrogen with binding energies substantially lower than what is typically observed for hydride formation. Among the more promising material classes, the Center demonstrated that catalyzed hydrogen molecule dissociation followed by "spillover" onto lightweight receptor support materials enabled ambient temperature storage with binding energies in the range of 10 to 25 kJ/mol. Although the phenomenon of spillover has been known for many decades, Center partners demonstrated that this material class could be used to store substantial (> 30 g/L and 4 wt%) amounts of hydrogen at near ambient temperature and at nominal pressure. The Center demonstrated spillover both experimentally and by thermodynamic principles as a process for ambient temperature, reversible hydrogen storage. However, the materials have tended to be very sensitive to synthetic processing conditions, resulting in substantial irreproducibilities.

Furthermore, the intrinsic nature of the spillover storage mechanisms makes hydrogen refill rates, material stability/durability, and intrinsic material costs challenging issues that must be adequately resolved. Nonetheless, once these issues are addressed, initial analyses indicate that storage systems with more than 75% of the material capacities could be achieved. Because the potential spillover material storage limits are ~80 g/L and ~8 wt%, and ultimately fill rates, materials costs, and durability are tractable issues, it should be possible to construct spillover-material based hydrogen storage systems that meet DOE's 2015 targets.

As mentioned previously, the Center's focused development efforts identified a substantial number of materials/material classes that should not be investigated further based on a number of considerations, including a detailed selection criteria developed specifically for sorption materials. Based on the nature of the Center's development of hydrogen storage mechanisms (rather than specific materials), the exact number of materials down-selected is difficult to identify. Through these efforts, the Center was able to quickly identify the few selected material classes and their required properties and stress them for present and future development. For example, regardless of the specific elements used, a pure physisorption material needs to have more than 3,000 m²/g specific surface area. This requirement alone eliminates hundreds of elements that are just too heavy to be able to meet this requirement if only a physisorption-based hydrogen storage mechanism is used. Furthermore, through calculations and a limited number of specific experimental investigations, it became clear that only correctly coordinated boron-substituted in graphitic carbon is a viable route to improved hydrogen storage for substituted

carbon materials, and thus the use of other lightweight elements should not be investigated. In terms of carbon materials, this eliminated the need to perform experimental investigations on hundreds of potential element/process combinations for this material class. Similarly, the Center has focused on identifying in Table 1 the material classes and their corresponding properties that should be investigated in present and future development efforts.

With currently demonstrated bulk material packing densities and hydrogen storage properties, sorbent materials will substantially decrease the volume and pressure now used for high-pressure (350 to 700 bar) compressed tanks, and thus could significantly reduce overall system costs. Future selection criteria should focus further on identifying materials that can be used to meet DOE Ultimate targets. In addition to the specific performance issues for each material class discussed previously, developing material synthetic processes and pathways that are scalable, inexpensive, and reproducible—and produce materials that can meet the DOE system cost targets—remains a challenge that must be aggressively pursued in all cases.

Again, in general, the main issues for sorbents are the relatively low dihydrogen binding energies, which directly affect storage temperature. This adversely impacts system costs, volumetric capacity, and available gravimetric capacity. Thus, the main focus of future applied development efforts must be enhancing and/or optimizing hydrogen binding energies. This focus will require balancing improved hydrogen storage system costs and capacities with perhaps adversely affected material contamination sensitivity, durability, refill rates, and material costs issues.

Table ES-1. Summary of Sorbent Material Classes Recommendations for Further Applied Research and Development for On-Vehicle Refuelable Hydrogen Storage Systems. All material results (unless specifically stated) are measured reversible excess surface capacities and based on either a measured or reasonably assumed bulk density.

Material Class/ Mechanism	Example Materials	Material Results to Date (volumetric and wt%)	Recommended Development Path
Physisorbents	Greater than 3000 m ² /g with pore sizes between 0.7 and 1.2 nm	>50 g/L, >7 wt% excess capacity at 77K and ~50 bar	Only materials that have the potential to exceed those already demonstrated should be investigated further.
Substituted/ Heterogeneous materials	Predominately BC _x materials; exposed metals in metal organic frameworks (MOFs) and covalent organic frameworks (COFs)	~30 g/L, ~4 wt% excess capacity at 77 K and 50 bar. >40 g/L, >6 wt% at 195K possible	Only efforts that focus on viable routes to incorporating properly coordinated elements in high surface area structures should be pursued.
Multiple Dihydrogen Sorption sites	Coordinated but unsaturated metal centers like Ca-graphene, Ca-COF, Metalloporphyrines, Sc or Ti, B-doped fullerenes	Theoretical potential to have >100 g/L, >10 wt% at ~298K, ~10 bar	Substantial synthetic development is required to catch up with theoretical predictions. Only the most synthetically viable and stable materials should be developed initially.
Spillover	Catalyst (Pt, Ru, Ni) integrated with porous carbon structures and/or MOFs	>30 g/L, >4 wt% excess capacity at 298K, 100 bar	Efforts should focus on improving reproducibility, hydrogen uptake rates (e.g. hydrogen diffusion on the receptor materials), and catalyst integration.

INTRODUCTION

Significant improvements over currently available hydrogen storage technologies are required if hydrogen-fueled vehicles are to be broadly competitive across the full light-duty vehicle fleet. The hydrogen storage targets and technology barriers presented in DOE's Multi-Year Research, Development and Demonstration (RD&D) Plan¹ (the FCT Program Plan) for the Fuel Cell Technologies (FCT) Program state the critical application needs and goals. At this time, no known storage system can simultaneously meet all the capacity, operability, transient performance, cost, safety, and efficiency requirements for on-board, light-duty vehicular hydrogen storage systems. Similarly, improvements in hydrogen storage systems are needed for stationary power, portable power, and early market applications.

Nanostructured high-surface-area sorbent materials containing carbon, boron, lightweight metals, oxygen, and other elements show promise for breakthrough performance in hydrogen storage. However, the limits of performance remain unclear based on a lack of understanding of both the factors governing their performance and the design principles for synthesizing the materials and constructing the required systems.

The DOE-funded Hydrogen Sorption Center of Excellence (HSCoE) is developing on-board reversible sorbent materials.² A guiding principle in developing the required materials is that a continuum of energies exists for hydrogen bound to substrates and molecules (see Figure 1).

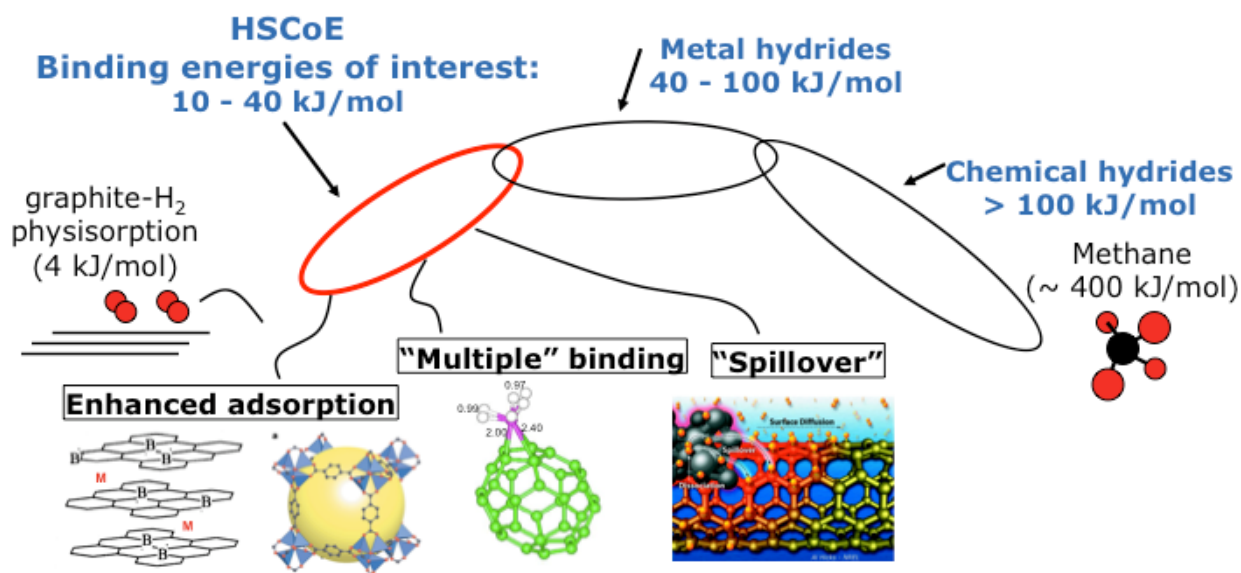


Figure 1. Depiction of the range of binding energies and several of the nanostructured materials of interest to the HSCoE.

On the weak side of the continuum is non-dissociative physisorption, which is due purely to van der Waals (vdW) forces (~ 4 kJ/mol). On the opposite end is the full C-H chemical bond in methane with an energy of ~ 400 kJ/mol. Between these two limits, with nominal binding energies between 10 and 40 kJ/mol, are:

- Physisorption (related to key parameters affecting vdW forces)
- Enhanced dihydrogen binding via the formation of complexes that exhibit electron transfer interactions from both the hydrogen and adsorbate
- Weak, reversible, chemical bonding of mono-atomic hydrogen to lightweight receptor materials (via a “spillover” mechanism). (See Figure 2 and Figure 3)

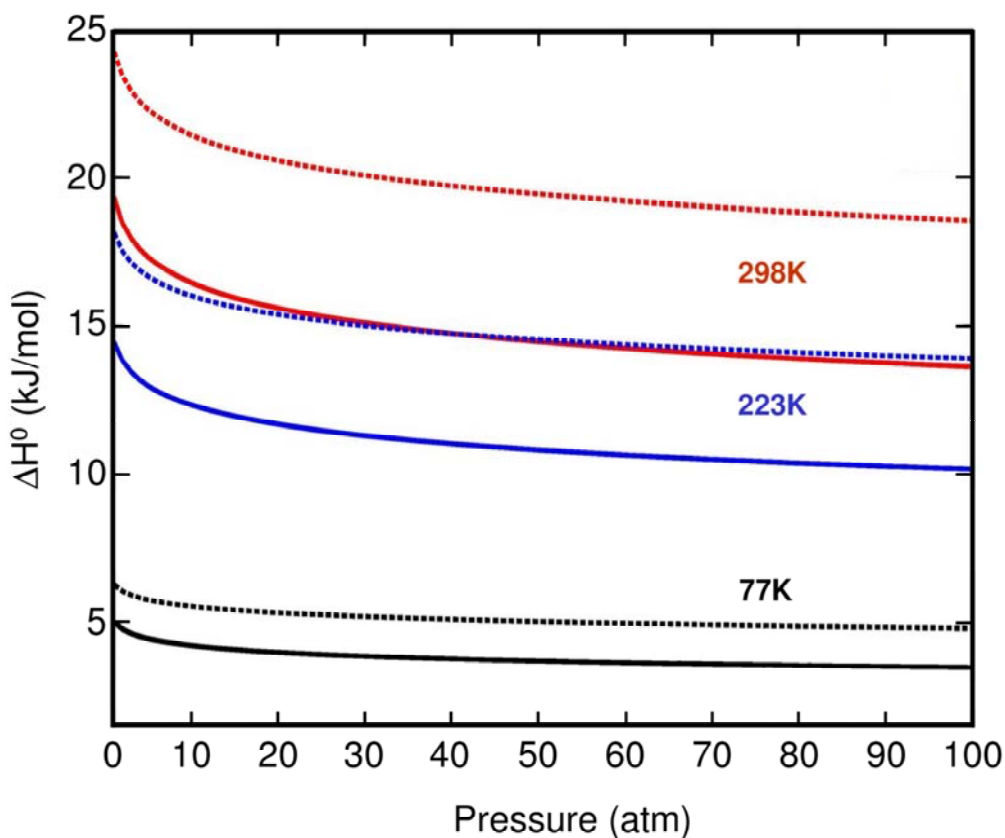


Figure 2. The optimal enthalpy for hydrogen storage depends on the pressure, temperature, and sorption interaction (i.e., entropy: e.g. dotted lines $\Delta S = -10R$, and solid lines $\Delta S = -8R$). For example, as shown in this plot (recreated from S.K. Bhatia, & A.L. Myers, *Langmuir*, 2006, 22, 1688) if materials with enthalpies between ~ 13 and 25 kJ/mol can be made, then ambient temperature hydrogen storage is possible with pressures between ambient and 100 bar. For lower binding energies, lower storage temperatures will be required.

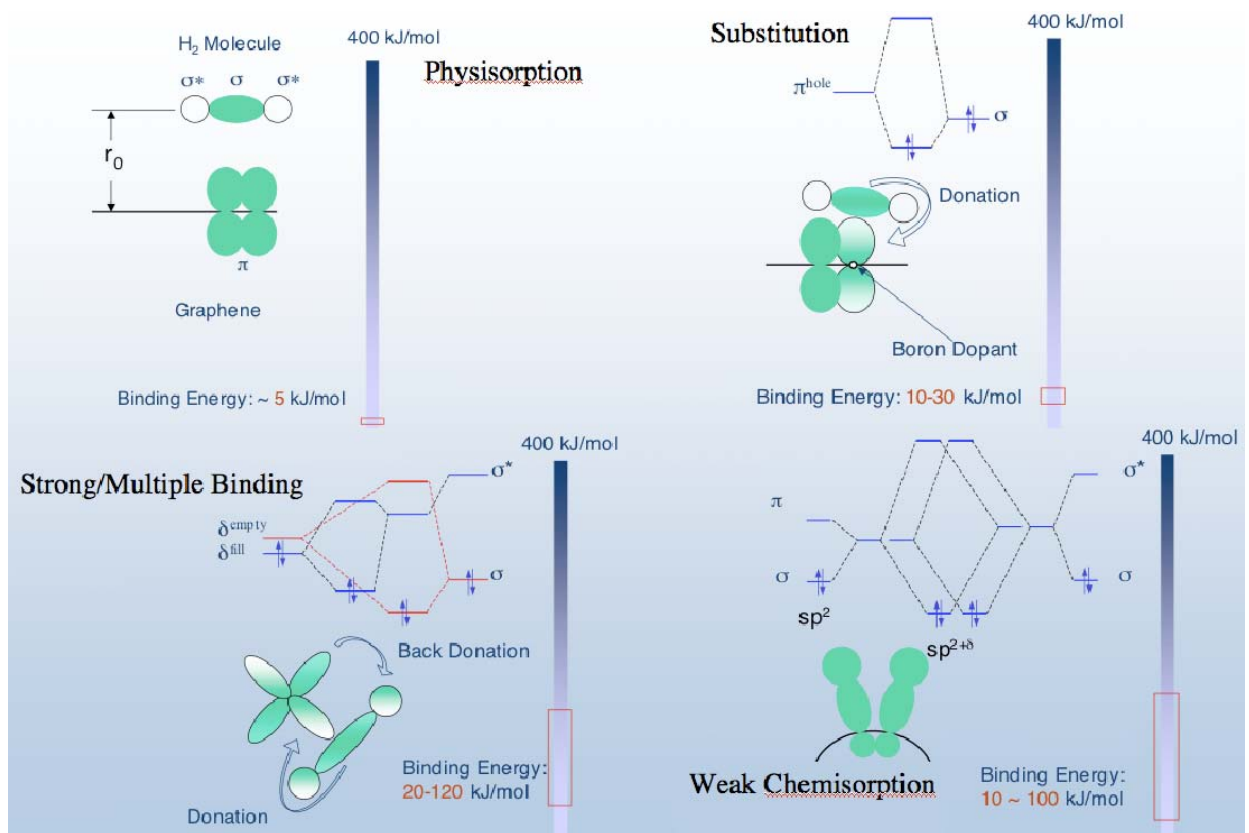


Figure 3. Illustrations of the four types of sorbent binding mechanisms investigated by the HSCoE.

The DOE goals may be met with sorbent materials if: (i) the energy for hydrogen adsorption can be designed to be in an nominal optimal range ($\sim 10\text{--}40$ kJ/mol: depending upon the entropy, desired operating pressure, and temperature; e.g., see Figure 2)³; and (ii) efficient volumetric arrangement (see Figure 4) of a sufficient number of suitable binding sites can be achieved with a low-weight material.

These goals are difficult to reach in conventional high-surface-area adsorbents like most activated carbon and metal-organic frameworks (MOFs) that are limited by low-physisorption binding energies, heterogeneity of the adsorbent surfaces and adsorption sites, and excessive macroporosity and poor volumetric packing.

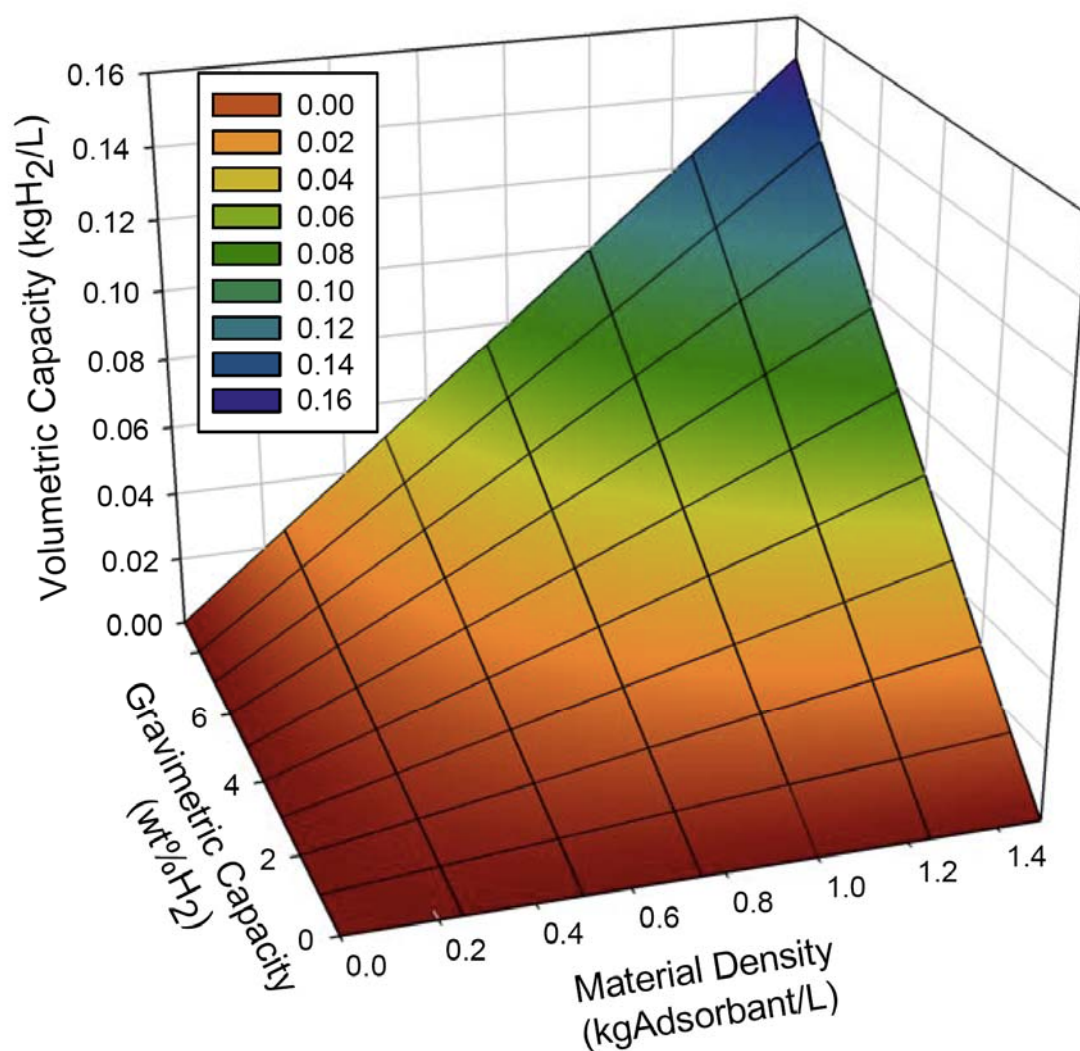


Figure 4. Graph from Argonne National Laboratory showing the dependence of volumetric density on gravimetric and bulk density for sorption materials. The plot indicates that to have the potential to meet DOE 2015 volumetric target (0.04 kgH₂/L, yellow band on chart), bulk material densities between 0.7 and 1 g/L will be required for sorbent materials with 6 to 7 wt% gravimetric capacities.

The HSCoE addresses the following technical barriers as defined by the FCT Program Plan.

General:

- A. Weight and Volume
- B. Cost
- C. Efficiency
- D. Durability/Operability
- E. Charging/Discharging Rates
- J. Thermal Management
- M. Reproducibility of Performance.

Reversible Materials-Based Storage System:

- P. Lack of Understanding of Hydrogen Physi- and Chemisorption.

As a general rule, sorbent materials have relatively low (e.g., less than 25 kJ/mol) dihydrogen enthalpies of adsorption (i.e., binding energies) where cryogenic temperatures and moderate pressures (i.e., 30 to 50 bar) are required. Therefore, thermal management (e.g., heat dissipation and rates during filling), delivered pressure, delivery rates, and refueling rates are not controlling issues. Thus, sorbent materials have the potential to be used to meet the vast majority of DOE hydrogen storage targets (see Appendix I), if cost and volumetric and gravimetric net available capacity issues can be adequately addressed.

The Center was charged with developing materials that would meet the former DOE FY2010 hydrogen storage system targets. In addition, the Center is investigating viable routes that may be used to meet DOE's Ultimate storage targets (including net available capacity of 70 g H/L system and 7.5 percent by weight system) and is also identifying potential early market applications that will benefit from sorbent materials. As discussed later in this document, sorbents may be used to enhance hydrogen storage capacities and other properties, with the caveat that the hydrogen storage system be designed to take full advantage of the material's capabilities as well as the specific performance needs for the application.

APPROACH AND RESEARCH ACTIVITIES

From the outset, in order for the Center to select among a relatively large number of potential sorbent materials, researchers placed more emphasis on identifying and developing mechanisms that lead to higher volumetric capacity and more favorable operating conditions rather than on specific, individual materials. This enabled efficient and rapid progress by focusing resources on identifying and optimizing specific properties and critically evaluating hydrogen storage material classes. This is why the Center was organized into four focused efforts, each of which is designed to efficiently address a specific set of issues associated with a specific hydrogen sorption mechanism (see Figure 3).

These focused research efforts are complementary, with lessons learned and materials developed in one effort often being applicable to another. For example, for physisorption the main issues are optimized pore sizes and very high specific-surface areas. Similar issues arise for other

sorbent material classes, and thus lessons learned for physisorption materials are directly applied to other Center development activities. The key advantage of the mechanism-focused approach is that selection criteria can be identified for each material class based on a limited amount of experimental and calculation work. This enables identification of the most promising materials and thus elimination of the vast majority that will not be able to meet DOE goals. This approach substantially reduced the Center's overall work while prioritizing development efforts.

Engineered Nanospaces

In almost all hydrogen sorption materials with the potential to meet DOE targets, almost every atom will need to be accessible and lightweight. Thus, materials with high specific-surface area will be required. In addition, to meet volumetric targets, the sorption sites will need to be arranged to minimize the amount of open space (see Figure 4). This suggests that porous structures should be optimized to allow hydrogen egress in and out, but the hydrogen should be in contact with some kind of sorption site. Thus, the materials should have minimal macroporosity (pores greater than ~50 nm diameter) or mesoporosity (pores between 2 and 50 nm diameter), and, depending on the specific sorption mechanism, the materials should have pore sizes between 0.7 and ~1.2 nm.⁴

In general, to allow sorption on all surfaces of a pore, the distance between the surfaces should be at least twice that of the kinetic diameter of dihydrogen (2.89 Å). In addition, multilayer adsorption effects, H-H repulsion, and other space-optimization considerations suggest that the pore sizes may need to be ~1.2 nm. Calculations⁵ suggest that some enhanced binding may occur if the pore structure is on the order of 0.7 to 1.2 nm.

The "engineering nanospaces" effort designs and synthesizes lightweight, high-surface-area, optimal-pore-size materials. Results from this effort are applicable to almost all sorption materials. The effort focuses on how to stabilize large quantities of hydrogen directly by physisorption. Researchers investigated methods to optimize sorption properties and increase dipole-dipole interaction (i.e., van der Waals) binding energies via appropriate geometrical pore structures by arraying high-surface-area structures (e.g., scaffolds). This was done by forming high-surface areas directly during synthesis, or by creating porosity in dense structures. The key to these efforts included optimizing sorption sites and optimizing space to enhance binding without loss of volumetric capacity.

Specific activities for the engineered nanospace effort involved performing theoretical modeling⁶ and experiments to determine potential mechanisms for higher storage capacities and to provide guidance for materials development. In addition, these efforts developed and/or improved scalable and reproducible synthesis methods of nanoporous materials. Several different synthetic pathways were investigated, including templated carbon/boron,⁷ polymers,⁸ metal-organic frameworks (MOFs),⁹ aerogels,¹⁰ single-wall nanohorns (SWNHs),¹¹ and scaffolded single-wall nanotubes (SWNTs).¹² Synthesized materials were characterized to determine their hydrogen storage properties and, when appropriate, to identify unique sorption mechanisms. In some cases, this involved optimizing materials for other sorption processes beyond physisorption.

Substitution

The Center formed the “substitution” development effort to focus on increasing the intrinsic binding energy of storage materials, and thus their storage capacity at higher temperatures. In general, increasing the intrinsic heats of dihydrogen adsorption is difficult, and the Center identified only a few potential pathways.

For most pure materials, or materials with electronic configurations that induce no significant adsorption, the primary adsorption mechanism is physisorption, which typically has enthalpies below 5 kJ/mol for interaction with a single surface. Enhanced physisorption binding energies (i.e., 5 to 10 kJ/mol) are often observed with high specific-surface-area materials. This is primarily a result of interaction with multiple adsorption sites that then limits the total volumetric capacity. In general, physisorbed dihydrogen on single surfaces has relatively low binding energies, and capacity requires operation at lower cryogenic temperatures and higher intermediate pressures. Typically, increased binding energies, lower temperature, and higher pressure are required to overcome the intrinsic repelling force between dihydrogens to yield higher storage capacities on the sorbent surface at a specific temperature and/or pressure.

To go beyond pure physisorption requires enhanced electron interactions between the sorption material and dihydrogen. In general, heterogeneous elemental structures or surface functionalization can induce enhanced electron interactions. However, after relatively comprehensive investigations, very few material systems were identified with the potential to enhance dihydrogen binding.^{13,14}

In general, the exchange of a different atom species in an elementally homogeneous lattice induces an electronic perturbation that may enhance dihydrogen binding. For example, the empty p orbitals on boron (B)-substituted [for] carbon induces electron donation from H₂ to provide a reasonable enhancement in binding (i.e., 10 to 15 kJ/mol) and capacities. However, it was determined that only boron substituted with a sp² or similar coordination produced the enhanced dihydrogen binding. Other B-C or C-C coordination,¹³ the presence of other elements such as nitrogen (N) in the lattice, or other (except for Be) substituted lightweight elements (e.g., Li, N, O, F, Na) in carbon lattices do not enhance dihydrogen binding. Furthermore, in addition to needing to be in the correct coordination state, calculations predict that enhanced binding may occur only if the B remains both electronically and structurally “frustrated” such that the B atoms are out of the plane of the carbon matrix, thus potentially expanding the lattice.

In addition to direct substitution, initial efforts identified that materials with intercalated and/or absorbed ions may enhance dihydrogen binding. For example, anions with high charge/volume ratio (e.g., fluoride)¹⁵ can donate electron density to s*-orbitals of dihydrogen. Similarly, other intercalated species (e.g., alkali and alkaline metals, anions) may induce charge interactions to improve hydrogen adsorption enthalpies.¹⁶ In some cases, it is theorized that molecular dopants complexed with nanostructures can generate sufficient electric fields to enhance H₂ storage. Finally, some of these substituted or functionalized materials may improve sorption of other elements/molecules for different hydrogen mechanisms associated with back-donation^{17,18} and/or spillover.

Based on initial predictions and experimental results, the Center partners developed scalable synthesis methods to form substituted and intercalated materials that demonstrate enhanced dihydrogen storage properties. Boron substitution was achieved by either starting with chemical compounds with high concentrations of B and forming high specific-surface-area materials, forming boron-substituted activated and graphitic carbons (e.g., BC₃), or substituting boron for carbon atoms in preformed materials. In addition, the Center partners developed anion-intercalated graphitic and other intercalated/functionalized materials with enhanced hydrogen storage properties.

Strong/Multiple Dihydrogen Binding

The final set of methods to improve dihydrogen binding is characterized by forward- and back-electron donation from the sorption material that induces a significant molecular bond stretching between the hydrogen atoms. Typically, this is achieved when the sorption sites are electronically and coordinately unsaturated. These types of sorption sites can bind a dihydrogen molecule more strongly (10 to 200 kJ/mol), but more importantly, can also bind multiple dihydrogen molecules to a single sorption site.^{17,18} This method enables a substantial increase in volumetric densities if these sites can be densely arrayed. As stated previously, the Center focused on materials with an optimal range between ~10 and 40 kJ/mol to enable reversible near-ambient temperature and pressure hydrogen storage.

In general, the specific partially coordinated atom sites needed for strong and multiple dihydrogen binding can be attained in a number of ways. These include stabilizing single metal atoms on high-surface materials (e.g.,¹⁹ Li/THF co-intercalation compounds or Ca on graphene lattices^{18,13}) or in crystalline structures such as MOFs or metallocarbohedrenes (Met-Cars). Thus, two of the Center's tasks focused on methods to develop hydrogen interactions with coordinated but unsaturated metal centers and to design and synthesize these types of sorbents. This involved using calculations to identify and guide tractable reactions that balance reactivity with stability and capacity.

The Center investigated integrating appropriate metal centers with binding energies to 40 kJ/mol, with materials such as aerogels, carbon nanohorns, carbon nanotube scaffolds, polycyclic aromatic hydrocarbons, graphene, and MOFs. These efforts included utilizing the higher Coulomb repulsion between alkaline metals to facilitate metal/substrate binding and/or enhancing charge transfer to stabilize the metal/substrate interaction with substitutional integration of different atoms in the support materials. One key issue with the use of open metal centers is the fact that their higher reactivity makes them susceptible to an array of issues. Such issues include agglomeration of the metals and reaction with contaminants, both of which eliminate the hydrogen storage enhancement, which makes durability and synthetic processing more challenging.

Weak Chemisorption/Spillover

The Center also actively investigated methods to efficiently store dissociated hydrogen. In general, dissociated or atomic hydrogen forms strong bonds with other materials (e.g., metal hydrides or chemical hydrides) that require high temperatures (e.g., more than 500K) or catalysts to break bonds. However, it is possible for hydrogen atoms to be adsorbed to surfaces in such a way that the bonding is weaker²⁰ and conducive to nominal reversible storage capacities at near-

ambient temperature and under moderate pressure.²¹ From a practical standpoint, a catalyst is typically needed to dissociate the dihydrogen gas; this is a known technology in the chemical process industry. However, because most common industrial catalysts (e.g., Pt, Pd, Ni) are relatively heavy and expensive (e.g., platinum group metals), reaching the DOE targets will require catalysts that are appropriately integrated with a lightweight and compact material such as carbon or boron so that the dissociated hydrogen can “spillover” and be stably and reversibly stored, primarily on the lightweight receptor material.

Maximizing performance and costs via spillover involves focused development efforts to optimize catalyst performance and dispersion and to integrate with receptor material properties and hydrogen surface transport/diffusion mechanisms. This involves performing systematic experiments to quantify spillover processes, determining the causes for material degradation and irreproducibility, and developing scalable and reproducible synthesis methods of spillover materials. For example, due to the mechanisms associated with hydrogen diffusion on the receptor material surfaces, low refueling rates and small materials surface properties are major challenges that must be resolved. To address these issues, the Center leveraged modeling²² to identify and to construct new spillover materials with improved properties and to chemically modify known spillover materials to improve spillover performance.

SELECTION CRITERIA

The Center is working on material classes that could be used to meet DOE hydrogen storage system targets for light-duty vehicles. The primary classes include:

- Cryogenic Sorbents (nominally 77K storage)
- Substituted Materials
- Strong Binding/Multiple H₂ Metal Centers
- Weak Chemisorption/Spillover.

As stated in the Introduction, the adsorption binding energy significantly affects the hydrogen storage system cost, net available volumetric and gravimetric capacities, and operating conditions. Thus, as the binding energies increase, the gravimetric capacity increases at higher temperatures and lower pressures.

This critical point means that the selection criteria used for each material class must be adjusted, because, on balance, meeting the DOE targets becomes easier with higher dihydrogen binding energies. Thus, within each material class, the Center developed a set of selection criteria for the most critical issues, and recommended down-selected materials based on these selection criteria or other issues identified by the Center (see Appendix II). The selection criteria allow materials to be developed that do not yet meet some of DOE’s hydrogen storage targets. In addition, the selection criteria do not replace the DOE hydrogen storage targets. In most cases, the materials being developed must have a clear potential to either meet the DOE hydrogen storage targets or provide useful insights into specific properties of interest to help make materials that can meet the DOE targets.

Cryogenic Sorbents (nominally 77K storage)

1. The material's volumetric storage capacity should be approximately 0.03 kg H₂/L, with a material excess gravimetric storage capacity of approximately 0.03 kg H₂/kg, in a temperature range of 77–200K, and a nominal pressure range of 30–100 bar—with a *clear potential* for further improvement.
2. The high-pressure adsorption isotherm should be >80% reversible, i.e., at least 80% of the stored hydrogen is desorbed or discharged between 77 and 200K, at nominal fuel cell operating pressures (i.e., ~100 to 4 bar).
3. The desorption or discharge rate at 77–200K should be more than 0.4 g/s for a material reservoir containing 5 kg H₂.
4. The charge rate should have 90% of the H₂ adsorbed by the material at 77–200K within 3.3 minutes for storage of a total of 5 kg H₂.
5. Full-scale commercial manufacturing material cost projections should be less than half the system cost targets.

Substituted Materials

1. The initial binding energy should be in the range of 10–25 kJ/mol, and the material should operate within a temperature range of 77–353K and pressure range of 30–100 bar. There should be a *clear potential* for volumetric and gravimetric capacity optimization in excess of the DOE 2015 targets for the given operating range.
2. The high-pressure adsorption isotherm should be >80% reversible, i.e., at least 80% of the stored hydrogen is desorbed or discharged between 77 and 353K, for nominal fuel cell operating pressures.
3. The desorption or discharge rate at 77–200K should be more than 0.4 g/s for a material reservoir containing 5 kg H₂.
4. The charge rate at 77–353 K should meet or be within 90% of the DOE target of 3.3 minutes for storage of a total of 5 kg H₂.
5. Full-scale commercial manufacturing material cost projections should be less than half the system cost targets.

Strong Binding/Multiple H₂ Metal Centers

1. The initial binding energy should be in the range of 10–40 kJ/mol, and the material should operate within a temperature range of 77–353K and pressure range of 30–100 bar. There should be a *clear potential* for gravimetric and volumetric capacity optimization in excess of the DOE 2015 targets for the given operating range.
2. The high-pressure adsorption isotherm should be >80% reversible, i.e., at least 80% of the stored hydrogen is desorbed or discharged between 77 and 353K, for nominal fuel cell operating pressures.
3. The desorption or discharge rate at 77–353K should be more than 0.4 g/s for a material reservoir containing 5 kg H₂.
4. The charge rate at 77–353K should meet or be within 90% of the DOE target of 3.3 minutes for storage of a total of 5 kg H₂.
5. Full-scale commercial manufacturing material cost projections should be less than 75% of the system cost targets.

Weak Chemisorption/Spillover

1. The material's volumetric storage capacity should be approximately 0.01 kg H₂/L with a gravimetric storage capacity of approximately 0.01 kg H₂/kg, a possible temperature range of 298–353K at 100 bar, and with a *clear potential* for further improvement.
2. The high-pressure adsorption isotherm should be >80% reversible, i.e., at least 80% of the stored hydrogen is desorbed or discharged with a temperature that does not exceed 353K, for a nominal fuel cell operating pressure.
3. The desorption or discharge rate at 298–353 K should be more than 0.4 g/s for a material reservoir containing 5 kg H₂.
4. The charge rate at 298–353K should not exceed 10 hours for a full charge of 5 kg H₂. In this case, since hydrogen loading is still a substantial development effort for spillover materials, charge rates have been adjusted to enable work to be performed on materials that have the potential to meet DOE targets.
5. Full-scale commercial manufacturing material cost projections should be less than 75% of the system cost targets.

RESULTS AND DISCUSSION

Substantial work in developing and characterizing nanostructured materials has demonstrated their potential to have more than ~30 g/L and ~7 wt% hydrogen storage excess material capacities at 80 to 100K and 30 to 100 bar conditions.^{7,9} Based on this body of work, it is clear that increasing a material's specific-surface area is necessary, but it is not by itself sufficient for achieving high volumetric hydrogen storage capacities. Optimized pore sizes in the range of approximately 0.7 to 1.2 nm are also required to provide some potential adsorption enthalpy enhancements that may enable multilayer adsorption and minimize open volumes where hydrogen is not being bound to a surface.

Optimized pore sizes also enhance the material's ability to be packed at higher densities without loss of storage capacity to improve volumetric capacity further. Finally, electronic and surface functionalization may also enhance the adsorption properties for both hydrogen and other atoms and molecules that can be integrated with the high-surface-area materials to enhance hydrogen storage capacity. Results are summarized below for:

- Optimizing structures
- Increasing dihydrogen binding energy
- Optimizing weak chemisorption.

Optimizing Structures

In general, numerous synthetic methods have been used to create high specific-surface-area materials with the appropriate properties for good hydrogen storage. Typically, the synthetic methods used involve formation of porous structures from gas or solution phases and/or creation of pores from solids. Some of the more specific techniques include those described below.

Superactivated Carbon

By far, the most common way to synthesize porous structures is to start with relatively solid materials and process them to create high surface-area materials. The history of activated and superactivated carbons²³ spans hundreds of years and will not be discussed here. Suffice it to say that the state-of-the-art for hydrogen storage is embodied in materials such as AX-21,²⁴ which typically has specific surface areas in excess of 3,000 g/m² and material excess hydrogen storage capacities at 77K of between 5 and 6 wt% (15 to 20 g/L; based on measured bulk densities of ~0.3 g/ml).

The main issue with commercially available superactivated carbon is the relatively broad pore size distribution that includes substantial amounts of mesoporosity and some macroporosity. In general, materials with uniform pore sizes in the range of 0.7 to 1.2 nm are optimal for hydrogen storage, and thus all Center efforts involving similar pyrolysis processes have focused on making materials with optimum uniform pore sizes. For example, pyrolyzation techniques of chemicals such as polyetheretherketone (PEEK)²⁵ and inexpensive carbon sources such as corncobs²⁶ have been optimized to form materials with the pore size distributions closer to optimal. Although the main issue (that materials with higher specific-surface areas typically have large pore sizes) still remains, the Center has demonstrated that materials with improved pore sizes enhance hydrogen storage capacities.

Aerogels

The use of aerogel synthesis techniques¹⁰ offers inexpensive and scalable processing that has the ability to tune pore sizes. These materials, which are also being used as scaffolds for metal hydrides, demonstrate reasonable hydrogen storage capacities at 77K. However, achieving suitable material thermal conductivity, uniform small pore sizes, and integration of boron into the carbon structure are remaining challenges.

The introduction of materials such as carbon nanotubes has been demonstrated to improve electrical/thermal conductivity. Although carbon aerogels have been optimized to provide ~20 g/L (with measured bulk densities of ~0.3 g/ml) and ~5.5 wt% material excess capacity at 77K and ~50 bar, the use of single-element carbon or silica aerogels has been down-selected. In this case, the Center decided that further optimization with pure carbon aerogels would not provide significant capacity improvements, and that efforts should be focused on increasing hydrogen binding energies via substitution of elements such as boron and integration of coordinated metal centers.

Graphene and Ordered Carbon

The use of graphene (via exfoliation or intercalation), nanotubes, nanohorns, and/or fullerenes has been demonstrated to be a way to form relatively durable and thermally conductive hydrogen storage materials. Cost and the ability to attain the appropriate pore sizes remain substantial issues that have yet to be resolved. In sheet form, intercalated materials have demonstrated very favorable binding energy results. For example, Cs-intercalated graphite demonstrated ~12 kJ/mol dihydrogen binding for the entire range of storage capacity.²⁷ However, in this case, because the graphene layers are separated by less than 0.6 nm, there is insufficient room for two dihydrogen layers between the graphene layers, and thus the potential capacity is less than 40 g/L

and 4 wt% at ~77K and moderate pressures. Thus, if suitable layer-to-layer spacing (i.e., 0.7 to 1.2 nm) can be achieved, intercalated graphite offers an intriguing storage solution.

In a similar way, carbon nanotubes and fullerenes may be good hydrogen storage materials if they can be arranged with optimum spacing. Scaffolds with nanotubes,⁶ fullerenes, and/or graphene have been designed that have the potential to be used to meet the DOE 2015 targets. Even so, appropriate synthetic methods must be developed to actually form the requisite structures.

Finally, in the case of nanotubes and fullerenes, the predicted higher availability of the π -electron due to the strained sp^2 coordination of the curved surfaces provides enhanced dihydrogen binding.²⁸ However, due to the sensitivity of this type of enhancement to functional groups and surface passivation, the exact amount of enhancement has been difficult to quantify. Estimates of a few percent to ~100% enhancements have been predicted.

Metal Organic Frameworks

Chemical synthesis of high specific-surface-area materials has progressed tremendously since the Center's inception. For example, metal organic frameworks (MOFs) and similar materials⁹ have been developed with more than twice the specific-surface-area of superactivated carbons. These materials have demonstrated more than 7 wt% excess hydrogen storage capacities, but typically their low crystal density, and thus bulk density (e.g., ~0.3 g/ml), limits their volumetric densities to less than 30 g/L. In addition, porous polymers have been developed with more than twice (i.e., ~1.4 g/ml)⁸ the densities of superactivated carbons.

These results demonstrate that inherent improvements can be made with pseudo-ordered structures and substantially raise the bar for what hydrogen storage capacities can be achieved with high specific-surface-area materials with optimum pore structures.⁴ For example, once materials are made with optimum pore structures and specific-surface-areas in excess of 3,500 m^2/g , the Center expects capacities will be approximately 7 wt% (excess) and 70 g/L at 77K. The latter will be higher than that of liquid hydrogen, but at much higher temperature. As exemplified here, it may be that sorbents may ultimately have a greater impact on volumetric density than on gravimetric density compared to other gas compression or liquefaction physical approaches.

Thin Films on Templates

Several other synthetic methods are used to form the requisite porous materials. Perhaps one of the more intriguing methods involves synthetic processes that deposit thin films of lightweight materials on “templates” that have optimal pore structures. In this way, the optimal pore structures are obtained via the template. Typically, the heavier materials of the template are then removed, leaving behind the lighter-weight deposited material. Although relatively new, these techniques have been used to demonstrate materials with excellent hydrogen storage properties.⁷

Additional improvements in engineering design and/or material gravimetric capacities will be required for high surface-area sorption materials to meet DOE's 2015 gravimetric system targets (5.5 wt%). From a practical standpoint, material availability and low atomic mass will be needed to create inexpensive sorbents with high specific-surface-areas.

In general, carbon is an inexpensive material, and high-specific-surface-area materials are commercially produced at ~\$1/Kg today. Thus, for carbon, the raw materials are not a significant factor in hydrogen storage system costs, leaving the system hardware as the main cost issue.

Initial work performed by TIAX LLC as part of the EERE Hydrogen Storage System Analysis Working Group (SSAWG)²⁹ indicates that sorption-based tank system costs (~\$15/kWh) need to be significantly reduced to meet DOE cost targets. However, the analysis to date has not been optimized to the material. If optimized high specific-surface-area materials with sufficient capacity are used, the system costs can be substantially reduced by decreasing the operational system pressure to ~50 bar and increasing tank capacity to ~10Kg H₂. In this scenario, using an initial analysis performed by TIAX LLC in 2007,³⁰ increasing the tank capacity to ~10Kg H₂ should reduce overall costs by ~25% to ~\$11/kWh.

Furthermore, carbon fibers used to strengthen the tank may be reduced and thus reduce tank cost fiber reductions by perhaps a factor of five to ~\$1.5/kWh. In addition, the lower pressure may reduce the balance-of-plant (BOP) component costs from ~\$2/kWh to perhaps <\$1.5/kWh. If processing costs were to decrease more than twofold (with improved designs and materials) to <\$1/kWh, and the media costs were more in line with present commercial activated carbon costs of <\$1/kWh it may be possible with these assumption to make an ~10 Kg H₂ tank for the DOE 2015 target of ~\$4/kWh. The latter two assumptions are within the sensitivity range of TIAX's analysis, while the first two are projections of the decreased costs associated with reducing the system operating pressure from 250 bar to 50 bar.

A detailed analysis must be performed to validate these assumptions, but this initial set of assumptions demonstrates a potential path for meeting the DOE 2015 cost targets with physisorption based materials. Furthermore, as seen from this analysis, as storage temperatures and pressures approach ambient, the overall system costs should decrease, even if more thermal management components are needed. Thus, the Center has focused on developing materials with higher binding energies that enable ambient-temperature and pressure storage; such materials should have a better chance of meeting the DOE targets.

Increasing Dihydrogen Binding Energy

To increase dihydrogen binding beyond what is typically achieved with physisorption, more “chemical” type bonding must occur. In the case of dihydrogen, this means enhanced electron sharing between the gas molecule and the sorption material. This can only be achieved by creating structures in the material that are electronically out of equilibrium (i.e., reactive or frustrated). Unfortunately, this is relatively difficult and thus only a few approaches work.

Even though the Center performed relatively exhaustive searches, when considering all the other hydrogen storage targets, sp²-coordinated boron in carbon and coordinated (but electronically unsaturated) single-metal 1st row transition atoms are the only ways to significantly enhance dihydrogen binding with lightweight elements. The main challenges with these approaches include being able to uniformly disperse these higher binding sites in such a way that they are accessible to the dihydrogen, are stable and do not degrade with time/refueling cycles, and

provide relatively uniform dihydrogen binding throughout as much of the material storage capacity range as possible. This latter point is important from an engineering perspective so that the net available capacity can be maximized over as small a temperature and pressure range as possible, which reduces the overall system costs.

In general, sorbent materials typically have a broad binding energy range (e.g., high specific-surface-area sorbents typically have a few sites with ~ 8 - 10 kJ/mol and then the binding quickly decreases to ~ 4 kJ/mol at higher coverage). Typically, as the binding energy range increases, the storage temperature and/or pressure range will also need to increase. Promising approaches to increasing dihydrogen binding are described below.

B-Substituted for Carbon

Calculations and experimental measurements both show that stronger dihydrogen binding between 10 and 15 kJ/mol¹³ occurs when B is substituted with sp^2 coordination with carbons. This is sufficient to substantially increase the storage temperature compared to typical cryo-compressed materials, and it may be possible to meet DOE hydrogen storage capacity targets with BC₃-like materials at 150 to 250K temperatures. Any significant storage temperature increase towards ambient temperature significantly reduces weight and costs, thus making it easier to meet DOE system targets.

In general, if the binding energy increases occur with relatively small changes in low entropy and is in the range of 10 to ~ 30 kJ/mol, there will be limited impact on heat transport issues even at ambient temperatures. Therefore, the main challenge is being able to create materials with high substitution concentrations (>20 atom%) and high specific-surface areas ($>1,000$ m²/g) with the substituted element in the correct electronic state. Because the specific concentration and specific-surface-area requirements depend on many factors, including the binding energy, it is difficult to quantify the exact properties needed. As a general rule, as the binding energy increases, the more tightly the hydrogen can be packed on the surfaces., and thus the less specific-surface area is required for a given temperature and pressure.

For dihydrogen, besides beryllium (Be), other compositions like nitrogen-substituted carbons do not significantly increase binding. To form the requisite B-C materials, approaches similar to those discussed for creating high-specific-surface-area materials with optimized pore sizes have been investigated. In general, pyrolyzation and templating of B-C precursors have produced ~ 500 m²/g materials with $\sim 15\%$ B. However, materials with higher specific-surface areas have lower boron concentrations. Attempts to sublime boron into carbon materials have not proven to be reproducible. Furthermore, most materials made to date demonstrate multiple binding states. This is probably because B goes into amorphous and other carbon coordinations more easily than sp^2 . However, it is the higher energy sp^2 coordination that has the greater electronic affinity and perhaps the structural stress needed for enhanced dihydrogen binding.

Heterogeneous Compositions That Enhance Other Binding

Although other lightweight atomic substitutions in carbon do not enhance dihydrogen binding, they can increase binding of other elements and molecules. For example, as with B-C compounds, nitrogen-substituted [for] carbons and some structures in crystalline materials such as MOFs can have a higher affinity for single-metal atoms or molecules. This method can be

used to coordinate elements and molecules that in turn enhance dihydrogen binding. For example, calculations indicate that F^-/BF_4^- have dihydrogen isosteric heats of adsorption of ~ 12 kJ/mol.¹⁵ This is sufficient to substantially increase hydrogen storage capacities at higher temperatures than liquid nitrogen temperature. Unfortunately, after a focused effort to engineer such materials, the limited storage capacities achieved suggested that, at this time, this material should be down-selected and the Center should perform no further work on it. Along these lines, it is believed that charge-compensated structures can be synthesized that affect the dihydrogen electronic structure sufficiently to enhance storage. However, no experimental validation of these effects has been demonstrated to date.

Coordinated Metal Centers

The final class of materials that enhance dihydrogen binding was first experimentally identified by Kubas et al.³¹ and involves creating materials in which individual metal atoms are coordinated to, or in, structures to keep them from agglomerating, but with electrons that are not fully compensated. Although initial experimental work demonstrated enhanced dihydrogen adsorption, the key experimental and theoretical findings are that this approach can be used to enhance binding of multiple (more than two) dihydrogen molecules with a single metal atom.^{17,19}

This enhanced binding can occur at the metal atom site itself, or potentially, be charge transferred to the matrix material, which may enhance adsorption over the entire exposed surface.¹⁶ The structurally coordinated but electronically unsaturated metal centers can be stabilized at higher energy binding sites on or within a material (e.g., boron- or nitrogen-substituted sites in carbon, or “exposed” sites in materials such as MOFs,³² Metallo-carbohedrenes, or macromolecules). These types of metal centers enable even ambient-temperature dihydrogen storage. Metal clustering and reaction with other elements reduce or eliminate the enhanced capacities, and thus materials must be designed to stabilize the metal centers.

The calculations used to make these initial predictions¹⁷ are in good agreement with experimental results that have observed adsorption of two or more dihydrogen molecules.¹⁹ Furthermore, similar calculations have predicted that Ca has unique hydrogen storage properties; specific materials incorporating Ca are predicted to have more than 10 wt% and 100 g/L hydrogen storage capacities.¹⁸ Although the observed storage capacity has yet to be experimentally determined for these materials, the implication from the theoretical work indicates that the dihydrogen binding energy is sufficiently high to enable reversible storage at ambient temperatures and relatively low pressures (e.g., 10 to 50 bar), whereas the entropy and other factors should be appropriate so that heat generation during refueling should not be a significant issue.

In general, a few other first-row transition metals are also good candidates for hydrogen storage materials. However, based on work to date, it is imperative that approaches be used to stabilize the coordination of the metal centers. Calculations and synthetic experience are used to predict new energetically stable materials and to identify viable synthetic routes.

Optimizing Weak Chemisorption

Reversible storage at near-ambient temperature and nominal pressure can also be accomplished by weak chemisorption of atomic hydrogen with sorbent materials.²¹ This chemisorption could possibly be achieved via a hydrogenation process. However, when gas-phase hydrogen (H₂) is used, catalysts or autocatalytic materials are typically required to dissociate the dihydrogen molecules, and then the atomic hydrogen “spills over” and is stored on receptor materials.

This process has been observed in part in the catalytic processes used in the petroleum and petrochemical process industries. Only recently has this process been demonstrated to create moderate storage capacities at ambient temperature and ~100 bar pressure. Hydrogen discharge rates via spillover storage are predicted to be able to meet DOE system targets.²¹ However, hydrogen charge or refill rates and total storage capacity must be improved.

Furthermore, because the binding energies for spillover are relatively moderate (i.e., 10 to 25 kJ/mol), heat generation during refueling should not be a significant issue. A detailed mechanistic understanding of all the spillover reaction steps is being developed to provide the insights necessary to improve the storage-uptake rates and total available capacity. A thermodynamic framework for the spillover process is well developed for atomic hydrogen stored on receptor materials,²² catalyst-assisted hydrogen dissociation, and hydrogen transport to the receptor materials from the catalysts.³³ These components have been validated using known results with spillover on the MoO₃.²⁰

Computationally, MoO₃ is an analogous model system for carbon and MOF receptor materials. The main issue that needs to be understood (even though a couple of potential mechanisms have been identified) is how the hydrogen travels along the receptor material’s surfaces.³⁴ Current experimental investigations involve methods to improve reproducible catalyst integration with the receptor materials, receptor-surface functionalization effects, and hydrogen transport on the receptor. Incorporation with specific functional groups has been shown computationally and experimentally to enhance or reduce spillover effects.

For example, the use of carbon “bridges” between the catalysts and the receptor substrate more than doubled the capacity of the spillover material to more than 4 wt% at ambient temperature and ~100 bar for an MOF-based material.²¹ In addition, experimental results indicate that improved catalysts, integration processes, and/or surface-functional groups improved spillover rates and capacities.

The Center will continue performing systematic experiments to investigate structural, surface functionalization and physisorption effects for spillover. In addition, the Center will continue developing specific characterization procedures to ensure that side chemical reactions and measurement baseline-drift issues are not skewing the results. With some processing conditions, an irreversible set of chemical reactions can account for some, or all, of the initial hydrogen uptake observed during initial exposure to hydrogen. These chemical reactions typically produce by-products such as water or methane, which can be easily detected in the effluent during discharging.

In addition, due to the relatively long times associated with hydrogen loading on some spillover materials, it is critical to have extremely good thermal control of the measurement system to ensure that pressure changes observed are not related to changes in temperature. Based on the experimental results obtained so far, spillover has the potential to be used to meet DOE targets using a potentially near ambient temperature material.

RECOMMENDATIONS FOR FUTURE RESEARCH DIRECTION

The Center recommends that development efforts for specific material classes be continued where viable routes exist for synthesizing sorbents that can be used to meet the appropriate set of targets. The specific selection criteria for future efforts should focus on the DOE 2015 and the Ultimate Full-Fleet hydrogen storage targets. As noted previously, the focus has been, and should remain, on capacity, transient performance (including thermal management) and costs. We recommend this because the majority of the other DOE 2015 and Ultimate targets for sorbents will be more of a system-engineering issue than an intrinsic material property issue.

For example, even when dihydrogen binding energies are substantially increased to enable near-ambient-temperature storage, these binding energies (typically 10 to 25 kJ/mol) and the associated entropies of dihydrogen are low enough that the relatively small amount of heat generated during refueling should be easily removed with the typical sorption material's intrinsic thermal conductivity properties and/or appropriately designed integration of thermal conductivity materials in condensed "pelletize" materials. In addition, because most sorbent materials will likely operate at moderate pressures (i.e., 10 to 100 bar), delivery rates and system pressures should not be significant issues.

In general, a range of temperature and pressure can be used as long as the materials and systems can be constructed to meet the DOE targets. However, typically, the closer to ambient the system operating conditions, the less expensive the system costs. This must be traded against overall system performance, which includes the potential need for added heat removal.

This need for balance leads to five specific recommendations.

Recommendation 1 – Develop only a select set of materials in which the primary storage mechanism is physisorption.

The Center recommends that present and future development should be performed only on a select set of materials in which the primary storage mechanism is physisorption. To meet the DOE 2015 targets, the only physisorption materials that should be considered for development are those that can have specific-surface areas greater than 3,000 m²/g, optimized uniform pore sizes in the range of ~0.7 to ~1.2 nm, and excess material hydrogen storage capacities greater than 50 g/L and 7 wt% at cryogenic temperatures (~80–200 K) and moderate pressures (less than 100 bar).

Although it may be possible to meet the DOE 2015 system targets with high-specific-surface-area materials, isosteric heats of adsorption between 10 and 25 kJ/mol will be required to

increase storage temperatures above ~100K to significantly improve system capacity and/or costs. Near ambient temperatures will be required to meet DOE Ultimate full-fleet storage targets. Such targets can be met in a number of ways, including developing specific heterogeneous materials, coordinated but unsaturated metal centers, and weak hydrogenation processes such as spillover.

Recommendation 2 – Develop substituted/heterogeneous materials that have demonstrated hydrogen binding energies in the range 10 – 25 kJ/mol.

As stated earlier, for pure carbon systems, only a few elements (e.g., boron substituted in sp^2 coordination) substantially enhance dihydrogen binding. However, other heterogeneous systems (e.g., certain MOFs) have demonstrated enhanced dihydrogen binding.¹⁴ In general, the principle is well established; the main issues include access and creating enough high-binding energy sites to substantially increase capacities.

In addition, these heterogeneous materials also demonstrate substantial stabilization of single-metal centers and other absorbed species that improve hydrogen storage. Thus, the Center recommends that researchers should develop substituted/heterogeneous materials that can be used to enhance dihydrogen isosteric heats of adsorption in the range of 10–25 kJ/mol. These materials will enable near-ambient-temperature (150–250K) hydrogen storage. Development efforts should focus on creating materials with the appropriate chemical and electronic structures, sufficient composition, and high specific-surface areas. These materials will potentially decrease system hardware costs and constraints and may be used to meet DOE’s 2015 hydrogen storage system targets (40 g H₂/L; 5.5 wt%).

Recommendation 3 – Develop materials for hydrogen storage by spillover.

Ambient-temperature storage via catalytic hydrogen dissociation and transfer to high-specific-surface-area receptor materials (i.e., spillover) demonstrate 10 to 30 kJ/mol reversible hydrogen binding energies, which enable ambient-temperature storage. Furthermore, because the binding energies for spillover are much lower than for typical metal or chemical hydrides, thermal management issues for heat removal during refueling and delivery rate issues should be moderate, and thus should not significantly impact the overall storage system.

Although some of the processes involved have been demonstrated experimentally and by thermodynamic principles, additional development is needed to further understand and improve atomic hydrogen transport on the receptor material (for uptake/refill and discharge kinetics) and to improve the performance reproducibility and effectiveness of the synthetic processes. Once these issues are addressed, initial analyses indicate that because spillover enables ambient-temperature storage, systems with more than 75%³⁵ of the material capacities can be achieved using basic pressurized (~100 bar) tanks.

Initial analysis indicates that excess material storage capacities of more than 7 wt% should be possible with spillover. In addition, because spillover should be applicable to materials with more than 1 g/ml bulk density, storage systems with more than 50 g/L and more than 5.5 wt% capacities should be achievable at ambient temperature and ~100 bar. Thus, with inexpensive

carbon-based materials and the development of inexpensive highly dispersed catalysts (e.g., nanoparticle Ni), spillover materials should be usable in systems that meet DOE's 2015 targets. Thus, the Center recommends that spillover or equivalent materials continue to be developed for hydrogen storage.

Recommendation 4 – Develop materials for multiple dihydrogen storage on designated sites.

Multiple-dihydrogen adsorption on designed sites provides a reasonable path toward meeting DOE's Ultimate full-fleet targets, with the proviso that this may require substantial development efforts. Several inexpensive material systems have been predicted that may be used to meet these targets at near-ambient temperature. One prediction includes the use of inexpensive Ca with inexpensive carbon supports to form materials that may be able to store hydrogen at ambient temperature with twice the gravimetric and volumetric densities compared to liquid hydrogen. Such a structure, if it is possible to synthesize and stabilize, promises to be a tremendous breakthrough. Thus, while substantial efforts will be needed to form the novel structures, development of multiple-dihydrogen adsorption on designed sites should be continued because the resulting structures could meet DOE Ultimate targets. Meeting those targets will enable hydrogen to become a viable energy carrier for transportation and other important renewable energy applications.

Recommendation 5 - Develop materials in concert with designs for hydrogen storage systems.

Compared to compressed (350 to 700 bar) or cryo-compressed hydrogen storage technologies, with demonstrated material packing densities and storage properties, the main benefits of sorption materials include substantial (twofold) reductions in volume (see Figure 4), reductions in pressure (~20-fold), and a fourfold or more increase in storage temperature. All this substantially improves system costs, resonance times for boil-off, and resolution of engineering-design issues.

Thus, development efforts should continue to optimize the materials for specific storage systems. Based on the successes achieved since the Center's inception, researchers have created sorption materials that have the potential to meet DOE's new 2010 targets, assuming that storage systems are optimized for the sorbent material being used. If sorbent materials are to be used to meet the DOE 2015 and Ultimate targets, it will be even more imperative that storage systems be optimized for the new sorbent materials with higher binding energies and other substantially different but critical performance characteristics.

Conclusion

At the time of the Center's inception, the required hydrogen storage performance criteria used to identify potential development materials were strict. Based on this and a number of other factors, a substantial amount of materials have been down-selected that should not be developed further. However, a limited number of viable routes exist to synthesize sorbent materials that can likely be used to meet DOE's 2015 and even DOE's Ultimate full-fleet on-board system targets.

Sorbent materials, which will be refilled on-vehicle, enables the potential for substantially higher refueling efficiencies (and thus lower costs) since storage material transport and regeneration will not be needed; as may be the case for off-vehicle regeneration. Thus, the Center believes that the on-vehicle refueling capability of sorbent materials is a tremendous advantage that should be exploited for hydrogen storage. However, to fully exploit this advantage, it is imperative that development efforts focus on reducing material and system costs. This cost reduction can be achieved by improving material storage capacities at near ambient temperatures. Furthermore, any future efforts must also investigate the material properties related to hydrogen storage systems, so that thermal conductivity, heat dissipation, refill and discharge rates, durability, and other engineering issues can be fully quantified.

Table 1: List of materials investigated that should be considered (Go Decision) for future materials development and hydrogen storage system analysis and design. The maximum reversible hydrogen capacity achieved for each system as well as the reason for the selection is provided.

System	Partner(s) Involved	Predicted Capacity ^a	Predicted ΔH (kJ/mol- H_2) ^a	Observed ΔH (kJ/mol- H_2)	Maximum Reported Hydrogen Capacity ^c	Status
Nanoporous (<1.2 nm pore size) materials (e.g., pyrolyzed, templated, polymer, etc.)	Duke, UMC, ANL, Rice, ORNL, NREL	5–8 wt%, 50 to 80 g/L	4–8	4–8	1 wt% (293 K, 100 bar) ⁿ >7 wt%, >50 g/L (77 K, ~50 bar) ^m >3000m ² /g	SSAWG indicates that it could meet 2015 system targets.
B-C materials with high SSA and B>20 atom% in correct coordination	PSU, NREL, APCI, ANL, Duke, LLNL, UMC	6–9 wt% 50 to 80 g/L	4–12	4–12	0.6 wt% (293 K, 100 bar) ⁿ ~3.8 wt% (77 K, ~50 bar), ^m only had ~500 m ² /g	Could meet DOE 2015 system targets at near-ambient T if SSA and B increased.
Coordinated metal centers; metal atoms on B-Cs, Ca-Graphene, Met-Cars, opened MOFs, etc.	NREL, TAMU	5 to 11 wt% 50 to 120 g/L	10 - 40	10 - 35	4.5 wt%, 37 g/L (77 K, 45 bar) ^m ~0.2 wt% (300K, 2 bar & 5 g/m ²) ^{n, b} ~10 times higher than AC	Could meet DOE ultimate targets at ambient T if stable materials can be made.
Spillover on catalyst-integrated materials	UM, NREL, ORNL, LLNL	8 wt% 80 g/L	10–25	10-25	4 wt% (298 K, 100 bar) ⁿ ~2 times increase at 200 bar measured ^d ~550m ² /g	Could meet DOE 2015 targets at ambient T with better catalysts/ materials.

- a. Predicted storage capacities and ΔH are based on first principle models with an accurate accounting of probable reversible hydrogen storage capacity for idealized conditions. The idealized conditions (e.g., pressure and temperature) will depend upon several factors, including the ΔH and entropy of the storage materials/system.

- b. The specific material formed had virtually no porosity, but showed that ambient-temperature storage by even a limited number of higher energy binding sites has a substantial impact on capacity. Superactivated carbon with more than 3,000 m²/g has 10 times less hydrogen storage at the same conditions. Other materials have been formed with much higher specific-surface areas.
- c. In general, other properties (e.g., thermal conductivity, rates, bulk densities) of the sorbent materials were not quantified because no specific issues were observed during the measurements. Thus, volumetric capacities can be assumed from the gravimetric results by assuming 0.5 to 1 g/L bulk densities for the materials. This level of bulk density has been achieved in a number of sorbent materials and should be achievable for most other materials made.
- d. In general, spillover tends to be somewhat linear with pressure. Recent unpublished measurements at NREL demonstrated that a Ru/AC material that had ~1.1 wt% at ~100 bar had ~2 wt% at 200 bar pressures at ambient temperature. This suggests that for spillover, capacity will need to be traded with pressure to construct an optimized system.
- m. Maximum excess adsorption quantities
- n. Not a maximum excess adsorption quantity, just a directly measured value at the temperature and pressure provided.

REFERENCES AND SELECTED PUBLICATIONS ON MATERIALS INVESTIGATED BY THE HSCoE

Note that this report and thus the references provided in this report were not meant to be comprehensive in review, and so represent only examples of the vast amount of literature available for the topics discussed.

- ¹ Multi-Year Research, Development and Demonstration Plan: Planned Program Activities for FY2005–2015. <http://www1.eere.energy.gov/hydrogenandfuelcells/mypp/index.html> (accessed September 23, 2009).
- ² “GRAND CHALLENGE” FOR BASIC AND APPLIED RESEARCH IN HYDROGEN STORAGE”, Funding Opportunity Announcement DE-PS36-03GO93013, September 2003.
- ³ S.K. Bhatia, A.L. Myers, *Langmuir* [online] **2006**, *22*, pp.1688–1700.
- ⁴ High-Pressure Hydrogen Storage in Zeolite-Templated Carbon Hiroto Nishihara, Peng-Xiang Hou, Li-Xiang Li, Masashi Ito, Makoto Uchiyama, Tomohiro Kaburagi, Ami Ikura, Junji Katamura, Takayuki Kawarada, Kazuhiko Mizuuchi, and Takashi Kyotani. *J. Phys. Chem. C*, **2009**, *113* (8), pp.3189–3196.
- ⁵ e.g., (i) Serguei Patchkovskii, John S. Tse, Sergei N. Yurchenko, Lyuben Zhechkov, Thomas Heine, Gotthard Seifert. Graphene Nanostructures as Tunable Storage Media for Molecular Hydrogen. *PNAS* [online] **2005**, *102*, pp.10439–10444.
- ⁶ e.g., (i) B. Yakobson, IV. C Hydrogen Storage, *DOE Annual Hydrogen Storage Report 2009*. (ii) A.K. Singh, J. Lu, R. Aga, B.I. Yakobson. Comparative Evaluation of Carbon-Foams Hydrogen Storage Capacity through Monte-Carlo Simulations. In preparation. (iii) O.V. Pupysheva, A.A. Farajian, B.I. Yakobson. Fullerene Nanocage Capacity for Hydrogen Storage (cover article). *Nano Letters* [online] **2008**, *8*, pp.767–774.
- ⁷ e.g., (i) Zhuxian Yang, Yongde Xia, Robert Mokaya. Enhanced Hydrogen Storage Capacity of High Surface Area Zeolite-like Carbon Materials. *J. AM. CHEM. SOC.* **2007**, *129*, pp. 1673–1679. (ii) L.J. Simpson, IV.C Hydrogen Storage, *DOE Annual Hydrogen Storage Report 2009*.
- ⁸ e.g., (i) Polyaniline. (ii) S. Yuan, S. Kirklín, B. Dorney, D.-J. Liu, L. Yu. Nanoporous Polymers Containing Stereo-contorted Cores for Hydrogen Storage. *Macromolecules* **2009**, *42*(5), pp.1554–1559. (iii) Y. Yuan, I. Cabasso, H. Liu. Surface Morphology of Nanostructured Polymer-based Activated Carbons. *J. Physical Chem. B* **2008**, pp.14364–14372.
- ⁹ e.g., (i) Antek G. Wong-Foy, Adam J. Matzger, Omar M. Yaghi. Exceptional H₂ Saturation Uptake in Microporous Metal-Organic Frameworks. *J. Am. Chem. Soc.* [Online] **2006**, *128*, pp.3494–3495. (ii) D.J. Collins, H.-C. Zhou. Hydrogen Storage in Metal-organic Frameworks. *J. Mater. Chem.* **2007**, *17*, pp.3154–3160.
- ¹⁰ e.g., (i) T.F. Baumann, M.A. Worsley, T.Y. Han, J.H. Satcher, Jr. High Surface Area Carbon Aerogel Monoliths with Hierarchical Porosity. *J. Non-Cryst. Solids* [Online] **2008**, *354*, pp.3513–3515. (ii) M.A. Worsley, J.H. Satcher, Jr., T.F. Baumann. Synthesis and Characterization of Monolithic Carbon Aerogel Nanocomposites Containing Double-walled Carbon Nanotubes. *Langmuir*[Online] **2008**, *24*, pp.9763–9766. (iii) Houria Kabbour, Theodore F. Baumann, Joe H. Satcher, Jr., Angelique Saulnier, Channing C. Ahn. Toward New Candidates for Hydrogen Storage: High-Surface-Area Carbon Aerogels. *Chem. Mater.* [Online] **2006**, *18* (26), p 6085.
- ¹¹ e.g., (i) A.A. Puzovskiy, D.B. Geohegan, D. Styers-Barnett, C.M. Rouleau, B. Zhao, H. Hu, M.D. Cheng, D.W. Lee, I.N. Ivanov. High Power Laser Vaporization Synthesis of Single Wall Carbon Nanotubes and Nanohorns. *Appl. Phys. A* [Online] **2008**, *93*(4), pp.849–855. (ii) D.B. Geohegan, A.A. Puzovskiy, D. Styers-Barnett, H. Hu, B. Zhao, H. Cui, C.M. Rouleau, G. Eres, J.J. Jackson, R.F. Wood, S. Pannala, J. Wells. In Situ Time-Resolved Measurements of Carbon Nanotube and Nanohorn Growth. *Phys. Stat. Sol. (b)* [Online] **2007**, *244* (11), pp.3944–3949.
- ¹² e.g., (i) P.F. Weck, E. Kim, N. Balakrishnan, H. Cheng, B.I. Yakobson. Designing Carbon Nanoframeworks Tailored for Hydrogen Storage. *Chem. Phys. Lett.* [Online] **2007**, *439*, pp.354–359. (ii) F. Ding, Y. Lin, P. Krasnov, B.I. Yakobson. Nanotube Derived Carbon Foam for Hydrogen Storage. *J. Chem. Phys.* [Online] **2007**, *127*, pp.164703. (iii) Ashley D. Leonard, Jared L. Hudson, Hua Fan, Richard Booker, L.J. Simpson, K.J. O’Neill, P.A. Parilla, Michael J. Heben, Carter Kittrell, Matteo Pasquali, James M. Tour. Nanoengineered Carbon Scaffolds for Hydrogen Storage. *J. Am. Chem. Soc.* [Online] **2008**, *131*(2), pp.723–728. (iv) Dmitry V. Kosynkin, Amanda L. Higginbotham, Alexander Sinitskii, Jay R. Lomeda, Ayrat Dimiev, B. Katherine Price, James M. Tour. Longitudinal Unzipping of Carbon Nanotubes to Form Graphene Nanoribbons. *Nature* [Online] **2009**, *458*, pp.872–876.

- ¹³ e.g., (i) Yong-Hyun Kim, Yufeng Zhao, Andrew Williamson, Michael J. Heben, S. B. Zhang. Nondissociative Adsorption of H₂ Molecules in Light-Element-Doped Fullerenes. *Phys. Rev. Lett.* [Online] **2006**, *96*, pp.016102. (ii) T.C. Mike Chung, Youmi Jeong, Qiang Chen, Alfred Kleinhammes, Yue Wu. Synthesis of Microporous Boron-Substituted Carbon (B/C) Materials Using Polymeric Precursors for Hydrogen Physisorption. *J. Am. Chem. Soc.* [Online] **2008**, *130*, pp.6668. (iii) A. Cooper, IV.C Hydrogen Storage, *DOE Annual Hydrogen Storage Report 2008*.
- ¹⁴ e.g., (i) Y. Liu, J.-H. Her, A. Dailly, A.J. Ramirez-Cuesta, D.A. Neumann, C.M. Brown. A Reversible Structural Transition of MIL-53 with Temperature Hysteresis, *J. Am. Chem. Soc.* [Online] **2008**, *130*, p 11813. (ii) N.J. Hess, M.R. Hartman, C.M. Brown, E. Mamontov, A. Karkamkar, D.J. Heldebrant, L.L. Daemen, T. Autrey. Quasielastic Neutron Scattering Experiments of Orthorhombic Ammonia Borane. *Chem. Phys. Letts.* [Online] **2008**, *459*, pp.85–88.
- ¹⁵ A. Cooper, IV.C Hydrogen Storage, *DOE Annual Hydrogen Storage Report 2008*.
- ¹⁶ Sun Q, Wang Q, Jena P. Functionalized Heterofullerenes for Hydrogen Storage. *App. Phys. Lett.* [Online] **2009**, *94*, p. 013111.
- ¹⁷ e.g., (i) Yufeng Zhao, Yong-Hyun Kim, A.C. Dillon, M.J. Heben, S.B Zhang. Hydrogen Storage in Novel Organometallic Buckyballs. *Phys. Rev. Letts.* [Online] **2005**, *94*, p 155504. (ii) Cheng-Gen Zhang, Renwu Zhang, Zhi-Xiang Wang, Zhen Zhou, Shengbai B. Zhang, Zhongfang Chen. Ti-Substituted Boranes as Hydrogen Storage Materials: A Computational Quest for the Ideal Combination of Stable Electronic Structure and Optimal Hydrogen Uptake. *Chem. Eur. J.* **2009**, *15*, pp.5910–5919. (iii) Yufeng Zhao, Y.-H. Kim, L.J. Simpson, A.C. Dillon, S.-H. Wei, M.J. Heben. Opening Space for H₂ Storage: Cointercalation of Graphite with Metal and Small Organic Molecules. *Phys. Rev. B* [Online] **2008**, *78*, pp.144102. (iv) Y. Liu, H. Kabbour, C.M. Brown, D.A. Neumann, C.C. Ahn. Increasing the Density of Adsorbed Hydrogen with Coordinatively Unsaturated Metal Centers in Metal-Organic Frameworks. *Langmuir* [Online] **2008**, *24*, p 4772. (v) Y. Zhao, M.T. Lusk, A.C. Dillon, M.J. Heben, S.B. Zhang. Boron-Based Organometallic Nanostructure: Hydrogen-Storage Properties and Structure Stability. *Nano Lett.* [Online] **2008**, *9*, pp.157–161. (vi) Yufeng Zhao, Y.-H. Kim, L.J. Simpson, A.C. Dillon, S.-H. Wei, M.J. Heben. Opening Space for H₂ Storage: Cointercalation of Graphite with Metal and Small Organic Molecules. *Phys. Rev. B* [Online] **2008**, *78*, p 144102.
- ¹⁸ (i) Y.-H. Kim, Y.Y. Sun, S.B. Zhang. Ab initio Calculations Predicting the Existence of an Oxidized Calcium Dihydrogen Complex to Store Molecular Hydrogen in Densities up to 100 g/L. *Phys. Rev. B* [Online] **2009**, *79*, p 115424. (ii) Y.Y. Sun, Kyuho Lee, Yong-Hyun Kim, S.B. Zhang. Ab initio Design of Ca-Decorated Organic Frameworks for High Capacity Molecular Hydrogen Storage with Enhanced Binding. *Appl. Phys. Lett.* [Online] **2009**, *79*, p 115424. (iii) M. Yoon, S. Yang, C. Hicke, E. Wang, D. Geohegan, Z. Zhang. Calcium as a Superior Coating Metal in Functionalization of Carbon Fullerenes for High-Capacity Hydrogen Storage. *Phys. Rev. Lett.* [Online] **2008**, *100*, p 206806.
- ¹⁹ (i) Ahmad Hamaed, Michel Trudeau, David M. Antonelli. H₂ Storage Materials (22KJ/mol) Using Organometallic Ti Fragments as σ -H₂ Binding Sites. *J. Am. Chem. Soc.* [Online] **2008**, *130*, pp.6992–6999. (ii) Lee, K.; Lucking, M.; Sun, Y.Y.; Chen, Z.; Zhang, S. Structural Stability and Hydrogen Storage Properties of Ti Anchored on Silica. *Nano Lett.* **2009**.
- ²⁰ (i) Chen, L.; Cooper, A.C.; Pez, G.P.; Cheng, H. J. On the Mechanisms of Hydrogen Spillover in MoO₃. *Phys. Chem. C*. [Online] **2008**, *112*, p. 1755. (ii) Chen, L.; Pez, G.P.; Cooper, A.C.; Cheng, H. A Mechanistic Study of Hydrogen Spillover in MoO₃ and Carbon-based Graphitic Materials. *J. Phys.: Condens. Matter* [Online] **2008**, *20*, p 064223.
- ²¹ e.g., (i) A.J. Lachawiec, Jr., R.T. Yang. Isotope Tracer Study of Hydrogen Spillover on Carbon-Based Adsorbents for Hydrogen Storage. *Langmuir* [Online] **2008**, *24*, p. 6159. (ii) Y.W. Li, R.T. Yang. Hydrogen Storage in Metal-Organic Frameworks and a Covalent-Organic Framework. *AIChE Journal* **2008**, *54*, p 269. (iii) Y.W. Li, R.T. Yang. Hydrogen Storage on Platinum Nanoparticles Doped on Super-Activated Carbon. *J. Phys. Chem. C*. [Online] **2007**, *111*, p. 11086. (iv) L.F. Wang, R.T. Yang. New Sorbents for Hydrogen Storage by Hydrogen Spillover – A Review. *Energy & Environmental Science, Roy. Soc. Chem. Cambridge* **2008**, *1*, p 268. (v) Y.H. Wang, R.T. Yang. Increased Hydrogen Spillover by Gaseous Impurity -Benson-Boudart Method for Dispersion Revisited. *J. Catalysis* **2008**, *260*, p 198. (vi) R.T. Yang, Y.H. Wang. Catalyzed Hydrogen Spillover for Hydrogen Storage. *J. Am. Chem. Soc.* [Online] **2009**, *131*, p 4224.
- ²² e.g., (i) C.K. Lin, Z.Z. Yang, T. Xu, Y.Z. Zhao. An in Situ Electrical Study on Primary Hydrogen Spillover from Nanocatalysts to Amorphous Carbon Support. *Appl. Phys. Lett.* [Online] **2008**, *93*, p 233110. (ii) Y. Lin, F. Ding, B.I. Yakobson. Hydrogen Storage by Spillover on Graphene as a Phase Nucleation Process. *Phys. Rev. B* **2008**,

-
- 78, p 041402-R. (iii) Chen, L.; Cooper, A.C.; Pez, G.P.; Cheng, H.J. Mechanistic Study on Hydrogen Spillover onto Graphitic Carbon Materials. *Phys. Chem. C*. [Online] **2007**, 111, p 18995 (2007).
- ²³ e.g., see Schwarz, J.A. *Final Report for the Tasks XC-1-1108-1 and XAE-3-13346-01* (National Renewable Energy Laboratory, Golden, Colorado) 1994.
- ²⁴ (i) P. Bénard, R. Chahine. *Scr. Mater.* 2007, 56, p 803. (ii) P. Bénard, R. Chahine. *Int. J. Hydrogen Energy* **2001**, 26, p 849.
- ²⁵ (i) J. Liu, IV.C Hydrogen Storage, *DOE Annual Hydrogen Storage Report 2009*. (ii) Thomas P. McNicholas, Simiao Zhang, Yanqin Wang, Lin Simpson, Alfred Kleinhammes, Yue Wu, Jie Liu. Effect of Surface Area and Microporosity of Microporous Carbon Materials Prepared from Decomposition of PEEK Polymer on the Hydrogen Storage Capacity and Binding Energy. In Preparation, **2009**.
- ²⁶ Pfeifer, P.; Burrell, J.W.; Wood, M.B.; et al. High-surface-area Biocarbon for Reversible On-board Storage of Natural Gas and Hydrogen. *Life-Cycle Analysis for New Energy Conversion and Storage Systems Conference Proceedings, Boston, MA* **2007**, pp.63–74.
- ²⁷ C. Ahn, IV.C Hydrogen Storage, *DOE Annual Hydrogen Storage Report 2009*.
- ²⁸ Y. Zhao, Y.-H. Kim, S.B. Zhang. Theory of Hydrogen Storage in Nanoscale Materials. In *Frontiers in Nanoscience and Nanotechnology*, Vol. 3.
- ²⁹ See for example the *DOE Annual Hydrogen Reports* for years 2005–2009.
- ³⁰ See S. Lasher, K. McKenney, Y. Yong, B. Rancatore, S. Unnasch, M. Hooks, TIAX LLC, *DOE Hydrogen Program Annual Merit Review 2007*.
- ³¹ Kubas, G. J. Metal–dihydrogen and σ -bond coordination: the consummate extension of the Dewar–Chatt–Duncanson model for metal–olefin π bonding. *Journal of Organometallic Chemistry* **2001** 635, pp.37–68.
- ³² e.g., (i) M. Dinca, A. Dailly, Y. Liu, C.M. Brown, D.A. Neumann, J.R. Long. Observation of Cu^{2+} - H_2 Interactions in a Fully Desolvated, Sodalite-type Metal-organic Framework. *Angewandte Chemie* [Online] **2007**, 46, p 1419.
- ³³ A.K. Singh, M.A. Ribas, B.I. Yakobson. H-spillover through the Catalyst Saturation: An ab initio thermodynamics study. *Nano Lett.* [Online] **2009**, 3, p 1657.
- ³⁴ e.g., (i) L.J. Simpson, IV.C Hydrogen Storage, *DOE Annual Hydrogen Storage Report 2009*. (ii) D. West, K. Lee, S.B. Zhang. Hole Mediated Diffusion of H on SP^2 Carbon Networks. *Phys. Rev. Lett.* [Online] **2009**.
- ³⁵ Internal DOE Storage System Analysis Working Group Report, 2009.

APPENDICES

Appendix I: Updated Table (June 2009) of DOE On-Board Hydrogen Storage System Targets for Light-Duty Vehicles

Technical System Targets: On-Board Hydrogen Storage for Light-Duty Vehicles				
Storage Parameter	Units	2010	2015	Ultimate
System net Gravimetric ^a	kWh/kg (kg H ₂ /kg system)	1.5 (0.045)	1.8 (0.055)	2.5 (0.075)
System Volumetric Capacity: Usable energy density from H ₂ (net useful energy/max system volume)	kWh/L (kg H ₂ /L system)	0.9 (0.028)	1.3 (0.040)	2.3 (0.070)
Storage system cost ^b (& fuel cost) ^c	\$/kWh net (\$/kg H ₂) \$/gge at pump	4* (133) 2-3	2* (67) 2-3	TBD 2-3
Durability/Operability <ul style="list-style-type: none"> • Operating ambient temperature ^d • Min/max delivery temperature • Cycle life (1/4 tank to full) ^e • Cycle life variation ^f • Min delivery pressure from storage system; FC= fuel cell, ICE= internal combustion engine • Max delivery pressure from storage system^g 	°C	-30/50 (sun)	-40/60 (sun)	-40/60 (sun)
	°C	-40/85	-40/85	-40/85
	Cycles	1000	1500	1500
	% of mean (min) at % confidence	90/90	99/90	99/90
	Atm (abs)	4FC/35 ICE	3FC/35 ICE	3FC/35 ICE
Atm (abs)	100	100	100	
Charging/discharging Rates <ul style="list-style-type: none"> • System fill time (for 5-kg H₂) • Minimum full flow rate • Start time to full flow (-20°C)^h • Start time to full flow (20°C)^h • Transient response 10%-90% and 90% -0%ⁱ 	min (Kg H ₂ /min)	4.2 min (1.2 kg/min)	3.3 min (1.5 kg/min)	2.5 min (2.0 kg/min)
	(g/s)/kW	0.02	0.02	0.02
	s	5	5	5
	S	15	15	15
	s	0.75	0.75	0.75
Fuel Purity (H ₂ from storage) ^j	% H ₂	99.99 (dry basis)		
Environmental Health & Safety <ul style="list-style-type: none"> • Permeation & leakage ^k • Toxicity • Safety • Loss of useable H₂ ^l 	Scch/h	Meets or exceeds applicable standards		
	(g/h)/kg H ₂ stored			

*The storage system costs are currently under review and will be changed at a future date.

Note: Targets are based on the lower heating value of hydrogen; targets are for a complete system, including tank, material, valves, regulators, piping, mounting brackets, insulation, added cooling capacity, and/or other balance-of-plant components. Unless otherwise indicated, all targets are for both internal combustion engine and fuel cell use, based on the low likelihood of power-plant-specific fuel being commercially viable. Also note that while efficiency is not a specified target, systems must be energy efficient. For reversible systems, greater than 90% energy efficiency for the energy delivered to the power plant from the on-board storage system is required. For systems regenerated off-board, the energy content of the hydrogen delivered to the automotive power plant should be greater than 60% of the total energy input to the process, including the input energy of hydrogen and any other fuel streams for generating process heat and electrical energy.

Footnotes to Table

Useful constants: 0.2778kWh/MJ, ~33.3kWh/gal gasoline equivalent.

^a Generally the ‘full’ mass (including hydrogen) is used; for systems that gain weight, the highest mass during discharge is used.

^b 2003 US\$; total cost includes any component replacement if needed over 15 years or 150,000-mile life.

^c 2005 US\$; includes off-board costs such as liquefaction, compression, regeneration, etc.; 2015 target based on H₂ production cost of \$2 to \$3/gasoline gallon equivalent untaxed, independent of production pathway.

^d Stated ambient temperature plus full solar load. No allowable performance degradation from –20C to 40C. Allowable degradation outside these limits is TBD.

^e Equivalent to 200,000; 300,000; and 300,000 miles respectively (current gasoline tank spec).

^f All targets must be achieved at end of life.

^g For delivery to the storage system, in the near term, the forecourt should be capable of delivering 10,000 psi (700 bar) compressed hydrogen, liquid hydrogen, or chilled hydrogen (35 to 77K) and up to 5,000 psi (350 bar). In the long term, it is anticipated that delivery pressures will be reduced to between 50 and 150 atm for solid state storage systems, based on today’s knowledge of sodium alanates.

^h Flow must initiate within 25% of target time.

ⁱ At operating temperature.

^j The storage system will not provide any purification, but will receive incoming hydrogen at the purity levels required for the fuel cell. For fuel cell systems, purity meets SAE J2719, Information Report on the Development of a Hydrogen Quality Guideline in Fuel Cell Vehicles. Examples include: total non-particulates, 100 ppm; H₂O, 5 ppm; total hydrocarbons (C₁ basis), 2 ppm; O₂, 5 ppm; He, N₂, Ar combined, 100 ppm; CO₂, 1 ppm; CO, 0.2 ppm; total S, 0.004 ppm; formaldehyde (HCHO), 0.01 ppm; formic acid (HCOOH), 0.2 ppm; NH₃, 0.1 ppm; total halogenates, 0.05 ppm; maximum particle size, <10 μm, particulate concentration, <1μg/L H₂. These are subject to change. See Appendix on Hydrogen Quality in the DOE EERE Hydrogen Fuel Cells and Infrastructure Technologies Program Multiyear Research, Development and Demonstration Plan (www.eere.energy.gov/hydrogenandfuelcells/mypp/) to be updated as fuel purity analyses progress. Note that some storage technologies may produce contaminants for which effects are unknown; these will be addressed as more information becomes available.

^k Total hydrogen lost into the environment as H₂; relates to hydrogen accumulation in enclosed spaces. Storage system must comply with CSA/HGV2 standards for vehicular tanks. This includes any coating or enclosure that incorporates the envelope of the storage system.

^l Total hydrogen lost from the storage system, including leaked or vented hydrogen; relates to loss of range.

Appendix II: Recommended Down-Selected Materials by Class

Table 1: List of physisorption-based high-specific-surface area materials that were considered and discontinued (No-Go Decision). The maximum reversible hydrogen capacity achieved for each, as well as the reason for the down-select is provided.

System	Partner(s) Involved	Predicted Capacity ^a	Predicted ΔH (kJ/mol- H_2) ^a	Observed ΔH (kJ/mol- H_2)	Maximum Reported Hydrogen Capacity	Status
Pure carbon single-wall nanotubes (SWNTs)	NREL, Rice, Duke, APCI, NIST, UNC	5–10 wt%	16–46	19.6	0.01 wt% (223 K, 0 bar) ⁿ 3 wt% (77 K, 20 bar)	Discontinued; predicted reversible capacity not observed.
Fe-decorated carbon multi-wall nanotubes (MWNTs)	NREL	Not Predicted	Not Predicted	50	0.04 wt% (273 K, 0 bar) ⁿ	No longer considered; high reversible capacity not achieved.
Co-decorated SWNTs	NREL	Not Predicted	Not Predicted	27.9	0.01 wt% (223 K, 0 bar) ⁿ	No longer considered; high reversible capacity not achieved.
Small-diameter, cut single-wall nanotubes	APCI	7 wt. %	8–18	8–11	1.5 wt. % (77 K, 1 atm) ⁿ 0.5 wt. % (298 K, 115 bar) ⁿ	Discontinued; high adsorption enthalpy not achieved.
Undoped activated carbon aerogels	LLNL, CalTech	6+ wt%	Not Predicted	~6 kJ/mol	5.3 wt% (77 K and 30 bar) ^m 0.8 wt% at RT and 100 bar	Reached maximum capacity that was below DOE target.
Double-wall carbon nanotubes	Duke	Not Predicted	Not Predicted	Not Predicted	0.11 wt% (77K, 2 bar) ⁿ	Reported improvement in DWNTs not observed in measurements.

- a. Predicted storage capacities and ΔH are based on first principle models with an accurate accounting of probable reversible hydrogen storage capacity for idealized conditions. The idealized conditions (e.g. pressure and temperature) will depend upon several factors including the ΔH and entropy of the storage materials/system.
- m. Maximum excess adsorption quantities
- n. Not a maximum excess adsorption quantity, just a directly measured value at the temperature and pressure provided.

Table 2: List of substituted materials that were considered and discontinued (No-Go Decision). The maximum reversible hydrogen capacity achieved for each system as well as the reason for the down-select is provided.

System	Partner(s) Involved	Predicted Capacity ^a	Predicted ΔH (kJ/mol-H ₂) ^a	Observed ΔH (kJ/mol-H ₂)	Maximum Reported Hydrogen Capacity	Status
Multiple wall enhanced binding	Caltech	~ 4 wt%	4 to 15	4 to 13	1.5 wt% (77 K and 3 bar) ⁿ	Model systems, provide good data, cannot meet capacity targets
B-doped SWNTs produced from B-containing graphite target	NREL, NIST	4 wt% (capacity for 10 kJ/mol - H ₂)	10	4	2 wt% (77 K, 20 bar) ⁿ	Discontinued; at 1.8 at%, maximum boron loading was too low.
Li, N, O, Na, etc. substituted carbon	NREL	~7 wt%	4	Not Measured	Not Measured	These substituted elements do not increase binding compared to just pure C
Lithium-doped SWNTs	APCI	Not Predicted	Not Predicted	6.5 – 10.5	0.7 wt.% (77 K, 1 bar) ⁿ	Discontinued; small observed capacity.
F-intercalated carbons	APCI	1 – 8 wt%	4 – 24 (for range of 1 – 8 wt%)	8 – 14	0.24 wt% at 298 K, 100 bar)	Discontinued; small observed capacity.

- a. Predicted storage capacities and ΔH are based on first principle models with an accurate accounting of probable reversible hydrogen storage capacity for idealized conditions. The idealized conditions (e.g., pressure and temperature) will depend upon several factors including the ΔH and entropy of the storage materials/system.
- m. Maximum excess adsorption quantities
- n. Not a maximum excess adsorption quantity, just a directly measured value at the temperature and pressure provided.

Table 3: List of strong/multiple H₂ binding metal center materials that were considered and discontinued (No-Go Decision). The maximum reversible hydrogen capacity achieved for each system as well as the reason for the down-select is provided.

System	Partner(s) Involved	Predicted Capacity ^a	Predicted ΔH (kJ/mol-H ₂) ^a	Observed ΔH (kJ/mol-H ₂)	Maximum Reported Hydrogen Capacity ⁿ	Status
Fe(C ₆₀)	NREL	3.5 wt%	60	4	1 wt% (77 K, 85 bar)	Discontinued; theoretical capacity/structure not observed.
Li(C ₆₀)	NREL	9 wt%	6	6	0.2 wt% (77 K, 2 bar) 0.8 wt% (300 K, no overpressure)	Discontinued; high reversible capacity not observed due to LiH formation.
Na(C ₆₀)	NREL	Not Predicted	Not Predicted	Not Measured	1 wt% (300 K, no overpressure)	No longer considered; high desorption temperature.
Ca(C ₆₀)	ORNL, NREL	8.4 wt%	20	6	0.25 wt% (77 K, 2 bar) 1 wt% (300 K, no overpressure)	Discontinued: high reversible capacity not observed due to CaH formation.
K(C ₆₀)	NREL	Not Predicted	Not Predicted	Not Measured	0.004 wt% (RT, 2 bar) 0.06 wt% (77 K, 2 bar)	No longer considered; high desorption temperature and low capacity.
Sc(C ₆₀)	NREL	Not Predicted	Not Predicted	Not Measured	0.02 wt% (RT, 2 bar) 0.04 wt% (77 K, 2 bar)	No longer considered; high desorption temperature and low capacity.
Cr(C ₆₀)	NREL	Not Predicted	Not Predicted	Not Measured	0.02 wt% (RT, 2 bar) 0.31 wt% (77 K, 2 bar)	No longer considered; high desorp. temp. and low capacity.
Co(C ₆₀)	NREL	Not Predicted	Not Predicted	Not Measured	0.01 wt% (RT, 2 bar) 0.12 wt% (77 K, 2 bar)	No longer considered; high desorption temperature and low capacity.

System	Partner(s) Involved	Predicted Capacity ^a	Predicted ΔH (kJ/mol- H_2) ^a	Observed ΔH (kJ/mol- H_2)	Maximum Reported Hydrogen Capacity ⁿ	Status
HKUST-1	NIST, U Sydney, A.U.	~4 wt %		6.6	3.26 wt % (77 K, 30 bar)	Binding strength too low.
Co-TCTHF	NIST, U Sydney, A.U.	Not Predicted	Not Predicted	9.6	1.2 wt % (77 K, 1 bar)	Low surface area
Nickel metal complexes on functionalized inorganic aerogel supports	NREL, LLNL	Not Predicted	Not Predicted	20.5 (@ low H_2 coverage)	0.29 wt% (77 K, 2 bar)	Upon scaling up of the synthesis of the Ni-supported aerogel materials, the new H_2 binding sites were not reliably reproduced and metal agglomeration was not avoided.
Organometallic scandium (Sc) complex with multiple dihydrogen ligands via solution chemistry	NREL	~9 wt %	~29	Not Measured	Not Measured	Sc sites were not coordinatively and electronically unsaturated in materials synthesized.

- a. Predicted storage capacities and ΔH are based on first principle models with an accurate accounting of probable reversible hydrogen storage capacity for idealized conditions. The idealized conditions (e.g. pressure and temperature) will depend upon several factors including the ΔH and entropy of the storage materials/system.
- n. Unless specifically stated, the material capacities listed are not a maximum excess adsorption quantity, just a directly measured value at the temperature and pressure provided.

Table 4: List of spillover materials that were considered and discontinued (No-Go Decision). The maximum reversible hydrogen capacity achieved for each system as well as the reason for the down-select is provided.

System	Partner(s) Involved	Predicted Capacity	Predicted ΔH (kJ/mol- H_2)	Observed ΔH (kJ/mol- H_2)	Maximum Reported Hydrogen Capacity ⁿ	Status
Ti-6Al-4V-decorated SWNTs	NREL	Not Predicted	Not Predicted	Not Measured	3.76 wt% (77 K, 85 bar)	No longer considered; high desorption temperature.
Pd-doped nanofibers	NIST, ORNL (not center)	Not Predicted	Not Predicted	Not Measured	Not Measured	Did not observe much spillover H using neutrons.
NaAlH ₄ -doped AX-21	UM	Not Predicted	Not Predicted	Not Measured	<1% (298 K, 100 atm)	No longer considered; H ₂ amount too low.
Pt-NaAlH ₄ -doped AX-21	UM	Not Predicted	Not Predicted	Not Measured	1% (298 K, 100 atm)	No longer considered; H ₂ amount too low.
LiCl-doped MOF-177	UM	Not Predicted	Not Predicted	Not Measured	-	Lower than undoped MOF
Pt-bridged MCM-41 (mesoporous silica, BET~1200)	UM	Not Predicted	Not Predicted	Not Measured	0.65% (298 K, 100 atm)	No longer considered; H ₂ amount too low.
Pt-bridged COF-1	UM	Not Predicted	Not Predicted	Not Measured	0.7% (298 K, 100 atm)	No longer considered; H ₂ amount too low.
Hg-Pd codoped AX-21	UM	Not Predicted	Not Predicted	Not Measured	Not Measured	Adding Hg decreased spillover compared to Pd alone
Pt-doped Activated Carbon Fibers (Osaka Gas)	UM	Not Predicted	Not Predicted	Not Measured	Not Measured	No longer considered; H ₂ amount too low.
Pd-doped on MOF-177	UM	Not Predicted	Not Predicted	Not Measured	Not Measured	Succeeded in reducing Pd <200 C, but H ₂ amt. too low.
Pt-bridged ZIF-8	UM	Not Predicted	Not Predicted	Not Measured	0.95% (298K,100 atm)	Although ZIF-8 is the only H ₂ O-stable MOF, but capacity is too

System	Partner(s) Involved	Predicted Capacity	Predicted ΔH (kJ/mol- H_2)	Observed ΔH (kJ/mol- H_2)	Maximum Reported Hydrogen Capacity ⁿ	Status
						low to continue
Pt-bridged MIL-53	UM	Not Predicted	Not Predicted	Not Measured	0.92% (298K, 100 atm)	No longer considered; H_2 amount too low.
Pt-doped on N-doped carbon	UM	Not Predicted	Not Predicted	Not Measured	Not Measured	No longer considered; H_2 amount too low.

n. Unless specifically stated, the material capacities listed are not a maximum excess adsorption quantity, just a directly measured value at the temperature and pressure provided.